1. General Information

The first conference on « Tracers and tracing methods » was organized in Nancy (France) in November 1998 by the Laboratory of Chemical Engineering Sciences. The idea was that tracing techniques were employed in a large variety of scientific and technical fields and that a forum for users from different disciplines was needed. Even though it was a purely national event, it met with some success, with over 100 participants and 65 presentations.

Extension was accordingly made to the international tracer community in the next edition, which was also held in Nancy (May 2001) and was equally successful. The now well-established "Tracer" conference became truly international in the 3rd edition, organized in Ciechocinek (Poland) by the Institute of Nuclear Chemistry and Technology (June 2004); after another French edition (Tracer 4, Autrans, October 2006, organized by the Atomic Energy Commission), the Tracer 5 conference will move to the American continent in 2008.

Fundamental developments

•Tomography, Tracer camera visualization and particle tracking

•Validation of computational fluid dynamics by tracer experiments, numerical residence time distribution

•New Tracers and detectors, improvement of existing tracing methods; reactive tracers, experiments and interpretation

•Data treatment and modeling

•Geology, hydrogeology, oilfield and geothermal applications

•Chemical engineering

•Environment

•Food engineering, bio-engineering and biological applications

Organizers

Scientific Committee

Hervé Andrieu (LCPC, Paris, France)
Jerzy Baldyga (Warsaw University of Technology, Poland)
Henri Berthiaux (ENSTIMAC, Albi, France)
Tor Bjornstad (IFE, Kjeller, Norway)
Dmitri Bugai (Institute of Geological Siences, Kiev, Ukraine)
Hector Constant (University of Caracas , Venezuela)
Milorad Dudukovic (Washington University, Saint Louid, USA)
Jean-Paul Gaudet (LTHE, Havana, Cuba)
Dries Hills (NECSA, Pretoria, South Africa)
Joon-Ha Jin (International Atomic Egency, Viena, Austria)
Zvonimir Kolar (University of Technology, Delf, The Netherlands)
Faiçal Larachi (Université de Laval, Québec, Canadá)
Jaean-Pierre Leclerc (CNRS-LSGC-INPL-ENSIC,Nancy, France)
Jack Legrand (GEPEA, Nantes, France)
Alain Line (INSA-Tolouse, France)
Harish Jagat Pant (BARC, Mumbai, India)
Pascal Pilot (Rhodia, Center de Recherches et de Technologies de Lyon, France)
Jean-Michel Rosant (Ecole Centrale de Nantes, France)
Michel Sardin (CNRS-LSGC-INPL-ENSIC, Nancy, France)
Daniel Schweich (CNRS, CPE-Lyon, France
Jean-Marc Schweiter (IPF,Solaize, France)
Torben Sevel (Force Institute, Denmark)
Zdzislaw Stegowski (AGH University of Science and Technology, Krakow, Poland)
Jovan Thereska (Viena, Austria)
Jiry Thyn (University of Pracha, Czech Republic)
Oliver Tillement (Université Lyon-1 , France)
Christelle de Traversay (Générale de Eaux, France)
Jiyuan Tu (RMIT University, Melboume, Australia)
Peixin Zhang (CIAE,Beijiing, China)

Scientific Coordination

Amenônia Maria Ferreira Pinto (Centro de Desenvolvimento da Tecnologia Nuclear)
Rubens Martins Moreira (Centro de Desenvolvimento da Tecnologia Nuclear)

Technical Support

Arivaldo M. Sacramento (Centro de Desenvolvimento da Tecnologia Nuclear - ams@cdtn.br)
Paulo César Horta Rodrigues (Centro de Desenvolvimento da Tecnologia Nuclear - pchr@cdtn.br)
Virgílio Lopardi Bomtempo (Centro de Desenvolvimento da Tecnologia Nuclear - vlb@cdtn.br)

Audit

Amenônia Maria Ferreira Pinto (CDTN, Belo Horizonte, Brazil)
George Menacho (Technical Manager, Santiago, Chile)
Joon Ha Jin (IAEA, Vienna, Austria)
Jean-Pierre Leclerc (CNRS-LSGC-INPL-ENSIC, Nancy, France)
Jovan Thereska (Consultant, Vienna, Austria)

Philippe Berne (CEA, Grenoble, France)
Rien van Genuchten (UFRJ, Rio de Janeiro, Brazil)
Rubens Martins Moreira (CDTN, Belo Horizonte, Brazil)
Tor Bjornstad (IFE, Kjeller, Norway)
Virgílio Lopardi Bomtempo (CDTN, Belo Horizonte, Brazil)
Wilson Aparecido Parejo Calvo (IPEN, São Paulo, Brazil)

Local Organizers

Cláudia Marques Peixoto (Centro de Desenvolvimento da Tecnologia Nuclear - cmp@cdtn.br)
Jacinta Maria de Souza (Centro de Desenvolvimento da Tecnologia Nuclear - souzajm@cdtn.br)

Sponsors

Support

Laboratoire des Sciences du Génie Chimique de Nancy

Société Française de Génie des Procédés

Commissariat à l'Énergie Atomique

Institute for Nuclear and Energy Research

TOWN OF TIRADENTES

Tiradentes is the most charming city of Minas Gerais is historical circuit. With a little more than 7 thousands inhabitants and a preserved colonial architecture, it looks like a movie village full of little houses, balconies, carriages and lanterns. All protected by São José hill which can be seen from anywhere in the city.

Considered a Historical Heritage in 1938 by the Institute of National Historical and Artistic Heritage (IPHAN), the city became famous in the decade of 80, since then the number of tourists there increased and by 'maria-fumaça' (an old historical type of train), by car, by bus or by plane, these tourists arrived in Tiradentes.

Some of these tourists fell in love with Tiradentes and decided to stay. They closed their shops, dropped their jobs in the big cities and brought a modern touch to the streets made of stones and to the old big houses.

In this way, the first restaurants of international food, the luxurious hotels and the handcraft, made with the demolished material of Oficina de Agosto (August Workshop), were given start. With the gastronomic festival and the Cinema Exhibition, since 1998, the city was, definitely, established as a cultural destination.

2. Lectures

- Iqbal Hussain Khan

– Deputy Chief Engineer, Pakistan Atomic Energy Commission
– Head Industrial Applications Group of Radiation and Isotope Application Division (RIAD), Pakistan Institute of Nuclear Science and Technology (PINSTECH)

The laboratory has the capability to provide Radioisotope Technology based services, at par with international quality, to various industries in the country. The services include:

A. Leakage detection in Heat Exchangers, Relief valves, buried pipelines, etc.
B. Efficiency Assessment of industrial systems, chemical reactors, water treatment plants by RTD analysis
C. Fluid Distribution studies of Packed-bed towers
D. Mixing Time/Blending time, Dead volume, Bypassing studies in industrial systems
E. Flow rate measurements in pipes
F. Wear/Erosion/Corrosion monitoring in industrial systems (on-line monitoring) by TLA Technique
G. Wear of automobile engine parts and effect of lubricant oils on wear rates
H. Inter-well Tracing for Enhanced Oil recovery
I. Gamma Column scanning (Trayed columns, Packed -bed columns, strippers/fractionators, etc.)
J. Separator/Process vessel Performance Assessment
K. Level/Interface Determination of hydrogenous materials in closed vessels
L. Pipeline pigging to locate blockages
M. Pipe Scanning/Vessel Scanning

Trouble-shooting in process industry using sealed radioactive sources & radiotracers

- Jorge M. Menacho

Received his B.Sc. in Chemistry from the University of Chile in 1974 and his D.Sc. in Metallurgical Engineering from the University of Concepción in 1985. He then joined the Pennsylvania State University (1985-1986) working in the field of mathematical modeling of comminution processes.

Since 1973 up to 1994 he worked for the Mining and Metallurgical Research Center (CIMM) in Chile and thereafter he founded De Re Metallica Engineering, a consulting company in extractive metallurgy where he currently holds the Technical Manager position. He has also been involved in academic activities at the University of Concepción, the University of Santiago and the National Commission for Science and Technology (CONICYT) in Chile. Dr. Menacho holds 15 patents in Chile and the U.S., several of which are currently being applied in industry. His field of interest includes R&D and the engineering aspects of hydrometallurgy and mineral processing with emphasis in the development and application of mathematical models to industrial processes.

- Leclerc, Jean-Pierre

Jan. 02 - Today Deputy-Director of the LSGC (Laboratory of Chemical Engineering Sciences)
The Laboratory of Chemical Engineering Sciences (LSGC) is a research unit of the French National Centre for Scientific Research (CNRS) com posed of around 60 researchers, 45 Engineers, technicians and administrative staff and around 60 PhD students. Its objectives are to develop the fundamental knowledge necessary for optimal operation of processes aiming at physicochemical or biochemical transformation of raw materials into useful products.

Jan. 1997 – Dec. 03 Head of PROGEPI
PROGEPI (Centre of promotion of process engineering in industry) is the centre of transfer of technologies of the LSGC. Its objective is the transfer of know-how to industry, applying research methods to practical industrial applications. PROGEPI is composed of a team of 5 engineers assisted by the total know-how of the 105 permanent staff of the LSGC. It has already performed over 350 industrial contracts.

Senior researcher:
Specialty: tracing methods and modeling for chemical and environmental engineering
- Development of the tracing methodology and interpretation
- Modeling of hydrodynamic heat and mass transfer and chemical reactions in complex reactors
- Development of processes for the treatment of highly polluted industrials wastes

Author or co-authors of 45 publications in international journals, 50 conference presentations in international and national meetings, 14 invited conferences and 80 industrial reports.
Numerous humanitarian missions in the field of water supply and sanitation
Personal interest: Fishing, diving, mountaineering, travels

- Michael Schubert

Department of Analytical Chemistry
UFZ - Centre for Environmental Research Leipzig-Halle

Dr. Michael Schubert, Environmental Scientist (BSc - Geology, MSc - Geochemistry, PhD - Geochemistry), is experienced in the investigation and the assessment of contaminated sites and lake sediments. Special experiences in the investigation and evaluation of subsurface contamination by Non-Aqueous Phase-Liquids (NAPLs). Skilled in geochemical analysis of soil and water samples. This is backed up by a graduate qualification in geology, mineralogy and geochemistry
Areas of interest: water samples, analysis, soil samples, analysis, sediments, lakes, assessment, non-aqueous phase-liquids (NAPL), NAPL (non-aqueous phase-liquids), Mineralogy;Geology;Geochemistry, contaminated sites, assessment

- Ramon Aravena, Ph. D.

Research Professor Earth Sciences, University of Waterloo

Dr. Aravena is a Research Professor in the Department of Earth Sciences, University of Waterloo with 20 years experience in the application of isotope techniques in hydrology. He has been involved in numerous groundwater studies in Latin America, Canada and the U.S. related to evaluation of groundwater resources and groundwater protection.
He worked for 10 years for the Atomic Energy Commission of Chile. Dr. Aravena has been consulting for 10 years as part of the expert pool of the International Atomic Energy Agency, Vienna, Austria, for their projects worldwide. He is the author and co-author of over 70 referee publications and over 30 technical papers. He serves as a reviewer for several journals including Water Resources Research, Ground Water, Journal of Hydrology, Journal of Contaminant Hydrology and Geochimica Cosmochimica Acta.
His current research focus on groundwater contamination caused by agricultural and urban activities using environmental isotopes as tracers to provide information about sources and processes that affect nitrate and organic compounds in groundwater.

- Rubens Martins Moreira

Doutor em Engenharia Química pela North Carolina State University (1976) e Pesquisador do Centro de Desenvolvimento da Tecnologia Nuclear – CDTN .

Coordenador da Pós-Graduação de Mestrado em Ciência e Tecnologia das Radiações, Minerais e Materiais do CDTN.

Atua Profissionalmente na área da Aplicação de Técnicas Nucleares aos seguintes temas:

A. processos de transporte no meio ambiente
B. sistemas industriais,
C. desenvolvimento e medição de traçadores radioativos,
D. modelagem matemática;

com ênfase em exploração de petróleo e poluição de águas

- Tor Bjørnstad, Professor Dr. Philos.:

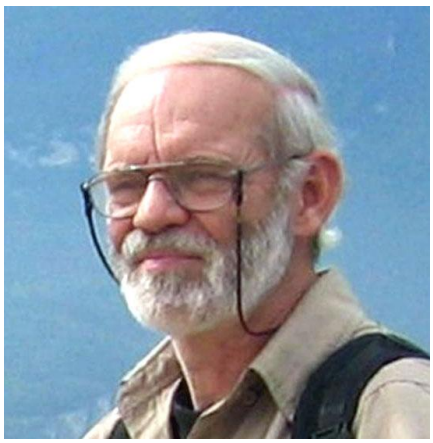

- Head of Department for Reservoir and Exploration Technology at Institute for Energy Technology (IFE) in Norway,
- Professor in Nuclear Chemistry/Radiochemistry at University of Oslo.

35 years experience in radiochemistry at different universities and research institutions. More than 20 years experience in petroleum-related activities. Keywords are:

A. Development of tracer methods for reservoir evaluation (interwell studies), near-well flow and residual oil saturation studies, well operations including drilling, completion and well work-over, process studies (heat exchangers, separators, scrubbers), multiphase transport in pipelines.
B. flow assurance problems including mineral scaling, radioactive scale and related problems,
C. EOR-methods including polymers, surfactants, CO_2 etc,
D. radioanalytical chemistry,
E. chemical separation methods.

3. Papers

3.1. ES – Environmental Section

ES01	Boron quantification in wood: an application of radiotracers Celso Vargas, Mario Conejo, Roger Moya, Joon Ha Jin
ES02	Using tracer experiments to determine deep saline aquifers caprocks characteristics for carbon dioxide storage P. Bachaud, Ph. Berne F. Renard, M. Sardin, J.P Leclerc
ES03	Using tracer experiments for compartmental modeling of an aerated sludge channel reactor Y. Le Moullec, O. Potier, C. Gentric, J.P. Leclerc
ES04	A non uniform flow velocity equation and its applications to mass transport in natural streams A. Constain, A. Carvajal and J. Carvajal
ES05	Groundwater recharge assessment using environmental tracing methods Mónica P D´ELIA, Ofelia C TUJCHNEIDER, Marta del C PARIS, Marcela A PEREZ & Susana GERVASIO
ES06	Use of 24Na in the determination of the moisture carryover In Angra 1 nuclear power station steam generators Anselmo Miranda, Enio Magalhães Freire
ES07	Liquid and gas residence time distribution in a two-stage bioreactor with cell recycle Lamia BEN GAIDA, Christophe ANDRE, Carine BIDEAUX, Sandrine ALFENORE, Xavier CAMELEYRE, Carole MOLINA-JOUVE, Luc FILLAUDEAU
ES08	Gamma-ray survey in the characterization of an area contaminated by mercury in Descoberto-MG, Brazil Carlos A. de Carvalho Filho, Peter M. Fleming, Otávio E. de Aquino Branco, and Mauro C. Trindade
ES09	99mTc mud labelling and its application in hydrodynamic studies of fine suspended sediment in brazil J.V. Bandeira, L.H. Salim, C.S. Sabino, E.G. Agudo, P.E. Aun, V.L. Mendes
ES10	Orinoco River suspended sediment studies using 99mTc – Venezuela Maria Léa Machado, Jefferson Vianna Bandeira, Lécio Hannas Salim Rubens M.Moreira
ES13	Environmental tritium as a tracer for the verification of groundwater flow models Cota, S., Velásquez, L.N.M., Minardi, P., Bomtempo, V.L.
ES14	Tracer techniques as a contribution for studying the hydrological behavior of a São Francisco River sub-basin - PART I Marcos Machado Drumond; Paulo César Horta Rodrigues;Cláudio Costa Camargos and Paulo Sérgio Pelogia Minardi

ES14	Tracer techniques as a contribution for studying the hydrological behavior of a São Francisco River sub-basin - PART II Marcos Machado Drumond; Paulo César Horta Rodrigues, Cláudio Costa Camargos and Paulo Sérgio Pelogia Minard
ES14	Tracer techniques as a contribution for studying the hydrological behavior of a São Francisco River sub-basin - PART III Marcos Machado Drumond; Paulo César Horta Rodrigues, Cláudio Costa Camargos and Paulo Sérgio Pelogia Minardi
ES15	Use of terrestrial epiphytic community to biomonitor of atmospheric pollution at steel valley region, Minas Gerais State Maria Adelaide R. V. Veado, Alex A. F. da Costa, Millôr G. Sabará, Maria Ângela de B. C. Menezes, Gabriela F. Lopes
ES16	Natural radioactivity of coastal sediments as "Tracer" in dynamic sedimentology Dr. Jovan Thereska
ES17	Soil-plant transfer factors of typical Brazilian crops Vanusa M. F. Jacomino*, Kerley A. P. Oliveira, Maria Ângela de B. C. Menezes, Maria H. T. Taddei, Maria C. Siqueira, Marcos Roberto L. Nascimento, Fabiana F. Dias, David F. da Silva, Maria Eleonora Deschamps, Jaime W. V. Mello

BORON QUANTIFICATION IN WOOD: AN APPLICATION OF RADIOTRACERS

Celso Vargas (1), Mario Conejo (2), Roger Moya (3), Joon Ha Jin (4)

SUMMARY

Protecting wood from attacks of termites and other agents is of relevance for wood industry. This protection is made by the introduction in the wood of some chemicals with specific properties. One important research subject is the development of new methods to effectively cure wood in a long lasting way. The other is the proposals of new methods for quantification the amount of chemicals absorbed by hydrophilic pores and other dynamic processes that take place in a wood piece, so that we may assure the permeability of wood to a specific chemical. The application of low energy and short half-life radiotracers, such as technecium-99, is an important method to achieve this quantification. In this paper we report our results in several tests conducted in the Non-destructive Testing Lab at the Costa Rica Institute of Technology.

MATERIAL AND METHODS

Plantation description and tree sampling: three different sample species from pure plantations located at several part of Costa Rica were utilized in these experiments. Samples were selected from plantations with an initial planting density of 1111 trees/ha (3x3 m spacing); at the moment of evaluation the stands aged 8-17 years and a density of 240-515 trees/ha (Table 1). A second thinning was applied in representative plot of all species, approximately 9 were felled. At sampled age, these species did not present heartwood (Moya, 2008), only sapwood is found in all cross section.

Table 1 - Conditions and management of the plantations used.

Specie	Bombapcosis quinata	Terminalia amazonia	Vochysia guantemalisis
Age (Years)	17	14	8
Density (trees/ha)	240	452	515
Total height (m)	21.6	21.40	22.7
DBH (cm)	31.3	22.59	18.5
Gravity specific	0.32	0.49	0.32

Sawing pattern and wood samples: Logs were sawn using the pattern described in figure 1. This is commonly used in Costa Rica to obtain wood to be used for furniture industries and other uses. In all boards used, 6 samples (2.5 thick x 2.5 cm width and 30 cm in length) were extracted as pointed out in figure 1. It was checked that all samples were formed of sapwood. This means that all logs are 100 % permeable to chemical compounds. Aiming at guarantying homogeneity in the samples, green wood samples were conditioned in a room at 22 ºC and 66 % of relative humid. They were kept for 60 days approximately. Finally, all samples reached the moisture content (MC) of 12 %. Three experiments were conducted, one for each specie selected.

[1] The Costa Rica Institute of Technology, Costa Rica, email:celvargas@itcr.ac.cr
[2] The Costa Rica Institute of Technology, Costa Rica, email:conejo@itcr.ac.cr
[3] The Costa Rica Institute of Technology, Costa Rica, email:rmoya@itcr.ac.cr
[4] International Atomic Energy Agency, Vienna, email:J-H.Jin@iaea.org

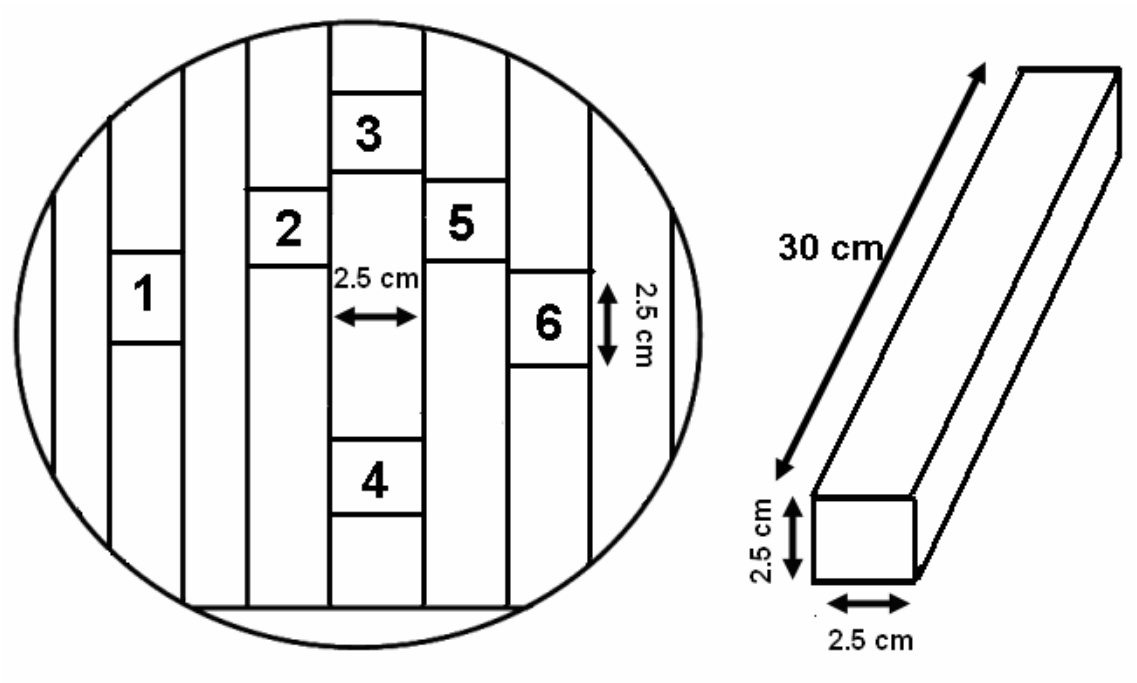

Figure 1 - Sawing pattern and samples obtained from log

Pressure treating

Six samples per species with dimensions of 2.5 x 2.5 x 30 cm were systematically taken from each log. The samples were treated with boron preservatives at 2.8% vv/vv concentration. Chemical solution was prepared in the following way: it was mixed borax (Sodium tetraborate decahydrate $Na_2\ B_4\ O_4\ -10H_2O$) with boric acid (H_3BO_3), then, water was added (24 litres) until it reached a concentration of 2,6 %. Then, it was stirred until these components dissolved completely. Finally, it was added techneciun 99 as radiotracer.

On the other hand, all samples were placed into an experimental preservation tank under a pressure of 690 kPa (approximately 100 psi), according to CCA preservation methods (AWPA, 1981). The initial weight and volume of these samples had been recorded. The treatment schedule involved subjecting the charge to vacuum (−55 kPa) for 15 minutes, flooding with the preservative solution and application of a pressure of 1300 kPa for 120 minutes. The pressure was then released and the solution drained from the cylinder. The samples were again held in vacuum (−55 kPa) for 5 minutes (15/120/15). The marked samples were weighed again after the treatment and tested for determining the penetration of preservative.

Absorption and preservation determination

Standard method for estimating the amount of chemicals absorbed is by calculating the difference between weights before and after treatment. The absorption, expressed as an average weight per unit volume of sample, was calculated using the formula below:

$$\text{Absorption} = \frac{\text{Total absorption} \times \text{Concentration of Boron}}{\text{Volume of wood sample (m3)}}\ \text{kg/m}^3$$

Next, these samples are dried to obtain the net dry salt retention that indicates the amount of toxic ingredient taken up by timbers treated with that preservative. Alternatively, it is the amount of toxic ingredient fixed in wood after treatment. Determination of net dry salt retention was based on the volume of chemical absorption by tested samples. It is calculated by the formula below:

$$\text{Retention} = \frac{\text{Weight of chemical absorbed} \times \text{Concentration of solution}}{\text{Volume of wood pieces}}\ \text{kg/m}^3$$

Fine-grained approach

It is concluded from the above description that standard method for determining the amount of chemical absorbed by wood is by averaging this chemical in the whole sample under analysis. If we want to determine more precisely the amount of chemical absorbed in a determine point of the sample, it is necessary to destroy the sample to make the estimation and data extrapolation. It was our goal to use radiotracers to provide a more fine-grain method for determining at any point of the sample the amount of chemicals absorbed.

To achieve this we used one arrangement of two detectors, 2 X 2 inches, Ludlum, collimated so that the area of detection reduce to a 1 X 1 inch (picture 1). So that, two wood samples were analyzed simultaneously. Each sample was marked in twelve parts each of 1 X 1 X 1 and was systematically measured by 5 minutes. To inspect the whole sample, it takes 60 minutes. After the measurement, each sample was sectioned in twelve parts, each of them was analyzed the standard method for absorption and preservation determination.

With the aim of reducing error estimation, background radiation was measured by an hour. In all cases we put in boron solution (24 liters) a sufficient amount of Tc-99 to assure that the determination be as precise as possible. It was used between 4 and 5 mCi of Tc-99. In all cases, no problems of detection were faced.

To establish the correlation between absorption and counts is the main objective of these tests. If this correlation can be established, it is possible to predict, by inspecting some sections of a sample, the amount of chemical composed absorbed. An appropriate knowledge of the main features of wood is required.

RESULT ANALYSIS

Following the procedure indicated above, the correlation between absorption/retention and counts average was positively established. We will introduce the results corresponding to every one of the species selected. Let start with the Vochysia guantemalisis. The following graphic shows an important level of linear correlation between these to factors. The only exception is the sample 4 (see Annexes 1) in which we didn't identify a pattern for accounting deviation from the tendency. As can be observed, in this sample there is no correspondence between retention and counts. Retention range locates between 15 g/m3 to 39 g/m^3, but counts per minute is very high, between 500 counts to 700 counts. But on the other hand, this sample presents an important degree of consistency in each its segments analysed. This could indicate that this sample has some particularities that are responsible for the differences in density observed. All the other samples analysed corresponding to this species present a higher degree of correlation between these two parameters. It is important to mention that during species experiment, we made a mistake: we sub-estimated the amount of solution applied during the wood treatment, so the immersion was not complete. In this sense, for future experiments it is necessary to repeat the treatment of these species.

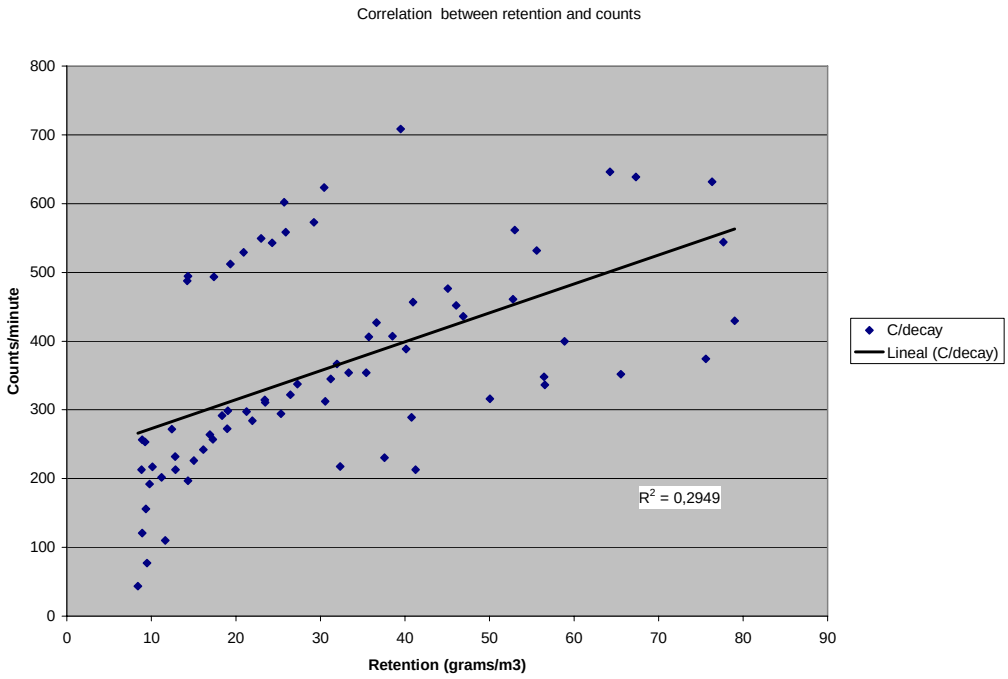

The correlation between retention and counts for the Bombapcosis quinata species is shown on the following graphic. As can be seen this sample present an important variation from averages in retention and counts. But at the same time an important degree of consistency between all segments is observed. The higher count obtained is 855 but this is correlated with the retention and absorption values obtained.

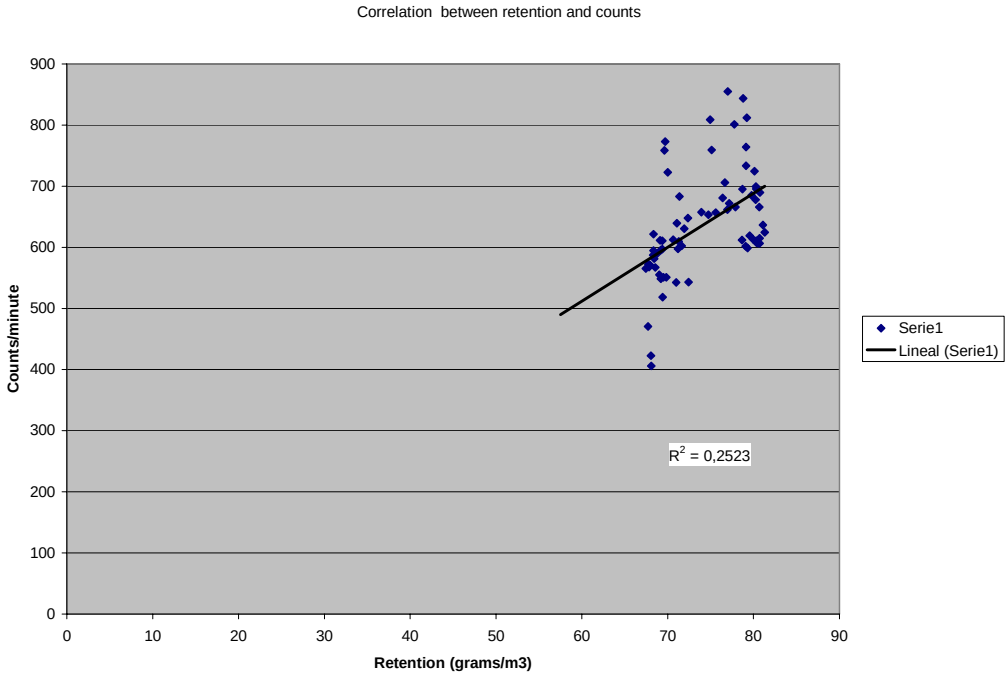

Finally, the correlation between absorption and counts for the third specie Terminalia amazônia, is shown in the following graphic. As can be seen, this species presents the better correlation between retention and counts. En effect, as higher retention obtained, the higher counts, and viceversa.

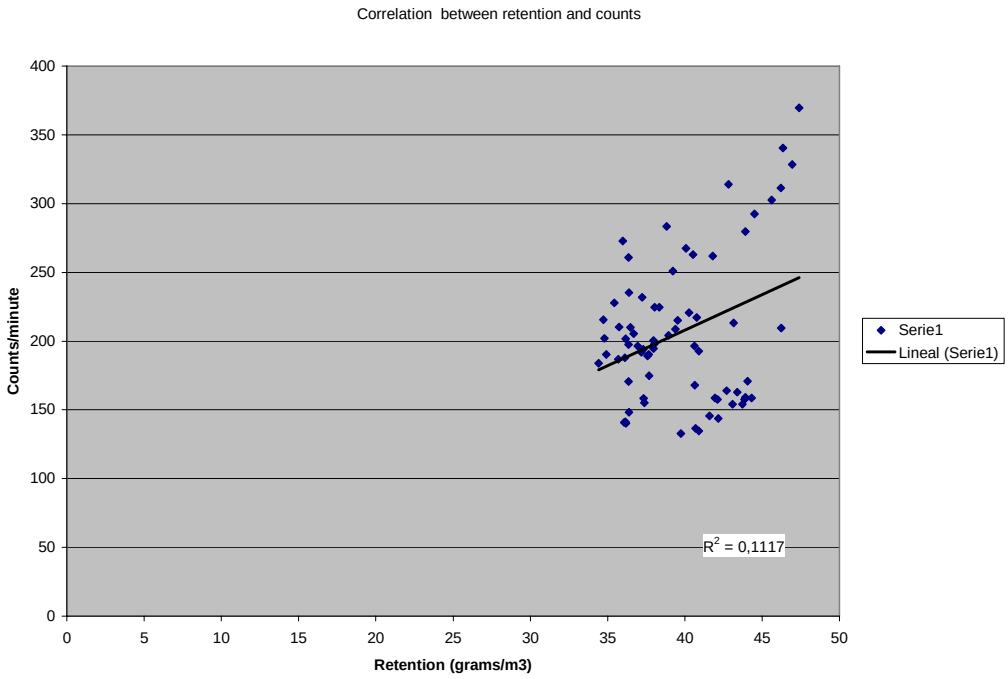

In the following graphic it can be observed an important degree of correlation between retention and counts in the three species analysed.

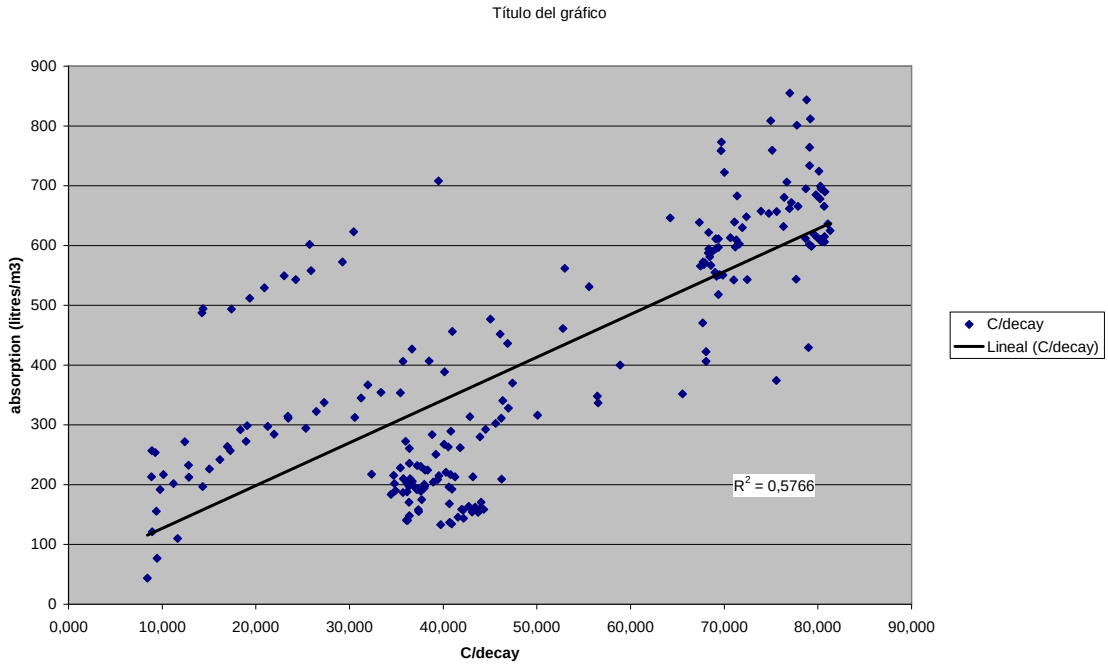

DISCUSSION

From the information available on wood, the following principle applies: as less density in wood, the more retention observed. That is, retention is inversely related to density. Applying this criterion to the species selected, the following order is satisfied:

Vochysia guantemalisis is less dense than Bombapcosis quinata and this is less dense than Terminalia amazônia. Then it is expected more retention in the first, than the second and even less in the third. This order is satisfy in the tests conducted, except for the first species. We attribute this diversity in retention to the fact that these samples were not completely immersed during the

treatment. We consider that fact, explains the wide range of retention values and counts obtained. It is important to verify this hypothesis with new experiments.
We may summary our findings considering all the samples and segments, the following results related to retention, absorption and counts.

Species	Absorption Maximum (l/m3)	Absorption average (l/m3)	Absorption Minimun (l/m3)	Counts/minute Mininum	Counts/minute Average	Counts/minute Maximum
Bombapcosis quinata	394,92	330,6620978	286,8097796	132,928002	206,3108116	369,792509
Vochysia guantemalisis	658,35	246,3265409	70,14568006	43,46436877	363,1433845	708,322982
Terminalia amazônia	677,57	616,6710015	479,3624812	406,0983258	637,9617507	855,249947
Total General	677,57	403,9978603	70,14568006	43,46436877	402,4719823	855,249947

Species	Retention (g/m3) Minimun	Retention (g/m3) Average	Retention (g/m3) Maximum
Bombapcosis quinata	34,41717355	39,6794517	47,39044846
Vochysia guantemalisis	8,417481607	29,5591849	79,00154698
Terminalia amazônia	57,52349774	74,0005202	81,30834681
Total General	8,417481607	48,4797432	81,30834681

REFERENCES

Flores-Vindas, Eugenia (1994) La Planta: Estructura y Función. Editorial Tecnológica de Costa Rica. Cartago, Costa Rica.

Moya, R. (2008). Informe de Proyecto de Investigación: Maderas de Reforestación. Centro de Investigación en Integración Bosque Industria. (en prensa)

Terminalia
amazonia

Annexes

1 Data from specie Vochysia guantemalisis

Sample	Section	Absorption/section (g)	Absorption (l/m3)	Chemical retention (grams preservants/m3)	wood Density (g/cm3)	Counts/S
C1	1	9,7264	561,096	67,331	0,328	638,978299
C1	2	6,265	441,582	52,990	0,310	561,805175
C1	3	6,0799	375,482	45,058	0,301	476,595321
C1	4	4,7288	320,956	38,515	0,300	407,043863
C1	5	4,2931	266,343	31,961	0,302	366,776746
C1	6	3,402	227,436	27,292	0,291	337,655493
C1	7	3,0601	195,573	23,469	0,295	311,082083
C1	8	2,2971	152,930	18,352	0,286	291,591706
C1	9	1,8838	119,360	14,323	0,281	197,172696
C1	10	1,4816	97,202	11,664	0,279	110,04478
C1	11	1,292	78,867	9,464	0,273	77,0494665
C1	12	1,0735	70,146	8,417	0,268	43,4643688
C2	1	11,0876	636,122	76,335	0,302	631,870874
C2	2	7,0429	463,238	55,589	0,272	531,472404
C2	3	6,2927	390,742	46,889	0,272	436,048978
C2	4	5,3513	334,383	40,126	0,270	388,749484
C2	5	4,676	295,184	35,422	0,269	353,799439
C2	6	4,1205	254,636	30,556	0,263	312,58881
C2	7	3,4535	210,939	25,313	0,255	294,566059
C2	8	2,8369	182,904	21,949	0,294	284,119792
C2	9	2,3487	141,225	16,947	0,270	264,032505
C2	10	1,6647	106,654	12,798	0,262	232,22998
C2	11	1,3227	84,548	10,146	0,262	216,966767
C2	12	1,198	73,697	8,844	0,257	212,911874
C3	1	5,2381	297,505	35,701	0,294	406,261709
C3	2	3,0339	194,995	23,399	0,295	314,437635
C3	3	3,0432	177,161	21,259	0,289	297,737623
C3	4	2,5087	158,036	18,964	0,281	272,555533
C3	5	2,5243	143,846	17,262	0,281	257,093217
C3	6	2,1138	134,479	16,138	0,288	242,120737
C3	7	2,1429	125,270	15,032	0,287	226,474878
C3	8	1,7085	107,166	12,860	0,279	212,734515
C3	9	1,5709	93,418	11,210	0,294	201,818118
C3	10	1,2296	81,396	9,767	0,300	192,167249
C3	11	1,2854	77,985	9,358	0,312	155,7559
C3	12	1,2502	74,443	8,933	0,296	120,96882
C4	1	5,6747	329,135	39,496	0,338	708,322982
C4	2	3,9185	253,572	30,429	0,327	623,322117
C4	3	3,2692	214,277	25,713	0,338	602,013383
C4	4	3,7212	243,675	29,241	0,320	572,595921
C4	5	3,3801	215,825	25,899	0,351	558,357017
C4	6	3,1801	202,208	24,265	0,328	543,161621
C4	7	3,1788	191,686	23,002	0,314	549,222754
C4	8	2,677	174,190	20,903	0,311	529,097854
C4	9	2,6757	161,296	19,356	0,326	511,79302
C4	10	2,3029	145,022	17,403	0,319	493,668246
C4	11	1,9317	119,520	14,342	0,312	494,39048

Sample	Section	Absorption/section (g)	Absorption (l/m3)	Chemical retention (grams preservants/m3)	wood Density (g/cm3)	Counts/S
C4	12	2,005	118,840	14,261	0,309	487,4837
C7	1	9,3609	535,214	64,226	0,354	645,955509
C7	2	6,5191	439,665	52,760	0,343	460,982628
C7	3	6,5969	383,887	46,066	0,356	451,696179
C7	4	5,574	341,372	40,965	0,337	456,436807
C7	5	5,2828	305,355	36,643	0,331	426,823488
C7	6	4,7482	277,944	33,353	0,323	354,085457
C7	7	4,0439	260,185	31,222	0,316	345,07095
C7	8	3,5084	220,571	26,468	0,313	322,252561
C7	9	2,5741	158,822	19,059	0,312	298,535302
C7	10	1,6194	103,512	12,421	0,312	271,77653
C7	11	1,2859	77,076	9,249	0,298	253,499004
C7	12	1,1825	74,170	8,900	0,306	256,661403
C8	1	11,2352	647,292	77,675	0,363	543,859054
C8	2	10,0681	658,346	79,002	0,366	429,417334
C8	3	7,9651	490,720	58,886	0,570	399,972277
C8	4	10,272	629,789	75,575	0,369	374,152057
C8	5	8,6236	546,170	65,540	0,371	351,585543
C8	6	8,0557	471,197	56,544	0,368	336,570233
C8	7	7,0556	470,291	56,435	0,399	347,938452
C8	8	6,3931	417,184	50,062	0,382	316,333124
C8	9	5,5094	339,936	40,792	0,354	289,157971
C8	10	5,7896	313,073	37,569	0,351	230,600975
C8	11	4,9908	269,643	32,357	0,310	217,63226
C8	12	6,3965	343,630	41,236	0,354	213,156599

2. Data from Bombapcosis quinata

Sample	Section	Absorption/section (g)	Absorption (l/m3)	Chemical retention (grams preservants/m3)	wood Density (g/cm3)	Counts/S
P1	1	10,0631	569,558	45,613	0,393	621,76164
P1	2	9,5781	572,958	39,225	0,417	589,708742
P1	3	8,9198	576,624	40,276	0,406	595,737291
P1	4	9,2546	569,634	40,615	0,409	594,326633
P1	5	8,8274	565,196	39,528	0,416	567,949485
P1	6	8,8781	562,159	38,020	0,417	565,391004
P1	7	9,02	564,427	37,583	0,417	572,480686
P1	8	9,1449	570,328	37,656	0,409	581,301943
P1	9	9,0842	569,050	37,964	0,411	587,646474
P1	10	8,7247	578,184	36,358	0,411	596,831231
P1	11	9,3905	575,886	34,723	0,406	611,494536
P1	12	9,931	578,124	40,517	0,403	610,986443
P2	1	10,8876	641,761	41,810	0,353	855,249947
P2	2	10,9865	656,547	40,913	0,353	843,993712
P2	3	9,6331	647,987	42,715	0,355	801,322789
P2	4	10,3257	659,401	43,859	0,349	764,270779
P2	5	10,6637	659,261	44,324	0,343	733,633902
P2	6	10,8954	656,011	43,911	0,338	695,083382
P2	7	9,5496	643,006	43,719	0,331	671,854773

Sample	Section	Absorption/section (g)	Absorption (l/m3)	Chemical retention (grams preservants/m3)	wood Density (g/cm3)	Counts/S
P2	8	11,5539	668,677	43,092	0,343	677,875619
P2	9	10,2986	672,977	42,122	0,345	689,924657
P2	10	10,8491	669,581	40,644	0,343	695,028927
P2	11	10,4398	667,509	38,933	0,341	724,362713
P2	12	10,5002	668,980	38,810	0,341	699,679168
P3	1	12,3041	660,997	47,390	0,334	598,728731
P3	2	10,4316	663,074	36,366	0,339	618,914976
P3	3	11,063	655,426	35,433	0,341	611,836119
P3	4	9,4	658,872	35,746	0,342	601,785841
P3	5	12,8634	669,258	34,794	0,334	610,568689
P3	6	11,2063	671,496	36,129	0,332	606,780039
P3	7	11,4012	672,585	35,697	0,333	614,987186
P3	8	10,6925	669,633	34,417	0,331	607,12182
P3	9	9,8192	666,190	34,904	0,326	613,347509
P3	10	11,4308	677,570	36,685	0,331	624,845501
P3	11	11,2024	675,570	37,225	0,330	636,398529
P3	12	12,3399	672,530	46,216	0,330	606,502365
P4	1	10,4941	580,712	42,832	0,391	773,223988
P4	2	8,6254	580,350	38,347	0,391	758,778269
P4	3	9,5384	583,493	37,685	0,389	722,495262
P4	4	9,7288	594,891	37,379	0,389	683,378075
P4	5	9,1161	592,395	36,191	0,388	639,341697
P4	6	9,5441	588,877	36,143	0,386	612,852633
P4	7	9,3089	596,818	36,080	0,381	602,423175
P4	8	9,641	593,201	36,374	0,380	597,397838
P4	9	9,4095	594,148	37,322	0,379	609,343377
P4	10	10,2047	599,490	36,355	0,374	630,241009
P4	11	9,6476	602,940	36,162	0,371	648,181204
P4	12	9,8013	569,558	40,085	0,366	657,282534
P5	1	9,3609	535,214	45,613	0,400	543,384768
P5	2	10,4606	650,976	39,225	0,401	542,725459
P5	3	9,6504	603,776	40,276	0,410	550,63921
P5	4	9,0732	591,657	40,615	0,407	518,284676
P5	5	9,4675	582,107	39,528	0,411	422,774314
P5	6	8,9872	578,278	38,020	0,420	406,098326
P5	7	9,4228	567,175	37,583	0,414	470,434372
P5	8	9,1254	567,308	37,656	0,411	548,520926
P5	9	9,1227	564,143	37,964	0,412	551,159103
P5	10	9,1713	576,575	36,358	0,410	554,798152
P5	11	9,0417	579,131	34,723	0,409	567,173783
P5	12	9,0883	575,190	40,517	0,417	571,183647
P6	1	9,4271	571,406	41,810	0,325	811,98136
P6	2	11,5382	566,059	40,913	0,320	808,940787
P6	3	11,0607	659,951	42,715	0,320	759,232314
P6	4	9,3028	624,527	43,859	0,327	706,23031
P6	5	10,4173	625,866	44,324	0,330	680,577733
P6	6	10,3409	638,968	43,911	0,335	661,572801
P6	7	10,5576	636,567	43,719	0,332	656,769153
P6	8	9,6341	641,393	43,092	0,341	653,582738
P6	9	10,9259	629,919	42,122	0,335	665,710145
P6	10	10,1806	622,893	40,644	0,337	685,197681
P6	11	11,0901	648,958	38,933	0,334	695,739308
P6	12	10,6259	664,758	38,810	0,334	665,882138

3. Data from Terminalia amazônia,

Sample	Section	Absorption/section (g)	Absorption (l/m3)	Chemical retention (grams preservants/m3)	wood Density (g/cm3)	Counts/S
A1	1	6,1625	380,110	46,350	0,499	302,516472
A1	2	5,0892	326,872	35,972	0,518	250,901072
A1	3	5,1122	335,632	36,370	0,528	220,622734
A1	4	5,4695	338,458	36,475	0,493	196,449005
A1	5	5,167	329,396	36,955	0,470	214,964623
A1	6	4,8274	316,832	37,179	0,457	197,762789
A1	7	4,8382	313,195	37,301	0,453	189,294664
A1	8	4,7636	313,800	37,975	0,453	190,240609
A1	9	5,049	316,363	39,398	0,470	194,590409
A1	10	4,4348	302,983	40,758	0,451	197,429400
A1	11	4,6697	289,356	38,045	0,442	215,578588
A1	12	5,5614	337,641	44,511	0,446	263,002410
A2	1	5,6493	348,417	46,938	0,495	261,887716
A2	2	5,414	340,941	46,240	0,496	192,583195
A2	3	5,396	355,960	44,062	0,499	163,958696
A2	4	5,5836	365,492	43,393	0,504	157,443160
A2	5	5,6899	369,368	42,166	0,512	158,657373
A2	6	5,6725	365,928	40,899	0,499	159,185085
A2	7	5,5457	364,328	39,742	0,501	154,003466
A2	8	5,5302	359,103	40,687	0,495	154,208501
A2	9	5,4009	351,014	41,582	0,488	157,534044
A2	10	5,2746	338,700	41,952	0,481	167,853857
A2	11	4,9702	324,438	43,163	0,490	204,254752
A2	12	5,2482	323,418	43,922	0,468	283,534933
A3	1	6,4413	394,920	46,350	0,411	369,792509
A3	2	5,0488	303,053	35,972	0,410	260,890479
A3	3	4,3933	295,273	36,370	0,435	227,903014
A3	4	4,8314	297,886	36,475	0,436	210,146254
A3	5	4,3688	289,947	36,955	0,407	201,874051
A3	6	4,9872	301,076	37,179	0,493	187,962782
A3	7	4,353	297,477	37,301	0,463	186,701614
A3	8	4,6513	286,810	37,975	0,423	183,831321
A3	9	4,4574	290,867	39,398	0,414	190,216824
A3	10	4,8864	305,707	40,758	0,412	205,573012
A3	11	4,7408	310,209	38,045	0,402	231,920083
A3	12	6,3463	385,132	44,511	0,398	311,462138
A4	1	5,3418	356,936	46,938	0,437	313,934523
A4	2	5,2314	319,561	46,240	0,424	224,57194
A4	3	4,7286	314,045	44,062	0,424	174,840825
A4	4	4,8442	311,488	43,393	0,433	155,153026
A4	5	4,7697	301,592	42,166	0,419	140,133373
A4	6	4,6301	301,193	40,899	0,422	141,379589
A4	7	4,7285	300,669	39,742	0,431	140,676595
A4	8	4,8227	303,113	40,687	0,414	148,307022
A4	9	4,9837	311,013	41,582	0,431	158,294765
A4	10	4,7577	302,957	41,952	0,420	170,701427
A4	11	4,8174	301,348	43,163	0,407	201,767832
A4	12	5,7123	334,039	43,922	0,407	267,458863
A5	1	6,3462	386,251	46,350	0,450	340,356012
A5	2	4,7173	299,766	35,972	0,449	272,679507

Sample	Section	Absorption/section (g)	Absorption (l/m3)	Chemical retention (grams preservants/m3)	wood Density (g/cm3)	Counts/S
A5	3	4,5729	303,086	36,370	0,453	235,352261
A5	4	4,6346	303,955	36,475	0,449	209,987463
A5	5	4,7043	307,958	36,955	0,449	196,357023
A5	6	4,8081	309,823	37,179	0,459	191,807092
A5	7	4,6764	310,844	37,301	0,467	194,041281
A5	8	4,7718	316,456	37,975	0,478	200,490423
A5	9	5,0599	328,315	39,398	0,515	208,636736
A5	10	5,1425	339,648	40,758	0,537	217,108614
A5	11	4,8235	317,038	38,045	0,510	224,684938
A5	12	5,862	370,922	44,511	0,507	292,508543
A6	1	6,2695	391,149	46,938	0,507	328,330715
A6	2	6,0476	385,334	46,240	0,526	209,548207
A6	3	5,3898	367,186	44,062	0,513	170,847266
A6	4	5,7024	361,605	43,393	0,485	162,784762
A6	5	5,1389	351,385	42,166	0,472	143,828821
A6	6	5,5378	340,826	40,899	0,468	134,63352
A6	7	4,7605	331,182	39,742	0,469	132,928002
A6	8	5,2451	339,060	40,687	0,472	136,620916
A6	9	5,1767	346,518	41,582	0,466	145,491038
A6	10	5,3082	349,602	41,952	0,460	158,577515
A6	11	5,3041	359,690	43,163	0,460	213,121772
A6	12	5,8381	366,017	43,922	0,454	279,704591

USING TRACER EXPERIMENTS TO DETERMINE DEEP SALINE AQUIFERS CAPROCKS TRANSPORT CHARACTERISTICS FOR CARBON DIOXIDE STORAGE

P. Bachaud[1,2], Ph. Berne[1], P. Boulin[1,3,4], F. Renard[5,6], M. Sardin[2], J.P. Leclerc[2]
[1] CEA, LITEN, L2T, F-38054 Grenoble, France
[2] LSGC, Nancy-Université, CNRS - 1 rue Grandville, BP 20451, 54001 Nancy Cedex, France
[3] Agence nationale pour la gestion des déchets radioactifs (Andra), Parc de la Croix Blanche, 92298 Châtenay-Malabry, France
[4] Laboratoire d'étude des Transferts en Hydrologie et Environnement, CNRS/INPG/IRD/UJF-UMR 5564, BP n° 53, 38041 Grenoble Cedex 9, France
[5] LGCA-CNRS-OSUG - University Joseph Fourier, Grenoble I BP 53, 38041 Grenoble, France
[6] Physics of Geological Processes, University of Oslo, Oslo, Norway

ABSTRACT

It is shown how a simple gas tracer technique can contribute to the determination of transport characteristics of tight rock formations. Main obtained parameters are intrinsic permeability and the Klinkenberg coefficient; permeability as low as 10^{-21} m^2 is easily attainable. Some information is also gained on diffusion characteristics and porosity. An example of application is given using caprocks from a deep saline aquifer in the Paris basin.

INTRODUCTION

Storage of carbon dioxide in deep saline aquifers is a promising technique to reduce greenhouse gas emissions. To be accepted by the public, long-term safety has to be proven. Safety predominantly depends on the sealing efficiency of the caprock formation above the aquifer, hence the need to thoroughly determine the physico-chemical properties of that formation. Among these properties, permeability is obviously important since it will largely control the flux of CO_2 that may escape under the influence of the pressure excess in the CO_2 bubble. Determination of the diffusion properties is also required since they will govern how dissolved CO_2 may migrate through the pore water to the outside.

Measurement of permeability is quite a routine procedure in high permeability rocks such as hydrocarbon reservoirs or aquifers. However, the permeability of caprocks is so low that conventional techniques are difficult to apply, not to say wholly inadequate. The aim of the present study is to illustrate how the use of a particular gas tracer technique can contribute to the measurement of low permeabilities and, to some extent, of diffusion coefficients. This technique is applied to measure the transport properties of a carbonate caprock with permeability lower than 10^{-19} m^2.

MATERIAL

The samples used here come from the Charmottes oilfield located about 100 km south-east of Paris (France). They are part of the top of the Dogger (Bathonian and Callovian geological units) and were taken at four different depths between 1900 and 2000 m.

The samples are compact and highly consolidated micritic marls. Mineralogical analysis showed that they contain carbonates (calcite and ankerite) with various proportions of quartz and minor clays. Mercury porosimetry tests were made and yielded low values of about 2 to 5 %. Pore size distributions were found unimodal with a peak well under 100 nm.

Whether these carbonated rocks can actually be considered as a good confining medium for CO_2 sequestration is unsure. Working with these samples is nevertheless interesting because one of the problems with caprocks is the complex chemical interactions with the fluid that are expected to produce both dissolution and precipitation of minerals. These interactions will be enhanced and made more easily observable by the nature of the samples. In addition, the samples are used as a model system to develop measurement methodologies.

"CONVENTIONAL" TECHNIQUES FOR PERMEABILITY MEASUREMEN

"Conventional" techniques for the measurement of permeability involve imposing a pressure gradient across a sample and measuring the resulting flux. They can be divided into:

- steady-state tests: the pressure gradient is kept constant and the flow rate is measured once a constant value is reached,
- pulse tests: the sample is placed between two closed reservoirs; a pressure step is applied to one of them and the fluid is let to flow into the second one while the pressure difference is monitored.

According to Davy et al. (2007), the former technique can be used down to 10^{-19} m^2; below that value, the latter technique should be preferred; the price to pay is that the tests are more complicated to make and to interpret.

Both techniques can be used with liquids or gases. In our case, gases are advisable because i) we are indeed interested in permeability to a non-wetting fluid (supercritical CO_2) ii) this implies working with dry samples, which are much easier to prepare and handle than water-saturated ones.

The samples porosity and pore size values reported above suggest that:

- permeability will indeed be low, probably in the 10^{-19} to 10^{-20} m^2 range (the latter value can be obtained for example using the Kozeny-Carman porosity-permeability relationship),
- a wide class of pores have sizes close to the mean free path of the gas molecules, which means that molecular (as opposed to viscous) flow will occur.

The latter effect requires that a correction (the so-called Klinkenberg correction – Klinkenberg, 1941) be introduced in Darcy's law (written here for a perfect gas):

$$J = -\frac{k}{\mu}\left(1+\frac{b}{p}\right)\frac{p}{RT}\frac{\partial p}{\partial z} \qquad (1)$$

where J is the molar flux, k the intrinsic permeability, μ the dynamic viscosity, p the pressure, b the Klinkenberg factor, R the gas constant, T the temperature and z the abscissa along the sample axis.

In the case of a steady-state test, equation (1) is easily integrated into:

$$J = \frac{k}{\mu RTe}\left(1+\frac{b}{p_m}\right)\frac{p_1^2 - p_0^2}{2} \qquad (2)$$

where p_1 and p_0 are respectively the upstream and downstream pressure, p_m their arithmetic mean and e the thickness of the sample. Plotting the apparent permeability k_{app} defined by:

$$k_{app} = J\frac{2\mu RTe}{p_1^2 - p_0^2} \qquad (3)$$

against $1/p_m$ should therefore yield a straight line:

$$k_{app} = k\left(1+\frac{b}{p_m}\right) \qquad (4)$$

from which the coefficients k and b can easily be estimated.

To give an example, the flux of air through a sample 1 cm thick and 3 cm in diameter with $k = 10^{-20}$ m^2, $b = 10^6$ Pa, $p_1 = 10^6$ Pa, $p_0 = 10^5$ Pa, $T = 300$ K, is only about 2 standard cubic centimetres per hour, which makes accurate measurements challenging.

AN ALTERNATIVE "TRACER" TECHNIQUE

Basic principle

The "tracer" technique differs from the previous ones by the use of two different gases: the first one, say helium, is used to maintain a pressure gradient upstream the sample, while the other one, e.g. nitrogen, flushes the downstream side with a known and constant flow rate (Figure 1). If the mole fraction of gas 1 in gas 2, x, can be measured, the molar flux of gas 1 through the sample, J_1, is simply given by:

$$J_1 = \frac{x}{1-x} J_2 \qquad (5)$$

where J_2 is the (imposed) molar flux of gas 2.

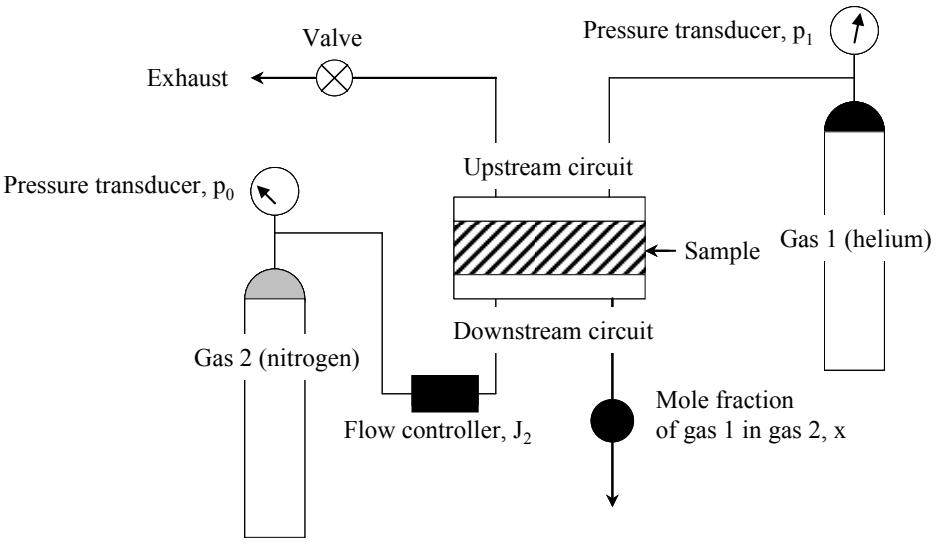

Figure 1: "Tracer" technique for the measurement of permeability.

This technique is an adapted version of the "continuous dilution method" commonly used to measure flow rates with tracers (AIEA, 1990), with the sole difference that the objective here is to measure the flow rate of the "tracer" (gas 1). It is also often used to measure transport properties through polymers (Flaconneche et al., 2001).

Using a mass spectrometer, mole fractions of helium in nitrogen down to 50 ppm (5.10^{-5} mol/mol) can be measured fairly easily. An helium flow rate of 0.2 standard cm^3/hr, one order of magnitude lower than the one mentioned above, is then measurable if a reasonable nitrogen flow rate of about 50 standard cm^3/min is used. In other words, a permeability of 10^{-21} m^2 is easily measured.

Elementary model for data interpretation

Interpretation of this tracer experiment however requires some caution since the gases are now submitted to an extra gradient due to the concentration difference between the upstream (pure helium) and the downstream (almost pure nitrogen) sides of the sample. Gas diffusion may therefore play some role and should be taken into account.

A simple way is to break the gas flux into convective and diffusive parts, respectively J_c and J_{1d} (gas 1) and J_{2d} (gas 2). J_c is again given by equation (1), where μ now is the viscosity of the mixture and, strictly speaking, dependent on volume fraction x. A simple expression for J_{1d} and J_{2d} could be the following form of Fick's law:

$$J_{1d} = -D\frac{\partial}{\partial z}\left(\frac{px}{RT}\right) \quad J_{2d} = -D\frac{\partial}{\partial z}\left(\frac{p(1-x)}{RT}\right) \qquad (6)$$

where D is an effective molecular diffusion coefficient that should be inversely proportional to pressure according to the kinetic gas theory (Bird et al., 1960):

$$D = D_0 \frac{p_0}{p} \tag{7}$$

D_0 being the value of D at reference pressure p_0, taken for instance as the downstream pressure. The system is completed by the molar balance equations for gas 1 and for the mixture:

$$\frac{\partial}{\partial t}\left(\frac{\varepsilon x p}{RT}\right) = -\frac{\partial}{\partial z}\left(x J_c + J_{1d}\right) \tag{8}$$

$$\frac{\partial}{\partial t}\left(\frac{\varepsilon p}{RT}\right) = -\frac{\partial}{\partial z}\left(J_c + J_{1d} + J_{2d}\right) \tag{9}$$

where ε is the accessible porosity.

This model is certainly oversimplified since it does not account for all the phenomena of gas diffusion in porous media (Boulin, 2008). It is however adopted here because it is mathematically manageable and yet able to capture the main trends.

Suppose now that a steady-state tracer experiment is performed where the flux of gas 1, J_1, is measured. It is again possible to derive an apparent permeability:

$$k_{app} = J_1 \frac{2\mu RTe}{p_1^2 - p_0^2} \tag{3bis}$$

The steady-state version of equations (8) and (9) yields an analytical solution provided that the concentration dependence of μ is neglected, which is not a strong assumption in the case of helium and nitrogen since their viscosities are very similar (respectively 1.9 and 1. 8.10^{-5} Pa.s at ambient temperature). This solution reads:

$$k_{app} = k\left[\left(1 + \frac{b}{p_m}\right) + \frac{2\alpha}{\left(p_1 / p_0\right)^2 - 1} \log\left(\frac{p_1}{p_0}\right)\right] \frac{\exp(\xi)}{\exp(\xi) - 1} \tag{10}$$

with:

$$\xi = \frac{\left(p_1 / p_0\right)^2 - 1}{2\alpha}\left(1 + \frac{b}{p_m}\right) + \log\left(\frac{p_1}{p_0}\right) \tag{11}$$

where α is a dimensionless parameter that can be interpreted as the inverse of a Péclet number:

$$\alpha = \frac{D_0 \mu}{k p_0} \tag{12}$$

Equations (10) looks substantially different from equation (4); however it has a particular behaviour at large upstream pressure: expression (11) grows to infinity when p_1 is much larger than p_0; the exponential terms in equation (10) therefore cancel out. At the same time, the log term in equation (10) becomes vanishingly small. Equation (10) therefore reduces to equation (4):

$$k_{app} = k\left(1 + \frac{b}{p_m}\right) \tag{4bis}$$

The practical consequence is that the high pressure points from a tracer experiment will fit on a straight line on the k_{app} vs. $1/p_m$ graph, from which the intrinsic permeability and the Klinkenberg coefficient can again be derived very simply.

Diffusion characteristics

Diffusion is somehow present in our interpretative model. To investigate how it affects k_{app} and under which conditions is it possible to measure it, the function k_{app}/k vs. p_0/p_m has been plotted

for various values of coefficients α and b (Figure 2). For low values of α, the straight line predicted by equation (4bis) is indeed observed. As α increases, the low pressure part of the curve shows some deviation from linearity. The larger α, the stronger the deviation and the shorter the straight part of the curve. This effect tends to be stronger when b is small.

What is observed here is obviously the effect of the diffusion flux. Figure 2 shows that, provided the adequate pressure range is explored, the k_{app}/k versus p_0/p_m curve is actually sensitive to α, or, in other words, that the diffusion coefficient D_0 can be obtained by parametric adjustment. Using the tracer technique, one can therefore get information not only on the permeation parameters, but also on the diffusion properties of the studied material.

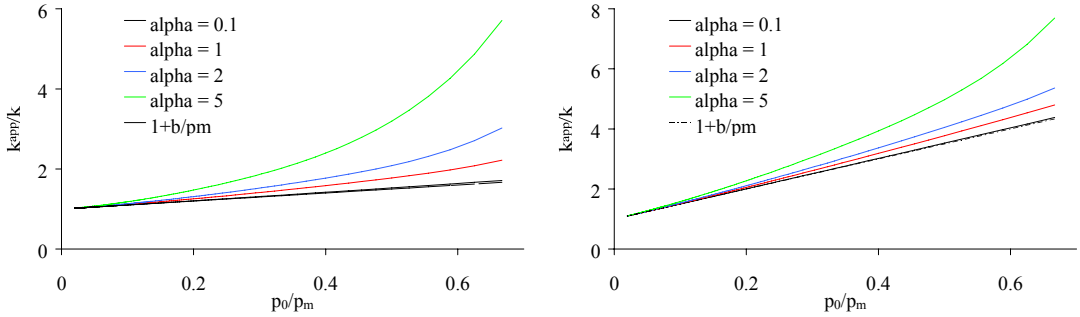

Figure 2: k_{app}/k versus p_0/p_m for different values of α

Left: $b/p_0 = 1$ - Right: $b/p_0 = 5$.

For this information to be really exploitable, a more realistic model for diffusion should be used. In that case, determination of the actual coefficient of mutual molecular diffusion of the gases is possible. This quantity does however not correspond to the initial problem: the transport of dissolved CO_2 in the pore water of caprocks. One possible way to bridge this gap is to introduce the notion of formation factor, equal to the ratio of the molecular diffusion coefficient of a species in a porous medium to its equivalent in a free fluid (Bear, 1972). Provided that all the species involved (helium and nitrogen under gas form, dissolved CO_2) have access to the same porous network, the formation factor should be the same for all. The gas tracer experiment enables to determine it; the desired diffusion coefficient is then just the product of this value by the diffusion coefficient of dissolved CO_2 in brine. The equal formation factor assumption is however a very strong one, and there are indications that it might not be generally valid (Boulin, 2008).

TWO EXAMPLES FROM EXPERIMENTS

The first experiment shown here was conducted on a very low porosity sample (less than 3 %) composed chiefly of carbonated materials. The sample was placed in a triaxial cell and an isotropic confinement pressure of 200 bar was applied. Downstream pressure p_0 was atmospheric pressure; upstream pressure varied from 2.5 to 125 bar. The main objective of this experiment was to measure intrinsic permeability k.

The results are shown on Figure 3. Visually, the data points group along a straight line on a k_{app}/k vs. p_0/p_m graph; they are actually well represented by a linear equation ("linear fit" on Figure 3). The parameters of the linear fit yield $k = 2.1\ 10^{-19}$ m^2 and $b = 19$ bar (or $b/p_0 = 19$).

As demonstrated in the previous section, the diffusion coefficient D_0 is related to curvature of the k_{app}/k vs. p_0/p_m line, which means that D_0 cannot be determined from this experiment (or lower values for the upstream pressure should have been used). The k and b parameters from the linear fit were however combined with various values of D_0, ranging from 10^{-9} to $2.\ 10^{-8}$ m^2/s, to yield the group of dotted curves on Figure 2. Upon examination, it appears that the actual D_0 coefficient should be less than 10^{-9} m^2/s; coefficient α should therefore be less than 0.9, which is indeed in the lower range in Figure 2.

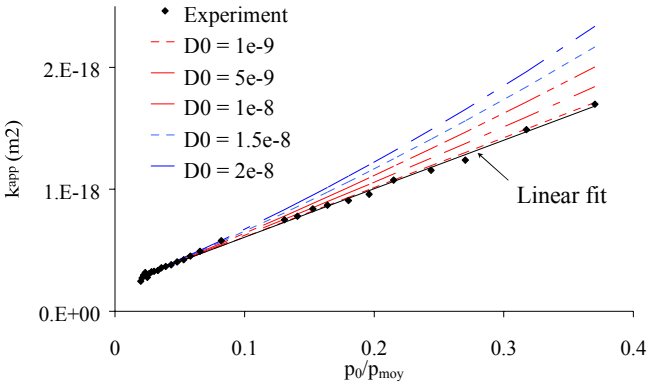

Figure 3: k_{app}/k versus p_0/p_m, 1st sample.

The second experiment involved a rock sample from the same geological layer, but extracted at a different location. Porosity and clay content were much higher (about 18 and 50 % respectively). The same experimental set-up was used. Downstream pressure was 2 bar, confinement pressure 90 bar and upstream pressure ranged from 2.4 to 44 bar. This time measurement of the complete set of parameters (k, b and D_0) was desired.

The results are given by Figure 4. The effect of diffusion is now clearly visible in the low pressure part of the graph. Non-linear fitting of equation (10) proved quite successful and yielded $k = 6.5\ 10^{-19}$ m^2, $b = 43$ bar and $D_0 = 8.4\ 10^{-9}$ m^2/s.

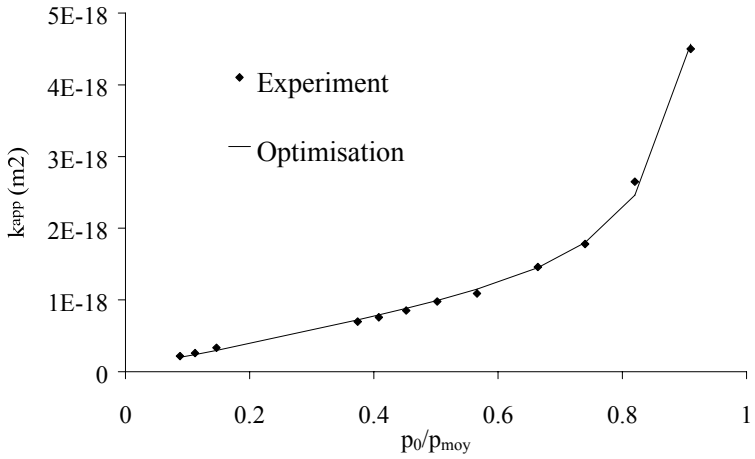

Figure 4: k_{app}/k versus p_0/p_m, 2nd sample.

EXPLOITATION OF THE TRANSIENT PART OF THE TRACER EXPERIMENT

So far only the steady-state part of the tracer experiment has been exploited. The experiment is however by nature a transient one (successive pressure steps are applied on the upstream side). If the tracer flux is continuously monitored, a graph like the one on Figure 5 is obtained.

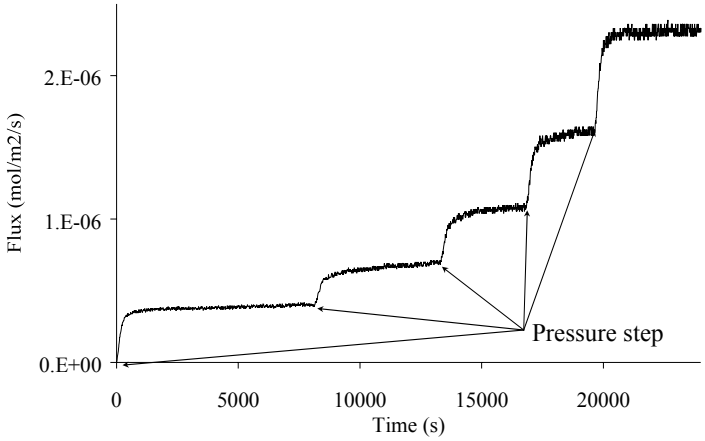

Figure 5: Tracer flux as a function of time.

Response after each pressure step comprises a transient part followed by a plateau. The transient part is governed by equations (8) and (9). In these equations, all the parameters connected with fluxes J_c, J_{1d} and J_{2d} can be known thanks to the analysis of the plateaux in Figure 5. The only remaining unknown is therefore the accessible porosity ε, that can be determined by a suitable model adjustment technique.

This method was successfully used by Boulin (2008) and has provided valuable results. It needs however further investigation, since the relationship between the porosity values yielded by this method and by other techniques like mercury intrusion remains to be confirmed.

CONCLUSION

The main findings of this work are the following:

- using a laboratory experiment based on a simple tracer technique, it is possible to measure very low gas permeabilities; in the numerical example given, permeability down to 10^{-21} m^2 was found easily attainable but lower values can certainly be measured with more optimised operating parameters (i.e. larger samples);
- provided the adequate pressure range is used, data are quite easy to exploit in terms of intrinsic permeability taking into account the Klinkenberg correction;
- experimental data at low pressure gradient also provides information on diffusion processes, but their processing is more difficult and requires a reliable model;
- if transient responses are monitored, accessible porosity can in addition be estimated.

REFERENCES

AIEA, 1990, Guidebook on radioisotope tracers in industry, Technical Report Series n° 316, International Atomic Energy Agency, Vienna.

Bear, J., 1972, Dynamics of Fluids in porous media, Dover Publications, New York.

Bird, R.B., Stewart W.E., Lightfoot, E.N., 1960, Transport phenomena, Wiley and Sons, New York.

Boulin, P.F., 2008, Experimentation et modélisation du transfert d'hydrogène à travers des argiles de centre de stockage de déchets radioactifs, PhD dissertation, Institut Polytechnique de Grenoble.

Davy, C.A., Skoczylas, F., Barnichon, J.D., Lebon, P., 2007, Permeability of macro-cracked argillite under confinement: gas and water testing, Physics and Chemistry of the Earth, 32, pp. 667-680.

Flaconneche, B., Martin, J., Kloppfer, M.H., 2001, Transport properties of gases in polymers: experimental methods, Oil & Gas Science and Technology, 56, pp. 245-259.

Klinkenberg, L.J., 1941, The permeability of porous media to liquids and gas. Drilling and production practice, American Petroleum Institute, pp. 200-213.

USING TRACER EXPERIMENTS FOR COMPARTMENTAL MODELING OF AN AERATED SLUDGE CHANNEL REACTOR

Y. Le Moullec, O. Potier, C. Gentric, J.P. Leclerc*
Laboratoire des Sciences du Génie Chimique, CNRS-Nancy-Université,
1, rue Grandville BP 20451, 54001 Nancy, France
*: corresponding authors Leclerc@ensic.inpl-nancy.fr

ABSTRACT:

This paper presents an intermediate solution between the simple systemic approach and the complex CFD modelling to simulate hydrodynamics, heat and mass transfer and chemical reactions in reactors. This approach, named compartmental approach, is based on information derived both from tracer experiments and CFD simulations. It has been applied to the complex behaviour of a biological wastewater treatment plant. The mapping of the compartmental modelling has been determined following three rules: flow direction should not change along a compartment boundary, physical scales should not go too far from an average value in each compartment and the compartmental model RTD should match the experimental one. Flowrates connecting compartments have been determined from CFD velocity and turbulence fields. The simulations of the biological reactions obtained with the model have been compared successfully with experimental concentration profiles of chemical oxygen demand, oxygen, nitrate and ammonium along the length of the reactor. The proposed method can be extended to numerous complex reactors for which CFD still remains too complex and classical systemic model lacks of predictability.

Keywords: Tracer, Compartmental modeling, Wastewater treatment plant, Computational Fluid Dynamics, Residence Time distribution

INTRODUCTION

Two main different methods are currently used to model the hydrodynamics of reactors. The first one, based on direct interpretation of tracer experiments, consists in describing the flow behavior using a combination of properly interconnected elementary reactors. This approach has been detailed by Levenspiel (1999) for simple models composed of few different modules in series or parallel and has been developed later for more complex models by several authors (for example Claudel et al., 2003). It can be further used to simulate chemical reaction and it gives rapidly with few efforts the main behavior of the reactor. It is a functional description of the flow since the location of the main features is not specified. The second approach is based on Computational Fluid Dynamics (CFD) modeling. Numerous developments and improvements have been performed during the last fifteen years and this method is now commonly used for hydrodynamics simulation of chemical reactors. This type of models is based on a structural description of the reactor given by a detailed meshing. But this method still remains difficult to handle when one wants to simulate hydrodynamics, heat and mass transfer and chemical reactions all together due to the high computational load.

This paper presents an intermediate solution in order to find a reasonable trade-off between an accurate description of the local phenomena and a limited calculation time. It is based on quantitative information coming from tracer experiments and CFD simulations. This idea has been used several times to develop complex compartmental models derived from tracer experiments. In these models, both the types of the elementary reactors and the order of magnitude of the parameters are justified or qualitatively estimated using CFD simulations. However these models remain a functional description of the main global trends of the reactor but not of the local effects which are sometimes preponderant. Moreover, the rules used to develop the model are not well defined; they depend both on the researcher sensitivity and knowledge. The present work proposes a method to develop a structural and functional compartmental model based not only on qualitative

information but on quantitative information derived from tracer experiment and CFD simulations using a well defined methodology. The proposed method has been validated by modeling concentration profiles in an activated sludge channel reactor for wastewater treatment. Due to the complex coupling between hydrodynamics, mass transfer and biological reactions, it is a perfect reactor to test the robustness of the proposed approach. Similar approaches have been proposed by Debangshu et al. (2006) for a simple chemical reaction in a single phase stirred tank reactor and Rigopoulos et al. (2003) for a non reactive bubble column.

EXPERIMENTAL SET-UP

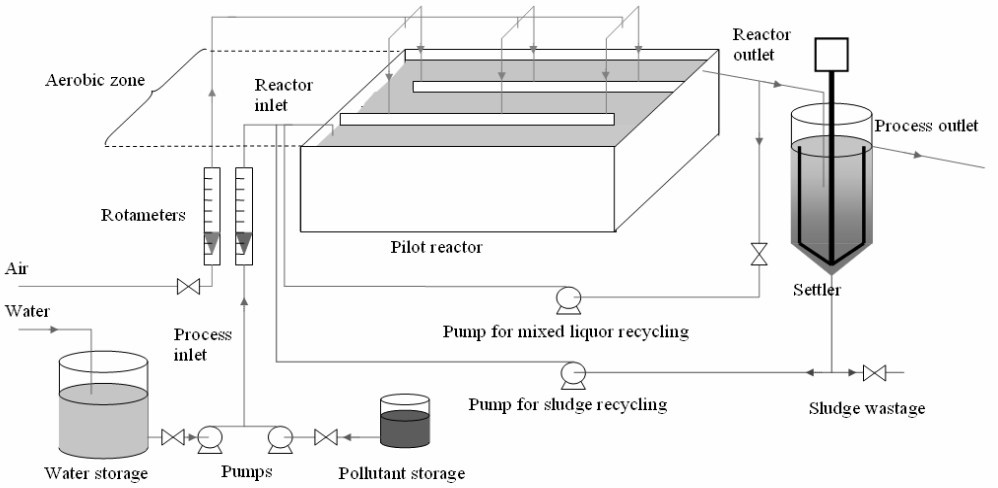

Figure 1: Scheme of the experimental set-up

The selected reactor is a channel reactor with a very long length compared to its height and width. The wastewater to be treated flows along the length and air is injected at the bottom. The total length of the bench scale reactor is 3.6 m with a rectangular section of width and height respectively equal to 0.18 m and 0.2 m (Figure 1). One side of the walls is fitted with stainless-steel tubes where 1 mm holes have been drilled every centimeter to ensure a sufficient aeration. The mixed liquor is partially recycled at the inlet. A settler of 0.88 m^3 is used to clarify the mixed liquor and to produce sludge which is also partially recycled at the reactor inlet. The mixed liquor and sludge recycling rates are respectively 4 and 1 to ensure a significant amount of biomass in the reactor and to obtain a reactor behavior similar to those observed in industrial treatment plants.

REACTOR HYDRODYNAMICS

The biological kinetics is described by Monod equations with apparent reaction orders greater than zero. Thus, the pollution removal efficiency depends on the hydrodynamics. Tracer experiments have been done in the reactor using a concentrated solution of sodium chloride as a tracer and conductivity probes as inlet and outlet detectors to measure the Residence Time Distribution (RTD). The global hydrodynamics is well represented by the plug flow reactor with axial dispersion model. A general correlation has been established to predict the axial dispersion coefficient as a function of the operating and geometric parameters (Le Moullec et al., 2008a). The liquid velocity field, liquid turbulence characteristics (k and □) fields and gas fraction field, as well as the numerical RTD have been determined by CFD simulations and successfully compared to experimental measurements (Le Moullec et al., 2008b).

MASS TRANSFER AND BIOLOGICAL REACTIONS

The oxygen transfer coefficient has been measured by the sulphite method. In fact, the numerical value calculated from CFD simulations using the Higbie's film penetration theory led to an overestimation of the mass transfer coefficient of 30%.

The biological kinetics model selected for the present work is the ASM1 model (Henze et al. 2001). It considers 12 different compounds and 8 kinetics processes (ρ_i, i=1 to 8) which are summarized in table 1. Biomass is composed of heterotrophic, autotrophic and inert biomass. Heterotrophic biomass grows with the consumption of soluble biodegradable pollution and oxygen (aerobic processes) or nitrate (anoxic process). Autotrophic biomass grows with the consumption of ammonium and oxygen and produces nitrate. Both heterotrophic biomass and autotrophic biomass decay into inert biomass, particulate biodegradable pollution and particulate nitrogen pollution. Both particulate biodegradable pollution and particulate organic nitrogen are hydrolysed in the presence of heterotrophic biomass into, respectively, soluble biodegradable pollution and soluble organic nitrogen. Finally soluble organic nitrogen is transformed into ammonium by the action of heterotrophic biomass.

In our calculations, the standard advised set of values, as recommended by the IWA, is used for stoechiometric and kinetics coefficients (Copp, J.B., 2001) has been used.

Table 1: Brief description of the compounds of the ASM1 model

Notation	Description	Involved in process
S_I	Soluble inert pollution	none
S_S	Soluble biodegradable pollution	Aerobic and anoxic growth (ρ_1 and ρ_2), Hydrolysis (ρ_7)
X_I	Particulate inert pollution	none
X_S	Particulate biodegradable pollution	Decay (ρ_4 and ρ_5), Hydrolysis (ρ_7)
$X_{B,H}$	Heterotrophic biomass	Aerobic and anoxic growth (ρ_1 and ρ_2), decay(ρ_4)
$X_{B,A}$	Autotrophic biomass	Aerobic growth (ρ_3), decay (ρ_5)
X_P	Inert biomass	Decay (ρ_4 and ρ_5)
S_O	Dissolved oxygen	Aerobic growth of $X_{B,H}$ and $X_{B,A}$ (ρ_1 and ρ_3)
S_{NO}	Nitrate and nitrite	Anoxic growth of $X_{B,H}$ and aerobic growth of $X_{B,A}$ (ρ_2, ρ_3)
S_{NH}	Ammonium	Aerobic growth (ρ_3), Ammonification (ρ_6)
S_{ND}	Soluble organic nitrogen	Ammonification (ρ_6), Hydrolysis (ρ_8)
X_{ND}	Particulate organic nitrogen	Decay (ρ_4 and ρ_5), Hydrolysis (ρ_8)

COMPARTMENT MODELING

The compartmental modeling methodology developed in this paper is summarized in figure 2. The reactor is described as a network of functional and spatially localized compartments. The model is based on the determination of compartments in which key parameters are homogeneous within a given tolerance. The first step is a complete CFD simulation of the hydrodynamics of the reactor (without chemical reactions). The most significant physical parameters that we need to take into account are based on the process knowledge. In our case, we considered:

- The gas fraction since gas transfer between phases has a preponderant role and the gas fraction is inhomogeneous on a slice of the reactor.
- The liquid velocity.

- Liquid turbulence (k and ε) because previous studies (Le Moullec et al., 2008 b) have shown that the axial dispersion coefficient was mainly turbulent.

In the present case, the hydrodynamic characteristics are constant along the reactor, i.e., the number of perfect mixing reactors derived from RTD measurements is strictly proportional to the length of the reactor for a given set of operating parameters (Potier et al., 2005). Thus the reactor can be divided into a succession of slices. The number, the shape and the connectivity of the compartments in a slice are determined by coupling the knowledge of the process, CFD simulations and image analysis to determine the homogeneity of physical scales. By construction, key parameters gradients along the boundaries between compartments are very low. Each slice is divided into 4 compartments corresponding to the main features of the reactor behavior. The first zone is a large liquid phase recirculation zone with high velocity magnitude, high turbulent kinetics energy (k). The second one is a liquid phase zone located at the centre of the first one with low velocity magnitude and low turbulent kinetics energy (k). The third one is a gas-liquid zone with high velocity magnitude and high turbulence, where oxygen transfer occurs. Finally, the fourth one is composed of the two dead corners at the opposite side of the sparger device, with low velocity magnitude and low turbulent kinetics energy (k).

The flowrates between compartments due to convective transport are computed straightforwardly from CFD simulations. The turbulent exchange between two compartments, corresponding to turbulent dispersion is more difficult to estimate. We made an analogy similar to the one used in the systemic approach, i.e. the equivalence between the plug flow with axial dispersion model and the perfect mixing cells in series with backmixing model (Potier et al., 2005). Equation 1 gives the backmixing rate α needed to simulate a series of J_{app} perfectly mixed reactor without backmixing from J reactors with a backmixing rate α.

$$J_{app} = \frac{J}{1+2\alpha - \frac{2\alpha\left(1+\alpha\right)}{J} + \frac{2\alpha^{1+J}\left(1+\alpha\right)^{1-J}}{J}} \qquad (1)$$

With this analogy, since the compartments are considered by pairs, the apparent number of compartments is deduced from equation (1) and is calculated as follows:

$$x = \frac{2\left(1+\alpha_{i,j}\right)}{1+2\alpha_{i,j}} \qquad (2)$$

where $\alpha_{i,j}$ is the turbulent backflow rate between compartments i and j.

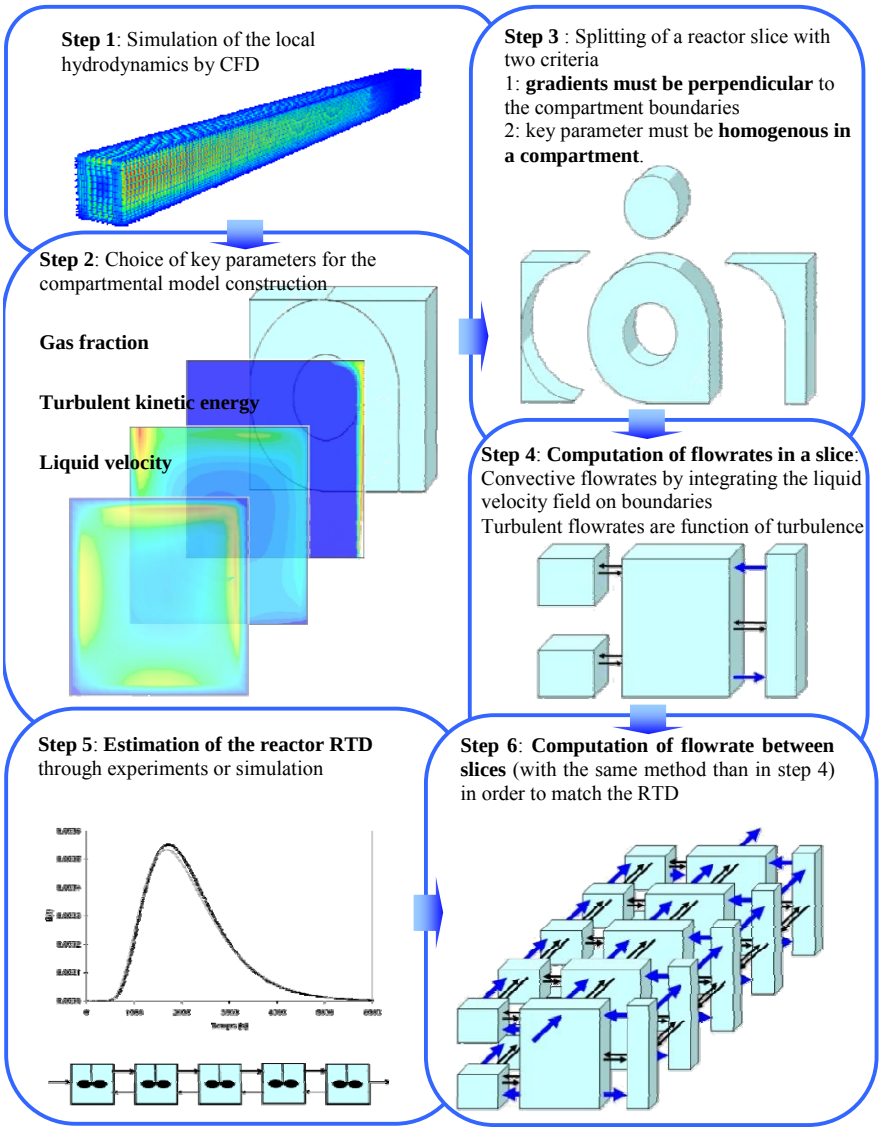

Figure 2: Description of the compartment modeling methodology

Following the same analogy, the Peclet number can be approximated to 2x+1 (as Peclet = 2J+1) leading to equation (3):

$$2(x-1) = Pe = \frac{u_{t,i,j}\Delta L_{i,j}}{D_t} = \frac{u_{t,i,j}\Delta L_{i,j} Sc_t \varepsilon}{C_\mu k^2} = \frac{\alpha_{i,j} Q_{i,j} \Delta L_{i,j} Sc_t \varepsilon}{S_{i,j} C_\mu k^2} \quad (3)$$

Where Pe is the Peclet number, $u_{t,i,j}$ represents an equivalent fluid velocity between compartments i and j due to turbulence, $\Delta L_{i,j}$ is the distance between the center of the compartments i and j, Sc_t is the Schmidt turbulent number (= 0.7), C_μ a constant of the k-ε turbulence model (= 0.09), ε the turbulent dissipation rate, k the turbulent kinetics energy, $S_{i,j}$ the surface between compartments i and j, $Q_{i,j}$ a nominal flowrate between compartments i and j and $\alpha_{i,j}$ the fraction of this flowrate due to turbulent mixing. Finally, $\alpha_{i,j}$ can be deduced from (2) and (3) with the following expression:

$$\alpha_{i,j} = \frac{\sqrt{A^2 + 8A}}{4A} - \frac{1}{4}, \quad A = \frac{Q_{i,j}\Delta L_{i,j} Sc_t \varepsilon}{2 S_{i,j} C_\mu k^2} \quad (4)$$

Once the structure of the slices has been determined, the number of slices is calculated by fitting the simulated RTD to the experimental one. CFD RTD results can also be used. An iterative procedure has been carried out: a number of slices is assumed, this allows to calculate the convective flowrates and turbulent backmixing rates between compartments. The process is repeated until the calculated RTD matches the experimental one.

RESULTS AND DISCUSSIONS

The simulations of biological reactions obtained with the compartmental model have been compared to experimental data in terms of the evolution of chemical oxygen demand (COD), suspended solid (SS), total nitrogen (TN) and oxygen concentration (S_O) along the length of the reactor with a satisfactory agreement (figure 3).

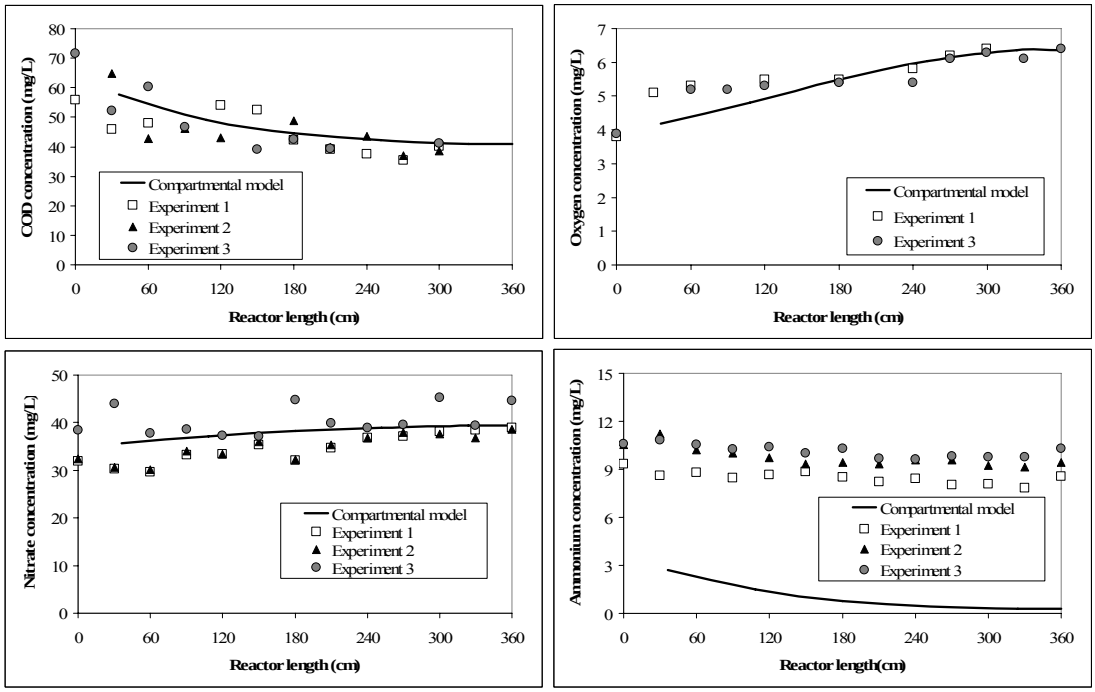

Figure 3: Experimental and simulated concentration profiles of COD (figure 3a top-left), Oxygen (figure 3b top-right), Nitrate (figure 3c bottom-left), and Ammonium (figure 3d bottom-right)

CONCLUSIONS

For several years, tracer experiments have been interpreted with simple models based on interconnected elementary reactors (perfect mixed reactors, plug flow reactors…). This approach still used for the simulation of chemical reactors is now forsaken on behalf of reactive CFD approach. However, if CFD allows taking into account the impact of local geometry or local flow characteristics, it remains time-consuming and difficult to apply when numerous simulations are required. A new approach has been developed to model the flow behavior of complex reactors by using simultaneously local information derived from CFD and global information derived from tracer experiments. It has been validated in the complex case of a biological gas-liquid-solid wastewater treatment reactor, by simulating successfully the concentration profiles of COD, oxygen and nitrate, even if the discrepancy between experimental and theoretical ammonium concentrations has not been explained at this level. This method needs to be validated for other complex reactors such as FCC for example but it opens also new opportunities when detailed description of the flow behavior in strongly non homogenous systems is required or when numerous simulations are required to test several similar configurations for scale-up or scale-down.

REFERENCES

Claudel S., Fonteix C., Leclerc J.P., Lintz H.G., "Application of the possibility theory to the compartment modelling of flow pattern in complex processes", Chemical Engineering Science, vol. 58, 4005-4016, 2003.

Copp, J.B. (2001) COST 'Simulation Benchmark' Manual, IWA Publishing.

Debangshu, G., Dudukovic, M.P., Ramachandran, P.A., Mehta, S., and Alvare, J. (2006) Cfd-based compartmental modelling of single phase stirred-tank reactors. AIChE Journal, 52 :1836-1846.

Henze, M., Gujer, W., Mino, T., van Loosedrecht, M. (2001) Activated Sludge Models ASM1, ASM2, ASM2d and ASM3, IWA Publishing.
Le Moullec, Y., Potier, O., Gentric, C., Leclerc, J.-P. (2008 a) A general correlation to predict axial dispersion coefficients in aerated channel reactors, Water Research, 42 (6-7), 1767-1777.
Le Moullec, Y., Potier, O., Gentric, C., Leclerc, J.-P. (2008 b) Flow field and residence time distribution simulation of a cross-flow gas-liquid wastewater treatment reactor using CFD, Chemical Engineering Science, 63 (9), 2436-2449.
Levenspiel O., (1999). Chemical Reaction Engineering, 3°ed., John Wiley & Sons, New York.
Potier, O., leclerc, J.P., Pons, M.N., (2005). Influence of geometrical and operational parameters on the axial dispersion in an aerated channel reactor. Water research, 39, 4454-4462.
Rigopoulos, S., Jones, A. (2003) A hybrid CFD-reaction engineering framework for multiphase reactor modelling: basic concept and application to bubble columns. Chemical Engineering Science, 58, 3077- 3089.

A NON UNIFORM FLOW VELOCITY EQUATION AND ITS APPLICATIONS TO MASS TRANSPORT IN NATURAL STREAMS

A. Constain[5], A. Carvajal[6] and J. Carvajal[7]

ABSTRACT

It is possible to find a more general equation for mean velocity of flow stating a Galilean composition of velocities that allows to define the Non-Fickian process as a virtual one accomplishing restrictions that usually current theories do not. This new equation links the dispersion coefficient and advective mean velocity by means of a random walk definition using theories proposed by I. Prigogine in last years of XX century. This equation contains a state function that allows to know when the tracer has reached the "complete mixing" condition being a very powerful theoretical tool to study contaminant dynamic models. The researchers explain how they have developed a software tool that may be applied in real time stream studies using NaCl and Rhodamine WT as tracers. Also a detailed experiment is documented.

INTRODUCTION

The simplified one-dimension diffusion-advection equation describes the mass balance in a control volume when a diffusion process takes place.

$$\frac{\partial C}{\partial t} + U_x \frac{\partial C}{\partial X} = E \frac{\partial^2 C}{\partial X^2} \qquad (1)$$

It is a well known fact that when there are not sources or sinks of mass, the solution of this differential equation is the Fick´s function

$$C(x,t) = \frac{M}{A(4\pi E\, t)} e^{\frac{(X-U_x t)^2}{4Et}} \qquad (2)$$

This function resembles a perfect symmetric Gaussian curve, which is not certainly the shape of an experimental asymmetric tracer curve in Figure 1. This fact leads to a main question: ¿Does diffusion follow a Fick´s dynamics?

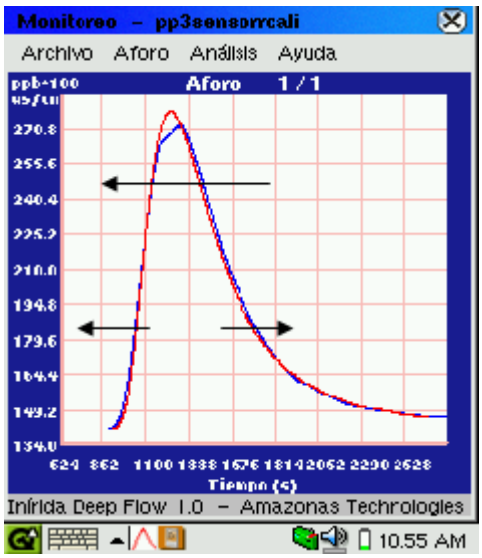

Figure 1.

[5] Professor, University of La Salle, Bogota. R+D Director, Amazonas Technologies, Cali, Colombia (www.amazonastech.com)
[6] Engineering Director, Amazonas Technologies, Cali, Colombia
[7] Manager, Director, Amazonas Technologies, Cali, Colombia

This asymmetry leads to consider a displacement of mass center for this moving system (which would be the responsible for the asymmetry). Then one can asks the way in which some agent does work to obtain this change of configuration of mass regarding the standard Gaussian curve. This agent does not exist as part of spreading plume itself because this is a fully irreversible process and all internal energy wastes all in heat, or in other words the free energy in a isothermal way is null (dF=0) in equilibrium. Then one has to ask for an external agent doing this work, but by definition equation (1) holds only for conservative process, i.e: one in which sinks or sources of mass are zero. The conclusion should be then that this external agent also does no exist. Then, if as was shown before, none agent may does work: ¿How can appear the displacement of mass center in the moving tracer plume? The only way in which this asymmetry may appear is if it is a virtual process without waste of energy.

From early times of mechanics such a process exist associated with the relative motion of inertial (non accelerated systems) and is called the Galilean composition of velocities. If the asymmetry of curve is associated with this composition its description may be different depends on state of motion of observer. For a fixed observer in the border of stream he (or she) sees the coming plume as an additive composition of Ux, the advective one-direction velocity of flow and the velocity of diffusion of tracer in the same direction, +Vdiff. Once the peak has passes by this point, the observer sees a sustractive composition of Ux and -Vdiff in oposite directions. The result of this composition is a stepper coming curve but slower falling going curve due to the different times spending in each motion, as is shown by the arrows of Figure 1.

Now, when a Galilean process takes place as in this case, always appears a function relating the two velocities involved. Also, the diffusion velocity may be put as the ratio of two characteristics parameters for one standard deviation, Δ and T:

$$\phi = \frac{V_{diff}}{U_x} = \frac{\left(\frac{\Delta}{\tau}\right)}{U_x} \tag{3}$$

If one takes a Random Walk motion model for diffusion knowing that I. Prigogine has given a universal status for it, a new equation for flow mean velocity may be written:

$$U_x = \frac{1}{\phi}\sqrt{\frac{2E}{\tau}} \tag{4}$$

Now, clearing E and putting it in Fick´s equation it holds:

$$C(x,t) = \frac{M}{Q\phi\, t\sqrt{2\pi\beta}}\, e^{\frac{(X-U_x t)^2}{2\beta\phi^2 U_x^2 t^2}} \tag{5}$$

Here β is a constant relating τ and t, found in a Poisson´s analysis of T. Svedberg`s work on Brownian motion. It can be proven that this function is solution of following differential equation:

$$\frac{\partial C}{\partial t} + U_x \frac{\partial C}{\partial X} = 2E \frac{\partial^2 C}{\partial X^2} \tag{6}$$

But this equation only differs from (1) in a constant, meaning that is the same balance structure. Then equation (5) is also a Gaussian because equation (6) defines a Gaussian nature, but equation (5) also describes an asymmetric tracer curve, as in Figure 1 (smooth line superimpossed on broken, experimental one). This implies only that the Non Fickian motion is indeed a virtual motion without any thermodynamic significance. It can be said that the Randon Walk motion has such universal nature that its description does not depends on the state of motion of observer: It has to be a Galilean invariant. From this statemen it follows that the tracer plume always has Gaussian nature, including the so called “Convective period” in which current theories do not admit validity of equation (1) and (2).

By the other hand, the Φ function is actually a state function which describes the thermodynamic evolution of tracer plume through the stream (at least in the chosen reach)

$$\oint_C d\phi = 0 \tag{7}$$

Following the evolution of Gibbs potential, the Φ function also can describes the steps in which the tracer taken as an idea gas (van`t Hoff model) reaches successive

DEVELOPMENT

Researchers have developed a software tool to apply presented theories. This instrument named INIRIDA DEEP FLOW works in a real time basis taken signals simultaneously from Conductivity or Rhodamine WT probes. The tracer curves are displayed in an interactive Hand PC screen. The tool produces a theoretical model which is drawn over experimental curve, depending on convergence of two curves the user may take measurement as good. The tool can store about 200 field journeis. Several pictures of 4 experiments in a large mountain river in Colombia (Pance river, Cali) are shown in following pages. Figure 2.

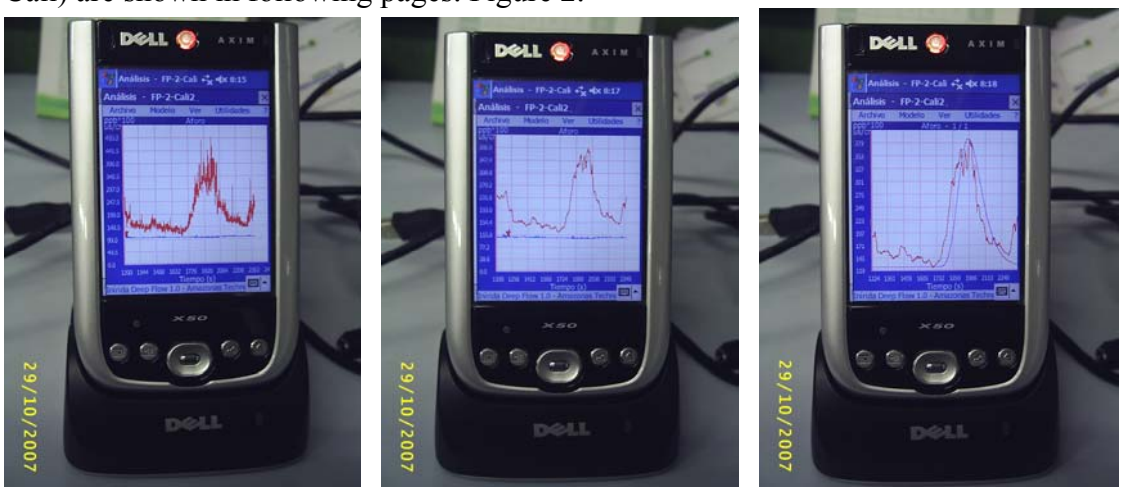


20/12/2007

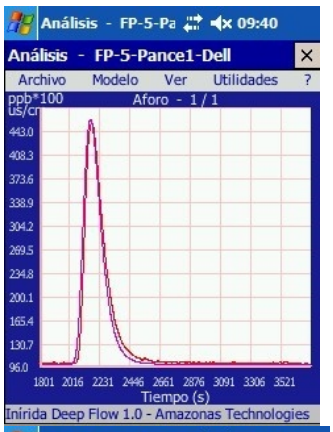
Análisis - FP-5-Pa 09:40
Análisis - FP-5-Pance1-Dell
Archivo Modelo Ver Utilidades ?
ppb*100
us/cr
Aforo - 1 / 1
443.0
408.3
373.6
338.9
304.2
269.5
234.8
200.1
165.4
130.7
96.0
1801 2016 2231 2446 2661 2876 3091 3306 3521
Tiempo (s)
Inírida Deep Flow 1.0 - Amazonas Technologies


Resultados 09:40
Análisis - FP-5-Pance1-Dell
Resultados
Aforo - 1 / 1
Datos
M (Masa) = 10 gr
L (Longitud) = 475.5 m
Resultados
Q (Caudal) = 18.2267 m3/s
U (Velocidad Media) = 1.273 m/s
Ex (Dispersión Long.) = 8.3011 m2/s
C (Concentración) = 1.011 ppb
T (Temperatura) = 17.8 °C
t (Tiempo) = 00:10:00
<< Registrar >>

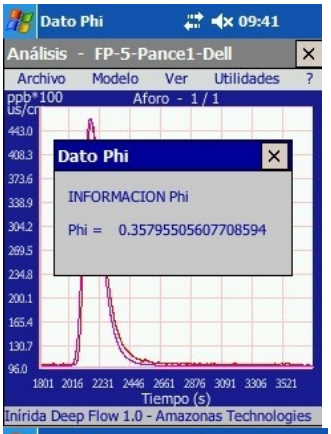
Dato Phi 09:41
Análisis - FP-5-Pance1-Dell
Archivo Modelo Ver Utilidades ?
Aforo - 1 / 1
Dato Phi
INFORMACION Phi
Phi = 0.35795505607708594
Tiempo (s)
Inírida Deep Flow 1.0 - Amazonas Technologies

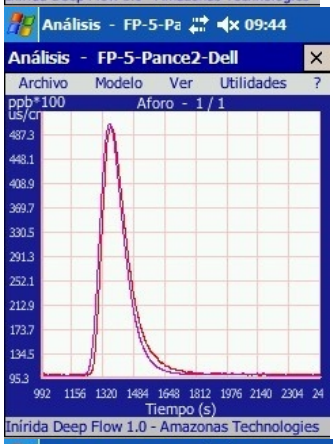
Análisis - FP-5-Pa 09:44
Análisis - FP-5-Pance2-Dell
Archivo Modelo Ver Utilidades ?
ppb*100
us/cr
Aforo - 1 / 1
487.3
448.1
408.9
369.7
330.5
291.3
252.1
212.9
173.7
134.5
95.3
992 1156 1320 1484 1648 1812 1976 2140 2304 24
Tiempo (s)
Inírida Deep Flow 1.0 - Amazonas Technologies


Resultados 09:44
Análisis - FP-5-Pance2-Dell
Resultados
Aforo - 1 / 1
Datos
M (Masa) = 10 gr
L (Longitud) = 475.5 m
Resultados
Q (Caudal) = 16.3806 m3/s
U (Velocidad Media) = 1.271 m/s
Ex (Dispersión Long.) = 8.0237 m2/s
C (Concentración) = 1.018 ppb
T (Temperatura) = 19.1 °C
t (Tiempo) = 00:06:52
<< Registrar >>

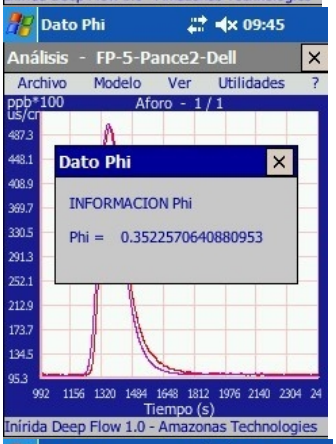
Dato Phi 09:45
Análisis - FP-5-Pance2-Dell
Archivo Modelo Ver Utilidades ?
Aforo - 1 / 1
Dato Phi
INFORMACION Phi
Phi = 0.3522570640880953
Tiempo (s)
Inírida Deep Flow 1.0 - Amazonas Technologies

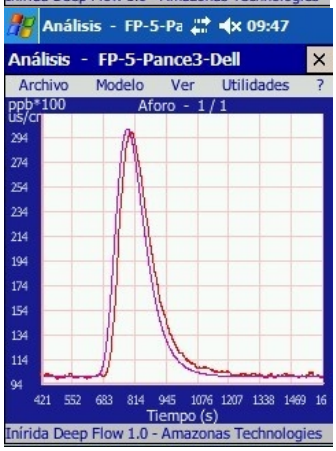
Análisis - FP-5-Pa 09:47
Análisis - FP-5-Pance3-Dell
Archivo Modelo Ver Utilidades ?
ppb*100
us/cr
Aforo - 1 / 1
294
274
254
234
214
194
174
154
134
114
94
421 552 683 814 945 1076 1207 1338 1469 16
Tiempo (s)
Inírida Deep Flow 1.0 - Amazonas Technologies


Resultados 09:47
Análisis - FP-5-Pance3-Dell
Resultados
Aforo - 1 / 1
Datos
M (Masa) = 5 gr
L (Longitud) = 475.5 m
Resultados
Q (Caudal) = 16.4300 m3/s
U (Velocidad Media) = 1.276 m/s
Ex (Dispersión Long.) = 8.2628 m2/s
C (Concentración) = 1.007 ppb
T (Temperatura) = 19.1 °C
t (Tiempo) = 00:05:46
<< Registrar >>

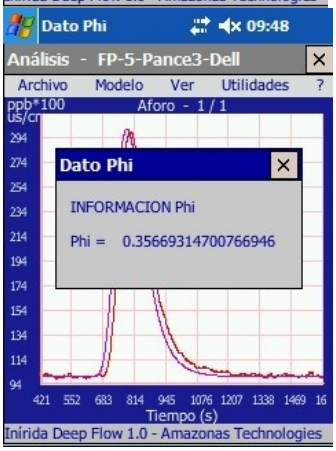
Dato Phi 09:48
Análisis - FP-5-Pance3-Dell
Archivo Modelo Ver Utilidades ?
Aforo - 1 / 1
Dato Phi
INFORMACION Phi
Phi = 0.35669314700766946
Tiempo (s)
Inírida Deep Flow 1.0 - Amazonas Technologies

Figure 2.

First part of photo section shows the PC screen processing a curve using a filter to clean the shape and displaying the theoretical model over real curve. Second part shows different views from the river and the tracer pouring. Third part shows the 4 sets of measurements as they appear in screen. Following is presented the data taken in this journey, congruent with the equations developed in this paper.

Table 1

Pouring	Width, WM	Distance, XM	Mass, MG	Mean Velocity, UxM/s	Φ	Discharge QM3/s	Peak Concentration, Cp,Ppb	Longitudinal dispersion Coefficient, E,M2/s
1.- Rhodamine WT	22	475.5	10	1.27	0.36	18.2	364.4	8.30
2.- Rhodamine WT	22	475.5	10	1.27	0.35	16.4	411.6	8.02
3.- Rhodamine WT	22	475.5	5	1.28	0.36	16.4	200.0	8.26
4.- Rhodamine WT	22	475.5	5	1.24	0.35	16.9	173.2	7.77

CONCLUSIONS

1. – There is a major drawback considering that asymmetric shapes of tracer curve in stream flow may be described as a real process. If tracer development is fully irreversible then no any energy can be used to do work against interaction forces within the tracer cloud, and also if the process is taken as a conservative one, there no exist any external agent to do that work.
2. – The only way to get simultaneously an asymmetric curve and a zero work against interaction forces is to considering a kinematic effect driven by the general Galileo`s principle. In this way the asymmetry is only a result of velocity composition which gives descriptions depending on motion state of observers. Randon Walk motion then may be a Galilean invariant allowing describing a space without absolute reference in the case of mass transport in streams.
3. -This leads to a set of equations that may be applied to link mass transport parameters with hydraulic ones.
4. -As is described in this paper, these equations work properly with real time measurements done in a large river mountain in southern Colombia.
5. -To apply these equations a software tool was developed. This tool named INIRIDA DEEP FLOW contains a hand computer and two different probes (conductivity and fluorescence) operated through a digital interface. The experiments were done using Rhodamine WT tracer.

6. –This method may be applied with other type of tracer (radioactive tracer for example)

REFERENCES

1.- Constain A, Carvajal J. and Carvajal A. 2007. An accurate measurement of discharge using conservative tracers. Flucome 2007, Tallahasse, USA.
2.- Constain A, Carvajal J. and Carvajal A. 2008. A thermodynamic method to measure mixing length using conservative tracers in streams. RIVER FLOW 2008, Cesme, Turkey.
3.- Constain A, Carvajal J. and Carvajal A. 2008. Naturaleza, comportamiento y métodos de medición de la dispersion en los cauces naturales. XXIII Congreso latinoamericano de Hidráulica e Hidrologia, Cartagena, Colombia.

ACKNOWLEDGEMENTS

We are in debt with Fomipyme, the Colombian government agency to Entrepreneur development which is funding this research. Also with COLCIENCIAS, the goverment S & T. Agency

GROUNDWATER RECHARGE ASSESSMENT USING ENVIRONMENTAL TRACING METHODS

[(1)]Mónica P D´ELIA, [(1,2)] Ofelia C TUJCHNEIDER, [(1, 2)] Marta del C PARIS,
[(1)] Marcela A PEREZ & [(2)]Susana GERVASIO
[(1)] Facultad de Ingeniería y Ciencias Hídricas (FICH) - Universidad Nacional del Litoral (UNL).
Ciudad Universitaria CC 217 (3000) Santa Fe, Argentina.
TE: 54-342-4575246 - FAX: 54-342-4575224 - e-mail: mdelia@fich.unl.edu.ar
[(2)]Consejo Nacional de Investigaciones Científicas y Técnicas, Argentina.

ABSTRACT

Groundwater resources are very important to the economic development in many regions, and sometimes is the only available one. Under natural conditions groundwater recharge is balanced by discharge, but this equilibrium is often affected by pumping. So, groundwater recharge and discharge need to be assessed in order to manage the aquifer system properly. Environmental tracers (^{18}O, ^{2}H, Cl, tritium) can provide information related to the sources of groundwater and location of recharge areas and can be used to estimate recharge rates and the time of residence of groundwater. The objective of this work is to present the assessment of groundwater recharge using environmental tracers, particularly oxygen-18, deuterium, tritium and chloride, in a flat area in Santa Fe, Argentina, and thus contribute to the knowledge of the groundwater system providing qualitative and quantitative criteria to base management and protection.

INTRODUCTION

Under natural conditions groundwater recharge is balanced by discharge, but if the extraction of groundwater exceeds the amount of recharge, water level declines and consequently, the groundwater reservoir decrease. Besides, salt water intrusion from other reservoirs can take place and groundwater quality would become unacceptable for different uses. So, groundwater recharge and discharge need to be assessed in order to manage the aquifer system properly.

Environmental tracers can provide information related to the sources of groundwater and location of recharge areas and can be used to estimate recharge rates and the time of residence of groundwater. The oxygen and hydrogen isotopes (^{18}O, ^{2}H) of the water molecules themselves are tracers of water movements and they are very useful to determine the sources, mechanism and seasonality of recharge and the interaction between surface water and groundwater. Chloride is a major ion that behaves conservatively and it is also a good tracer of groundwater movement. The mass balance of chloride is used to infer recharge mechanism and to estimate the magnitude of chloride addition to the aquifer. To identify the moment from which groundwater was recharged, some chronological tracers like ^{3}H or ^{36}Cl are used.

The objective of this work is to present the assessment of groundwater recharge using environmental tracers, particularly oxygen-18, deuterium, tritium and chloride, in a flat area in Santa Fe, Argentina, and thus contribute to the knowledge of the groundwater system providing qualitative and quantitative criteria to base management and protection.

DEVELOPMENT

Study Area

The study area is located in the center of the Santa Fe province, Argentina. It is a flat area of 500km^2 with a slope of about 0.2 to 0.3%, and 1% in areas near to the Salado River (Figure 1). Although surface water resources are available in the region, human activities (agriculture, live stock, industry, human consumption) are strongly dependant on groundwater, principally from the semiconfined aquifer.

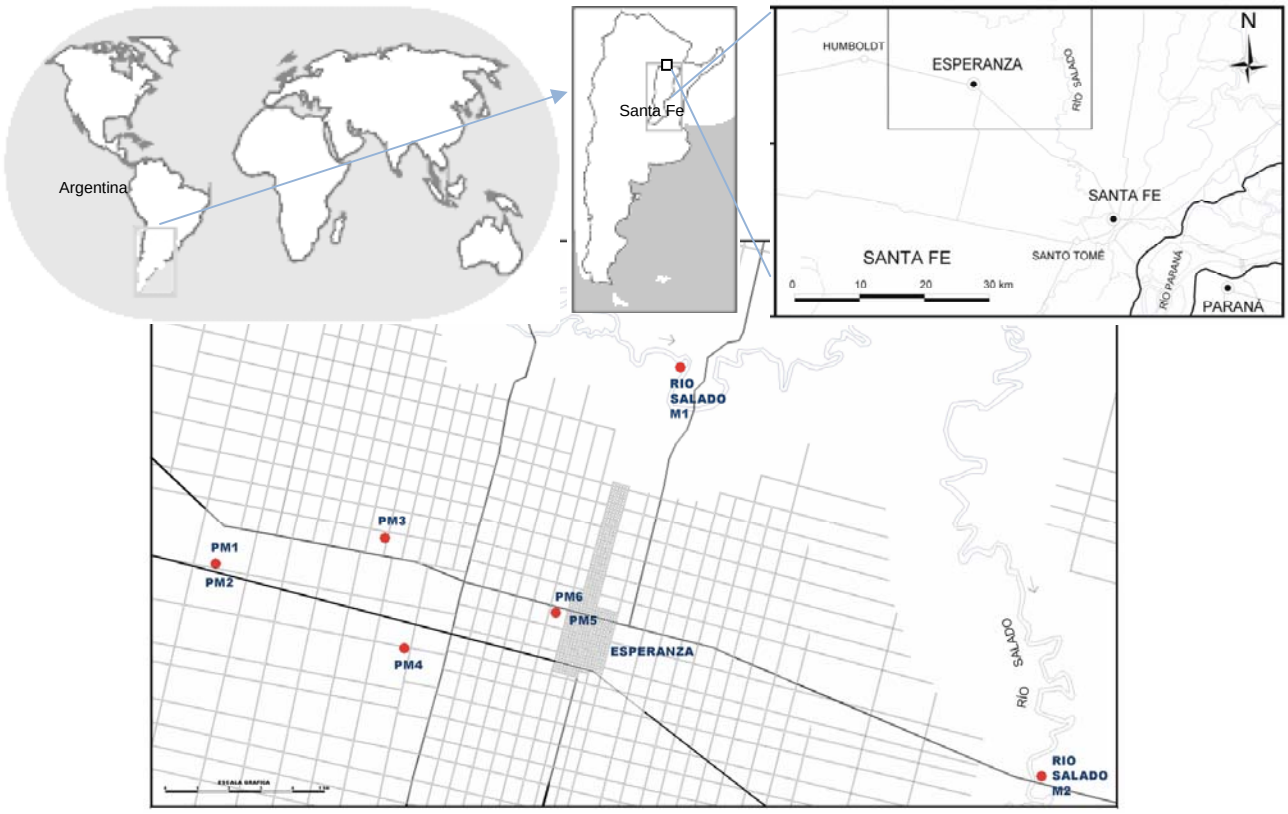

Figure 1. Location of the study area and the groundwater and surface water sample points.

The aquifer in the area is multilayer. Miocene clays and sands of marine origin are considered as the hydrogeological basement of the system. Over these sediments, there is an aquifer of about 24m of Pliocene fluvial sands that is semiconfined by clays of 3m thickness. An unconfined aquifer composed by Pleistocene silts, loess and clays of aeolian an lacustrine origin are over the aquitard and it is 15 m thickness approximately. The groundwater flow direction is from the West to the East and groundwater is principally sodium bicarbonated (Fili et al.,1999; Tujchneider et al., 2006). The predominant soil is deep and well drainage, principally formed by silts. The climate of the region is moderate and humid. Average annual rainfall is approximately 960mm for 1904-1996; a maximum amount of 1710mm was registered in 1914 and a minimum of 423mm in1906. A gradual increasing of annual precipitation was observed from 1960s. The greater average month precipitations occur during summer and autumn (100-140mm) and winter is the dry season (less than 35mm). Mean annual temperature is about 18°C, the higher average month temperature is 25 ºC and corresponds to January and the lower one is 12 ºC and corresponds to June and July. The origin of the principal air masses that produce precipitation in the region during the summer is the subtropical Atlantic Ocean anticyclone. Besides, mainly in winter and the beginning of spring, air masses coming from Atlantic Ocean (cold maritime polar masses) enter to the continent (hotter than the air masses) and origin convective instability.

MATERIALS AND METHODS

Precipitation samples are being monthly collected in Santa Fe station since October 1998 to analyze stable isotopes, tritium and chloride concentrations. This station is located in the FICH-UNL Campus, Santa Fe, Argentina, 30 km east of the study area. It belongs to the Global Network for Isotopes in Precipitation (GNIP) of the International Atomic Energy Agency (IAEA) and World Meteorological Organization (WMO). On the other hand, during field works (2003-2005), groundwater samples were collected in 6 monitoring wells, one production well P6 and two sections of Salado River (Figure 1). PM1 and PM5 correspond to the unconfined aquifer and PM2, PM3, PM4, PM6 and P6 to the semiconfined one. Monitoring wells are located at the outermost limits of the water utility well-field which pumps water from the semiconfined aquifer.

Stable isotopes (^{18}O and ^{2}H) and tritium analyses of rainfall and surface water samples were performed at the Instituto de Geocronología y Geología Isotópica-Consejo Nacional de Investigaciones Científicas y Técnicas (INGEIS-CONICET) and results (1998-2002) are published by the IAEA. Month chloride concentrations of precipitation for 2000-2006, were determined at the Unidad de Vinculación Tecnológica (VINTEC) Laboratory. Stable isotopes and ^{3}H analyses of groundwater samples were performed at the Environmental Isotopes Laboratory of the University of Waterloo (EIL-UW) and chloride concentrations of groundwater were determined at the Aguas Provinciales de Santa Fe (APSF) Laboratory. Stable isotopes analyses are reported in ∂ units expressed as per mile (‰) deviations with respect to the international standard (SMOW). Tritium is reported in TU that corresponds to an abundance of 10^{-18} ^{3}H per ^{1}H atoms. The analytical error is ±0.1 ‰ for ^{18}O, ±1.0 ‰ for ^{2}H and ±0.5 TU for ^{3}H for EIL-UW determinations; and ±0.2 ‰ for ^{18}O and ±1.0 ‰ for ^{2}H for INGEIS-CONICET. The Chloride in water and wastewater ASTM D-517-67 Method was used to determine chloride concentration in precipitation. The analytical error is ±0.05mg/l.

An analysis of $\partial^{18}O$, $\partial^{2}H$ and tritium contents of groundwater in relation with those of precipitation were done. The chloride concentration in rainfall was also analyzed. Recharge to the unconfined aquifer was calculated using chloride mass balance with a zero-dimensional mixing cell model (Cook and Herczeg, 1998). Finally, one-dimensional mixing cell model was used to preliminary estimate the regional recharge to the semiconfined aquifer between two sections (coincident with two monitoring wells) along the groundwater flow.

RESULTS AND DISCUSSION

Month precipitation of Esperanza station (1998-2006) is shown in Figure 2. It is observed that higher amounts of month precipitation (more than 100 mm) correspond principally to summer and autumn, and 2002-2003 was a very humid year in which an extraordinary flood of Salado River took place. Annual precipitations are also listed in Figure 2.

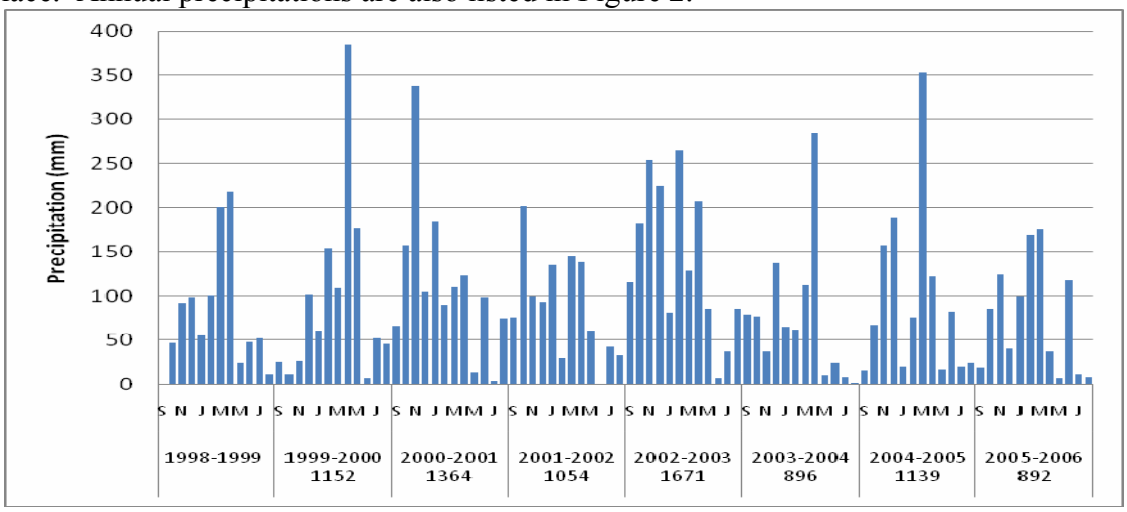

Figure 2. Month and annual precipitation- Esperanza (1998-2006)

Environmental tracers in rainfall, surface water and groundwater

Stable Isotopes

The local meteoric water line (Santa Fe LMWL) was defined by D´Elia (2006) for 1998-2002 period (Figure 3). The expression of this line is: $\partial^2H = 8.22\ \partial^{18}O + 13.76$ (‰) similar to the Global Meteoric Water Line (GMWL). $\partial^{18}O$ values range between -9.3‰ and 1.0‰ with an average of -4.5‰; and ∂^2H between -66‰ and 14‰ with an average of -23.1‰. The slope of the LMWL is closed to 8, the annual weighted mean isotopic composition of precipitation in the region results in $\partial^{18}O$= -5.3‰, ∂^2H= -29.5‰ and the weighted average contents of stable isotopes were calculated seasonally (Figure 3).

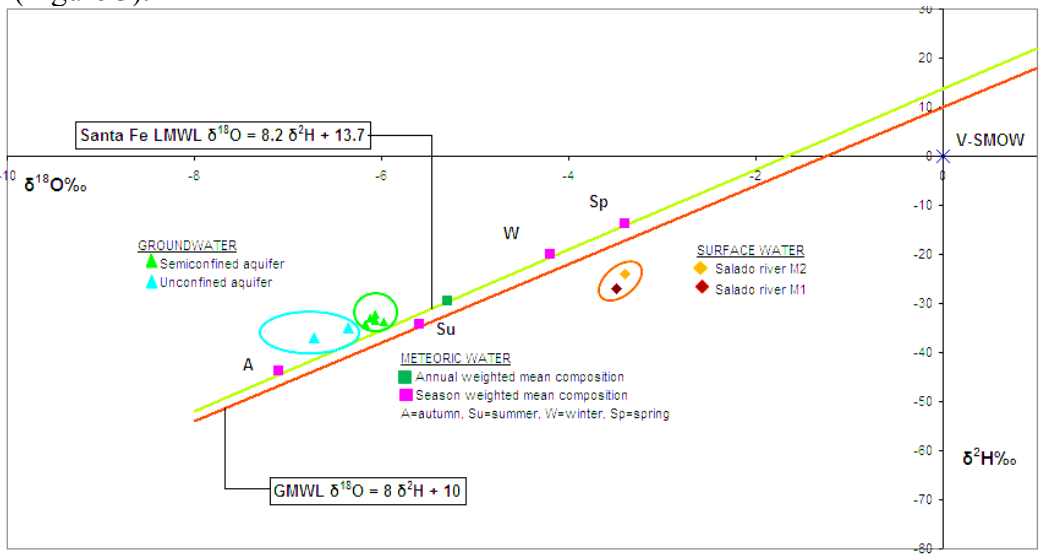

Figure 3. Local meteoric water line

$\partial^{18}O$ of groundwater ranges between -6.3‰ and -5.9‰ and ∂^2H varies between -37‰ and -32.3‰. These values are not significantly different from the annual weighted mean isotopic composition of precipitation in the region and are aligned to the LMWL, indicating that recharge came principally

from precipitation and no significant evaporation took place during recharge process. On the other hand, theses values are near to those corresponding to the autumn and summer weighted average contents of precipitation, suggesting that groundwater recharge occurred mainly during these seasons. Stable isotopes of Salado River are below to the LMWL indicating that surface water was affected by evaporation processes after the precipitation took place (Figure 3).

Tritium

The IAEA and the Centro de Desenvolvimento da Tecnologia Nuclear/Comissao Nacional do Energia Nuclear (CDTN/CNEN) do Brazil (2001) reported the average tritium content of several stations in Brazil and Argentina between the 1950s and 2000 and showed that higher values are closed to 10 TU in the 1960s and then decline to approximately 3 TU. In a recent study, Dapeña & Panarello (2007) informed tritium concentrations of rainfall for Santa Fe GNIP station for 2000-2002, observed higher contents (more than 10 TU up to 22 TU) from August 2000 to May 2001 which then decline to 3 TU and remark that the higher contents were not due to natural factors and probably came from Atucha I Nuclear Central (located 400 km to the South East of Santa Fe Station).

^{3}H content of groundwater coming from the semiconfined aquifer are <0.8 TU, those of the unconfined aquifer are 3.2 TU and 3.9 TU, and the corresponding to the production well is 1.3 TU. Considering a qualitative interpretation of ^{3}H data, it is possible to point that time residence of groundwater of semiconfined aquifer is more than 50 years (recharge prior to 1952); unconfined groundwater is a mixture between submodern and recent recharge -the tritium contents of rainfall reported by the CDTN/CNEN (2001) for South American Stations and by Dapeña & Panarello (2007) for Santa Fe Station also prove this assumption. Groundwater tritium content of P6 suggests a mixture between the unconfined and semiconfined aquifers. This fact is strengthened if the increasing of NO_3 content groundwater in the semiconfined aquifer -probably coming from the unconfined aquifer which is locally affected by industries and septic systems-, is taken into account.

Chloride

In Argentina, coastal zones located at the South-East of the study area, present chloride concentrations of rainfall ranging between 10 and 37 mg/l (Bocanegra & Martinez, verbal communication) and several investigations carried out in inland zones show that chloride concentration of precipitation decline to values near to 6 mg/l, 4 mg/l and 1mg/l, proving the natural gradient from coastal to inland zones. The present work is the first one that specifically considers the chloride concentration in rainfall in the area. The annual mean distribution of rainfall and the month average chloride concentrations are presented in Figure 4. It is observed that the lower the precipitation the higher chloride concentrations. The mean chloride concentration of the series resulted in 0.73 mg/l. The weighted mean chloride concentration of the series results in 0.21 mg/l, 0.20 mg/l for summer, 0.30 mg/l for autumn, 0.12 mg/l for winter and 0.19 mg/l for spring.

The mean chloride concentration of groundwater was 13.3 mg/l and 26 mg/l for the unconfined and semiconfined aquifer respectively. Mean annual precipitation (1239 mm) and surface runoff (170 mm) for 2000-2007, weighted mean chloride concentration in precipitation of summer and autumn and chloride concentration of groundwater (4.3 mg/l) in PM5 were considered to estimate the mean annual recharge to the unconfined aquifer which resulted in 63 mm. This amount of recharge is similar to the value (69 mm) obtained using the groundwater level fluctuation method (D´Elia et al., 2007). On the other hand, mean annual regional recharge to the semiconfined aquifer results in 41 mm.

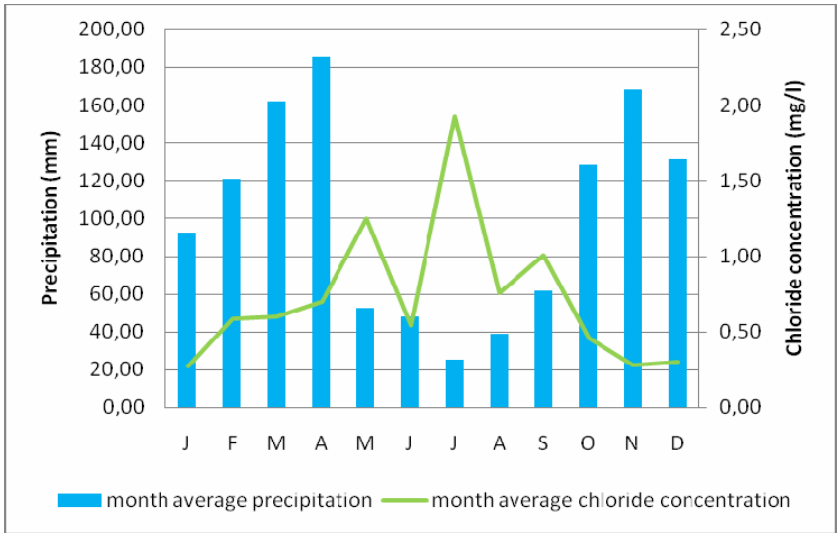

Figure 4. Annual mean distribution of rainfall and month average chloride concentrations Santa Fe (2000-2006)

CONCLUSION

The environmental tracing methods used in this work allow assess the groundwater recharge in the central sector of the Santa Fe province, Argentina, in which all the activities are dependent on groundwater.

The analysis of $\partial^{18}O$ and $\partial^{2}H$ in groundwater in relation to the LMWL shows that recharge comes from precipitation, occurs mainly during summer and autumn and no significant evaporation takes place during recharge process. Tritium contents indicate that the time residence of groundwater of the semiconfined aquifer is more than 50 years and the unconfined groundwater is a mixture between submodern and recent recharge. Tritium content in groundwater of the production well (P6) suggests a mixture between the unconfined and semiconfined aquifers. Thus, in addition with the presence of nitrate in groundwater, it is possible to corroborate the relation between both aquifers; and point the hypothesis that there is a discontinuity of the aquitard in the east of the area (Tujchneider, verbal communication).

If it is considered that monitoring wells -which are located at the outermost limits of a pumping field-, are not affected directly by pumping and the aquitard is a continuous layer, the increasing of chloride concentration in the groundwater flow direction would suggest a local recharge from the aquitard (despite of the practically undetectable tritium contents of the semiconfined aquifer). The chloride mass balance method allows to preliminary estimate regional recharge to the semiconfined aquifer (41mm) and recharge to the unconfined aquifer (63 mm/year).

The results of this study contribute to the knowledge of the groundwater system providing qualitative and quantitative criteria to base management and protection. Detailed investigations will be carry out in order to estimate more accurately the groundwater recharge to the semiconfined aquifer coming from the aquitard and from the unconfined aquifer where this layer is not present. Discharge, groundwater extractions and requirements to different uses and their relation with groundwater ecosystems will be also investigated.

ACKNOWLEGMENT

To Grupo de Investigaciones Geohidrológicas and Centro de Informaciones Meteorológicas (FICH-UNL) for the information given and to the IAEA for the support for the isotopes determinations.

REFERENCES

1) Centro de Desenvolvimento da Tecnologia Nuclear/Comissao Nacional do Energia Nuclear do Brazil, 2001. Informe del Taller Proyecto para la Protección Ambiental y Desarrollo Sostenible

del Sistema Acuífero Guaraní-Proyecto RLA/8/035 "Preparatory Activities for Guaraní Aquifer Project. Belo Horizonte, 4 al 7 de diciembre de 2001. 47pp.
2) Cook P. & Herczeg L. 1998. Groundwater chemical methods for recharge studies. Part 2 of the Basics of recharge and discharge. CSIRO Publishing. 24pp.
3) Dapeña C. & Panarello H. 2007. Composición isotópica de la precipitación de la estación Santa Fe. Red Nacional de Colectores. Argentina. Proceedings V Congreso Argentino de Hidrogeología: 187-198.
4) D´Elia M. 2006. Recarga a los acuíferos. Análisis de metodologías de cuantficación en áreas de llanura húmeda. Thesis of Master in Water Resources Engineering-Facultad de Ingeniería y Ciencias Hídricas-Universidad Nacional del Litoral. 193pp.
5) D´Elia M., Tujchneider O., Paris M. & Perez M. 2007. Evaluación de la recarga a los acuíferos en un sector del centro de la provincia de Santa Fe, Argentina. Proceedings V Congreso Argentino de Hidrogeología. Paraná, Entre Ríos, Argentina. 479-488.
6) Fili M,Tujchneider O, Perez M, Paris M, D´Elia M. 1999. Estudio del sistema de aguas subterráneas en el área de Esperanza-Humboldt y zona de influencia. Servicio Especializado de Asistencia Técnica. Convenio Aguas Provinciales de Santa Fe y Universidad Nacional del Litoral. Informe Final.
7) Tujchneider O, Paris M, Perez M, D´Elia M. 2006. Singularidad constitutiva de sistemas geohidrológicos de llanura y la gestión de los recursos hídricos subterráneos. Revista Latino-Americana de Hidrogeología. Vol. 5: 117-121.

USE OF NA24 IN THE DETERMINATION OF THE MOISTURE CARRYOVER IN ANGRA1 NUCLEAR POWER STATION STEAM GENERATORS

Authors: Anselmo Miranda - Physicist - Eletronuclear - Eletrobrás Termonuclear S.A.,
miranda@eletronuclear.gov.br
Enio Magalhães Freire – Physicist - SBF 1080.

SUMMARY

Angra Nuclear Power Station, in Brazil, is constituted of Unit 1 (657 MWe, reactor in operation since 13/mar/1982), Unit 2 (1350 MWe, reactor in operation since 14/jul/2000) and Unit 3 (1350 MWe, in construction). As part of the commissioning tests of Unit 1 it was measured, together with Westinghouse, the moisture carryover in the two steam generators, with the use of the radioactive tracer sodium carbonate Na_2CO_3 injected in the feedwater and collected in the steam sample lines leaving the steam generators. A correlation between the measured activities in the feedwater line and in the steam lines lead to the determination of the steam moisture carryover. The sodium carbonate sources were produced in the CDTN (Nuclear Technology Development Center) of CNEN, in Belo Horizonte-MG. Such commissioning test, carried out two times, confirmed the final result of 0,172 % moisture carryover with "steam probe", a temporary steam sampling collector, and 0.222% with sampling through installed Plant systems. Both results were less than the assumed value of 0,25% in the scope of supply of the steam generators. Each source were 4,5 g, 1,0 Ci and 2,0 Ci, measured during the addition in the feedwater. They were transported inside specific shield (338 kg), by truck, with special logistic arrangements taking into account the 10 hours transit time and the half-life of the sources (15 hours), with time enough for their valid utilization in the tests. During the tests the ETG – Turbine-Generator Building of the Plant was considered radioactive controlled area. In the first test the tracer was injected at 21:20 hours of 20/06/85 and at 21:20 hours of 23/06/85 the ETG was released for access without necessity for radiological control. At the 10:00 hours of 26/06/85 the area in the proximity of the tanks utilized for injection of the sources was also released. In 25 years of operation of the Plant, inspections do not indicate the presence of erosion of the turbine blades that could have been caused by excess of humidity in the steam, demonstrating the effectiveness of the tests performed during commissioning of the Plant. Also, the daily calculations of the reactor thermal power, which depend on the moisture carryover values have being demonstrated coherence.

ABSTRACT

Hereby its presented the chronology, methodology and the results of the moisture carryover test, performed as part of the commissioning of Angra Nuclear Power Station, Unit 1, in Brazil, with the use of sodium carbonate, Na_2CO_3, as radioactive tracer. The source of Na_2CO_3 was produced in the Reactor IPR-R1 of CNEN/CDTN - Nuclear Technology Development Center, in Belo Horizonte, MG. The results obtained were 0.172% with steam probe and 0.222% with samples taken from the plant process sampling systems. Both results were smaller than the contractual value of 0.25% assumed within the scope of supply of the plant equipments.

INTRODUCTION

Unit 1 is a 2 loop PWR pertaining to Furnas Centrais Elétricas S.A. at the time of the test and currently belongs to Eletronuclear - Eletrobrás Termonuclear S.A. In the two Steam Generators (SG) is produced dry and saturated steam, that after the high-pressure turbine is superheated and reused in the two low pressure turbines, then condensed in the condensers, cooled by sea water. By the contract of supply the steam saturated steam should not contain more than 0.25% moisture carryover. The test was carried through 2 times, in 25-26/oct/1984 and 20-21/jun/1985. The tracer was injected into the SG feedwater system. Sodium, being not volatile, remains in water droplets that constitutes the humidity of the steam and is detected in the steam that leaves the steam generators, before the turbines. The specific activities of the feedwater and the steam had been

measured using a multichannel analyzer Camberra-8000, with Ge-Li detector. Carryover can be expressed as:
CO(%) = (liquid mass in the steam)/(steam mass+liquid mass in the steam).

PROCEDURE

The tests, consisted of the following phases:

4.1 Irradiation of the sources in Reactor IPR-R1 of the CDTN, in Belo Horizonte.
4.2 Logistic of terrestrial transport until the Plant, considering the half life of the source.
4.3 Injection of the source in the chemical addition tanks in the feedwater lines, hydrazine tank for SG1 and morpholyne tank for SG2.
4.4 During the test, all the ETG was transformed into radiological controlled area.
4.5 Collections of samples and data for determination of the following parameters:

Item	Parameter	Description	Unit
A	If	Specific feedwater activity	□Ci/cm^3
B	Ib1	Specific blowdown activity SG1	□Ci/cm^3
C	Ib2	Specific blowdown activity SG1	□Ci/cm^3
D	W1	Feedwater flow of SG1	lb/h
E	W2	Feedwater flow of SG2	lb/h
F	Is1	Specific activity of Steam SG1	□Ci/cm^3
G	Is2	Specific activity of Steam SG2	□Ci/cm^3

1. CALCULATIONS:

The following formulas for the calculation of the moisture carryover was applied (Moisture Carryover):

CO (%) = (50 x (A) x (D+E) x (1/B +1/(CxR))/(D+E/R),

with steam probe, being R=F/G, and .

CO (%) = (100 x (A) x (D+E)) /(B x D + C x E),

for normal process sampling.

2. RESULTS AND CONCLUSIONS

- The chronology of the 1st Test, as a reference, is described below:

<u>25-26/SEP/1984</u>
08:00 - 2 Sources of Na-24, as Na_2CO_3, 1 Ci each, left Belo Horizonte.
18:00 – The sources arrived in Angra 1.
21:10 - Opening of the shielded transport container.
21:50 - Sources were poured into the hydrazine and morpholyne tanks.
22:00 - Initiated the injection in the SG feedwater lines.
23:45 - Finished “flushing” of the addition tanks, with 30 mrem/h in the CF-9 - SG1 and 30 mrem/h in the CF-3 - SG2.
01:20 Opening of the valves of SG steam and purge systems sampling.
02:20 Specific activity of SG1 = 1.9E-3 □Ci/cm^3
02:45 - 15:15 - Collections of Samples and calculations
<u>27/SEP/84</u>

At 17:00 hours the access to the Turbine-Generator Building were released without radiological control.

05/OCT/84

At 15:00 hours tanks CF-3 and CF-9 were released for normal operations.

- The first test was considered preliminary for optimization for the second test. It was also used for calibration of the SG operational levels.
- The results of the 2nd test are described in Table 1 below.
- The activities of the sources for the 2nd test were 2 Ci each.
- The final average values of the 2nd test were 0.172% with "steam probe" and 0.222% for the process sampling, both below the contractual value of 0,25%.
- The steam probes were temporarily supplied by Westinghouse. They were also used for comparison between the moisture carryover of individual Steam Generators.
- The R-15 radiation monitor, located in the discharge of the condenser vacuum pumps did not indicate release of radioactivity for the environment during the tests.
- As it was performed, the test, satisfies also the ASME Code.
- The test could be repeated as part of the commissioning of the new Steam Generators to be installed in Angra 1, in case such decision is made by Eletronuclear.
- The final results consider best operating conditions for steam generator levels.
- The values and concepts presented in this paper are simplified, for didactical purposes. The original values and formulas are found in Angra 1 files, as described in the references below.

3. REFERENCES

1. Angra 1 – Steam Generator Moisture Carryover Test Procedure – IT-RC-37, Westinghouse Electric Corporation and Furnas Centrais Elétricas S.A. 23/mar/1984.
2. Angra 1 – Procedimento de Proteção Radiológica Durante o "Steam Generator Moisture Carryover Test" PR-O/T 001.84, Furnas, 19/sep/84.
3. Freire, E. M. e Nascimento, Jorge – Determinação do Teor de Umidade do Vapor de Angra 1, utilizando o Na-24 como Traçador Radioativo - Simpósio Sobre Integração Regional de Energia Nuclear, ANS – Latin American Section, Rio de Janeiro, 1993.

TABLE 1.1 - FIRST SET OF MEASUREMENTS

Date			20.jun.85	20.jun.85	20.jun.85	20.jun.85
Time			22:30	23:00	23:30	24:00
Pt	Reactor Thermal Power	%	101.0	101.0	101.0	101.0
Pe	Generator Electric Power	MWe	655	655	655	655
Pv	Pressure in the steam header	kg/cm^2	61	61	61	61
If	Feedwater Specific Activity	$\mu Ci/cm^3$	1.06E-5	1.02E-5	5.64E-6	5.78E-6
W1	Feedwater Flow SG1	lb/h	4.096E+6	4.085E+6	4.089E+6	4.085E+6
N1	Level SG1	%	58.6	58.9	58.7	58.5
Ib1	SG1 blowdown Specific activity	$\mu Ci/cm^3$	4.43E-3	4.12E-3	4.13E-3	4.08E-3
Is1	Specific activity SG1 (Steam Probe)	$\mu Ci/cm^3$	1.86E-5	1.38E-5	9.86E-6	1.09E-5
W2	Feedwater flow SG2	lb/h	E. 109E+6	4.120E+6	4.098E+6	4.119E+6
N2	Level SG2	%	59.6	59.4	59.4	59.5
Ib2	Specific activity SG2 purge	lb/h	2.42E-3	2.00E-3	1.50E-3	1.16E-3
Is2	Specific activity SG2 (Steam Probe)	$\mu Ci/cm^3$	< 9.7E-8	< 9.2E-8	< 1.0E-7	< 1.10E-7
CO	Carryover, process	%	0.310	0.334	0.244	0.273
CO	Carryover, with steam probe	%	0.241	0.250	0.182	0.191

TABLE 1.2 - SECOND SERIES OF MEASURES

Date			21.jun.85	21.jun.85	21.jun.85	21.jun.85
Hour			01:30	02:00	02:30	03:00
Pt	Reactor Thermal Power	%	99.3	99.6	99.4	99.4
Pe	Generator Electric Power	MWe	649	649	649	649
Pv	Pressure in the steam header	kg/cm^2	61	61	61	61
If	Feedwater Specific Activity	$\mu Ci/cm^3$	1.62E-6	3.21E-6	1.90E-6	2.26E-6
W1	Feedwater Flow SG1	lb/h	4.02E+6	4.038E+6	4.020E+6	4.038E+6
N1	Level SG1	%	58.6	58.7	59.0	58.9
Ib1	Specific activity of purges of the SG1	$\mu Ci/cm^3$	2.20E-3	1.50E-3	1.48E-3	1.73E-3
Is1	Specific activity SG1 (Steam Probe)	$\mu Ci/cm^3$	4.65E-6	2.63E-6	2.50E-6	4.30E-6
W2	Feedwater flow SG2	lb/h	4.029E+6	4.036E+6	4.044E+6	4.018E+6
N2	Level SG2	%	59.1	59.2	59.1	59.0
Ib2	Specific activity SG2 purge	lb/h	7.49E-4	7.40E-4	7.50E-4	6.22E-4
Is2	Specific activity SG2 (Steam Probe)	$\mu Ci/cm^3$	< 9.5E-8	< 9.8E-8	< 1.0E-7	< 1.0E-7
CO	Carryover, process	%	0.110 (Annulled)	0.287	0.171	0.192
CO	Carryover, with steam probe	%	0.077 (Annulled)	0.222	0.134	0.136

TABLE 1.3 - THIRD SERIES OF MEASURES

Date			21.jun.85	21.jun.85	21.jun.85	21.jun.85
Hour			05:30	06:00	06:30	07:00
Pt	Reactor Thermal Power	%	100.3	100.1	100.1	100.1
Pe	Generator Electric Power	MWe	653	653	653	650
Pv	Pressure in the steam header	kg/cm^2	61	61	61	61
If	Feedwater Specific Activity	□Ci/cm^3	9.81E-7	1.00E-6	1.53E-6	1.48E-6
W1	Feedwater Flow SG1	lb/h	40.070E+6	40.048E+6	40.059E+6	40.066E+6
N1	Level SG1	%	59.0	58.7	58.6	58.9
Ib1	Specific activity of purges of the SG1	µCi/cm^3	1.02E-3	1.00E-3	9.96E-4	9.67E-4
Is1	Specific activity SG1 (Steam Probe)	µCi/cm^3	2.25E-6	2.85E-6	2.43E-6	2.29E-6
W2	Feedwater flow SG2	lb/h	4.068E+6	4.079E+6	4.075E+6	4.064E+6
N2	Level SG2	%	59.3	59.3	59.2	59.0
Ib2	Specific activity SG2 purge	lb/h	3.84E-4	3.77E-4	3.42E-4	3.16E-4
Is2	Specific activity SG2 (Steam Probe)	µCi/cm^3	< 9.80E-8	< 1.10E-7	< 1.15 E-7	1.06E-7
CO	Carryover, process	%	0.140	0.145	0.229	0.231
CO	Carryover, with steam probe	%	0.103	0.107	0.167	0.167

TABLE 1.4 - FOURTH SERIES OF MEASURES

Date			21.jun.85	21.jun.85	21.jun.85	21.jun.85
Hour			12:30	12:45	13:00	13:15
Pt	Reactor Thermal Power	%	99.8	99.8	100.1	100.1
Pe	Generator Electric Power	MWe	650	650	653	653
Pv	Pressure in the steam header	kg/cm^2	61	61	61	61
If	Feedwater Specific Activity	$\mu Ci/cm^3$	6.57E-7	6.30E-7	5.43E-7	4.99E-7
W1	Feedwater Flow SG1	lb/h	4.036E+6	4.034E+6	4.051E+6	4.037E+6
N1	Level SG1	%	60.2	60.4	60.4	60.4
Ib1	Specific activity of purges of the SG1	$\mu Ci/cm^3$	4.16E-4	3.83E-4	3.53E-4	3.54E-4
Is1	Specific activity SG1 (Steam Probe)	$\mu Ci/cm^3$	1.28E-6	1.22E-6	1.18E-6	1.10E-6
W2	Feedwater flow SG2	lb/h	4.060E+6	4.070E+6	4.071E+6	4.046E+6
N2	Level SG2	%	59.8	59.8	59.5	59.7
Ib2	Specific activity SG2 purge	lb/h	1.57E-4	1.44E-4	1.40E-4	1.38E-4
Is2	Specific activity SG2 (Steam Probe)	$\mu Ci/cm^3$	< 9.4E-8	< 9.7E-8	< 9.8E-8	< 1.0E-7
CO	Carryover, process	%	0.230	0.240	0.214	0.203
CO	Carryover, with steam probe	%	0.176	0.185	0.167	0.159

LIQUID AND GAS RESIDENCE TIME DISTRIBUTION IN A TWO-STAGE BIOREACTOR WITH CELL RECYCLE

Lamia BEN GAIDA[1], Christophe ANDRE[2], Carine BIDEAUX[1], Sandrine ALFENORE[1], Xavier CAMELEYRE[1], Carole MOLINA-JOUVE[1], Luc FILLAUDEAU[1]
[1]Laboratoire d'Ingénierie des Systèmes Biologiques et des Procédés (LISBP)
(CNRS UMR5504, INRA UMR792, INSA), Toulouse, France.
[2]Ecoles des Hautes Etudes d'Ingénieur (HEI), Lille, France.

ABSTRACT

Hydrodynamic behaviour of a two-stage bioreactor with cell recycle (TSCB) was investigated. Residence time distribution (RTD) and Internal Age Distribution (AID) of gas and liquid phases were performed with accurate tracing methods and under specific operating conditions and process modes (batch and continuous modes with and without recirculation between first and second stages). From experiments, RTD and analytical solution were formulated, and systemic analysis carried out. Results demonstrated that the magnitude of mean residence time and variance were strongly different between gas (≈1min) and liquid (≈100min) phases. RTD of gas phase showed that both reactors exhibited independent behaviour, and RTD could be described by two single and simple models (plug flow in series with j CSTR) with constant parameters (α, j) whatever investigated operating conditions (VVM, Re and Re_{mixing}). For liquid phase, experiments will enable to identify mixing time (batch mode) as well as the mean residence time and variance in continuous modes. RTD for permeate and purge flow and IAD in the first and second reactors were obtained and formulated. Under selective assumptions, a systemic analysis of liquid RTD lead to propose a reactor model in close relation with TSCB structure. In a first step, model parameters will be identified under continuous mode without recirculation and then, validated with recycle between two stages.

Keywords: residence time distribution, internal age distribution, tracing methods, liquid, gas, bioreactor, high cell density.

INTRODUCTION

The application of three phase reactors (solid, liquid and gas) is well established in a wide variety of chemical processing operations such as, production of fine chemical, wastewater treatment and fermentation processes. For these last cases, increasing cell density in bioreactors is useful to improve the overall productivity of continuous modes processes particularly the bio-ethanol production which has to be competitive according to energetic, economical and environmental criteria. Another determinant factor to optimise the overall performance of biological process is the configuration of the bioreactor. The performance of bioreactors is, however, strongly influenced by the complex interactions between gas and liquid hydrodynamics as well as the solids (microorganism) activities [10].

Theoretical approaches [8, 9] showed that recycle two-stage continuous fermentations with membrane separator would be potentially the most efficient system for improving ethanol productivity in high cell density cultures. An innovative two-stage bioreactor with cell recycle (TSCB) was developed to study the behaviour of Saccharomyces cerevisiae under high cell concentration, taking into account the management of growth, ethanol production and cell viability [1, 2]. The first stage of the bioreactor was dedicated to cell growth without oxygen limitation and at non-inhibitory ethanol concentration. The second stage was dedicated to high ethanol productivity. The high cell density was so obtained by an ultra filtration module coupled to the second reactor under micro-aeration condition. The innovative part of the bioprocess consists of the use of a recycle loop from the second stage to the first one to manage cell viability and activity.

In the present work, a global hydrodynamic study was carried out with the TSCB (Fig. 1). RTD and IAD formulations constitute efficient tools to give new insights in complex hydrodynamic

phenomena occurring in the bioreactor. From experiments, RTD and analytical solution were formulated and discussed, and systemic analysis carried out. Reactor models were proposed for gas and liquid phases.

DEVELOPMENT

Theory : RTD and IAD

The residence time distribution (RTD) is a chemical engineering concept introduced by Danckwerts [3]. The concept of RTD can be used to obtain hydrodynamic data and to assess the degree of mixing and flow patterns within any reactors [6]. The models derived from tracer experiments are often limited to simple elementary reactors such as perfect mixing cells in series [7], plug flow with axial dispersion [12], mixing cells in series exchanging with a dead zone [5] or simple compartment models [6].

In our study, analysis of RTD profile can be used to determine the deviations from ideal reactor behaviour and to give indications about the modifications that the system needs to overcome distribution problems.

RTD profiles may be measured by monitoring the evolution of an inter tracer through the bioreactor. The RTD function, E(t), can be evaluated dividing the tracer concentration c(t) in the exit stream of the bioreactor (in our case the exit permeate and bleed) by the total mass of tracer injected in the feed (Eq. 1).

The average residence time was given by the first moment of the RTD function E(t), Γ^i also called mean residence time, t_s. This parameter may be calculated by determining the area under the curve of a plot of t E(t) as a function of time (Eq. 2). The theoretical mean holding time, τ was calculated as the ratio of the reactor volume, V to the volumetric flow rate, Q (Eq. 3)

$$E(t) = \frac{c(t)}{\int_0^\infty c(t)\cdot dt} \quad \text{Eq. 1,} \qquad \Gamma^1 = t_s = \int_0^\infty t \cdot E(t)\cdot dt \quad \text{Eq. 2 and} \qquad \tau = \frac{V}{Q} \quad \text{Eq. 3}$$

In this study, the results where the values of τ differed significantly from the mean residence time, t_s (above 10%) were rejected.

The general equation (Eq. 4) defines the central moments of order i. The higher order centred moments, $\Gamma^{i'}$, can provide significant information about the behaviour of the function E(t). For example, the second central moment, $\Gamma^{2'}$ is referred to as the variance, σ^2 which describes the spread of the RTD curve. The centred moments of third order, $\Gamma^{3'}$ represent deviation from a symmetrical distribution (skewness) and of fourth order, $\Gamma^{4'}$ spreading of the RTD. However, the quality of signals led to non significant or reliable results for centred moments of third and fourth order.

Internal age distribution, I(t) was also defined to describe the reactor contents. This function has a similar definition as E(t): the fraction of fluid within the reactor with an age of t is I(t) dt. The relation between E(t) and I(t), and between F(t) and J(t) can be determined from the mass balance (Eq. 6 and 7):

$$\Gamma^{j'} = \int_0^\infty (t - t_s)^i \cdot E(t)\cdot dt \quad \text{Eq. 4 and} \qquad I(t) = \frac{1}{\tau}\left(1 - \int_0^t E(t)\cdot dt\right) \quad \text{Eq. 5}$$

$$\text{With} \quad E(t) = -\tau \frac{dI(t)}{dt} \quad \text{Eq. 6 and} \quad J(t) = \tau \cdot I(t) = 1 - F(t) \quad \text{Eq. 7}$$

Simulation of complex compartment models

A software package (DTS Progepi v4.2 software) has been developed to simulate the response to an input of any complex network of elementary reactors properly interconnected [5]. Processes with multiple inlets or outlets can be modelled by convolution and optimization procedures. The

software may also be used to determine the parameters of the different models giving the same response, and the subsequent test of the physical soundness of these parameters leads to the choice of a realistic model. In addition, automatic generation of RTD needs both analysis of the RTD curves (tail, number of peaks, etc.) and physical information about the process itself (presence of agitator, dead volume, etc.). A very good knowledge of the geometry of the reactor is thus necessary in order to establish a model as faithful as possible to the real flow, and permitting to draw some useful information for future experiments.

MATERIALS AND METHODS

Experimental set-up

Experiments were carried out using the pilot plant (Fig. 1) which was composed of four major parts: the first and second bioreactors, the filtration and permeate loops. The TSCB included a first, R1 (Chemap CMF100, 5 l) and a second bioreactor, R2 (SGI, 8L) controlled by a CB5 control unit (B. Braun Biotech International, pH, dissolved oxygen, mixing, temperature). The second reactor (R2) was connected to a filtration loop (6.5L, ∅=25.4mm) composed of two parallel modules (Rhodia - Orelis company - Miribel, France, Kerasep-K01-B-X2, Al_2O_3-TiO_2 ceramic membrane, $\varnothing_{int}$ 6mm, 7 channels, $\varnothing_{ext}$ 25mm, 1178mm length, UF cut-off: 150kDa, unit surface: 0.155m²) and a tubular heat exchanger including temperature regulation. Transmembrane pressure was adjusted to get an accurate permeate flow-rate by a counter pressure valve. Permeate was extracted and partially recycled in R2 reactor.

Peristaltic pumps (Masterflex model, Q ranging from 0 to 10 l/h) were used to enable the circulation of the liquid phase as feed Q_w, circulation Q_{12} and Q_{21}, second stage bleed Q_{pg} and permeate Q_p. Flow rate in filtration loop was achieved with a volumetric pump (PCM pump, Moineau M6000C4, Q_{max}=5m^3/h). Two mass flow meters (Micromotion serie R, Coriolis effect) measured the total flow in the filtration module and the permeate flow. Each reactor was equipped with an inlet air flow meter (Bronkhorst high-tech, Instrutec type F, $Q_{max\text{-}R1}$=5Nl/min and $Q_{max\text{-}R2}$=2.5Nl/min). The experimental set-up was also connected to a computer with homemade software performing the on–line acquisition of the controlled parameters (stirring rate, pH, temperature, inlet air flow, dissolved oxygen, liquid level regulation), and monitored the peristaltic pumps. The control of feed flow, Q_{Feed}, circulation flow from R1 to R2, Q_{12} and outlet flow, Q_{Bleed} and $Q_{Permeate}$, allowed us to keep the working volume constant.

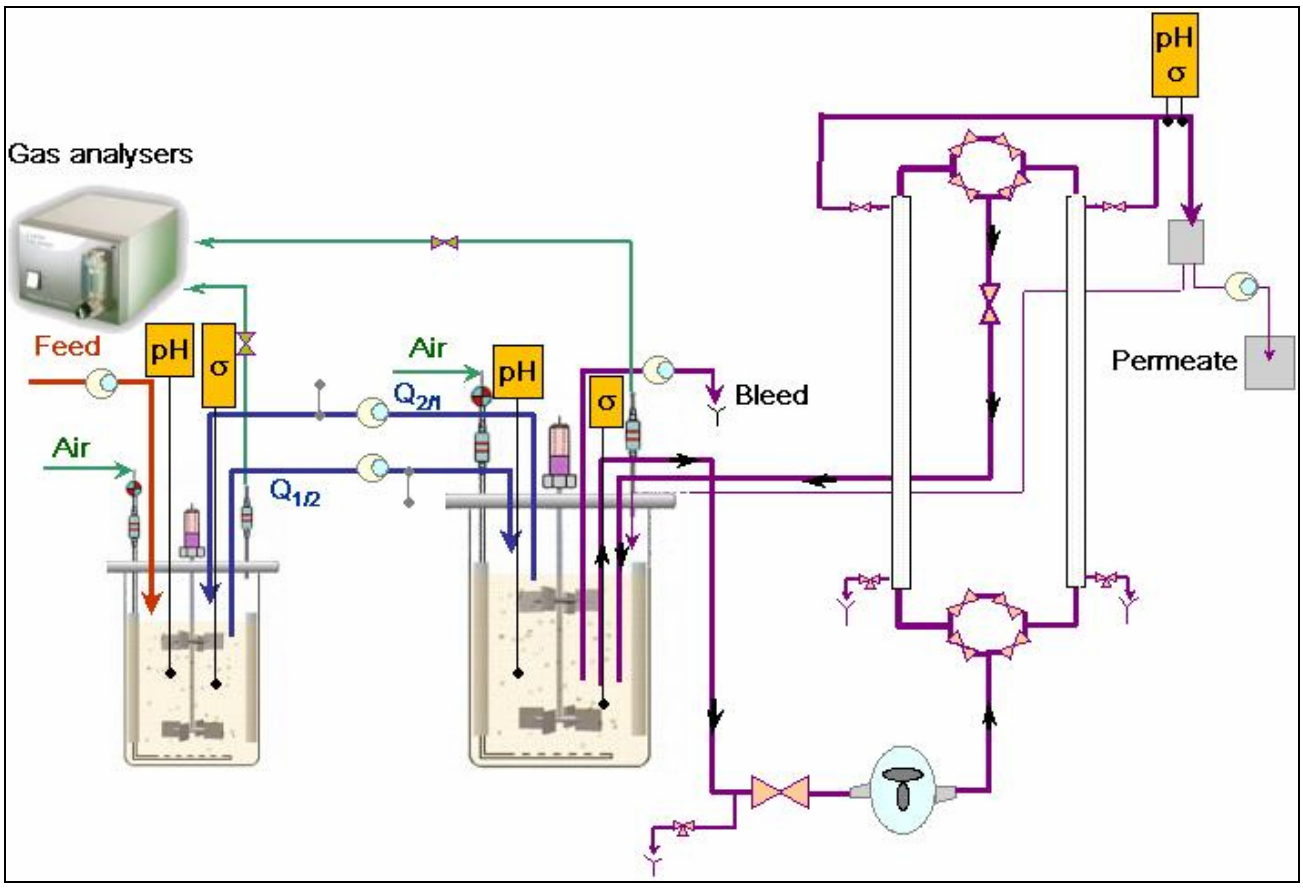

Fig. 1 : Overview of experimental TSCB set-up and specific instrumentation for RTD investigation

Table 1: Average operating conditions in experiments a, b, c and d.

Parameters	Units	Exp(a)	Exp(b)	Exp(c)	Exp(d)
Q_{21}	[l/h]	1	4.1	1	4
Q_{12}	[l/h]	2.56	9.11	2.56	9.79
Q_{Loop}	[l/h]	2500	2600	1100	2600
$Q_{Permeate}$	[l/h]	1.38	4.95	1.38	5.7
Q_{Bleed}	[l/h]	0.18	0.06	0.18	0.09
Q_{Feed}	[l/h]	1.56	5.01	1.56	5.79
Rpm_R1	[tr/min]	700	900	850	900
Q_{Air}_R1	[l/min]	1.5	1.7	0.15	2.6
Q_{Air}_R2	[l/min]	2	3.8	0.6	0.8
V_{R1}	[L]	4.5	4.5	4.5	4.5
$V_{(R2+Loop)}$	[L]	5+6.5	5+6.5	5+6.5	5+6.5
T	[°C]	30	30	30	30

Parameters	Units	Exp(a)	Exp(b)	Exp(c)	Exp(d)
a	[/]	0.39	0.45	0.39	0.44
$Re_{mixing-R1}$	[/]	36400	46800	44200	46800
$Re_{loop-R2}$	[/]	46600	48700	20700	48000
Re_{perm}	[/]	1800	1900	1400	2300
VVM-R1	[1/min]	0.33	0.38	0.03	0.58
VVM-R2	[1/min]	0.17	0.33	0.05	0.07

OPERATING CONDITIONS FOR TRACING EXPERIMENTS

RTD and IAD experiments were carried out under 4 operating conditions (a, b, c and d, Table 1), identified and selected among 8 experiments established during microorganism culture and ethanol production [1, 2], and 3 process modes: batch, continuous with recycle and without recycle (Q_{21}=0). Experimental RTD and IAD were conducted with TSCB without biological activity and following the methodology described by Thereska [11].

The tracing methods (Fig. 1) were respectively a step of oxygen or nitrogen concentration as gas tracer, injected at the inlet of the reactor R1 or R2, and a pulse (Dirac) of NaCl/NaOH concentration as liquid tracer, injected rapidly with a syringe at R1 inlet. In each experiment, the quantity of tracer injected was controlled. For gas phase, oxygen/nitrogen concentration at R1 and R2 outlets were simultaneously monitored with two gas analyzers (Innova Air Tech Instruments, Type 1313). Percentage of dissolved di-oxygen inside R1 and R2 reactors and permeate loop were measured using 3 dissolved oxygen electrodes (Hamilton type Oxyferm FDA120, OxyProbe Serie Dissolved Oxygen Sensor and Ingold n°322 756800/83264). For liquid phase, the tracer concentration was measured simultaneously by conductivity (Kemotron type 9147, Conducell 4USF-PG215 and PG325) and pH (Hamilton type Easyferm plus VP/120, pH FermProbe F-615-B130-DH and F-635-B325-DH) electrodes located on different zones of the bioreactor (R1, R2 and permeate extraction). All sensor signals were electrically conditioned and collected using an on-line data-acquisition system (Agilent technologies, Loveland, Colorado, USA, type 34970A with specific cards 34901A and 34907A). A PC (Dell, Intel(R) Core(TM)2 CPU, T56001@ 1.83GHz) equipped with a software driver (Benlink Data Logger, version 3.00.02) were used for the configuration and the acquisition of data.

Hydrodynamic conditions in TSCB were firstly characterized by conventional dimensionless numbers (Re, Re_{mixing}, recirculation rate) and VVM. These parameters were related to operating conditions (i.e. mixing rate, gas flowrate, liquid flowrate, recirculation).

Recirculation rate: $$a = \frac{Q_{21}}{Q_{12}}$$ *Eq. 8 and Aeration rate:* $$VVM = \frac{Q_{air}}{V_{liq}}$$ *Eq. 9*

Reynolds numbers: $$\mathrm{Re}_{mixing} = \frac{\rho \cdot N \cdot d^2}{\mu}$$ *Eq. 10 and* $$\mathrm{Re} = \frac{\rho \cdot U \cdot d_h}{\mu}$$ *Eq. 11*

Two flow regimes were observed, (i) a highly turbulent flow regime inside R1 due to mixing ($36000<Re_{Mixing-R1}<47000$) and inside R2 due to flow-rate in the filtration loop ($20000<Re_{Loop-R2}<50000$) and (ii) a close laminar flow regime inside the permeate extraction loop ($1400<Re_{Permeate}<2400$). It was also deduced that the rate of recirculation between R1 and R2, was almost constant for all operating conditions whereas VVM exhibits a wide range of value in both reactors.

RESULTS AND DISCUSSIONS

Analytical solution: RTD and IAD formulation

In a first step, data analysis and RTD formulation were realized, inlet and outlet RTD signals, x(t) and y(t) were formulated. Measured parameters (electrical conductivity, gas percentage) were converted into concentration values. Concentration profiles, c(t) were obtained as a function of time and reduced and normalized signals established, E(t) and E(θ). Then, experimental residence time distributions, E(t) or cumulative, F(t) and the internal age distribution, I(t), under different operating conditions and process modes could be compared and characterized by a set of moments (mean residence time) and centred moments of order i.

RTD of gas phase

Experiments demonstrated that R1 and R2 exhibit independent behaviour. None gas passage between R1 and R2 was been observed as shown in Figure 2A. For an infinite time (300-400s), $F_{R1}(t)$ tends to unit value whereas $F_{R2}(t)$ remains null after a nitrogen step in R1. Holding time, τ, mean residence time, t_s and reduced variance, β^2_{exp} were determined (Table 2), and demonstrated different hydrodynamic behaviour between R1 and R2, under investigated conditions. A larger spread of RTD signal was noticeable in R2 which seems correlated to physical structure of filtration loop associated with R2. A gas retention inducing liquid hold-up was corroborated by holding time and mean residence time ratio of 1.5 in R1 and 1.8 in R2. Under highly turbulent flow or mixing, these ratios stand at constant values whatever VVM.

RTD curves of gas phase showed that there is not any significant difference between RTD curves, E(t) versus process mode (batch, continuous with and without recycle) and between normalized RTD curves, E(θ) whatever operating conditions (Figure 2B). From these results, R1 and R2 under investigated conditions demonstrated that both reactors exhibit a single hydrodynamic behaviour. However, dissolved oxygen sensors located in R1 and R2 indicated that a short delay exists between inlet and outlet in both reactors.

In conclusion, both reactors behaviour could be assumed as a plug flow reactor associated with j CSTR whose model parameters should remain constant whatever the investigated operating conditions. In addition, gas volume and retention could be estimated through model parameters.

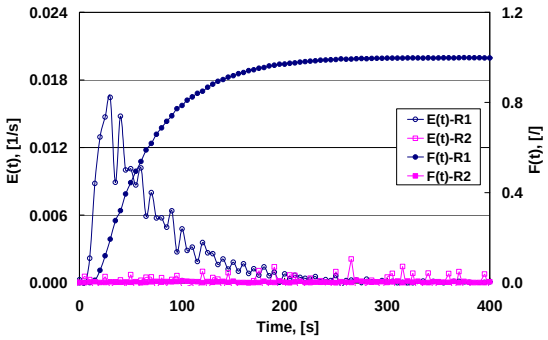

(2-A)

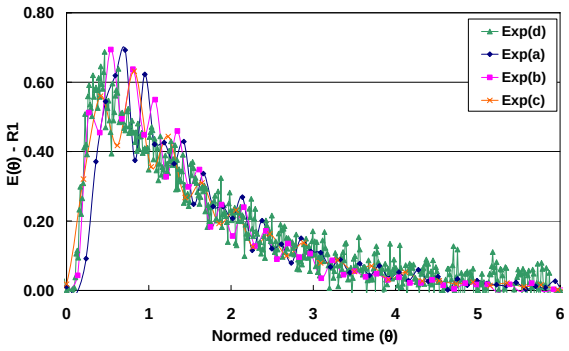

(2-B)

Fig. 2 : Residence time distribution, E(t) and cumulative, F(t) of gas phase in R1 and R2 (Fig. 2-A), (experiment a) and reduced RTD, E(θ) in TSCB (experiments a, b, c and d) in continuous mode with recycle.

RTD and IAD of liquid phase

Hydrodynamics of liquid phase appeared complex in TSCB and required an appropriate methodology to identify several parameters (mixing time, mean residence time and variance, impact of recycle). In the future, experiments will lead to (i) determine the mixing time in batch mode, (ii) identify model parameters in continuous mode without recycle, (iii) validate models in continuous mode with recycle and (iv) investigate different operating conditions.

Both reactors (R1 and R2) and outlets (bleed and permeate) were considered. In figure 3-A, the experimental residence time distribution, E(t) or cumulative, F(t) and the internal age distribution cumulative, J(t) were reported for experiment (a) in continuous mode without recycle. Mass balance between internal age distribution and cumulative residence time distribution was verified. RTD and IAD curves exhibited high spread value, which should be carefully considered during bioreaction. In a first step, only R1 reactor was considered. The evolution of normalized and reduced liquid RTD at the outlet of R1 had a single behaviour whatever various operating conditions (Figure 3-B). R1 behaviour was close to a CSTR with a reduced variance equal to 0.97 ±0.16.

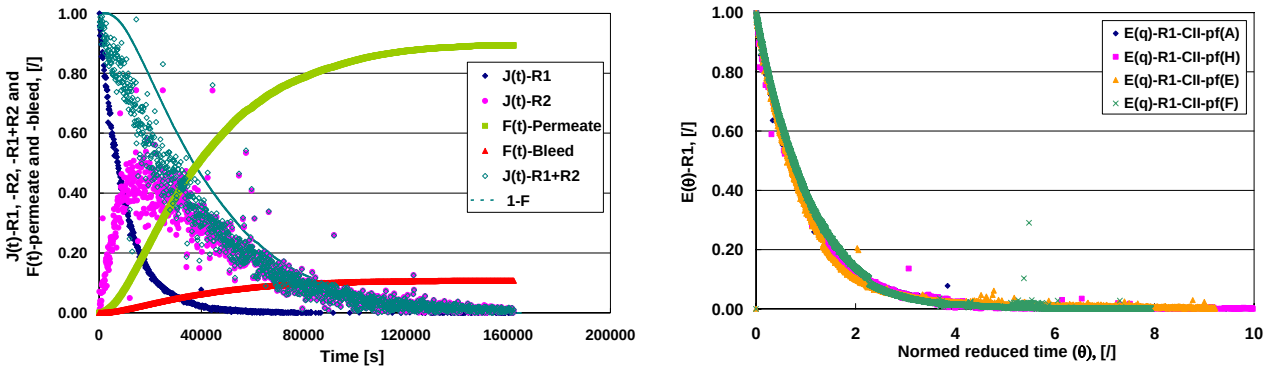

(3-A) (3-B)

Fig. 3: IAD, J(t) and RTD, F(t) of liquid phase in TSCB (Exp. A-Fig. 3-A) and liquid normalized and reduced RTD, E(θ) in R1 (Exp. A, b, c and d, fig.3-B) under continuous mode without recycle.

SYSTEMIC ANALYSIS OF RTD

In a second step, the reactor behaviour was described with a RTD analysis based on DTS Progepi v4.2 software [4]. RTD formulation stands as an efficient tool to give new insights in hydrodynamic phenomena occurring in TSCB. In order to quantify the degree of mixing and to investigate the hydrodynamic behaviour of the reactor for gas and liquid phases, a systemic analysis was performed. Two different models for gas and liquid phases were assumed based on (i) physical structure of the CSTR, (ii) experimental RTD and IAD results and (iii) assumptions about hydrodynamic behaviour. For each experiment, curves fitting of both models and parameters identification were realized by minimizing the sum of square residual (SSR). Model parameters were discussed versus operating conditions and process modes.

Gas phase

For gas phase, a single model was assumed for R1 and R2 (Figure 4) and structured as a cascade of PF reactor (τ_{PFR}) in series with j CSTR (τ_{CSTR}, j). This model was chosen because it is simple and closely correlated to the physical structure of the process and perfectly fit experimental data (Figure 5).

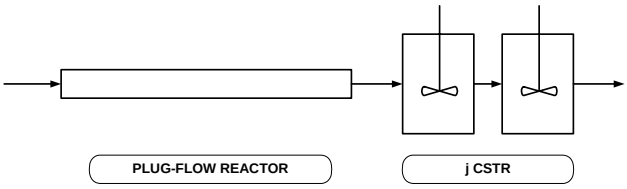

Fig. 4: Reactor model for RTD of gas phase in R1 and R2

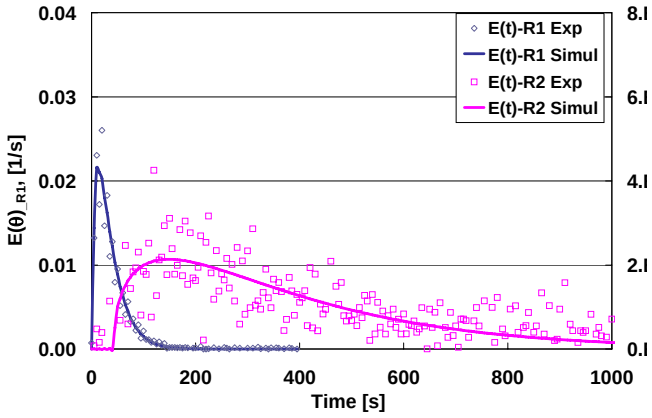

Fig. 5 : Experimental and simulated E(t) in R1 and R2 for gas phase, continuous mode with recycle (exp.a)

The corresponding expression of the transfer function G(s) and E(t) were formulated by Eq.12 and Eq.13.

$$G(s)=\frac{\exp(-s.\tau_{PFR})}{\left(1+\left(\frac{s.\tau_{CSTR}}{j}\right)\right)^{j}}$$ *Eq. 12,* $$E(t)=H(t-\tau_{PFR}).\left(\frac{j}{\tau_{CSTR}}\right)^{j}.\frac{(t-\tau_{PFR})^{j-1}.\exp\left(\frac{-j.(t-\tau_{PFR})}{\tau_{CSTR}}\right)}{(j-1)!}$$ *Eq. 13*

With Van der Laan's relations (Eq. 14), a simple relation between □ and □^{2} was established. The most advantage of this simple model is that only two parameters j and □are used, if the knowledge of mean residence time is assumed to be equal to holding time, τ.It is the plug reactor contribution, in term of residence time (Eq. 15) from which reduced variance may be deduced (Eq. 16).

$$\Gamma^{1}=-G'(0)=(\tau_{PFR}+\tau_{CSTR})=\tau$$

$$\Gamma^{2}{}'=G''(0)=\tau^{2}+\frac{\tau_{CSTR}^{2}}{j}$$ *Eq. 14,* $$\alpha=\frac{\tau_{PFR}}{\tau_{PFR}+\tau_{CSTR}}$$ *Eq. 15 and* $$\beta^{2}=\frac{(1-\alpha)^{2}}{j}$$ *Eq. 16*

In table 2, the holding time, τ, experimental data, t_s, β^2_{exp} and model parameters, τ_{PFR}, τ_{CSTR} and j were reported and differences between experiments and models were calculated. Experimental and model mean residence times exhibited close values for R1 and R2 (difference < 5% except for the experiment (d) in R2). In the same way, calculated reduced variances showed a good agreement with experimental data for R1 (average error < 10%) which was not the case for R2 in spite of a good fitting with experimental data.

Table 2: Experimental and identified model parameters for gas RTD in R1 and R2.

		Experiments					Model				Deviations [%]	
	Exp	τ [s]	t_s [s]	β^2_{exp} [/]	τ_{PFR} [s]	τ_{CSTR} [s]	j [/]	τ_{Tot} [s]	α [/]	β^2 [/]	$\frac{t_s - \tau_{Tot}}{t_s}$	$\frac{\beta^2_{exp} - \beta^2_{calc}}{\beta^2_{exp}}$
R1	(a)	42.1	67.7	0.54	6.9	55.7	1.66	62.6	0.11	0.48	7.4	12.6
	(b)	37.1	52.6	0.58	5.1	45.6	1.47	50.8	0.10	0.55	3.6	5.0
	(c)	420.8	646.3	0.61	52.4	571.6	1.46	624.0	0.08	0.57	3.4	5.4
	(d)	24.3	37.8	0.72	2.4	34.0	1.45	36.3	0.07	0.60	4.0	15.8
R2	(a)	90	148.0	1.53	36.2	141.9	1.19	178.1	0.20	0.53	3.2	65.3
	(b)	47.4	98.1	1.73	14.6	78.8	1.41	93.4	0.16	0.51	4.8	70.8
	(c)	300	505.7	1.61	64.2	412.0	1.75	476.2	0.13	0.43	5.8	73.4
	(d)	225	437.9	1.61	42.8	341.7	1.45	384.5	0.11	0.54	12.2	66.3

RTD of gas phase in R1 and R2 could be described by a simple reactor model whose parameters α and j remained almost constant under investigated conditions (Table 3).

Table 3: Average identified parameters for RTD of gas phase in R1 and R2

	α, [/]	j, [/]	Re, [/]	VVM, [min^{-1}]
R1	0.09	1.51	$36400<Re_{mixing}<46800$	$0.03<VVM_{R1}<0.58$
R2	0.15	1.45	$20700<Re_{loop}<48700$	$0.05<VVM_{R2}<0.33$

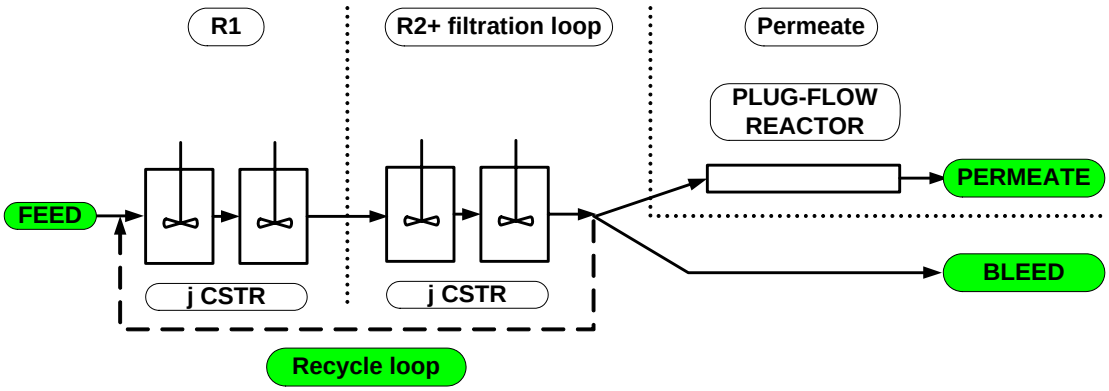

Fig. 6: Considered reactor model for liquid phase in TSCB

Liquid phase: proposal of reactor model

From experiments carried out in continuous mode without recycle and the first RTD and IAD curves, a reactor model could be proposed. Reactor model was based on the physical structure of TSCB and integrated 2 successive j CSTR in series with exchange loop, followed by a plug flow reactor (Fig. 6). This reactor model had been validated for experiment (a) and comparison between experimental and simulated data showed good agreements. However, others operating conditions need to be investigated in the hydrodynamic behaviour understanding in order to get insight of liquid phase in TSCB.

CONCLUSION

RTD and IAD formulations for liquid and gas phases stand as an efficient tool to give new insights in hydrodynamic phenomena occurring in TSCB and to investigate interaction between physical and biological phenomena. From experiments, RTD and analytical solution were formulated, and systemic analysis carried out. Results demonstrated that the magnitude of mean residence time and associated variance were strongly different for gas (≈1min) and liquid (≈100min). Reactors model have been proposed for gas and liquid phases. RTD of gas phase showed that both reactors exhibited independent behaviour, and could be simulated by a single model (plug flow in series with j CSTR) with constant parameters (α, j) whatever investigated operating conditions range (VVM, Re and Re_{mixing}). For liquid phase, RTD for permeate and purge flow and IAD in the first and second reactors have been obtained and formulated. Under assumptions, a systemic analysis of liquid IAD and RTD led to propose a reactor model in close relation with TSCB structure. In the future, model parameters will be fully identified under continuous mode without recirculation and so that the proposed model could been applied with recycle between two stages. These parameters will then be confronted to experiments carried out with biological activity (cells concentration and viability, ethanol production rate, specific growth rate).

REFERENCES

Aldiguier A.S., (2006) Activité bio-catalytique en haute densité cellulaire de Saccharomyces cerevisiae pour l'intensification de la production de bio-éthanol, Thesis 820. INSA, Toulouse, France.

Ben Chaabane F., Aldiguier A.S., Alfenore S., Cameleyre X., Blanc P., Bideaux C., Guillouet S.E., Roux G., Molina-Jouve C. (2006) very high ethanol productivity in an innovative continuous two-stage bioreactor with cell recycle. Bioprocess and Biosystems Engineering Journal, 29(1), 49-57.

Danckwerts P.V. (1953) Continuous flow systems, distribution of residence times. Chemical Engineering Science, 2(1), 1-13.

Leclerc J.P., Detrez C., Bernard A., Schweich D. (1995) un logiciel d'aide à l'élaboration de modèles d'écoulement dans les réacteurs. Revue de l'Institut Français du Pétrole, 50(5), 641-654.

Leclerc J.P., Claudel S., Lintz H.G.., Potier O. and Antoine B. (2000) Theoretical interpretation of residence time distribution measurements in industrial processes. Oil & Gas Science and Technology – Rev. IFP, 55(2), 159-169.

Levenspiel O. (1999) Nonideal flow, In: Chemical Reaction Engineering, 3rd Ed., John Wiley & Sons Inc.

Lin W., Weinell C.E., Hansen P.F.B., Dam-Johansen K. (1999) Hydrodynamics of commercial scale CFB boiler-study with radioactive tracer particles. Chemical Engineering Science, 54(22), 5495-5506.

Nishiwaki A., Dunn I.J. (1998) Analysis of two-stage fermentor with recycle for continuous ethanol production. Chemical Engineering Communications, 168, 207-227.

Nishiwaki A., Dunn I.J. (1999) Analysis of the performance of a two-stage fermentor with cell recycle for continuous ethanol production using different kinetic models. Biochemical Engineering Journal, 4, 37-44.

Pareek V.K., Yap Z., Brungs M.P., Adesina A.A. (2001) Particle residence time distribution (RTD) in three-phase annular bubble column reactor, Chemical Engineering Journal, 56, 6063-6071.
Thereska J. (1998) L'application des radiotraceurs dans les unités industrielles. Bilan et Perspectives. Récent Progrès en Génie des Procédés : traceurs et méthodes de traçage, Nancy, Ed. Lavoisier Tech et Doc, 12(61), 1-7.
Van Hasselt B., Calis H.P.A., Sie S.T., van den Bleek C.M. (1999) Gas- and liquid-phase residence time distribution in three-levels-of-porosity reactor. Chemical Engineering Science, 54(21), 5047-5053.

GAMMA-RAY SURVEY IN THE CHARACTERIZATION OF AN AREA CONTAMINATED BY MERCURY IN DESCOBERTO-MG, BRAZIL

Carlos Alberto de Carvalho Filho1, Peter Marshall Fleming1
Otávio Eurico de Aquino Branco1 and Mauro Campos Trindade2

[1] Center of Nuclear Technology Development (CDTN/ CNEN)
Av. Presidente Antônio Carlos 6627, Pampulha
31270-901, Belo Horizonte, MG
cacf@cdtn.br; pmf@cdtn.br; oeab@cdtn.br

[2] Geological Survey of Brazil, (CPRM), Goiânia Regional Branch
Rua 148, 485 - Setor Marista, Goiânia, Brasil CEP.: 74170-110
mauro@go.cprm.gov.br

ABSTRACT

After an intensive rain period occurred in December 2002 in the rural zone of the Municipality of Descoberto, State of Minas Gerais, Brazil, was observed he arising of metallic mercury in the slope on the right margin of the Rico stream, an affluent of the Grama stream, belonging to the Paraíba do Sul River basin. The site was characterized as Contaminated Area and the results of chemical analyses determined the interruption of the catchment of public municipal water and the interdiction of an area of about 8,000 m2. According to local people reports and based upon historical reconstitution, it was found out that gold mining works were carried out in the region from the 19th century until early 20th century. The mercury used in the concentration of gold imposed a great environmental problem. In 2006, the Detailed Investigation of the site was concluded, showing that the highest mercury concentrations occurred in the auriferous gravels found along old structures known as “canoas”, which were used to concentrate and depurate the gold. In this process, the miners used to throw the metallic mercury straight into the “canoas” in order to promote the amalgamation between gold and mercury. This product was then collected and burned, and the gold, recovered. Mercury is also found in soil, close to the gravel layers, but in lower concentrations than gravels. The Contaminated Area comprises about 800 m2 and is characterized by mercury concentrations in soil and gravel higher than the proposed remediation limit, which is of 10mg/kg and was established by risk analysis. The contamination reaches no more than 1 m deep from the ground surface. The existence of the radioactive mineral monazite (Ce, La, Y, Th) PO4 as a constituent of the gravel allowed the use of a gamma detector (SRAT SPP2 Gamma Scintilometer) as an important tool for the determination of the spatial distribution of the gravel contaminated by mercury. This paper aims at presenting the results obtained by the radiometric survey done in the Contaminated Area in order to demonstrate how this survey can be useful in investigating the gold-bearing gravels with monazite occurring in the old gold mining works in the region of Descoberto/MG, which are potential sources of contamination by mercury. The reference (background) for the total gamma counting rates values for soils in the region ranged between 40 and 60 cps (counts per second), while the higher value measured in the gravel was of 500 cps.

INTRODUCTION

Mercury was found in the soil of a farm located in the municipality of Descoberto, southeast of Minas Gerais State, Brazil, after an intensive rain period that occurred in December 2002 (Figure 1). The place where the metal was found is located on the right bank of the Rico stream, a tributary of the Grama stream which, in turn, launches its waters in the Rio Novo river, that belongs to the Paraiba do Sul River basin. The initial site investigation was held by the Environmental State Foundation - FEAM, resulting in the site characterization as a contaminated area and the interruption of the water catchment from the Grama stream and its distribution to the city of

Descoberto, in addition, to interdict and fence an area of approximately 8,000m2, involving the contaminated site (Figure 2).

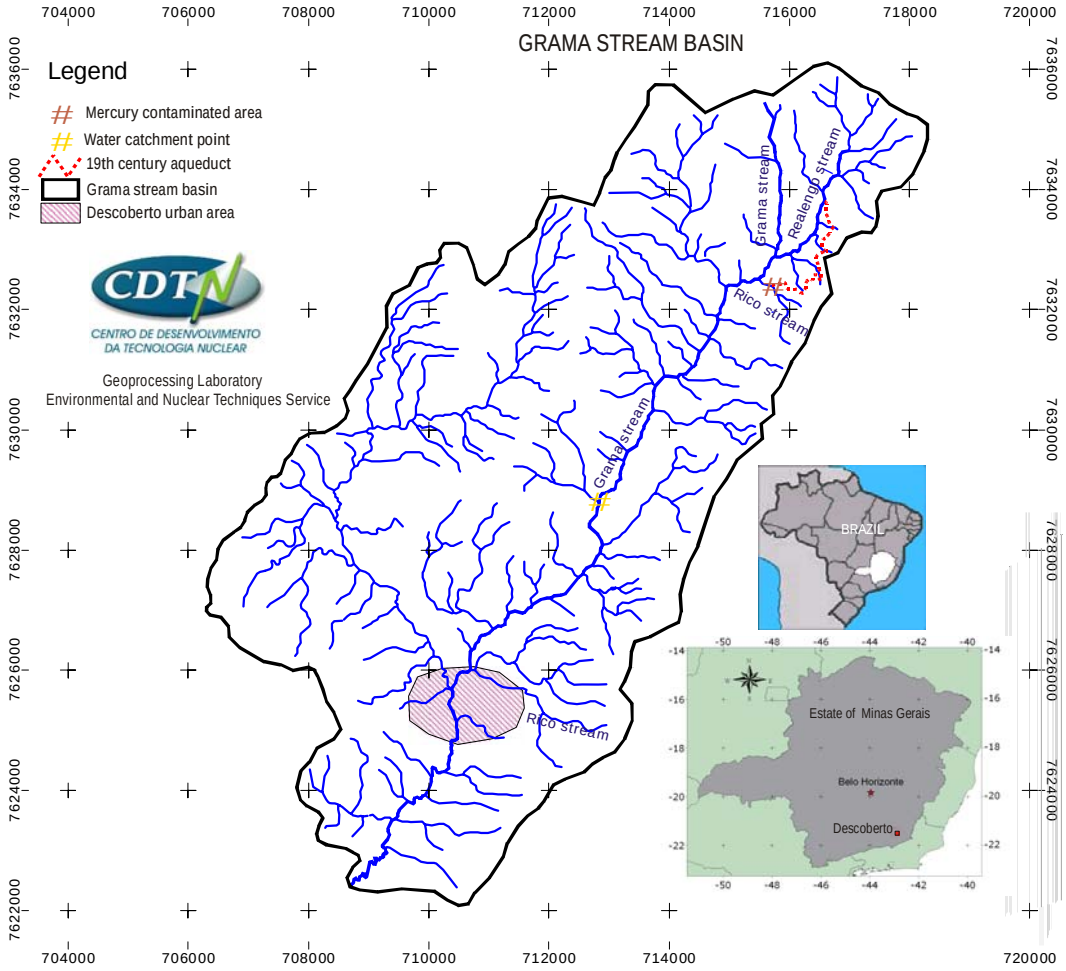

Figure 1: Localization of the municipality of Descoberto, Minas Gerais State, and the contaminated area by mercury in Grama stream basin.

After the mercury contamination of the site was confirmed and its approximated extension was observed, the Detailed Investigation of the Contaminated Area has began in August 2003. For this Investigation, FEAM counted with the partnership of the Center of Development of the Nuclear Technology (CDTN) and also with the Geological Survey of Brazil (CPRM). The Detailed Investigation was concluded in October 2006 (FEAM & CDTN, 2006), and it was verified that the contaminated area is approximately 800 m2, characterized by mercury concentrations in soil and gravel, above the target of remediation (10 mg/kg), established by the risk analysis which was performed. The contamination reaches a maximum depth of 1 m from the ground surface (Figure 2).

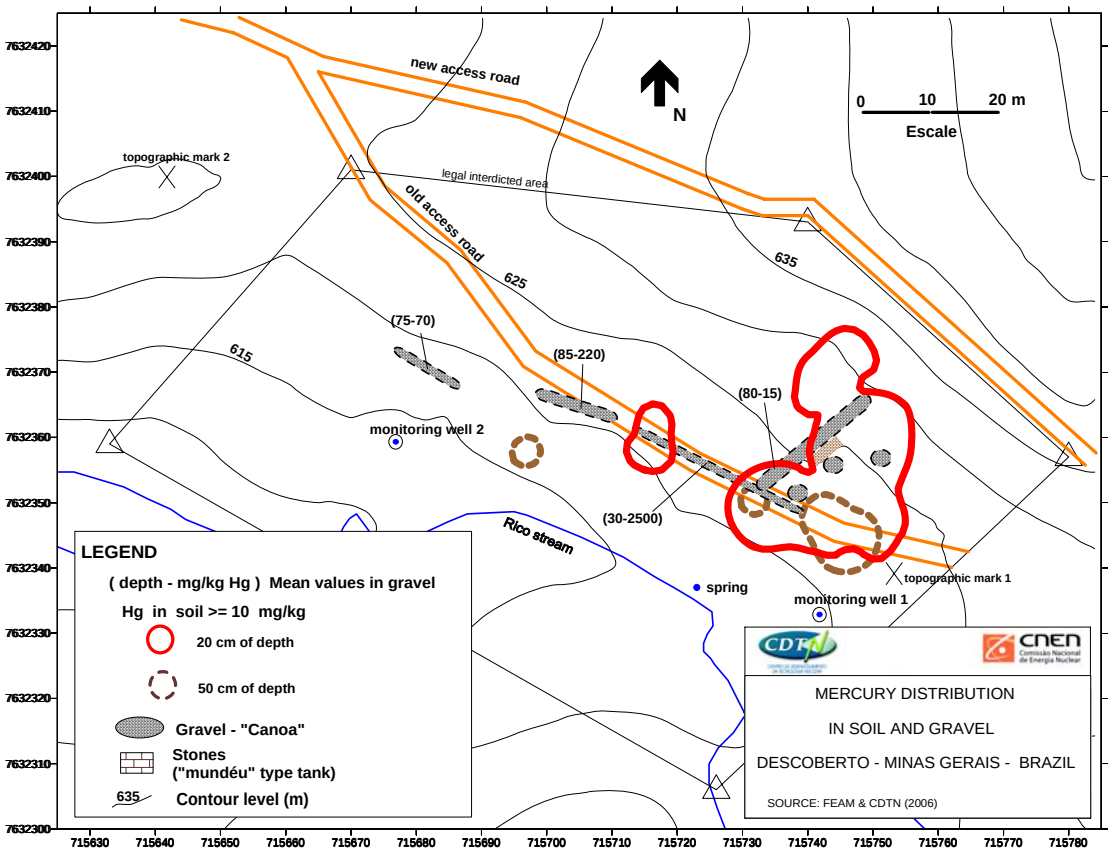

Figure 2: Localization of the contaminated area (interdicted) and the mercury distribution in soil and gravel in the site.

Since the confirmation of mercury presence in the rural area of Descoberto/MG, many uncertainties about the origin of that environmental contamination appeared. It is fundamental to the implementation of detailed diagnosis, the knowledge of the contamination origin and the environmental compartments potentially impacted by old activities that caused the contamination. Several activities were carried out mainly aimed at characterizing the existing environmental liabilities (Branco et al., 2005; FEAM & CDTN, 2006), it current and potential impact and also to implement mitigatory procedures to prevent the spread of contamination (Trindade et al., 2005). Among these activities it is pointed out the historical studies (Carvalho Filho et al., 2005), the collection and analysis of environmental samples (soil, deep and surface waters, plants and sediment), the topographic survey and the granulometric and mineralogic tests of natural and contaminated soil samples.

These activities showed that the focus of mercury contamination occurs in the gravel, arranged in structures called "canoas" where due to the method adopted, the gravel was washed to concentrate ore, and the amalgamation process was applied in order to obtain a better gold recovery (FEAM & CDTN, 2006). Mercury was spread from the gravel (mining hotspot) into the surrounding soil, due to natural processes of erosion and transport and also by human action. The distribution of spatial mercury contamination in both soil and the gravel is shown in Figure 2. The area enclosed by the continuous lines represent the concentrations of Hg in soils higher than 10 mg/kg, to a superficial depth of 20 cm, and the area enclosed by dashed lines match the concentration of Hg in soils, 50 cm deep.

Tests carried out in soil and gravel from the contaminated area, by X-Ray Difratometry analysis showed the presence of heavy minerals associated with the gravel, whose highest concentrations of mercury were recorded. Among these minerals, the monazite (Ce, La, Y, Th) PO4 is found, which is a radioactive mineral due to the presence of thorium in its composition. Due to the radioactive characteristics of this mineral, a radiometric survey of the contaminated area was performed in order to evaluate the use of this technique in the detection of gravel with monazite and thus to

identify the places of greatest potential of mercury concentration. This work presents the results of this radiometric survey.

MATERIALS AND METHODS

A Gamma scintilometer SRAT SPP2 was used for the radiometric survey. The measurements were made with the equipment placed about 10 cm above the ground surface. A rectangular grid was delimited on the ground and was used as a guide for the field measurements. The grid (Figure 3) is a matrix of 7 lines, N45oW direction (numbered 1 to 7) and 8 lines, N45oE direction (labeled A to H). Each node of the grid was fixed by a picket on the ground during the plani-altimeric survey carried out by CDTN in 2004 (FEAM & CDTN, 2006).
The radiometric survey was performed with the equipment in use along the lines of the grid mentioned above. Preferably, in each node of the grid, a measure of the total gamma count rate, in counts per second (cps) was registered. Other measures were made outside the points cited above in order to improve the data.

RESULTS AND DISCUSSIONS

Table 1 shows a list of points with the radiometric measurements in the surface field. Some considerations are listed below:

a. The points of type C4, A6, B5 etc. refer to nodes of the gride;

b. The points of type XYn refer to the auxiliary radiometric measurements held between the points of the grid;

c. The points of type Zn are located around the contaminated area. These points resulted in gamma measurements range between 40 to 50 cps;

d. The radiometric points on the banks of the Rico stream were identified as corr-n;

e. The points of type ptn refer to radiometric measurements done exclusively during a complementary survey;

f. The radiometric measure held in point F3 registered 70 cps on the surface of the ground. At that point, a small hole until the top of the gravel was dug. At this point, considering depth, a radiometric measure of 500 cps was obtained due to the proximity to the gravel (“canoa” 2, Figure 3);

g. Measures were taken at the point H2 and near a drainage ditch, beside H2. The measures reached 70 cps on the surface of the ground and reached 400 cps inside the ditch. This ditch (60 cm in depth) intercepted a gravel layer;

h. At the point near the spring, the radiometric record was carried out beside the existing water pipe (PVC pipe), reaching 180 cps.

In Figure 3, the curves for the total gamma counts in soil surface are shown, defined from the data interpolation presented in Table 1. In relation to the results shown in Figure 3, it was observed that:

a. The value found in soil for the natural (background) total gamma counting rate was about 40 cps to 60 cps;
b. The radiometrics spots represent total gamma values above 60 cps. The highest count was registered and reached to 400 cps on “canoa” 1 on a point where the gravel arises along the old access road;

c. The major axis of the radiometric spot shows SE-NW direction, which coincides with the main gravels direction (“canoas”) and the curve of iso-concentration of 0.8 mg/kg Hg. The gravel arising on the old road, in the vicinity of the points C4 and D4, facilitated the spread of such material along that route, following the NW declivity;
d. From the major axis, on the “canoas”, the spot has extensions to SW, coinciding with the natural slope of the land. The gravel was moved upstream to downstream by the action of natural phenomena such as, erosion, transportation and deposition;
e. It was observed that in some locations downstream of “canoas” (SW), the radiometric spot moved to SW more than the curve of 0.8 mg/kg. This may be due to high retention capacity of mercury by the soils of the region (FEAM & CDTN, 2006). Thus, while the gravel with monazite was carried downstream from the ground toward the Rico stream, the mercury was retained in soils surrounding the gravel.

Table 1: Radiometric survey in the mercury Contaminated Area – UTM Datum Corrego Alegre 23K.

Point	UTM East	UTM West	Total Gamma cps	Point	UTM East	UTM West	Total Gamma cps	Point	UTM East	UTM West	Total Gamma cps	Point	UTM East	UTM West	Total Gamma cps
A4	715746.6	7632335.9	60	G1	715682.7	7632357.0	50	E3	715709.1	7632356.0	60	XY18	715708.7	7632364.4	70
A5	715753.6	7632343.0	70	G2	715689.6	7632364.4	60	E3/E4	715713.7	7632360.2	70	corr-5	715700.0	7632347.8	50
A6	715762.2	7632350.1	40	G3	715697.2	7632371.5	60	E4	715718.3	7632364.3	40	XY19	715712.5	7632364.4	60
B3	715732.4	7632335.7	50	H1	715675.1	7632364.4	70	E5	715725.4	7632371.6	40	Z1	715625.0	7632354.5	50
B4	715739.4	7632343.1	60	H2	715682.9	7632371.5	70	F2	715697.0	7632357.2	50	Z2	715640.0	7632350.0	50
B5	715747.2	7632350.1	50	Well N.1	715738.0	7632333.0	40	F3	715704.3	7632364.4	70	Z3	715660.0	7632340.5	50
B6	715753.6	7632357.1	40	Spring	715723.0	7632337.0	180	Z5	715625.0	7632340.0	40	Z4	715680.0	7632345.0	50
B7	715760.1	7632364.4	30	X Y1	715687.4	7632371.5	70	Z6	715640.0	7632340.0	40	corr-38	715737.2	7632318.0	50
C3	715725.6	7632343.4	200	XY4	715680.1	7632368.9	150	Z7	715660.0	7632340.0	50	pt1	715669.0	7632412.0	50
C4	715732.4	7632350.2	90	XY5	715723.2	7632355.1	100	Z8	715753.3	7632339.1	40	pt2	715683.0	7632392.0	50
C5	715739.5	7632357.2	70	XY7	715724.0	7632356.0	120	Z9	715641.8	7632399.9	40	pt3	715686.0	7632377.0	50
C6	715747.3	7632365.0	50	XY6	715724.9	7632356.8	180	Z10	715675.1	7632404.8	40	pt4	715675.0	7632382.0	50
C7	715753.8	7632371.5	30	XY8	715726.0	7632358.0	100	Z13	715652.6	7632346.5	50	pt5	715661.0	7632376.0	50
D3	715718.2	7632350.2	60	XY10	715733.1	7632350.9	200	Z14	715665.4	7632349.5	50	pt6	715661.0	7632364.0	50

Point	UTM East	UTM West	Total Gamma cps	Point	UTM East	UTM West	Total Gamma cps	Point	UTM East	UTM West	Total Gamma cps	Point	UTM East	UTM West	Total Gamma cps
D4	715725.3	7632357.2	100	XY12	715734.5	7632352.3	180	Z21	715676.8	7632359.3	40	pt7	715707.0	7632379.0	50
D5	715732.4	7632364.5	50	XY14	715735.9	7632353.7	70	Z22	715633.0	7632359.0	40	pt8	715716.5	7632359.6	70
D6	715739.4	7632371.4	40	XY15	715737.2	7632354.9	50	Z23	715670.0	7632401.0	40	pt9	715718.0	7632359.0	70
D7	715746.7	7632378.8	50	XY16	715726.7	7632355.9	400	Z24	715740.0	7632393.0	40	corr-21	715730.3	7632317.4	50
E2	715704.7	7632355.4	120	XY17	715731.1	7632351.5	100	Z25	715780.0	7632357.0	40	corr-34	715725.5	7632331.3	50
corr-16	715703.2	7632345.5	50	corr-33	715714.3	7632340.0	50	corr-18	715721.8	7632335.5	50	Z26	715726.0	7632306.0	40

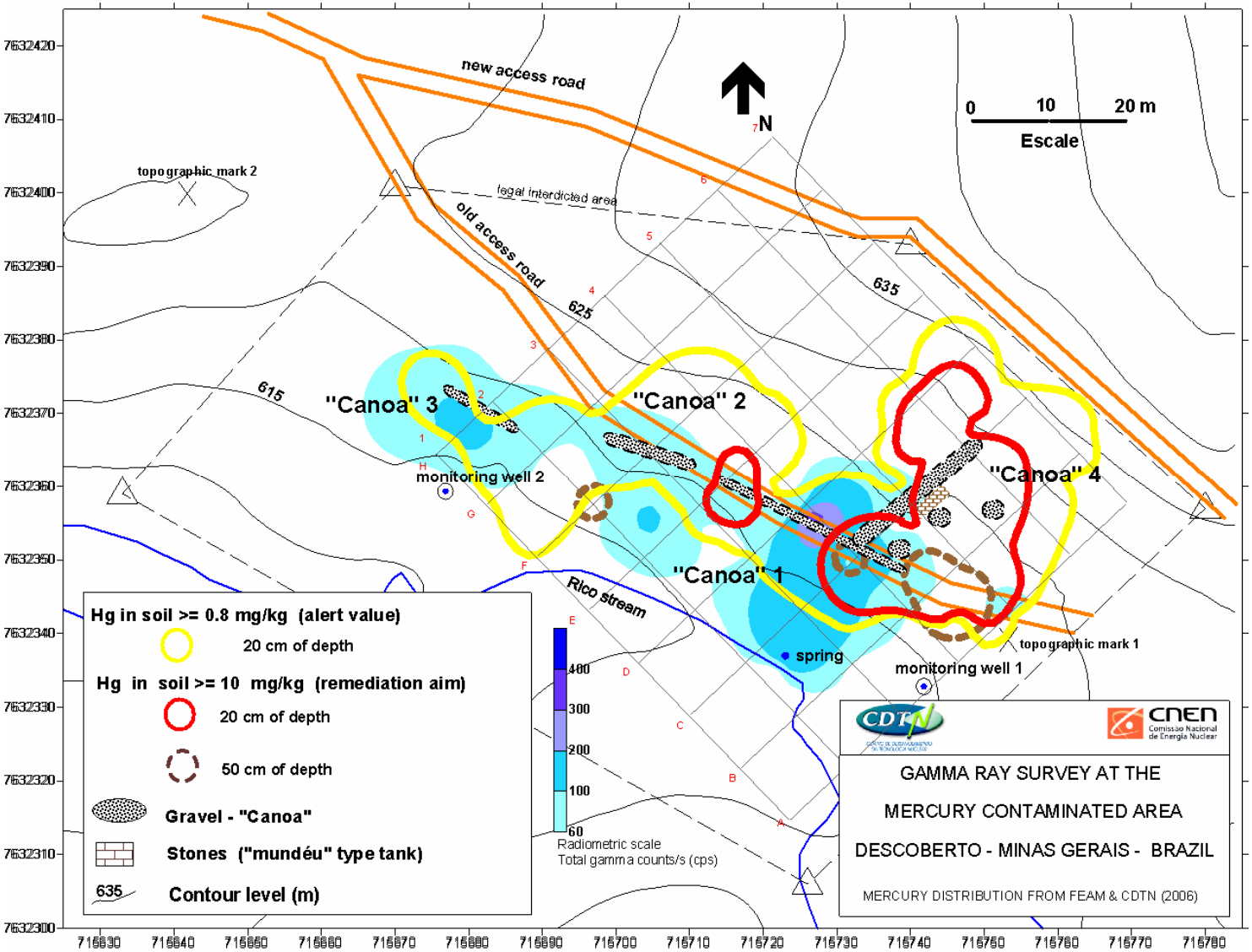

Figure 3: Radiometric survey and mercury Contaminated Area characteristics.

CONCLUSIONS

The gravel with monazite arranged in the “canoas” for gold recovery (with Hg), previously identified in surveys carried out in the field, was confirmed by radiometric survey (total gamma measures). The radiometric measurement in ground surface could indicate the location of these “canoas” which occur from the surface to 85 cm deep. It is concluded that more detailed surveys should be carried out in the Contaminated Area aiming at identifying other structures used in gold recovery.

It is emphasized that the evaluation of the applicability of this technique in the studied areas shows its effectiveness in the identification of similar sources of contamination as in this study, and not identified yet, allowing the implementation of more accurate diagnosis of environmental liabilities and the adoption of more effective actions of environmental control.

ACKNOWLEDGMENTS

The authors acknowledge the Descoberto City Hall, the National Council for Scientific and Technological Development - CNPq and the Minas Gerais State Agency for Research and Development - FAPEMIG for the support given to the development of this work.

REFERENCES

Branco, O. E. A., Carvalho Filho, C. A., & Trindade, M. C Evaluation of Mercury Contamination In Soils: The Case of The Rural Area of The Municipality of Descoberto, State of Minas Gerais, Brazil. XIII Internatational Conference on Heavy Metals in The Environment (ICHMET), Rio de Janeiro – RJ, Brazil, 05-09 June 2005, p. 237.

Carvalho Filho, C. A., Branco, O. E. A., & Trindade, M. C – Contamination by Mercury From Past Gold Mining Activities at Descoberto, State of Minas Gerais, Brazil: Historical Reconstitution. XIII Internatational Conference on Heavy Metals in The Environment (ICHMET), Rio de Janeiro – RJ, Brazil, 05-09 June 2005, p. 192.

FEAM & CDTN (2006). Diagnóstico da contaminação ambiental em Descoberto, Minas Gerais, em decorrência do afloramento de mercúrio em dezembro de 2002. Relatório Final FEAM nº RE-DIMOG-022/2006, CDTN nº 958/2006, Belo Horizonte, 199p.

Trindade, M. C, Branco, O. E. A & Carvalho Filho, C. A. – Control Measures Implemented In Area Contaminated With Mercury from Past Gold Mining Activities in The State of Minas Gerais, Brazil. XIII Internatational Conference on Heavy Metals in The Environment (ICHMET), Rio de Janeiro – RJ, Brazil, 05-09 June 2005, p. 458.

^{99m}Tc MUD LABELLING AND ITS APPLICATION IN HYDRODYNAMIC STUDIES OF FINE SUSPENDED SEDIMENT IN BRAZIL

J.V. Bandeira[8], L.H. Salim[9], C.S. Sabino[10], E.G. Agudo[11], P.E. Aun[12], V.L. Mendes[13]

ABSTRACT

The feasibility of using ^{99m}Tc, broadly applied in Nuclear Medicine, for labelling mud, through the chemical reduction of the TcO_4^- eluted from Mo/Tc generators, was studied in laboratory and in field conditions (Bandeira et al., 1999a), (Bandeira et al., 1999b). The hydrodynamic behaviour of labelled and non-labelled sediment was compared in the laboratory (Bandeira, 2001), (Bandeira et al., 2002). ^{99m}Tc has $T_{1/2}$ =6.02 h and gamma-ray energy = 140 keV, being suitable for studying the transport of fine suspended sediment in water environment (rivers, estuaries, bays and open coast). After labelling natural sediment in the field, it is released in the water and its movement is followed by "in situ" detection, using stationary scintillation detectors at suitable depths and fixed locations (Eulerean detection), or measured with detectors in moving boats (Lagrangean detection), allowing the calculation of advection, dispersion and sedimentation rate parameters.

This kind of study, when associated with information on hydrodynamic parameters, e.g.: river, tidal, wind and wave currents, are powerful tools for the understanding and quantification of sediment transport in suspension. It also can be used to study the effect of human interventions, such as dredging of reservoirs, access channels and harbours, and the dumping of dredged materials in the water environment. Besides that, it can be used to optimize dredging works, evaluating the technical and economical feasibility of dumping sites and its environmental impact. It is also a valuable support in the calibration and validation of mathematical models for sediment dynamics.

This technique has been used to evaluate dredging activities in the accreted Pampulha reservoir in Belo Horizonte-MG, Brazil, and the dumping of the dredged sediment in the watercourse downstream the reservoir dam. (Bandeira, 2004).

1 – INTRODUCTION

In the aquatic environment, heavy metals and many organic compounds are usually associated to the fine sediment phase (silt and clay). The fate of these contaminants will be associated with the dynamic behaviour of suspended or bottom sediments in polluted streams. The study of suspended sediment behaviour is an activity to be included in many environmental studies. Of special interest is the study of individual discharges of contaminants associated to suspended sediments, the short-term dispersion of contaminated material dredged from harbours and reservoirs when dumped into water bodies and the behaviour of natural sediment in suspension in bays, estuaries or reservoirs. Tracking for few hours the contaminated suspended sediments introduced into the streams or in the coastal area by individual discharges could allow the quantitative in situ determination of the advection, dispersion, dilution and sedimentation rates (Aun & Bandeira, 1995). These parameters are important for the calibration and validation of hydrodynamic models which consider simultaneously the solid and liquid phases.

Radioactive tracers are used to label fine sediment and some of them, such as: ^{198}Au, ^{46}Sc and ^{51}Cr, have been employed to study the dynamics of suspended sediments. The labelling technique consists in adsorbing the tracer, in an appropriate chemical form, onto the sediment (Bougault, 1970).

[8] Senior **Researcher - Nuclear Technology Development Centre - CDTN/CNEN - Cidade Universitária - Pampulha - P.O.Box 941 Zip Code 30123-970 - Belo Horizonte, MG - Brazil - Tel. 55 31 3069-3120 - E-mail: jvb@cdtn.br**

[9] **Idem... - Tel. 55 31 3069-3246 - E-mail: salimlh@cdtn.br**

[10] **Idem...(Retired) - Tel. 55 31 3491-1752 - E-mail: sachayersabino@hotmail.com**

[11] **Senior Researcher -Isotope Hydrology Section. IAEA (Retired) - Tel. 55 35 3433-5508 E-mail: garciaagudo41@gmail.com**

[12] **Idem.of [1].(Retired) - Tel. 55 31 3221-.2176 - E-mail: pedro.aun@gmail.com**

[13] **Chemical Technician - Idem.of [1].(Retired)... - Tel. 55 31 3291-7727 - E-mail: vlmendes@uai.com.br**

^{99m}Tc in the form of TcO_4^- (pertechnetate) has been used for water tracing in short-term hydrological studies (Garcia-Agudo, 1997), (Borroto et al., 1999), (Airey et al., 2003), (Borroto, 2004), and seems to be a rather easy radionuclide to be obtained even in countries where nuclear reactors are not available, because of its extended use in Nuclear Medicine. A first attempt on using ^{99m}Tc as a tracer for sediments was made in Montevideo Bay, Uruguay, in 1997 (Bandeira & Pinto, 1997), (Pinto & Bandeira, 1998). The objective of this application was to study the behaviour of the natural fine sediment in suspension in Montevideo Bay, which is very polluted, obtaining parameters (advection velocity, dispersion and sedimentation rate) to calibrate a mathematical model. The radioisotope originally selected to label the fine sediment in the Montevideo Bay experiment was the ^{198}Au, scheduled to be irradiated in IPEN/CNEN nuclear reactor, in São Paulo, Brazil, and transported to Montevideo City by plane. Nevertheless, due to an unforeseen reason, the material did not arrived in time to be used in the programmed experiment. In this way, the two alternatives left were: cancel the work or try an alternative tracer. The second option was chosen and the team searched for another radioisotope to label the mud. As in Uruguay there is no nuclear reactor facilities, the radioisotopes used in Nuclear Medicine and received from Argentina by the Centre of Nuclear Medicine of the University of the Republic of Uruguay (UdelaR) were the only option. In this way, from the radioisotopes received, the ^{99m}Tc was chosen by its half life and gamma-ray energy. But, being eluted as TcO_4^-, it was necessary to perform a chemical reduction with $SnCl_2.2H_2O$ to transform it in an electropositive colloidal compound, allowing its sorption by the fine sediment, which is electronegative. The field experiment, performed with this improvised radiotracer attained its main objectives (Bandeira & Pinto, 1997).
After this first use, the Nuclear Technology Development Centre (CDTN) of the Brazilian Nuclear Energy Commission (CNEN), under the IAEA Research Contract BRA-10891, performed a detailed research in laboratory for the labelling of fine sediment with ^{99m}Tc (Bandeira et al., 1999a,b), (Bandeira, 2001) which will be briefly shown in sequence.

2 – LABORATORY STUDIES FOR LABELLING MUD WITH ^{99m}Tc

The methodology for the validation of the use of the fine sediment labelled with 99mTc as a tracer for the natural fine sediment in suspension was divided into two parts:
1- Labelling yield as a function of different factors;
2- Hydrodynamic behaviour of labelled and not labelled sediment.

2.1 – Labelling yield as a function of different factors

The main results obtained from the development of the labelling technique, as described in Bandeira et al (1999a, 1999b) are shown in sequence.
2.1.1 Type of reductor - it is easily possible to label fine sediment with 99mTc with yields higher than 99%, using stannous chloride - SnCl2.2H2O - as the reducing agent (Figure 1).

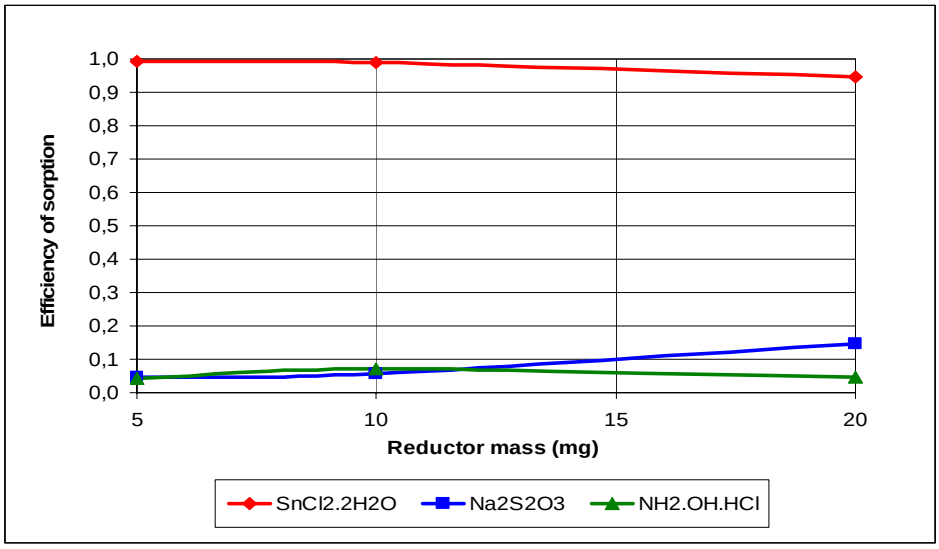

Figure 1 - Effect of reducing agent nature for the sorption of 99mTc in fine sediments

The reduction of Tc(VII) with Sn(II) is produced according to the following equations (Sekine et al., 1993):

$$3\ Sn\ (II) + 2\ Tc\ (VII) = 3\ Sn\ (IV) + 2\ Tc\ (IV) \quad (1)$$

In aqueous solution a colloidal compound is formed after reduction.

$$TcO^{2+} + 2\ H_2O = TcO(OH)_2 + 2H^+ \quad (2)$$

Most probably this is the chemical species which is adsorbed onto the sediment after reduction of the pertechnetate.

2.1.2 Amount of reductor - With increasing concentrations of reducing agent, there is a decrease in the efficiency of sorption, possibly due to the competition of the Sn(II) cations with the reduced technetium species for the active sites in the sediment (Figure 2).

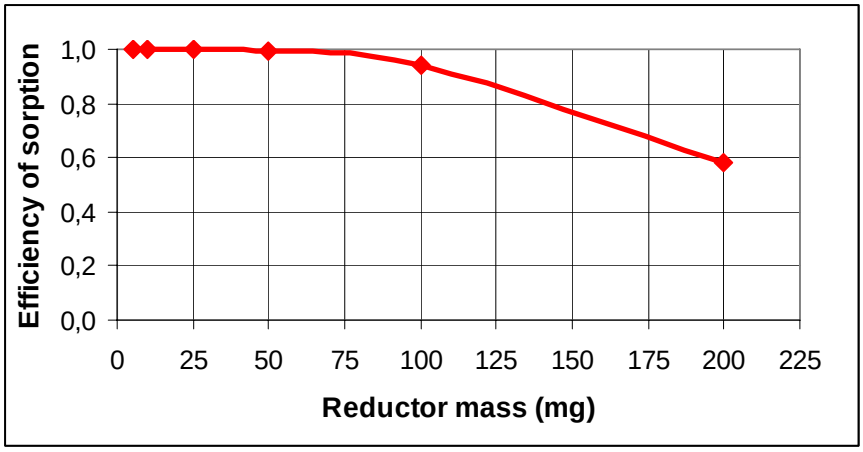

Figure 2 - Variation of sorption of ^{99m}Tc in 100 mg of sediment with mass of $SnCl_2.2H_2O$

2.1.3 Effect of pH - In practical applications, the pH of the labelling solution must be above 5, i.e. in the range found in most natural waters and because, for lower pH values, the yield decreases (Figure 3).

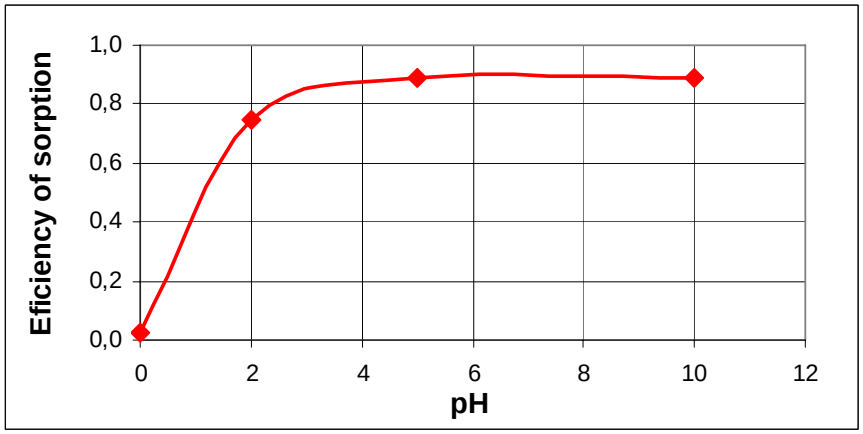

Figure 3 - Effect of pH in the sorption of ^{99m}Tc

2.1.4 Influence of sediment concentration - Increasing the concentration of suspended sediment to be labelled increases the adsorption yield, the highest yields obtained with sediment concentrations being greater than 15 g/l (Figure 4).

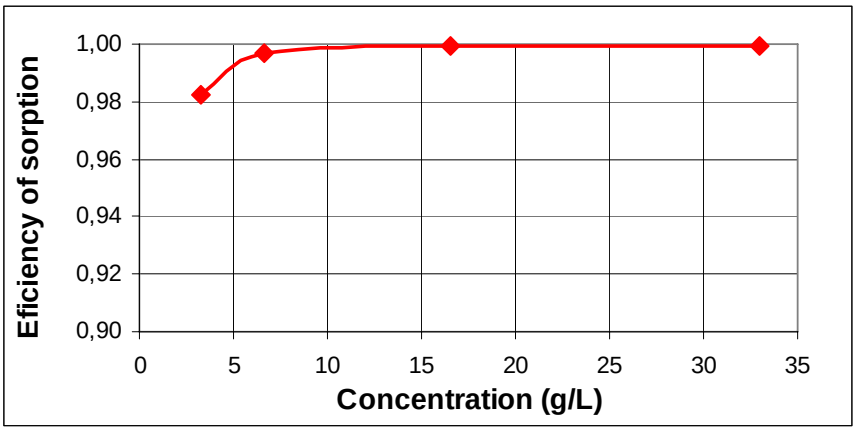

Figure 4 - Influence of the concentration in the sorption of ^{99m}Tc by fine sediment

2.1.5 Influence of contact time - Sorption of the reduced species of 99mTc is not instantaneous but is rather fast. In laboratory tests to evaluate the influence of contact time, yields above 95% were obtained stirring the suspended sediment with the Tc(IV) solution for at least 5 minutes (Figure 5).

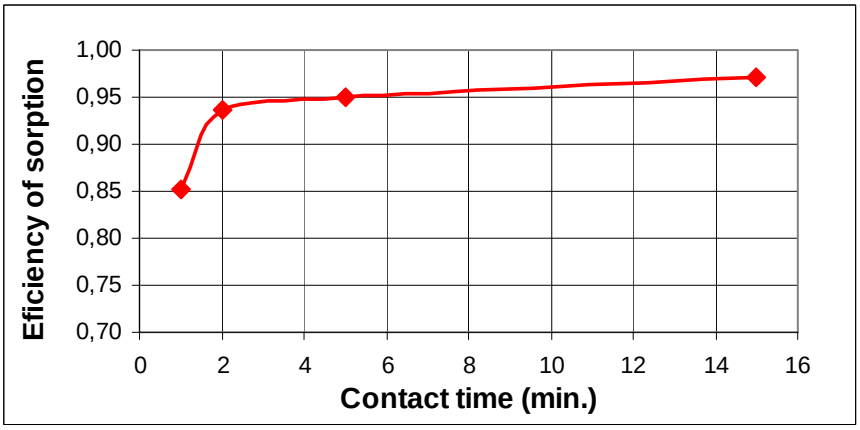

Figure 5 - Influence of the contact time in the sorption of ^{99m}Tc by fine sediment

2.1.6 Labelling stability - Labelling is only slowly reversible: significant desorption was not observed after agitation, for two hours, of sediment at three different concentrations typical of natural streams (50, 200 and 1000 g/L). The increase of activity in the supernatant with time was measured and indicated a release of radioactivity of less than 10% after the indicated agitation time (Figure 6).

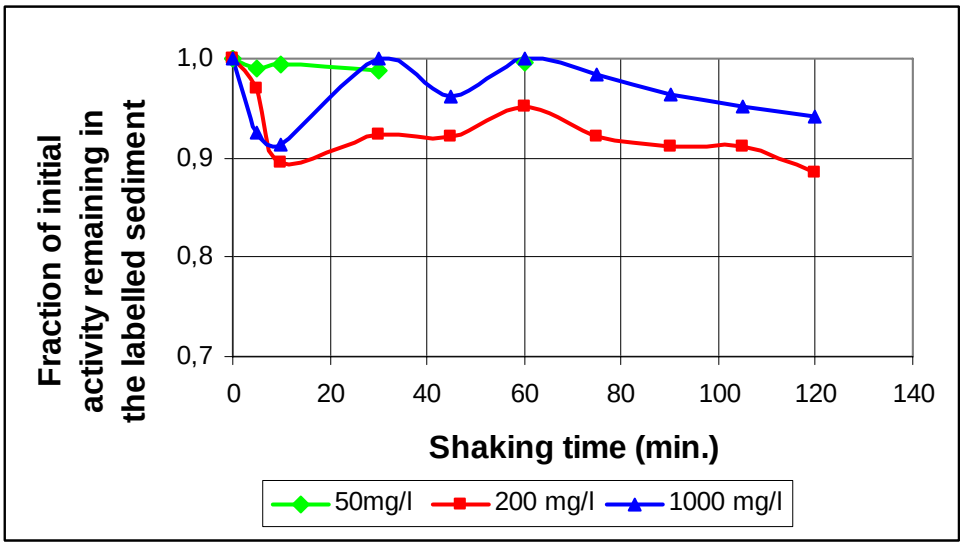

Figure 6 - Desorption of ^{99m}Tc in river water for different sediment concentrations

2.2 – Comparison of the hydrodynamic behaviour of the labelled and not labelled sediment

The comparison was performed in the Sedimentology Laboratory of CDTN through sedimentation tests using test tubes of 1 L and Andreasen pipettes (Figure 7) and considering the Stokes Law (Migniot, 1968), (Bougault, 1970), (Caillot et al. 1978).

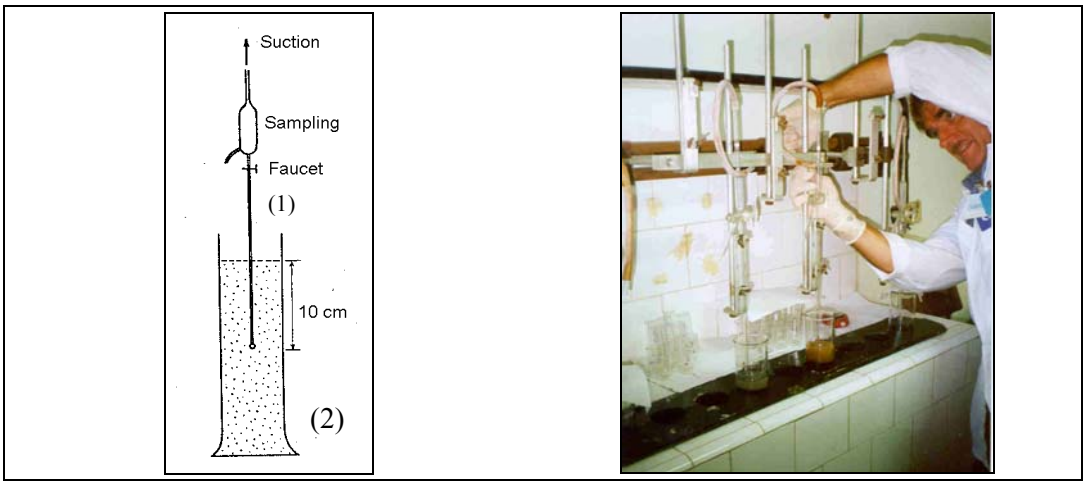

Figure 7 - Andreasen pipette (1) & test tube (2)

Labelling without flocculation, which promotes the same sedimentation behaviour of the natural (Figure 8) and the labelled (Figure 9) sediment was only achieved using small quantities of SnCl2.2H2O dissolved in proportionally small volumes of HCl (0.3%), in the reduction of 99mTcO4- (Bandeira, 2001), (Bandeira et al., 2002).

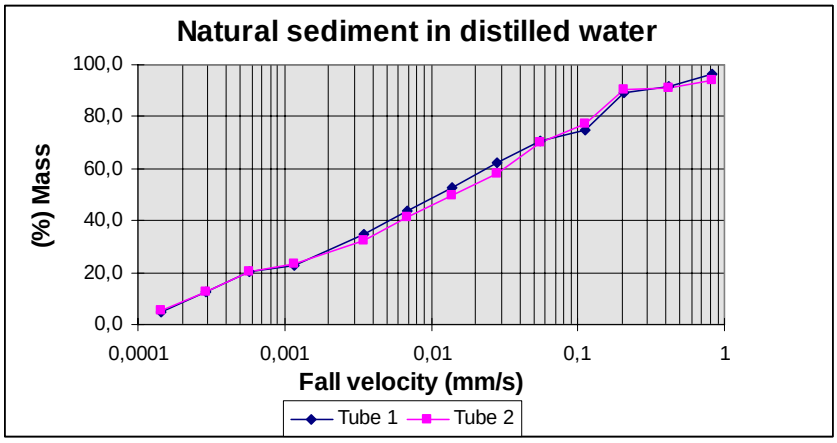

Figure 8 - Sedimentation of natural sediment in distilled water

$M = 11.077Ln(W) + 100.9$ $R^2 = 0.9929$ (trend line - Tube 1)
$M = 10.971Ln(W) + 99.628$ $R^2 = 0.9856$ (trend line - Tube 2)

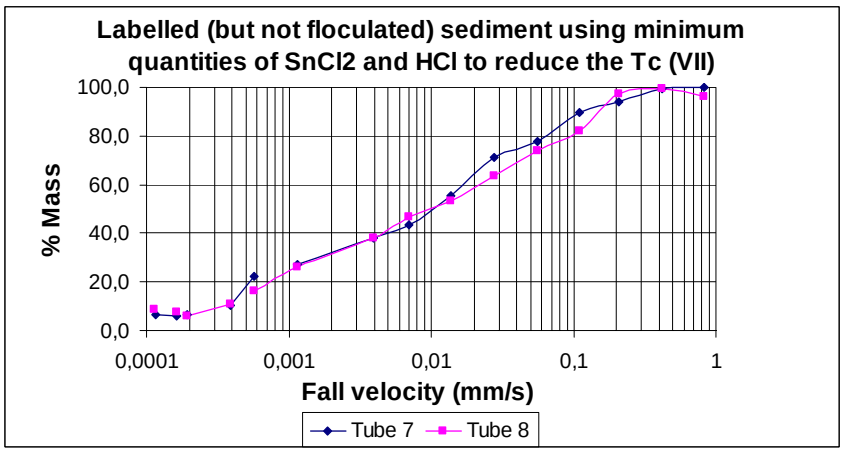

Figure 9 - Sedimentation of labelled sediment in distilled water

$M = 12.285Ln(W) + 111.52$ $R^2 = 0.9890$ (trend line - Tube 7) - HCl (0.3%)

$M = 11.57Ln(W) + 105.90$ $R^2 = 0.9832$ (trend line - Tube 8) - HCl (0.3%)

3 – **PAMPULHA RESERVOIR DREDGING STUDIES USING ^{99m}Tc – BRAZIL**

The study was performed to evaluate the viability of an environmental and perennial solution to dredge the fine sediment that accretes (400,000 m3/year) the Pampulha reservoir, in Belo Horizonte, Brazil, which is in an accelerated process of reduction of its liquid volume and water surface (Figure 10). With this tendency, the reservoir could lose, in a near future, two of the main purposes for which it was built: flood damping and leisure region, with its water surface indubitably linked to the buildings designed in the 1940 decade by the famous Brazilian Architect Oscar Niemeyer, forming the Architectonic Complex which is the landmark of the modern Brazilian Architecture.

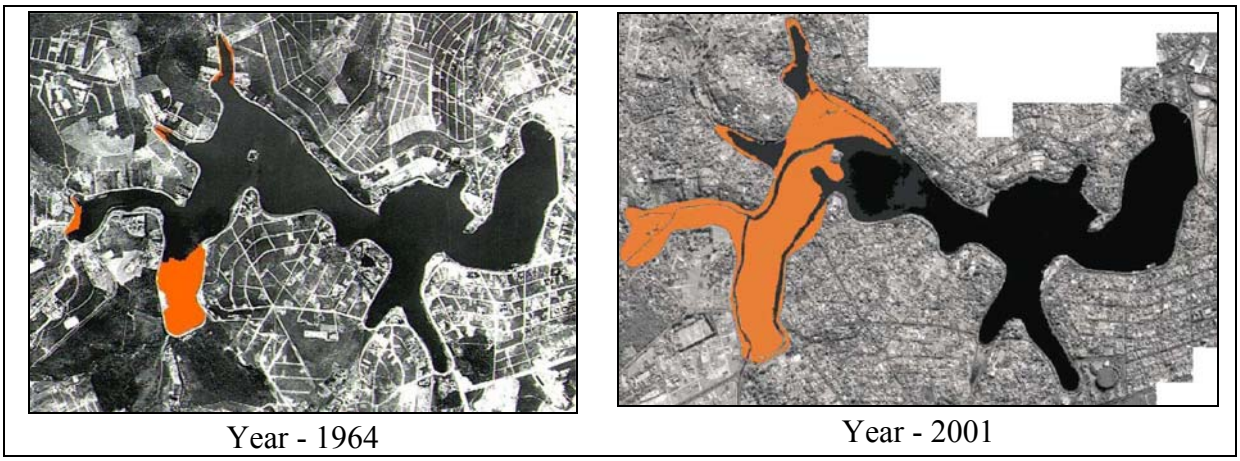

Year - 1964 Year - 2001

Figure 10 – Pampulha Reservoir Accretion (in orange), Belo Horizonte, Brazil

There is no available area inland to dump the dredged material from the reservoir. The watercourses downstream the dam are the natural way for the sediment that accretes the reservoir if the dam were not constructed. In this way, field experiments, with simultaneous and instantaneous injections of sediment and water, labelled, respectively, with 99mTc and Rhodamine WT, were performed, in dry season, in 2000 and 2001, to measure the hydro-transport capability downstream the dam, in a stretch of 25km. They allowed comparing the different hydrodynamic behaviours of the mud in suspension and the water transporting it (Bandeira, 2004). A recent mathematical model (Sing & Beck, 2003) was applied and calibrated to the data obtained: advection velocity and longitudinal dispersion. Through convolution, the sediment dumping in suspension using hydraulic dredging system was simulated, calculating also, the physical environmental impacts: increase of sediment concentration and the possibility of deposition. The measurement of physical-chemical parameters of the water, allowed to evaluate the possibility of desorption of the metals adsorbed in the sediment to be dredged and dumped downstream. It was concluded that there is no impediment for the dumping of the dredged fine sediment in the watercourses downstream (Bandeira, 2004).

4 – **CONCLUSIONS**

The labelling of fine sediment with 99mTc has been successfully accomplished and the labelled sediment has the same hydrodynamic behaviour as the natural one. The labelling yield was quite high (over 90%) and relatively irreversible without significant desorption, during, at least, two hours.

A new application for this radioactive tracer, widely used in Nuclear Medicine, is now available in the field of Sedimentology for which fine sediments are instrumental in the transportation of heavy metals and other pollutants in the water environment (Förstner & Schoer, 1984). 99mTc is easy to use due to its simple handling:

- Low gamma ray energy (140 keV) implying moderate shielding and ease of manipulation in field conditions by simple elution from the ^{99}Mo/Tc generator;
- Availability even in places where there are no nuclear facilities, due to its widespread application in Nuclear Medicine. Indeed, the possibility of using second week ^{99}Mo generator (already used for one week in the Nuclear Medicine laboratory) facilitates the use of this tracer in environmental studies.
- Convenient half life of the ^{99}Mo parent nuclide (66 h), which makes it possible to obtain ^{99m}Tc from the ^{99}Mo generator for one week or more in field studies. This illustrates the portability of the tracer when compared with, for example, ^{198}Au obtained by irradiation in nuclear reactors.

The work performed in the laboratory research and almost all the field work for Pampulha dredging reservoir studies, used second week generators obtained, at no cost, from Nuclear Medicine laboratories. The reason is that the 99mTc detector for environmental applications is placed into the water, in 4π geometry and, for medical applications it is situated externally to the patient. So, the necessary concentrations for environmental use (Bq/mL of water) are much lower (10-7) than in Nuclear Medicine utilization (Bq/mL of blood) (Bandeira, 2004).

ACKNOWLEDGEMENTS

The research was conducted in the laboratories of the Nuclear Technology and Development Centre (CDTN), Brazilian Nuclear Energy Commission (CNEN), Belo Horizonte, Brazil, and was partially sponsored by the International Atomic Energy Agency (IAEA), Vienna, Austria, through the Research Contract BRA-10891.

The 99mTc used for the laboratory research and for part of field work was donated by ECOGRAF and ECOAR Nuclear Medicine laboratories (Dr. Ivana Sena Nascimento), Belo Horizonte, Brazil, and obtained mostly from second week 99Mo generators.

REFERENCES

1. AIREY, P.; Hughes, C.; Kluss, T.; Duran, E.; Miller, B.; Chiuenta, S.; Nielsen, A.F.; Hollins, S. (2002). “Evolving role of radiotracers in coastal zone studies”. Journal of Applied Radiation and Isotopes, v.58, p. 401-406.
2. Aun, P.E.; Bandeira, J.V. (1995). “The role of nuclear techniques in sedimentological studies and some applications in Latin America”, in IAEA-TECDOC-818: “Use of nuclear techniques in studying soil erosion and siltation” – Vienna, 1995.
3. Bandeira, J.V.; Pinto, G.G. (1997). “Estudio de La Calidad Ambiental de La Bahía de Montevideo – Estudios Sedimentológicos con la Aplicación de Técnicas Nucleares”. End-of-Mission Report. IAEA Technical Cooperation Project URU/8/009. (In Spanish).
4. Bandeira, J.V.; Pinto, G.G.; Sabino, C.S.; Agudo, E.G. (1999a). “The use of ^{99m}Tc as an adsorbable tracer for studying the dynamics of fine sediments in suspension”. In: International Symposium on Isotope Techniques in Water Resources Development and Management, 10-14 May 1999, Vienna. Proceedings… Vienna: IAEA, 1999. 1 CD-ROM.
5. Bandeira, J.V. Pinto, G.G.; Sabino, C.S.; Agudo, E.G. (1999b). “A utilização do ^{99m}Tc como um traçador adsorvível para o estudo da dinâmica de sedimentos finos em suspensão”. In: SIMPÓSIO BRASILEIRO DE RECURSOS HÍDRICOS, 13, 1999, Belo Horizonte. Anais...São Paulo: ABRH, 1999b. 1 CD-ROM. (In Portuguese).
6. Bandeira, J.V. (2001). “The use of the ^{99m}Tc as an adsorbable tracer for studying the dynamics of fine sediments”. Final Report: IAEA Research Contract BRA-10891.
7. Bandeira, J.V.; Sabino, C.S.; Aun, P.E.; Mendes, V.L.; Agudo, E.G. (2002). “Development of a technique for using ^{99m}Tc as an adsorbable tracer for hydrodynamic studies of fine sediments in suspension”. Journal of Applied Radiation and Isotopes, v.57, p. 85-92.
8. Bandeira, J.V. (2004). “Development of Nuclear and Correlate Techniques for Urban Hydrology Studies - Applications in Pampulha Hydrographic Basin and Velhas River, MG”.

Doctorate Thesis in Sanitation, Environment and Hydric Resources – Federal University of Minas Gerais - UFMG, Belo Horizonte, Brasil. (In Portuguese).
9. Borroto, J.; Domínguez, J.; Pérez, E.; Fernández, G.; García-Agudo, E. (1999). "Behavior of ^{99m}Tc in highly polluted surface waters: field and laboratory studies". In: International Symposium on Isotope Techniques in Water Resources Development and Management, 10-14 May 1999, Vienna. Proceedings... Vienna: IAEA, 1999. 1 CD-ROM.
10. Borroto, J. (2004). "Comportamiento del ^{99m}Tc como radiotrazador en aguas superficiales y residuals". Doctorate Thesis in Chemical Sciences. Instituto Superior de Tecnologías y Ciencias Aplicadas. Facultad de Ciencias y Tecnología Nucleares (INSTEC), Departamento de Radioquímica, La Habana, Cuba (In Spanish).
11. Bougault, H. (1970). "Étude de la sorption de quelques radioéléments artificiels par les sédiments pélitiques en vue de son application au marquage radioactif de ces matériaux", PhD Thesis, Faculté des Sciences de l´Université de Paris. (In French).
12. Caillot, A; Aun, P.E.; Moreira, R.M.; Castro, J.O.N.M; Bandeira, J.V.; Dolabella, R.O.P.; Bomtempo, V.L.; Mendes, V.L.; Chagas, E.A; Pinto, A.M.F.; Gomes, R.S.; Souza, A.D.; Costa, D.A.; Aun, L.R.; Neto, A.F. (1978). "Laboratory and in situ studies of the hydrodynamic behaviour of fine particles in suspension using radioactive tracers – Application to the particular study of dredging spoil disposal of Recife harbour (Brazilian Northeast)". End-of-Mission Report, IAEA TC Project BRA/8/018 (in French).
13. García-Agudo, E. (1997). "Use of tracers and environmental isotopes in surface water pollution studies". In: IAEA Consultant's Meeting, Vienna. Report. Vienna: IAEA, 1997.
14. Förstner, U.; Schoer, J. (1984). "Some typical examples of the importance of the role of sediments in the propagation and accumulation of pollutants". In: Research Co-Ordination Meeting on the Role of Sediments in the Accumulation and Transport of Radionuclides in Waterways, 1982, Mol, Belgium. Introductory lectures: sediments and pollution in waterways. General Considerations. Vienna: IAEA, 1984. p.137-158 (IAEA-TECDOC 302).
15. Migniot, C. (1968). "Study of the physical properties of very fine different sediments and of their behaviour under hydrodynamic actions". Houille Blanche, 7, pp. 591-620 (in French).
16. Pinto, G.G.; Bandeira, J.V.; Antola, R.S.; Malek, A.; Ameigenda, B.S.; Parada, M.L.B.; Fraga, H.A.; Del Monte, D.; Firpo, A.; Cabral, W.; Odino, R.; Postiglione, M.; Magnani, G.D.L.; Gorfain, J.B.; Cruz, A.; Longoni, H.; Cane, H.; D'Angelo, J.; Ramirez, F.; Tapia, L.A.; Tasende, S.M.; Garcia, P. (1998). "Estudios sedimentológicos en la región de la bahía de Montevideo, con el empleo de técnicas nucleares y trazadores radiactivos y fluorescentes" - III Meeting in Sediment Engineering, Belo Horizonte, Brasil. (In Spanish).
17. Sekine, T., Watanabe, K., Yoshihara, K., Kim, J.I. (1993). "Complexation of technetium with humic acid". Radiochimica Acta 63, 87-90 (1993).
18. Singh, S.K.; Beck, M.B. (2003). "Dispersion coefficient of streams from tracer experimental data". Journal of Environmental Engineering, v. 129, n.6, p.539-546, June 2003.

ORINOCO RIVER SUSPENDED SEDIMENT STUDIES USING ^{99M}TC – VENEZUELA

M.L. Machado[14], J.V. Bandeira[15], L.H. Salim[16], R.M. Moreira[17]

ABSTRACT

The paper presents the main results obtained from the suspended sediment transport study, using the natural sediment labelled with ^{99m}Tc as a tracer, and performed in the stretch Guarguapo – Barrancas – Ya-Ya of the Orinoco River, in Venezuela, in April 2006, at the end of the low water season. The following characteristics of the behaviour of fine sediment in suspension were obtained: advection velocity, dispersion coefficient, sedimentation rate and dilution. These parameters are important for environmental studies, taking into account that the fine sediment is the main carrier of heavy metals and other pollutants in the water environment.
The Orinoco River basin region is presently undergoing a fast industrial development with many industries being installed in the river margins and the results obtained with the studies could be used for preliminary designs of outfalls for industrial effluents which will discharge particulate material with a density similar to the fine sediment or for pollutant material that can be adsorbed by the fine sediment.

1 – INTRODUCTION

In April 2006, under the framework of IAEA TC Project VEN/8/019: "Management of Sediments throughout the Navigation Channel of the Orinoco River" radiotracer studies were performed in Orinoco River, Venezuela, in the stretch Guarguapo – Barrancas – Ya-Ya (Figure 1) in order to evaluate bottom and suspended sediment transport (Bandeira, Salim & Brisset, 2006). The broad objective of the former study was related with the choice of a dumping site for the material dredged from the ship channels. The specific objective of the latter was to study the following characteristics of the behaviour of fine sediment in suspension: advection velocity, dispersion coefficient, sedimentation rate and dilution, taking into account that the fine sediment is the main carrier of heavy metals and other pollutants in the water environment (Förstner & Schoer, 1984). The Orinoco River basin region is presently undergoing a fast industrial development with many industries being installed in the river margins.
In relation to the suspended sediment study, two sub-superficial injections of mud labelled with ^{99m}Tc ($T_{1/2}$ =6.02h and gamma-ray energy = 140keV) were performed (figures 2 & 3). The initial activities used during the injections were respectively, 2.1 and 1.6Ci. The detection was performed by a boat positioned by GPS with scintillation detectors placed at 1.5m (probe 1) and 0.5m (probe 2) below the water surface. The measured count rates were corrected for the background and radioisotope decay.

[14] Senior Researcher - Nuclear Technology Development Centre - CDTN/CNEN - Cidade Universitária - Pampulha - P.O.Box 941 Zip Code 30123-970 - Belo Horizonte, MG - Brazil - Tel. 55 31 3069-3345 - E-mail: mlm@cdtn.br
[15] Idem... - Tel. 55 31 3069-3120 - E-mail: jvb@cdtn.br
[16] Idem... - Tel. 55 31 3069-3246 - E-mail: salimlh@cdtn.br
[17] Idem... - Tel. 55 31 3069-3132 - E-mail: rubens@cdtn.br

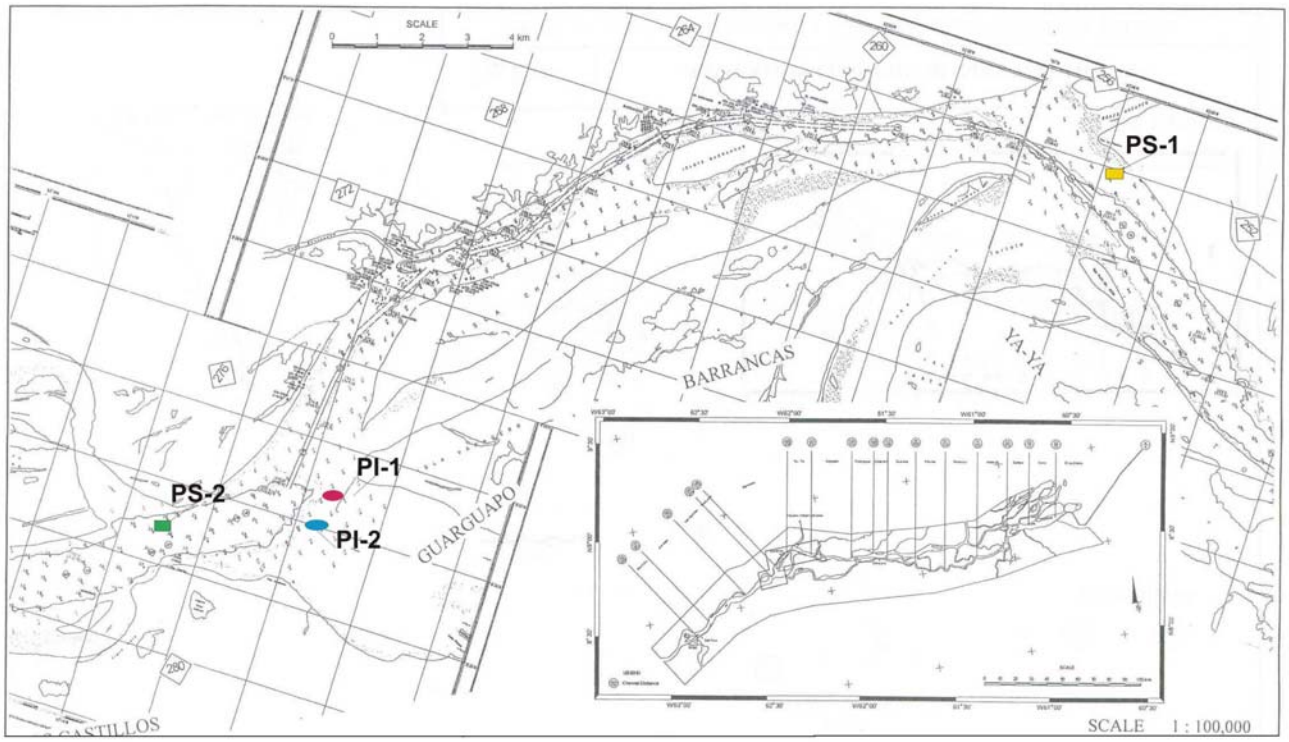

Figure 1 - Map of the sector Guargapo – Barrancas – Ya-Ya
PI-1 and PI-2 (bottom sediment injection points)
PS-1 and PS-2 (suspended sediment injection points 1 & 2, respectively)

Figure 2 - Labelled mud mixer & injector
Obs: the mud in the bucket is not yet labelled

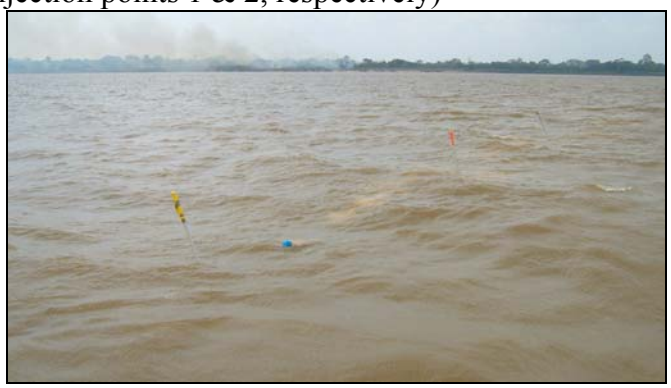

Figure 3 - Just after injection & floating indicators

2 – PARAMETERS MEASURED FROM THE SUSPENDED SEDIMENT EXPERIMENTS

2.1 – Advection velocity

The advection of the suspended particles was determined from measurements of the displacement of the puffs of radioactively tagged particles. Thus, the distance from the injection point to the position of the maximum count rate of each crossing of the cloud (Δs) was plotted as a function of the time from the injection (Δt). The advection velocity ($\overline{U}$) was obtained by the inclination of the straight line adjusted to the points (figures 4a & 4b).

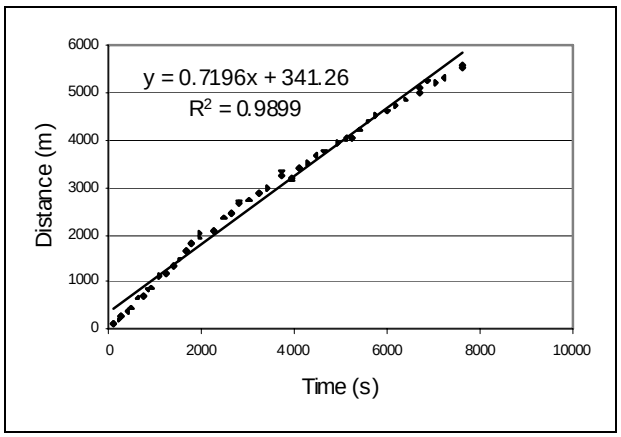

(a) Injection 1 at PS-1

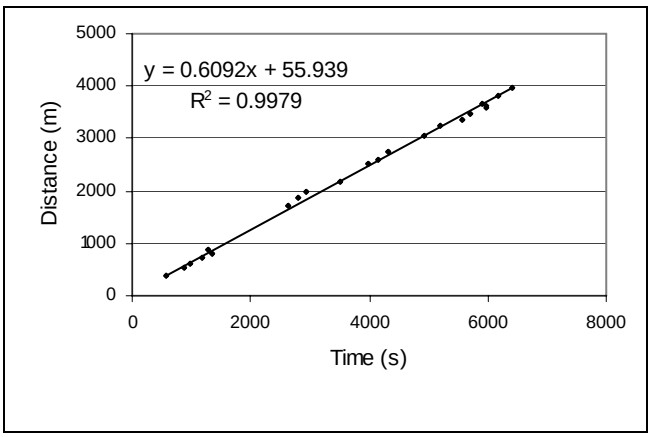

(b) Injection 2 at PS-2

Figure 4 - Travel distance of radioactive cloud in function of time

Table 1 presents, for both injections and considering, for each one, the ensemble of measurements of both probes, the values of velocity together with the corresponding values of the correlation coefficients.

Table 1 - Advection velocity of the sediment cloud and correlation coefficients

Injection	Probe	Advection velocity $\overline{U}$ (m/s)	R^2	R
1	1 & 2	0.72	0.9899	0.9949
2	1 & 2	0.61	0.9979	0.9989

2.2 – Dispersion coefficient

Each crossing of the radioactive cloud provides an approximately Gaussian distribution of the count rates. The dispersion coefficient is related with the rate of variance growth as the cloud expands. This increase could be expressed by a general law with the form of:

$$\sigma^2 = A^2 t^{2m} \tag{2.1}$$

where A and m are adjustable constants obtained by least squares fit.

Taking into account the correlation coefficient values of the present study, one could assert that this function is suitable to represent the growth of the variance with time.

For each crossing (longitudinal or transversal) the variance of this distribution was determined in two different ways a) adjusting the curve to a Gaussian distribution using linear regression; b) by the definition of variance.

The dispersion coefficient D is related to the rate of variance growth by the following expression:

$$D = \frac{1}{2}\frac{d\sigma^2}{dt} \tag{2.2}$$

Combining (2.1) and (2.2), one obtains:

$$D = m\, A^2\, t^{2m-1} \text{ or } D = A'\, t^{m'} \tag{2.3}$$

where: $A' = mA^2$ and $m' = 2m - 1$.

The constant values of these expressions were obtained by least squares fit and are shown in tables 2 & 3 (values considering the curve adjustment to a Gaussian distribution) and in tables 4 & 5 (considering the definition of variance).

Table 2 - Constant values (adjustment to a Gaussian distribution) - transversal crossings

Injection	Probe	A'	M'	A	M	R^2	R
1	1	3.784E-02	0.4322	0.2299	0.7161	0.8485	0.9211
1	2	2.614E-02	0.4808	0.1879	0.7404	0.8441	0.9187
2	1	2.330E-05	1.3230	0.00448	1.1615	0.8188	0.9049
2	2	6.388E-04	0.9088	0.0259	0.9544	0.7876	0.8875

Table 3 - Constant values (adjustment to a Gaussian distribution) - longitudinal crossings

Injection	Probe	A'	M'	A	M	R^2	R
1	1	5.278E-03	0.8777	0.0750	0.9388	0.8078	0.8987
1	2	6.478E-03	0.8014	0.0848	0.9007	0.9222	0.9603

After the second injection, for operational reasons of the detection, it was possible only to perform two longitudinal crossings of the cloud. This fact made impossible the determination of the parameters representing the growth of the variance in this direction.

Table 4 - Constant values (considering the definition of variance) - transversal crossings

Injection	Probe	A'	M'	A	M	R^2	R
1	1	8.496E-03	0.5650	0.1042	0.7825	0.9056	0.9516
1	2	8.739E-03	0.5496	0.1062	0.7748	0.8942	0.9456
2	1	4.288E-05	1.1660	0.00629	1.0830	0.8890	0.9429
2	2	8.166E-05	1.0938	0.00883	1.0469	0.9080	0.9529

Table 5 - Constant values (considering the definition of variance) - longitudinal crossings

Injection	Probe	A'	M'	A	M	R^2	R
1	1	7.365E-03	0.7276	0.0923	0.8638	0.8663	0.9308
1	2	7.409E-03	0.6935	0.0935	0.8467	0.9159	0.9570

Taking into account the values of the correlation coefficients obtained and presented in tables 2 to 5, one could asseverate that the function $\sigma^2=A^2\ t^{2m}$ is adequate to represent the variance growth in function of time. Furthermore, the correlation coefficient values obtained, considering the definition of variance, are always higher than the ones obtained for the adjustment to a Gaussian distribution. Figures 3a & 3b highlight this fact.

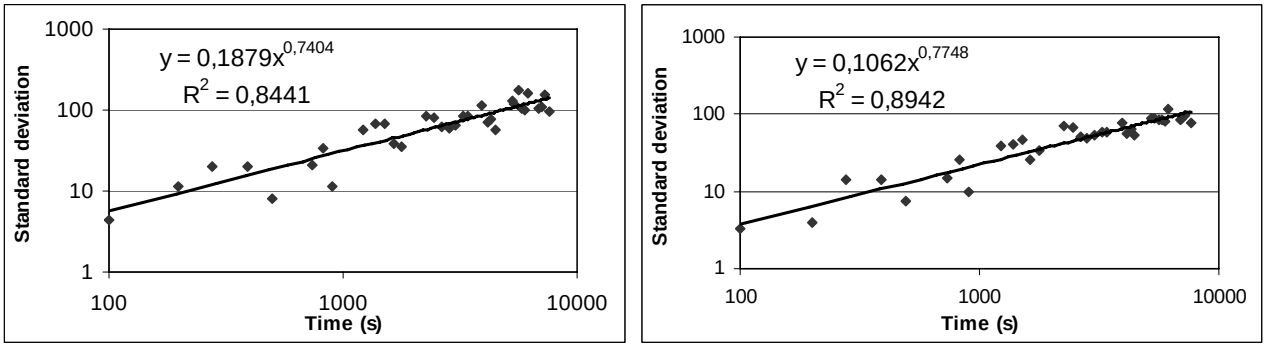

(a) Adjustment to a Gaussian distribution (b) Considering the definition of variance

Figure 5 - Date of variance and correlation coefficients. Injection 1 - Probe 2

2.3 – Sedimentation rate

The sedimentation rate is determined from the decrease of the maximum count rate with time. In this way, the maximum count rates obtained for each cloud crossing were plotted, in a logarithmic scale as a function of time, and the envelopes to the peaks were drawn. These envelopes approximately correspond to the true variation of the peaks with time since the crossings only occasionally hit the maximum concentration of the tracer.
The sedimentation rates were obtained adjusting the envelope curve determined for each injection and probe level, to the following expression:

$$R_{\max} = \frac{R_0}{t - t_0} \exp\left[-S_R \left(t - t_0\right)\right] \tag{2.4}$$

where:

$R_{\max}$ - Maximum count rate in each crossing;

R_0 - Constant;

t - Time span after injection;

t_0 - Virtual time of injection;

S_R - Sedimentation rate.

The adjustment is performed using three parameters: R_0, S_R and t_0 (Caillot et al., 1972, 1978), (Caillot, 1973), (Tola, 1981), (Tola et al., 1987). The value of S_R obtained by this method corresponds to the sedimentation rate:

$$S_R = -\frac{dM}{Mdt} \tag{2.5}$$

Where M is the total mass of the sediment dumped in suspension at the time t, and S_R represents the fraction of the total material that settles per unit~~y~~ of time, being expressed in (g/ton)/s.

Figures 6a & 6b illustrate this adjustment and Table 6 shows the optimum values of R_0, S_R and t_0 determined for each case.

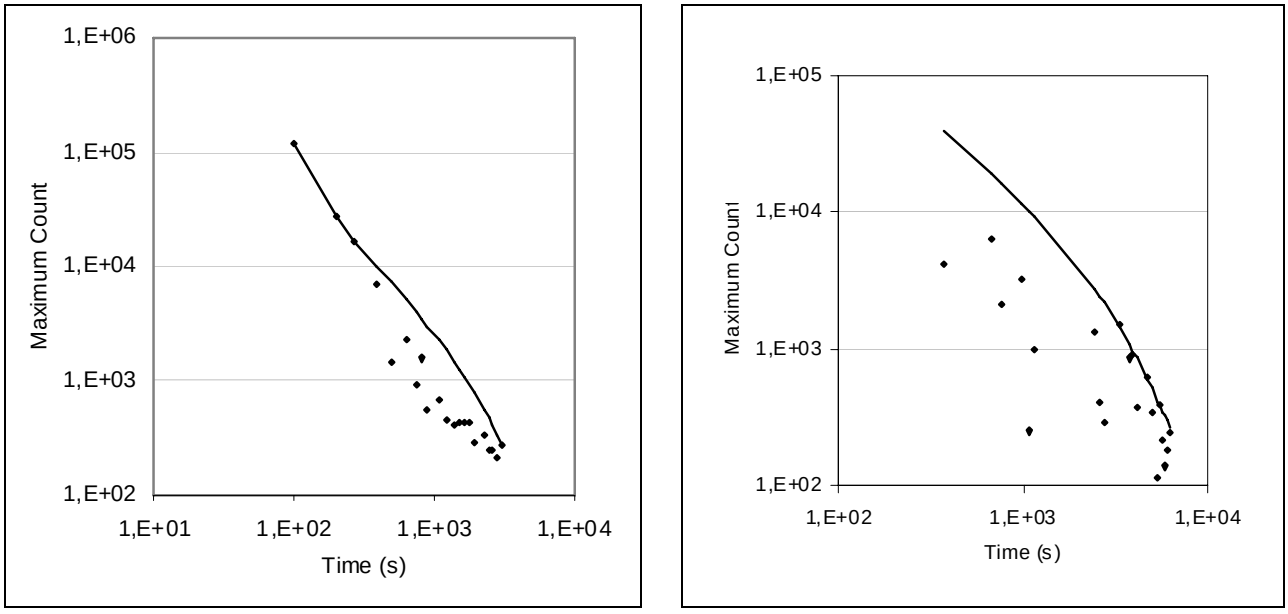

(a) Injection 1 - Probe 1 (b) Injection 2 - Probe 1

Figure 6 - Maximum count rates as a function of time

Table 6 - Sedimentation rate and associated parameters

Injection	Probe	Depth. (m)	S_R (g/ton/s)	T_0	R_0
1	1	1.5	520	68	3.83E+06
1	2	0.5	532	71	3.63E+06
2	1	1.5	372	0.5	1.67E+07
2	2	0.5	421	0.3	2.05E+07

Two other parameters derived from the sedimentation rate were inferred: the necessary time (T_{half}) for half of the suspended sediment dumped (M_0) to settle below the diameter of the sphere of influence of the scintillation detector and the distance travelled from the dumping site, for this occurrence (L_{half}). The calculated values for these two parameters, in each case, are shown in Table 7, together with the mean advection velocity values (item 2.1).

$$T_{half} = \frac{\ln 2}{S_R} \tag{2.6}$$

$$L_{half} = \overline{U}\, T_{half} \tag{2.7}$$

where $\overline{U}$ represents the average advection velocity.

Table 7 - Values of T_{half} and L_{half}

Injection	Probe	Depth (m)	S_R (g/ton/s)	$\overline{U}$ (m/s)	T_{half} (min)	L_{half} (m)
1	1	1.5	520	0.723	22.2	963
1	2	0.5	532	0.720	21.7	937
2	1	1.5	372	0.609	31.1	1136
2	2	0.5	421	0.609	27.4	1001

2.4 – Dilution

The minimum dilution attained at a given point of the water body is the relation between the initial concentration of the discharged solids (C_0) and the concentration at this point.

$$S = \frac{C_0}{C} \tag{2.8}$$

The evaluation of C_0 would lead to take a sample of the labelled mud. As the labelling and the injection are almost a simultaneous process it is difficult, for operational reasons, to sample the labelled mud and determine, with accuracy, the amount of labelled mud for field conditions. One utilizes the concentration of the first pick detected instead of C_0. As the relation between the tracer concentration and the count rates is given by a constant factor, the minimum dilution (S_m), a conservative value, is given by the following relation:

$$S_m = \frac{R_1}{R} \tag{2.9}$$

where R_1 is the count rate of the first peak detected, as fast and as near as possible the injection point and R is the maximum count rate value determined for each subsequent cloud crossing. In reality the effective dilution is always higher. Figure 7 shows the minimum dilution values as function of distance in a semi logarithmic scale for the date corresponding to the Injection 1,

considering the measurements of both probes. The straight line under the points represents the minimum dilution as a function of distance (dilution follows an exponential law). Nevertheless, a reasonable supposition is that this exponential growth has a limit and the dilution tends to the stability.

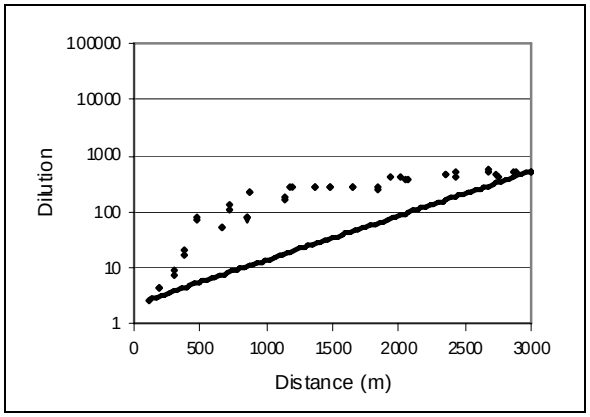

Figure 7 – Dilution as a function of distance.

2.5 – Synthesis of results

Tables 8 & 9 summarize the main results obtained, respectively, for the injections 1 & 2.

Table 8 - Results of suspended sediment studies – Injection 1

Injection	Probe	Sedimentation rate (S_R)	Dispersion coefficient		Dilution	Advection velocity	T_{half}	L_{half}
		(g/ton/s)	D_L (m^2/s)	D_T (m^2/s)	D	A_V (m/s)	(min)	(m)
1	1 (1.5 m)	520	1.3731	0.4949	500	0.723	22.2	963
1	2 (0.5 m)	532	1.0811	0.4500		0.720	21.7	937

Table 9 - Results of suspended sediment studies – Injection 2

Injection	Probe	Sedimentation rate (S_R)	Dispersion coefficient		Dilution	Advection velocity	T_{half}	L_{half}
		(g/ton/s)	D_L (m^2/s)	D_T (m^2/s)	D	A_V (m/s)	(min)	(m)
2	1 (1.5 m)	372	-	0.2783	30	0.609	31.1	1136
2	2 (0.5 m)	421	-	0.2646		0.609	27.4	1001

Where:

D_L & D_T = Longitudinal & transversal dispersion coefficients for the time T_{half}.

One can observe that the value of D_L, for both levels of detection, for Injection 1 (Table 8) is more than twice the corresponding value for D_T, as expected. The values of D_T obtained for Injection 2 are lower than the corresponding ones for Injection 1 which presented higher values of advection velocity than Injection 2. The dilution value calculated for Injection 2, considering both probes, is much lower than the corresponding for Injection 1, for two main reasons: delay in obtaining the first crossing of the cloud (lower value of C_0 or R_1); lower advection velocity during the experiment of Injection 2.

3 – CONCLUSIONS

^{99m}Tc, broadly used in Nuclear Medicine for diagnosis purposes, and developed for labelling mud (Bandeira, 2004), (Bandeira et al., 2008), proved to be an efficient tracer for field survey in a huge environment, as Orinoco River. ^{99m}Tc is easy to be used due to its simple handling and availability:

- Low gamma ray energy (140 keV) implying moderate shielding and ease of manipulation in field conditions by simple elution from the ^{99}Mo/Tc generator;
- Availability even in places where there are no nuclear facilities, due to its widespread application in Nuclear Medicine;
- Being injected in the veins of human patients for diagnosis purposes (activities up to 40 mCi), it has public acceptance for being used in environmental studies. Furthermore, the necessary concentrations for environmental use (Bq/mL of water) are much lower (10^{-7}) than in Nuclear Medicine utilization (Bq/mL of blood) (Bandeira, 2004). The reason is that the ^{99m}Tc detector, for environmental applications, is placed into the water, in 4π geometry, increasing tremendously the counting efficiency and, for medical applications, it is situated externally to the patient. In this way, for many environmental studies, second week generators obtained for free, from Nuclear Medicine laboratories are enough.
- Convenient half life of the ^{99}Mo parent nuclide (66 h), which makes it possible to obtain ^{99m}Tc from the ^{99}Mo generator for one week or more in field studies. This illustrates the portability of the tracer when compared with, for example, ^{198}Au obtained by irradiation in nuclear reactors.

The results obtained for the behaviour of the natural sediment in suspension, at the end of the low water season of the Orinoco River (April), could be used for preliminary designs of outfalls for industrial effluents which will discharge particulate material with a density similar to the fine sediment or for pollutant material that can be adsorbed by the fine sediment.

ACKNOWLEDGEMENTS

The work was performed under the framework of IAEA TC Project VEN/8/019, with the “Instituto Nacional de Canalizaciones – INC” of Venezuela as the Counterpart Institution, providing a strong support in all phases of the studies through Eng. Roberto Savelli Ciatteo (Project Counterpart) and Eng. Juan Carlos Rojas (Hydrographic support) and supplying one of the survey boats (L.F. Piacoa). The Central University of Venezuela – UCV participated also of the studies (Phys. Hector Constant Machado; Phys. Eddie Avilán; Techn. Gustavo Landaeta), supplying also nuclear detection equipment. “Fundación La Salle – FLASA” of Venezuela provided one of the survey boats (Hermano Gines) and its Oceanographer, Aitzol Arellano, participated of the field works. Dr. Patrick Brisset (CEA-DETECS, Saclay, France) participated in all phases of the TC Project as one of the IAEA experts.

REFERENCES

1. Bandeira, J.V. (2004). “Development of Nuclear and Correlate Techniques for Urban Hydrology Studies - Applications in Pampulha Hydrographic Basin and Velhas River, MG”. Doctorate Thesis in Sanitation, Environment and Hydric Resources – Federal University of Minas Gerais - UFMG, Belo Horizonte, Brasil. (In Portuguese).
2. Bandeira,J.V.; Salim, L.H.; Brisset, P. (2006). “Management of Sediments throughout the Navigation Channel of the Orinoco River - Bottom and Suspended Sediment Transport Evaluation, in Orinoco River, Using Radioactive Tracers”. End-of-Mission Report. IAEA Technical Cooperation Project VEN/8/019. Vienna: IAEA, 2006. 24p.
3. Bandeira,J.V et al. (2008). “^{99m}Tc mud labelling and its application in hydrodynamic studies of fine suspended sediment in Brazil”. To be presented at 5th International Conference on Tracers and Tracing Methods (Tracer5). Tiradentes, MG – Brazil, 2-6 November, 2008.

4. Caillot, A. et al. (1972). “Étude des gravières marines – Approche théorique du transport en suspension, mode de depouillement des mesures de traceurs radioactifs - Fascicule 2”. Comissariat a L’Energie Atomique et Centre National d’Exploitation des Oceans, France.
5. Caillot, A. (1973). “Sediment labelling with radioactive isotopes”. In: INTERNATIONAL ATOMIC ENERGY AGENCY. Tracer techniques in sediment transport. Vienna:IAEA, 1973. p. 169-176 (IAEA TECDOC-145).
6. Caillot, A. et al. (1978). “Étude au laboratoire et in situ du comportement hydrodynamique des fines particules en suspension à l´aide de traceurs radioactifs - Application au cas particulier du rejet des produits de dragage du port de Recife (N-E du Brésil)”. Belo Horizonte, Brasil: Centro de Desenvolvimento da Tecnologia Nuclear; Divisão de Radioisótopos. Rapport Final de Mission – AIEA, BRA/8/018.
7. Förstner, U.; Schoer, J. (1984). “Some typical examples of the importance of the role of sediments in the propagation and accumulation of pollutants”. In: Research Co-Ordination Meeting on the Role of Sediments in the Accumulation and Transport of Radionuclides in Waterways, 1982, Mol, Belgium. Introductory lectures: sediments and pollution in waterways. General Considerations. Vienna: IAEA, 1984. p.137-158 (IAEA-TECDOC 302).
8. Tola, F. (1981). “The use of radioactive tracers in dynamic sedimentology”. In: IAEA Regional Seminar on the Use of Isotope Techniques in Water Resources Development, 1980, Athens. Proceedings... Vienna: IAEA, 1981.
9. Tola, F. et al. (1987). “Study of the evolution of dredged material discharges by means of radioactive tracers”. In: Symposium on Isotope Techniques in Water Resources Development, 1987, Vienna. Proceedings... Vienna: IAEA, 1987. p. 663-682.

ENVIRONMENTAL TRITIUM AS A TRACER FOR THE VERIFICATION OF GROUND WATER FLOW MODELS

Cota[18], S., Velásquez[19], L.N.M., Minardi[1], P.S.P., Bomtempo[1], V.L.

ABSTRACT

This paper aims to present the verification of the ground water flow model of the Bauru aquifer by comparing the transit times calculated by the model and the ones estimated for water samples from wells exploiting the Bauru aquifer in the area of the municipality of Araguari, situated at 569 km west of Belo Horizonte, the capital of Minas Gerais state, Brazil. Located at the north-northeastern border of the mesozoic sedimentary basin of Paraná River, between Paranaíba and Araguari rivers, Araguari is mainly supplied for public use and irrigation by the exploitation of the Bauru granular aquifer, and, in a minor scale, Serra Geral volcanic fractured aquifers.
The Bauru aquifer flow model was developed using the MODFLOW model and transit times for fifteen wells were calculated by the MODPATH model based on the modeled data. Transit times for water samples were estimated by applying the well-established tracer technique based on environmental tritium (^3H) technique, using data of isotope in precipitation of selected GNIP – Global Network of Isotopes in Precipitation/IAEA - stations (Brasília, Porto Alegre and Kaitoke) as input data for the exponential model.

INTRODUCTION

The mathematical modeling of the ground water flow is a powerful tool to help understanding the dynamics of the water in aquifers, estimating long-term impacts of the water exploitation, planning the proper management of water resources and predicting the fate of contamination plumes and the effectiveness of remediation techniques. Taking into account that the calibration process does not necessarily lead to a unique and widely applicable model, it is advisable to verify how well the calibrated model is able to predict a set of data other than the one used for building the model.
This paper aims to present the verification of the ground water flow model of the Bauru aquifer by comparing the transit times calculated by the model and the ones estimated by the measurement of natural tritium concentration in water samples from wells exploiting the Bauru aquifer in the municipality of Araguari, situated at 569 km west of Belo Horizonte, the capital of Minas Gerais state, Brazil. According to Izbicki et al. (2004), this technique has been mostly successful when applied for large regional flow systems with relatively simple well-defined flow paths.

BACKGROUND

The municipality of Araguari, Minas Gerais, has its economy based upon agricultural and industrial activities, in which the production of soy-beans, corn, coffee, fruit and cattle are outstanding. Groundwater resources are intensively used (Figure 1), due to technical and economical constraints to use surface water from Rivers Araguari and Paranaíba as a result of the large difference of about 300m in altitudes between the river valleys and the plateau. Two main aquifer systems have been individualized in the study area, both of them related to Mesozoic unities of the sedimentary basin of Paraná river (Figure 2). The lower aquifer, Serra Geral, corresponds to the basaltic rocks of São Bento Group and the upper aquifer, Bauru, is represented in this region by the sandstones of Marília Formation (Bauru Group).

[18] Centro de Desenvolvimento da Tecnologia Nuclear, Comissão Nacional de Energia Nuclear – CDTN\CNEN
[19] Instituto de Geociências, Universidade Federal de Minas Gerais – IGC/UFMG

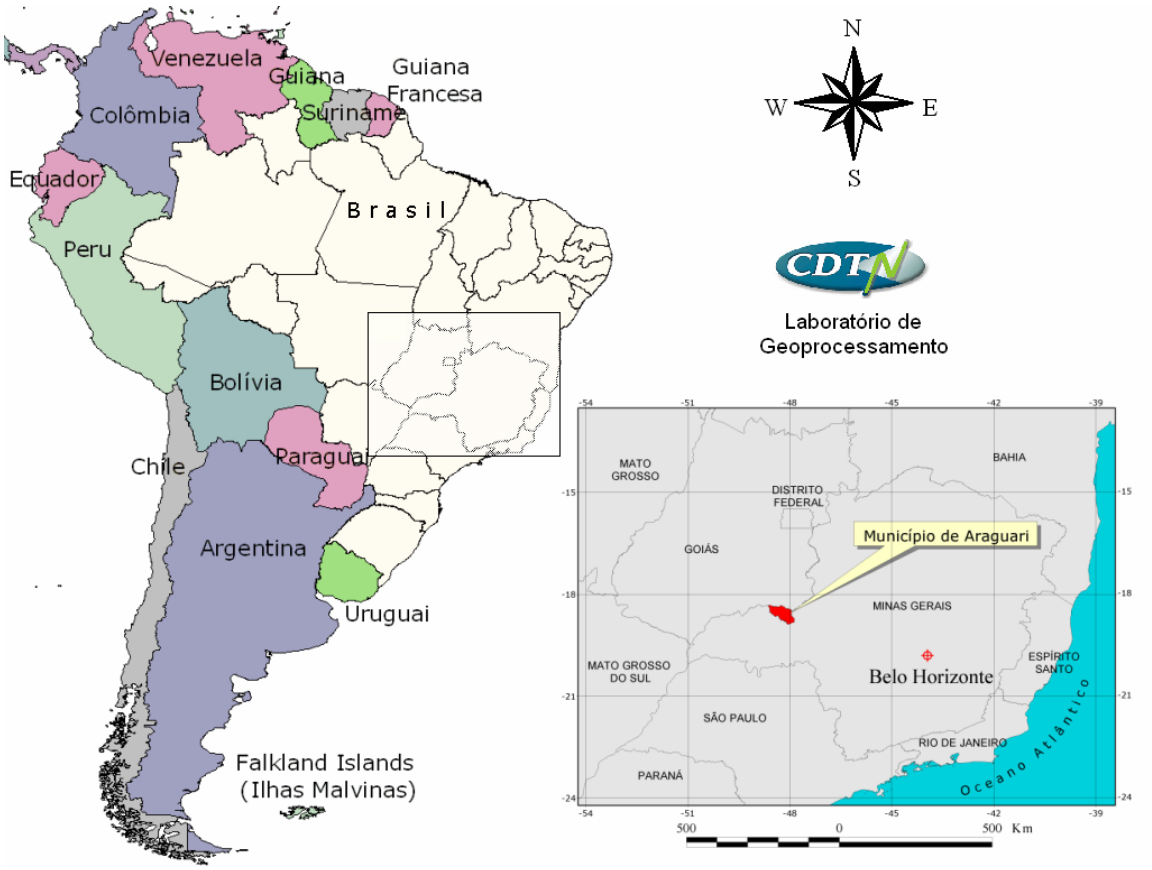

Figure 1. Localization map of the area.

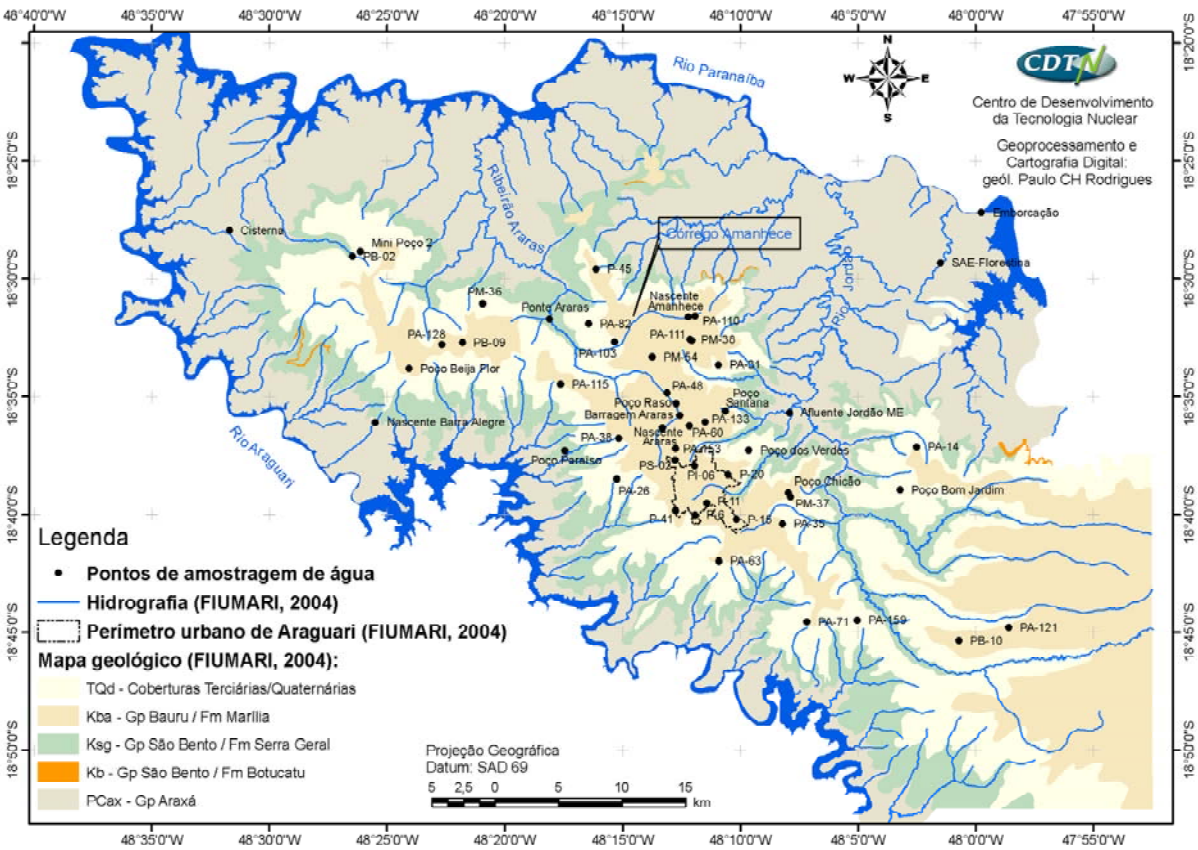

Figure 2. Geological map and location of the water sampling points.

An extensive investigation was carried out in the area, during the years 2004-2005, namely "Evaluation of Water Resources of the Guarani Aquifer System in the Municipality of Araguari, MG, Brazil" (UFMG et al., 2006). The main objective of this Project was the collection of reliable technical and scientific information about the region in order to contribute to the implementation of a consistent water management program by local and state authorities. The Project was developed with the support of GEF/Fund of Universities (BNPPW), in the framework of the Guarani Aquifer Project. Two products of this Project, the Bauru groundwater flow model and the transit time for water samples from the Bauru aquifer by means of environmental tritium determination, were used on the development of the present paper, along with the estimation of transit times based on particle tracking modelling, as described below.

METHODOLOGY

The groundwater flow modelling of the Bauru aquifer was carried out by using MODFLOW (McDonald and Harbaugh, 1988), applying the software Visual MODFLOW, version 4.1.0 (Waterloo Hydrogeologic, Inc., 2005). The model, comprising a total area of 2,958 km2, was built in such a way to reproduce the piezometric map obtained by plotting the data of hydraulic heads of 22 tubular wells, measured in the beginning of the winter time, characterizing a situation in which the aquifer reaches its higher level. The model was constituted by only one layer; the top was established by means of topographic surveys of the area, varying from an altitude of 500m to more than 1,000m, considering a mean saturated thickness of 39-40m in the central part of the plateau, and nule at its borders.

Along the whole limit of the active area of the dominium, boundary conditions of Drain type were applied in order to simulate all the water springs and courses along the Bauru aquifer limits, as well as the main drainages represented by Rivers Araras and Amanhece. Water extraction by pumping the tubular wells was not taken into account in the model, once the piezometric data used to calibrate it represent a situation in which the aquifer was considered at rest. For the modelling purposes, the aquifer was considered as homogeneous and isotropic, bearing a hydraulic conductivity of 2.13x10-3cm/s and an effective porosity of 12%. Further details about the modelling conditions may be seen in Cota et al. (2007).

The stationary solution of the hydraulic heads in the aquifer was obtained from a single initial value for the whole area. The deviations of the potentiometric values of the calibrated model from those measured ranged from -8,97m to 9.94m (Figure 3). Greater differences were observed for wells labelled as 51, PA-74, ARA-370 and ARA-261. The mean absolute error for the calibration was less than 5m (mean quadratic error of 5.84m; normalized mean quadratic error of 7.64%). The estimated piezometric surface can be seen in a color graduation in Figure 4.

Natural (environmental) tritium concentrations in 51 water samples from surface and groundwater origin were measured (Figure 2) by liquid scintillation counting. The residence time (or transit time) of the water was estimated taking into consideration the correlation with available natural tritium data from GNIP (Global Network of Isotopes in Precipitation) stations of Brasília and Kaitoke (New Zealand). The exponential (or total mixture) model was used to estimate the transit time of the samples and 31 of them, collected from Bauru aquifer, were used to interpolate values and prepare the iso-concentration curves shown in Figure 5, together with the estimated water ages.

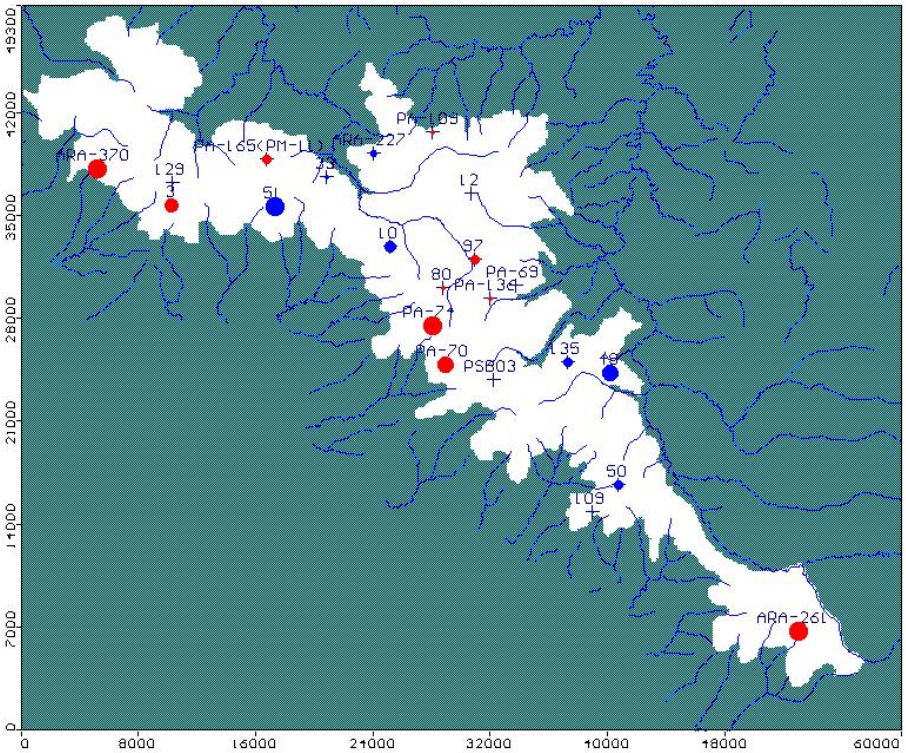

Figure 3. Deviations between calculated and observed values. Blue and red circles represent positive and negative deviations, respectively.

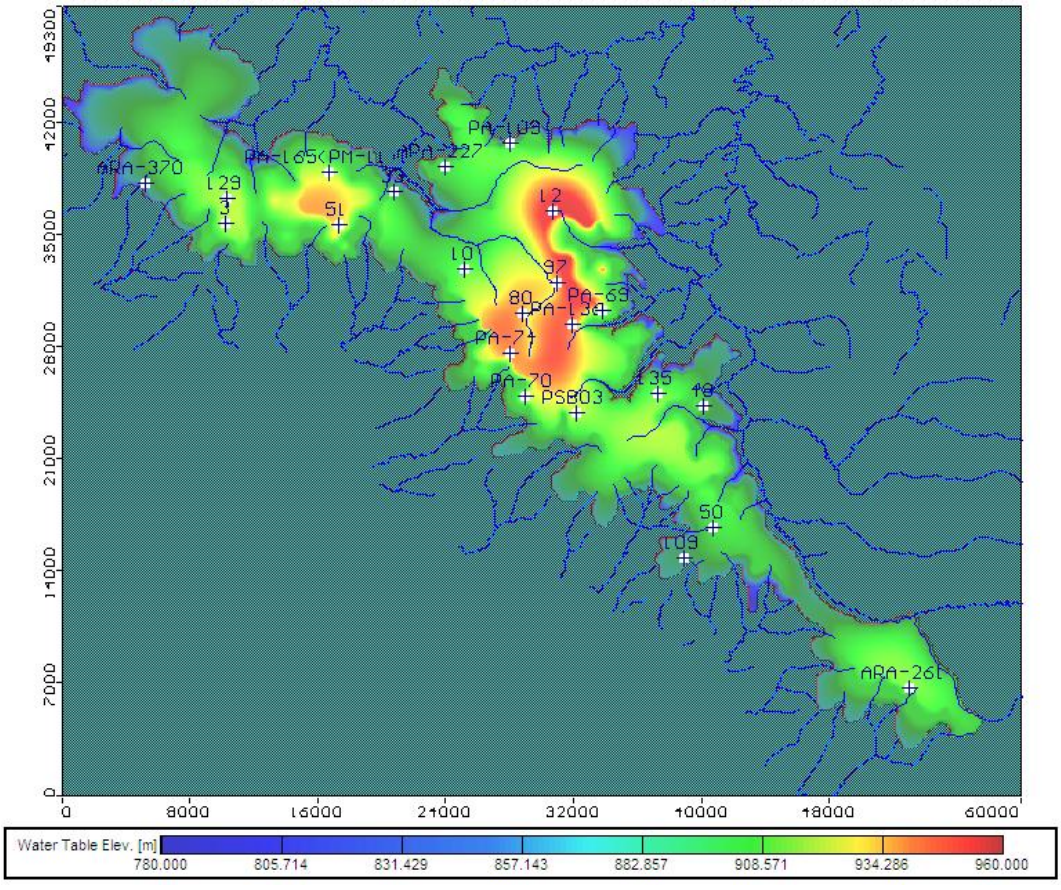

Figure 4. Simulated piezometric surface for the Bauru aquifer.

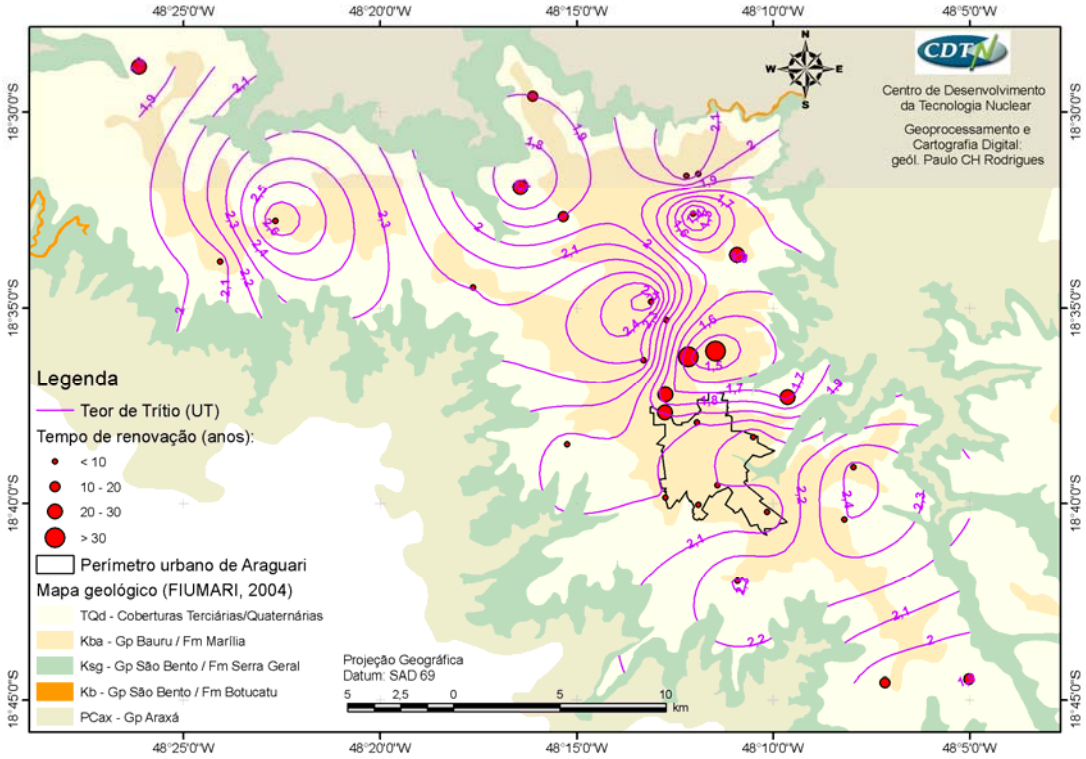

Figure 5. Tritium iso-concentration curves and transit times for the Bauru aquifer.

From the 31 wells exploiting from Bauru aquifer with estimated transit time, 15 wells were selected to be compared with the transit times calculated by the groundwater flow model. This choice was based on the availability of reliable information about the exploited aquifers, total depth and length and position of the filters. Using the model of particle tracking MODPATH, and a combination of forward and backward particles, pathlines from the recharge point to each filter of the 15 wells were obtained (Figure 6) and the transit time for each filter was calculated. An average value of transit time was estimated by averaging the values for each filter considering the filter length.

RESULTS AND ANALYSIS

The results of the comparison between the transit times calculated by the mathematical model and estimated by tritium concentrations are shown in Table 1 and Figure 7. Table 1 shows also the transit time calculated by the model for each filter, as well as the range of values of transit time estimated for the confidence interval of tritium concentrations as informed by the laboratory.

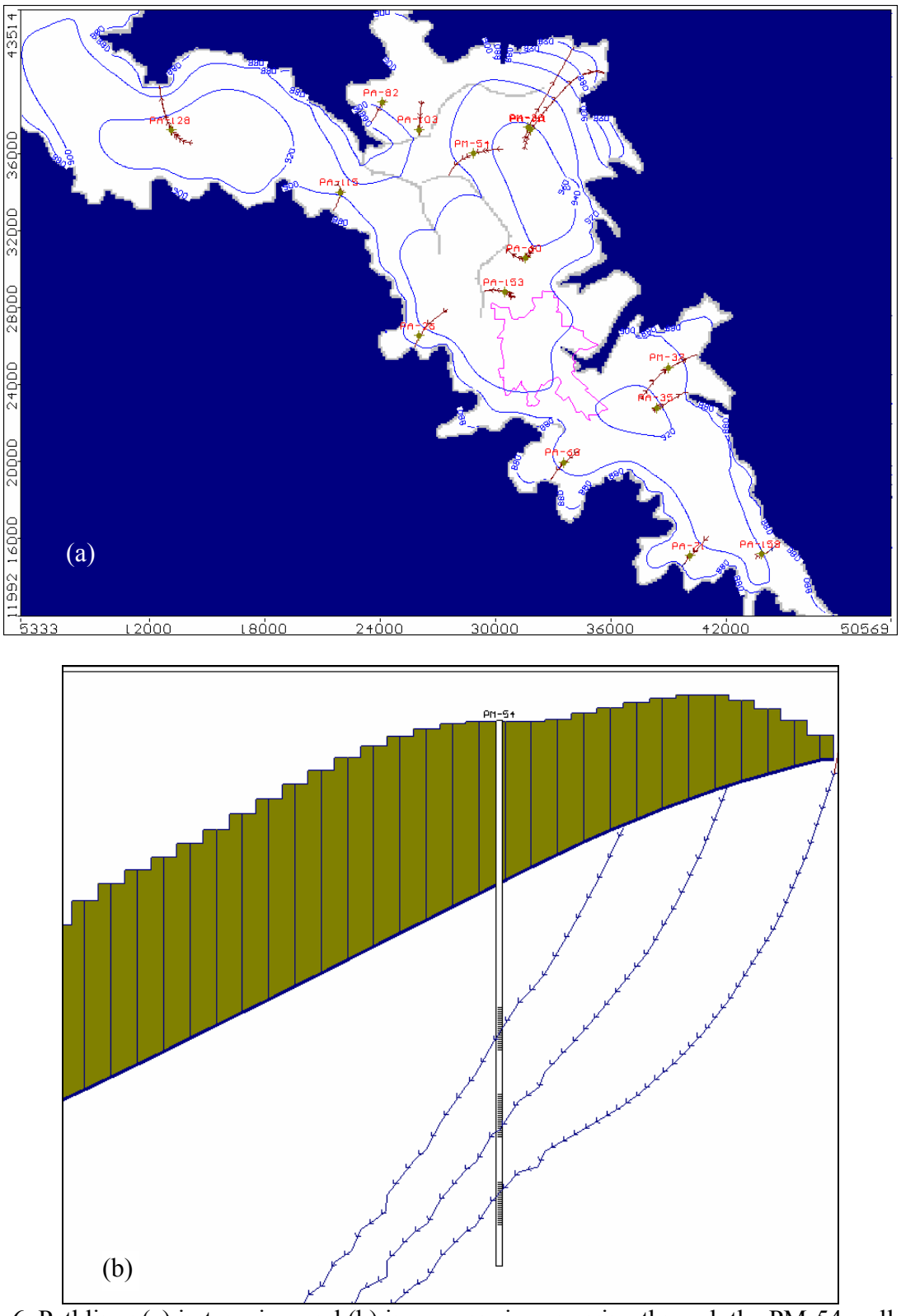

Figure 6. Pathlines (a) in top view and (b) in a cross view, passing through the PM-54 well (time-marks show an one-year interval).

Table 1. Results of the comparison between the Transit Times (TrT) based on flow model and tritium estimative.

Well	Filters	Filter depths (m)		Filter lengths (m)	Model TrT (yr)	Average Model TrT (yr)	Tritium TrT ranges (yr)
PA-159	Filter 1	29.5	33.5	4	6		
	Filter 2	37.5	41.5	4	15		
	Filter 3	45.5	49	3.5	26	15	5 - 28
PA-35	Filter 1	28	36	8	5		
	Filter 2	40	44	4	14		
	Filter 3	48	52	4	20	11	<5
PA-111	Filter 1	30	34	4	23		
	Filter 2	28	45	17	55	49	45 - 60
PM-38	Filter 1	24	54	30	26	26	18 - 40
PA-153	Filter 1	28	52	24	30		
	Filter 2	56	58	2	80	34	18 - 40
PA-103	Filter 1	19	23	4	5		
	Filter 2	27	31	4	14		
	Filter 3	35	39	4	25		
	Filter 4	43	47	4	49	28	5 - 28
PA-60	Filter 1	30	34	4	22		
	Filter 2	42	46	4	48		
	Filter 3	50	54	4	70	47	28 - 53
PA-128	Filter 1	28	36	8	24		
	Filter 2	40	44	4	38		
	Filter 3	48	58	10	68	47	<5
PA-115	Filter 1	23	27	4	0		
	Filter 2	31	35	4	4		
	Filter 3	39	43	4	27	10	<8
PM-54	Filter 1	26	30	4	12		
	Filter 2	34	38	4	23		
	Filter 3	42	46	4	40	25	<18
PA-82	Filter 1	12	16	4	10		
	Filter 2	20	24	4	11	11	18 - 42
PM-37	Filter 1	34	36	2	35		
	Filter 2	42	46	4	77	63	28 - 53
PA-26	Filter 1	21	27	6	38	38	5 - 25
PA-71	Filter 1	17	21	4	5		
	Filter 2	25	29	4	16		
	Filter 3	33	37	4	36	19	5 - 25
PA-63	Filter 1	30	34	4	1		
	Filter 2	44	48	4	14		
	Filter 3	52	56	4	29	15	<5

The transit time calculated by the flow model for seven of the fifteen wells fell into the range of transit time estimated by tritium using the exponential model. For another six wells, the calculated transit times are greater than the upper limit of the range, although in the same order of magnitude. For just a single well, the calculated transit time was less than the lower limit of the estimated range, but again with the same order of magnitude.

Thus, it is possible to verify that, for 14 of 15 wells, there was a reasonable agreement between the results yielded by both methods. It means that the results are perfectly acceptable, even for the case of hydrogeological study in a local scale.

Factors influencing the results can be related to the lack of reliable information about filters and well depths, analytical uncertainties, to inherent errors of the flow model calibration process and of

the ground water age estimates, such as lack of data from a local GNIP station and the type of model used (total mixture, in this case). Another possible reason for the differences observed could to be related to the influence of pumping. Since the flow model did not consider pumping, the transit times calculated did not reflect this effect.

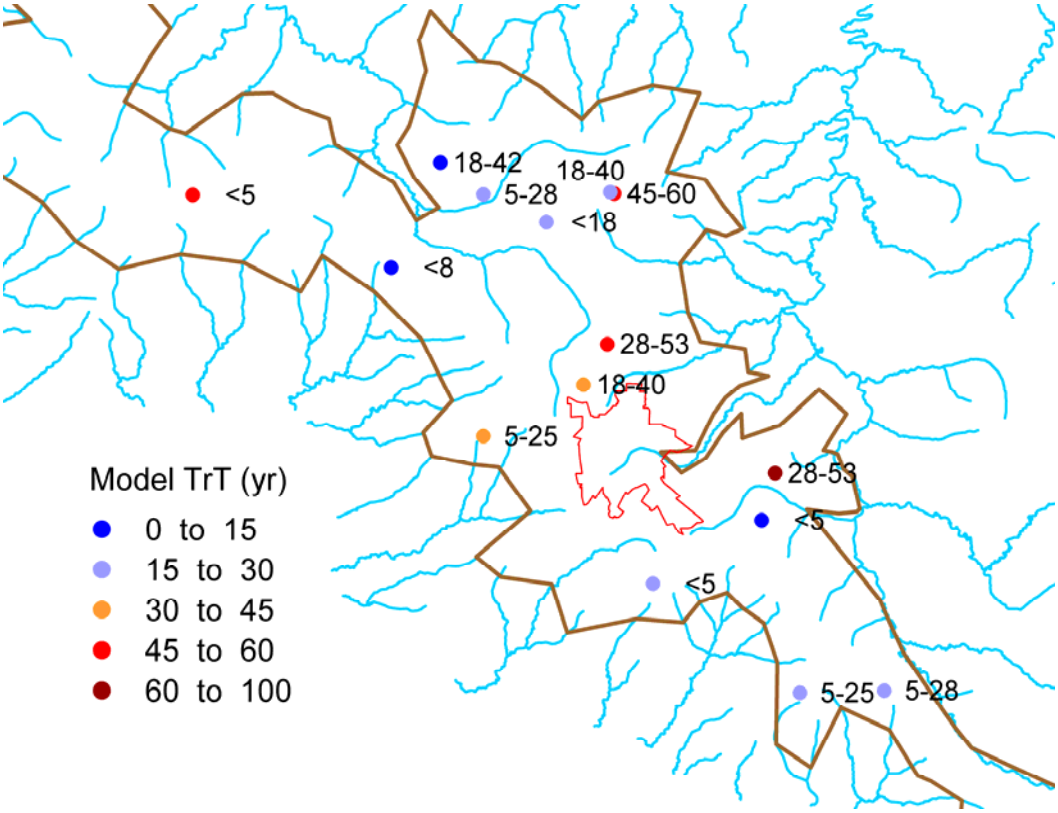

Figure 7. Comparison between transit times calculated by the mathematical model (Model TrT) and estimated by tritium concentrations (range indicated in the map).

CONCLUSIONS

The transit time calculated by the flow model for seven of the fifteen wells fell into the range of transit time estimated by tritium using the exponential model. For another six wells, the calculated transit times are greater than the upper limit of the range, although in the same order of magnitude.
As a result of the comparison of the methodologies, it is possible to verify that, for 14 of 15 wells, there was a reasonable agreement between the results yielded by both methods. It means that the results are perfectly acceptable, even for the case of hydrogeological study in a local scale.
In order to obtain more suitable results the authors consider to be mandatory an absolute control of the water entrance depths, the strata permeability, the pumping time to collect a homogeneous sample and a fairly good calibration of the flow model.

REFERENCES

1. Cota, S. , Carvalho Filho, C. A., Branco, O.E.A., Velásquez, L.N.M. Simulação matemática de fluxo de água subterrânea no aquífero Bauru no município de Araguari, MG. XVII Simpósio Brasileiro de Recursos Hídricos, 2007.
2. Izbicki, J.A., Stamos, C.L., Nishikawa, T., Martin, P. Comparison of ground-water flow model particle-tracking results and isotopic data in the Mojave River ground-water basin, southern California, USA. Journal of Hydrology, 292, pp. 30-47, 2004
3. McDonald, M. G., Harbaugh, W. A modular three-dimensional finite-difference ground-water flow model. Techniques of Water-Resources Investigation, Book6, chapter A1 USGS. Washington D.C, U.S.A., 576p., 1988.

4. UFMG (Universidade Federal de Minas Gerais); CDTN (Centro de Desenvolvimento da Tecnologia Nuclear), UFMT (Universidade Federal do Mato Grosso). Avaliação dos recursos hídricos do Sistema Aqüífero Guarani no município de Araguari, Minas Gerais, Brasil. Proyecto para la Protección Ambiental y Desarrollo Sostenible Del Sistema Acuífero Guaraní, Fondo de Universidades, SG/OEA, Informe Final, 2006.
5. Waterloo Hydrogeologic. Visual MODFLOW User's manual, versão 4.1.0, Waterloo, Canadá, 2005.

ACKNOWLEDGMENTS

The authors would like to express their gratitude to GEF/Fund of Universities for supporting the Araguari Project in the framework of Guarany Aquifer System Environmental Protection and Sustainable Development Project. The support of IAEA for the isotopic analyses of the water samples has also to be acknowledged. They are also indebted to the Municipality of Araguari and to SAE, the autonomous water and sewage supply company, for the use of their installations and all the administrative support to develop the fieldwork.

TRACER TECHNIQUES AS A CONTRIBUTION FOR STUDYING THE HYDROLOGICAL BEHAVIOR OF A SÃO FRANCISCO RIVER SUB-BASIN - PART I

Marcos Machado Drumond[20]; Paulo César Horta Rodrigues[21]; Cláudio Costa Camargos[22] and Paulo Sérgio Pelogia Minardi[23]

ABSTRACT

A research program that has been developed by CDTN/CNEN, since 1997, in order to study the hydrological behavior of a São Francisco river sub-basin is presented in this paper. This program involves a series of research projects which main objectives are to use tracer techniques, available in CDTN/CNEN, to increase the knowledge on the hydrological behavior of a typical basin of the Minas Gerais State central region as well as to improve, or to adapt, methodologies that, although developed in basins with different characteristics from the Brazilian basins, have been used in our country to quantify hydrological phenomena. A summary of three already developed research projects and their results are presented here. The paper was divided in three parts, one for each research project. In this first part, it is presented the project entitled "Application of Tracer Technique to Flood Studies in the Juatuba Representative Basin", which had as main objectives the determination, with the tracer technique, of the Time of Concentration and the Instantaneous Unit Hydrograph - basic parameter in flood studies - and to evaluate the empirical formulas used in Brazil to estimate these parameters.

1 – INTRODUCTION

The Nuclear Technology Development Center - CDTN/CNEN has been developed, since 1997, a Research Program entitled "Hydrologic Studies using Tracer Techniques in Juatuba Representative Basin". This program involves a series of research projects and has the following objectives: i) improving/adaptation of methodologies that, although developed in basins which have different characteristics from the Brazilian basins, are used in our country to quantify hydrological phenomena; ii) hydrological characterization of Juatuba river basin that is a experimental basin situated on the São Francisco river upstream region; and iii) diffusion of the tracer techniques which, although their great potential to accomplish hydrological studies, is not much used in Brazil yet.

Being a valuable tool to determine directly hydrological parameters and to calibrate and validate numerical models used in the simulation of the dynamics of surface waters, routings, times of residence, erosion and transport of sediments, the tracer techniques act an important role to improve the understanding of hydrological phenomena. Considering the lack of hydrological data and researches on Brazilian basins, mainly referring to small ones, this tool assumes an even bigger importance.

The object of study, Juatuba Representative Basin, has characteristics similar to other basins situated in a vast region in the center of Minas Gerais State (see Figure 1-A) and, for this reason, it was chosen by the Brazilian Government to represent these basins from the hydrological point of view. Therefore, the basin was equipped with a reasonable dense net of hydrometric stations that has been operated since the beginning of 80's and whose data consist in the better file of small basins information of Minas Gerais State. Thus, the results obtained with the research can be extended for other basins of the region where no data are available.

[20] **Researcher of the Nuclear Technology Development Center - CDTN/CNEN – Cidade Universitária – Pampulha – Caixa Postal 941 – 30123-970 – Belo Horizonte, MG – Brazil – Tel. 55 31 3069.3131 – E-mail: drumond@cdtn.br**

[21] **Idem – Tel. 55 31 3069.3126 – E-mail: pchr@cdtn.br**

[22] **Idem – Tel. 55 31 3069.3220 – E-mail: ccc@cdtn.br**

[23] **Idem – Tel. 55 31 3069.3219 – E-mail: pspm@cdtn.br**

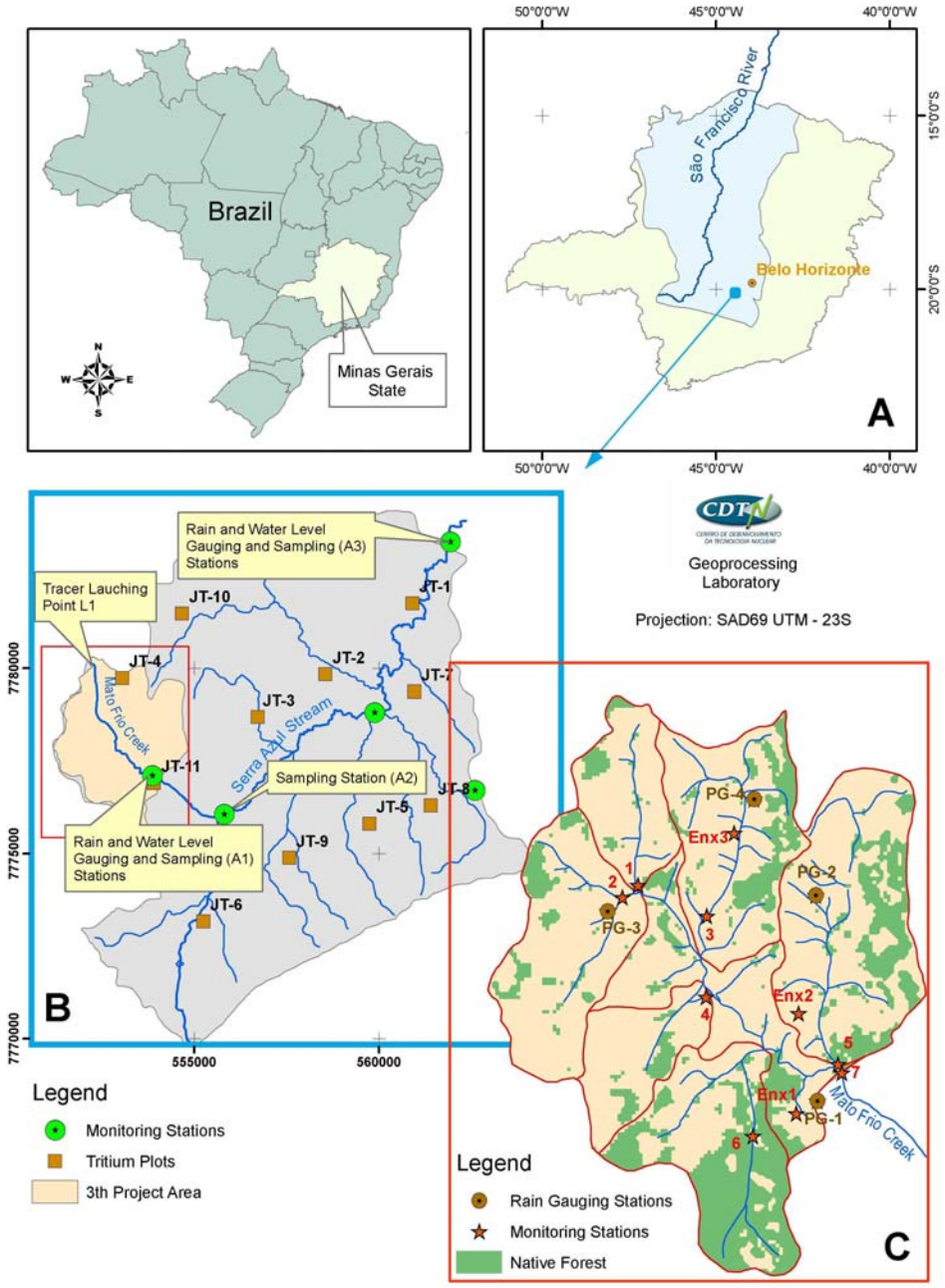

Figure 1 - Juatuba Representative Basin and the Study Area

Into that research program, which has a wider feature, three research projects with more specific objectives were developed. Two of them have counted on the support of the FAPEMIG - Research Support Foundation of Minas Gerais State and are already concluded. The first one, entitled "Application of Tracer Technique to Flood Studies in the Juatuba Representative Basin", began in August 1997 and was concluded in August 2000. The second one, entitled "Determination of Infiltration and Evapotranspiration Rates using Artificial Tritium in the Juatuba Representative Basin", began in November 1999 and was concluded in October 2003. The third research project, entitled "Study of the Runoff Formation using Natural Tracers in the Juatuba Representative Basin", supported by FINEP - Financier of Studies and Projects, began in March 2006 and its conclusion is foreseen for 2008. In this paper, divided in three parts, a synthesis of these research projects and a summary of their results are presented. In this Part I, it is presented the first project.

2 – FIRST RESEARCH PROJECT

As it is known, the stream peak discharge is a basic parameter in hydraulic projects and also to define safe quotas against flooding occurrences. Therefore, to determine this parameter it is necessary to use trustworthy methodologies which present results as next as possible to the reality since these results have implications to the population security as well to the economic costs of the projects. The increasing frequency of the flooding occurrences in the Brazilian cities and roads are not only an evidence of deficient urban planning but also of deficient draining projects. Indeed, this fact indicates the necessity of a revision and adaptation of the methodologies used in Brazil for forecasting the peak discharge, which were developed for other countries basins.
Considering this context, it was elaborated the project "Application of Tracer Technique to Flood Studies in the Representative Basin of Juatuba", which had the following objectives: i) to use the tracer technique to measure directly the Time of Concentration; ii) to verify the possibility of determining the Unit Hydrograph, based on the response of the basin to a tracer instantaneous injection; iii) to evaluate the empirical methods used in Brazil to estimate these basic parameters of the flood studies.

2.1 – Site description

The Juatuba river basin is situated about 50km on west direction from Belo Horizonte and is formed by the Serra Azul and Mateus Leme stream sub-basins. For carrying out the first research project, a parcel of the Serra Azul sub-basin situated upstream of the COPASA MG - Minas Gerais Sanitation Company reservoir (see Figure 1-B) was chosen. This parcel has a drainage area of about 110km^2 and is equipped with four rain gauge stations and two water-level gauge stations operated by ANA-Water National Agency since the 70's.

2.2 – The Time of Concentration determination

The time of concentration was measured using a methodology similar to that one used by Pilgrim (1966), that is, launching the tracer, during the occurrence of intense rain events, in the springs of the Serra Azul stream (point L_1 in Figure 1-B) and monitoring the tracer cloud passing, by collecting water samples with automatic samplers in three points situated downstream (points A_1, A_2 and A_3 in Figure 1-B). After analyzing the water samples in laboratory, the graphic "Tracer concentrations in the samples x Time" was constructed to enable the determination of the time of concentration, assuming that it is equal to the interval of time between the instant of the tracer launching and the instant of the passage of the tracer concentration peak (see Figure 2).

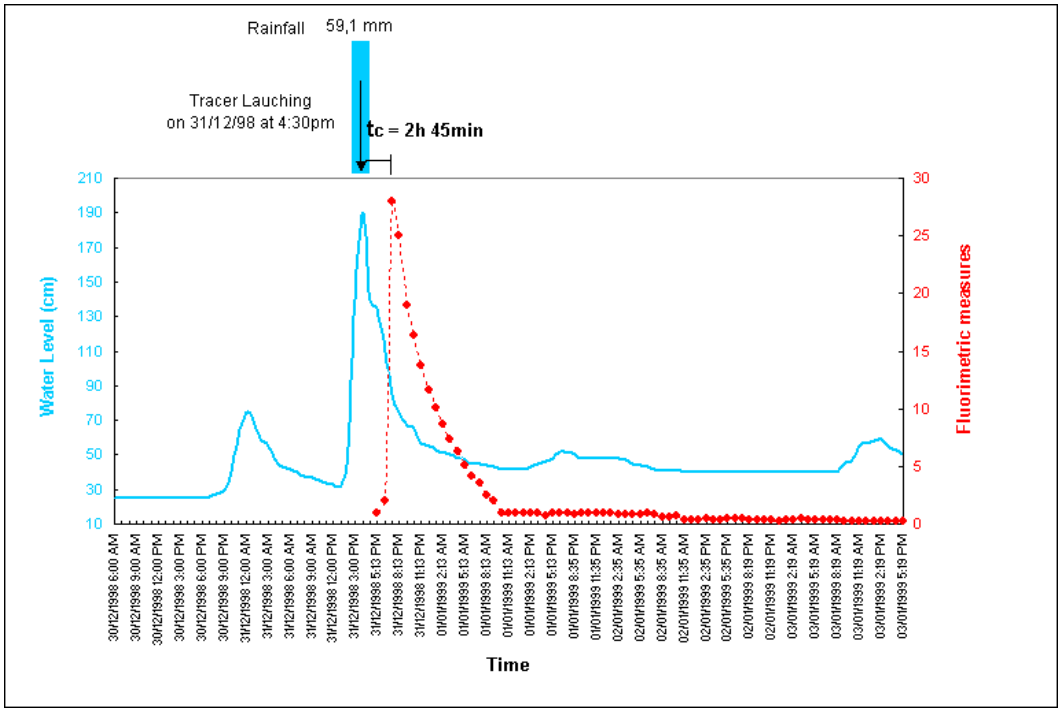

Figure 2 - Determination of the time of concentration in the sampling station A1

The chosen tracer to carry out the experiment was a fluorescent solution of Rhodamine WT 20%, which has the following advantages: easy handling, not toxic, can be detected by fluorimeters in very low concentrations (10 parts for trillion) and low adsorption capacity.
To solve the difficulty of foreseeing the intense rain occurrences, a local inhabitant, who knows very well the rain regime of the region, was contracted and instructed to make, during the occurrence of intense rain events, the tracer launching and to turn on the automatic samplers. After the collecting campaign is completed, he contacted the project team, who picked up the collected samples and brought them to CDTN laboratories to make the fluorimetric analyses.
As evidenced by Pilgrim (1966), the time of concentration decays with the flood discharge increasing and tends asymptotically for a constant value for the bigger discharges. Thus, 19 measuring campaigns were carried out during the period 1998-2002. The result obtained in each flood event was plotted against the respective peak discharge and, then, obtained the final value for the time of concentration at the three sampling stations.

2.3 – The Unit Hydrograph determination

According to Pilgrim (1966), the tracer concentration curve obtained after an instantaneous tracer injection has the same form of the Instantaneous Unit Hydrograph – IUH and, for this reason, it can be used to the determine the Unit Hydrograph, which is another important parameter in flood studies. To test this hypothesis, the tracer concentration curves obtained with the experiments, during the flood events close to the ideal conditions of the Unit Hydrograph Theory (Chow et al., 1988), were used. Based on these curves a unit hydrograph was established and, then, compared with another one established by Drumond (1994) for the Station A_3, based on 20 flood hydrographs selected among flood registers for a period of 10 years.
Initially, the tracer concentration curves were normalized by dividing the ordinates by the area under the curve to obtain the IUH's with ordinates in units of T^{-1}. These normalized graphics were settled with the coincident peaks and then an average IUH was calculated. Once this average IUH was established, the final unit hydrograph was determined by a convolution for the 2 hours unit period, which was the same used by Drumond (1994) for establishing the unit hydrograph based on the flood registers.

3 – RESULTS

Based on the results obtained in the experimental phase, it was possible: i) to determine directly the time of concentration; ii) to evaluate the performance of the main empirical formulas used in Brazil for estimating the time of concentration; iii) to establish the relation of the time of concentration with the lag-time for the study basin; and iv) to confirm the possibility of obtaining the instantaneous unit hydrograph by just one tracer launching during a flood occurrence.

As mentioned previously, the time concentration values obtained in the 19 measuring campaigns carried out in the period from 1998 to 2002 were plotted against the respective peak discharges and, then, the following final values for the time of concentration at the three sampling stations were found:

- Station A1 (draining area of 10,5 km^2): t_c = 1,8 hours;
- Station A2 (draining area of 32 km^2): t_c = 3,5 hours;
- Station A3 (draining area of 110 km^2): t_c = 15,5 hours.

In order to evaluate the performance of the empirical formulas normally used to estimate the time of concentration, three of them – Kirpich, Soil Conservation Service and Ventura – were chosen to establish a comparison with the values obtained by means of the experiments for the stations A_1 and A_3, which were equipped with gauging stations. The two first formulas were chosen because they are frequently used by Brazilian hydrologists and the third one because it has presented good results in another study carried out in the Juatuba basin (Drumond, 1994). The results obtained with these three formulas as well the comparison with the values obtained with the tracer technique are presented in Table 1.

Table 1 - Comparison of the times of concentration obtained with empirical formulas and with the tracer experiments

	Station A_1	Error*	Station A_3	Error*
Tracer	1.8 h		15.5 h	
Kirpich	0.9 h	- 50%	5.0 h	- 68%
SCS	3.9 h	+ 117%	36.0 h	+ 132%
Ventura	2.7 h	+ 50%	17.2 h	+ 11%

* Error = (Formula value - Tracer value) / Formula value

As it can be observed, the Kirpich formula would underestimate the time of concentration values, while the Soil Conservation Soil formula would overestimate them considerably. So, among the three formulas, only the Ventura formula gives, for the station A_3, a value of the time of concentration next to that one obtained with the tracer technique.

Another parameter that is very used in flood studies is the Lag-Time (t_L), defined as the interval of time between the center of mass of the rain event and the discharge peak. This parameter is used, for example, in the Soil Conservation Service method for establishing a synthetic unit hydrograph of the basin. According to SCS, the lag-time is equal to 60% of time of concentration ($t_L = 0{,}6\ t_C$). For the purpose of verifying this relationship in the study basin, the lag-times of the flood events registered during the time of concentration measurements were determined based on the available rainfall and water-level registers. The mean values obtained for this coefficient were 0,51, for Station A_1, and 0,66, for Station A_3. It has to be noted that they are not so different from that one of the SCS.

In order to compare the unit hydrograph obtained with the tracer technique and the unit hydrograph obtained in 1994, this one was also normalized and then compared as shown in Figure 3.

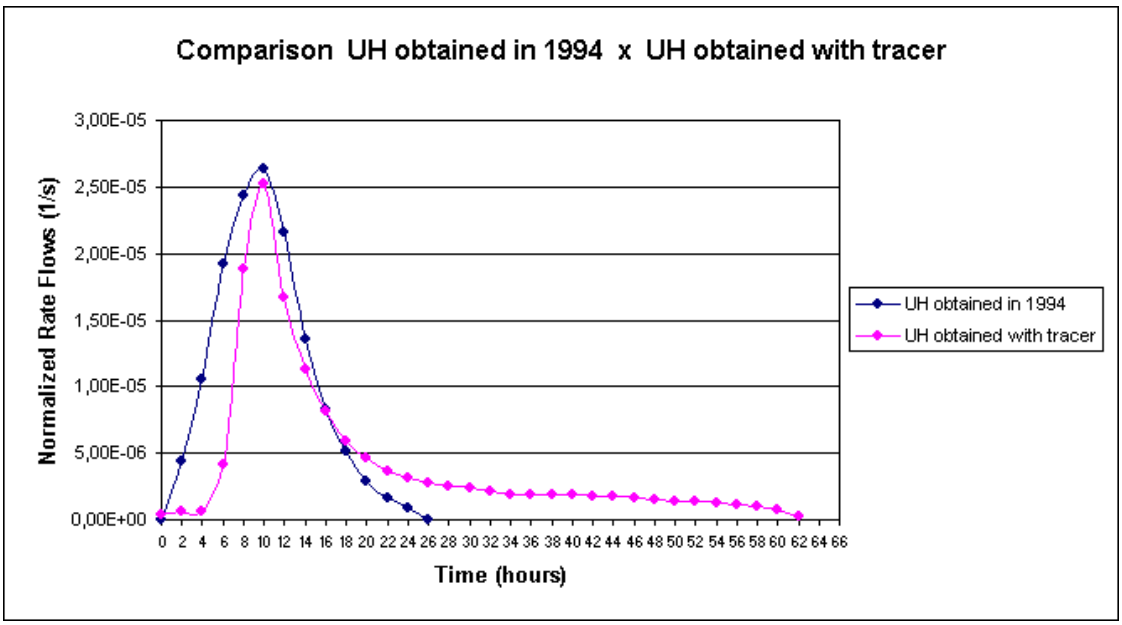

Figure 3 - Comparison of unit hydrographs obtained with hydrologic data and with the tracer technique

As it can be observed, the unit hydrograph established with the tracer experiments comes close to that one established with hydrological data. This indicates that the tracer concentration curve obtained with tracer instantaneous injections can really be used to define the unit hydrographs of the basin. The obtained results therefore indicate that the tracer technique can be used not only to determine the time of concentration but also to establish unit hydrographs in a relatively simple and direct way.

4 – CONCLUSIONS

The obtained results show not only the potential of the tracer technique for measuring directly parameters as the time of concentration and the unit hydrograph, very important in flood studies, but also the errors that can be committed when one uses here methodologies developed in basins with different characteristics from the Brazilians ones.

It should be mentioned also that the results obtained with the tracer techniques were also very useful for calibrating and validating numerical models, which are another important tool for studying hydrological phenomena.

ACKNOWLEDGEMENTS

The authors express their gratitude for the valuable team of the Juatuba Project, especially: to the Engineers Andréa Barbalho, Antônio Fioravante Neto, Elenísio Fonseca, Geraldo Godinho Pinto, Lécio H. Salim, Maria Léa Machado; to the Geologist Walter de Brito; to the Technicians Duarte Costa, Francisco Carvalhaes, Namir Vieira, Raquel Mingote, Zilmar Lula; and to the Drivers Augusto Lúcio, Antônio Queiroz and Geraldo Braga, of the CDTN/CNEN; to the Scholarship holders Amanda Barsante, Ana Luiza Cunha, Ettore Brescia, Gustavo Amaral, Guillerme Heleno, Ívina Andrade, João Paulo Garofilo, José Roberto Cabral, Leandro Silva, Lígia Faria, Lorena Costa, Priscila Moura, Rossana Vasconcellos, Silvani Oliveira, and Rafaella Teixeira; and to the field observers Otávio Custódio Borges and Ana Maria Q. Borges; whose contribution was, and continues being, essential for the accomplishment of the work.

The authors manifest, also, their sincere gratefulness to FAPEMIG - Research Support Foundation of Minas Gerais State, to the FINEP - Financier of Studies and Projects, to the COPASA - Minas Gerais Sanitation Company, to ANA - Waters National Agency and to CPRM - Mineral Resources Research Company, for the support given to the research projects; and to the UFMG Engineering School Professors Dr. Bruno Versiani, Dr. Márcio Baptista, Dr. Nilo Nascimento, Dr. Mônica Leão and Dr. Terezinha Galvão, for their contribution to the work.

REFERENCES

CHOW, V. T.; MAIDMENT, D. R.; MAYS, L. W. (1988) “Applied hydrology”. New York: McGraw-Hill,. 572 p.

DRUMOND, M.M. (1994) “Análise comparativa de metodologias para o estudo de vazões de enchentes: Determinação e sintetização de hidrogramas unitários na bacia representativa de Juatuba – MG”. Dissertação (Mestrado em Saneamento e Meio Ambiente) - Escola de Engenharia, Universidade Federal de Minas Gerais, Belo Horizonte, 115 p.

PILGRIM D.H. (1966) “Radioactive tracing of storm runoff on small catchment, I e II. Experimental Technique and Discussion of Results”. Journal of Hydrology, v.4. p. 289-326.

TRACER TECHNIQUES AS A CONTRIBUTION FOR STUDYING THE HYDROLOGICAL BEHAVIOR OF A SÃO FRANCISCO RIVER SUB-BASIN - PART II

Marcos Machado Drumond[24]; Paulo César Horta Rodrigues[25]; Cláudio Costa Camargos[26] and Paulo Sérgio Pelogia Minardi[27]

ABSTRACT

A research program that has been developed by CDTN/CNEN, since 1997, in order to study the hydrological behavior of a São Francisco river sub-basin is presented in this paper. This program involves a series of research projects which main objectives are to use tracer techniques, available in CDTN/CNEN, to increase the knowledge on the hydrological behavior of a typical basin of the Minas Gerais State central region as well as to improve, or to adapt, methodologies that, although developed in basins with different characteristics from the Brazilian basins, have been used in our country to quantify hydrological phenomena. A summary of three already developed research projects and their results are presented here. The paper was divided in three parts, one for each research project. In this second part, it is presented the project entitled "Determination of Infiltration and Evapotranspiration Rates using Artificial Tritium in the Juatuba Representative Basin", which had the following objectives: i) to measure directly the infiltration rates using a tracer method; ii) to establish, based on the results of the rain, runoff and infiltration direct measurements, a water balance and, then, to estimate the real evapotranspiration of the study basin; and iii) to evaluate the performance of the indirect methods used in Brazil to estimate the real evapotranspiration.

1 – INTRODUCTION

The Nuclear Technology Development Center - CDTN/CNEN has been developed, since 1997, a Research Program entitled "Hydrologic Studies using Tracer Techniques in Juatuba Representative Basin". This program involves a series of research projects and has the following objectives: i) the improving/adaptation of methodologies that, although developed in basins which have different characteristics from the Brazilian basins, are used in our country to quantify hydrological phenomena; ii) the hydrological characterization of Juatuba river basin that is a experimental basin situated on the São Francisco river upstream region; iii) the diffusion of the tracer techniques which, although their great potential to accomplish hydrological studies, is not much used in Brazil yet.

Being a valuable tool to determine directly hydrological parameters and to calibrate and validate numerical models used in the simulation of the dynamics of surface waters, routings, times of residence, erosion and transport of sediments, the tracer techniques act an important role to improve the understanding of hydrological phenomena. Considering the lack of hydrological data and researches on Brazilian basins, mainly referring to small ones, this tool assumes an even bigger importance.

The object of study, Juatuba Representative Basin, has characteristics similar to other basins situated in a vast region in the center of Minas Gerais State (see Figure 1-A) and, for this reason, it was chosen by the Brazilian Government to represent those basins from the hydrological point of view. Therefore, the basin was equipped with a reasonable dense net of hydrometric stations that has been operated since the beginning of 80's and whose data consist in the better file of small basins information of Minas Gerais State. Thus, the results obtained with the research can be extended for other basins of the region where no data are available.

[24] **Researcher of the Nuclear Technology Development Center - CDTN/CNEN – Cidade Universitária – Pampulha – Caixa Postal 941 – 30123-970 – Belo Horizonte, MG – Brazil – Tel. 55 31 3069.3131 – E-mail: drumond@cdtn.br**

[25] **Idem – Tel. 55 31 3069.3126 – E-mail: pchr@cdtn.br**

[26] **Idem – Tel. 55 31 3069.3220 – E-mail: ccc@cdtn.br**

[27] **Idem – Tel. 55 31 3069.3219 – E-mail: pspm@cdtn.br**

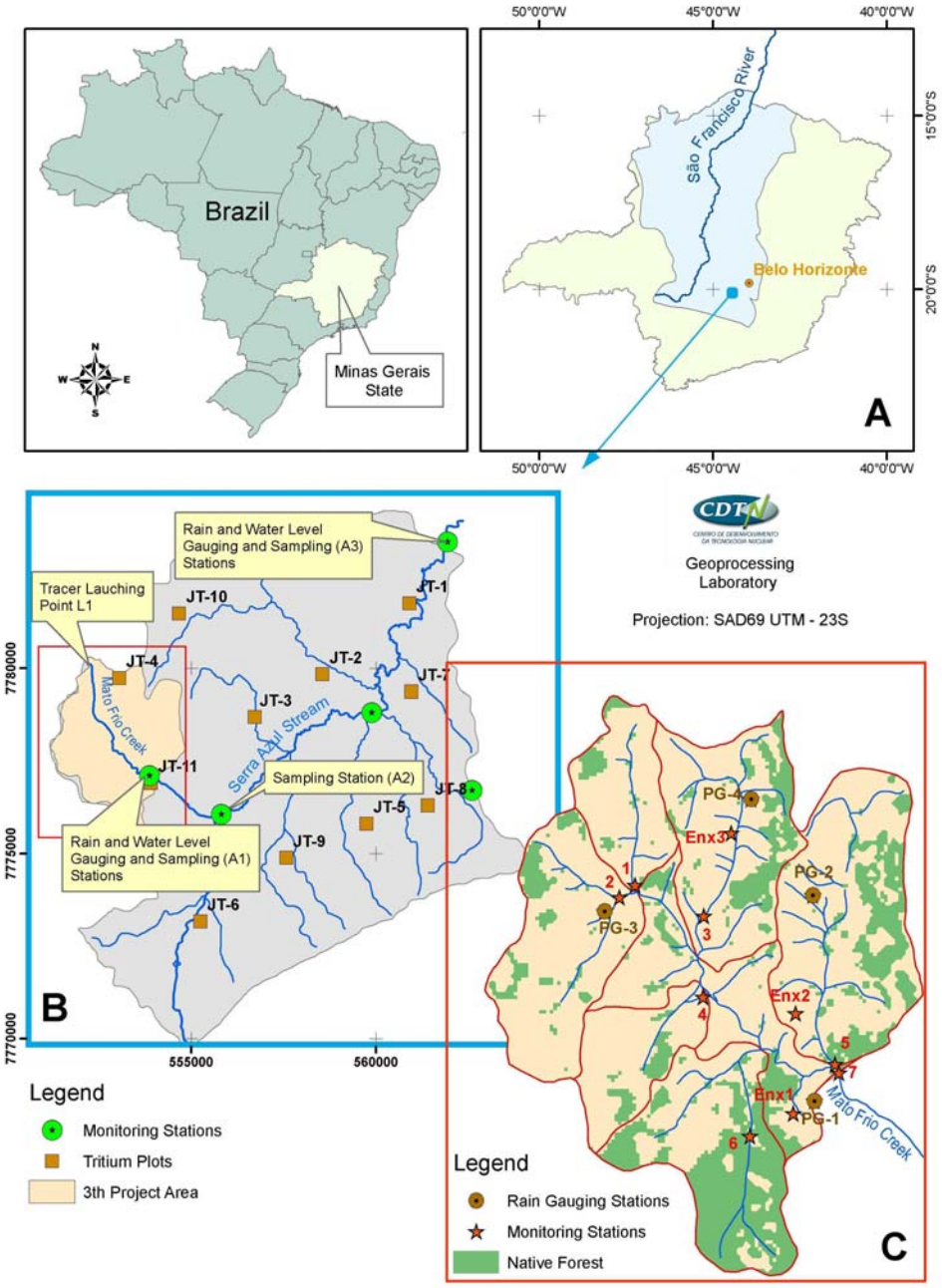

Figure 1 - Juatuba Representative Basin and the Studying Area

Into that research program, which has a wider feature, three research projects with more specific objectives were developed. Two of them have counted on the support of the FAPEMIG - Research Support Foundation of Minas Gerais State and are already concluded. The first one, entitled "Application of Tracer Technique to Flood Studies in the Juatuba Representative Basin", began in August 1997 and was concluded in August 2000. The second one, entitled "Determination of Infiltration and Evapotranspiration Rates using Artificial Tritium in the Juatuba Representative Basin", began in November 1999 and was concluded in October 2003. The third research project, entitled "Study of the Runoff Formation using Natural Tracers in the Juatuba Representative Basin", supported by FINEP - Financier of Studies and Projects, began in March 2006 and its conclusion is foreseen for 2008. In this paper, divided in three parts, a synthesis of these research projects and a summary of their results are presented. In this Part II, the second project is presented.

2 – SECOND RESEARCH PROJECT

The Infiltration and Evapotranspiration Rates are fundamentals to estimate hydrological parameters such as the groundwater reservoir recharges and the effective precipitation, that is, the excess rainfall used in flood studies. Despite their importance, these parameters, as well as the concentration time, have been estimated in Brazil indirectly, using only empirical formulas which were developed for other countries basins.

Considering this fact, it was created the second research project, "Determination of Infiltration and Evapotranspiration Rates using Artificial Tritium in the Representative Basin of Juatuba", that had the following objectives: i) to measure directly the infiltration rates using a tracer method; ii) to estimate the real evapotranspiration on the study basin based on a water balance established with the results of the direct measurements of the rain, runoff and infiltration rates; and iii) to evaluate the performance of the indirect methods used in Brazil to estimate the Real Evapotranspiration.

2.1 – Site description

The Juatuba river basin is situated about 50km on west direction from Belo Horizonte and is formed by the Serra Azul and Mateus Leme stream sub-basins. For carrying out the second research project the same area of the first one was chosen, that is, a parcel of the Serra Azul sub-basin situated upstream of the COPASA MG - Minas Gerais Sanitation Company reservoir (see Figure 1-B). This parcel has a drainage area of about 110km^2 and is equipped with four rain gauge stations and two water-level gauge stations operated by ANA-Water National Agency since the 70's.

2.2 – The Infiltration Rate determination

The methodology used to determine the infiltration rates was similar to that one adopted by Araguás-Araguás et al. (1995) in a study carried out in the Amazon basin and also used by CDTN in a study developed in the Montes Claros region (CDTN, 1996). Initially, eleven 3m x 6m plots, which represent the different physiographic characteristics of the basin, were chosen (see these plots sites in the Figure 1-B).

Over each plot it was sprinkled the tracer solution, that is, 1mCi of tritium diluted in 50 liters of tracer-free water (see Figure 2). Subsequently, about 400 liters of tracer-free water were added, in order to push down the labeled layer and reduce the loss of tracer due to evaporation. The tritium launchings took place in November 1999 (plots JT-1, 2, 3, 5 and 6) and November 2001 (plots JT-4, 7, 8, 9, 10 and 11), in the beginning of rainy period, in order to monitor the infiltration processes during two complete hydrologic years. For monitoring the labeled layer displacement into the unsaturated zone, five soil cores collecting campaigns were carried out, using a motorized auger (Figure 2), in the following periods of time: two days, one month, three months, six months and one year after the tritium launchings.

Figure 2 - Tracer launching and soil cores collecting with a motorized auger

The soil cores were taken in each 15cm depth layer, in predetermined points in the interior of the plots. After collecting, the soil cores were weighed in loco and conditioned in flasks to determine

later, in the CDTN laboratories, the tritium concentrations and the soil moisture. The results of the tritium analyses were plotted and, then, determined the positions of the tracer cloud (see Figure 3), as well the water content in the layer above of the labeled layer.
Assuming a piston-like flow, the labeled layer acts like a boundary between the old soil moisture and the fresh incoming water contributed by precipitation and can not be by-passed in the vertical direction (Saxena, 1995). Thus, the soil moisture volume above the labeled layer can be assumed as being the parcel of the rain that infiltrated less the evapotranspiration losses.

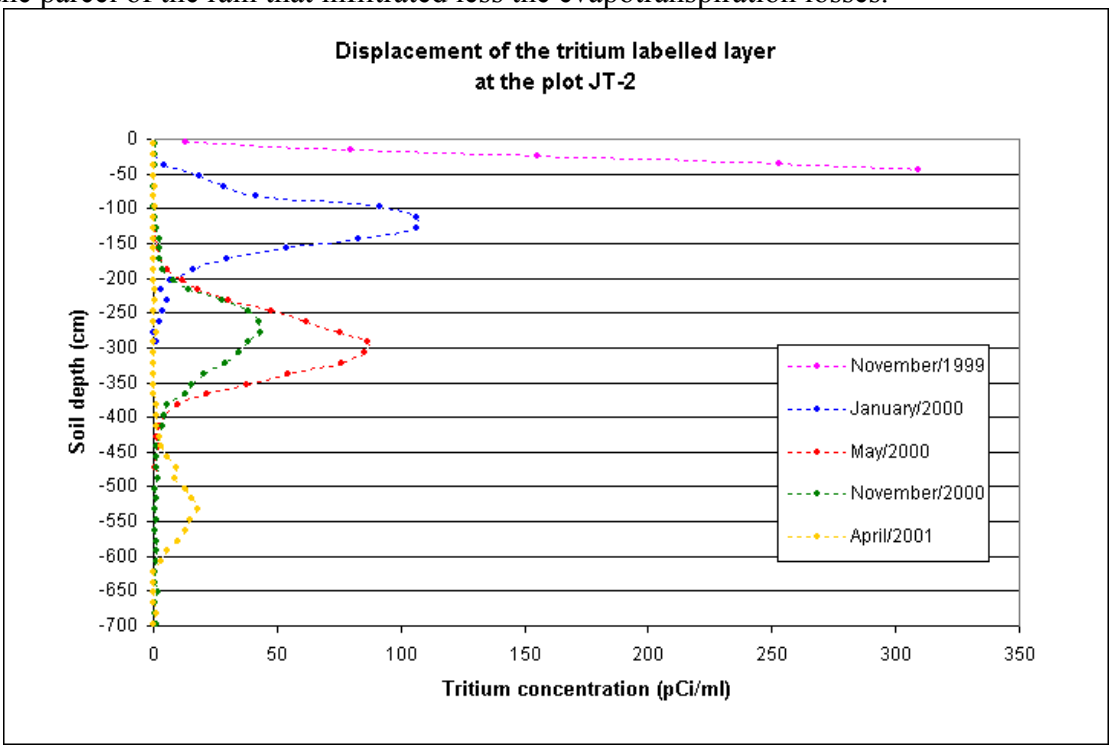

Figure 3 - Displacement of the labeled layer from Nov/1999 to Apr/2001 at the plot JT-2

2.3 – The Real Evapotranspiration estimation

Based on the infiltration results obtained with the tracer experiments for the 1999-2000 and 2001-2002 hydrologic years and on the rain and surface runoff data obtained, for the same period, from the gauging stations existing in the basin, a water balance was established in order to calculate the evapotranspiration losses.
Once this water balance was done, it was possible to calculate the annual real evapotranspiration for the study basin as a whole and to evaluate the performance of the main indirect methods used in Brazil to estimate the real evapotranspiration.

3 –RESULTS

In Table 1, it is presented a summary of the results obtained with the tracer experiments carried out to determine the infiltration rates as well the precipitation, at each plot, for the 1999-2000 and 2001-2002 hydrologic years.
It should be noted that the results obtained in the plots JT-1 and JT-11 were not satisfactory due to the existence of a gravel layer in the soil that drained laterally the labeled water, hindering its vertical displacement.

Table 1 - Summary of the results obtained with the infiltration experiments

Hydrologic Year 1999-2000			
Plot	Precipitation Height (mm)	Infiltration Height (mm)	% Infiltrated
JT 1	1600.5	-	-
JT 2	1650.7	693.3	42.0%
JT 3	1613.8	496.9	30.8%
JT 5	1679.8	638.9	38.0%
JT 6	1632.5	497.4	30.5%
	Weighed mean =	601.0	36.3%
Hydrologic Year 2001-2002			
Plot	Precipitation Height (mm)	Infiltration Height (mm)	% Infiltrated
JT 4	1446.5	567.1	39.2%
JT 7	1294.2	434.9	33.6%
JT 8	1452.7	685.3	47.2%
JT 9	1421.7	370.3	26.0%
JT 10	1386.6	602.2	43.4%
JT 11	1442.7	174.3	12.1%
	Weighed mean =	531.6	38.3%

In order to evaluate the infiltration height in the basin as a whole, it was calculated a weighed mean of the obtained infiltration results for each period. The weighed means were calculated considering the soil and vegetal cover characteristics of the plots and the areas occupied by these characteristics in relation to the basin total area.

The occupied areas for each soil and vegetal cover type and their respective percentages were obtained based on the classification of satellite images, GIS resources available in CDTN, cartographic and bibliographical information and observations made during field trips. The obtained mean infiltrated heights were then: 601.0mm, for the hydrologic year 1999-2000, and 531.6mm, for 2001-2002.

Based on these results and on the mean precipitation heights (1650.5mm, for the period of 1999-2000, and 1403.8mm, for 2001-2002) and the superficial runoff heights (98.0mm, for 1999-2000, and 83.3mm, for 2001-2002), obtained with the gauging stations data, it has established a water balance to estimate the real evapotranspiration in the study basin. The following equation was used for that:

$$EVT_R = PPT - (INF + RNF_{SUP}) \quad (1)$$

where EVT_R is the annual real evapotranspiration height, in mm; PPT is the annual precipitation height, in mm; INF is annual infiltration height, in mm; and RNF_{SUP} is the annual superficial runoff height, in mm.

Thus, the obtained real evapotranspiration heights were: 951.5mm (57.6% of the total precipitation), for the hydrological year 1999-2000, and 788.9mm (56.2% of the total precipitation), for 2001-2002.

To establish a comparison of these values with those results which would be obtained if the indirect methodologies used in Brazil were adopted, it was calculated the real evapotranspiration with another water balance based only on the Potential Evapotranspiration calculated with Penman-Monteith, Thornthwaite, Blaney-Criddle and Hargreaves empirical formulas. The results obtained with this methodology and the values calculated with the first water balance are presented in Table 2.

Table 2 - Comparison of the real evapotranspiration heights obtained with the tracer experiment and with the indirect methodology

	Experiment	Penman-Monteith	Thornthwaite	Blaney-Criddle	Hargreaves
1999 – 2000	951.5mm	858.6mm	826.5mm	1143.2mm	429.7mm
2001 – 2002	788.9mm	803.0mm	798.0mm	1017.5mm	460.8mm

As it can be observed, the indirect methodology gave reasonable results of the real evapotranspiration only when it was used the Penman-Monteith and the Thornthwaite formulas, for the period of 2001-2002. If the Blaney-Criddle formula were adopted, the value of the real evapotranspiration would be overestimated up to 29% (for the period 2001-2002); and, if the Hargreaves formula were adopted, it would occur the opposite, that is, the value of the real evapotranspiration would be underestimated up to 55% (for the period 1999-2000).

Another indirect methodology frequently used to estimate the real evapotranspiration is based on evaporation pan data. Usually, the evaporation pan Class A data and an empirical coefficient are adopted to calculate the real evapotranspiration. According to FAO - Food and Agriculture Organization the recommended coefficient for basins with the same Juatuba Representative Basin characteristics is 0.85 (Allen et al., 1998). However, the obtained values for this coefficient, based on the real evapotranspiration determined with the experiments and on the values registered in evaporation pan Class A existing in the basin, were 0.61, for the period 1999-2000, and 0.52, for the period 2001-2002.

4 – CONCLUSIONS

The obtained results show not only the potential of the tracer technique for measuring hydrological parameters such as the infiltration and evapotranspiration rates but evidence also the errors that can be committed when methodologies developed for basins with different characteristics from the Brazilian ones are used.

It should be mentioned that the results obtained with the tracer techniques were also used for calibrating and validating hydrological simulating models, which are another important tool for studying hydrological phenomena.

ACKNOWLEDGEMENTS

The authors express their gratitude for the valuable team of the Juatuba Project, especially: to the Engineers Andréa Barbalho, Antônio Fioravante Neto, Elenísio Fonseca, Geraldo Godinho Pinto, Lécio H. Salim, Maria Léa Machado; to the Geologist Walter de Brito; to the Technicians Duarte Costa, Francisco Carvalhaes, Namir Vieira, Raquel Mingote, Zilmar Lula; and to the Drivers Augusto Lúcio, Antônio Queiroz and Geraldo Braga, of the CDTN/CNEN; to the Scholarship holders Amanda Barsante, Ana Luiza Cunha, Ettore Brescia, Gustavo Amaral, Guillerme Heleno, Ívina Andrade, João Paulo Garofilo, José Roberto Cabral, Leandro Silva, Lígia Faria, Lorena Costa, Priscila Moura, Rossana Vasconcellos, Silvani Oliveira, and Rafaella Teixeira; and to the field observers Otávio Custódio Borges and Ana Maria Q. Borges; whose contribution was, and continues being, essential for the accomplishment of the work.

The authors manifest, also, their sincere gratefulness to FAPEMIG - Research Support Foundation of Minas Gerais State, to the FINEP - Financier of Studies and Projects, to the COPASA - Minas Gerais Sanitation Company, to ANA - Waters National Agency and to CPRM - Mineral Resources Research Company, for the support given to the research projects; and to the UFMG Engineering School Professors Dr. Bruno Versiani, Dr. Márcio Baptista, Dr. Nilo Nascimento, Dr. Mônica Leão and Dr. Terezinha Galvão, for their contribution to the work.

REFERENCES

1. ARAGUÁS-ARAGUÁS, L. ROZANSKI, K.; BEDMAR, A.P.; VITAL, A.R.T.; TANCREDI, A.C.; FRANKEN, W. (1995). "Changes of soil water balance due to forest clearing in the central Amazon region" in Proceeding of the XXVI Congress of the IAH. Solutions'95. Managing the effects of man's activities on groundwater. (Ed.IAH) IAH, Edmonton, 1-6.
2. CNEN/CDTN, (1996) "Characterization of karstic basins in a semi-arid region", Proj. de Coop. Técnica CDTN/AIEA-BRA/8/024, Belo Horizonte.
3. SAXENA, R. K. (1995) "Use of a mechanistic model to simulate soil moisture and tritiated water transport in a wheat field" in Proceedings of the International Symposium on Isotopes in Water Resources Management. Vienna, Austria: IAEA.

TRACER TECHNIQUES AS A CONTRIBUTION FOR STUDYING THE HYDROLOGICAL BEHAVIOR OF A SÃO FRANCISCO RIVER SUB-BASIN - PART III

Marcos Machado Drumond[28]; Paulo César Horta Rodrigues[29]; Cláudio Costa Camargos[30] and Paulo Sérgio Pelogia Minardi[31]

ABSTRACT

A research program that has been developed by CDTN/CNEN, since 1997, in order to study the hydrological behavior of a São Francisco river sub-basin is presented in this paper. This program involves a series of research projects which main objectives are to use tracer techniques, available in CDTN/CNEN, to increase the knowledge on the hydrological behavior of a typical basin of Minas Gerais State central region as well as to improve, or to adapt, methodologies that, although developed in basins with different characteristics from the Brazilian basins, have been used in our country to quantify hydrological phenomena. A summary of three already developed research projects and their results are presented here. The paper was divided in three parts, one for each research project. In this third and last part, it is presented the project entitled "Study of the Runoff Formation using Natural Tracers in the Juatuba Representative Basin", which has the following objectives: i) to test the methodology that uses the tracer technique to separate the surface and groundwater runoff parcels of flood hydrographs; ii) to test the use of natural tracers, as electric conductance and isotopes (^{18}O and ^{2}H), to make the runoff separation; and iii) to establish a comparison between the results obtained with this methodology and the results that would be obtained by the graphical methods.

1 – INTRODUCTION

The Nuclear Technology Development Center - CDTN/CNEN has been developed, since 1997, a Research Program entitled "Hydrologic Studies using Tracer Techniques in Juatuba Representative Basin". This program involves a series of research projects and has the following objectives: i) the improving/adaptation of methodologies that, although developed in basins which have different characteristics from the Brazilian basins, are used in our country to quantify hydrological phenomena; ii) the hydrological characterization of Juatuba river basin that is a experimental basin situated on the São Francisco river upstream region; iii) the diffusion of the tracer techniques which, although their great potential to accomplish hydrological studies, is not much used in Brazil yet.

Being a valuable tool to determine directly hydrological parameters and to calibrate and validate numerical models used in the simulation of the dynamics of surface waters, water paths, times of residence, erosion and transport of sediments, the tracer techniques act an important role to improve the understanding of hydrological phenomena. Considering the lack of hydrological data and researches on Brazilian basins, mainly referring to small ones, this tool assumes an even bigger importance.

The object of study, Juatuba Representative Basin, has characteristics similar to other basins situated in a vast region in the center of Minas Gerais State (see Figure 1-A) and, for this reason, it was chosen by the Brazilian Government to represent these basins from the hydrological point of view. Therefore, the basin was equipped with a reasonable dense net of hydrometric stations that has been operated since the beginning of 80's and whose data consist in the better file of small basins information of Minas Gerais State. Thus, the results obtained with the research can be extended for other basins of the region where no data are available.

[28] **Researcher of the Nuclear Technology Development Center - CDTN/CNEN – Cidade Universitária – Pampulha – Caixa Postal 941 – 30123-970 – Belo Horizonte, MG – Brazil – Tel. 55 31 3069.3131 – E-mail: drumond@cdtn.br**

[29] **Idem – Tel. 55 31 3069.3126 – E-mail: pchr@cdtn.br**

[30] **Idem – Tel. 55 31 3069.3220 – E-mail: ccc@cdtn.br**

[31] **Idem – Tel. 55 31 3069.3219 – E-mail: pspm@cdtn.br**

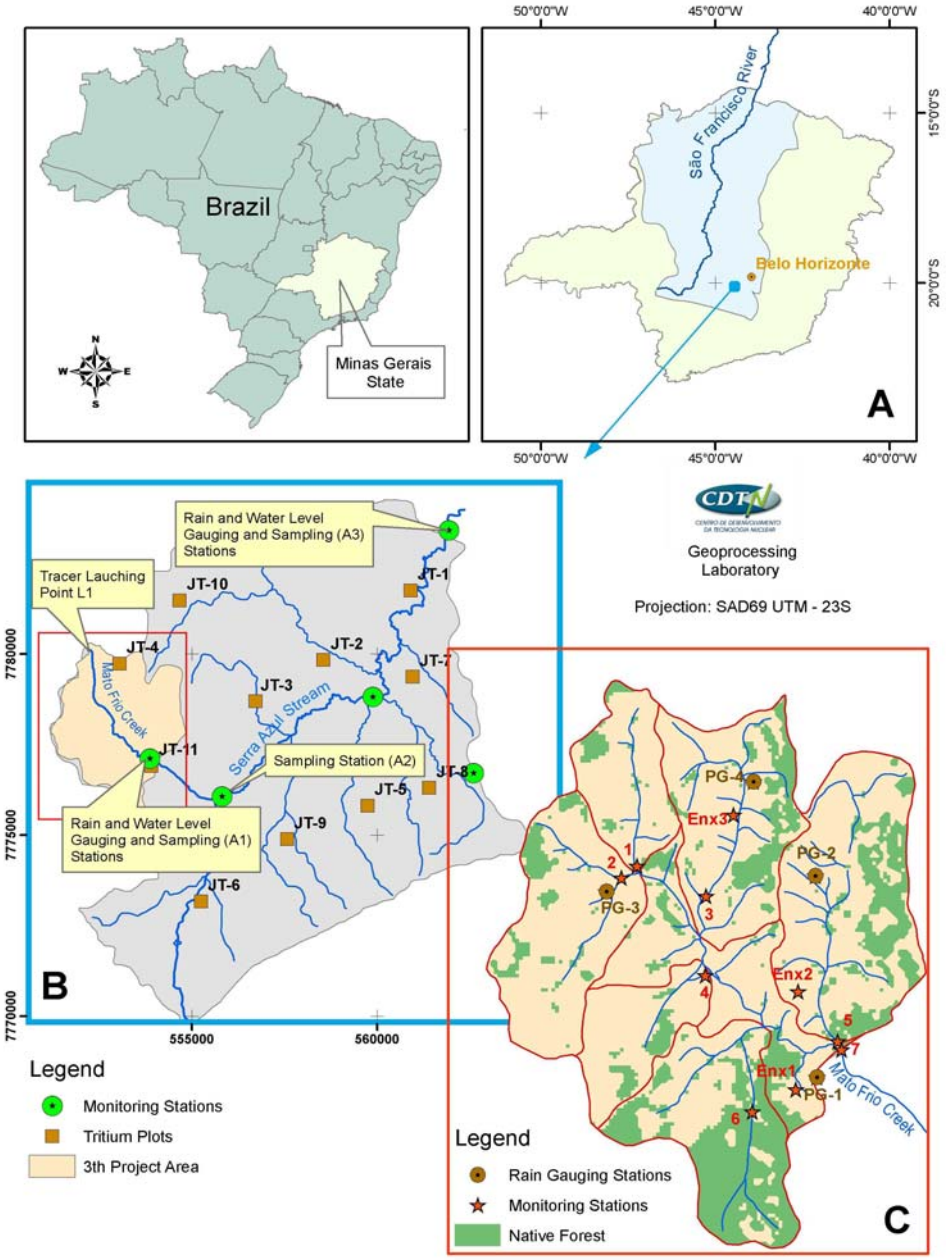

Figure 1 - Juatuba Representative Basin and the Studying Area

Into that research program, which has a wider feature, three research projects with more specific objectives were developed. Two of them have counted on the support of the FAPEMIG - Research Support Foundation of Minas Gerais State and are already concluded. The first one, entitled "Application of Tracer Technique to Flood Studies in the Juatuba Representative Basin", began in August 1997 and was concluded in August 2000. The second one, entitled "Determination of Infiltration and Evapotranspiration Rates using Artificial Tritium in the Juatuba Representative Basin", began in November 1999 and was concluded in October 2003. The third research project, entitled "Study of the Runoff Formation using Natural Tracers in the Juatuba Representative Basin", supported by FINEP - Financier of Studies and Projects, began in March 2006 and its conclusion is foreseen for 2008. In this paper, divided in three parts, a synthesis of these research projects and a summary of their results are presented. In this Part III, it is presented the third project.

2 – THIRD RESEARCH PROJECT

In respect of flood studies, one of the main difficulties that hydrologists have to deal with is quantifying the surface and groundwater runoff parcels of the flood hydrographs. The involved processes in the runoff generation are, even today, a controversial matter and have been object of study in the main international research centers. In view of this, it was created the third research project, "Study of the Runoff Formation using Natural Tracers in the Representative Basin of Juatuba", which is still in progress.

The main objectives of this third project are: i) to test the methodology that uses the tracer technique to make the separation of the surface and groundwater runoff parcels of flood hydrographs; ii) to test the use of natural tracers, such as electric conductance and isotopes (^{18}O and ^{2}H), to make the runoff separations; iii) to establish a comparison between the results obtained with this methodology and those results that would be obtained by the graphical method, generally used in Brazil; and iv) to implant a monitoring stations net at the Serra Azul springs and, based on the data obtained there, to establish a comparison between the hydrological behavior of a sub-basin still covered by native forest and the behavior of other small adjacent sub-basins, whose vegetal cover is already degraded by the anthropic action.

2.1 – Site description

To carry out this third research project it was chosen a parcel of the Mato Frio creek sub-basin which is situated at the Serra Azul springs and has a drainage area of about 10,5km^2. In order to evaluate the influence of the soil and vegetal cover characteristics as well the anthropic action on the flood formation, the study area was sub-divided in six sub-areas according to its main six streams (see Figure 1-C). Their respective draining areas vary from 0.8km^2 to 2.3km^2. It may be noted that one of these sub-areas (Station 6) is almost entirely covered by the native forest. So, it will be possible to compare the hydrological behavior of a preserved area with the adjacent areas which have suffered the anthropic action.

2.2 – The Hydrograph Separation using the tracer technique

The use of the tracer technique for identify the runoff origin is already well established (Pilgrim et al., 1979; Eshleman et al., 1993 and Matsubayashi et al., 1993). The method is based on the fact that, during a storm, the flow rate is constituted by a part of the rain that flows rapidly, generally over the surface, and by a infiltrated part that flows slowly. The faster part is normally identified as "superficial runoff" and the slower one as "groundwater runoff". These two parts have distinct chemical characteristics and, for this reason, they can be identified in the Nature. The parcel of the rain that flows superficially evaporates more and, besides this, has a small time of contact with the soil, incorporating less salts. Meanwhile, the infiltrated parcel evaporates less and, flowing slowly, incorporates more salts available in the soil. Thus, the superficial runoff have, generally, bigger isotope concentration and lesser salt concentrations while, with groundwater runoff, it occurs the inverse. The differences of concentration of these substances present in waters, theoretically, can be used to quantify the two parcels of the flood hydrographs, by solving simultaneously the continuity and mass balance equations, that is:

$$Q_T(t) = Q_{Sup}(t) + Q_{Grw}(t) \tag{1}$$

$$Q_T(t).C_T(t) = Q_{Sup}(t).C_{Sup}(t) + Q_{Grw}(t).C_{Grw}(t) \tag{2}$$

where Q is the runoff, C is the tracer concentration in the waters, and the indices T, Sup and Grw indicate, respectively, Total, Superficial and Groundwater.

Considering that the isotope analyses are relatively expensive and that the electric conductance had shown a good potential to be used as tracer in preliminary tests in the study basin and, besides this, it can be easily determined, it was adopted primarily to carry out the study. To verify the validity of

the results obtained with the electric conductance, tests using the isotopes ^{18}O and ^{2}H as tracer, in some flood events, were also planned.

So, in order to register the flow rate and electric conductance variations in the streams, seven monitoring stations were established. In the six sub-areas it was installed a weir, to measure flow rates, as well as a probe equipped with a datalogger and three sensors, for continuous registering the water level, electrical conductance and temperature variations (see the localization of the Stations in Figure 1-C). At the basin outfall, where it previously had a level water gauge station operated by ANA – Water National Agency, a water level, electrical conductance and temperature probe was also installed (Station 7). In order to measure the variations of the superficial runoff, three stations equipped with electrical conductance and temperature probe were additionally established (Stations Enx.1,2and3).

In order to register the rainfall events, three rain gauge stations were installed in the study area (Stations PG-2, 3 and 4). Besides these stations it has been also used another one located near the basin outfall which has been operated by ANA since the 70's (Station PG-1). In Figure 2, it can be observed more details of some of these stations.

Station 5

Station 6

Station Enx. 2

Station PG 2

Figure 2 - Details of some of the monitoring stations used in the third project

The data have been downloaded monthly, with a portable computer, and then processed in the office. The monitoring stations have been operated since October 2006 and will be operated, at least, until the end of rainy period 2008-2009. During the 2006-2007 and 2007-2008 rainy periods, 26 flood events were recorded. The respective flood hydrographs were registered and have been used to make the runoff separation with the tracer technique. Some of the obtained results are presented in the following item.

3 –RESULTS

In order to give an example of the already obtained results of the hydrograph separation with the tracer technique, it was selected one of the greatest observed floods in the period that occurred on 25/12/2006 and was caused by a 70mm height and 50min duration rainfall.
In Figure 3, the flood hydrographs as well the electrical conductance registers and the hydrograph separations for the sub-basins 2 and 5 are presented (the superficial runoff in green and the groundwater runoff in brown color).

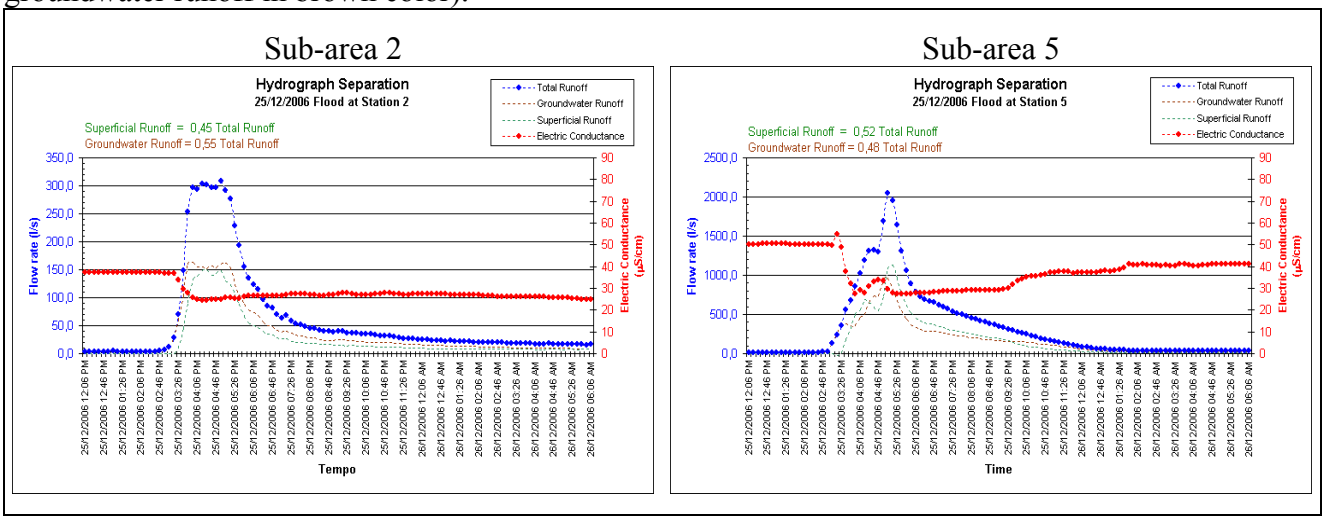

Figure 3 – Hydrograph separation of the 25/12/2006 flood

It may be observed that it was registered an electrical conductance increasing on the flood beginning for the station 5. It is due probably to the first precipitated waters which may have leached the available salt on the ground surface. Nevertheless, it does not occurred on the station 2 due, probably, to the dilution of this initial runoff by a reservoir existing upstream of the station.
In Table 1 it is presented a comparison of the runoff separation with the tracer technique results and those ones which would be obtained with the conventional graphical method.

Table 1 – Parcels of superficial and groundwater runoff on the 25/12/06 flood hydrographs

Method	Station 2		Station 5	
	Superficial.	Groundwater	Superficial	Groundwater
Tracer	45%	55%	52%	48%
Conventional	82%	13%	90%	10%

As it can be noted, the groundwater runoff results obtained with the tracer technique are considerably higher than the usual values for the small draining area basins, where, according to the Hortonian hypothesis, the superficial runoff contribution is usually bigger than the groundwater runoff. Nevertheless, these results coincide in magnitude with the results obtained by other authors (e.g.: Matsubayashi et al., 1993 and Eshleman et al., 1993). Thus, in spite of its preliminary character, the obtained results indicate that the groundwater runoff can have a contribution to the flood formation more significant than usually considered and, in this case, its response to precipitation events may be faster than it is supposed.

4 – CONCLUSIONS

The obtained results with the Juatuba Representative Basin researches have demonstrated not only the potential of the tracer techniques to study the hydrological processes which occur in the basin scale and to determine directly basic hydrological parameters (e.g., time of concentration, unit hydrographs, infiltration and evapotranspiration rates, runoff origin, among others), but also

demonstrated the errors that can be committed when one uses here methodologies developed in basins with different characteristics from the Brazilians ones.
Finally, it has to be mentioned that the results obtained with the tracer techniques were also used to calibrate and to validate numerical models, which are another important tool for studying hydrological phenomena.

ACKNOWLEDGEMENTS

The authors express their gratitude for the valuable team of the Juatuba Project, especially: to the Engineers Andréa Barbalho, Antônio Fioravante Neto, Elenísio Fonseca, Geraldo Godinho Pinto, Lécio H. Salim, Maria Léa Machado; to the Geologist Walter de Brito; to the Technicians Duarte Costa, Francisco Carvalhaes, Namir Vieira, Raquel Mingote, Zilmar Lula; and to the Drivers Augusto Lúcio, Antônio Queiroz and Geraldo Braga, of the CDTN/CNEN; to the Scholarship holders Amanda Barsante, Ana Luiza Cunha, Ettore Brescia, Gustavo Amaral, Guillerme Heleno, Ívina Andrade, João Paulo Garofilo, José Roberto Cabral, Leandro Silva, Lígia Faria, Lorena Costa, Priscila Moura, Rossana Vasconcellos, Silvani Oliveira, and Rafaella Teixeira; and to the field observers Otávio Custódio Borges and Ana Maria Q. Borges; whose contribution was, and continues being, essential for the accomplishment of the work.
The authors manifest, also, their sincere gratefulness to FAPEMIG - Research Support Foundation of Minas Gerais State, to the FINEP - Financier of Studies and Projects, to the COPASA - Minas Gerais Sanitation Company, to ANA - Waters National Agency and to CPRM - Mineral Resources Research Company, for the support given to the research projects; and to the UFMG Engineering School Professors Dr. Bruno Versiani, Dr. Márcio Baptista, Dr. Nilo Nascimento, Dr. Mônica Leão and Dr. Terezinha Galvão, for their contribution to the work.

REFERENCES

1. ALLEN, R.G.; PEREIRA, L.S.; RAES, D. e SMITH, M. (1998) “Crop evapotranspiration – guidelines for computing water requirements”. Rome: FAO Irrigation and Drainage paper, 56. FAO – Food and Agriculture Organization of United Nation, 300 p.
2. ESHLEMAN, K.N., POLLARD, J.S. e O’BRIEN, A. K. (1993) “Determination of contributing areas for saturation overland flow from chemical hydrograph separations”. Water Resouces Research, Vol 29, n.10, pp. 3577-3587.
3. MATSUBAYASHI, U., VELASQUEZ, G.T. e TAKAGI, F. (1993) “Hydrograph separation and flow analysis by especifc electrical conductance of water”. Journal of Hydrology, 152, pp.179-199.
4. PILGRIM D.H., HUFF, D.D., e STEELE, T.D. (1979) “Use of specific conductance and contact time relations for separating flow components in storm runoff ”. Water Resouces Research, Vol 15, pp. 329-339.

USE OF TERRESTRIAL EPIPHYTIC COMMUNITY TO BIOMONITOR OF ATMOSPHERIC POLLUTION AT STEEL VALLEY REGION, MINAS GERAIS STATE, BRAZIL

Maria Adelaide R. V. Veado[1], Alex A. F. da Costa[1], Millôr G. Sabará[2]
Maria Ângela de B. C. Menezes[2], Gabriela F. Lopes[1]
[1] University Center of Minas Gerais East, Av. Presidente Tancredo de Almeida Neves, 3500, CEP 35170-056, Coronel Fabriciano, Brazil.
mariavasc@unilestemg.br, mgsabara@unilestemg.br
[2] Center of Nuclear Technology Development – Brazilian National Comission of Nuclear Energy, Av. Presidente Antônio Carlos, 6.627, CEP 31270-901, Belo Horizonte, Brazil.
menezes@cdtn.br

ABSTRACT

This work was carried out for verification of the presence of inorganic contamination in atmospheric pollution through a biomonitor of metals in industrial area pollution, Steel Valley region, Minas Gerais State, Brazil. The studied cities have been: Ipatinga; Fabriciano Colonel; Timóteo; Santana do Paraíso e Marliéria. Terrestrial epiphytic community, Sphagnum sp., samples have been used as a biomonitor. The samples were collected in trees Oiti (Licania tomentosa) and Angico (Piptadenia rígida), very common in studied region. The results indicate high concentrations of the elements Al, Au, Co, Cr, Cu, Fe, Hg, Mn, Mg, Cr, Zn, V and Th when compared with the values cited in the literature. The biomonitor, terrestrial epiphytic community, showed an excellent capacity for metals retention by atmospheric contamination.
Key words: NAA, biomonitor, terrestrial epiphytic community, metals, atmospheric pollution.

1. INTRODUCTION

The "Vale do Aço" (literally Steel Valley) represents one of Brazil's most outstanding smelting resources. The Steel Valley is located between two confluent rivers (Piracicaba and Doce), which constitute, by their tributary streams, the water supply of its half a million inhabitants. Ore smelting may well be harmful to people causing slow but chronic poisoning. This region is home to the largest steel making complex in Latin America. Three of the five largest companies in Minas Gerais state, "Companhia Siderúrgica Belgo Mineira", "Arcellor Mittal" and "USIMINAS", are located there. Furthermore, we can find the largest open-pit mine in the world operated by the "Companhia Vale do Rio Doce". These industrial conglomerates have an important role in Brazilian exports of iron ore, steel, and cellulose (Cenibra). Metal smelting is considered one of the most important anthropogenic sources of heavy metal pollution to the environment worldwide [1, 2]. This has been attributed to emissions from both smelter stacks and dispersive sources such as stockpiles and waste heaps [3]. Metal is transferred to environmental compartments, such as air; river water, sediment, and fish. It can also eventually enter the human body through the food chain or direct ingestion, which will pose a threat to human health. Many studies have reported high levels of Al, As, Fe, Cr, Co, Hg, Zn, Cu, Sb, Th and U in environmental samples in hydrographic basins and lakes in Brazil [4, 5, 6, 7, 8].

2. MATERIAL AND METHOD

The biomonitor, terrestrial epiphytic community, Sphagnum sp., samples, has been collected in the surrounding areas of the main industries in the cities of Ipatinga, Timóteo, Coronel Fabriciano, Santana do Paraíso and Marliéria, as illustrated in the figures 1. In the City of Marliéria the samples has been collected in the State Park of the Doce River, PERD, area of ambient preservation, distant of the urban centers of approximately 20 km. The terrestrial epiphytic community samples has been collected in trees Oiti (Licania tomentosa) and Angico (Piptadenia rígida), very common in studied region, see figure 2. The samples were collected in 17 points and two season: summer - January

(rainy) and winter - June (dry) of 2007. The samples has been removed of the trees trunks in a height of approximately 1,80 m, collected in 5,0 cm^2 using a stainless steel spatula. A surgical glove was used for to prevent contamination. After the samples has been conditioned in polystyrene bottles and stored at 4º C. In Laboratory they has been opened, washed with bidistilled water, dried at 40 °C, triturated and aliquot a representative one of approx. 0,30 g has been weighed for the analyses.

2.1 Neutron Activation Analysis – NAA

In this work the NAA was applied using the TRIGA MARK I IPR – R1 reactor at the Nuclear Technology Development Center of the National Council of Nuclear Energy (CDTN/CNEN), in Belo Horizonte, capital, Minas Gerais State, Brazil. At 100 kW the flux of neutrons is 6.6 10^{11} n. cm^{-2}. s^{-1}. The irradiation and measuring conditions were chosen as a function of the samples analyzed and the elements determined. The scheme used for analysis was: Short half-lives – $T_{1/2}$: 5 minutes of irradiation; Waiting time: 2 - 20 minutes (Al, Cl, Cu, V); Waiting time - 1 hour (Mn); Middle half-lives and Long half-lives - $T_{1/2}$: 8 hours of irradiation; Waiting time: 24 hours (As, Au, Br, K, Na, Mo, Sb, U); Waiting time: 10 days (Ba, Co, Cr, Cs, Fe, La, Rb, Sc, Sr, Zn, Th).

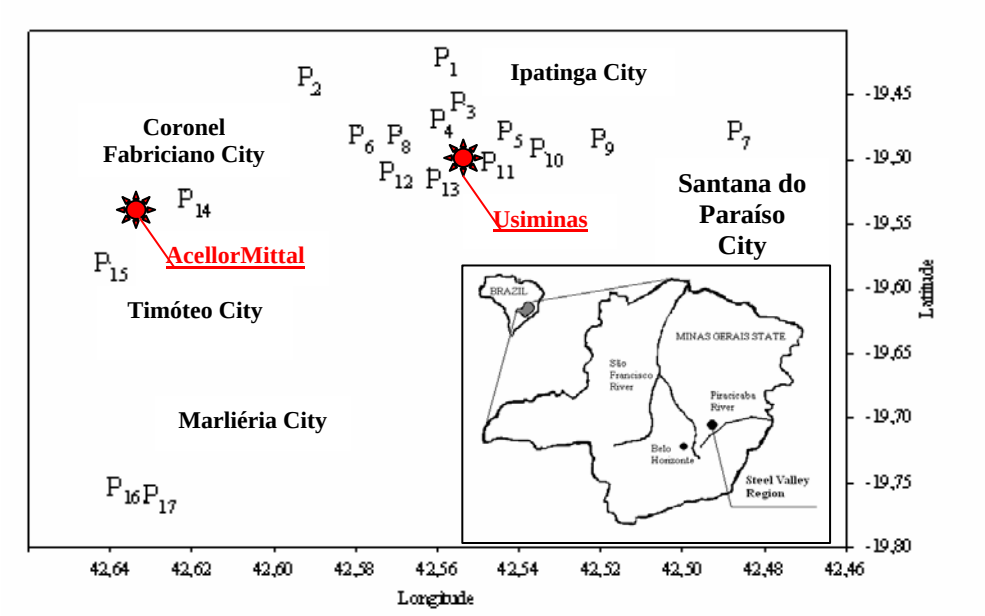
P1
Ipatinga City
P2
P3
P4
P5
P6
P8
P9
P10
P11
P12
P13
P7
Coronel
Fabriciano City
P14
AcellorMittal
P15
Timóteo City
Usiminas
Santana do
Paraíso
City
Marliéria City
P16 P17
BRAZIL
MINAS GERAIS STATE
São
Francisco
River
Piracicaba
River
Belo
Horizonte
Steel Valley
Region
-19,45
-19,50
-19,55
-19,60
-19,65
-19,70
-19,75
-19,80
Latitude
42,64
42,62
42,60
42,58
42,56
42,54
42,52
42,50
42,48
42,46
Longitude


P1
IPATINGA CITY
P2
P3
P4
P6
P8
P5
P9
P7
CORONEL
FABRICIANO
CITY
USIMINAS
P12
P10
P11
P13
P14
SANTANA
DO
PARAÍSO
CITY
ACELOR
MITTAL
TIMÓTEO
CITY
P15
DOCE RIVER
STATE PARK
MARLIÉRIA
CITY
P16
P17
Image



The gamma radioactivity was measured with a 100 cm^3 coaxial ultra-pure germanium crystal detector coupled to a 4096 pulse-height. The "Canberra" Gennie 2000 software was used to analyse the spectra. Gold monitors were used for short irradiations and Sodium monitors for long irradiations. The concentrations were calculated using K0LABSUE software, written in Turbo adapted to the conditions of both the nuclear reactor and the radiochemistry laboratory in CDTN/CNEN [9].

3. RESULTS AND DISCUSSION

The average results are showed in Table 1. Samples collected in the Piedade Mountain (1751 m), located in the Caeté city, at a distance of 100 km, had been analysed to compare with the results obtained in this work. Results of recent papers [10, 11, 12, 13] had been also used to compare. The figures 1 to 16 show the results of Al, As, Co, Cu, Fe, Hg and Th in the rainy and dry season 2007. The results indicate high concentrations of the elements Al, Au, Co, Cr, Cu, Fe, Hg, Mn, Mg, Cr, Zn, V and Th when compared with the normal values cited in the literature. The results show high concentrations for Al, Co, Cr, Cu, Fe and Th in dry seasons, June 2007. The biomonitor used in this work, has showed a excellent capacity for metals retention by atmospheric contamination and a good biomonitor will can indicate the presence of the pollutant and also attempt to provide additional information about the amount and intensity of the exposure. For Al, Fe and Th, the results indicate an increase of the concentrations in the dry station (approximately 3 times more) and high concentrations in all sampling sites. Hg concentration increase in P12 (Ipatinga City – Near the Usiminas). In P17 in the rainy season the Hg the high concentration is in (Marliéria City) in the dry season, we can relate these results with the predominant wind direction an region. For the elements Co, Cr, Cu, Fe, Mn, V, Ti and Zn we can attributed the atmospheric pollution at the local industries.

Table 1. The average results obtained in biomonitor samples (n=6 and $\sigma \sim 5\%$), $\mu g.g^{-1}$.

	Stell Valley (average)	Serra da Piedade, Caeté*	Áustria [10]	Italy [11]	WHO [12]	ATSDR [13]
Al	3048 - 95113	1400	394	-	218	50-200
As	0.41 - 6.15	0.43	0.15	-	1	5-20
Co	0.37 - 12.25	0.27	0.27	-	49	15-50
Cr	2 - 493	11	0.99	1.9	17 - 76	5-30
Cu	7 - 99	-	-	5.4	141	20-100
Fe	2407 - 73500	3300	503	-	-	>1000
	Stell Valley (average)	Serra da Piedade, Caeté*	Áustria [10]	Italy [11]	WHO [12]	ATSDR [13]
Hg	0.45 - 6.83	0.14	0.049	-	3	1-3
Mn	150 - 2160	139	-	-	-	300-500
Th	1 - 33	0.25	-	-	-	-
Ti	109 - 4206	45	-	-	-	-
V	3 - 71	2	1.14	3.6	203	5-10
Zn	96 - 523	85	33.2	25	73	100-400

* Piedade Mountain (1751 m).

4. CONCLUSION

The multi-elementary analysis technique NAA was applied to determine the major and trace elements concentrations and to clearly shown the contamination by metals in biomonitor samples from industrial area in Steel Valley region. This pollution is credited to the tons of waste without treatment poured into air from several industries. The biomonitor used in this work, has showed a excellent capacity for metals retention by atmospheric contamination.

ACKNOWLEDGEMENTS

This work was supported by CNPq, UNILESTEMG and FAPEMIG. The analyses were carried out at the Center of Nuclear Technology Development – National Committee of Nuclear Energy, in Belo Horizonte city, Minas Gerais State, Brazil.

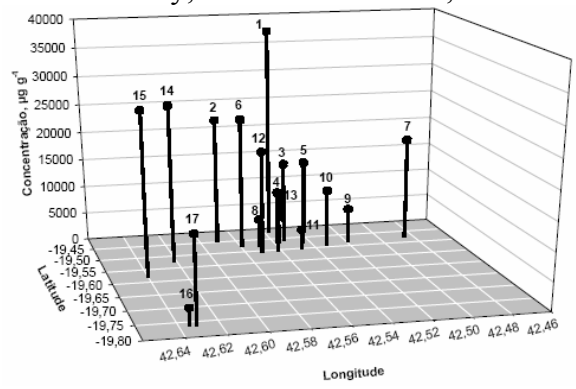

Fig. 1. Results of Al, January 2007.

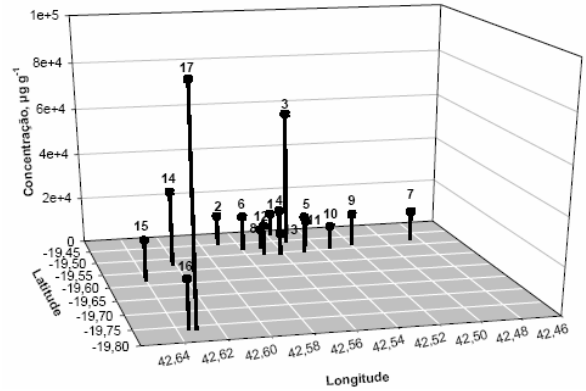

Fig. 2. Results of Al, June 2007.

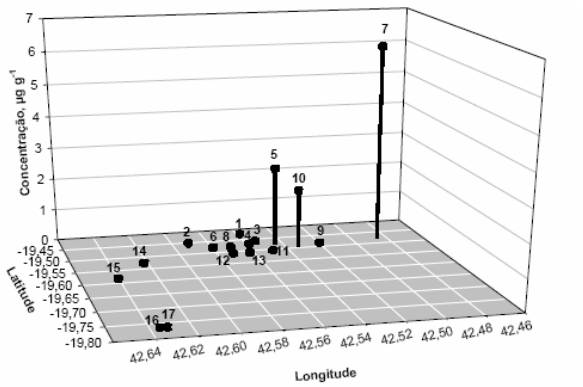

Fig. 3. Results of As, January 2007.

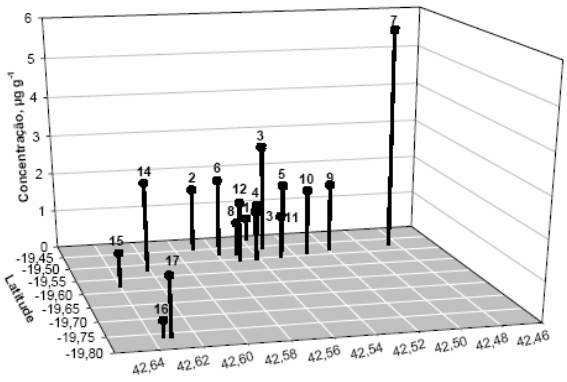

Fig. 4. Results of As, June 2007.

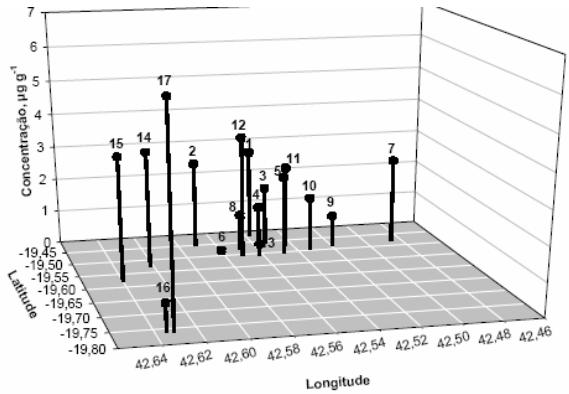

Fig. 5. Results of Co, January 2007.

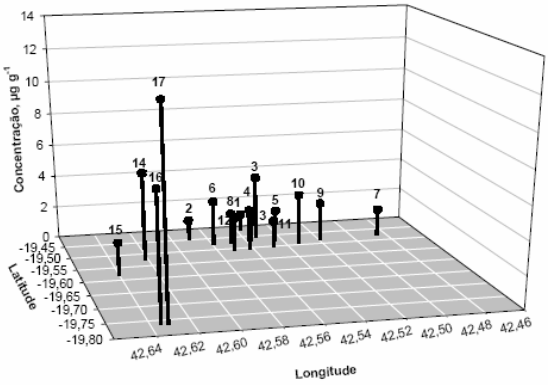

Fig. 6. Results of Co, June 2007.

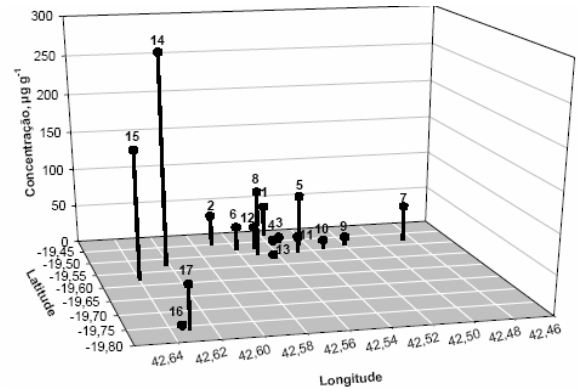

Fig. 7. Results of Cr, January 2007.

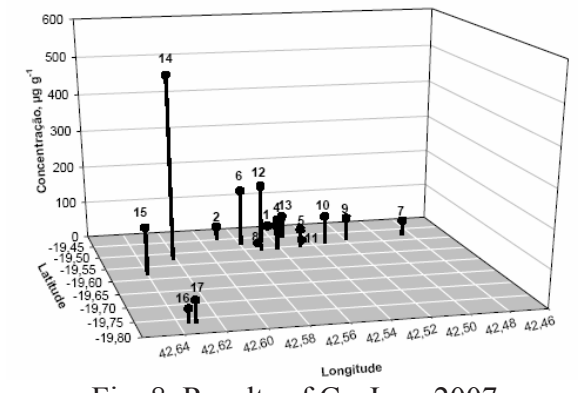

Fig. 8. Results of Cr, June 2007.

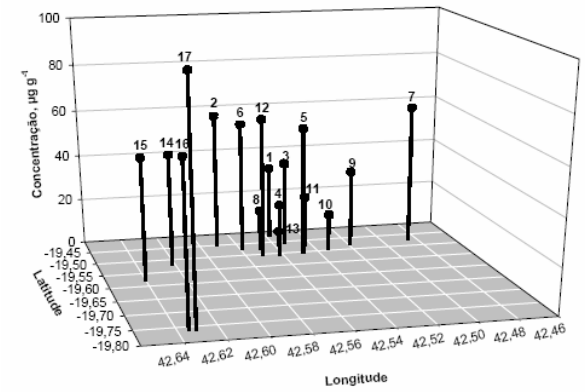

Fig. 9. Results of Cu, January 2007.

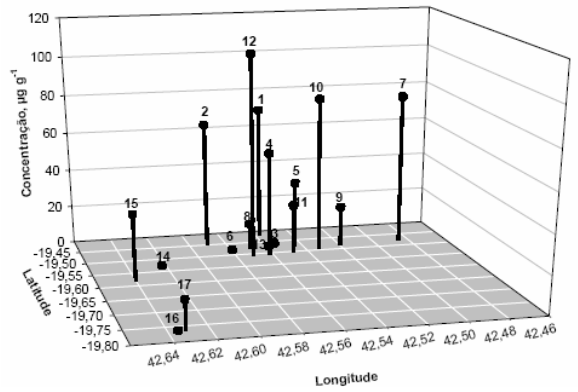

Fig. 10. Results of Cu, June 2007.

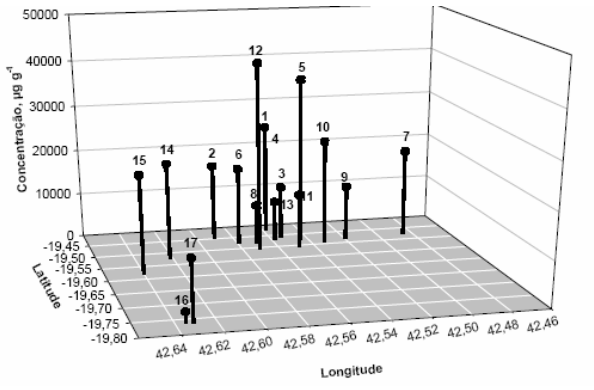

Fig. 11. Results of Fe, January 2007.

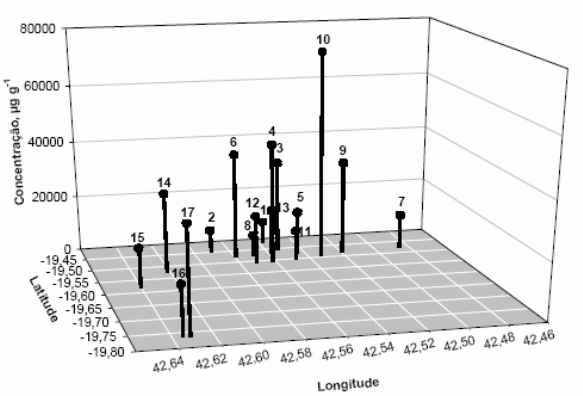

Fig. 12. Results of Fe, June 2007.

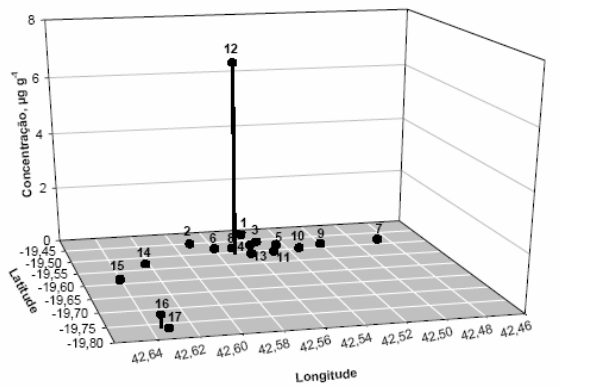

Fig. 13. Results of Hg, January 2007.

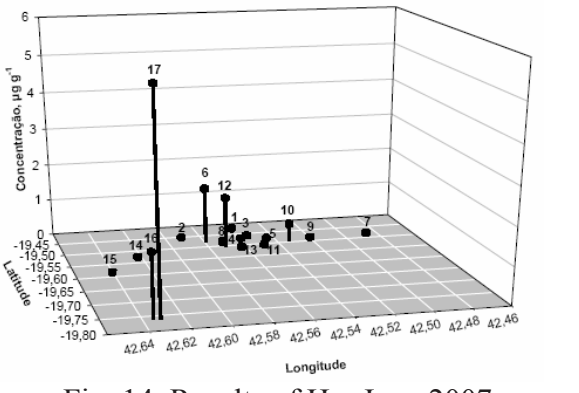

Fig. 14. Results of Hg, June 2007.

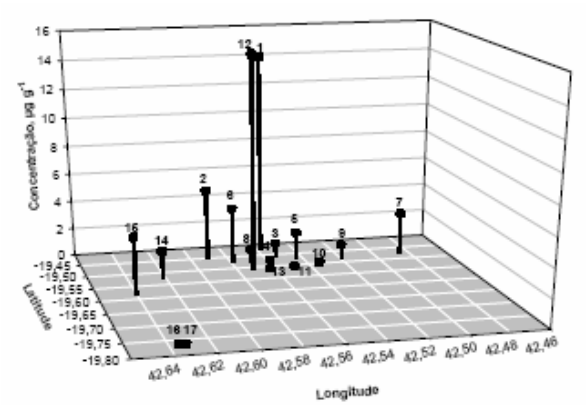

Fig. 15. Results of Th, January 2007.

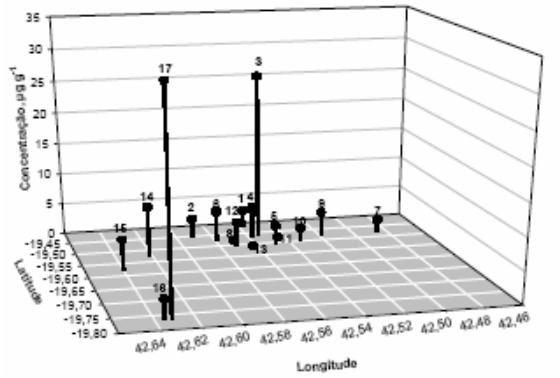

Fig. 16. Results of Th, June 2007.

REFERENCES

[1] J. S. Rieuwerts, M. Farago, "Heavy metal pollution in the vicinity of a secondary lead smelter in the Czech Republic", Appl. Geochem v.23, p.17 [1996].

[2] T. Sterckeman, F. Douay, N. Proix, H.Fourrier, "Vertical distribution of Cd, Pb and Zn in soils near smelters in the north of France", Environ. Pollut., v.107, p.377 [2000].

[3] J. S. Rieuwerts, M. Farago, "Lead contamination in smelting and mining environments and variations in chemical forms and bioavailability" Chem. Speciation and Bioavailability, v.7, n.4, p.113, [1996].

[4] M. A. R. V. Veado, I. A. Arantes , M. R. M. G. Almeida, R. A. Miguel, M. I. Severo, H. L. Cabaleiro, "Metal Pollution in environment of Minas Gerais", Envir. Monitor. and Assessment, v.26, p.255 [2006].

[5] M. A. R. V. Veado, A. H. Oliveira, G. Revel, G. Pinte, S. Ayrault, P. Toulhoat, "Study ofnwater and sediment interactions in the Das Velhas river, Brazil – major and trace elements", Water S.A., v. 26, p.255 [2000].

[6] C. P. Jordao, M. G. Pereira, A. T. Matos, B. J. L. Pereira, "Influence of domestic and industrial waste discharges on water quality at Minas Gerais State, Brazil", Braz. Chem. Soc., v.16, p.241 [2005].

[7] M. A. T. Queiroz, "Bioacumulacão de metais pesados no Rio Piracicaba, Minas Gerais, Aplicando a Analise por ativação neurônica instrumental", Master Science Thesis, Curso de Mestrado em Engenharia Industrial, Centro Universitário do Leste de Minas Gerais, UnilesteMG, Coronel Fabriciano, Brasil, (in portuguese), 105p., [2006].

[8] A. A. F. Costa, "Uso da comunidade epifítica terrestre para biomonitorar a poluição atmosférica na região do Vale do Aço, Minas Gerais", Master Science Thesis, Curso de Mestrado em Engenharia Industrial, Centro Universitário do Leste de Minas Gerais, UnilesteMG, Coronel Fabriciano, Brasil, (in portuguese), 86p., [2006].

[9] R. A. Miguel, "Otimização da técnica de Analise por Ativacao Neurônica Instrumental e Adequação do software K0Labsue, método paramétrico do K0", Master Science Thesis, Curso de Mestrado Ciências e Técnicas Nucleares, Universidade Federal de Minas Gerais, Belo Horizonte, Brasil, 145p., (in portuguese), [2003].

[10] V. Krommer, H. G. Zechmeister, I.Roder; S.Scharf, A. Hanus-Illnar, "Monitoring atmospheric pollutants in the biosphere Wienerwald by a combined approach of biomonitoring methods and technical", Chemosphere, v.67 p.1956 [2007].

[11] M. Schintu, A. Cogoni, L. Durante, C. Cantaluppi, A. Contu, "Moss (Bryum radiculosum) as a bioindicator of trace metal deposition around an industrialized area in Sardinia (Italy), Chemosphere, v. 60, p. 610 [2005].

[12] Word Health Organization: http://www.who.int/phe/health_topics/outdoorair_aqg/en/index.html

[13] ATSDR: Agency for Toxic Substances and Diseases Registry: http://www.atsdr.cdc.gov/index.html

NATURAL RADIOACTIVITY OF COASTAL SEDIMENTS AS "TRACER" IN DYNAMIC SEDIMENTOLOGY

Dr. Jovan Thereska
Institute of Nuclear Physics, Tirana, Albania

BACKGROUND

Radiometric measurement of gamma natural radiation is a simple and fast technique for lithological mapping of the sea bottom that could provide useful information about the origin and transport of sediments (1).

Natural radioactivity of sea bottom sediments can provide:

- granulometric selection of sediments,
- depth limit of wave effect on the sediments on the sea bottom,
- direction and distance of distribution of fluvial sediments,
- accretion and erosion zones along the coast line.

Natural radioisotopes distributed in sediments are uranium-238 (and its family), thorium-232 (and its family) and potassium-40 (2). The radioactive decays of these three radioisotopes show that:

- 1 g U-238, (in equilibrium), emits 33 300 gammas/s and 84 000 betas/s, with energy from some tens KeV till several MeV;
- 1 g Th-232, (in equilibrium), emits 17 400 gammas/s and 15 000 betas/s, with energy from some tens KeV till several MeV;
- 10 g potassium (natural potassium contents 0.0118% K-40) emit 33 gammas/s with energy 1,46 MeV and 275 betas/s with maximal energy of 1,35 MeV.

The concentrations of U-238, Th-232 and K-40 in sediments vary with sediment nature and origin. In the coastal sediments of Albania, there were found these values (3):

Silts:

- U-238 – 3-5 ppm;
- Th-232 – 10- 12 ppm;
- K – 1- 2°/o;

Sands:

- U-238 – 1-2 ppm;
- Th-232 - 5-6 ppm;
- K – 0.5- 1%.

Based on these concentrations and decays, it can be calculated that the major contributor of gamma natural radioactivity of sediments is Th-232 (over 55%), thus Th-232 is the "natural tracer" of sediment dynamics. Th-232 is always in equilibrium and is very resistant against chemical and mechanical agents, so it makes it a reliable tracer for long period transport of sediments.

50 keV was the detection system threshold for online gamma total measurement, while the spectrometric gamma natural radioactivity of samples taken from the sea bottom and beaches was measured in the following windows:

- 1.36-1,60 MeV for the K-40 (photopick 1,46 MeV),
- 1,65 –1,95 MeV for U-238 (photopick 1,76 MeV)
- 2,40 – 2,80 MeV for Th-232 (photopick 2,62 MeV)

The scope of the study was to validate the natural radioactivity method for tracing sediment transport. Natural radioactivity investigation was undertaken in two important areas of the Adriatic Sea littoral of Albanian cost, in the gulfs of Durres and Vlora, where complex studies (radiotracers included) were carried out in the frame of the maintenance of existing Durres harbour, and the design of the new harbour in Vlora (4). Fig. 1 shows the beaches of Durres (left) and Vlora (right) where the natural radioactivity of sediments was measured online on sea bottom from depth 2-3 m till 20-25 m.

Fig. 1. Gulf of Durres (left) and of Vlora (right)

2. RADIOMETRIC MEASUREMENTS

2. 1. Online radiometric mapping of the sea bottom

The gamma measurements were performed in dynamic that means from moving boat with average speed of 1.5 m /s, according to profiles perpendicular to coastal line. The detection probe (NaI (Tl) scintillator 2”x2”) was mounted in a special support, which kept constant distance probe-sea bottom of 5cm (Fig. 2).

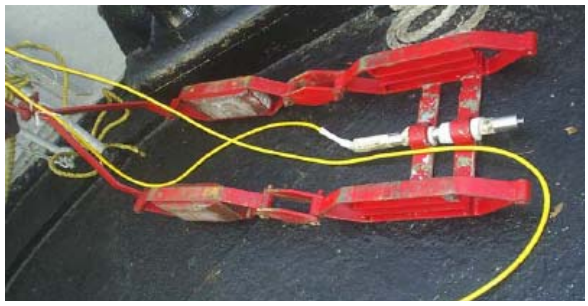

Fig. 2. Detection probe and detection equipment.

Each profile had a length of several kms. It was proved that for rather homogeneous zones the count rate obtained in dynamic is the same with that in static. Taking into account the boat speed of 1.5 m/s and the measuring interval of 30 seconds, it results that each measured value was representing around 50 m length, that is acceptable in radiometric mapping of relatively large natural zones where sharp changes in sediment size and nature are not expected. Radiometric profiles (250 m from each other) were performed in the map scale of 1: 25000, with a position error of 1 mm (equivalent of 25 m) that is acceptable.

2. 2. Treatment of radiometric field data

The plot of radiometric data was treated according to following methods.

a).Treatment with Gauss chart.

For each lithology the distribution of count rates is normal one, that means its graph in Gauss chart is linear, with a mean value characteristic for that kind of sediment. Two count rate populations are considered significantly different when $I_1^* + s_1 < I_2^* - s_2$, where I_1^*, I_2^*, - are the mean values of two successive populations ($I_2^* > I_1^*$) and s_1, s_2 – are their standard deviations. Each radioactive population corresponds to particular sediment (lithology). To correspond a lithology to radioactivity several sediment samples were taken from the sea bottom and analysed in laboratory (granulometric analysis).

b) Treatment with regressive analysis (trend surface analysis)

Trend surface analysis is in most respects similar to normal regression analysis. "Trend" means the least squares trend. Given a set of data, and the desire to produce some kind of "model" of that data (model, in this case, meaning a function fitted through the data) there are a variety of functions that can be chosen for the fit. The trend surface analysis methods can be used to e.g., derive a

continuous smooth surface from irregular data or isolating regional trends from local variations. Trend surface for natural radiation values are approached with a polynomial:

$$X(ui, vj) == P(ui, vj) + aij,$$

where: X (ui, vj) – count rate I measured at bottom point (ui, vj); P (ui, vj) – most probable value; aij – error.

3. RESULTS OF MEASUREMENT OF NATURAL RADIOACTIVITY OF SEDIMENTS

3.1. Radiometric maps in gulfs of Vlora and Durres

Figure 3 shows three radioactivity classes for sediments of Vlora and Durres.

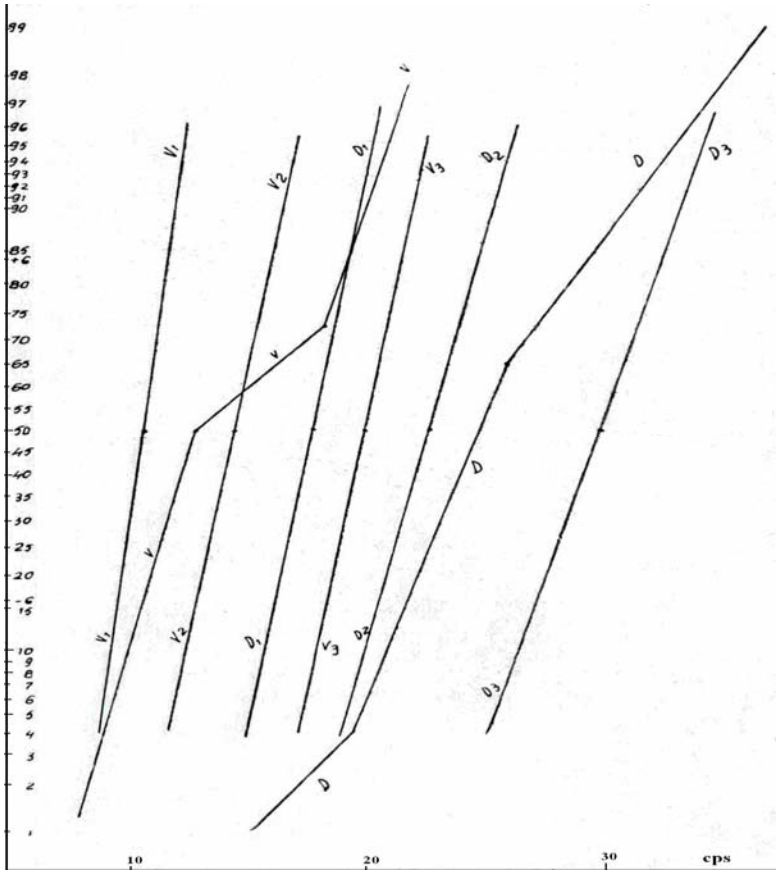

Fig. 3. Statistical distribution of sediment radioactivity's in Vlora and Durres.

Taking samples from these zones, the following relation radioactivity- lithology (granulometric classes of sediments) was found:

Vlora:

I_1* = 11 ± 1 cps (sand grain size 100-200 μm)

I_2* = 14.5 ± 1.5 cps (sand grain size 63-100 μm)

I_3* = 19.5 ± 1.5 cps (silt <63 μm)

There is a zone with mixed grain sizes, called alevrit (mixture of silt with very fine size of sand). The following correlation was found between count rates I(cps) and silt (argil) content in the alevrit Cs(%):

$$I(cps) = 14.5 + 0.05 \times Cs(\%)$$

Durres:

I_1* = 17.5 ± 1.5 cps (sand grain size 63-100 μm)

I_2* = 21.5 ±2 cps (alevrit = 50% fine sand + 50% silt)

I_3* = 28 ± 3 cps (silt < 63 μm)

The relation count rates – silt content for Durres was found as follows:

$$I(ips) = 17.5 + 0.105 \times Cs(\%)$$

Fig. 4 presents isocount trend surfaces for bottom sea sediments in gulfs of Vlora and Durres.

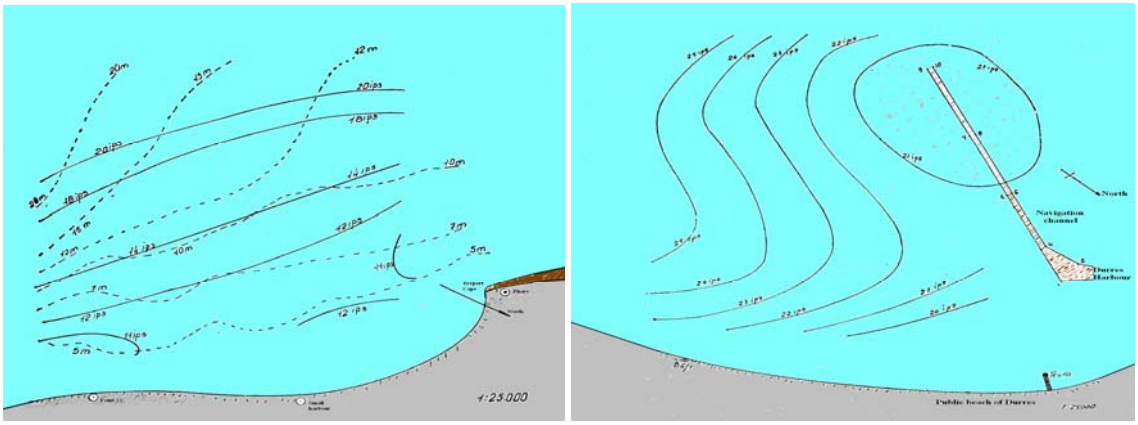

Fig. 4. Isocount trend surfaces for sediments in gulfs of Vlora (left) and Durres (right).

The isocount trend surfaces in Vlora are parallel with bathymetry lines, passing gradually from sand to alevrits till silt (>20 cps after 15 m depth). This picture is result of wave action coming mostly from south-west direction perpendicular to the coast line, which seems to be the predominant factor of sediment transport normal with beach line. There is no evidence of the sediment transport along the shore, at least after 2-3 m. depth.
The isocount map in Durres gulf shows curved lines perpendicular to the shore line and bathymetry, that is characteristic for alongshore transport of alevrit sediments near the sea bottom.
Main conclusions obtained from the mapping of gamma natural radioactivity in Vlora and Durres gulfs are:
- Sediments in Vlora have a lower radioactivity for the same granulometry than in Durres, that reflects their origins from different land stratifications,
- Gulfs of Vlora and Duress have different lithological distributions; the sea bottom of Vlora consists mostly of sand, while sea bottom of Durres contains mostly alevrits (mixage mof fine sand and silt),
- In Vlora gulf there is a sediment selection in profiles normal to the coast line, resulting under influence of the waves perpendicular to the shore line.
- In Durres gulf there is not any sediment selection in profiles normal to the coast line; it could be explained as an alongshore transport of alevrit sediments near the sea bottom towards the harbour and its channel.

3.2. Radiometric profiles in the Durres navigation channel

Radiometric measurements along the navigation channel (on its axes and both sides) to the port of Durres (4 km long) were performed to obtain the silting map (Fig. 5). In fact, the channel was almost inexistent because it was filled up with sediments (estimated around 1 million m^3 sediments).

Fig. 5. Gulf of Durres, the harbour, the navigation channel and the main direction of sediment transport under the action of waves coming from the south-east.

The results of four profiles measured at different periods were:

- Profile 1: The average I_{ch}= 22.6 ± 0.5 cps (correlation coefficient r=0.22)
- Profile 2: The average: I_{ch} = 22.4 ± 0.4 cps (r= 0.22)
- Profile 3: The average: I_{ch}= 22.1 ± 0.3 cps (r = 0.25)
- Profile 4: The average: I_{ch} = 22.2 ± 0.3 cps (r = 0.20)

For the whole channel the average value was calculated I_{ch} = 22.3 ± 0.5 cps. This value of radioactivity is characteristic for alevrits (mixture of very fine sand with silt in different proportions).

There was a very good reproducibility of the measurements, which make them very reliable for interpreting even relatively small differences.

There was observed a significant difference between the average activities of the first (harbour entry) and second (large sea) part of the channel: I_{ch1} = 24.1± 0.5 cps (nearly 70% silt), while the second part: I_{ch2} = 20.5 ± 0.5 cps (nearly 30% silt). This indicates that the first part of the channel (half of it near the harbour) is silted more than the second part.

The average activities of two parallel profiles, both sides of the channel, was found 21.0 ± 0.5 cps that means similar with the activity of sediment within the second part of the channel. Comparison of radioactivity distributions within the channel and both sides of it indicates that first half part of the channel is prone to higher silt deposition. The silt deposited mostly in the first part of the channel is coming very probably from the gulf centre (because they have the same radioactivity). The waves coming from the south-east move silt towards the harbour, where it settles down trapped by harbour structures.

3.3. Radiometric results of sediments south of Vjosa river

There is a river out of gulf of Vlora, nearly 15 km north of it (Fig.6). Vjosa river has changed its position two times in the last century; the actual river mouth is located nearly 5 km in the north of the old river mouth. Consequently, the old mouth is undergoing on important erosion process under the wave actions.

Fig. 6. Location of Vjosa river mouth in the north of gulf of Vlora

The radiometric measurement of beach sediments south of Vjosa river was carried out (from dunes till 1.5 m water depth). The aim was to investigate the fluvial sediment transport and see if any alongshore pathway away from the mouth of the river happened, as well as to localize if possible the erosion and accretion zones south of Vjosa river mouth. Fig. 7 shows the results of radiometric survey of the beaches south of Vjosa river.

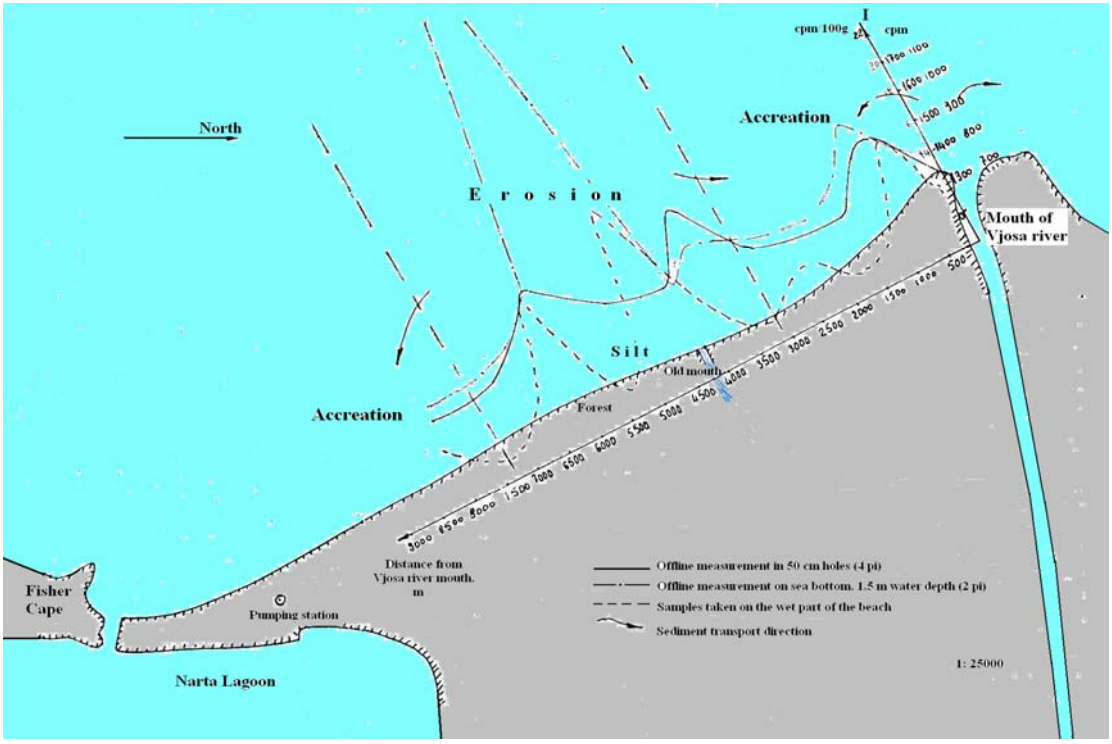

Fig. 7. Distribution of radioactivity of sediments in the south of Vjosa river.

Along each normal profile, the radioactivity was measured in two stations: near the sand dunes, with NaI 3"x3" detector introduced 50 cm under the surface (4 π geometry), and on the sea bottom (depth 1.5m). Samples were taken also at the wet part of the beach and analysed in laboratory. Both online measurements in dunes and sea bottom have almost similar trends, while the sampling data have some deviations that were more related with sampling technique and relatively small quantity of samples that do not represent the whole site.

Fig. 7 indicates some phenomena that could be related with local erosion and accumulation processes, as well as allowing to judge for the zone of influence of river sand transport. An erosion zone nearly 5 km south of Vjosa river mouth (where it is the old river mouth) (Fig. 8) helped the interpretation of the radiometric data.

Fig. 8. Trees and forest in the sea showing erosion of this zone

Taking into account the alteration of accretion and erosion zones along the littoral south of Vjosa river mouth, it could be assumed that there is not any dominant alongshore drift transport south of Vjosa river, thus Vjosa river influence is limited to a few km south of it.

4. GENERAL CONCLUSIONS

Natural radiometric survey of the sediments of sea bottom provided some qualitative sediment transport features, characteristics and parameters similar with those obtained with radiotracers, in particular the resultant direction and mechanism of sediment transport were made evident. This

simple and low cost technique can be used for sediment transport studies as complementary to other techniques.

The radiometric survey of the sediments of sea bottom and beaches in the gulfs of Vlora and Durres has provided the following major conclusions:

Vlora

1. Waves coming from the west move sends normal to the beach line. The influence of waves of this sector is up to depth 15 m, where is the boundary between sand and silt.
2. There was an accumulation zone from the Vjosa river mouth till nearly 3 km to the south, which was nourished by the fluvial sediments. From 3 to 7.3 km there was another zone, which seemed to be in erosion. In this zone, there was the mouth of old river of Vjosa that is not bringing any more sediment, and consequently the zone was under erosion. Further to the south is another accumulation zone nourished with sediments that are eroded above.
3. There were found alternating erosion and accretion zones south of Vjosa river that indicates more a local transport phenomenon than any long distance alongshore drift transport in the investigated zone.

Durres

1. There was not any visible granulometric selection of sea bottom sediments in the gulf of Durres.
2. There was an indication of sediment transport trend from south to the north of the gulf under the influence of waves coming from the south sector.
3. There was evidence of silting process, in particular in the first part of the navigation channel near the harbour.

REFERENCES

1. Giresse P. Applications des measures de radioactivite naturelle a la sedimentologie. Bull. Soc. Geol. De France, 7, VII, p. 668-673, 1965
2. Mahdavi A. The thorium, uranium and potassium contents of Atlantic and Gulf Coast Beach Sands. Chap. 5 in Natural Radiation Environment, University of Chicago Press, 1964
Martin J. M. Utilisation des radioelements naturels comme “traceurs” dans l’etude de quelques problemes de sédimentologie dynamique. Paris, 1966.
3. Thereska, J. 1981, Study of natural radioactivity in some zones of Albanian Adriatic shelf (in Albanian). M.Sc. Thesis, Institute of Nuclear Physics, Academy of Sciences, Tirana.
4. Caillot A., Kedhi. M., Thereska. J., et al. Etude des mechanismes sedimentaires dans le golfe de Durres au moyen de la radioactivite. Application a l’envasement du chenal au port de Durres. CEA, France, Institute de Physique Nucleaire, Albania. 1976.

SOIL-PLANT TRANSFER FACTORS OF TYPICAL BRAZILIAN CROPS

Vanusa M. F. Jacomino*, Kerley A. P. Oliveira, Maria Ângela de B. C. Menezes, Maria H. T. Taddei, Maria C. Siqueira, Marcos Roberto L. Nascimento, Fabiana F. Dias, David F. da Silva, Maria Eleonora Deschamps, Jaime W. V. Mello

ABSTRACT

Phosphogysum (PG) or agricultural gypsum (AG), a solid waste from the phosphate fertilizer industry, is used as a soil amendment, especially in soils from the Cerrado region, in Brazil. Nevertheless, such material may contain natural radionuclides and metals which can be transferred to soils, plants and water sources. This paper presents and discusses the results of physical and chemical analyses that were done in order to characterize samples of PG and two typical soils from the Cerrado region, Brazil, one clayey and one sandy. These analyses included: solid waste classification, evaluation of organic matter content, P, K, Ca, Mg, and Al concentrations, particle size distribution, and mineralogical composition. Natural radionuclides and metal concentrations in PG and soils samples were also measured. According to Brazilian Regulation ABNT Norm 10004/2004, the results showed that PG is classified as non-inert solid waste. The soils studied presented high acidity and low natural fertility. It was also observed that the activity concentration of natural radionuclides in PG was below the limit suggested for agricultural purposes. In addition, this study verified that natural radionuclides and metal concentrations in PG were lower than those concentrations verified in the clayey oxisol from Sete Lagoas, Minas Gerais State, Brazil. Soil-plant transfer factors of natural radionuclides were determined for three different types of crops: lettuce, soybeans and corn. For this, a set of greenhouses experiments were carried out during a period of one year. The obtained values varied from 4.7 E-04 for 238U (corn) to 9,6 E-02 for 210Pb (soybeans).

Keywords: Phosphogypsum, Natural radionuclides, crops, transfer factor

INTRODUCTION

The main raw material in Brazilian phosphoric fertilizer industries is the apatite present in rocks, of which approximately 80 % are of igneous origin (Canut, 2006). The most commonly used process in the production of phosphoric fertilizers is the attack of the phosphate rock with concentrated sulfuric acid and water. In this case, the main products from chemical reactions are phosphoric acid (H_3PO_4), simple super-phosphate (SSP), and triple super-phosphate (TSP). Dehydrated calcium sulphate (gypsum or phosphogysum) and hydrofluoric acid are by-products of phosphate rock processing.

The phosphogysum (PG) generation rate is approximately 4.8 tons for each ton of phosphoric acid produced. Annual world production is estimated to be 150 million tons, approximately 12 million tons of which are generated in Brazil. At present, this material is stored in piles located near the factories. However, this practice may represent a potential risk of contamination, mainly to organisms and hydrological systems located close to the pile.

Global demand has spurred interest in finding processes that generate great amounts of both phosphoric acid and chemical fertilizers. However, there are several important environmental concerns that remain unaddressed regarding PG disposal. These problems exist because phosphogysum, although being mainly composed of dehydrated calcium sulfate, also contains fluoride, heavy metals, and radionuclides (from the ^{238}U and ^{232}Th natural radioactive series). These impurities can percolate through the pile and contaminate groundwater, eventually causing damage to human health (Mazzilli et al., 2000). Another problem is ^{222}Rn exhalation, which can affect populations close to the piles (Santos et al., 2006), especially workers.

Research studies dealing with the development of possible uses for PG are ever more important, not just from an economic point of view, but also from technological and environmental points of views, since there are large amounts of this material worldwide. Besides the low cost, reutilization of PG

would contribute to the preservation of natural gypsum reserves, guaranteeing one of the basic principles of sustainable development: the preservation of natural resources for future generations.
The possibility of using PG in agriculture (FIRP, 1996, El-Mrabet et al. 2003, Papastefanou et al., 2006) has been the focus of research in several countries and in Brazil, especially in the agriculture of the Cerrado Region (Ribeiro et al., 2000; Ernani et al., 2001), where soils have characteristics which are compatible with the use of this material. In this system, fast mineralization of organic matter associated with intense leaching produces soils with naturally low fertility. These are acidic soils (pH between 4.3 and 6.2) with high levels of exchangeable aluminum and low levels of phosphorus available for plants; they are also poor in calcium and magnesium, elements involved in root development (Lopes & Cox, 1977, Silva &Azevedo, 2002).
According to Kochian et al., 2004, acidity is the largest limitation of soils in extensive tropical and temperate areas. Acidic soils take up about 3.95 billion acres, approximately 30 % of the continent's total area, not including polar areas (von Uexkull & Mutert, 1995). In general, formation of acidic soils results from many factors, with great importance given to climatic conditions. Tropical climate conditions favor fast alterations of the rock in which exchangeable bases are leached away and consequent acidification of soils occurs. In environments where there is a high rate of rainfall, soluble nutritients such as calcium, magnesium, potassium, and other alkaline elements can be leached (Lima & Cavalli-Molina, 2001).
When removal of cations occurs faster than their release rate due to weathering, the pH of the soil will decrease. At low pH, aluminum ions (Al^{3+}) are released into the soil solution and adsorbed by negative charges of clay particles in the soil. Excess aluminum can harm crop productivity. In addition, aluminum has an important role in fixation of phosphorus in well-drained soils (Cregan, 1980; Hochman et al., 1995).
Dominant species of soluble aluminum in well-drained soils mainly depends on soil pH. At strongly acidic conditions (pH < 4.0), it exists as Al^{3+}ion; with the elevation of the pH to 5.0, the prevailing species are $Al(OH)^{2+}$ and $Al(OH)^{2+}$ and, finally, the uncharged species $(AlOH)_3$º prevails in pH values above 5.0 (Marschne, 1991). Toxic concentrations of soluble aluminum in soils that negatively influence crops can be avoided with the addition of acidity correctives, which buffer the soil pH over 5.0.
Rocks that contain alkaline constituents such as oxides, hydroxides, carbonates or calcium, and/or magnesium silicates (Bellingieri & Bertin, 2003) are commonly employed to neutralize soil acidity. Calcareous materials are included in this category and are known as limestone that contains calcium and/or magnesium carbonates. However, it is more difficult and expensive for farmers to obtain limestone, mainly due to its use in more profitable industrial sectors, such as cement production, metallurgic sites, building sites, etc.
Various residues generated by industries have been studied as possible substitutes for limestone, among them the industrial waste phosphogysum (PG), or "agricultural gypsum" (AG), which it is the object of this study. In fact, PG can not be considered as a corrective for acidity, but solely a soil conditioner. Notwithstanding, addition of Ca and sulphates can contribute to a decrease of the Al saturation percentage in the system. In this case, toxic Al is moved down in the soil profile out of the roots zone, which allows deepen the root system and a better crop development. A deep root system is an important strategy for acquisition of water by crops in the Cerrado region, mainly during dry seasons. In natural conditions the presence of exchangeable Al^{3+} under the superficial layer of the soil impairs the growth of the roots. In this sense the use of PG is important and the limestone is not suitable to neutralize toxic Al^{3+} under the superficial layer (20 cm), because carbonates are less mobile than sulphates in the soil. The average PG composition is: free humidity (15-17 %); CaO (26-28 %); S (15-16 %); P_2O_5 (0.6-0.75 %), insoluble SiO_2 (1.26 %); Fluoride (0.63 %), and Al and Fe oxides (0.37 %) (Malavolta & Vitti, 1985).
According to the Brazilian Agricultural Research Corporation (EMBRAPA, 2000), the use of PG is justified in two situations from an agronomic point of view: (a) where there is a need to supply calcium and sulfur to plants; and (b) to decrease toxic concentrations of exchangeable aluminum in sub-superficial layers with consequent increase of calcium levels in those layers, which tends to

"improve" the environment for root growth. Response to PG is greater when saturation for Al^{3+} is above 30 % or when Ca level is lower than 0.4 $cmol_c\ dm^{-3}$ of soil, a common situation in soils from Cerrado region. However, it is worth mentioning that the merely agronomic evaluations may be inadequate in evaluating the environmental impact due to the use of PG in agriculture.

Solid waste production has significantly increased due to the expansion of industry to better meet demands of the modern societies. In this context, the reuse of wastes containing synthetic organic compounds, natural radionuclides or heavy metals is an important reason of concern; thus their application in soils is currently being studied. Taking into consideration the possible presence of such elements in PG, its use in agriculture requires additional studies in order to evaluate the mobility of radionuclides and heavy metals in the soil profile to the groundwater, and their absorption by plants.

Approximately 85 % of the great plateau at the Central Brazil is dominated by the "Cerrado" landscape, representing from 1.5 to 2 million km^2, or approximately 20 % of the country's surface. This ecosystem is similar to savannas. The climate is hot, semi-humid, and notably seasonal, with rainy summers and dry winters, with an annual rainfall of about 800 to 1600 mm. The soils are generally very weathered, chemically poor, and deep. The "Cerrado" landscape is characterized by extensive savanna formations interspersed with woods along rivers valleys. This region is one of the largest unexploited agricultural areas in Brazil.

Agriculture is one of the main economic activities in Brazil. Increase in agricultural productivity depends on the use of adequate technologies that can contribute to sustainable agriculture. In order to contribute for the regulation of the agricultural use of PG in Brazil, this project evaluated the environmental impact of its use in soils from Cerrado region and attempted to better understand transfer mechanisms of natural radionuclides and heavy metals in the soil/plant system.

The project comprises: 1) soil and PG sample collection, followed by their physical, chemical, and radiological characterization; 2) set up greenhouse experiments with lettuce, soybean, and corn plants; and 3) determination of soil-plant transference factors (FT). These factors are defined as the ratio between total radionuclide activity or concentration of metals present in the plants and total radionuclide activity or heavy metal concentrations present in the soil (IUR, 1989). The main objective of this report is to present and discuss results obtained in the first and second phases of the project.

MATERIALS AND METHODS

Samples of PG were collected in a fertilizer facility that produces phosphoric acid by means of a wet method. The phosphate rock used at the industrial site has igneous origin and comes from the Alkaline-Carbonate site in Tapira, MG, Brazil (Canut, 2006). Thirty samples were collected from the surface of the piles at different locations, according to the Environmental Protection Agency guidelines (EPA, 1988).

PG samples were then dried in the laboratory at 60 ºC for 48 hours and sieved through 30 and 60 mesh (590 and 250 μm). Afterwards, small fractions of the samples were mixed, and divided to form a composed sample. This sample was submitted to leaching and solubilization tests for waste classification. Brazilian regulations consider two waste categories have been established: (1) Class I - dangerous solid waste, with hazardous characteristics such as inflammability, corrosiveness, reactivity, toxicity, and/or pathogeneticity; (2) Class II – Harmless solid waste - IIA (non-inert) and IIB (inert), wastes that do not present any of the characteristics that were described previously.

Leaching and dissolution/solubilization tests were done according to ABNT NBR 10005/2004 and 10006/2004 Norms. All substances listed in the F and G Annexes of ABNT NBR 10004/2004 were analyzed and toxicity classification tests were done by leaching and dissolution of inorganic and organic substances (pesticides and other chemicals).

Soil samples were collected from two different locations in the Sete Lagoas municipal district (clayey yellow rhodic ferralsol (hapludox) - LVSL) and in the João Pinheiro municipal district (sandy rhodic ferralsol (hapludox) - LVTM), that represent typical soils from the Cerrado region. Soil samples were air dried and sieved through 2 mm mesh. Lime and different doses of PG were

applied to the soils and, after an incubation period, plants of lettuce, soy beans, and corn were cultivated in greenhouse pot trials.

Chemical characterization of soil samples was done by means of the following analyses: pH in water (1:2.5); P and K extractable by Mehlich 1; exchangeable Ca, Mg, and Al by extraction with 1 mol L^{-1} KCl; Sum of Exchangeable Bases (SB); Cationic Exchange Capacity at pH 7.0 (CEC); Index of Bases Saturation (V); Index of Aluminum Saturation (m), and Organic Matter Content (OM).

Several sieves with different meshes were employed for soil and PG particle size analysis: +60 #, +100 #, +150 #, +200 #, +270 #, +325 #, +400 #, +500 #, and -500 #. Samples were first manually disaggregated on a table using a cylindrical roll and then sieved in 16 meshes. A fraction of each sample was removed for mineralogical analysis by X-ray Diffraction technique (powder method). Those analyses were carried out using a Rigaku X-ray Diffractometer with a copper tube.

Identification of crystalline phases was done by comparing sample diffractograms with ICDD database (International Center for Diffraction Data / Joint Committee on Powder Diffraction Standards – JCPDS), (Sets 01 - 50; 2000). These analyses took into account intensities of main reflections and comparison of diffractograms in order to obtain relative amounts of different minerals in the samples.

Elemental composition of PG samples was determined by X-ray Fluorescence. Phosphate content was measured using a colorimetric method and humidity was determined through a gravimetric method.

Concentrations of toxic elements were determined including natural radionuclides (^{226}Ra, ^{228}Ra, ^{210}Pb, ^{210}Po, ^{238}U, and ^{232}Th), heavy metals (Ni, Pb, Cd, Hg, and Cr), and metalloids (As and Se). ^{226}Ra, ^{228}Ra, and ^{210}Pb activity concentrations in PG and soil samples were determined by Gamma Spectrometry using a CANBERRA HPGe detector (relative efficiency of 45 %) and Genie 2000 software for spectra analysis. Samples were sealed in plastic containers for 30 days, which is the time needed to assure radioactive balance between ^{226}Ra and its daughters, ^{214}Pb and ^{214}Bi. Energy photopeaks at 609 keV and 1,020 keV, and 351 keV were used to determine ^{226}Ra, corresponding to ^{214}Bi and ^{214}Pb, respectively. A 911 keV energy photopeak for ^{228}Ac ($T_{1/2}$ = 6.12 hours) was used to determine ^{228}Ra. A 46.5 keV energy photopeak was used for ^{210}Pb determination.

^{210}Po is an important element to be studied, since it is one of the most biologically active and toxic products from the uranium decay series, and strongly accumulates in the biota; for this reason it is a significant contributing source for radiation doses in humans (John Arthur III & Markham, 1984). Polonium concentration measurement was performed using a Canberra Alpha Spectrometry system, through determination of the powder deposited in a silver planchet, using a reducing HCl and ascorbic acid medium. Matrix purification was done by using a specific SR-Spec chromatographic resin from Eichrom.

^{232}Th activity concentrations in PG and soil samples were determined by Neutronic Activation Analysis technique (AAN), k_0 method (Menezes et al., 2003). Irradiation was applied in a TRIGA MARK I IPR-R1 reactor located at CDTN/CNEN, using 100 kW with a thermal neutron flow equivalent to 6.35 x 10^{11} neutrons cm^{-2} s^{-1}, for 8 hours. Samples were simultaneously irradiated with a flow of neutrons to monitor Al - Au (0.1 %) IRMM-530RA (5.0 mm diameter and 0.1mm thickness). After irradiation and an appropriate time for decline, the procedure followed medium and long half-life radionuclide determination. Gamma Spectrometry was done using an HPGe detector with 15 % efficiency. KAYZERO/SOLCO software was used for calculating the concentration of elements.

The ^{238}U activity concentration was determined through retarded neutron fission activation method, and samples were irradiated with a flow of thermal neutrons. This method uses fast irradiation followed by a reading of retarded neutrons. Samples were irradiated for 50 seconds, 30 seconds were allowed for decline time, and counting took 60 seconds. The irradiation process and counting utilized an automated pneumatic system. A $10BF_3$ detector was used to count retarded neutrons. Uranium concentration was calculated through linear regression, adjusted according to established

patterns. Quality control for soil analysis results was verified by analyzing a certified reference material, IAEA/Soil-7 (IAEA, 1984).
The Cr and Ni analyses were done by Inductively Coupled Plasma Atomic Emission Spectrometry, ICP-OES, using a Varian spectrometer model Liberty. Cd and Pb were done by Graphite Furnace Atomic Absorption Spectrometry, GF-AAS, using a Varian equipment, model 220 FS, equipped with a deuterium background corrector, GTA-110 furnace accessory, and automatic sampler. Conventional pyrolitically covered graphite tubes were used.
Toxic elements concentration measurement for As and Cr was done by Neutronic Activation Analysis technique (AAN), k_o method, as described above. For determination of other toxic elements such as Cd, Pb, Ni, and Se, PG and soil samples were analyzed using Atomic Absorption Spectrometry in a lead furnace (GFAAS). A Varian, FS-220 Spectrometer, with a GTA-100 lead furnace, equipped with a deuterium bottom corrector and automatic sampler was used. Conventional pyrolytically covered lead tubes were used. The accuracy of the method was evaluated by analyzing a reference material, 8704 Buffalo River Sediment.
Finally, determination of total mercury was performed by cold steam generation coupled with an Atomic Absorption Spectrophotometer (CVAAS) (Perkin Elmer FIMS 400). Samples were processed according to the adapted procedure of EPA (1983), which involved addition of 1.0 mL of MilliQ® water and 2.5 mL of a 3:7 mixture of concentrated nitric and sulfuric acids (0.0000005 % maximum Hg level) per approximately 200 mg of sample.
These samples were later heated to 75 °C for 4 h. After that, 4.0 mL of a 5 % (m/v) aqueous potassium permanganate solution was added along with 2.0 mL of 5 % (m/v) aqueous potassium persulfate solution. Samples were taken back to the greenhouse and maintained at 75 °C for one night. The excess of permanganate was eliminated by adding 1 mL of 20 % (m/v) hydroxylamine and the final volume was adjusted to 50.0 mL. An aliquot was centrifuged for 10 min (2,000 rpm) and the floating material was analyzed using CVAAS.
Calibration curves were prepared from a certified 1,000 μg/mL Hg standard solution from Merck (1.0 to 5.0 ηg/mL), measuring patterns in the same conditions of the samples. Method accuracy was verified by analyzing a CRM 320 reference material, a river sediment produced by BCR Community Bureau of Reference.
Soybeans and corn were chosen as a typical species of the Cerrado region. Lettuce was also included due to its low growing cycle and its great need for nutrients. Plants were cultivated in plastic pots filled with 2 kg of a mix of each soil, lime and phosphogypsum (PG). Four set of experiments were carried out for each crop cultivated with clayey or sand soil: 01 without PG, 01 with half of the PG recommended dose (according to EMBRAPA, the recommended dose is 0.5 $g.dm^{-3}$ for clayey soil and 0.2 $g.dm^{-3}$ for sand soil), 01 with the recommended dose and 01 with double of the recommended dose. Three seeds were sown in each pot. Plants were grown in a greenhouse throughout the experiment and were watered and fertilized with a nutrient solution as needed. The transfer factors (FT_{sp}) were estimated according to the relationship:

$$FT_{sp} = \frac{C_p}{C_s}$$

Where:

- Cp is the radionuclide concentration on edible part of the plant;
- Cs is the radionuclide concentration in soil

Different types of analyses were performed in order to determine the radionuclides concentration on the edible part of each crop and of the soil as showed in Table 1.

Table 1. Description of the each analytical method used to determine the concentration of radionuclides in soil and crops samples.

Radionuclides	Soil	Crops
^{238}U	NAA - DN	NAA – k0
^{232}Th	NAA – k0	NAA – k0
^{226}Ra	Gamma Spectrometry	Radiochemical separation followed by an alpha radiometry with a gas proportional counter
^{228}Ra	Gamma Spectrometry	Radiochemical separation followed by an beta radiometry with a gas proportional counter
^{210}Pb	Gamma Spectrometry	Radiochemical separation followed by an beta radiometry with a gas proportional counter
^{210}Po	Radiochemical separation followed by an alpha spectrometry	Radiochemical separation followed by an alpha spectrometry

NAA – DN: Neutron Activation Analysis by delayed neutrons method;
NAA – k0: Neutron Activation Analysis by k0 method

RESULTS AND DISCUSSION

Results from solid waste classification tests showed that PG was neither considered corrosive nor reagent, according to ABNT norms. It is classified as non-inert waste based on NBR 10004/2004 (Class II A, non-dangerous / non-inert) due to the presence of arsenic, fluoride, aluminum, iron, manganese, and sulfates above established limits for the dissolution/solubilization test.

The main physico-chemical characteristics of each soil are reported in Table 1. The results revealed that both soils were acidic and possessed low fertility levels (Table 2). This is related to the low levels of nutrients (Ca, Mg, K, and P), as well as low CEC values. Low base saturation indexes (V) indicated small proportions of exchangeable Ca^{2+}, Mg^{2+}, and K^{+} are occupying negative charges sites of the colloids. Conversely, exchangeable Al^{3+} ions are dominant, as indicated by relatively high Al saturation index (m > 30%)..The clayey soil presented slightly higher fertility, with higher Ca and organic matter (OM) levels. In general, both soils had high Al levels and potential acidity. These are typical characteristic of acidic Cerrado soils, where exchangeable Al is considered toxic for most cultivated plants.

Table 2. Physico-chemical characteristics of the soils used for each crop culture

Soil Type	Results											
	pH	P	K^+	Ca^{2+}	Mg^{2+}	Al^{3+}	H^+Al	SB	CEC	V	m	OM
		($mg.dm^{-3}$)	($cmol_c.dm^{-3}$)							(%)		g/kg
clay	5.18	1.5	0,02	0.90	0.06	0.48	8.3	0.97	1.45	10.5	33.1	4.43
sand	5.32	0.4	0,041	0.11	0.02	0.1	3.2	0.17	0.27	5.0	37	1.17

Mineralogical analyses revealed that PG is composed of gypsum (above 40 %), with significant presence of calcium sulfates, such as anydrite and bassanite. PG has a yellowish white coloration and analyses of granulometry distribution showed that it is mainly made up of particles between 53 and 74 µm in diameter.

The sandy soil presented a mineralogy dominated by quartz (above 30 %). Granulometry distribution analyses revealed that this soil contained particles varying from 105 to 250 µm in diameter. The main constituent of the clayey soil was kaolinite (more than 30 %), which was basically composed of fine particles of approximately 250 µm in diameter.

These results corroborated with those of the soil chemical characterization analyses, which indicated low CEC (Refer to Table 1). Mineralogical composition was typical of Ferralsols (hapludox) from the Cerrado region. Wasserman et al., (2002), demonstrated that presence of minerals such as kaolinite and gibbsite influences the transfer of pollutants in the soil-plant system. This fact can be related to the low capacity of those minerals to retain cations. On the other hand, Fe and Al oxides, such as goethite and gibbsite, may have high adsorption capacities through formation of "inner sphere" surface type complexes with some metals and metalloids in the soil, such as arsenic. These surface complexes are quite stable and can hinder the transfer of soil pollutants to plants as well as alter their bioavailability.

The results also revealed that the activity concentration of the radionuclides were very low (Table 3). As can be seen, PG concentration values for ^{226}Ra (251 Bq/kg) and ^{228}Ra (226 Bq/kg) were below the limit recommended by the US Environmental Protection Agency (EPA, 1988), which is 370 Bq/kg. In general, PG had ^{210}Pb activity concentrations comparable to those found for ^{226}Ra and ^{228}Ra.

Table 3. Results for natural radionuclides activity concentrations

Activity Concentration ($Bq.kg^{-1}$)	Samples		
	PG	Sandy Soil	Clayey Soil
^{226}Ra	251 ± 26	18 ± 2	69 ± 5
^{228}Ra	226 ± 29	34 ± 2	114 ± 5
^{210}Pb	206 ± 29	20 ± 5	50 ± 9
^{232}Th	27 ± 2	8.9 ± 0.3	29.3 ± 0.9
^{238}U	3.2 ± 0.9	1 ± 1	6 ± 1
^{210}Po	229.7 ± 26.3	< 10	43.51 ± 6.1

The ^{238}U concentration in PG was well below the concentration found in the clayey soil. It is important to mention that: (1) PG samples usually have low ^{238}U concentration compared to other

natural radionuclides. In phosphoric rock, members of the natural series of ^{238}U and ^{232}Th are in radioactive equilibrium. During acid attack to phosphoric rocks, phosphoric acid is enriched with ^{238}U, while ^{232}Th, isotopes of radium, and ^{210}Pb tend to concentrate in PG (Mazzilli, 2000); (2) Brazilian phosphoric rock has an igneous origin, with smaller ^{238}U concentrations than ^{232}Th concentrations; and (3) the clayey soil used in this study was developed from weathering of granite rocks over 2,700 million years old which typically present contents of ^{238}U from 5 to 10 ppm.

In general, the PG generated by phosphoric acid industries in Brazil has natural radionuclides activity concentrations well below those observed in other countries (Silva et al., 2001; Papastefanou et al., 2006). The largest ^{232}Th activity concentration in relation to ^{238}U activity concentration can be explained by the igneous origin of the rock used in the phosphoric acid production process.

Metal (Cd, Pb, Cr, Ni, and Hg) and metalloid (As and Se) concentrations in PG and soils samples are displayed on Table 4. For comparative purposes, limits for concentrations of toxic elements were also displayed (Brazilian Agriculture Department Normative Instruction, SDA number 27 from June 5th, 2006), as well as results for reference material analyses (Certified Value).

Table 4. Metal and metalloid concentration analyses.

Elements		Concentration (mg/g)			Concentration Reference Material [2] (mg/g)	
	Limit [1] (mg/g)	PG	Sandy Soil	Clayey Soil	Certificated Value	Experimental Value
As	20	< 8	3.4 ± 0.1	61 ± 2	13 ± 1 [1]	15 ± 1
Cd	8	< 0.1	< 0.1	< 0.1	2.9 ± 0.3 [2]	3.0 ± 0.1
Pb	300	< 0.5	2.9 ± 0.2	69.7 ± 0.2	150 ± 17 [2]	167 ± 3
Cr	500	< 17	38.2 ± 0,1	177 ± 47	60 ± 12 [1]	74 ± 1
Hg	2.5	< 0.025	< 0.025	0.063 ± 0.013	1.03 ± 0.13 [3]	1.03 ± 0.07
Ni	175	15.7 ± 1.5	12.4 ± 0.8	77 ± 4	43 ± 4 [2]	40 ± 2
Se	80	< 1.5	< 1.5	< 1.5	-	-

[1]Limits of concentration IAEA/Soil-7;

[2]Buffalo River Sediment (8704);

[3]CRM 320, BCR Community Bureau of Reference.

In all cases, concentrations of toxic elements found in the clayey soil were larger than those obtained in the sandy soil. That is probably due to the higher CEC and organic matter contents in the clayey soil. Concentrations of toxic elements present in plaster were, in general, smaller than in the soils studied, especially in the clayey soil. Concentrations of toxic elements in PG samples were below the limits established in MAPA Normative Instruction SDA number 27 (MAPA, 2006).

As previously mentioned, quality control for analytical results was verified by analyzing certified reference materials. Experimental results had similar values when compared to reference values, therefore indicating the accuracy of the methods employed.

Table 5 presents the final results of soil-plant transfer factors for each type of soil and each crop. As it can be verified the values of ^{232}Th and ^{210}Pb transfer factors for lettuce and soybeans were similar (approximately, 2.7E-03 for ^{232}Th and 9.0E-02 for $^{21}0Pb$). The values of ^{226}Ra and ^{228}Ra transfer

factors for soybeans were higher then those observed in lettuces probably that due to the fact that soybeans needs much more nutrients, as an example Ca. The transfer factors for corn plants were one order of magnitude lower then those from obtained for the other plants extremely low. It is important to point out that the transfer factor were estimated just for those conditions where the radionuclide concentration of soil or plant samples presented values higher the minimum detectable activity level (MDA).

Table 5. Soil-plant transfer factors.

Plants	U-238	Th-232	Ra-226	Ra-228	Pb-210	Po-210
	Clayey Soil					
Lettuce	-	2.7E-03	3.7E-02	2.2E-02	8.6E-02	5.2E-02
Soybeans	1.5E-03	2.7E-03	8.9E-02	7.1E-02	9.0E-02	-
Corn	-	4.7E-04	-	-	-	-
	Sand Soil					
Lettuce	-	6.3E-03	-	5.6E-02	8.6E-02	5.2E-02
Soybeans	7.4E-03	1.8E-03	9.1E-02	6.8E-02	9.6E-02	-
Corn	-	4.1E-04	-	-	-	-

CONCLUSION

Several analyses were carried out in order to evaluate chemical and physical characteristics of two different types of soils from the Cerrado region and phosphogysum (PG), which is a solid waste generated by phosphoric acid production industries in Brazil.

This study showed that PG is classified as non-Hazardous, non-Inert waste (Class IIA), with arsenic, fluorides, aluminum, iron, manganese, and sulfate concentrations in the solubilization test above the maximum limit established by ABNT Norm 10004/2004. Both types of soils (sandy and clayey Ferralsols) are acidic with low fertility and presented Al concentration level considered toxic to plants.

Mineralogical and granulometry analyses indicated that PG is mainly composed of gypsum (> 40 %) and particles varying from 53 to 74 μm in diameter.

The sandy soil is made up of quartz (> 30 %) and has particles varying from 105 to 250 μm in diameter. The main constituent of the clayey soil is kaolinite (> 30%) and has fine particles of approximately 250 μm in diameter.

The ^{226}Ra (251 Bq.kg^{-1}) and ^{228}Ra (226 Bq.kg^{-1}) activity concentrations in PG samples were well below EPA limits recommended for agricultural purposes (EPA, 1988). ^{210}Pb and ^{210}Po activity concentration values were similar to those values found for ^{226}Ra and ^{228}Ra.

The ^{238}U concentration in PG samples was bellow the concentration found in the clayey soil. ^{232}Th activity concentration was larger than ^{238}U, due to igneous origin of the rock which is used in the production of phosphoric acid. Activity concentration for natural radionuclides was larger in the clayey soil than in the sandy soil. The same was observed regarding the concentration of other toxic elements. These results were related to physicochemical characteristics of the soil samples. In addition, all values determined for Cd, Pb, Ni, and Cr were lower than the concentration limits established by the Brazilian Agriculture Department.

The results of the soil-plant transfer factors showed that, independently of the type of soil, it was the mobility of the radionuclides in these systems is low;

ACKNOWLEDGEMENTS

Funding for this study has been provided by Fosfertil industry and Conselho Nacional de Desenvolvimento Científico e Tecnológico (CNPq), grants nº 410021/2006-7.

REFERENCES

1. CANUT, M. (2006). Viability Study for the substitution of gypsum by phosphogysum as a building material, Master Dissertation, School of Engineer of the Federal University of Minas Gerais (UFMG), Belo Horizonte (2006).
2. MAZZILLI, B.; PALMIRO, V.; SAUEIA, C NISTI, M.B., (2000) Radiochemical characterization of Brazilian phosphogysum. Journal of Environmental Radioactivity, vol. 49, p.13-122.
3. SANTOS, A.J.G., MAZZILLI, B. P.; FÁVARO, D.I.T.; SILVA, P.S.C., (2006). Partitioning of radionuclides and trace elements in phosphogysum and its source materials based on sequential extraction methods. Journal of Environmental Radioactivity, vol. 87, p.52-61.
4. FLORIDA INSTITUTE OF PHOSPHATE RESEARCH (FIRP), 1996. The Economic benefit of phosphogysum use in agriculture in the Southeastern United States. Bartow. FL. FIPR Publication nº 01-124-119.
5. EL-MRABET R, ABRIL JM, PERIÁÑEZ R, MANJÓN G, GARCÍA-TENORIO R, DELGADO A, ANDREU.L. (2003). Phosphogysum amendment effect on radionuclide content in drainage water and marsh soils from southwestern Spain. Journal of Environmental Quality, vol. 2, p.1262-1268.
6. PAPASTEFANOU C, STOULOS S, IOANNIDOU A, MANOLOPOULOU M. (2006). The application of phosphogysum in agriculture and the radiological impact. Journal of Environmental Radioactivity, vol. 89, p.188-98.
7. RIBEIRO J.; OLIVEIRA, A., VILELA, L. and AYARZA, M.A. (2000). Nitrate adsorption in Cerrado oxisoils. Pesq. Agropec. Bras. vol.35 (6), Brasília, D.F.
8. ERNANI, P.R.; RIBEIRO, M.S.; and BAYER, C.. Chemical modifications in acid soils caused by addition of gypsum or limestone. Sci. agric., Oct./Dec. 2001, vol.58, no.4, p.825-831.
9. LOPES, A. J.; COX, F. R. (1977). A survey of the fertility status of surface soils under Cerrado vegetation of Brazil. Soil Sci Soc Am J, vol. 41, p.752-757.
10. SILVA, E.M. and AZEVEDO, J.A. (2002). Influence of the centrifugation time in the soil-water retention curve in Cerrado soils. Pesq. Agropec. Bras., vol. 37, (10), p. 1487-1494.
11. KOCHIAN, L.V., HOEKENGA, O.A., PINEROS, A.M. (2004). How do crop plants tolerate acid soils? Mechanisms of aluminum tolerance and phosphorous efficiency? Annu. Rev. Plant Biol. Vol. 55, p.459–93.
12. von UEXKULL HR & MUTERT, E. (1995). Global extent, development and economic impact of acid soils. Plant Soil, vol. 171, p.1–15.
13. LIMA E.C. and CAVALLI-MOLINA, S. (2001). Aluminum fitotoxicity: effects mechanisms of tolerance and its genetic control. Ciência Rural, vol. 31, p.531-541.
14. CREGAN, P.D. (1980). Soil acidity and associated problems - Guidelines for farmer recommendations. AGbulletin No. 7, New South Wales Department of Agriculture, Sydney.
15. HOCHMAN, Z.; CROCKER, G.J., DETTMAN, E.B. (1995). Predicting lime-induced changes in soil-pH from exchangeable aluminum, soil-Ph, total exchangeable cations and organic-carbon values measured on unlimed soils. Australian Journal of Soil Research, vol. 33 (1), p.31 – 41.
16. MARSCHNER, H. (1991). Mechanisms of adaptation of plants to acid soils. Plant and Soil, vol. 134, p.1-20.
17. BELLINGIERI, P. A.; BERTIN, E. G. (2003). Effects of the application of sewage, slags and limestone in the chemical properties of a soil cultivated with corn (Zea mays, L.). Científica, vol.31 (1), p. 81-89.

18. MALAVOLTA, E.; VITTI, G.C. 1985 Fosfogesso uso agrícola. In: SEMINÁRIO SOBRE CORRETIVOS AGRÍCOLAS, Piracicaba, 1984. Anais. Campinas: Fundação Cargill, p.161.
19. BRAZILIAN AGRICULTURAL RESEARCH CORPORATION (EMBRAPA), Soil Fertility (2000), http://sistemasdeproducao.cnptia.embrapa.br/FontesHTML/Milho/CultivodoMilho/fertilsolo.htm.
20. US EPA. UNITED STATES ENVIRONENTAL PROTECTION AGENCY. Background Information Document: Statistical Procedures for Certifying Phosphogysum for Entry Into Commerce, As Required by Section 61.207 of 40 CFR Part 61, Subpart R. EPA 402-R-98-008, Washington, DC (1988).
21. BRAZILIAN ASSOCIATION OF TECHNICAL NORMS (ABNT) 2004. NBR 10005: Procedures for obtaining leaching extracts from solid wastes, Rio de Janeiro, Brazil.
22. BRAZILIAN ASSOCIATION OF TECHNICAL NORMS (ABNT) 2004. NBR 10006. Procedures of waste solubilization, Rio de Janeiro, Brazil
23. BRAZILIAN ASSOCIATION OF TECHNICAL NORMS (ABNT), NBR 10004: Solid Waste - Classification, Rio de Janeiro (2004a).
24. W. JOHN ARTHUR III; O. DOYLE MARKHAM. (1984). Polonium-210 in the environment around a radioactive waste disposal area and phosphate ore processing plant. Health Physics, Vol. 46 (4), p.793-799.
25. MENEZES, M. A. B. C., SABINO, C. V. S., FRANCO, M. B., KASTNE, G. F. R, ROSSI, E. H. M. (2003). k_0-Instrumental Neutron Activation Analysis Establishment at CDTN, Brazil: A successful story. Journal of Radioanalytical and Nuclear Chemistry., vol. 257 (3) p. 627-632.
26. INTERNATIONAL ATOMIC ENERGY AGENCY (IAEA), Certified Reference Material IAEA/SOIL 7, (1984).
27. US EPA. UNITED STATES ENVIRONENTAL PROTECTION AGENCY. Method 3051, Microwave assisted acid digestion of sediments, sludges, soils and oils. Washington, DC, 1994.
28. WASSERMAN, M. A.; PEREZ, D. V.; LAURIA, D. C. (2002). Cultural inputs of ^{226}Ra and ^{228}Ra in tropical agricultural environments. Radioprotection – Colloquies. Proceedings of ECORAD 2001, v. 37, pp. 541-545
29. SILVA, N. C.; FERNANDES, E. A. N.; CIPRIANI, M.; TADDEI, M. H. T. (2001). The natural radioactivity of Brazilian phosphogysum, Journal of Radioanalytical and Nuclear Chemistry, vol. 249 (1), p.251-255.
30. MINISTÉRIO DA AGRICULTURA, PECUÁRIA E ABASTECIMENTO (MAPA). Brazilian Agriculture Department Normative Instruction, SDA number 27 from June 5th, 2006.

3.2. HS – Health Section

HS01	Comparation of blood residues effects in body tissues considering dose estimation three lutetium models M. F. Lima, E. B. Araújo and C. H. de Mesquita
HS02	New method for preparing a 35S in the form as a sulfite to be used as Tracer in medical and physiological research J Topkin, P Mitchel, JR Zeevaart, Z Szucs
HS03	Effect of the medicinal plant echinacea on the labeling of red blood cells with technetium-99m Maria Luisa Gomes, Glaucio Diré Feliciano, Simone Maia Evaristo and Mario Bernardo-Filho
HS04	Chemical and biological characterization of the lutetium-177 labeled bombesin derivative BBNp6 Priscilla Brunelli Pujatti, Josefina da Silva Santos, Jair Mengatti and Elaine Bortoleti de Araújo
HS05	Guide to radiopharmaceuticals interactions with other drugs Ralph S Oliveira
HS06	COMPARISON OF PC, TLC-RP AND HPLC-RP METHODS IN THE DETERMINATION OF THE RADIOCHEMICAL PURITY OF 99mTc-SESTAMIBI Almeida, E. V.;Fukumori, N. T. O.;Guirau, A.; Mengatti,J.;Matsuda, M. M. N.
HS07	Radiolabeling and quality control of 2-acetylpyridine N4-phenyl-thiosemicarbazone: a potent antitumoral agent Soares, M.A, Mendes, I. M. C., Beraldo H., Gouvêa dos Santos R1
HS08	Preparation of radioactive Gold-nanoparticles as a SPECT imaging agent Rafael Gontijo Furst Gonçalves, Marcella Araugio Soares, Paulo Roberto Ornelas da Silva, Arno Heeren de Oliveira, Andréa Vidal Ferreira, Ana Paula Alves, Marina Bicalho Silveira, Fabrício de Almeida Souza Vilas Boas, Klaus Krambrock, Luis Orlando Ladeira, Raquel Gouvêa dos Santos, Maurício Veloso Brant Pinheiro
HS09	159Gd- Gadodiamide: obtainment of a possible therapeutic radiopharmaceutical Daniel Crístian Ferreira Soares, Maria Ângela de Barros Correia Menezes, Raquel Gouvêa dos Santos, Gilson Andrade Ramaldes
HS10	195mPt- labeled cisplatin as a possible tool for glioblastoma treatment Soares M.A., Mattos J.L., Leal A.S., Santos R.G

lues effects in body tissues considering dose n three Lutetium models

M. F. Lima[1], E. B. Araújo and C. H. de Mesquita
Instituto de Pesquisas Energéticas e Nucleares (IPEN-CNEN/SP)
Av. Lineu Prestes, 2242, Cidade Universitária - CEP 05508-000 - São Paulo ï Brasil
mflima@ipen.br[1]

ABSTRACT

The lutetium biokinetic models for the estimative of the patient dose are described in the ICRP 30 and ICRP 78 reports. However, none of those models subtract the blood contained in the organ and that circulating in the organ neighborhood of the organ. Alternatively, the biokinetic data can be obtained by ópost-mortisô measurements of the radioactivity in the organs. However, this kind of sample is appropriated only for studies in animals; however, is not completely possible to avoid of the problem trying to remove all the blood on the organs. The present work is based on the Lanthanide model described in the ICRP 30, the Cerium model described in the ICRP 88 and the free Lutetium biokinectic experimental data presented by Jiménez. The MIRD protocol inside the **AnaComp™** software was used to calculate the transport of the element from fluids to other tissues and its elimination constant rate. The compartmental analysis theory helps to elucidate the dose overestimation due to the blood residues in the organs studies and to compare theoretical and experimental results. Firstly, hypothetical values of 0%, 5% and 10% of blood contained in the liver, bone and kidneys were chosen to generate the concentration response curves. Afterwards, these curves are used in the dose calculation, by interpolation of the dose in the tissues applying the reference values described in the ICRP 89 for regional blood contents in the bone (4%), liver (10%) and kidney (2%). Afterwards, a mamillar model was proposed to elucidate the data presented by Jiménez work. These results show that the three models present different results in absorbed doses. The expected doses using The ICRP models to the whole body are between 1.67 (ICRP 30) and 2.55 (ICRP 88) times the values obtained using Jiménez experimental data. The better agreement between ICRP models and experimental data was to the S*keleton:* 13.84Ÿ 17.07 mGy/MBq (ICRP 88) and *marrow +bone*: 14.16mGy/MBq (Jiménez), to the *liver:* 0.36→0.43 mGy/MBq (ICRP 30) and 0.62mGy/MBq (Jiménez) and to the *kidneys*: 20 times higher (ICRP 30) and between 4 and 1000 times higher (ICRP 88) than 0.0103mGy/MBq (Jiménez). These results show that general biokinetic models for Lutetium based in other chemical elements as suggested by ICRP 30 and ICRP 88 do not reflect the real radionuclide metabolic pathways. Consequently, the choice of representative tracers and modeling methods has to be priority in the biodistribution and dosimetric studies to approval new radiopharmaceuticals.

KEYWORDS: Biokinetic model, Compartmental analysis, MIRD protocol, Dose estimation, Lutetium.

ers described in ICRP (30 and 88) were defined only for the ithout the commitment with the physiologic aspects.[1, 2 and 3]

Recently one study of internal dosimetry of radiopharmaceuticals labeled with free ^{177}Lu published by Jiménez and coworkers come up with experimental data from biodistribution and dosimetry of ^{177}Lu in mice projected directly to the human. [4, 6]

This study is an important contribution to the ^{177}Lu biokinetics modeling because any radiopharmaceutical contained ^{177}Lu were included in the ICRP 80 Publication (International Commission on Radiological Protection), *Radiation dose to patients from radiopharmaceuticals*. [5]

The proposal of the present work is to compare the dose for ^{177}Lu calculated from models described in ICRP numbers 30 and 88 against a model, here proposed, developed in consistency with the data described by Jiménez and col. In this model, it was introduced two compartments for the bones represented by the bone marrow or the first superficial bone layer and the mineral bone.

All the data were modeled using the compartmental analysis code **AnaComp™** developed by one of the authors. [7]

2. 2. Methodology

2.1. ICRP 30 model

Biokinetics data to dose calculation, due to oral intake of Lanthanide model, presented in the ICRP30 show generic retention times (0.25 days = 2.772d^{-1}), where only the transferred fractions to destination compartment are specifically described. [2]

2.1. ICRP 88 model

Biokinetics data for dose calculation due to blood injection of Lutetium uses Cerium model presented in the ICRP88 [3]. The Cerium biological half life is 3,500 days (elimination from blood to excreta).

The transfer constant is:

$$k_{i,j} = \frac{\ln 2}{T_{1/2}b} R_j \qquad (1)$$

Where;

$k_{i,j}$ Transfer constant from original compartment *(i)* to destination compartment *(j)*;
$T_{1/2}b$ Biological half-life of chemical element (Lu) to human;
R_j Fraction of the initial injection transferred to destination compartment *(j)*.

Fig. 1 is an outline presentation of the four compartments model employed in this work. This model is supported by data from Tab. 1 and shows one same compartmental analysis scheme applicable to two models: Lanthanide group (ICRP 30) and Cerium (ICRP 88). The 4th compartment comprises the kidneys (ICRP 30) or other tissues (ICRP 88).

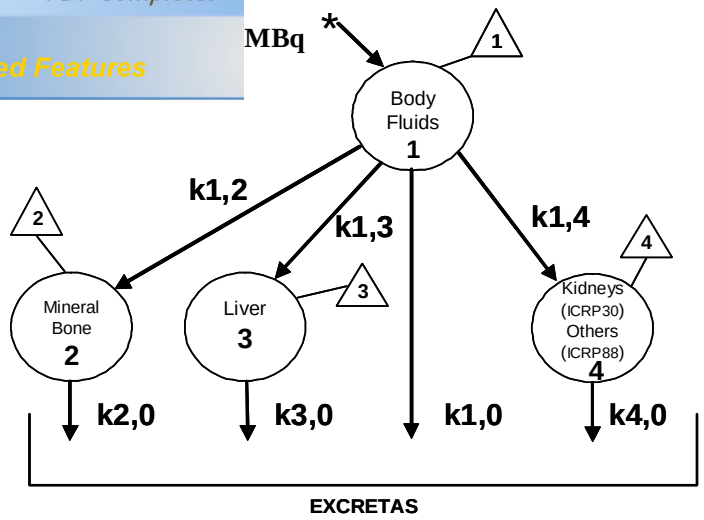

Figure. 1. Generic dosimetric compartmental model applicable to Lanthanides group according to ICRP 30 and Cerium ICRP 88.

Where:
* ↘ 1MBq injection de ^{177}Lu in the blood (time=0).
△ - Samplings.
k1,2- Transfer constant from blood to mineral bone.
k1,3- Transfer constant from blood to liver.
k1,4- Transfer constant from blood to kidneys (ICRP 30); blood-other tissues (ICRP 88).
k1,0- Removal constant from blood to excreta.
k2,0- Removal constant from bone to excreta.
k3,0- Removal constant from liver to excreta.
k4,0- Removal constant from kidneys to excreta.(ICRP 30); to other tissues-excreta (ICRP 88).

2.2. Proposed model

The model shown in Fig. 2 was developed to fit the data described by Jiménez and col. It considers the Lutetium that returns from the tissues to the body fluids removed by the blood stream. The phenomenon is remarkable only to some organs which was representative in terms of radioactivity concentration.

Jiménez experimental data projected directly from mice to the human was employed to feed the input data to **AnaComp** code.

2.2. AnaComp™ code data feeding

The code **AnaComp** [7] could be employed in different types of studies and it was firstly designed for metabolic studies. In dose calculations in organs and tissues, **AnaComp** uses the radionuclides data from **MIRD** protocol and it is capable to calculate the doses for seven human beings phantom models, from of the newly born to adults. The **MIRD** protocol inside in the **AnaComp** routines considers the whole body more 24 organs and tissues in the absorbed and effective dose calculation to the phantom models.

Tab. 1 gives the original values used in calculation following ICRP 30 and ICRP 88 and the experimental Jiménez data used to feed the **AnaComp** code for the dose estimation in organs and tissues according to a mamillar model shown in Fig. 2. [1, 3, 5]

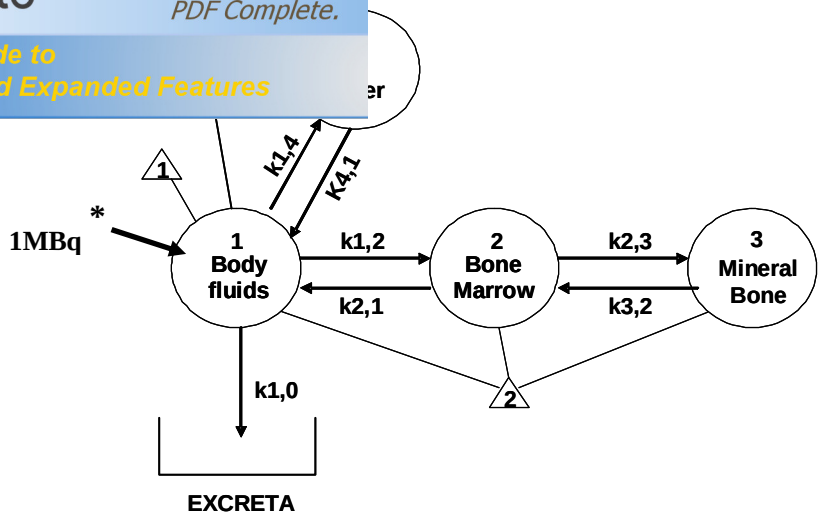

Figure. 2. Mamillar compartmental analysis scheme to Jiménez data

Where:
*↘ 1MBq injection de ^{177}Lu in the blood (time=0).
△ - Samplings,
k1,2- Transfer constant from blood to bone marrow.
k1,4- Transfer constant from blood to liver.
k1,0- Removal constant from body fluids to excreta.
k2,1- Transfer constant from bone marrow to body fluids.
k2,3- Transfer constant from bone marrow to mineral bone.
k3,2- Transfer constant from mineral bone to bone marrow.
k4,1- Transfer constant liver to blood.

Table 1. Transfer fractions of Lutetium in the whole body

Transfer Constant Between Compartments (Original→Destination) (days^{-1})		***Transferred Fractions***		***Transferred Fractions by Time (days^{-1})***	
ICRP 30	**ICRP 88**	**ICRP 30**	**ICRP 88**	**ICRP 30**	**ICRP 88**
2.772	2.772	0.6 (blood)	0.3 (blood)	k1,2=1.632	k1,2=0.8316
		0.02 (liver)	0.5 (liver)	k1,3=0.05544	k1,3=1.386
		0.05 (kidneys)	*NA*	k1,4=0.1386	*NA*
		0.33	0.2 (other tissues)	*NA*	k1,4=0.915

NA é not available in the publications

2.2. Modeling with hypothetical values of residual blood in the organs

The hypothetical values, after ex vivo samples washing, of 0%, 5% and 10% blood residues in the organs (mineral bone, liver and kidneys) were chosen to generate the following dose response curves from ICRP 30 and Jiménez data and after washing values of 0%, 5% and 10% blood residues in the tissues and organ (skeleton, liver and other tissues) to generate the following dose response curves from ICRP 88. [1,2]

Afterwards, polynomial interpolation of these curves are used to calculate the dose in the tissues applying the reference values for regional blood volumes and flow rates in adults from the ICRP 89 in the mineral bone (4%), total skeleton (7%), liver (10%) and kidneys (2%). [6]

ose fraction contribution of the residual blood in the organs) in the mineral bone; (3) in the skeleton; (4.1 and 4.2) in the

Skeleton:

$y = 1.071E^{-3}x^2 + 0.0115x + 27.873$ **(ICRP 30)** (2)

$y = 2E^{-5}x^2 + 0.323x + 13.838$ **(ICRP 88)** (3)

Liver:

$y = 1.14E^{-5}x^2 + 0.061x + 0.363$ **(ICRP 30)** (4.1)

$y = 1E^{-4}x^2 + 0.087x + 8.576$ **(ICRP 88)** (4.2)

Kidneys:

$y = 8.8E^{-6}x^2 + 0.026x + 0.234$ **(ICRP 30)** (5.1)

$y = 2.73E^{-1}x^2 + 0.273x + 0.041$ **(ICRP 88)** (5.2)

In this work, the proposed model considers that the entire blood fraction described in the ICRP 89 Publication remains in the dissected organs after the washing (3% in the bone, 4% in the bone marrow and 10% in the liver). The equations (6.1, 6.2, 6.3 and 6.4) created by **AnaComp** describe the ^{177}Lu biodistribution in the blood, bone marrow (or first layer of the cortical bone) and liver, respectively.

Blood:

$$f_1 = 99.12E^{-3.18t} + 0.585E^{-1.105t} + 0.138E^{-2.58D^{-3t}} + 0.152E^{-0.029t} \quad (6.1)$$

Bone marrow or first layer of cortical bone:

$$f_2 = 65.49E^{-3.18t} + 52.58E^{-1.105t} + 15.37E^{-2.58D^{-3t}} - 2.46E^{-0.029t} \quad (6.2)$$

Liver:

$$f_3 = 18.21E^{-3.18t} + 52.28E^{-1.105t} + 41.34E^{-2.58D^{-3t}} - 7.27E^{-0.029t} \quad (6.3)$$

Kidneys:

$$f_4 = 17.39E^{-3.18t} - 0.301E^{-1.105t} + 2.37E^{-2.58D^{-3t}} + 15.32E^{-0.029t} \quad (6.4)$$

3. Results

Tab. 2 shows data given from **AnaComp** simulations of Lutetium concentration in organs and tissues as a function of post injection time in the blood stream following ICRP 30 and ICRP 88 models and Jiménez experimental data.

oncentrations in organs and tissues as a time function following ICRP 30, ICRP 88 models and Jiménez data.

ICRP 30					JIMÉNEZ				ICRP 88				
Time (days)	**Body Fluids (Blood)**	**Mineral Bone***	**Liver**	**Kidneys**	**Time (days)**	**Body Fluids (Blood)**	**Skeleton ****	**Liver**	**Time (days)**	**Body Fluids**	**Skeleton ****	**Liver**	**Other Tissues**
	100%	**0%**	**0%**	**0%**		**100%**	**0%**	**0%**		**100%**	**0%**	**0%**	**0%**
0	100	0	0	0	0	100	3	10	0	100	0	0	0
0.01	97.267	1.640	0.055	0.01	0.0833	2.1796	38.6345	16.7968	0.01	97.267	0.822	1.367	0.547
0.05	87.057	7.765	0.259	0.065	1	1.023	42.4011	9.8436	0.1	75.790	7.263	12.105	4.842
0.1	75.790	14.526	0.485	0.120	7	0.0264	32.1194	1.6601	1	6.254	28.120	46.867	18.747
0.5	25.007	44.99	1.45	0.367	14	0.00995	20.8636	1.004	10	0	29.943	49.904	19.962
1	6.254	56.24	1.874	0.446					100	0	29.412	49.020	19.608
3	0.024	59.954	1.998	0.416					500	0	27.166	45.277	18.111
7	0	59.921	1.997	0.316					1000	0	24.599	40.997	16.399
20	0	59.767	1.992	0.128					2000	0	20.168	33.613	13.445
60	0	59.295	1.976	0.008					4000	0	13.557	22.595	9.038
100	0	58.827	1.961	0					8000	0	6.126	10.210	4.084
									10000	0	4.118	6.863	2.745

***Cortical and trabecular bones.**
****Cortical and trabecular bones, red marrow and other skeleton parts.**

Comp and **MIRD** protocol as absorbed doses/injected activity
n in the whole body, bone marrow, cortical bone, liver and
man of 73.7 kg.

The expected doses using the ICRP models to the whole body are between 1.67mGy/MBq (ICRP 30) and 2.55mGy/MBq (ICRP 88) times the values obtained using Jiménez experimental data.

The absorbed dose in the skeleton calculated using ICRP 88 and Jiménez experimental data (marrow +bone) shows that Cerium model to bone is acceptable: 13.84Ÿ 17.07mGy/MBq (ICRP 88) and 14.16mGy/MBq (Jiménez).

The absorbed dose in the liver calculated using ICRP 30 shows a better concordance with Jiménez: 0.36→0.43mGy/MBq (ICRP 30) and 0.62mGy/MBq (Jiménez).

To the kidneys, the absorbed doses calculated using Jiménez data is 20 times lower than the absorbed doses calculated using ICRP 30 model and between 4 and 1000 times lower than the absorbed dose calculated using ICRP 88 model.

Table 3. Comparison of absorbed doses calculated using **AnaComp™** and **MIRD** protocol due to ^{177}Lu biodistribution in the human considering ICRP 30, ICRP 88 and Jiménez data.

Organ/Tissue	Absorbed Dose (mGy/MBq)		
	ICRP 30	ICRP 88	JIMÉNEZ
Bone marrow		13.84Ÿ 17.07*	1.9361
Cortical bone	27.87→27.89		12.2556
Liver	0.36→0.43	8.58→9.44	0.62031
Kidneys	0.23→0.29	0.041→10.48	0.0103
Whole body	0.1849	0.2817	0.1106

é .Skeleton

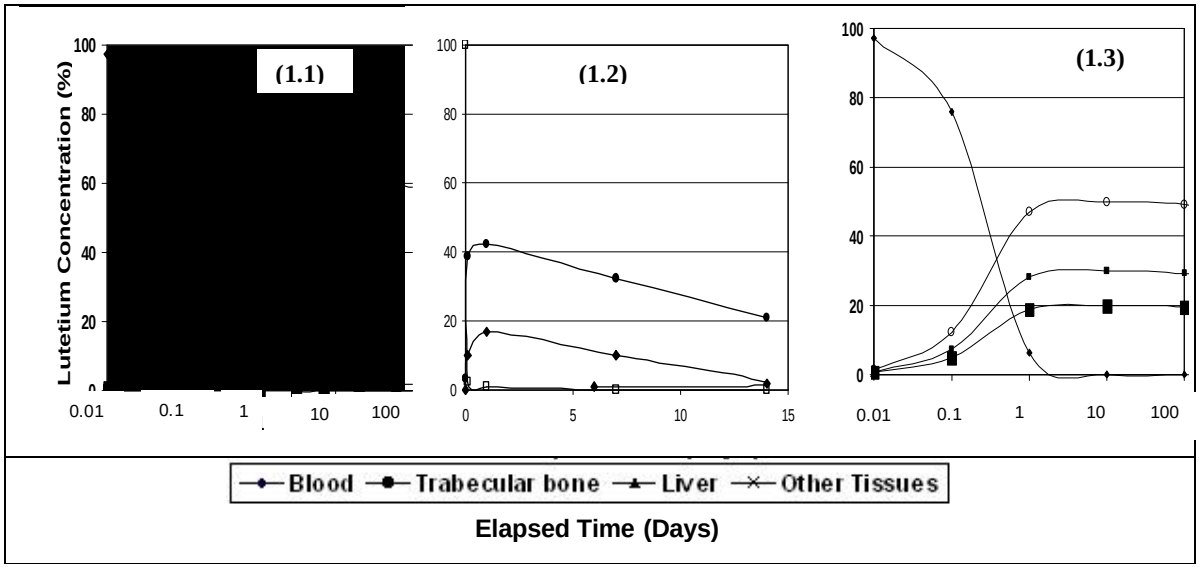

Figure 3. **AnaComp** plot of retention/elimination of Lutetium as a time function by body fluids, mineral bone, liver and kidneys, following ICRP 30 (1.1) and Jiménez (1.2) and body fluids, skeleton and other tissues following ICRP 88 (1.3) models.

h beta emitters have been used on base of results obtained til more specific studies. A classical example is the ^{119}In as tracer of the ^{90}Y. [9]

On base of results presented in this work, the general biokinetic models for Lutetium based in other chemical elements as suggested by ICRP 30 and ICRP 88 do not reflects the real radionuclide metabolic paths.

The present work indicated that the absorbed dose in the kidneys estimated in the present radionuclide therapy using Lutetium salts have to be reevaluated.

The use of a compartment that represents a tin superficial layer between bone marrow and cortical bone would be considered in the modeling of the bone seachers chemical elements used in radionuclide therapy.

Consequently, the choice of representative tracers and modeling methods has to be priority in the biodistribution and dosimetric studies to approval new radiopharmaceuticals.

Ackonowledgments: The authors gratefully acknowledge Dr. A. M. Rojo, Dr. G. M. Deluca, Dr. J. Crudo and Lic. Y.V. Jiménez for sharing the raw data modeled in this work.

REFERENCES

[1] LIMA, M. F., ARAUJO, E. B. MESQUITA, C. H., Efeito do Resíduo de Sangue nos Órgãos e sua Repercussão na Estimativa de Dose, DOSIMN 2008, Recife (2008).
[2]INTERNATIONAL COMMISSION ON RADIOLOGICAL PROTECTION, Limits for intakes of radionuclides by workers, Publication 30, Part 3, Pergamon, New York (1989).
[3] INTERNATIONAL COMMISSION ON RADIOLOGICAL PROTECTION, Doses to the embryo and fetus from intakes of radionuclides by mother, Publication 88, Elsevier, Oxford (2001)
[4] JIMENEZ,Y.V., ROJO, A. M., DELUCA, G. M., CRUDO, J., Biokinetic study of free ^{177}Lu in NIH mice, DOSIMN 2008, Recife (2008).
[5] INTERNATIONAL COMMISSION ON RADIOLOGICAL PROTECTION, Radiation dose to patients from radiopharmaceuticals, Publication 80, Pergamon, Oxford (1999). Addendum 2 to ICRP Publication 53.
[6] JIMENEZ,Y.V., Dosimetria interna de radiofarmacos marcados con ^{177}Lu, Instituto Balsero, Comision Nacional de Energia Atomica, Universidad de Cuyo, Buenos Aires (2007).
[7] AnaComp™, Manual do Programa AnaComp, v. 4.0, 1996.
[8] INTERNATIONAL COMMISSION ON RADIOLOGICAL PROTECTION, Basic anatomical and physiological data for use in radiological protection, Publication 89. Annals of the ICRP, 32, No. 3-4, Pergamon, Oxford (2002).
[9] PAUWELS, S., Practical Dosimetry of Peptide Receptor Radionuclide Therapy with ^{90}Y-Labeled Somatostatin Analogs, 15th IRIST Meeting, Rotterdam (2002).

New method for preparing a ^{35}S in the form as a sulfite to be used as Tracer in medical and physiological research

J Topkin[a], P Mitchel[a], Z Szucs[a], JR Zeevaart[b]
[a]Radiochemistry, South African Nuclear Energy Corporation (Necsa), PO Box 582, Pretoria, South Africa;
[b]CARST, North West University, Mafikeng Campus, P.Bag X2046, Mmabatho 2735, South Africa

Introduction

Labeled sulfite is used in preparing ^{35}S labeled medical and physiological chemical compounds which may provide information on the effectiveness and distribution of these compounds [1]. As sulfite, the labeled ^{35}S is stabilised as a sodium salt (see figure 1) which is chlorinated to form sulfonyl chlorides. This is then further reacted with amines to form sulfonamides [2].

Small amounts of ^{35}S measured in mC serves as starting material for the preparation of sulfur tracers. The chemical equivalent of typical amounts used for preparation of radiological tracers of ^{35}S is about 1000 mC equivalent to 0.06571 g. One stable tracer form of sulfur is the labeled sodium sulfite form. Typical techniques used for the preparation of labeled sulfite involve reduction of barium sulfate ($Ba^{35}SO_4$) with red phosphorus [3]. This chemical reaction between barium sulfate and red phosphorus is very reactive and difficult to control. Better techniques [1] were developed based on the pyrolytic decomposition of $Cu^{35}SO_4$. The pyrolytic decomposition method starts by addition of the required amount of sulfur in the form of sulfuric acid to an abundance of copper metal pieces. After drying the active sulfuric acid and copper products, copper sulfate is formed on the copper surfaces. By heating these surfaces to above 400˚C in enclosed glassware, active sulfur dioxide is liberated (figure 2). This active sulfur dioxide is bubbled through a sodium hydroxide solution, leading to the formation of the sought after labeled sodium sulfite.

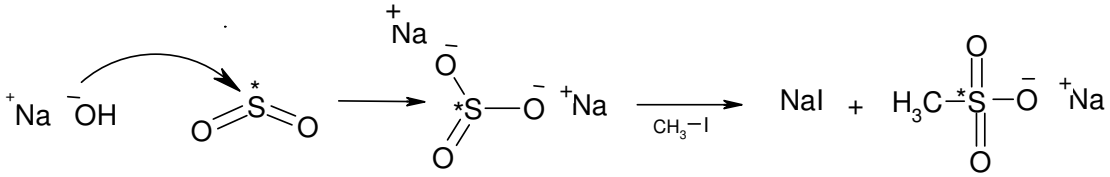

Figure 1: Schematic representation of the formation of sodium sulfite

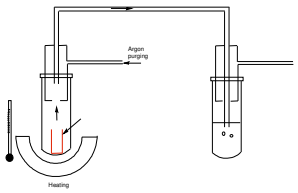

Figure 2: Thermal heating with resistant wire

Initially this pyrolytic method was used for the preparation of labeled sulfite but the following problems were experienced:

- The existing pyrex glassware had to be replaced by quartz glass since pyrex glassware cannot be used above 450˚C
- Heating electrically required long heating times of 3 to 5 hours.
- The yield of the active sulfur dioxide transferred to the sodium hydroxide was low in radiometric counts about **10%**, correlating with the results in literature.

This paper will present a new pyrolytic technique for the decomposition of $Cu^{35}SO_4$ to form sulfur dioxide. Advantages of using this technique are that the reaction time is reduced to 15 minutes and that higher yields of sulfur dioxide are achievable.

Background

The arc plasma usage for the ^{35}S preparation originated from an article by Kazutoshi Fujiwara et al [4] that used this technique for the successful removal of contamination from a stainless steel surface (see figure 3). The radioisotopes on a stainless steel surface were treated with arc plasma and the amounts of isotopes successfully removed were evaluated afterwards. The results indicated that by using this technique, approximately 80% of the radioisotopes on the steel surface could be removed.

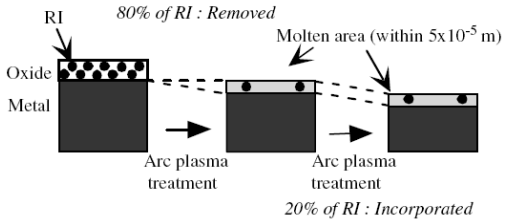

Figure 3: The successful removal of radioisotopes (RI) with arc plasma

New Arc Plasma Method

The new proposed method for preparation of sodium sulfite is similar to the arc plasma method described above. The difference is the layer of active copper sulfate on the surface of one of the electrodes is purposely formed to be removed by pyrolisation.

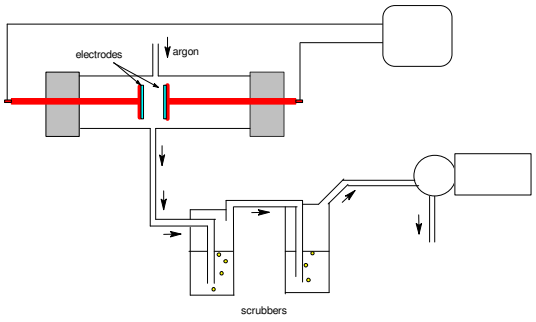

Figure 4: Schematic setup of the arc plasma method

In this method the pyrolytic decomposition of $Cu^{35}SO_4$ was achieved with an electric arc. The surface of a copper electrode was use to form copper(II) ^{35}sulfate which is then pyrolised to $^{35}SO_2$. Figure 5 shows photos of the actual tests conducted with this method. Initial results indicate that good pyrolysation occurs (see figure 6). Better results were achieved at a later stage by small changes in the experimental setup (figure 7).

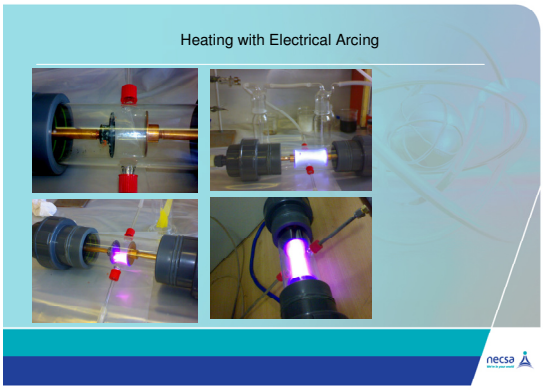

Figure 5: Tests with arc plasma

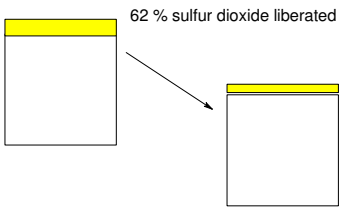

Figure 6: Initial results on tests with arc plasma showing a reduction of ^{35}S on an electrode that was spiked with the isotope

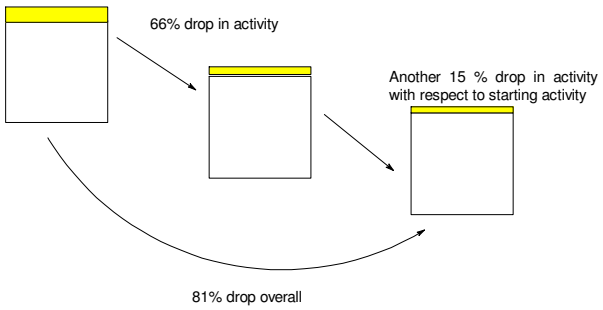

Figure 7 Better results achieved at a later stage with the arc plasma method

Figure 8 and Figure 9 shows the surfaces changes that occur during the arc plasma pyrolisation of $Cu^{35}SO_4$.

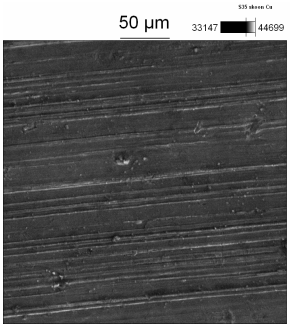

Figure 8 A clean copper surface without any addition of active sulfuric acid

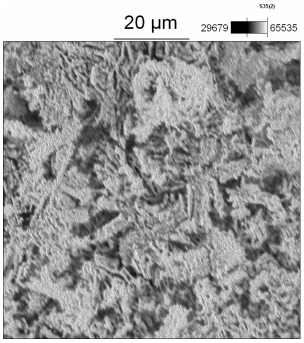

Figure 9 Discharged surface after pyrolytic decomposition of $Cu^{35}SO_4$

Conclusions

Initial results show that good pyrolysation of the active copper sulfate layer occurs with this quick method. The reaction time was reduced from 6 hours to 15 minutes. Higher yields of sulfur dioxide were liberated from the surface that was arced. Good prospects thus exists for an increased yield (from 10% to 80%) of sodium sulfite.

References

[1] Gueronniere, De L and Henry, E., R CEA, p.858, (1958)
[2] Organic Syntheses Coll. Vol 5, p.39, (1973), Vol 48, p8, (1968)
[3] Masakazu Tanase, Toshio Kase, Eiji Shikata and Hiroshi Amano, Preparation of ^{35}S-labeled Sulfite by pyrolization of Copper(II) Sulfate, Journal of Nuclear Science and Technology, 8(6), p.302 – 308 (June 1971)
[4] Kazutoshi Fujiwara, Shizue Furukawa et al, A new method for decontamination of radioactive waste using low-pressure arc discharge, Corrosion Science, Vol 48, p.1544 – 1559, (2006)

EFFECT OF MEDICINAL PLANT ECHINACEA ON THE LABELING OF RED BLOOD CELLS WITH TECHNETIUM-99m

Maria Luisa Gomes[1], Glaucio Diré Feliciano, Simone Maia Evaristo and Mario Bernardo-Filho

[1]Universidade do Estado do Rio de Janeiro, Instituto de Biologia Roberto Alcântara Gomes, Departamento de Biofísica e Biometria, Laboratório de Radiofarmácia Experimental Av. 28 de setembro, 87, Rio de Janeiro, RJ, 20551-030, Brasil. Fax number: 55 21 2543532 E.mail: malu-gomes@ig.com.br

ABSTRACT

The use of plants for the treatment of different diseases is a spread custom in the popular medicine and has increased in the last decades all over the world, but in some cases the biological effects of these plants are not known. The drug therapy could affect the blood elements labeling with technetium-99m (99mTc). This process has several important applications in Medicine like cardiovascular system analysis and detection of hemorrhage sites. Echinacea purpurea (Echinacea) is the most widely used herbal medicine in the treatment for acute upper respiratory infection based in its immunological properties. The aim of this study was to evaluate the influence of the extract of Echinacea on the morphology and labeling of red blood cells (RBC) in an in vivo study. Samples of heparinized blood were withdrawn from Wistar rats treated with Echinacea (180mg/kg) during 60 days and from the control group. Blood smears were prepared and evaluated in an optical microscope. The radioactivity in RBC were determined in a well counter and the %ATI was calculated. The analysis of the results shows that the treatment with Echinacea during 60 days could decrease the levels of RBC and hemoglobin, decrease the fixation of 99mTc in the RBC and alter the shape of RBC in comparison with the control group. The effects founded were statistically significant (Mann-Whitney test, $p<0.05$) and they could be explained by the biological properties of this studied extract of Echinacea.

Key words: Echinacea, red blood cells, morphology, technetium-99m.

INTRODUCTION

The use of plants for the treatment of diseases constitutes a line of Medicine known as Phytotherapy (Pitetti et al, 2001; Matos, 2002). A series of experiments have shown that the Phytotherapy can offer effectives solutions for different diseases with lower costs (Roman-Ramos et al, 1995). But, unfortunately, there are many plants whose effects are not known yet and their uses could affect the health (Lorenzo & Matos, 2002).

Echinacea purpurea (Echinacea) is the most widely used herbal for the treatment of acute upper respiratory infection all over the world. Echinacea extracts demonstrate significant immunomodulatory activities and the many pharmacological properties reported, are changes in the numbers and activities of macrophage, polymorphonuclear leukocytes and natural killer cells (Barrett, 2003).

In nuclear medicine, red blood cells (RBC) labeled with technetium-99m (99mTc) has several important applications, including imaging of the cardiovascular system, detection of gastrointestinal hemorrhage and localization of intramuscular hemangioma (Sampson, 1996). Red blood cells may be radiolabeled by a variety of techniques: in vivo, in vitro and a combination of the two methods. The choice of radilabeling technique is dependent on the type of clinical investigation (Sampson, 1999).

The use of the radionuclide 99mTc for labeling RBC is based on its optimal physics properties. 99mTc emit gamma ray appropriate for imaging and have a half life suitable for the duration of the clinical study. The 99mTc is most often eluted from 99Molybdenium/99mTechnetium (99Mo/99mTc) column type generators with 0.9% sodium chloride solution, in the form of 99mTc sodium pertechnetate ($Na^{99m}TcO_4$) (Sampson, 1999).

The labeling process with 99mTc needs a reducing agent. The stannous ion (Sn^{+2}) is frequently used (Hladik et al, 1987). RBC treatment can be carried out with stannous ion and afterwards with 99mTc, although the opposite can also be done. The 99mTc attach to the hemoglobin, mainly, to the beta chain, although 99mTc can also bind the erytrocyte membrane proteins (Caniné et al, 1993). Several of the cellular labeling steps have been well characterized. The band-3 protein, an anion transport system, and calcium channels may be the rays that the pertechnetate and the stannous ion, respectively, reach the interior of RBC (Callahan & Rabito, 1990).
There is growing evidence that patient drug therapy could affect the blood elements labeling and the biodistribution of labeled compounds. Certain drugs may result in a decrease in labeling efficiency, possibly by oxidation of the stannous ions may also be a cause of poor red cell labeling (Sampson, 1999). Natural products are also effective in alter the labeling procedures. It was reported that an extract of eggplant (Solanum melanogena) decrease the uptake of 99mTc in blood cells proteins due to the presence of oxidant components in the extract (Capriles et al, 2002). Paullinia cupana, popularly known as guaraná, decrease the uptake of 99mTc in red blood cells by damages in the plasma membrane (Oliveira et al, 2002).
The aim of this study was to evaluate the influence of the extract of Echinacea on the morphology of red blood cells and on the labeling of blood elements with 99mTc using in vivo assays that could explain better the biological effects of this plant.

MATERIAL & METHODS

Extract preparation

A commercial sample of dry powdered extract (360mg) made from the root of Echinacea purpurea (L) Moench, Compositae (Herbarium Laboratório Botânico, Brazil, lot 266512, validity Jan/2005) was diluted in 10mL of sodium chloride solution (NaCl, 0.9%) and after agitation followed by centrifugation (Alpha Ltda, Brasil), this preparation was filtered and the extract solution obtained was administered in the animals by oral via.

Morphology analysis

Histological preparations were carried out with the blood samples obtained from the control and treated animals. Blood smears were prepared, dried, fixed and staining (May-Grünwald-Giensa, Merck, Alemanha). After that, the morphology of red blood cells was evaluated under an optical microscope (Olympus BH2-RFCA, EUA) and the images were processed.

Labeling protocol

Samples of 0.5mL of the blood were incubated at room temperature for 1 hour with 0.5mL of stannous chloride (1.2 µg/mL) (Sigma Chemical Co., St. Louis, USA). After this period of time, 0.1mL of 99mTc, as sodium pertechnetate (3.7MBq) recently eluted from 99Mo/99mTc generator (Instituto de Pesquisas Energéticas e Nucleares, Comissão de Energia Nuclear, São Paulo, Brazil), was added and the incubation maintained for 10 minutes. These samples were centrifuged (1500 rpm) and plasma (P) and red blood cells (RBC) separated. Aliquots of 20µL of P and RBC were precipitated with 1mL of trichloroacetic acid (TCA) 5% and soluble (SF) and insoluble fractions (IF) were isolated. The radioactivity in P, RBC, SF-P, IF-P, SF-C and IF-C were determined in a well counter (Clinigamma, gamma counter, LKB, Wallac, Finland). After that, the percentage of radioactivity (%ATI) was calculated. The %ATI in P was calculated by dividing the radioactivity in P by the sum of the radioactivities in P and RBC. The %ATI in RBC was calculated by dividing the radioactivity in RBC by the sum of the radioactivities in P and RBC. The %ATI in SF-P was calculated by dividing the radioactivity in SF-P by the sum of the radioactivities in SF-P and IF-P. The %ATI in IF-P was calculated by dividing the radioactivity in SF-P and IF-P. The %ATI in SF-C was calculated by dividing the radioactivity in SF-C by the sum of the radioactivities in SF-C and IF-C. The %ATI in IF-C was calculated by dividing the radioactivity in SF-C and IF-C. The radioactivity assay was performed according to the national radiological protection norms (CNEN, 1998).

Statistical analysis
The means and standard deviations were determined. The groups (control and treated) were compared through Mann-Whitney test with significance level, $p<0.05$.

RESULTS

The distribution of radioactivity in the plasma and red blood cells from blood of control and treated animals is shown in table 1. The analysis of the results revels a significant decreased ($p<0.05$) in the uptake of 99mTc by the RBC.

Table 1 - Effect of Echinacea extract on the in vivo labeling of red blood cells and plasma with 99mTc

	Groups	
Blood constituents	Control	Experimental
Blood Cell	93.20 ± 2.98	77.16 ± 2.50
Plasma	6.80 ± 2.98	22.84 ± 2.50

The percentages of radioactivity (%ATI) in blood cells and plasma were calculated and statistical analysis ($p<0.05$) was used (Mann-Whitney test). Values are means ± standard deviations (n=4).
In the table 2 is shown the distribution of radioactivity in insoluble and soluble fractions of RBC. The analysis of the results indicates that there is a significant decrease ($p<0.05$) in the fixation of 99mTc in the IF-C.

Table 2 - Effect of Echinacea extract on the in vivo labeling of IF-C and SF-C with 99mTc

	Groups	
Blood constituents	Control	Experimental
IF-C	74,69 ± 2,80	69,04 ± 5,93
SF-C	25,31 ± 2,80	30,96 ± 5,93

The percentages of radioactivity (%ATI) in the insoluble (IF-C) and soluble (SF-C) fractions of RBC were calculated and statistical analysis ($p<0.05$) was used (Mann-Whitney test). Values are means ± standard deviations (n=4).
Figure 1 is a photomicrography of blood smears obtained from the control group and figure 2 is a photomicrography of blood smears obtained from animals that received aqueous extract of Echinacea during 60 days. The qualitative comparison of the shape of the RBC under optical microscopy showed important morphological alterations (area and perimeter) due to the treatment with Echinacea.

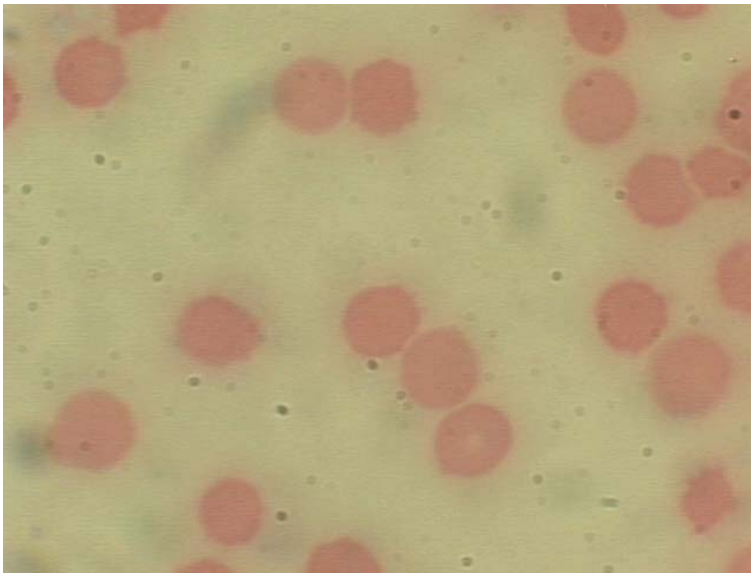

Figure 1 - Photomicrography of blood smears obtained from the control group. May-Grünwald-Giensa. 1000x.

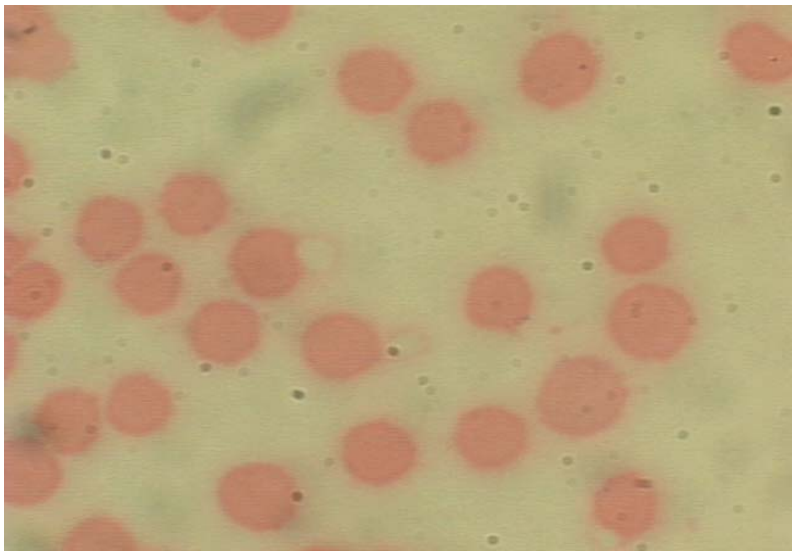

Figure 2 - Photomicrography of blood smears obtained from the animals treated with Echinacea extract (180mg/kg). May-Grünwald-Giensa. 1000x.

DISCUSSION

RBC labeled with 99mTc has been used in Nuclear Medicine images. This labeling procedure has shown an important model to evaluate the biological effects of drugs. Consequently, the ability of natural products to act as reduce or oxidant agent has been studied (Gomes et al, 2002; Diré et al, 2002; Moreno et al, 2002; Diré et al, 2003).

Evidence is now accumulating that patient medication can adversely affect the radiolabeling of red blood cells (Gleue et al, 1995). Most of the substances may interfere in the radiolabeling procedure by oxidation of the stannous ions, used for the reduction of 99mTc (Zimmer et al, 1981).

Is known that Echinacea has some active principles with antioxidative properties (Hu & Kitts, 2000), and because this is difficult to speculate that this extract could affect the labeling procedure by oxidation of stannous chloride.

The alterations on the morphology of RBC caused by the treatment with Echinacea could explain the effect in the labeling procedure. The damages in the plasma membrane caused by the referred

extract possible interferes with the incorporation of the 99mTc and/or stannous chloride into the RBC resulting in lower labeling efficiency.
The 99mTc transport into the RBC is trough the banda3 protein (Callahan & Rabito, 1990). This protein is responsible to the fixation of the cytoskeleton in the membrane. The alteration in the plasma membrane interferes, consequently, in the properties of the transport proteins (Gitirana, 2004).

REFERENCES

1. Barrett B. Medicinal properties of Echinacea: a critical review. Phytomedicine. 10(1):66-86, 2003.
2. Callahan RJ and Rabito CA. Radiolabeling of erythrocytes with technetium-99m: role of band-3 protein in the transport of pertechnetate across the cell membrane. J Nucl Med. 31: 2004-2008, 1990.
3. Caniné MC, Boasquevisque EM and Bernardo-Filho M. Binding sites of 51Chromium and 99mTechnetium to red blood cells: a comparative study. Acta Medica et Biologica. 41(4): 189-192, 1993.
4. Capriles PVSZ, Dias APM, Costa TEMM, Oliveira MBN, Faria MVC, Moura EG, Abreu BAL and Bernardo-Filho M. Effect of eggplant (Solanum melanogena) extract on the in vitro labeling of blood elements with technetium-99m and on the biodistribution of sodium pertechnetate in rats. Cell Mol Biol. 48(7): 771-776, 2002.
5. CNEN. Diretrizes Básicas de Proteção Radiológica NE - 3.01. Comissão Nacional de Energia Nuclear, Ministério das Minas e Energias, Rio de Janeiro, 1988.
www.cnem.gov.br/segurança/normas
6. Diré G, Lima EA, Pereira MJS, Oliveira MB, Pereira MJ, Moreno S, Mattos DMM, Jales RL, Bernardo-Filho M. Effect of a chayotte (Sechium edule) extract on the labeling of red blood cells and plasma proteins with technetium-99m: in vitro and in vivo studies. Cell Mol Biol. 48: 751-755, 2002.
7. Diré G, Lima EA, Gomes ML, Castro-Faria M, Jales RL, Bernardo-Filho M. Effects of a chayotte (Sechium edule) extract (macerated) on the labeling of blood constituints with technetium-99m, on the biochemistry of bloods of Wistar rats and on the action against the stannous chloride effect. J Animal Veterinary Advances. 2: 602-606, 2003.
8. Gitirana LB. Histologia: conceitos básicos dos tecidos. São Paulo, Atheneu, 2004.
9. Gleue AD, Spicer JA and Preston DF. The effect of cyclosporine on technetium-99m red blood cell labeling using the ultratag RBC in vitro kit. J nucl med Technol. 23: 22-25, 1995.
10. Gomes ML, Oliveira MBN, Bernardo-Filho M. Drug interactions with radiopharmaceuticals: effect on the labeling of red blood cells with technetium-99m and on the bioavailability of radiopharmaceuticals. Braz Arch Biol Technol. 45: 143-149, 2002.
11. Hladik III WB, Saha GB and Study KT. Essentials of Nuclear Medicine Sciences. Willians and Wilkins, Baltimore, London, 1987.
12. Hu C, Kitts DD. Studies on the antioxidant activity of Echinacea root extract. J Agric Food Chem. 48: 1470-1472, 2000.
13. Lorenzi H, Matos FJA. Plantas Medicinais no Brasil - Nativas e exóticas. Nova Odessa, Instituto Plantarum, 2002.
14. Matos FJA. Farmácias vivas. 4ª edição. Fortaleza, Edições UFC, 2002.
15. Moreno SRF, Freitas R, Diré G, Farah M, Lima E, Lima-Filho GL, Pereira MJ, Mandarim-Lacerda C, Rocha EK, Bernardo-Filho M: Evaluation of the effect of a Ginkgo biloba extract on the biodistribution of sodium pertechnetate in rats and on the morphology of red blood cells. In Technetium, rhenium and other metals in chemistry and nuclear medicine 6. Nicoline, M. and Mazzi, U. (eds.) Servizi Grafici Editoriali, Padova, Italy. 531-533, 2002.
16. Oliveira JF, Ávila AS, Braga ACS, Oliveira MBN, Boasquevisque EM, Jales RL, Cardoso VN and Bernardo-Filho M. Effect of extract of medicinal plants on the labeling of blood elements with

technetium-99m and on the morphology of red blood cells: I – a study with Paullinia cupana. Fitoterapia. 73: 305-312, 2002.
17. Pitetti R, Singh S, Hornyak D, Garcia SE, Herr S. Complementary and alternative Medicine use in children. Pediatr Emerg Care. 17: 165-9, 2001.
18. Roman-Ramos R, Flores-Saenz JL and Alarcon-Aguilar FJ. Anti-hiperglycemic effects of some edible plants. J Ethnopharmacol. 48: 25-32, 1995.
19. Sampson CB. Complications and difficulties in radiolabelling blood cells: A review. Nuclear Medicine Communications. 17: 648-658, 1996.
20. Sampson CB. Textbook of Radiopharmacy. Theory and Practice. 3rd edition. Edited by Charles B. Sampson. Gordon and Breach Science Publishers, Amsterdan, Netherlands. 530pp, 1999.
21. Zimmer AM, Spies M and Majewiski W. Effects of drugs on in vivo RBC labeling: a propose mechanism of inhibition. In Proceedings of the Second Intrnational Symposium of Radiopharmacy, Chicago, 1981.

CHEMICAL AND BIOLOGICAL CHARACTERIZATION OF THE LUTETIUM-177 LABELED BOMBESIN DERIVATIVE BBNP6

Priscilla Brunelli Pujatti*, Josefina da Silva Santos, Jair Mengatti and Elaine Bortoleti de Araújo
Directory of Radiopharmacy – Nuclear and Energetic Research Institute – IPEN / CNEN – São Paulo – Brazil
*E-mail address: priscillapujatti@yahoo.com.br

ABSTRACT

In designing radiometal-based peptides for cancer diagnostic and treatment, important factors to consider are the physical characteristics, cost and availability of the radionuclide and the radiolabeled molecule chemical and biological properties. In the field of radiolabeled peptides, bombesin analogs have become focus of interest because their receptors, specially gastrin-releasing peptide receptor (GRP), have been shown to be massively overexpressed in several human tumors. In this work we describe the radiolabeling with ^{177}Lu and some properties of the novel bombesin analog BBNp6 – DOTA-Y-BBN(6-14), where Y is a spacer of six aminoacids – in order to predict its target to tumor cells in animal tumor models. BBNp6 was labeled with high yield and kept stable after storing at 4ºC and in human serum at 37°C. This peptide exhibits low lipophilicity, in according to its partition coefficient, and in vivo pharmacokinetic studies showed a bicompartimental distribution model with fast blood clearance. These results suggest that BBNp6 has ideal characteristics for a radiopharmaceutical and can be applied in preclinical studies.

Keywords: Bombesin analogs, lutetium-177, GRP receptor.

1 INTRODUCTION

Radionuclides coupled to receptor-specific peptides are currently under investigation in clinical trials involving different tumors. They specifically localize receptors overexpressed on the plasma membrane and then internalize into cells. The prototypes of these peptides are somatostatin analogs (Zhang et al., 2007) and the success in the area of somatostatin receptor-positive tumor targeting with diagnostic and therapeutic radionuclides has stimulated research toward radionuclide targeting of alternative receptor systems overexpressed in tumors (Maina et al., 2005).

In designing radiometal-based radiopeptides for cancer diagnosis and treatment, important factors to consider are half-life, mode of decay, cost and availability of the radionuclide and the chemical and biological properties of the labeled molecule. In the field of radiolabeled peptides, bombesin appears as focus of interest. Bombesin peptide (BBN) is a 14-amino acid analog of human gastrin releasing peptide (GRP) originally isolated from the skin of the frog Bombina bombina in 1970. There are four known receptor subtypes of BBN, including the neuromedine B receptor (subtype 1), the GRP receptor (GRPr, subtype 2), the orphan receptor (subtype 3) and the BBN receptor (subtype 4) (Lane et al., 2008). GRPr expression is normally restricted to nonneuroendocrine tissues of the pancreas and breast, and neuroendocrine cells of the brain, gastrointestinal tract, lung and prostate, but it is not normally expressed by epithelial cells present in colon, lung or prostate (Lantry et al., 2006). In addition, gastrin-releasing peptide receptors are predominantely expressed in different human tumors, such as prostate cancer, gastrinoma, and breast cancer. This findings provide a possibility to apply bombesin-like peptides as a vehicle for delivery cytotoxic radiation doses into tumor cells (Zhang et al., 2004).

The application of ^{177}Lu isotope in medicine is spreading in a last few years. This radiolanthanide has been finding a continuously wider use in diagnosis and therapy. This increasing is probably due to its good radiation properties. Its half-life of 6.65 days permits to apply sophisticated procedures to synthesize and purify the radiopharmaceuticals requiring the use of more time and work. Besides, its beta radiation of 498 keV maximum energy is very suitable for cancer therapy ensuring the interacting range in a human tissue of about 670 m. The presence of modestly energetic and abundant (11%) gamma-radiation of 208 keV makes it suitable for gamma scintigraphy. As with

other radiolanthanides, it is relatively easy to conjugate the ^{177}Lu numerous biologically active compounds (Mikolajczak et al., 2003).
Studies with bombesin agonists and antagonists radiolabeled with lutetium-177 have been reported and have shown to reduce tumor growth in mice. Despite the variety of compounds synthesized, one with the optimal characteristics for systemic radiotherapy – including maximal tumor uptake and retention and minimal nontumor tissue uptake and retention – has yet to be reported. Most of the studied analogs exhibit high abdominal accumulation, specially in pancreas and intestine (Garayoa et al., 2007; Lantry et al., 2006; Rogers et al., 2003; Smith et al., 2003; Prasanphanic et al., 2007). This abdominal accumulation may represent a problem in clinical use of radiolabeled bombesin analogs probably due to serious side effects to patients. The aim of the present work is to develop a novel bombesin analog (BBNp6) – DOTA-Y-BBN(6-14) – radiolabeled with lutetium-177 (^{177}Lu) and to characterize its chemical and biological properties. Y is a spacer of six aminoacids which was inserted between the chelator and the binding sequence in order to improve bombesin in vivo properties.

2 MATERIALS AND METHODS

2.1 Reagents

DOTA-Y-BBN(6-14) was provided from piChem and $^{177}LuCl_3$ was obtained from IBD (Netherlands). All other chemicals and reagents required for experiments were of analytical grade and were purchased from Sigma Aldrich Chemical Co..

2.2 Radiolabeling of BBNp6

Preliminary studies were done to establish the ideal labeling conditions of labeled BBNp6. All reagents were prepared with Chelex 100 treated free metal water. Briefly, BBNp6 (20 □g), 0.4 mol/L sodium acetate buffer pH 4.5 and 92.5 MBq (2.5 mCi) of $^{177}LuCl_3$ (specific activity 871 – 920 GBq/mg) were heated at 90°C for 30 minutes.

2.3 Quality Control

Instant thin layer chromatography (ITLC) was applied to determine free lutetium, with citrate/citric acid buffer pH 5.0 as solvent (Rf of labeled peptide was 0.1-0.3 and Rf of free lutetium was 0.9-1.0). Radiochemical purity was also determined by HPLC (Shimatzu) using RP C_{18} columns (Waters, 4.0 x 150 mm, 5 □m) with radioactivity (Shell) detection, flow rate of 1.5 mL/minute with a linear gradient of 10-90% (v/v) 0.1% TFA / acetonitrile and 0.1% TFA / H_2O for 15 minutes.

2.4 Purification of ^{177}Lu-BBNp6

Reaction mixtures were purified on Sep-Pak C_{18} reversed phase extraction cartridge (Waters) as described by Zhang et al. (2004). The column was prewashed with 10 mL of ethanol and subsequently activated with 10 mL of distilled water. After application of the sample, the cartridge was washed with 10 mL of distilled water to remove free lutetium-177 followed by 5 mL of methanol to elute the labeled peptide. The solvent was evaporated and the dry residue was dissolved in saline.

2.5 Stability of radiolabeled BBNp6

To determine the ^{177}Lu-BBNp6 in vitro stability the preparation was stored at 4°C for different times (1 to 7 days) or human serum samples were spiked with ^{177}Lu-BBNp6 and incubated for 1, 4 and 24 hours, followed by ITLC analysis. All experiments were performed in triplicate.

2.6 Partition coefficient

The partition coefficient of radiolabeled BBNp6 was determined according Durkan et al. (2007), with some modifications. A 25 □L aliquot of radiolabeled peptide was added to a test tube containing 3 mL of each of n-octanol and water. The tube was vortexed for 1 hour at room temperature and then aliquots of each phase were taken for counting. The partition coefficient was

determined by the function: Partition coefficient = $\log_{10}$ (counts in n-octanol phase / counts in water phase). The experiments were performed in triplicate.

2.7 In vivo studies

2.7.1 Animals

Animal studies were performed in accordance with United Kingdom Biological Council's Guidelines on the Use of Living Animals in Scientific Investigations as well as institutional guidelines. Male Balb-c mice (4 to 6 weeks old, 20-25 weight, IPEN) were used for in vivo experiments.

2.7.2 Biodistribution studies

The radioactive analog (0.185 MBq/100□L/mouse) was injected intravenously in mice lateral tail vein. After different time intervals (1, 4 and 24 hours p.i.), the animals were sacrificed in groups of five and the blood was collected. Then, the mice were dissected and vital organs were isolated, weighed and their respective radioactivities were measured in an automatic gamma counter (Packard). The biodistribution of labeled BBNp6 was calculated as percentage uptake of injected dose per organ (%ID) and per gram of organ (%ID/g).

2.7.3 Pharmacokinetics

Kinetics studies were performed by measuring ^{177}Lu-BBNp6 in blood. Blood samples were collected 1, 5, 30, 60, 120, 240 and 1440 min after the intravenous injection and their radioactivities were measured as described early. The pharmacokinetics parameters were determined using Biexp software.

2.8 Statistical analysis

Statistical analysis were performed using Prism 3.0 software. Results were subjected to Student´s t-test and expressed as mean $\pm$ SD.

3 RESULTS

3.1 Radiolabeling of BBNp6 with Lutetium-177

BBNp6 was radiolabeled with high yield (98.70 $\pm$ 0.15%) and a specific activity of ~7.30 MBq/□g was achieved. Sep-Pak purification procedure did not alter the radiochemical purity of the methanol fraction.

The FIG. 1 shows a typical radioactive HPLC profile of ^{177}Lu-labeled BBNp4. The labeled peptide (Rt = 6.55 minutes) can be clearly separated from free lutetium (Rt = 1.15 minutes).

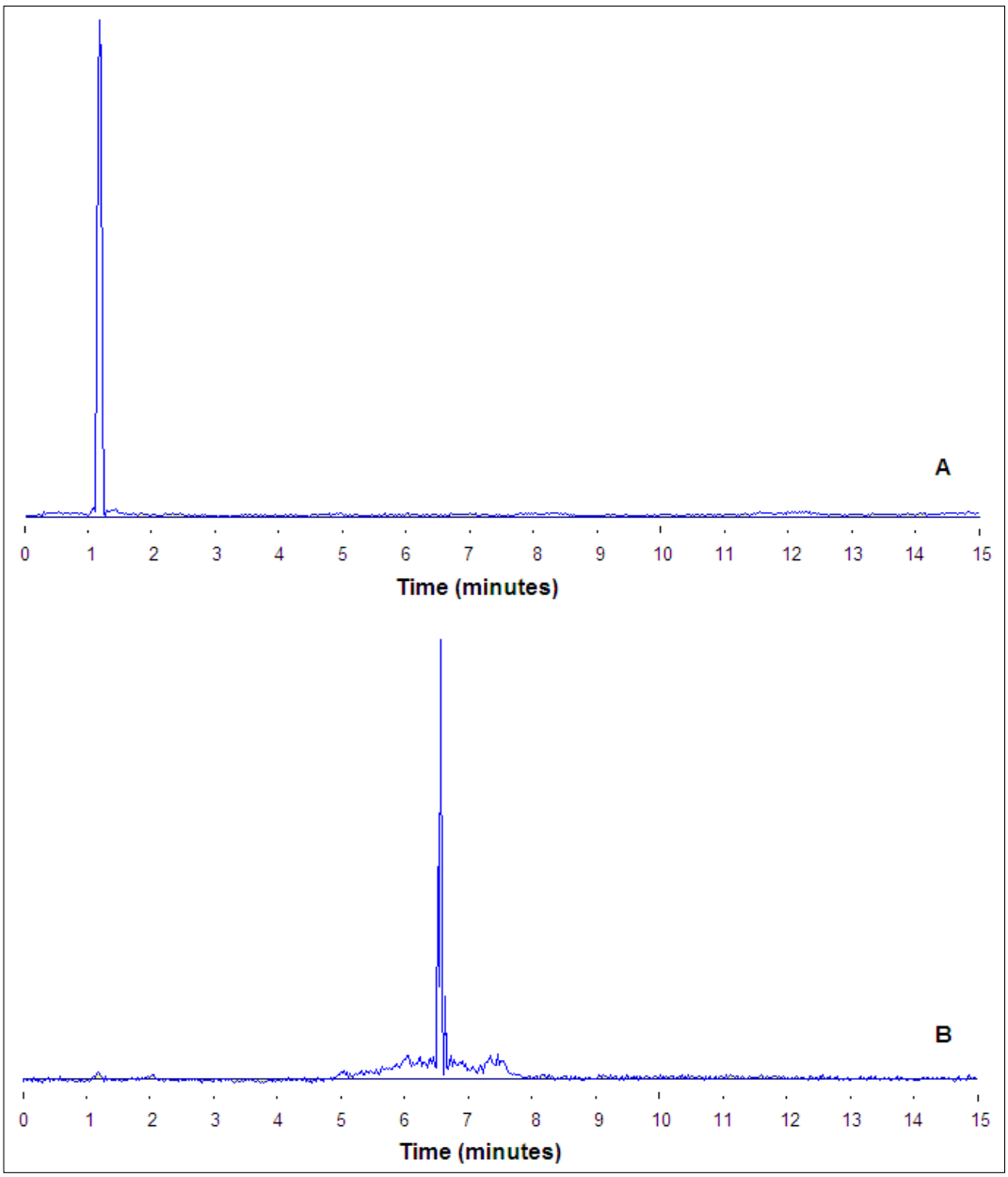

FIG. 1. HPLC chromatogram of (A) lutetium-177 and (B) ^{177}Lu-BBNp6.

3.2 Stability of ^{177}Lu-BBNp6

The stability of labeled peptide was evaluated by instant thin layer chromatography after storage at 4°C and incubation at 37°C in human plasma. The Table I shows the results obtained from the samples stored at 4°C at different times. ^{177}Lu-BBNp4 remain stable at this temperature and the radiochemical purity were higher than 90% for more than 168 hours (7 days) of storage.

Table I. In vitro stability of radiolabeled BBNp4 after storing a 4°C for different times.

	Incubation time at 4°C					
	Immediately	24 hours	48 hours	72 hours	96 hours	168 hours
Radiochemical Purity	98.9 ± 0.5	98.1 ± 0.8	96.2 ± 0.9	95.6 ± 0.6	94.1 ± 1.8	91.4 ± 1.1

After incubation of ^{177}Lu-BBNp6 with fresh serum, differences in the ITLC chromatogram were detected in all time intervals analyzed, suggesting a metabolic degradation of the labeled peptide by serum enzymes. These differences were used to calculate the radiochemical purity of the preparation and can be seen in the FIG. 2.

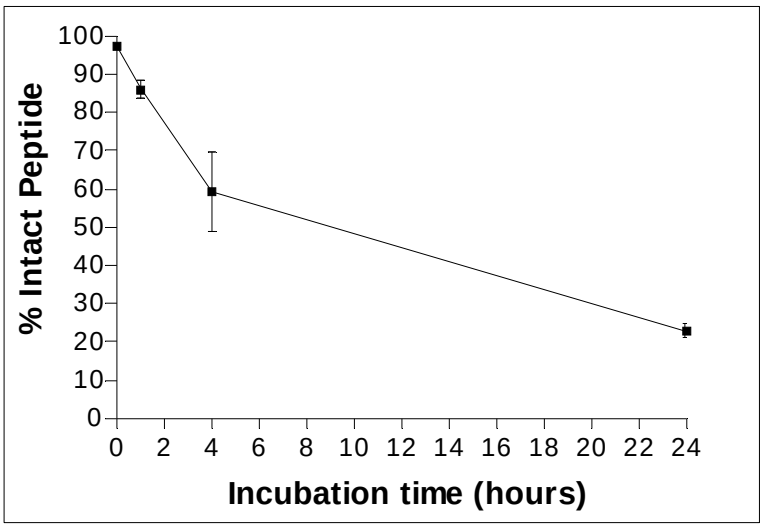

FIG. 2. Time-course degradation of ^{177}Lu-DOTA-Y-BBN(6-14) in human serum at 37°C. The radiochemical purity decreased to 86.1 $\pm$ 2.4, 59.3 $\pm$ 10.5 and 23.0 $\pm$ 2.0 after 1, 4 and 24 hours of incubation, respectively.

3.3 Partition coefficient determination

Partition coefficient results showed that the experimental partition coefficient of ^{177}Lu-BBNp6 was found as -2.94 $\pm$ 0.1, indicating that radiolabeled peptide exhibits low lipophilicity.

3.4 In vivo studies

Results from biodistribution studies using the ^{177}Lu-labeled peptide performed with Balb-c mice are presented in FIG. 3 as the percentage of injected activity per gram of organ (% IA/g). Appreciable radioactivity could be detected in the kidneys and intestine until 24 hours post injection, indicating peptide excretion by renal pathway and peptide binding to GRPr, mainly localized in pancreas and colon. Kidneys may be the critical organs for dosimetry. In addition, it could be observed low abdominal accumulation of ^{177}Lu-BBNp6, specially in pancreas.

Bone uptake is commonly assumed as a control of lutetium-labeled compounds stability in in vivo assays. This tissue actively uptakes free lutetium-177, being a good indicator of radiochemical purity, mainly at the initial time. Bone uptake of ^{177}Lu-BBNp4 was negligible when compared to pure $^{177}LuCl_3$ (Haley et al., 1964), confirming no contamination of free lutetium in the preparation.

To evaluate the pharmacokinetic of ^{177}Lu-BBNp6 in mice we performed kinetics studies by measuring the radiolabeled peptide in blood. The results of blood analysis are expressed in FIG. 4 and the calculated pharmacokinetics parameters are resumed in Table II. The amount of ^{177}Lu-BBNp6 present in plasma decreased rapidly and became almost undetectable at 60 minutes post injection. This rapid clearance is performed mainly by renal pathway, as described early in the biodistribution assay.

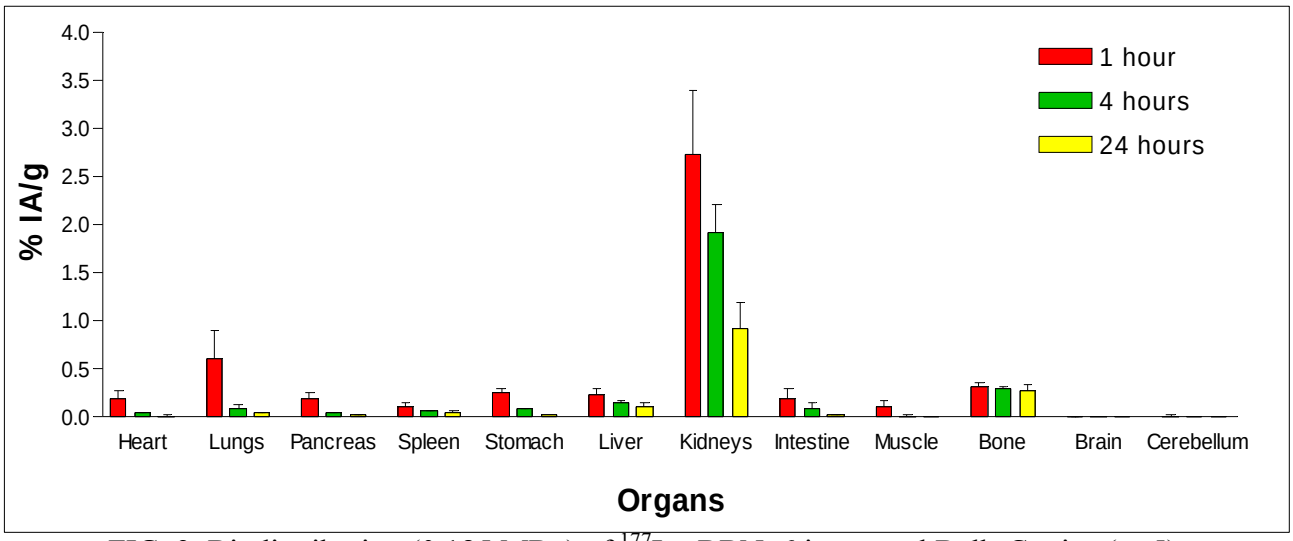

FIG. 3. Biodistribution (0.185 MBq) of ^{177}Lu-BBNp6 in normal Balb-C mice (n=5).

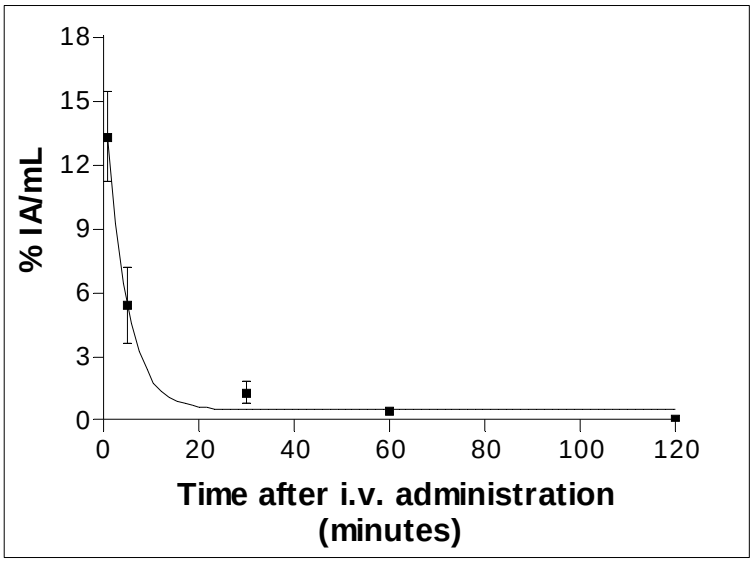

FIG. 4. Blood clearance kinetics of labeled BBNp6. Data analysis suggest a two-compartmental model (Biexp software).

Table II. Calculated pharmacokinetics parameters for ^{177}Lu-BBNp6 in male Balb-C mice. Blood sample data was adjusted by two phases with an exponential and a linear component.

Pharmacokinetics Parameters	Value for ^{177}Lu-BBNp6
Equation	$C(t) = 15105.62^{-2.20t} + 241.46^{-0.0030t}$
$T_{1/2}$ fast phase (h)	0.32
$T_{1/2}$ slow phase (h)	88.29
$^{*}K_{12}$ (h^{-1})	1.76
$^{**}K_{21}$ (h^{-1})	0.04

Pharmacokinetics Parameters	Value for ^{177}Lu-BBNp6
$^{***}K_{10}$ (h^{-1})	0.41
Distribution volum (mL)	493.62
Clearance ($mL.h^{-1}$)	4.74
$^{****}K_{ss}$ (h^{-1})	0.009

*Intravascular to extravascular space transfer constant; **Extravascular to intravascular space transfer constant; ***Intravascular space to excretion system transfer constant; ****Elimination rate constant

4 DISCUSSION

Radiopharmaceuticals for systemic therapeutic applications are designed to deliver a therapeutic dose of radiation to specific disease sites. The ionizing radiation (e.g., □- or □-particles) given off from such compounds can either damage cellular components in the target tissue directly or indirectly via the free radicals. However, the potentially destructive properties of a therapeutic radioisotope emission are not limited to their cellular targets (Chen et al., 2008) and the efforts in developing novel bombesin derivatives are concentrated in reducing their binding to non-target tissues. This selectivity is influenced by the length and composition of the spacer group.

In this work we described the radiolabeling, chemical and biological properties of the novel bombesin analog BBNp6. In the developing procedure of this new derivative we intended to insert a hydrophilic spacer between the chelator group (DOTA) and the aminoacidic bombesin sequence 6-14. The results of partition coefficient, pharmacokinetics analysis and biodistribution studies showed that ^{177}Lu-BBNp6 exhibits very low lipophilicity, rapid blood kinetic and fast renal excretion. So, the use of the six-aminoacid spacer group, in this case, influenced the biodistribution pattern of radiopeptide and determined low liver uptake and rapid clearance mainly performed by renal pathway.

An inconvenient of most studied bombesin analogs is their high in vivo uptake by pancreas and intestine due to the high density of GRP receptors in these mice tissues (Garayoa et al., 2007; Lantry et al., 2006; Rogers et al., 2003; Smith et al., 2003; Prasanphanic et al., 2007). Although GRPr are found in rodent pancreas but rarely in human pancreas, these receptors are present in high density in human colon (Waser et al., 2007) and colon dosimetry would constitute a problem for the clinical application of radiolabeled bombesin analogs in target radiotherapy. Biodistribution studies showed ^{177}Lu-BBNp6 uptake by the intestine, suggesting accumulation of the radiolabeled peptide in colon, but this bind was lower than that decribed for other bombesin derivatives (Garayoa et al., 2007; Lantry et al., 2006; Rogers et al., 2003; Smith et al., 2003; Prasanphanic et al., 2007). This lower pancreatic and intestinal uptake of ^{177}Lu-BBNp6 could means lower tumor affinity, but some studies have shown non linear relation between tumor uptake and pancreatic or intestinal uptake (Garayoa et al., 2007). So, BBN analogs which show low uptake by these organs can also bind to tumor cells that overexpress GRPr. These considerations and the results of the present study are encouraging to justify further evaluation of the radiolabeled peptide as a possible GRP-based tumor imaging and treatment agent.

5 REFERENCES

1. CHEN J, LINDER KE, CAGNOLINI A, METCALFE E, RAJU N, TWEEDLE MF, SWENSON RE. Synthesis, stabilization and formulation of 177Lu[Lu]-AMBA, a systemic radiotherapeutic agent for gastrin releasing peptide receptor positive tumors. Applied Radiation and Isotopes 66:497-505, 2008.
2. DURKAN K, LAMBRECHT FY, UNAK P. Radiolabeling of bombesin-like peptide with ^{99m}Tc: ^{99m}Tc-litorin and biodistribution in rats. Bioconjugate Chemistry 18:1516-1520, 2007.

3. GARAYOA EG, SCHWEINSBERG C, MAES V, RÜEGG D, BLANC A, BLÄUENSTEIN P, TOURWÉ DA, BECK-SICKINGER AG, SCHUBIGER PA. New [^{99m}Tc]bombesin analogues with improved biodistribution for targeting gastrin releasing-peptide receptor positive tumors. The Quartely Journal of Nuclear Medicine and Molecular Imaging 51:42-50, 2007.
4. HALEY TJ, KOMESU N, EFRUS M, KOSTE L, UPHAN HC. Pharmacology and toxicology of lutetium chloride. Journal of Pharmaceutical Sciences 53:1186-1188, 1964.
5. LANE SR, VEERENDRA B, ROLD TL, SIECKMAN GL, HOFFMAN TJ, JURISSON SS, SMITH CJ. ^{99m}Tc(CO)$_3$-DTMA bombesin conjugates having high affinity for the GRP receptor. Nuclear Medicine and Biology 35: 263-272, 2008.
6. LANTRY LE, CAPPELLETTI E, MADDALENA ME, FOX JS, FENG W, CHEN J, THOMAS R, EATON SM, BOGDAN NJ, ARUNACHALAM T, REUBI JC, RAJU N, METCALFE EC, LATTUADA L, LINDER KE, SWENSON RE, TWEEDLE MF, NUNN AD. 177Lu-AMBA: Synthesis and characterization of a selective 177Lu-labeled GRP-R agonist for systemic radiotherapy of prostate cancer. The Journal of Nuclear Medicine 47(7):1144-52, 2006.
7. MAINA T, NOCK BA, ZHANG H, NIKOLOPULOU A, WASER B, REUBI JC, MAECKE HR. Species differences of bombesin analog interactions with GRP-R define the choice of animal models in the development of GRP-R-targeting drugs. The Journal of Nuclear Medicine 46:823-830, 2005.
8. MIKOLAJCZAK R, PARUS JL, PAWLAK D, ZAKRZEWSKA E, MICHALAK W, SASINOWSKA I. Reactor produced ^{177}Lu of specific activity and purity suitable for medical applications. Journal of Radioanalytical and Nuclear Chemistry 257(1):53-57, 2003.
9. PRASANPHANIC AF, NANDA PK, ROLD TL, MA L, LEWIS MR, GARRISON JC, HOFFMAN TJ, SIECKMAN, GL, FIGUEROA SD, SMITH CJ. [^{64}Cu-NOTA-8-Aoc-BBN(7-14)NH$_2$] targeting vector for positron-emission tomography imaging of gastrin-releasing peptide receptor-expressing tissues. PNAS 104(30):12462-12467, 2007.
10. ROGERS BE, BIGOTT HM, MCCARTHY DW, MANNA DD, KIM J, SHARP TL, WELCH MJ. MicroPET imaging of a gastrin-releasing peptide receptor-positive tumor in a mouse model of human prostate cancer using a 64Cu-Labeled bombesin analogue. Bioconjugate Chemistry 14:756-763, 2003.
11. SMITH CJ, SIECKMAN GL, OWEN NK, HAYES DL, MAZURU DG, KANNAN R, VOLKERT WA, HOFFMAN TJ. Radiochemical investigations of gastrin-releasing peptide receptor-specific [^{99m}Tc(X)(CO)$_3$-Dpr-Ser-Ser-Ser-Gln-Trp-Ala-Val-Gly-His-Leu-Met-NH$_2$] in PC-3, tumor-bearing, rodent models: syntesis, radiolabeling and in vitro/in vivo studies where Dpr = 2,3-Diaminopropionic acid and X = H_2O or P(CH$_2$OH)$_3$. Cancer Research 63:4082-4088, 2003
12. WASER B, ELTSCHINGER V, LINDER K, NUNN A, REUBI JC. Selective in vitro targeting of GRP and NMB receptors in human tumours with the new bombesin tracer 177Lu-AMBA. European Journal of Nuclear Medicine and Molecular Imaging 34(1):95-100, 2007
13. ZHANG H, CHEN J, WALDHERR C, HINNI K, WASER B, REUBI JC, MAECKE HR. Synthesis and evaluation of bombesin derivatives on the basis of pan-bombesin peptides labeled with indium-111, lutetium-177, and yttrium-90 for targeting bombesin receptor-expressing tumors. Cancer Research 64:6707-6715, 2004
14. ZHANG H, SCHUHMACHER J, WASER B, WILD D, EISENHUT M, REUBI JC, MAECKE HR. DOTA-PESIN, a DOTA-conjugated bombesin derivative designed for the imaging and targeted radionuclide treatment of bombesin receptor-positive tumours. European Journal of Nuclear Medicine and Molecular Imaging 34:1198-1208, 2007.

GUIDE TO RADIOPHARMACEUTICALS INTERACTIONS WITH OTHER DRUGS

Ralph Santos-Oliveira[1],
[1]Radiopharmacist, Radiopharmacy, National Nuclear Energy Commission, Brazil.

ABSTRACT

Too many adverse reactions related to radiopharmaceuticals take place every day in hospitals routine, but many are not reported or even sensed. Information concerning these kind of reactions is not abundant and nuclear medicine staff is usually overwhelmed by this information. As every healthcare intervention carries some risk of harm, clinical decision making needs to be supported by a systematic assessment of the balance of benefit to harm. A systematic review that considers only the favourable outcomes of an intervention, without also assessing the adverse effects, can mislead by introducing a bias favouring the intervention that in the case o radiopharmaceuticals may to render a important factor related not even to the quality of the drug but even to the quality of the diagnosis. The results suggest a logical framework to make decisions in reviews that incorporate adverse reactions. Researchers undertaking a systematic review that incorporates adverse reactions must understand the rationale for the suggested methods and be able to implement them in their review. Beyond a world effort should be made to report as many cases of false positive and adverse reactions with radiopharmaceuticals as possible. Only if this is done a complete picture of false positive reactions with radiopharmaceuticals can be drawn.

INTRODUCTION

According to Mather (2001) radiopharmacy is scientifically recognised as an essential sub-speciality of nuclear medicine. Without radiopharmaceuticals, the "food" of nuclear medicine, no radiodiagnostic or radiotherapeutic procedures could be performed, and without progress in radiopharmacy medical speciality, like nuclear medicine, will, ultimately, wither and die. Radiopharmaceuticals serve two complementary roles. The first is a pragmatic one in which the labeled compound is administered to the patient and some aberrant physiological or biochemical process leads to an abnormal distribution of the compound. In the second role the radiopharmaceutical is a tracer for particular physiological or biochemical process and the time course of its distribution is used to quantity the biological process (Tweson & Krhon, 1998; Kortylewicz, 2007)

Radiopharmaceuticals have been in use for many years for the diagnosis and therapy of a wide variety of diseases (Sampson, 2003). In the early days of radiopharmacy, radipharmaceuticals were generally prepared "in-house" and were not regarded as true medicines. They were as often as not prepared on the open bench and proper quality testing was not officially recognised.

The last few decades have seen an immense growth in avalability and consumption of medicines. Whilst most consumers derive far more benefit than harm, a proportion of patients experience undesirable effects (adverse effects) from the use of medicines at recommended doses and frequencies (Wiffen et al., 2002). The radiopharmaceuticals are not diference, but the implications are so severe or more, because the interference is directly related to the quality of the exam which may result in adverse reaction.

Jones (1982) had already alerted to the fact that although ADRs (adverse reactions) can appear as isolated, specific clinical events that may be related to a number of factors in the patient's background and environment, in many situations it may not appear early as a detectable clinical event, but rather be clinically silent. With radiopharmaceuticals things are not different, since they are also drugs. Other descriptive characteristics of ADRs concern their acuteness or latency relative to drug exposure, their seriousness, and their frequency or incidence. The latter information, although highly desirable, is usually not well-defined for most adverse reactions, except the common ones defined in clinical trials. The incidence of rarer effects is known for just a few drugs, as only recently have epidemiological methods and studies been directed to this area.

MATERIALS AND METHODS

The location and the selection of studies by the authors is one of the most important step in a sytematic review. The authors need to develop a literature search strategy based on key elements in their research question: population, intervention (plus acceptable comparators), and outcomes. The review question determines the nature of the search strategy.

The collected studies were subjected to the following inclusion criteria: a) investigated the indication and drug interaction of treatment using radiopharmaceuticals; b) reported a comparison; c) reported findings and results in a manner that allowed quantitative analysis; and d)reported studies of cost-effectiveness.

A review of the literature, using some criteria of a systematic review was conduced for the drug interaction with radiopharmaceuticals. Were searched computerized databases for radiopharmaceuticals as MEDLINE, EMBASE, International Pharmaceutical Abstracts and Science Citation Index, published between 1956 and 2007 (April) using "radiopharmaceuticals/drug interactions", "radiopharmaceuticals/interactions" and many others. The searches were supplemented with manual searches of bibliographies of the published articles on major radiopharmacy textbooks, and in the Cochrane Database of Systematic Review. This review of the literature use a selection of the material collected. Was considered controlled trials, cohort studies, case-control studies and case series, in English, French, Deutsch and Portuguese language. The difficulties to find studies related to radiopharmaceuticals drug interaction, forced the acceptance of studies with low quality (less than 10 cases related in the study) but that provided information not found in other literature. Beside this, the criteria included studies of any study reports reporting prospective or retrospective monitoring of drug interaction with radiopharmaceuticals. All the papers were retrieved and reviewed.

RESULTS AND DISCUSSION

The search strategy identified 40 potentially relevant papers. Two reviews described more than 10 related-cases. Others authors published aspects of a single study in a number of related papers. All the publications included in this study were located through our replicate search and all met inclusion criteria.

The results are show below in the table 1, that sumarize all the principals studies related to radiopharmaceuticals and adverse reaction. It provide a fast way to look for and/or to consult after proceeding an exam using radiopharmaceuticals.

Table 1 – Sumary of the compounds that might interfer with radiopharmaceuticals.

Reference	Compound	Radiopharmaceuticals	Conclusion
Fisher et al.(1977)	Antiseptics iodine-based	Technetium-99	Positive: reduce the uptkake
Sampson & Hesselwood (1989)	Clorhexidine gluconate	Technetium-99	Positive: reduce the uptake
Slater et al. (1983)	Syringe and catheter components	All radiopharmaceuticals	Positive: reduce the radiopharamceuticals concentration in the sample
Millar, et al. (1983)	Syringe and catheter components	All radiopharmaceuticals	Positive: reduce the radiopharamceuticals concentration in the sample
Hladik et al (1987)	Spironolactone	Iodomethylnorcholesterol -131	Positive: increase the uptake
Fischer et al. (1982)	Spironolactone	Iodomethylnorcholesterol	Positive: increase the

Reference	Compound	Radiopharmaceuticals	Conclusion
		-131	uptake
Khafagi et al (1991)	Spironolactone	Iodomethylnorcholesterol -131	Positive: increase the uptake
Gross, et al (1981)	Spironolactone	Iodomethylnorcholesterol -131	Positive: decrease the uptake
Gross et al. (1981)	Contraceptive	Iodomethylnorcholesterol -131	Positive: increase the uptake
Sampson (1993)	Cortisone	Gallium-citrate-67	Positive: supression of the uptake
Waxman et al (1977)	Cortisone	Gallium-citrate-67	Positive: supression of the uptake
Sandler et al (1991)	Etidronate or pamidronate	Technetium-99-labelled-phosphate	Positive: reduce the increase
Hommeyer et al (1992)	Etidronate or pamidronate	Technetium-99-labelled-phosphate	Positive: reduce the uptake
Hesslewood & Leung (1994)	β-blockers	Thallous-201	Positive: reduce the uptake
Narahara et al (1989)	β-blockers	Thallous-201	Positive: reduce the uptake
Sampson (1990)	Heparinised catheter	Technetium-pyrophosphate-99m	Positive: reduce the uptake
Lentle & Scott (1979)	Heparinised catheter	Technetium-pyrophosphate-99m	Positive: reduce the uptake
Chacko et al (1977)	Heparinised catheter	Technetium-pyrophosphate-99m	Positive: reduce the uptake
Hegge et al (1978)	Heparinised catheter	Technetium-pyrophosphate-99m	Positive: reduce the uptake
Estorch et al (1990)	Doxorubicin	Antimyosin-indium-111	Positive: reduce the uptake
Reuland et al (1992)	Doxorubicin	Antimyosin-indium-111	Positive: reduce the uptake
Pope & Bratke (1981)	Opioid analgesics	Technetium-iminodiacetic-99m	Positive: reduce the uptake
Feezer (1982)	Phenobarbital and Bethanecol	Technetium-iminodiacetic-99m	Positive: increase the excretion
Hladik et al (1987)	Antibiotics and corticosteroids	Labelled-leukocytes	Positve: false-negative results
Chung et al(1991)	Antibiotics and corticosteroids	Labelled-leukocytes	Negative: no interference
Datz & Thorne (1986)	Antibiotics and corticosteroids	Labelled-leukocytes	Negative: no interference
Latham et al (1992)	Dipyridamole	Technetium-diethylenetriamine-pentact-acid-99m	Positive: affect the kdney handling.
Bobbinet et al. (1974)	Aluminium (antacids)	All radiopharmaceuticals	Positive: reduce the uptake.

Reference	Compound	Radiopharmaceuticals	Conclusion
Hesslewood & Leung(1994)	Iodide pharmaceuticals	Iodide-131 and Iodide-123	Positive: reduce the uptake
Sternthal et al (1980)	Perchlorate and pertechnetate ions	Iodide-sodium-131	Positive: reduce the uptake
Dorr et al.(1993)	Octreotide	Indium-pentetreotide-111	Positive: reduce the uptake
Sampson (1993)	Cyclosphosphamide; vincristine and cisplatin	Gallium-67	Positive: alters the pharmacokinetic
Khafagi et al.(1989)	Labetalol	I-MIBG-131	Reduce uptake
Gomes et al. (2001)	Mitomycin C	99m Tc radiopharmaceuticals, 99m Tc-diethylene-triaminepentaacetic acid (99mTc-DTPA), 99mTc-dimercaptosuccinic acid (99mTc-DMSA), 99mTc-glucioheptonic acid (99mTc-GHA)	99mTc-DTPA: Increase the uptake in pancreas, ovary, uterus, stomach, kidney, spleen, thymus, heart, lung, liver, thyroid and bone. 99mTc-DMSA: Decreased the uptake in all organs except brain 99mTc-GHA Increased the uptake in liver and decreased in stomach, thymus, heart and thyroid.
Moreno et.al (2007)	Extract of Uncaria tomentosa	Radiobiocomplex sodium pertechnetate	Increased uptake in pancreas and muscle Decreased the uptake in heart.
Moreno et al. (2007)	Extract of Ginko biloba	Sodium pertechnetate	Decrease the uptake in duodenum
Schroeder et al (2007)	Cigarrete smoke	FDG-18	Increase the uptake in lungs.

CONCLUSION

The results showed that too many drugs may to interfer with the radiopharmaceuticals metabolism or biodistribution, and for that, efforts most be made to minimize this type of event, even why this kind of event may cause a wrong interpretation of the exam results which can be very dangerous.
This review of literature for radiopharmaceuticals drug interactions intended as a guide for nuclear medicine staff referral and patient medication selection before, during or after a proceeding or use of radiopharmaceuticals. It is particularly important and useful to the daily routine of hospitals where rapid guide are very welcome.
In the lights of what was showed the drug interaction should be well documented and reported, and this information should be world-wide disseminated, because only a few studies were made in this direction and the amount of medicine that are used every day is so enormous that it seems impossible think that just 25 may really interfere with the radiopharmaceuticals.

REFERENCES

1. Bobbinet EB, et al. 1974. Lung uptake of tc-99m sulphur colloid in patients exhibiting presence of aluminium in plasma. J. Nucl.Med; 15: 1220-1222.

2. Chacko AK et. al 1977. Myocardial imaging with tc-99m pyrophosphate in patients on adiamycin treatment for neoplasia. J Nucl Med. 18:680-683.
3. Chung CJ et. al. 1991. Indium-111-labelled leukoccyte scan in detection of synthetic vascular graft infection: the effect of antibiotic treament. J Nucl Med ; 32:13-15.
4. Datz FL, Thorne DA.1986. Effect of antobiotic therapy on the sensitivity of indium-111-labelled leukocyte scans. J Nucl Med ; 27:1849-1853.
5. Dorr U et al.1993. Improved visualization of carcinoid liver metastases by indium-111 pentetreotide scintigraphy following treatment with cold somatostatin analogue. Eur J Nucl Med ; 20:431-433.
6. EARLY PJ 1995. Use of diagnostic radionuclides in medicine. Healthy Physics; 69(5):649-661.
7. Estorch M et al. 1990. Indium-111 antimyosin scintigraphy after doxorubicin theraphy in patientes with advanced breast cancer. J Nucl Med ; 31:1965-1969.
8. Feezer EA. 1982. Hepatobiliary imaging: general considerations. The view box, july issue, Dep. Nucl. Med, Wesley Medical Centre, 400pp.
9. Fischer SM et al. 1977. Unbinding of tc-99m by iodinated antiseptics. J. Nucl. Med, 18; 1139-1140.
10. Fischer M et.al. 1982. Adrenal scintigraphy in primary aldosteronism. Spironolactona as a cause of incorrect classification between adenona and hyperplasia. Eur J Nucl Med, 7:22-224, 1982.
11. Gomes ML et al. 2001. Study of the toxicological effect of mitomycin c in mice: alteration on the biodistribution of radiopharmaceuticals used for renal evaluations. Human & Experimental Toxicology; 20:193-197.
12. Gross MD et al. 1981.The roleof farmacologic manipulation in adrenal cortical scintigraphy. Semin. Nucl Med, 11: 128-148.
13. Hegge FN et al. 1978. Cardiac chamber imaging: a comparison of red blood cells labelled with tc-99m in-vitro an in-vivo. J. Nucl.Med, 21: 129-134.
14. Hesselwod S, Leung E. 1994. Drug interaction with radiopharmaceuticals. Eur. Jour. Nucl.Med; 21 (4):348-356.
15. Hladik WB et. al. 1987. Apud HLADIK, WB; SAHA, BG. Study KT, eds essentials of nuclear medicine science. Ed. Wiliams and Wilkins, Nova York .
16. Hommeyer SH et al. 1992. Skeletal nonvisualization in a bone scan secondary to intravenous etidronate therapy. J. Nucl. Med, 33: 740-750.
17. Jones JK.1982. Adverse drug reactions in the community health setting:approaches to recognizing, counseling, and reporting. Fam. Community Health 5: 58-67.
18. Keeling DH. 1990. Adverse reaction and untoward events associated with radiopharmaceuticals. In Textbook of radiopharmacy: theory and practice. Gordon and Breach, London, p.289-309.
19. Khafagi, F et al. 1991. The adrenal gland apud MAISEY, MN; BRITTON KE, GILDAY, DL. Clinical nuclear medicine, second edition. Ed. Chapman&Hall Medical, Londres, 1991.
20. Khafagi F et. al. 1989. Labetolol reduces iodine-131-mibg uptake by pheochromacytom and normal tissues. J.Nucl.Med; 30 (4): 481-489
21. Kortlylewicz JB 2007. Radioactive drugs in drug development research: quality assurance issues. Mini-Reviews in Medicinal Chemistry 7:231-244.
22. Latham TB et al. 1992. Effects of dipyrdamole infusion on human renal function observed using technetium-99m-dtpa. J.Nucl.Med; 33: 355-358.
23. Lentle BC, Scott JR. 1979. Iatrogenic alterations in radionuclide biodistribuition. Semin Nucl. Med; 9: 131-134.
24. Mather SJ 2001. Innovation in radiophatmacy:progress and constraints? Eur. Jour. Nucl. Med. 28 (4): 405-407.

25. Meyer GJ et al. 1995. PET radiopharmaceuticals in europe:current use an data relevant for the formulation of summaries of products characteristics (spcs). Eur. J. Nucl. Med; 22 (12): 1420-1432.
26. Millar AM; et al. 1983.. Failure in labelling of red cells with tc-99: interaction between intravenous cannulae and stannous pirofosfato. Eur J Nucl Med 8:502-504.
27. Moreno SRF et al. 2007. Effect of oral ingestion of an extract of the herb uncaria tomentosa on the biodistribution of sodium pertechnetate in rats. Braz. J Med Biol Res, 40 (1): 77-80.
28. Moreno SRF et al. 2007. Experimental model to assess possible medicinal herb interaction with a radiobiocomplex: qualitative and quantitative analysis of kidney, liver and duodenum isolated from treated rats. Food and Chemical Toxicology; .45:19-23.
29. Narahara KA et al. 1989. The effect of beta-blockade on single emission computed tomographic (SPECT) thallium-201 images in patients with coronary disease. Am. Heart J; 117:1030-1035.
30. Numerof P.1967. Radiopharmaceutical development in nuclear medicine. Lahey Clinic Foundation Bulletin; 16(4):321-326.
31. Pope R, Bratke J. 1981. Two tc-99mhda cases with delayded emtying into the doudenum. Monthly scan:College of Pharmacy, New Mexico, Monthly Newsletter, may/june.
32. Reuland P. 1992. Correlation of chemotherapy-induced kdney disorder and antimyosin antibody uptake in kidneys. J Nucl Med ; 33:309-311.
33. Sampson CB. 1993. Adverse reactions and drug interaction with radiopharmacuticals. Drug safety, 8 (4): 280-294.
34. Sampson CB. 1990. Drugs and chemicals wich affect the purity, biodistribuition and pharmacokinetics of radiopharmaceuticals. J. Biopharm Sci, 1(4): 381-390.
35. Sampson CB, Hesselwood SR.1989. Altered biodistribution of radiopharmaceuticals as a result of pharmacological or chemical interaction, J. Biopharm; 5: 132-151.
36. Sandler ED et al.1991. Duration of etidronate effect demonstrated by serial bone scintigraphy. J. Nucl. Med., 32:1782-1784.
37. Schoeder T et al. 2007. Pet imaging of regional 18-f-fdg uptake and lung function after cigarett smoke inhalation. J. Nucl. Med; 48: 413-419.
38. Slate DM et al. 1983. Syringe extractables, effects on radiopharmaceuticals. Lancet, n. II: 1431.
39. SIilberstein EB. 2001. Positron-emitting radiopharmaceuticals: how safe are they? Cancer Biotherapy and Radioharmaceuticals.16 (1): 13-15.
40. Sternthal E et al 1980. Supressing of thryoid radioiodine uptake by various doses of stable iodine. New England J. Med. ; 303: 1083-1088.
41. Tewson TJ, Krhon K.A. 1998. Pet radiopharmaceuticals: state-of-the-art and future prospects. Siminars in Nucl. Med. 28 (3): 221-234.
42. Waxman AS et al. 1977. Steroid induced supression of gallium uptake tumours of the central nervous system. J. Nucl. Med, 18: 618.

COMPARISON OF PC, TLC-RP AND HPLC-RP METHODS IN THE DETERMINATION OF THE RADIOCHEMICAL PURITY OF ^{99m}Tc-SESTAMIBI

Almeida, E. V.; Fukumori, N. T. O.; Guirau, A.; Mengatti, J.; Silva, C.P.G.; Matsuda, M. M. N
Radiopharmacy Directory - IPEN – CNEN/SP
Av. Professor Lineu Prestes 2242 - 05508-000 - São Paulo – SP – Brazil
erikavieira@usp.br

ABSTRACT

Technetium-99m hexakis 2-methoxy isobutyl isonitrile (^{99m}Tc-sestamibi) is a monovalent, cationic, lipophilic complex that consists of one atom of ^{99m}Tc in a +1 oxidation state and six molecules of 2-methoxy isobutyl isonitrile (MIBI). It is a promising radiopharmaceutical for myocardial perfusion imaging. The present study reports the comparison among three chromatographic methods for determination of ^{99m}Tc-sestamibi purity: paper chromatography (PC), thin layer chromatography – reversed phase (TLC-RP) and high performance liquid chromatographic reversed phase (HPLC-RP), 30 and 240 minutes after reconstitution of the sestamibi lyophilized reagent with sodium pertechnetate ($Na^{99m}TcO_4$). Sestamibi lyophilized kit and generator eluate were from IPEN-CNEN/SP (Brazil). All reagents were from Merck (Germany). A labelling kit was reconstituted by the addition of 2 mL generator eluate containing 111 MBq $Na^{99m}TcO_4$ and heating for 10 minutes in a boiling water-bath. The PC mobile phase was obtained with equal volumes of acetonitrile, 0.5 mol L^{-1} acetic acid and 0.35 mol L^{-1} sodium chloride, while 10 volumes of tetrahydrofuran, 20 volumes of ammonium acetate 0.05 mol L^{-1} solution, 30 volumes of methanol and 40 volumes of acetonitrile were mixed for TLC-RP. A 5µL sample was applied both for the PC and TLC-RP methods. The analysis by HPLC-RP was performed with a Shim-Pack VP-ODS colunm (150 mm x 4.6 mm i.d., 5 µm particle size). A 25 µL aliquot sample was injected and the mobile phase (20:35:45; v/v, acetonitrile, ammonium sulphate and methanol, respectively) was isocratically eluted, at 1.5 mL min^{-1} flow rate, continuously monitored by a radiation detector Bioscan. The time after labeling of the kit was not significant for the RCP values (up to de 0.27 %). The values TcO^-_4impurity were (0.35 ± 0.02)% by HPLC-RP and (1.86 ± 0.20)% by TLC-RP. The TcO_2 values were (0.52 ± 0.02)% by PC and (0.34 ± 0.02)% by TLC-RP. PC and TLC-RP RCP were (99.48 ± 0.09)% and (97.75 ± 0.08)%, respectively. A HPLC-RP analysis showed a labeling average efficiency of (99.36 ± 0.06)%. The identity of some radiochemical impurities of the ^{99m}Tc-sestamibi was confirmed by 3 different methods. PC, TLC-RP and HPLC-RP techniques are important aids in quality control of ^{99m}Tc-sestamibi radiopharmaceutical.

1. INTRODUCTION

Radiopharmaceuticals are substances without pharmacological activity that are used in Nuclear Medicine for diagnosis and therapy of several diseases. Diagnosis radiopharmaceuticals generally emit γ radiation or positrons (β^+) and their decay originate penetrating electromagnetic radiation that can cross the tissues and be externally detected (1). Technetium is a group VIIB transition element which has seven electrons beyond the noble gas electronic configuration. It exhibits multiple oxidation state from -1 to +7 and variable coordination number and geometries. In aqueous solution, the most stable oxidation states are +7 (TcO^-_4) and +4 (TcO_2) (2).

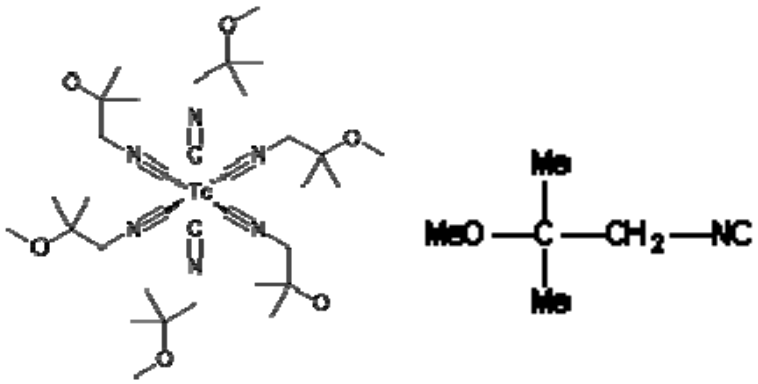

(A) (B)

Figure 1. Structure of Tc-sestamibi (A), MIBI (B) (5, 6).

Technetium-99m (^{99m}Tc) is the most frequently used radionuclide for in vivo imaging studies in Nuclear Medicine. Technetium-99m hexakis 2-methoxy isobutyl isonitrile (^{99m}Tc-sestamibi) (Fig. 1A) is a monovalent, cationic, lipophilic complex that consists of one atom of ^{99m}Tc in a +1 oxidation state and six molecules of 2-methoxy isobutyl isonitrile (MIBI) (Fig. 1B) (3).

It is a promising radiopharmaceutical for myocardial perfusion imaging and can be utilized in patients with acute myocardial infarction to quantify the amount of myocardium at risk. It is recommended at least 90% radiochemical purity (RCP) of ^{99m}Tc-sestamibi for clinical use (4). Several techniques can be used to quantify the RCP. Norenberg et al. (4) have assessed the RCP by Baker-Flex thin-layer using reagents and materials recommended in the package insert, Cardiolite DuPont. Hung et al. (7) have used Mini-Paper Chromatography (MPC) method using a cut paper strip as the stationary phase and $CHCl_3$/ THF as mobile phase.

The present study reports the comparison among three chromatographic methods for determination of ^{99m}Tc-sestamibi purity: paper chromatography (PC), thin-layer chromatography – reversed phase (TLC-RP) and high performance liquid chromatography reversed phase (HPLC-RP), 30 minutes and 4 hours after reconstitution of the sestamibi lyophilized reagent with sodium pertechnetate ($Na^{99m}TcO_4$).

2. EXPERIMENTAL

2.1. Materials

Sestamibi lyophilized kit was from IPEN-CNEN/SP (Brazil). Water was purified in a Milli-RX® system from Millipore (France). $Na^{99m}TcO_4$ was obtained by elution of a ^{99}Mo/^{99m}Tc generator (IPEN-CNEN/SP - Brazil). The activity of ^{99m}Tc was measured in a Capintec CRC-35R dose calibrator. 2-methoxy isobutyl isonitrile (MIBI) reagent was acquired from ABX (Germany). Tetrahydrofuran, ammonium acetate, methanol, acetic acid and other reagents were purchased from Merck (Germany).

2.2. Sample preparation

A MIBI kit (2 kits of three different lots A, B and C) was reconstituted by the addition of 2 mL generator eluate containing 3.0 mCi (111.11 MBq) of $Na^{99m}TcO_4$ and heating for 10 minutes in a boiling water-bath. After 30 and 240 minutes, an aliquot was taken for quality control. A 5 μL sample was applied both for PC and TLC-RP methods. For HPLC analysis, an 25 μL aliquot was injected.

2.3. Paper Chromatography

Paper Chromatography (PC) assays were carried out with silica gel impregnated with glass fiber sheets (5 cm x 20 cm). The PC mobile phase was obtained by mixture of same volumes of acetonitrile, 0.5 mol L^{-1} acetic acid and 0.35 mol L^{-1} sodium chloride solution. Radiochromatogram scanner (Bioscan Model B-AR-2000-1) was utilized to determine the values of radiochemical species in ^{99m}Tc-sestamibi experiment. Retention factor (R_f) for ^{99m}Tc-sestamibi was 0.8 to 1.0; impurities were R_f 0 to 0.1.

2.4. Thin Layer Chromatography

TLC was performed on an octadecylsilyl silica gel plate (20 cm long x 5 cm wide) (Whatman). The TLC mobile phase was a mixture of (10: 20: 30: 40) volumes of tetrahydrofuran, 0.05 mol L^{-1} ammonium acetate, methanol and acetonitrile. An 5 µL aliquot of the radioactive sample solution was applied on a 10 cm plate from origin. The radioactivity was monitored in the Radiochromatogram scanner (Bioscan Model B-AR-2000-1). Subsequently, the plate was cut in 0.6 cm length horizontal strips which were counted in an autogamma counter (Auto-Gamma Cobra II, 5002 Series, Packard). Retention factor (R_f) from ^{99m}Tc-sestamibi was 0.3 to 0.6. Apolar impurities and polar impurities had R_f of 0 to 0.1 and 0.9 to 1.0, respectively.

2.5. High Performance Liquid Chromatography

The HPLC system (LC 20AT Prominence) (Shimadzu, Japan) was composed by two pumps, autosampler (SIL 20A), system controller (CBM 20A), diode array (SPD M20A), and radiometric detector (Bioscan). The analysis by HPLC-RP was performed at room temperature with a Shim-Pack VP-ODS colunm (150 mm x 4.6 mm i.d., 5 µm particle size). A 25 µL aliquot sample was injected and the mobile phase (20:35:45; v/v, acetonitrile, ammonium sulphate and methanol, respectively) was isocratically eluted, at 1.5 mL min^{-1} flow rate, continuously monitored by a radiation detector Bioscan and U.V. detection was performed at 245 nm. The mobile phases were previously filtered in a Millex GV 0.22 µm pore 25 mm diameter disposable filter unit (Millipore). Each kit was analyzed in duplicate in the three methods.

3. RESULTS AND DISCUSSION

The labeling efficiency (Mean ± S.D (Standard Derivation)) determined by PC, TLC-RP and HPLC-RP methods at 30 and 240 minutes (two replicates) are presented in Table I.

Table I – Radiochemical purity of ^{99m}Tc-sestamibi by PC, TLC-RP and HPLC-RP methods

Lot	Time (Minutes)	PC (Mean ± S.D)	TLC-RP (Mean ± S.D)	HPLC-RP (Mean ± S.D)
A	30	99.40 ± 0.04	97.96 ± 0.05	99.49 ± 0.03
	240	99.62 ± 0.11	97.74 ± 0.11	99.22 ± 0.09
B	30	99.55 ± 0.01	98.07 ± 0.01	99.43 ± 0.02
	240	99.80 ± 0.02	97.88 ± 0.04	99.49 ± 0.13
C	30	99.49 ± 0.03	97.22 ± 0.02	99.16 ± 0.01
	240	99.84 ± 0.30	97.48 ± 0.05	99.21 ± 0.10

PC and TLC-RP RCP were (99.48 ± 0.09)% and (97.75 ± 0.08)%, respectively, (n = 6) at the 30 minutes after reconstitution, while at 240 minutes were (99.75 ± 0.43)% and (97.70 ± 0.20)%, respectively. HPLC-RP analysis showed a labeling average efficiency of (99.36 ± 0.06)% and (99.31 ± 0.32)%, at 30 and 240 minutes, respectively. The time after labeling was not significant for

the RCP values (up to 0.27 %) corresponding to lot A. Each method gave similar results for radiochemical purity. The difference between HPLC-RP and TLC-RP was 1.94% for lot C after 30 minutes labeling and 1.73% for 240 minutes, while the difference between HPLC-RP and PC was only 0.33% and 0.63%, at 30 and 240 minutes, respectively. From a clinical standpoint, it is important to note that none of the three methods presented RPC below the recommended level of 90%.

The results for radiochemical impurities TcO^-_4 and TcO_2 for assays performed on the commercial preparations of ^{99m}Tc-sestamibi are showed in Table II and Table III, respectively (duplicate).

Table II – Radiochemical impurity TcO^-_4 of ^{99m}Tc-sestamibi by TLC-RP and HPLC-RP methods.

Lot	Time (Minutes)	TLC-RP (Mean ± S.D)	HPLC-RP (Mean ± S.D)
A	30	1.74± 0.08	0.35 ± 0.03
	240	1.95 ± 0.08	0.48 ± 0.04
B	30	1.91 ± 0.09	0.32 ± 0.02
	240	1.79 ± 0.09	0.37 ± 0.01
C	30	1.93 ± 0.03	0.38 ± 0.01
	240	2.09 ± 0.05	0.34 ± 0.03

Table III – Radiochemical impurity TcO_2 of ^{99m}Tc-sestamibi by PC and TLC-RP methods.

Lot	Time (Minutes)	PC (Mean ± S.D)	TLC-RP (Mean ± S.D)
A	30	0.21 ± 0.00	0.32 ± 0.01
	240	0.18 ± 0.01	0.33 ± 0.01
B	30	0.15 ± 0.01	0.26 ± 0.02
	240	0.20 ± 0.04	0.32 ± 0.04
C	30	0.22 ± 0.01	0.46 ± 0.00
	240	0.17 ± 0.03	0.33 ± 0.01

The values for TcO^-_4 impurity were (0.35 ± 0.02)% and (0.40 ± 0.08)% by HPLC-RP and (1.86 ± 0.20)% and (1.94 ± 0.22)% by TLC-RP (Table II), at 30 and 240 minutes, respectively. TcO_2 values were (0.52 ± 0.02)% by PC and (0.34 ± 0.02)% by TLC-RP (Table III) at 30 mimutes, while at 240 minutes were (0.18 ± 0.08)% and (0.33 ± 0.06)% by PC and TLC-RP, respectively.

HPLC-RP analysis of the ^{99m}Tc-sestamibi is shown in Figure 2. While peak 2 is ^{99m}Tc-sestamibi, peak 1 is colloid technetium (TcO_2). Retention time of the product and radiochemical impurity were 5.991 minutes and 1.462 minutes, respectively.

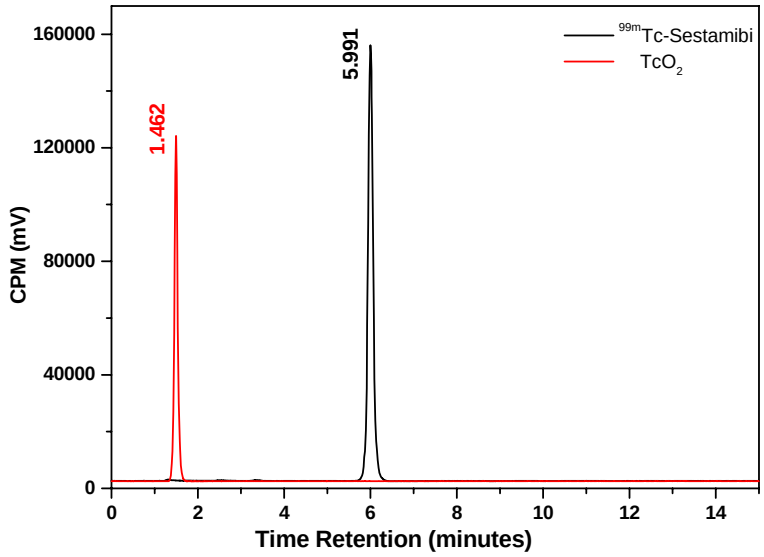

Figure 2. HPLC-RP spectrum. Peak 1: spike TcO_2. Peak 2: ^{99m}Tc-sestamibi 240 minutes post-reconstitution.

The spike confirmed the retention time of the radiochemical impurity TcO_2.

4. CONCLUSION

The identity of some radiochemical impurities of the ^{99m}Tc-sestamibi was confirmed by 3 different methods. Each method gave similar results for RCP, with labeling efficiency for ^{99m}Tc-sestamibi more than 90%. PC, TLC-RP and HPLC-RP techniques are important aids in the quality control of ^{99m}Tc-sestamibi radiopharmaceutical and can be utilized combined.

5. ACKNOWLEDGMENTS

We thank IPEN-CNEN/SP, CR and CNPq for financial support. E. V. A. is a recipient of a master fellowship from CNPq.

6. REFERENCES

1) Oliveira, R.; Santos, D.; Ferreira, D.; Coelho, P. M. B.; Veiga, F. “Radiopharmaceuticals and applications”. Brazilian Journal of Pharmaceutical Sciences, 42, 2, 152-165, 2006.
2) Owunwanne, A.; Patel, M.; Sadek, S. The handbook of radiopharmaceuticals. Chapman & Hallmedical, 1995.
3) Wackers, F. J.; Berman, D. S.; Maddahi J. Technetium-99m hexakis 2-methoxyisobutyl isonitrile: human biodistribution, dosimetry, safety and preliminary comparison to thallium-201 for myocardial perfusion imaging. Journal Nuclear Medicine, 30, 301– 311, 1989.
4) Norenberg, J. P.; Vaidya, M. P.; Hladik, W. B.; Pathak, D. R.; Born, J. L.; Anderson, T. L.; Carroll, T. R. The Effect of Selected Preparation Variables on the Radiochemical Purity of ^{99m}Tc-Sestamibi. Journal Nuclear Medicine Technology, 33, 34– 41, 2005.
5) Verduyckt, T.; Kieffer, D.; Huyghe, D.; Cleynhens, B.; Verbeke, K.; Verbruggen, A.; Bormans, G. Identity confirmation of ^{99m}Tc-MAG3, ^{99m}Tc-Sestamibi and ^{99m}Tc-ECD using radio-LC-MS. Journal of Pharmaceutical and Biomedical Analysis, 32, 669- 678, 2003.
6) Advanced Biochemical Compounds Product List of ABX- ABX
Available at:<http://www.abx.de/chemicals/product-list.html>. Access to: 8/10/2008
7) Hung, J. C.; Wilson, M. E.; Brown, M. L.; Gibbons, R. J. Rapid Preparation and Quality Control Method for Technetium-99m-2-Methoxy Isobutyl Isonitrile (Technetium.-99m-Sestamibi). Journal Nuclear Medicine, 32, 2162, 1991.

RADIOLABELING AND QUALITY CONTROL OF 2-ACETYLPYRIDINE N4-PHENYL-THIOSEMICARBAZONE: A POTENT ANTITUMORAL AGENT

Soares, M.A[1], Mendes, I. M. C.[2], Beraldo H.[2], Gouvêa dos Santos R.[1]
[1]Lab. Radiobiologia, Centro De Desenvolvimento da Tecnologia Nuclear, CDTN/CNEN, MG
[2]Departamento de Química, Universidade Federal de Minas Gerais

ABSTRACT

The aim of this work was to radiolabel Ph using ^{125}I as radiotracer and to carry out the quality control of radiolabeled molecule. Labeling was done by lactoperoxidase method and ^{125}I-Ph specific activity and radiochemical analyses were done using ascending chromatography in Whatman paper n° 1 as the stationary phase and methanol saturated with KI as mobile phase. Contaminants, mainly as $^{125}I^-$, were eliminated by anionic exchange chromatography. ^{125}I-Ph serum stability and interaction with blood plasmatic proteins were also analyzed. ^{125}I-Ph production was successful with 96% of radiochemical purity and high specific activity (17.6 TBq /mmol). ^{125}I-Ph showed to be a stable compound keeping its stability for 7 days, when stored at 2-4ºC. Moreover, ^{125}I-Ph was found to be stable at 37ºC in serum for at least 4 hours. The low binding to plasmatic proteins (7.9±1.1%), during 24 hours of incubation, suggests that ^{125}I-Ph can freely circulate in the blood stream, without main interferences on its biodisponibility. ^{125}I-Ph proved to possess indispensable characteristics for a possible antitumor radiopharmaceutical to be applied for non invasive tumour diagnosis. The next step will be to evaluate ^{125}I-Ph biodistribution and its capacity for tumour detection in vivo.
Keywords: N4-phenyl-2-acetylpyridine thiosemicarbazone, ^{125}I radiolabeling, quality control

1. INTRODUCTION

According to the World Health Organization (WHO, 2007), cancer accounts for 7 million deaths annually, being the second cause of death for disease in the majority of the countries, subsequent to the cardiovascular diseases.

The neoplasms basic knowledge is increasing quickly, however, few advances have been reached in clinical therapy and diagnosis of tumours. Application of radiotracer (radiopharmaceutical) highly specific for tumours constitutes a non invasive approach for early diagnosis of malignant tumours by molecular imaging (Thrall and Ziessman, 2003). Therefore, the development of alternative radiopharmaceuticals for tumour diagnosis is relevant in the attempt to improve prognosis and to increase the patient survival.

Thiosemicarbazones present a wide range of bioactivities including antibacterial, antimalarial, antiviral and antitumoral activities. Some authors described that thiosemicarbazones mechanism of action is due to their ability to inhibit DNA biosynthesis, possible by blocking the enzyme ribonucleotide reductase, binding to the DNA nitrogen bases, blocking base replication or creation of lesions in DNA strands by oxidative rupture (Lakvidou et al., 2001; .Storelli et al., 1977; French and Blanz, 1970).

Because of these potent bioactivities and chemical properties, thiosemicarbazones constitute a good template to develop a radiopharmaceutical. For this purpose, N4-phenyl-2-acetylpyridine thiosemicarbazone (Ph) must be radiolabeled with high specific activity and radiochemical purity. The aim of this work was to radiolabel Ph using 125I as radiotracer and to carry out the quality control of radiolabeled molecule.

2. MATERIALS AND METHODS

2.1. Reagents

All chemicals used were of analytical grade.

2.2. Ph radioiodination

The radioiodination of Ph was done by lactoperoxidase method according described by Santos et al. (1999). Briefly, Ph was reacted for two minutes with $3.7x10^6$ Bq of carrier-free $Na^{125}I$ in the presence of lactoperoxidase and H_2O_2 in 50mM phosphate buffer at pH 7.4. The reaction was stopped with phosphate buffer containing 1mg/mL BSA. Contaminants, mainly under the form of $^{125}I^-$, were eliminated by anionic exchange chromatography on Dowex 1-X8.

2.3. Radiochemical purity of ^{125}I-Ph

For the measurements of the ^{125}I-Ph labelling efficiency, ascending paper chromatography was performed using Whatman paper n° 1 as the stationary phase and methanol saturated with KI as mobile phase. A single drop of the shaken mixture was spotted at the origin of Whatman paper strip and the run developed in a glass jar for about 20 minutes. The strip was cut into 1-cm segments, and the radioactivity was measured in a gamma counter (Wallac – Window: 35keV – Counter efficiency: 80%). The percentage of ^{125}I-Ph was calculated by the relationship between the radioactivity present in the section with $R_f = 0$ and the total radioactivity.

2.4. Stability of ^{125}I-Ph complex

To measure the stability of the ^{125}I-radiolabeled Ph, a sample of this complex was incubated at 2-4ºC for 20 days. ^{125}I-Ph stability was measured, different times after incubation, by paper chromatography (described in 2.3).

2.5. In vitro serum stability of ^{125}I-Ph complex

To test the serum stability of ^{125}I-Ph in vitro, the complex was incubated in FBS at 37ºC for 1, 4, 6, 24 and 48 hours. Radiochemical purity was measured by paper chromatography (described in 2.3).

2.6. In vitro ^{125}I-Ph plasmatic protein binding

To determine the amount of ^{125}I-Ph plasmatic protein-binding in vitro, the complex was incubated in FBS at 37ºC for 24 hours. After this, 100mL fractions were removed and to these was added 200mL of ethanol to precipitate the proteins present. The sample was then centrifuged until the precipitated proteins formed pellet. The supernatant was removed from the pellet and both samples were counted on a gamma counter.

3. RESULTS

3.1 Radiochemical purity of ^{125}I-Ph

Because of the Ph non-polar characteristic, the complex ^{125}I-Ph stayed at the origin of the paper chromatography (Rf = 0.0) and presented a different profile compared with free $^{125}I^-$ (Rf= 0.8-1.0) (FIG. 1). The radiolabeling was fast, and paper chromatography showed a minimum of unlabeled $^{125}I^-$, resulting in a high enough radiochemical purity (96%) to perform in vitro and in vivo studies. ^{125}I-Ph recuperation after anionic exchange chromatography on Dowex 1-X8 was 34% and the complex specific activity was 17.6 TBq /mmol (TAB 1).

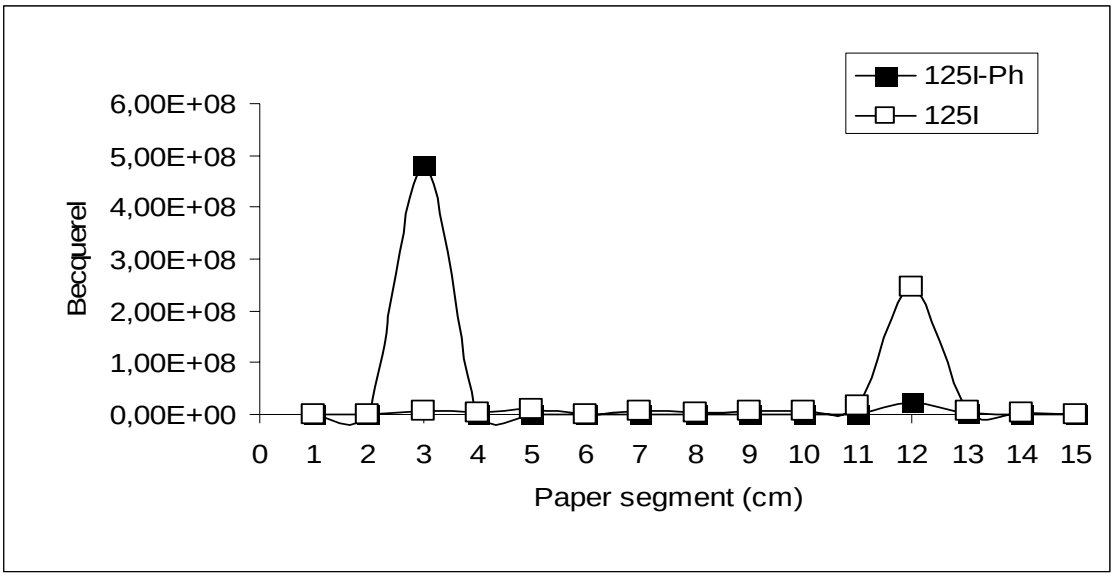

FIGURE 1. Paper chromatography using Whatman paper n° 1 as the stationary phase and methanol saturated with KI as mobile phase. ^{125}I-Ph remained at the origin of the paper chromatography (Rf = 0) and presented a different profile compared to free $^{125}I^-$.

TABLE 1: Ph ^{125}I-labeling characteristics

Recuperation after anionic exchange chromatography	Radiochemical purity	Specific activity
34%	96%	17.6 TBq /mmol

3.2. Stability of 125I-Ph complex

^{125}I-Ph was incubated at 2-4ºC for 20 days and its stability was measured different times after incubation. The complex ^{125}I-Ph showed to be a stable compound keeping its stability for at least 7 days (FIG.2). After 20 days of incubation ^{125}I-Ph stability was a little reduced but the complex remained with good radiochemical purity (85%).

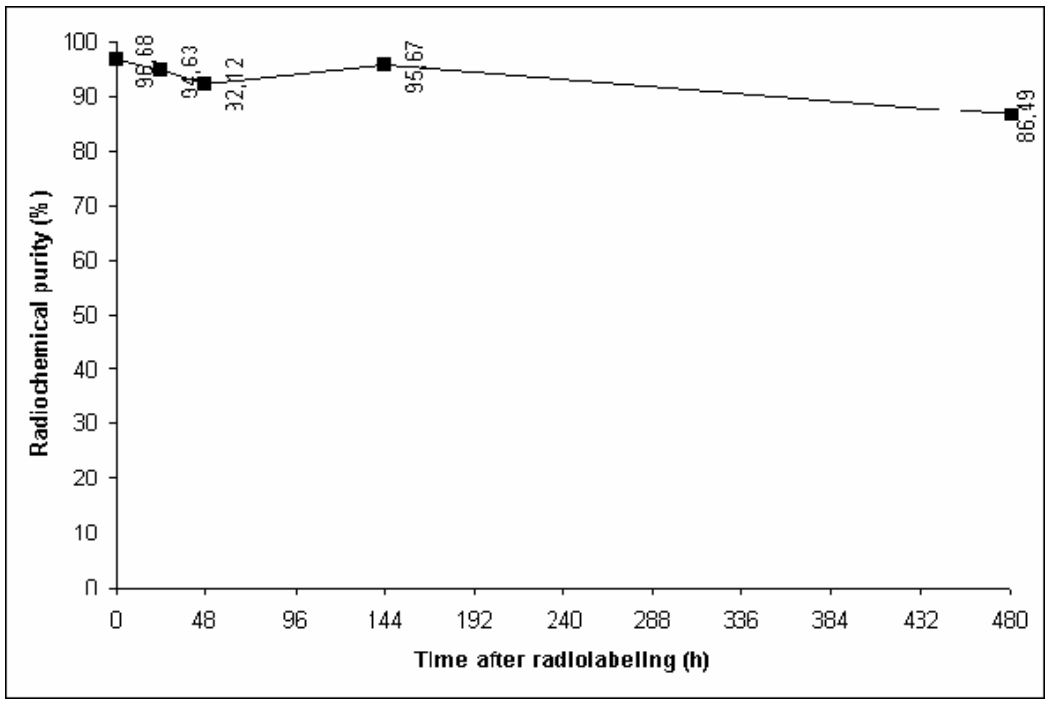

FIGURE 2. Stability of ^{125}I-Ph complex after incubation at 2-4ºC for 20 days. ^{125}I-Ph showed to be a stable compound keeping its stability for at least 7 days

3.3. In vitro serum stability of ^{125}I-Ph complex

Incubation of ^{125}I-Ph in FBS for 4 hours at 37ºC showed no loss of ^{125}I from the complex, which kept its radiochemical purity (FIG. 3). After 6 hours of incubation in FBS, ^{125}I-Ph stability was a little reduced (radiochemical purity: 86%), although this radiochemical purity remained constant for the next 48 hours.

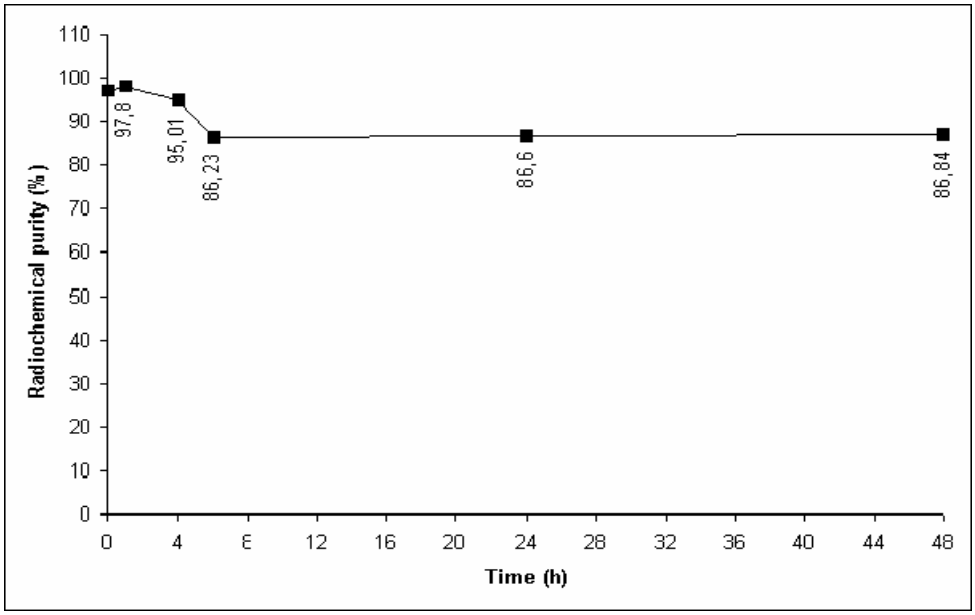

FIGURE 3. Stability of ^{125}I-Ph complex after incubation in FBS at 37ºC for 48 hours. . ^{125}I-Ph was found to be stable at 37ºC in serum for at least 4 hours.

3.4. In vitro 125I-Ph plasmatic protein binding

The drug's pharmacologic efficiency may be affected by the blood proteins binding. The less bound a drug is, the more efficiently it can traverse cell membranes. Only the unbound fraction exhibits pharmacologic effects (Rang et. Al., 2003).

To determine the amount of ^{125}I-Ph plasmatic protein-binding in vitro, the complex was incubated in FBS at 37ºC for 24 hours. After this, the proteins present were precipitaded and counted on a gama counter as well as the supernatant. The results showed a low binding of the complex to plasmatic proteins present in FBS (7.9±1.1% binding) (FIG. 4). This result suggests that ^{125}I-Ph can freely circulate in the blood stream, without main interferences on its biodisponibility.

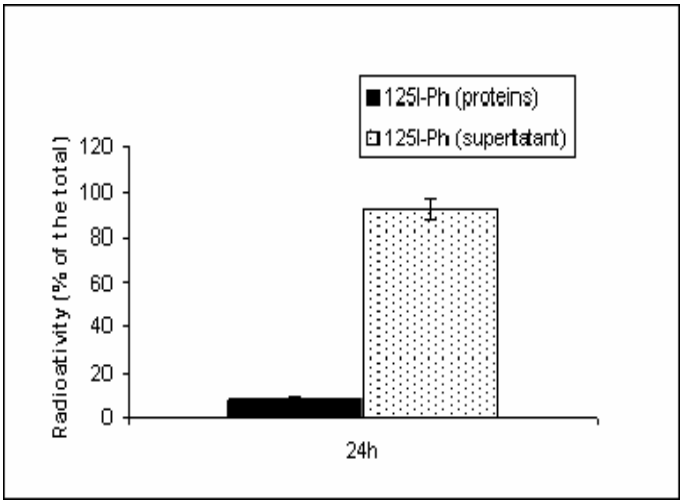

FIGURE 4. In vitro ^{125}I-Ph plasmatic protein binding. ^{125}I-Ph has low binding to plasmatic proteins present in FBS.

4. CONCLUSIONS

^{125}I-Ph proved to possess indispensable characteristics for an antitumor radiopharmaceutical to be applied for non invasive tumour diagnosis, such as high radiochemical purity (96%) and good specific activity (17.6 TBq /mmol). Besides this it can freely circulate in the blood stream, without main interferences on its biodisponibility. The next step will be to evaluate ^{125}I-Ph biodistribution and its capacity for tumour detection in vivo.

REFERENCES

1- A.C. Sartorelli, K.C. Agrawal; A.S.Tsiftsoglou, A.C. Moore. Characterization of biochemical mechanism of action of alpha (N)-heterocyclic carboxaldehyde thiosemicarbazones. Adv Enz Reg, 15, pp.117-139 (1977).

2- F.A. French, E. Blanz Jr. Carcinostatic activity of thiosemicarbazones of formyl heterocyclic compounds. 6.1-formyllisoquinoline derivates bearing additional ring substituints with notrs on mechanism of action. J. Med. Chem., 13, pp. 1117-1123 (1970).

3- H. P. Rang; M. M. Dale.; J. M. Ritter.; P. K. Moore. Absorção e biodistribuição dos fármacos. In: Farmacologia. 5. ed. Rio de Janeiro: Elsevier, (2003). Cap.7.

4- Iakovidou, Z; Papageorgiou, A; Demertzis, M A; Mioglou, E; Mourelatos, D; Kotsis, A; Nath Yadav, P; Kovala-Demertzi, D. Platinum(II) and palladium(II) complexes with 2-acetylpyridine thiosemicarbazone: cytogenetic and antineoplastic effects. Anticancer Drugs, 12, pp. 65-70 (2001).

5- J. T. Thrall; H. A. Ziessman. Oncologia. In: Medicina Nuclear. Rio de Janeiro: Guanabara Koogan, (2003). Cap. 9.

6- R.G. Santos, C.R. Diniz, M.N. Cordeiro, M.E. Lima, "Binding sites and actions of Tx1, a neurotoxin from the venom of the spider Phoneutria nigriventer, in guinea pig ileum," Braz. J. Med. Biol. Res., 32, pp.1565-1569 (1999).

7- WHO - World Health Organization, 2007. <http://www.who.int /cancer>.

ACKNOWLEDGEMENTS

The authors thank to Fundação de Amparo a Pesquisa do Estado de Minas Gerais (FAPEMIG) for financial support. MAS is a fellowship CNPq (DTI-CNEN).

PREPARATION OF RADIOACTIVE GOLD-NANOPARTICLES AS A SPECT IMAGING AGENT

Rafael Gontijo Furst Gonçalves[1*], Marcella Araugio Soares[2*], Paulo Roberto Ornelas da Silva[2*], Arno Heeren de Oliveira[1*], Andréa Vidal Ferreira[2**], Ana Paula Alves[2**], Marina Bicalho Silveira[2*], Fabrício de Almeida Souza Vilas Boas[2*], Klaus Krambrock[1**], Luis Orlando Ladeira[1**], Raquel Gouvêa dos Santos[2**], Maurício Veloso Brant Pinheiro[1*]

[1]* Depto Engenharia Nuclear , ** Depto Física, Universidade Federal de Minas Gerais

[2]*Laboratório de Radiobiologia, **Serviço de Reator e Irradiações , Centro de Desenvolvimento da Tecnologia Nuclear/ Comissão Nacional de Energia Nuclear, Caixa Postal 941, CEP 31123-970, Belo Horizonte, Minas Gerais, Brazil.

Abstract:

Nowadays, molecular imaging using radiopharmaceuticals has been a technique of choice for tumor diagnosis due to its higher resolution [Watanabe Y, Brain nerve 59 (3):209, 2007]. Colloidal gold nanoparticles (AuNPs) represent a novel technology in the field of particle-based tumor-targeting drug delivery, early-stage diagnosis and tumor radiotherapy. Gold nanoparticles or colloidal gold have been assayed in mice as X-Ray contrast agent for tumor diagnosis [Cai Q-Y et al, *Invest. Radiol*. 42:797, 2007]. However, the amount of gold in this technique is high (2.7 g kg^{-1} animal), becoming virtually impracticable for humans. In this study, we described our efforts to develop a radioactive AuNP probe with specific activity high enough to serve as an agent for single photon emission tomography (SPECT) imaging using just a few amount of gold (~ 10 mg kg^{-1} animal). In order to prepare the AuNPs, chloroauric acid solution ($HAuCl_4$) was reduced by sodium citrate and nanoparticles diameter was determined by atomic force microscopy (AFM) and optical absorption. AuNPs around 3 nm were produced and submitted to irradiation at TRIGA Mark IPR-R1 reactor for 8 hours, under a thermal and epithermal neutron flux of 6.6 x 10^{11} and 3.0 x 10^{10} n cm^{-2} s^{-1}, respectively. Under this flux the reaction $^{197}Au(n, \gamma)^{198}Au$ occurred producing radioactive gold nanoparticles. The induced activity obtained for the ^{198}AuNPs was around 800 $\mu Ci/mg_{Au}$ at the end of the irradiation. Radiochemical analysis was done by gamma spectrometry using a germanium detector. A surfactant agent, polivinylpirrolidone (PVP K30), was mixed to the AuNPs to keep the homogeneity of colloidal gold in physiological solution and to avoid further agglomeration. AFM showed diameters of 60-80 nm for PVP coated colloidal gold (AuNPs-PVP). ^{198}AuNPs-PVP were intravenously injected in Swiss mice and toxicology was evaluated at different periods post injection. The ^{198}AuNPs-PVP proved to be biocompatible without significant toxicity in the mice. Toxicological results state for the safe use of these nanoparticles for imaging diagnosis. Studies are ongoing to evaluate the potential use of ^{198}AuNPs-PVP as blood-pool SPECT imaging agent.

Keywords: ^{198}Au Nanoparticles, SPECT agent, toxicology

Financial support: FAPEMIG, CNEN, CNPq, CAPES

1 Introduction

Nanotechnology has emerged at the forefront of science research and technology development. In the last years, gold nanoparticles ($N_{Au}P$) have triggered great interest for application as blood imaging contrast. It has been shown the higher efficiency of stable-gold nanoparticles as contrast agent for tomography of blood flow, in comparison to iodine (Hanfield et al, 2006). It has been used around 67.5 mg/mouse (2.7 g Au-nanoparticles/kg animal) in the imaging studies using tomography. Despite its utility and great sensibility as contrast blood imaging agent, the amount of gold necessary to produce such images is very high. Considering the application of these nanoparticles for human imaging the amount of gold will be probably higher, which can evoke toxicological concerns.

In this present study we have hypothesized the use of radioactive gold nanoparticles could have some advantages in comparison to stable-gold nanoparticles such as: the need for reduced amount of gold, minor toxicological concerns and more sensitive detection by single photon emission tomography (SPECT).

As it is well recognized, risk evaluation is an important issue to be considered in the early stage of any new technology. Toxicological evaluation is an important approach to understand and assess the potential application as a human diagnosis tool. We produced radioactive gold nanoparticles by neutron activation and characterized them in order to evaluate its safety for future application for SPECT imaging. To evaluate the in vivo toxicological parameters of the gold nanoparticles coated with poly(*N*-vinyl-2-pyrrolidone), synthesized as described in this work, we investigate the hematological parameters after $N_{Au}P$ injection in mice.

2 Methods

Preparation of gold nanoparticles:

In a typical experiment, gold nanoparticles were synthesized by direct reduction of 5.7 mL $HAuCl_4$ aqueous solution (0.001 M) in sodium citrate (1.4%) and heated at 70 °C.

Poly (*N*-vinyl-2-pyrrolidone) (PVP K30) has been extensively used to stabilize colloidal particles of different materials in water and many non-aqueous solvents (Graf et al, 2003). $N_{Au}P$ were coated with PVP using a varied ratio of PVP/ $HAuCl_4$ in order to obtain nanoparticles well dispersed in phosphate-buffered saline at pH 7.4 for the toxicological assays .

The characterization of the gold nanoparticles was done by Atomic force microscopy (AFM).

Gold nanoparticles neutron activation:

$_{}N_{Au}P$ samples were irradiated in the carrousel of the TRIGA MARK I IPR-R1 reactor at CDTN /CNEN, under average thermal and epithermal neutron fluxes of 6.6×10^{11} $n.cm^{-2}.s^{-1}$ and 3.0×10^{10} $n.cm^{-2}.s^{-1}$ for 1 hour, respectively. After two days cooling-time, the gamma spectrometry was carried out in a gamma counter system with a HPGe detector.

Toxicological evaluation:

Healthy female Swiss mice were intravenously injected with saline (control group), 4.5 μg/mL PVP in saline or 920 μg NAuP (dispersed in 4.5 μg/mL PVP)/kg animal. The animals were observed during 30 days for behavioral and weight changing, lethality and toxicology. Animals were euthanized 1, 14 and 30 days after intravenous gold injections, blood was collected for hematological (haemoglobin, total white [WBC] and red [RBC] blood cell counts, neutrophil, lymphocyte, monocyte, and eosinophil counts, mean corpuscular volume, mean corpuscular haemoglobin, mean corpuscular haemoglobin concentration, platelets), and biochemical analysis (blood urea nitrogen, creatine, total protein, albumin, alanine aminotransferase (ALT), aspartate aminotransferase (AST), total bilirubin). Vital organs were dissecated and slices of tissues were prepared for microscopic study by formalin fixation, paraffin embedding, and haematoxylin/eosin staining.

All the animals used in this research were treated with the respect of the National Legislation for Animal Vivisection which works nowadays (Federal Law 6,638 since May 8th, 1979) and respecting the rules from the Brazilian School for Experimental Surgery (COBEA). This research has been approved by the Research Ethical Committee from State University of Minas Gerais (CETEA-UFMG).

3 Results

Gold nanoparticles characteristics

Gold nanoparticles synthesized by reducing a gold salt ($HAuCl_4$) with citrate rendered nanoparticles with average size of 3 nm (Fig1) as evidenced by AFM. It is well known that gold nanoparticles agglomerate when in saline solution. In order to avoid further agglomeration when diluted in phosphate-buffered saline at pH 7.4 for the in vivo assays, these nanoparticles were coated with PVP.

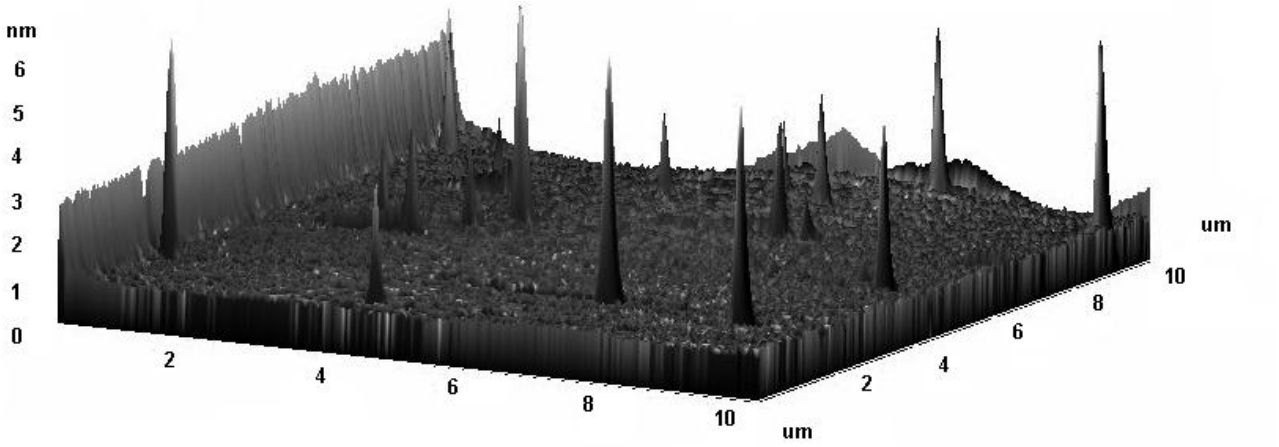

Figure 1. Atomic force microscopy analysis. Profile of gold nanoparticles synthesized by direct reduction with sodium citrate.

PVP-coated gold NPs could be homogeneously dispersed in phosphate buffer saline and an average range of 60-80 nm was obtained.

Radioactive gold nanoparticles

After neutron activation and counting, the spectrum range of gold nanoparticles was obtained and processed by the software Genie 2000. The photopeak characteristic of the radioisotope ^{198}Au can be seen at 412 keV (Fig. 2). The induced activity obtained for the ^{198}AuNPs was around 30 MBq.mg$_{Au}^{-1}$ (800μCi. mg$_{Au}^{-1}$) and 250MBq.mg$_{Au}^{-1}$ (4 mCi mg$_{Au}^{-1}$) at the end of 1 and 8 h irradiation, respectively. This activity is high enough to be applied in animal biodistribution assays and SPECT imaging.

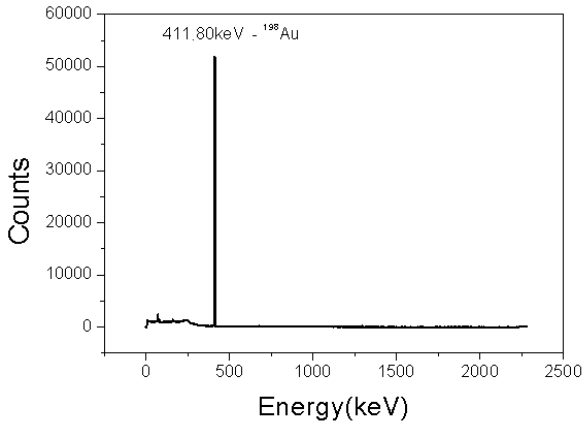

Figure 2.Gamma spectrum profile of ^{198}Au. Main line at 411.8 keV is shown.

Toxicological evaluation

Biocompatibility of $N_{Au}P$ was assessed by hematological (table 1), serum biochemical (table 2) and histopathological analysis. No behavioral alterations or lethality were observed up to 30 days post-injection.

Hematological and serum biochemical evaluation in mice showed no significant toxicity. Histopathological inspection presented only minor alterations in liver (data not shown).

Table I – Blood hemathology of mice intravenously injected with NAuP, sampled on days 2 and 14, compared with that of sham injected mice

Time post-injection	***Treatment***	***VG (%)***	***ER (10^6/ul)***	***HB (g/dl)***	***MCHC (%)***	***MCV (fl)***	***RDW (%)***	***PTP (g/dl)***
48 h	saline	32.0±5.6	7.9±1.2	12.8±1.2	40.1±3.3	40.3±1.1	17.4±1.6	6.0±0.3
	PVP	31.5±7.8	10.0±3.5	16.8±5.9	52.5±5.7	32.1±3.6	17.2±0.9	5.8±0
	NAuP	31.8±0.7	8.9±1.2	14.8±1.2	46.3±5.7	36.2±4.9	17.3±0.1	5.9±0.3
14 days	PVP	31.6±2.1	9.5±2.0	15.8±2.3	49.4±4.5	34.2±7.1	17.2±1.7	5.8±0.2
	NAuP	29.0±5.6	7.9±2.3	14.4±0	50.6±9.9	37.2±3.5	17.9±0.3	6.0±0.3

ER: erythrocytes, HB: haemoglobin, MCHC: mean corpuscular haemoglobin concentration, MCV: mean corpuscular volume, RDW: red cell distribution weight, PTP: platelet

Table II – Serum biochemistry values of mice intravenously injected with NAuP, sampled on days 2, 14 and 30 compared with that of sham injected mice

	Time post-injection	***TP (gdl^{-1})***	***ALB ($g\ dl^{-1}$)***	***BUN ($mddl^{-1}$)***	***CR ($mgdl^{-1}$)***	***TB ($mgdl^{-1}$)***	***AST (IU/L)***	***ALT (IU/L)***
Control		4.5 ± 0.5	2.6 ± 0.4	55.3 ± 2.0	0.4 ± 0.4	2.3 ± 1.2	71.3±27.0	44.7 ± 5.0
Group 1	Day 2	6.2 ± 0.3	2.8 ± 0.3	45.0 ± 10.0	1.45 ± 0.2	6.5 ± 0.4	15.0 ± 1.0	95 ± 0
	Day 14	5.0 ± 1.0	2.8 ± 0.5	52.5 ± 16.0	0.65 ± 0.6	2.1 ± 2.6	30.1±18.0	85.5±20.0
Group 2	Day 2	5.5 ± 0.5	2.8 ± 0.3	49.7 ± 22.0	0.98 ± 1	3.4 ± 3.5	95.3 ± 30	36.0±13.0
	Day 14	4.0 ± 0.7	2.0 ± 0.3	38.0± 5.0	0.1 ± 0	3.8 ± 2	42.0 ± 0	65.0 ± 0
	Day 30	5.1 ± 0.5	2.2 ± 0.1	140.0±16.0	2.0 ± 0.2	4.2 ± 0.4	8 ± 2	18.5 ± 0.5

Control: saline , Group 1: PVP, Group 2: NAuP, TP: total protein, ALB: albumin, , BUN: blood urea nitrogen, CR: creatine, TB: total bilirubin, AST: aspartate aminotransferase, ALT: alanine aminotransferase

Conclusions

Gold nanoparticles synthesized using the protocol described here proved to have good physical characteristics for imaging application (3-80nm). Neutron irradiation rendered $N^{198}AuP$ with specific activity of 0.03 - 0.25 GBq/mg_{Au} and good physical properties, as showed by AFM analysis. Toxicological evaluation showed that these nanoparticles were not significantly hematotoxic. On the other hand, mild toxicity were observed for the liver as evidenced by histological evaluation.

Take together all the results suggest that $N^{198}{}_{Au}P$ can be safely used as a radiopharmaceutical for SPECT imaging. Further studies involving biodistribution of $N^{198}{}_{Au}P$ are in development in order to evaluate this promising potential of $N^{198}{}_{Au}P$ for SPECT imaging.

Acknowledgments

The authors thank the financial support of the Comissão Nacional de Energia Nuclear (CNEN) and to FAPEMIG for financial support. RFG was a fellowship from CNPq . MAS is a fellowship from PCI/DTI-CNPQ-Comissão Nacional de Energia Nuclear.

References

Hanfield JF, Slatkin DN, Focella TM, Smilowitz HM, Gold nanoparticles: a new X-ray contrast agent, British Journal of radiology, 79:248-253, 2006

Graf C, Dirk L.J.V., Imhof A. and Van Blaaderen A., A general method to coat colloidal particles with silica *Langmuir* 19, 2003

^{159}Gd- GADODIAMIDE: OBTAINMENT OF A POSSIBLE THERAPEUTIC RADIOPHARMACEUTICAL

Daniel Crístian Ferreira Soares1, Maria Ângela de Barros Correia Menezes2*, Raquel Gouvêa dos Santos 2**, Gilson Andrade Ramaldes1.

Laboratório de Tecnologia Farmacêutica e Farmacotécnica – Faculdade de Farmácia – Universidade Federal de Minas Gerais - Avenida Presidente Antônio Carlos, 6627 – Pampulha – 31270-901, Belo Horizonte, Minas Gerais, Brazil.

*Serviço de Reator e Irradiações, **Laboratório de Radiobiologia, Centro de Desenvolvimento da Tecnologia Nuclear/ Comissão Nacional de Energia Nuclear, Caixa Postal 941, CEP 31123-970, Belo Horizonte, Minas Gerais, Brazil.

ABSTRACT

INTRODUCTION

The Gadodiamide®(General Electric Healthcare Company), a non-ionic complex (Figure 1) of low dissociation in aqueous solutions (Chang et al., 1992). Actually it is the most used as a MRI contrast agent due to its low osmolality and chemotoxicity (Meyer et al., 1990).

The gadolinium present in Gadodiamide is a mixture of the isotopes ^{152}Gd (0.20%), ^{154}Gd (2.18%), ^{155}Gd (14.80%), ^{156}Gd (20.47%), ^{157}Gd (15.65%), ^{158}Gd (24.84%) and ^{160}Gd (21.86%) (Browne, et al., 1986).

Submitting a natural gadolinium sample to an adequate neutron irradiation process, the radioisotope ^{159}Gd is observed, which is a beta (1.001 keV) and gamma (main energy 363.54 keV) emitter (Moralles et al., 1995). According to some published studies, these energies are suitable for the diagnosis and therapeutic applications (Thrall et al., 2001).

The aim of this paper was to verify if the specific activity of ^{159}Gd obtained by neutron irradiation would be suitable for its future use in radiopharmaceutical treatments.

EXPERIMENTAL

Radioactive gadodiamide obtaining

Gadodiamide samples, in triplicate, were irradiated in the carrousel of the TRIGA MARK I IPR-R1 reactor at CDTN /CNEN, under average thermal neutron flux of 6.6×10^{11} n.cm^{-2}.s^{-1} for 8 hours. After two days cooling-time, the gamma spectrometry was carried out in a gamma counter system with a HPGe detector. The gamma spectrum (Figure 1) is shown with the characteristic peak of ^{159}Gd in 363.54 keV (Blaauw, 1995). The gadodiamide complex integrity was verified by FTIR analysis

Antitumoral property in RT2 culture cells - MTT assay

In order to evaluate the antitumoral potential of radioactive gadodiamide, the RT2 tumor cells were thawed and grown in controlled atmosphere with CO_2 at 3% and temperature of 25 ° C using DEMEM (Dulbecco's modified Eagle medium) as culture medium. For MTT assay, RT2 cells (100 cells/well) were sown in the culture plates of 96 wells and incubated for 24 hours for adherence. After exposure for 48 hours of treatment with radioactive and non radioactive gadodiamide, the cells were subjected to the solution of MTT [bromide, 3 - (4,5-dimethyl-2-thiazolyl-2 ,5-diphenyl)-2H-tetrazolium] 0.5 mg / ml for 4 hours and viability assessed metabolic spectrophotometrically (infrared to 570 nm) after solubilization of the product formed in 100 μL of dimethyl sulfoxide (DMSO) in each well.

RESULTS AND DISCUSSION

After appropriate process of irradiation and counting, the spectrum range of gadodiamida was obtained and processed by the software statistically Genie 2000. The photopeaks characteristic of the radioisotope Gd-159 can be seen at 348.28, 363.50 and 560.80 KEV respectively (Figure 1). The energy found and their relative intensities were confirmed compared with figures published by Moralles et al., 1995. After irradiation, the specific activity reached was 40kBq.mg^{-1} and the chemical structure was kept intact as shown by FTIR analysis.

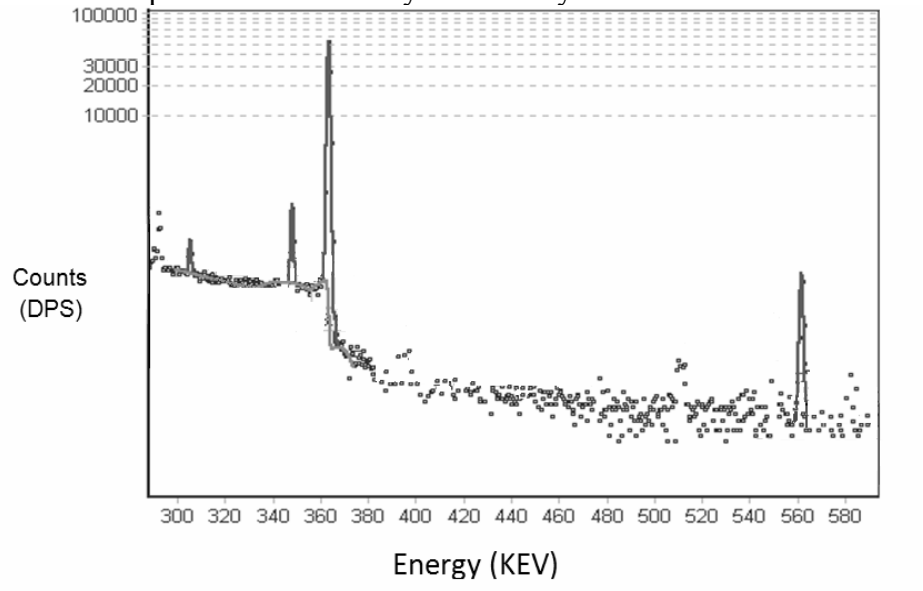

Figure 1 - Gamma spectrum of ^{159}Gd-Gadodiamide sample

The results of Antitumoral property of non radioactive and radioactive gadodiamide in RT2 cells is shown in tables 1 and 2 below.

Table 1- Citotoxicity of Non radioactive gadodiamide in RT2 cells

Gadodiamide concentration (mM)	Percent median survival of RTE 2 cells ± standard deviation (n = 8)
100	3,41 ± 1,58
50	5,55 ± 1,10
40	9,62 ± 2,22
30	14,48 ± 2,03
20	51,55 ± 4,77

Table 2- Citotoxicity of radioactive gadodiamide in RT2 cells

Radioactive gadodiamide concentration (mM)	Percent median survival of RTE 2 cells ± standard deviation (n = 8)
100	0.018 ± 0.002
50	0.031 ± 0.03
40	0.052 ± 0.04
30	0.082 ± 0.09
20	0.271 ± 0,12

CONCLUSION

^{159}Gd-Gadodiamide proved to have higher potency than non radioactive gadodiamide against malignant glioblastoma. We can see that there was an increase in cytotoxic action of gadodiamida according to ionizing radiation in an average of 170 times. From these results we can indicating that use of radiolabeled gadodiamide can be a promising therapeutic agent for tumor. More studies involving characterization, biodistribution and toxicity of radioactive gadodiamide should be conducted aiming the evaluation of the potential of ^{159}Gd-Gadodiamida as a new therapeutic radiopharmaceutical.

ACKNOWLEDGMENTS

REFERENCES

1) Alan J., 2005. Functional MRI using molecular imaging agents. Trends in Neurosciences. 28, 120-126.
2) Bardies, M., Chatal, J. F., 1994. Absorbed doses for internal radiotherapy from 22 beta-emitting radionuclides: beta dosimetry of small spheres. Physics in medicine and biology. 39, 961-981.
3) Blaauw, M., 1995. The IRI Gamma-ray Catalogue for INAA. Interfaculty Reactor Institute, University of Technology Delft, Delft, The Netherlands. ISBN 90-73861-32-2.
4) Browne E., Firestone, R.B., Shirley, V.S., 1986. Table of Radioactive Isotopes, John Wiley & Sons, Inc., New York
5) Brugger R.M., Shih J.A., 1989. Evaluation of gadolinium-157 as a neutron capture therapy agent. Strahlenther Oncology.165, 153-156.
6) Bushong, S. 1996. Magnetic Resonance Imaging: Physical and biological principles. Moseby: St. Louis, 368pp.
7) Dempsey, M.F., Condon B., Hadley, D. M., 2002 Seminars in Ultrasound, CT, and MRI, 23, 392-401.
8) Dicker, T., Siller, G. Saunders, N., 2002. Molecular and cellular biology of basal cell carcinoma. Australasian J. Dermatology. 43, 241-246.
9) Evan, G. I., Vousden, K. H., 2001. Proliferation, cell cycle and apoptosis cancer. Nature. 411, 342-348.
10) Friedlander, G., Kennedy, J.W., Macias, E. S. Miler, J.M.,1981. Nuclear and Radiochemistry. Wiley-Interscience, New York. 684pp.
11) Gangarosa, R. E., Minnis, J. E., Nobbe, J., Praschan, D., Genberg, R.W., 1987. Operational safety issues in MRI. Magnetic Resonance Imaging, 5, 287-292. Goorley, T., Nikjoo, H., 2000. Electron and photon spectra for three gadolinium-based cancer therapy approaches. Radiation Research. 154, 556-563.
12) Guo-Ping, Y., Leslie, R. Hoog, P., 2007. Magnetic resonance imaging contrast agents: Overview and perspectives. Radiography. 13, 15-19.
13) Hirohashi, S., Kanai, Y., 2003. Cell adhesion system and human cancer morphogenesis. Cancer Sci. 94, 575-581.
14) Le U. M., Cui Z., 2006a. Biodistribution and tumor-accumulation of gadolinium (Gd) encapsulated in long-circulating liposomes in tumor-bearing mice for potential neutron capture therapy. International Journal of Pharmaceutics. 320, 96-103.
15) Le, U. M., Cui Z., 2006b. Long-circulating gadolinium-encapsulated liposomes for potential application in tumor neutron capture therapy. International Journal of Pharmaceutics. 312, 105-112.
16) Menezes, M. Â. B. C., Sabino, C. V. S., Franco, M. B., Kastner, G. F., Rossi, E. H. M., 2003. K_0-Instrumental Neutron Activation Analysis Establishment at CDTN, Brazil: A successful story. Journal of Radioanal. Nucl. Chem. 257, 627-632.
17) Moralles, M. Pascholati, P. R. Vanin, V. R. Helene, O., 1995. Applied Radiation and. Isotopes. 46, 133-138.

18) Saha T. K., Ichikawa H., Fukumori Y., 2006. Gadolinium diethylenetriaminopentaacetic acid-loaded chitosan microspheres for gadolinium neutron-capture therapy. Carbohydrate Research. 341, 2835-2841.
19) Suzuki M., Sakurai Y., Masunaga S., Kinashi Y., Nagata K., Maruhashi A., Ono K., 2006. Feasibility of boron neutron capture therapy (BNCT) for malignant pleural mesothelioma from a viewpoint of dose distribution analysis. International Journal of Radiation Oncology Biology Physics. 66,1584-1589.
20) Takahashi K., Nakamura H., Furumoto S., Yamamoto K., Fukuda H., Matsumura A. Yamamoto Y., 2005. Synthesis and in vivo biodistribution of BPA–Gd–DTPA complex as a potential MRI contrast carrier for neutron capture therapy. Bioorganic & Medicinal Chemistry. 13,735-743.
21) Tokumitsu H., Hiratsuka J., Sakurai Y., Kobayashi T., Ichikawa H., Fukumori Y. Gadolinium neutron-capture therapy using novel gadopentetic acid±chitosan complex nanoparticles: in vivo growth suppression of experimental melanoma solid tumor. Cancer Letters, v.150, p.177-182, 2000.
22) Thrall, J. H., O'Malley, J. P., Zeissman, M. D., 2005. Nuclear Medicine. Third edition. (The Requisites in Radiology). Mosby Inc. USA. 704 pp.
23) Watanabe T., Ichikawa H., Fukumori Y., 2002. Tumor accumulation of gadolinium in lipid-nanoparticles intravenously injected for neutron-capture therapy of cancer. European Journal of Pharmaceutics and Biopharmaceutics, 54,119-124.
24) White, K., 1993. Safety in the design and operation of MRI systems Cryogenics, 33, 821-824.

^{195m}Pt- LABELED CISPLATIN AS A POSSIBLE TOOL FOR GLIOBLASTOMA TREATMENT

Soares M.A.[1], Mattos J.L.[1], Leal A.S.[2], Santos R.G[1]

[1] Laboratory of Radiobiology, [2] Division for Radiation Technology, Center for Development of Nuclear Technology CDTN/CNEN, CP 941, CEP 31123970, Minas Gerais, Brazil.

ABSTRACT

Gliomas are the most common and most deadly primary tumours found in the brain and carry a particularly poor prognosis. Because of its location beyond the reach of local control when it is first detected, these tumours have frustrated almost every attempt for successful therapy. By introducing radionuclides into the cells during the treatment with cisplatin, internal radiation and chemotherapy are possible at a low rate of toxicity. The proposal of this work was to investigate the antitumoral effect of neutron activated cisplatin at the TRIGA MARK-I IPR-RI and verify if the low-dose internal radio-chemotherapy produces additive effects on malignant glioblastoma cells.

The results obtained in the present work indicate that ^{195m}Pt-cisplatin kept its chemical stability upon neutron activation and was a very potent radiosensitizer evoking a supra additive effect. Treatment with internal radio-chemotherapy based on neutron activated cisplatin became possible a significant reduction of the cisplatin concentration required for effective inhibition of glioblastoma growth. Therefore production of radioactive cisplatin based on neutron activation may constitute a good strategy for the preparation of novel therapy for malignant glioblastoma.

Keywords: radioactive cisplatin, internal radiotherapy, glioblastoma

1 Introduction

Gliomas are the most common and most deadly primary tumours found in the brain and carry a particularly poor prognosis. They are classified into four clinical grades out of which the glioblastoma multiform (GBM) is the most aggressive one [1]. Glioblastoma is by far the most common glioma. This neoplasm infiltrates diffusely into regions of the normal brain rendering total surgical extirpation impossible. Because of its location beyond the reach of local control when it is first detected, these tumors have hampered almost every attempt to obtain a successful therapy. Despite recent attempts to improve chemotherapy and external radiotherapy, the median survival period of patients with cerebral glioblastoma is approximately 12 months [2]. The identification of novel therapeutic agents able to inhibit the growth of these tumours is therefore essential to improve the prognosis of glioma patients.

The antitumor activity of cis-dichlorodiamineplatinum(II) (CDDP, cisplatin) was discovered by Rosenberg et al (1969). It is particularly effective against testicular cancer and ovarian cancer. It is also used to treat cancer of the oesophagus, bladder, head and neck, including malignant glioma. However, the effectiveness of cisplatin against recurrent tumours is less than that observed against primary tumours [4], probably because of the presence of a population of cisplatin resistant cells. Additionally, in spite of its strong anticancer potency, chemotherapy with cisplatin associates many serious side effects, such as: nephrotoxicity, othotoxicity, nausea, neuropathy, allergy, etc.

Recently, the need of a multifactorial strategy for cancer treatment has been acknowledged and different treatment modalities are often combined to optimize treatment efficacy. An increase of anticancer potency has been observed by concomitant combination of irradiation and chemotherapeutic agents, including cisplatin [5,6]. This synergy enables the reduction of cisplatin dose, diminishing the side effects. Therefore, this combining-modality approach possesses therapeutic advantage for several types of malignant tumours.

Ionizing radiation interacts with tissue, thereby damaging DNA and other chemical structures. The success of radiotherapy in cancer patients largely depends on tumour radiosensitivity. Increasing the ratio between sensitivity of tumour cells versus normal cells to ionizing radiation would greatly improve cancer treatment. One of the approaches used to radiosensitize tumour cells is the combined application of

chemotherapeutic agents that alter DNA sensitivity to irradiation. Cisplatin, likewise other platinum-based anticancer drugs, appear to be excellent radiosensitizer [7]. Impressive response rates have been shown in radiochemotherapy with cisplatin and external irradiation, however, often at a expense of significant toxicity [8].

The internal radio-chemotherapy with its intrinsic selectivity and low irradiation dose rate to the target tissues has become an alternative and promising treatment option for some unresectable malignant tumours [9].

Despite the interaction with other molecules, the main target for cisplatin is DNA, on which the intra strand crosslink is assumed to be responsible for the biological activity [10]. By introducing radionuclides into the cells during the treatment with cisplatin, internal radiation and chemotherapy are possible at a low rate of toxicity. Because of its insertion into DNA, cisplatin itself is an optimal carrier molecule for the radionuclide once cisplatin and the radioactivity will act on the specific *target.*

Cisplatin has been used to treat malignant glioma, but internal radio-chemotherapy has not been used up to now. In the present report, we used neutronic activation to produce a radioactive analogue of cisplatin which emits Auger electron and gamma photon to verify if the internal radio-chemotherapy with this agent has sinergistic effect in comparison to cisplatin or irradiation alone.

2 Methods

2.1 Cisplatin neutron activation

Neutron activation was done on cis-dichlorodiamino platinum - II (cisplatin) as described by Leal et al [11]. A sample of cisplatin (2.0 mg) was irradiated inside of the TRIGA MARK I IPR R-1 reactor housed at the CDTN, applying an average thermal and epithermal neutron flux of 6.4×10^{11} and 4.4×10^{10} neutrons cm^{-2} s^{-1}, respectively, at 100 kW. The irradiation time was 8 h.

2.2 Evaluation of maintenance of the chemical stability upon neutron activation

Cisplatin was dissolved in PBS containing 0.5% DMSO and subject to gel filtration chromatography on Sephadex G10. Eluted fractions were monitored by UV spectrometry. Unmodified and ^{195m}Pt-cisplatin chromatographic profiles were compared.

2.3 Cell culture

Malignant RT2 glioblastoma cells were maintained in Dulbecco's Modified Eagle's Medium (DMEM- Gibco), supplemented with 10% fetal bovine serum and antibiotics (50 U mL^{-1} penicillin/50 µM streptomycin), in a water jacketed incubator with humidified atmosphere of 5% CO_2/95% air at 37 °C. For all experiments, cells were seeded at appropriate concentrations to ensure exponential growth.

2.4 Evaluation of antitumoral activity

2.4.1 Morphological analysis of tumour cells

For phase contrast microscopy, representative fields of cells were photographed using a TS100 (Nikon) microscope. Cells stained with 4`,6`-diamidino-2-phenylindole (DAPI) were visualized using suspensions of treated or control cells placed in tissue culture dishes. Cells were fixed with methanol, rinsed with PBS and methanol, stained with DAPI in methanol and observed using fluorescence microscopy (Nikon) under UV illumination.

2.4.2 Cytotoxic activity of native and neutron activated cisplatin on glioblastoma cells

To compare the IC_{50}-values the cytotoxic effects were quantified using a 3-(4,5-dimethiol-2-thioazolyl)-2,5-diphenyl tetrazolium bromide (MTT) colorimetric assay. Tests using DMSO (0.5% in DMEM) as negative control were carried out in parallel.

2.4.3 Cytostatic activity on glioblastoma cells

The capacity of the compounds to inhibit cell proliferation (cytostatic effect) was evaluated by clonogenic assay. Glioblastoma cells were treated with unlabeled or ^{195m}Pt-cisplatin, colonies were fixed in methanol and stained with 0.07% Giemsa after 7-10 days outgrowth.

2.5 Statistical analysis

Data were reported as mean $\pm$ SD, expressed as percentage of cell viability and proliferation relative to the untreated control. All tests were performed in triplicates with full agreement between the results. The statistical significance was assessed using Student's *t*-test ($p<0.05$).

3 Results

3.1 Cisplatin neutron activation

The final specific activity for cisplatin after neutron activation under the conditions described here was of approximately 87kBq mg^{-1}. Chromatographic analysis (fig.1) presents the same profile for both native and radioactive cisplatin, indicating that chemical structure was preserved after neutron activation.

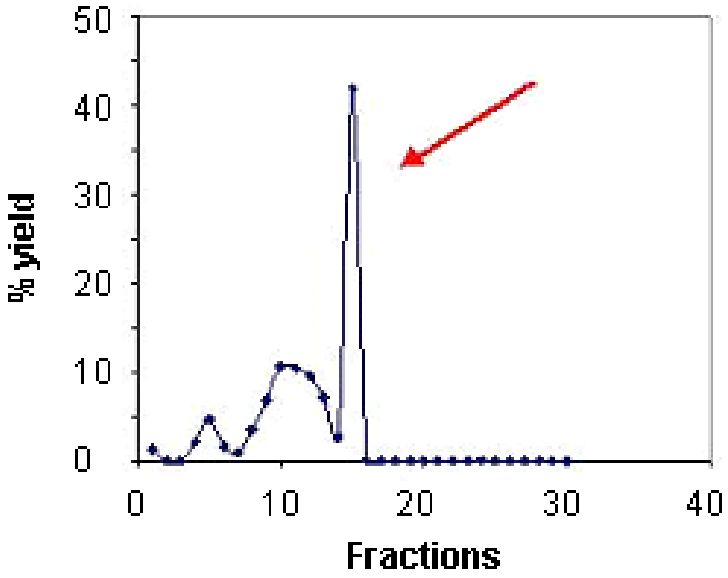

Fig 1- Profile of ^{195m}Pt-cisplatin under gel filtration chromatography

3.2 Native and ^{195m}Pt- cisplatin induce morphological alteration and cell death

The morphology of control and treated glioblastoma cells is depicted in Fig 2. A wide range of phenotypic modifications was observed in glioblastoma cells after exposure to cisplatin. During both treatments, it could be observed retraction of cytoplasmatic expansions, detachment, leading to round shaped cells, cell shrinkage and membrane blebs formation. Reduction of the number of cells after treatment was also observed. All of these morphological changes are associated to cell death probably by apoptosis.

As seen in Fig 2b, no DNA fragmentation was observed in untreated cells, but treated glioblastoma exhibited extensive DNA fragmentation following exposure to the native and the radioactive cisplatin.

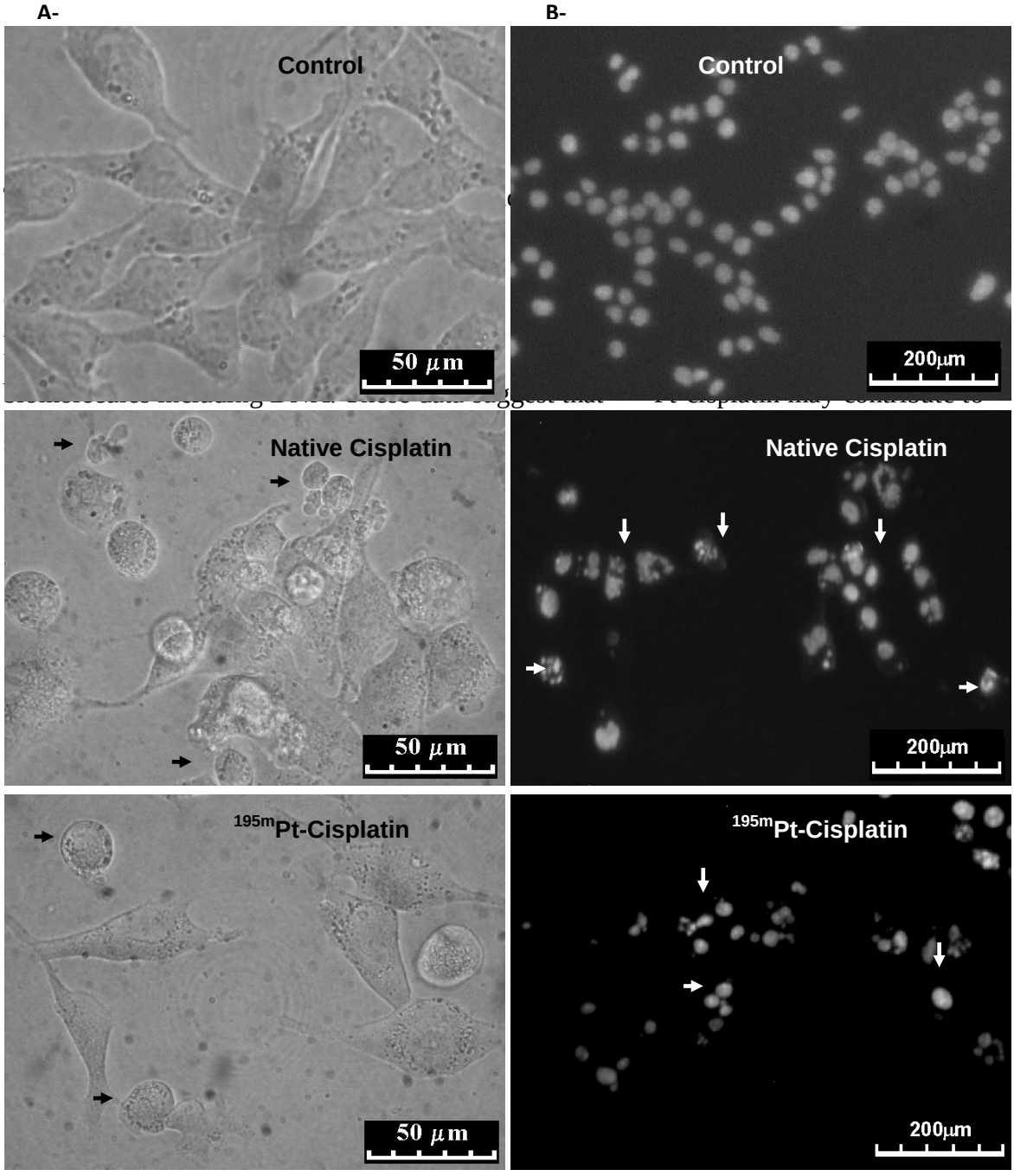

Fig 2: Cells treated with ^{195m}Pt-cisplatin exhibit morphological and nuclear changes characteristic of apoptosis. RT2 cells were treated with native and ^{195m}Pt-cisplatin. After 48h treatment (3μM) cells were observed under phase contrast microscopic or fixed and stained with DAPI as described in Materials and methods. It can be observed retraction of cell expansions, rounding cell, blebs (black arrows), chromatin condensation, nuclear fragmentation and apoptotic bodies (white arrows).

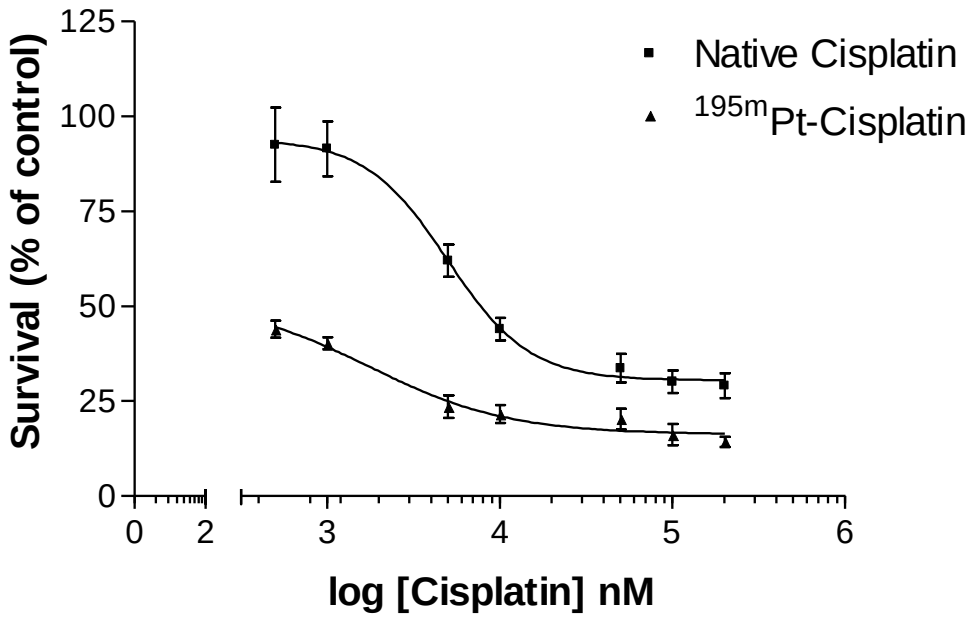

Fig 3: ^{195m}Pt-cisplatin induces cell death in glioblastoma cells more efficiently than native cisplatin. Cells were grown and treated with native and ^{195m}Pt-cisplatin as described in Materials and methods. Survival was measured by MTT assay

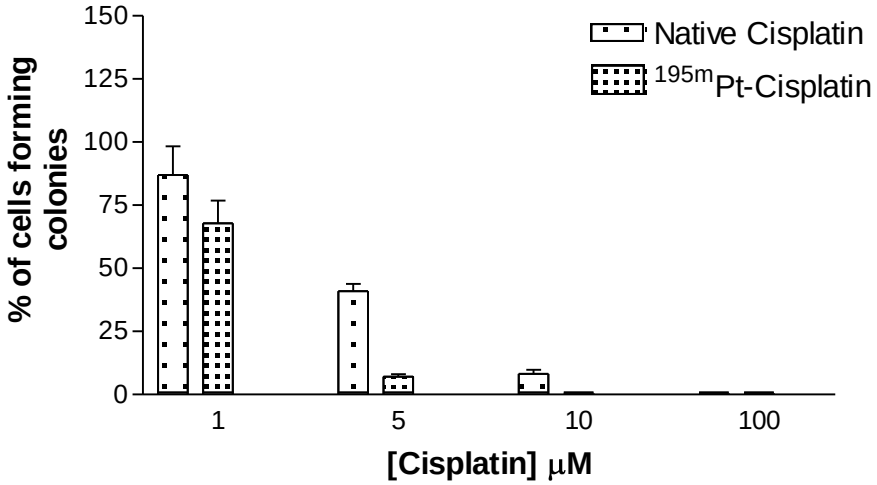

Fig 4- . ^{195m}Pt-cisplatin inhibits colony formation in glioblastoma cells more efficiently than native cisplatin. Cells were grown and treated with native and ^{195m}Pt-cisplatin as described in Materials and methods. Colonies were stained with Giemsa.

3.3 Antitumour activity

The cytotoxic effects of the studied compounds against glioblastoma are depicted in Fig 3 and 4. The data show that ^{195m}Pt-cisplatin was more potent (IC_{50} 1.75 μM) than native cisplatin (IC_{50} 4.96 μM) to inhibit cell survival (Fig 3) and cell proliferation (Fig 4). One of the reasons for this difference in activity could be the high LET particles such as electron auger. Cisplatin is well known to interact with biomolecules including DNA. These data suggest that ^{195m}Pt-cisplatin may contribute to strategically deliver radioactivity into tumour cells.

4 Conclusions

In the present study, the neutron activation of cisplatin proved to enhance its action on glioblastoma cells. Considering the poor prognosis of glioblastoma patients and the resistance of these tumors to conventional therapies, the results presented here are very encouraging and suggest that further studies should be performed to validate the use of ^{195m}Pt-cisplatin to improve the prognosis of these patients.

Production of radioactive cisplatin based on neutron activation may constitute a good strategy for the preparation of novel therapy for malignant glioblastoma.

5 Acknowledgements

This work was supported in part by Centro de Desenvolvimento da Tecnologia Nuclear-Comissão Nacional de Energia Nuclear. MAS was supported by a fellowship from PCI/CNEN. JLM was supported by a fellowship from Fundação de Amparo à Pesquisa do Estado de Minas Gerais (FAPEMIG), Brazil

6 Bibliography

[1] Levin V.A., Leibel S. *In*: De Vita V.T., Hellman S., Rosenberg S.A. (Eds). Cancer: Principles and Practice of Oncology, Lippincott, Philadelphia, 1993, pp. 1697-1737

[2] Winger M.J., MacDonald D.R., Cairncross J.G.. Supratentorial anaplastic gliomas in adults: the prognostic importance of extent of resection and prior low-grade glioma. *J. Neurosurg* 1989; 71:487-93.

[3] Rosenberg B., Van Camp L., Trosko J.E., Mansour V.H.. Platinum compounds: a new class of potent antitumor agents. *Nature* 1969; 222, 385-386.

[4] Amer M.H., Al-Sarraf M., Vaitkevivius V.K.. Factors that affect response to chemotherapy and survival of patients with advanced head and neck cancer. *Cancer*, 1979; 43(6):2202-6.

[5] Bachaud J.M., Chatelen E., Canal P., Albin N., Yardeni E., David J.M., et al. N Radiotherapy with concomitant continuous cisplatin infusion for unserectable rumors of the upper aerodigestive tract: results of phase I study *Am. J. Clin. Oncol* 1997; 20 (1): 1-5.

[6] Gorodetsky R., Levy-Agababa F., Mou X., Vexler A.M.. Combination of cisplatin and radiation in cell culture: Effect of duration of exposure to drug and timing of irradiation. *Int J Cancer* 1998; 75:635-642.

[7]Ali H., van Lier J.E.. Metal complexes as photo- and radiosensitizers. *Chem Rev* 1999; 99(9):2379-2450.

[8] Wheeler R.H., Spencer S. Cisplatin plus radiation therapy. *J. Infus Chemother* 1995; 5(2):61-66.

[9] Chatal J.F., Hoefnagel C.A.. Radionuclide therapy, Nuclear Medicine Sextet, *The Lancet* 1999; 354:931-935.

[10] Zamble D.B., Lippard S.J.. Cisplatin and DNA repair in cancer chemotherapy. *Trends in Biochem* Sci 1995; 20:435-9.

[11] Leal A.S., Júnior A.D.C., Abrantes F.M., Menezes M.A.B.C., Ferraz V., Cruz T.S. et al. Production of the radioactive antitumoral cisplatin. Applied *Radiation and Isotopes* 2005; 64:178-181.

3.3. IS – Industrial Section

IS01	Axial mixing performance of continuous phase in a pulsed sieve plate extraction column using gallium chloride as radiotracer Ghiyas-ud-Dina, Imran Rafiq Chughtai, Mansoor Hameed Inayat, Iqbal Hussain Khan
IS03	Industrial radiotracer generators Kristin Fure, Sindre Hassfjell and Tor Bjørnstad
IS04	Application of radiotracer methodology to study mixing and segregation in a rotary mixer in glass industry Luis Eduardo Barreira Brandão, Lidia Vasconcellos, Álvaro Serafim de Sousa
IS05	Using tracer data to improve petroleum reservoir models Olaf Huseby, Elin Rein , Øyvind Dugstad and Jan Sagen
IS06	Tracers for enhanced oil recovery in the Northeast Brazil Maria Aparecida de Melo, Ivonete Pereira Gonzalez da Silva, Amenonia Maria F. Pinto
IS08	Radiolabelled [Ni(Cn)4]2-for Water Tracing: Synthesis and Quality Examination Kjersti Jevanord and Tor Bjørnstad
IS09	Profile analysis of fluids displacement in a Phase separation tank applying the radiotracer technique Ricardo Elias de Miranda Candeiro, Luís Eduardo Barreira Brandão, Éder Fernando da Silva
IS10	Studies on Separation of Tracer Concentrations of Radiolabelled [Co(Cn)6]3- from Radiolabelled Scn- in Water Samples Tor Bjørnstad, Odd B. Michelsena), Dag Ø. Eriksen and Gonglay Yan
IS12	Analytical model for tracer transport in formations having conductive geological faults Manuel Coronado and Jetzabeth Ramírez-Sabag
IS13	RTD of the gas phase in a 130 m³ self-aerated flotation cell Francisco Díaz, Juan Yianatos, Felipe Contreras
IS14	Application of radioactive tracers in pulp follow up during a digester blowing in a multiple batch-digester pulp mill Francisco Díaz V., Darren Ledermann M, Hernán Arriagada C.
IS15	Comparative study of the catalytic powder behavior at two different risers of FCC plants Francisco Pablo Ramírez García
IS16	Development of new and alternative tracers for oil reservoirs Lauris L. Silva, Claudio L. Donnici, J. Danilo Ayala, Cíntia H. Freitas, Rubens M. Moreira, Amenônia M. F. Pinto
IS17	Synthesis of the indium complexes for using as an activable tracer in the oil secondary recuperation Júnia de O. Alves, Rubens M. Moreira

IS18	Comparison of Several Models/Software For Interpretation of a Tracer Test in a Five-Spot Laboratory Set-Up Ph. Berne, J.P Leclerc
IS19	Tracers for wormhole characterization and gel treatment design and evaluation, in oil secondary recovery M.B. Peralta, C. Procak, M.V. de la Fuente y C. Somaruga
IS20	Hydrodynamic Characteristics of SDU Enterprise “Heriberto Duquesne” by the radiotracer method Griffith J, Derivet M; Cuesta J, Flores J, Valdés J.
IS21	Implementation and automatization of a flow-through experimental setup for the evaluation of new tracers for oil reservoir characterization Bruno Resende Debien, Aimoré Dutra, Letícia Tasmo Perigolo and Rubens Martins Moreira
IS22	Methodology for Injection of Radioactive Tracer in Oil Reservoirs Alberto A. Barreto, Amenônia M. Ferreira Pinto, Rubens M. Moreira, Bruno G. Batista

AXIAL MIXING PERFORMANCE OF CONTINUOUS PHASE IN A PULSED SIEVE PLATE EXTRACTION COLUMN USING GALLIUM CHLORIDE AS RADIOTRACER

Ghiyas Ud Din[1,3,*], Imran Rafiq Chughtai[2], Mansoor Hameed Inayat[2], Iqbal Hussain Khan[3]

[1]Department of Nuclear Engineering, Pakistan Institute of Engineering and Applied Sciences [PIEAS], P.O Nilore, Islamabad, Pakistan

[2]Department of Chemical and Materials Engineering, Pakistan Institute of Engineering and Applied Sciences [PIEAS], P.O Nilore, Islamabad, Pakistan

[3]Isotope Applications Division, Pakistan Institute of Nuclear Science and Technology [PINSTECH], P.O Nilore, Islamabad, Pakistan

ABSTRACT

Axial mixing performance of continuous phase in a liquid-liquid extraction pulsed sieve plate column has been investigated. Residence Time Distribution (RTD) analysis of continuous phase has been carried out for a wide range of pulsation frequency and amplitude in a liquid-liquid extraction pulsed sieve plate column operating with water as continuous and kerosene as dispersed phase using radiotracer technology. The column was operated in the emulsion region and ^{68}Ga in the form of gallium chloride eluted from a ^{68}Ge/^{68}Ga generator was used to trace the continuous phase (water). Axial Dispersion Model (ADM) with open-open boundary condition and two point measurement method was used to model the continuous phase hydrodynamics. A comparison of experimental and model RTD functions and their respective Mean Residence Time (MRT) revealed that the Axial Dispersion Model is a suitable model to describe the continuous phase hydrodynamics in a pulsed sieve plate extraction column.

Keywords: Axial mixing; liquid-liquid extraction; pulsed sieve plate column; Residence Time Distribution (RTD); radiotracer; ^{68}Ga

INTRODUCTION

Pulsed columns are considered efficient liquid-liquid extraction equipments as they offer large interfacial area, high mass transfer coefficient, high turbulence and minimum radial gradients. They find a great deal of applications in petroleum, nuclear, chemical, metallurgical, pharmaceutical, food processing and bio-processing industries. Phases are

* Corresponding author: Tel.: +92-51-2207381 (Ext. 3332), Fax: +92-51-2208070.
E-mail addresses: fac192@pieas.edu.pk, ghiyasuddin@hotmail.com (G. U. Din).

subject to flow counter currently to achieve high concentration gradients for efficient mass transfer in this kind of equipments but axial mixing in both phases lowers the process efficiency by lowering solute concentration gradients. The presence of axial mixing in this kind of extractors is inevitable as it is caused by the geometrical and operating parameters. Therefore, a considerable academic and industrial interest exists in the measurement of axial mixing in such equipments. A usual process engineering approach is to model the system as plug flow with some degree of back mixing superimposed on it (Levenspiel and Smith, 1957; Levenspiel, 1999) and the concept of Residence Time Distribution (RTD) analysis is an important tool for the estimation of axial mixing (Danckwerts, 1953). The holdup and slip velocity are other important parameters in the design and operation of pulsed extraction columns.

The issue of axial mixing in the continuous phase of liquid-liquid extraction columns has been under research (Kim and Baird, 1976a, 1976b; Hafez et al., 1979; Parthasarathy et al., 1984; Srinikethan et al., 1987). Effect of various geometrical and operating parameters on the axial mixing of continuous phase has been reported in these investigations. Most of these studies have been carried out using conventional tracers which do not provide on-line information. Low sensitivity and poor statistics are other disadvantages associated with this methodology.

Radiotracer technology offers state of the art technique for industrial process optimization and trouble shooting due to high sensitivity, on-line measurement, better statistics and high benefit to cost ratio. The unique ability of this technology is that it can provide information that may not be obtained by other techniques. This technology has been widely used in developed countries to help solve industrial problems (Blet et al., 1999; Dudukovic, 2000; Berne and Thereska, 2004; Kim et al. 2005). It is also flourishing in developing countries (Pant et al., 2000; Farooq et al. 2003; Moreira et al., 2007) but facing a major constraint due to the unavailability of radiotracers at the time of requirement. For countries that do not possess radioisotope production facilities, it is necessary to import the radiotracers and long time involved in this process rules out the possibility of achieving potential benefit of this technology. Medical radionuclide generators such as ^{99}Mo/^{99m}Tc and ^{113}Sn/^{113m}In provide a partial solution to the problem but radiotracers from these generators have limited applications in industry because of their relatively short half lives, low gamma energies and adsorption on solid surfaces depending on the chemical and physical conditions. Hence, there is a need to explore some more nuclear genetic relationships that may form the basis for the development of radionuclide generators for industrial process investigations. Keeping in view of these considerations, a novel

industrial radionuclide generator (IRG) system (^{68}Ge/^{68}Ga) especially for industrial process investigations has been developed (IAEA, 2007). The concept of ^{68}Ge/^{68}Ga generator is already in the market for nuclear medicine applications especially for Positron Emission Tomography (Nakayama et al., 2003; Mathias and Green, 2008) but it is rather new in the field of industrial process investigations. The special feature of this IRG is that it has been made cost economical by compromising the biological factors; therefore, it is not useful for in-vivo applications. This IRG system produces ^{68}Ga radiotracer in the form of gallium chloride with dual gamma energy 0.511 MeV. A major attraction of this IRG lies in the half-lives of mother (270 days) and daughter (67.6 minutes). So the life of this IRG spans over a period of around two years and due to high gamma energy of the daughter it is useful in industrial systems having thick metallic walls. Moreover, the short half-life of daughter ensures quick decontamination of the systems under investigation. Although ^{99m}Tc in the form of sodium pertechnatate proved to be a good water tracer while working on the hydrodynamics of dispersed phase (water) in the pulsed sieve plate extraction column (Din et al., 2008a) but this radiotracer failed to provide a sufficient signal at the system outlet due to large degree of dilution as the water is subject to flow as continuous phase in the present scenario. However, thick lead shield collimators with fine collimation are required to counter high back ground level, which may arise during the course of experiments.

The present study is focused to investigate the axial mixing performance of continuous phase (water) in a pulsed sieve plate extraction column using ^{68}Ga in the form of gallium chloride as radiotracer. Residence Time Distribution experiments for the continuous phase have been carried out for a wide range of pulsation frequency and amplitude for this purpose. The holdup of continuous phase and slip velocity has also been reported.

MATERIALS AND METHODS

The schematic diagram of pulsed sieve plate extraction column under investigation is shown in Fig. 1. The internal diameter of the column is 5×10^{-2} m and height is 2 m. Two separating chambers, one at the top and the other at the bottom of the column are also part of this apparatus. The column is fitted with regularly spaced (5×10^{-2} m) sieve plates, which help to increase the interfacial area between the two immiscible liquids. The column was operated counter currently with heavy phase (water) as continuous and light phase (kerosene) as dispersed phase. The kerosene which is fed into the lower separating chamber with the help of a metering pump flows upwards through the sieve plate column to the upper separating chamber where it overflows to a collection vessel. Similarly water is fed into the top separating chamber via a metering pump from where it flows downwards

through the column to the lower separating chamber, and then through a balance leg into a collection vessel. A pulse unit located at the base of lower separating chamber provides vertical pulses to the flowing fluids. The column was operated in the emulsion regime i.e. dispersed phase remained dispersed throughout the plate stack and no coalescence into layers occurred at the plates. A liquid-liquid interface was allowed to form at about 10 cm above the heavy phase inlet and this interface level was stabilized with the help of the balance leg before starting the experiment.

^{68}Ga in the form of gallium chloride is a novel radiotracer in the field of industrial process investigation; therefore, validation of radiotracer was carried out by thoroughly mixing a minute quantity of ^{68}Ga in equal amounts of water and kerosene with the help of a stainless steel stirrer in a glass beaker. Upon separation and measurements, the radiotracer was found suitable as water tracer in water-kerosene environment. Also, no adsorption of radiotracer was experienced on the glass walls and stainless steel stirrer upon rinsing them with fresh water and kerosene. About 0.25 mCi of ^{68}Ga eluted from a ^{68}Ge/^{68}Ga generator was injected in the form of an instantaneous pulse to carry out RTD experiments for measuring the axial mixing performance of continuous phase (water) as per experimental setup shown in Fig. 1. The experiments were carried out for a range of pulsation frequency and amplitude as given in Table 1. The movement of radiotracer was monitored for every second with the help of lead collimated NaI(Tl) (2'' x 2'') scintillation detectors mounted at D1, D2 and D3 as shown in Fig. 1. The data was acquired on-line using a multi-channel data acquisition system and stored in a computer for further processing.

The tracer data from detectors D2 (column inlet) and D3 (column outlet) was corrected for background, radioactive decay and normalized. The experimental Mean Residence Time (MRT) of the system was calculated by the difference of first moments of outlet and inlet response curves. Mathematical expression for the first moment in discrete form can be written as:

$$\textit{First Moment} = \frac{\sum_i t_i C_i \Delta t_i}{\sum_i C_i \Delta t_i} \qquad (1)$$

Where

C = Tracer concentration (counts/s in present case)

t = Time of measurement (s)

Δt *= Time interval between the two measurements (s)*

i = 0, 1, 2, 3, ……

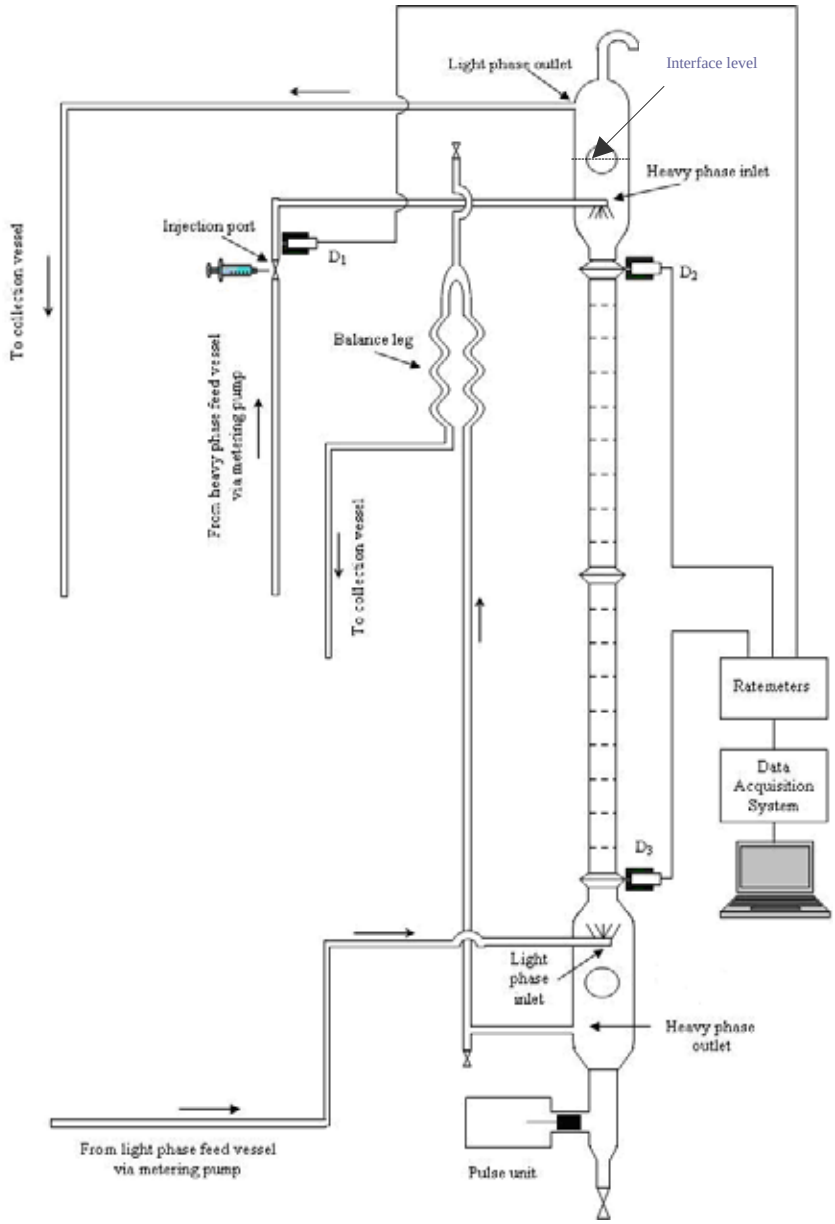

Fig. 1. Schematic diagram of pulsed sieve plate extraction column

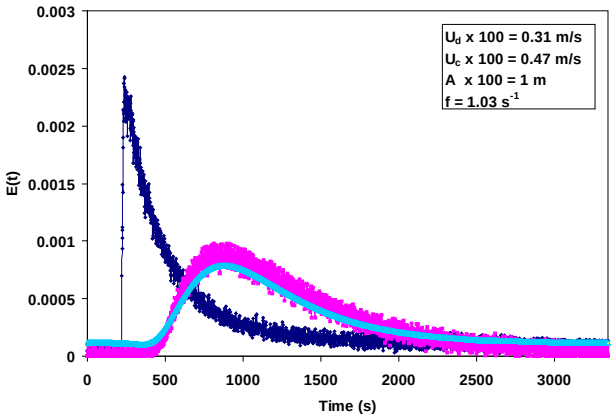

Fig. 2. Typical normalized RTD function curves at the input (D2) and output (D3) with model output response of continuous phase in the pulsed sieve plate extraction column

Table 1.

Internal diameter of the column (m)	5×10^{-2}
Length of the column (m)	2
Number of sieve plates	38
Plate spacing (m)	5×10^{-2}
Plate diameter (m)	5×10^{-2}
Hole size (m)	2×10^{-3}
Average number of holes	140 per plate
Average free area (%)	25
Range of pulsation frequency (s^{-1})	1.03 - 2.16
Range of pulsation amplitude (m)	0.6×10^{-2} - 1.4×10^{-2}
Dispersed phase superficial velocity (m/s)	0.31×10^{-2}
Continuous phase superficial velocity (m/s)	0.47×10^{-2}

Overall holdup of the phase under investigation was calculated on the basis of experimental MRT using the following relationship:

$$H_c = \frac{\bar{t}Q_c}{V_R} \qquad (2)$$

Where

H_c = *Continuous phase holdup*

$\bar{t}$ = *Mean residence time*

Q_c = *Continuous phase flow rate*

V_R = *Effective reactor volume*

The slip velocity averaged over the whole column was estimated as (Treybal, 1981; Venkatanarasaiah and Varma, 1998):

$$V_s = \frac{U_d}{(1-H_c)} + \frac{U_c}{H_c} \qquad (3)$$

Where

V_s = *Slip velocity*

H_c = *Continuous phase holdup*

U_d = *Dispersed phase superficial velocity*

U_c = *Continuous phase superficial velocity*

The RTD is a probability distribution function that describes the amount of time a fluid element spends inside a reactor. It helps in troubleshooting of reactors and characterizes the mixing and flows within the reactors. If an impulse of tracer is injected at the inlet of a system at time *t = 0* and its concentration is measured as a function of time at the outlet, then *E(t)* representing the probability for a tracer element to have a residence time between the time interval *(t, t+dt)* is defined as:

$$E_i(t) = \frac{C_i(t)}{\int_0^\infty C_i(t)dt} \qquad (4)$$

Such that

$$\int_0^\infty E_i(t)dt = 1 \qquad (5)$$

Where

i = 0, 1, 2, 3, …….. , n

$C_i(t)$ = *Tracer concentration*

$E_i(t)$ = *Residence Time Distribution function*

RTD models have been playing a vital role for industrial process investigations for decades. They provide macroscopic lumped sum description, which is sufficient for many engineering calculations. The plug flow is an ideal condition for the flow of phases in an extraction column but some degree of axial mixing is always inevitable. ADM was used to model the subject system.

The basic general differential equation of the one dimensional ADM for fluid flow in the dimensionless form is as follows:

$$\frac{\partial C}{\partial \theta} = \frac{1}{Pe}\frac{\partial^2 C}{\partial X^2} - \frac{\partial C}{\partial X} \qquad (6)$$

Where

C = Dimensionless tracer concentration = $\frac{c(t)}{c(0)}$

Pe = Peclet number = $\frac{uL}{D}$

u = Mean linear velocity

X = Dimensionless axial coordinate = $\frac{x}{L}$

D = Axial dispersion coefficient

c(t) = Tracer concentration at time t

c(0) = Initial tracer concentration

The flow conditions are not plug type before and after the inlet (D_2) and outlet (D_3) boundaries, therefore, open-open boundary condition can be chosen in present situation. A uniform radial concentration in the continuous phase is assumed due to large length to diameter ratio.

A solution of Eq. 6 for open-open boundary condition in dimensionless form is given as under with a detailed analysis given by (Levenspiel and Smith, 1957; Levenspiel, 1999):

$$E(\theta) = \sqrt{\frac{Pe}{4\pi\theta}}\exp\left(\frac{-Pe(1-\theta)^2}{4\theta}\right) \qquad (7)$$

A Residence Time Distribution analysis software package “RTD” developed by IAEA (2004a) was used for modeling in the present investigations. This model calculates the RTD response of a system to an arbitrary pulse of tracer by convoluting the input function with impulse response of the model (Levenspiel, 1999; IAEA, 2004a, b). The ADM in this

software package adopts two points measurement methodology and optimizes two parameters, the MRT and Pe. The software uses the least square curve fitting method to fit the model RTD function (Eq. 7) onto the experimental data and obtains the optimum model parameters. Fig. 2 shows typical normalized RTD function curves obtained at the input (D_2) and output (D_3) with model output response of continuous phase in response to an instantaneous pulse injection at (D_1).

Due to the random nature of radioactive decay process, any measurement of radiation is subject to some degree of statistical fluctuation. These inherent fluctuations represent an unavoidable source of uncertainty in all nuclear measurements. Uncertainty associated in the measurement of radiation and its propagation in subsequent calculations has been worked out using standard methods and shown as error bars in respective results (Knoll, 2000; Bevington and Robinson, 2003). The metering pumps used for the flow of fluids and pulsation in the pulsed sieve plate column were calibrated before the experiments and errors associated in the measurement of flow rate, pulsation frequency and amplitude have been considered negligible.

RESULTS AND DISCUSSION

Fig. 3(a) shows the effect of pulsation frequency on the MRT of continuous phase when U_c, U_d and pulsation amplitude are kept constant. It has been observed that increase in pulsation frequency decreases the MRT of the continuous phase. The axial mixing in continuous phase decreases with increase in pulsation frequency when U_c, U_d and pulsation amplitude are not changed. This phenomenon can be seen by the increasing Peclet number in Fig. 3(b).

As pulsation frequency increases, the droplet population density of dispersed phase inside the column increases; hence increase the dispersed phase holdup. The increase in holdup of dispersed phase with increase in pulsation frequency has already been reported while working on the hydrodynamics of dispersed phase on the same column with water as dispersed and kerosene as continuous phase (Din et al., 2008b). The increase in dispersed phase holdup decreases the proportion of continuous phase inside the column (Fig. 3c) leading to a decrease in the MRT of continuous phase (Eq. 2).

Moreover, increase in dispersed phase holdup with increase in pulsation frequency leads to decrease the slip velocity when U_c, U_d and pulsation amplitude are kept constant Fig. 3(d). This may also be due to the reason that increase in droplet population density of dispersed phase inside the column leads to the situation where velocity fields around the droplets interfere with each other. Also, decrease in the size of a droplet increases the

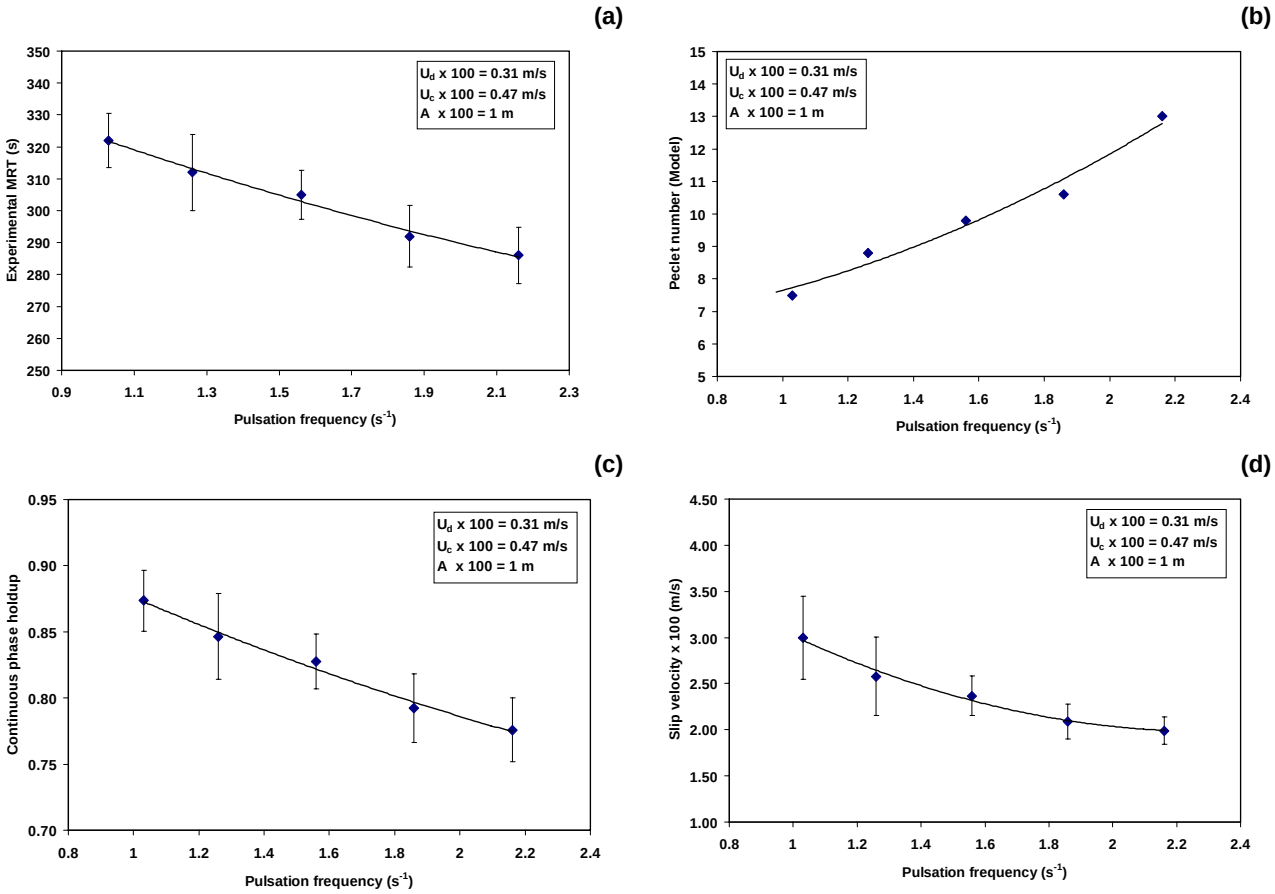

Fig. 3. Effect of pulsation frequency on the (a): MRT of continuous phase, (b): Peclet number of continuous phase, (c): continuous phase holdup, (d): slip velocity

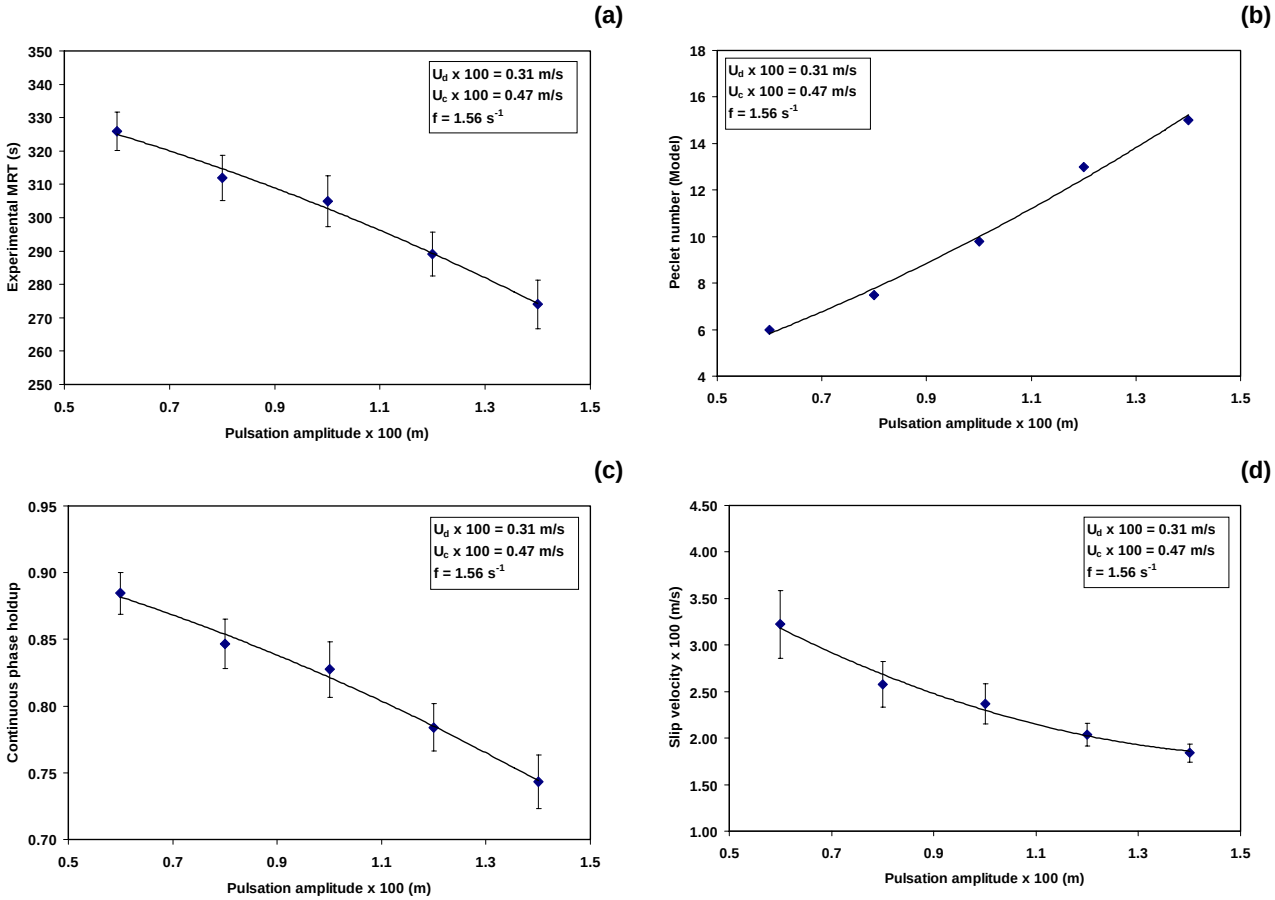

Fig. 4. Effect of pulsation amplitude on the (a): MRT of continuous phase, (b): Peclet number of continuous phase, (c): continuous phase holdup, (d): slip velocity

drag on this droplet and hence decreases its velocity to move counter currently through the continuous phase; therefore, slip velocity decreases with increase in pulsation frequency.

Fig. 4(a-d) shows the effect of pulsation amplitude on the MRT, Peclet number, holdup of continuous phase and slip velocity when U_c, U_d and pulsation frequency are not changed. Increase in pulsation amplitude also leads to an increase in droplet population density inside the column, therefore, similar trends in MRT, Peclet number, holdup and slip velocity have been observed and phenomena can be explained on the basis already described above.

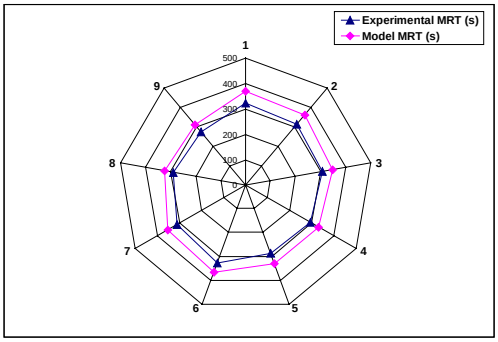

Fig. 5. Comparison of experimental and model MRTs

A comparison of experimental and model MRTs of various RTD experiments carried out during these investigations has been given as a radar plot shown in Fig. 5 which shows a good agreement between experimental and model MRTs.

CONCLUSIONS

(a) ^{68}Ga in the form of gallium chloride is a suitable radiotracer for labeling water phase in water-kerosene environment.

(b) The axial mixing in the continuous phase of a liquid-liquid extraction pulsed sieve plate column decreases with increase in pulsation frequency and amplitude.

(c) The holdup of continuous phase decreases with increase in pulsation frequency and amplitude.

(d) The slip velocity decreases with increase in pulsation frequency and amplitude.

(e) The model estimated MRTs are in good agreement with experimentally measured MRTs which means that ADM is a suitable model for the system under investigation.

ACKNOWLEDGEMENTS

The authors are grateful to the Higher Education Commission [HEC], Islamabad, Pakistan for financial support in accomplishment of this study. The authors are greatly indebted to the International Atomic Energy Agency (IAEA) for partially supporting this work under the framework of Coordinated Research Project No. 14348 on *"Evaluation of industrial radionuclide generators and validation of radionucilde generator-based radiotracers for industrial applications"* and for the provision of RTD analysis software package. Special thanks are due to Dr. Joon-Ha Jin, Technical Officer, Industrial Applications and Chemistry

Section, Division of Physical and Chemical Sciences, IAEA in this regard. The cooperation and technical assistance extended by Pakistan Institute of Nuclear Science and Technology [PINSTECH] and Pakistan Institute of Engineering and Applied Sciences [PIEAS] is thankfully acknowledged.

REFERENCES

Berne, P., Thereska, J., 2004. Simulation of a radiotracer experiment by flow and detection-chain modelling: a first step towards better interpretation. Appl. Radiat. Isot. 60 (6), 855-861.

Bevington, P.R., Robinson, D.K, 2003. Data reduction and error analysis for the physical sciences. Mc Graw Hill Co. Inc., New York.

Blet, V., Berne, P., Tola, F., Vitart, X., Chaussy, C., 1999. Recent developments in radioactive tracers methodology. Appl. Radiat. Isot. 51 (6), 615-624.

Danckwerts, P.V., 1953. Continuous flow systems, distribution of residence times. Chem. Eng. Sci. 2 (1), 1-13.

Din, G.U., Chughtai, I.R., Inayat, M.H., Khan, I.H., 2008. Axial dispersion, holdup and slip velocity of dispersed phase in a pulsed sieve plate extraction column by radiotracer residence time distribution analysis. Appl. Radiat. Isot. 66, 1818-1824.

Din, G.U., Chughtai, I.R., Inayat, M.H., Khan, I.H., 2008. Study of axial mixing, holdup and slip velocity of dispersed phase in a pulsed sieve plate extraction column using radiotracer technique. 6$^{th.}$ International conference on isotopes held in Seoul, Korea from 12-16 May, 2008.

Dudukovic, M.P., 2000. Opaque multiphase reactors: experimentation, modeling and troubleshooting. Oil & Gas Sci. Tech. 55(2), 135-158.

Farooq, M., Khan, I.H., Din, G.U., Gul, S., Palige, J., Dobrowolski, A., 2003. Radiotracer investigations of municipal sewage treatment stations. Nukleonika 48 (1), 57-61.

Hafez, M.M., Baird, M.H.I., Nirdosh, I., 1979. Flooding and axial dispersion in reciprocating plate extraction column. Can. J. Chem. Eng. 57, 150-158.

International Atomic Energy Agency, 2004a. Integration of tracing with computational fluid dynamics for industrial process investigation, Tecdoc-1412. IAEA, Vienna, Austria.

International Atomic Energy Agency, 2004b. Radiotracer applications in industry - A guidebook, Technical Report Series No. 423, IAEA, Vienna, Austria.

International Atomic Energy Agency, 2007. Report of the first research coordination meeting of the CRP on evaluation and validation of radioisotope generators-based radiotracers for industrial applications. IAEA, Vienna, Austria.

Kim, H.S., Shin, M.S., Jang, D.S., Jung, S.H., Jin, J.H., 2005. Study of flow characteristics in a secondary clarifier by numerical simulation and radioisotope tracer technique. Appl. Radiat. Isot. 63 (4), 519-526.

Kim, S.D., Baird, M.H.I., 1976a. Axial dispersion in a reciprocating plate extraction column. Can. J. Chem. Eng. 54, 81-89.

Kim, S.D., Baird, M.H.I., 1976b. Effect of hole size on hydrodynamics of a reciprocating perforated plate extraction column. Can. J. Chem. Eng. 54, 235-237.

Knoll, G.F., 2000. Radiation detection and measurement. John Wiley & Sons, New York.

Levenspiel, O., 1999. Chemical reaction engineering. John Wiley & Sons, New York.

Levenspiel, O., Smith, W.K., 1957. Notes on the diffusion-type model for the longitudinal mixing of fluids in flow. Chem. Eng. Sci. 6 (4-5), 227-235.

Mathias, C.J., Green, M.A., 2008. A convenient route to [68Ga]Ga-MAA for use as a particulate PET perfusion tracer. Appl. Radiat. Isot. doi:10.1016/j.apradiso.2008.06.004.

Moreira, R.M., Pinto, A.M.F., Mesnier, R., Leclerc, J.-P., 2007. Influence of inlet positions on the flow behavior inside a photoreactor using radiotracers and colored tracer investigations. Appl. Radiat. Isot. 65 (4), 419-427.

Nakayama, M., Haratake, M., Ono, M., Koiso, T., Harada, K., Nakayama, H., Yahara, S., Ohmomo, Y., Arano, Y., 2003. A new ^{68}Ge/^{68}Ga generator system using an organic polymer containing N-methylglucamine groups as adsorbent for ^{68}Ge. Appl. Radiat. Isot. 58 (1), 9-14.

Pant, H.J., Saroha, A.K., Nigam, K.D.P., 2000. Measurement of liquid holdup and axial dispersion in trickle bed reactors using radiotracer technique. Nukleonika 45 (4), 235-241.

Parthasarathy, P., Sriniketan, G., Srinivas, N.S., Varma, Y.B.G., 1984. Axial mixing of continuous phase in reciprocating plate columns. Chem. Eng. Sci. 39 (6), 987-995.

Srinikethan, G., Prabhakar, A., Varma, Y.B.G., 1987. Axial dispersion in plate-pulsed columns. Bioprocess Eng. 2 (4), 161-168.

Treybal, R.E., 1981. Mass transfer operations. Mc Graw Hill Book Company, Inc., New York.

Venkatanarasaiah, D., Varma, Y.B.G., 1998. Dispersed phase holdup and mass transfer in liquid pulsed column. Bioprocess Eng. 18 (2), 119-126.

INDUSTRIAL RADIOTRACER GENERATORS

Kristin Fure, Sindre Hassfjell and Tor Bjørnstad
Institute for Energy Technology (IFE), Kjeller, Norway

ABSTRACT

This paper describes a project at Institute for Energy Technology, in its initial phase. The goal is to make radiotracer generators for tracing processes primarily in the oil industry utilizing radionuclide generators. The project addresses the need for automatic and unmanned monitoring in relation to the e-field concept and short-lived radiotracers for multiple phases; oil, water, gas or even sand distributed by unmanned radionuclide generators is the achievement. Four radionuclide nuclear "genetic" relationships are selected for this purpose: $^{68}Ge \rightarrow ^{68}Ga$, $^{113}Sn \rightarrow ^{113m}In$, $^{137}Cs \rightarrow ^{137m}Ba$ and $^{144}Ce \rightarrow ^{144}Pr$. These radionuclides are chosen due to their desirable nuclear properties (half-life, radiation type and –energy).

INTRODUCTION

Radiotracers are excellent tools for measuring flow and trace leakages in industrial facilities. Among the advantages are high accuracy, low detection limits, on-line measurements without perturbing the system and well-known detector technology. Despite their benefits, rather few short-lived radiotracers are in use. The reason is often accessibility. Lack of nearby production facilities like particle accelerators and nuclear reactor facilities impedes the use of short-lived radiotracers. Radiotracers produced from a radionuclide generator overcome this problem. In a radionuclide generator a longer-lived radionuclide produces a shorter-lived radionuclide that may either be used as a radiotracer directly or incorporated in a more complex radiotracer molecule. By choosing right pair of nuclides and automation of the process, many of the problems which are associated with radiotracers, like waste and radiation exposure may also be minimized or even eliminated.

TRACERS IN THE PETROLEUM INDUSTRY

A tracer may be defined as any substance who's atomic or molecular, physical, chemical or biological properties provide for the identification, observation and study of the behavior of various physical, chemical or biological processes (dispersion of concentration, flow, kinetics and

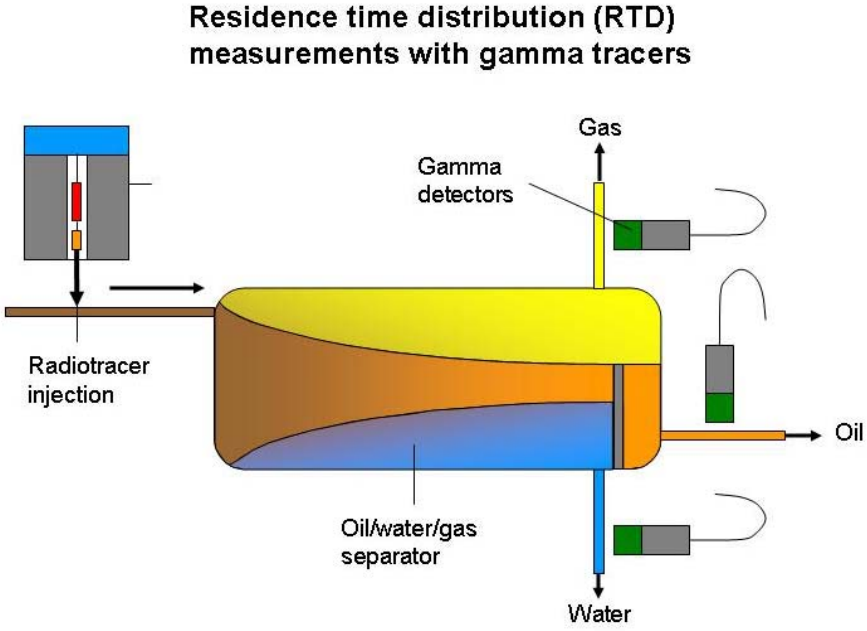

Figure 1 Quality control of multiphase separator by RTD measurements

dynamics, chemical reactions, physiological interactions etc.), which occur either instantaneously or in a given laps of time [i]. See references [ii], [iii] and [iv] on present frontier knowledge on tracer technology and its application in industry and geospherical investigations. A general overview of tracer technology in the oil field application is found in the book by B. Zemel [v]. While much have been done on development of tracers for oil field characterization, tailor-made tracers for process studies has not seen the same degree of development, and there is a considerable potential to further improve the experimental tracer technology in combination with Residence Time Distribution (RTD) technology.

Due to this situation and the concept of e-fields where the goal is to remotely control and operate production equipment, there is now a continuously strengthening industrial request for more tracer material and new types of applications in this field. IFE has a long tradition in developing tracers, especially for the petroleum industry. IFE's Department for Reservoir and Exploration Technology has made the tracer technology area the subject for its main research focus, and are eager to take this discipline into a new era with development of novel technology.

THE RADIOTRACER GENERATOR

A radionuclide generator is a chemical/physical/mechanical devise that is based on nuclear "genetic" mother-daughter relationship. In the nuclear "genetic" relationship, one radionuclide (the mother) produces another radionuclide (the daughter) by radioactive decay. In a radionuclide generator the nuclear properties are such that the mother nuclide has a longer half-life (less unstable) than the daughter nuclide (more unstable). This entails that the daughter will "grow in" until equilibrium between the activities of the two nuclides are reached. Depending on the differences in half-life of the two nuclides the mother-daughter relationship belongs either to a secular equilibrium were the half-life of the mother is much longer than that of the daughter, or transient equilibrium were the half-life of the mother is the same or slightly longer than the half-life of the daughter. The most useful genetic relationships for radionuclide generator in the industry are

the one with secular equilibrium. The nuclear chart contains more than 110 such mother-daughter relationships, some of them useful for industrial purposes. From the nature of the radioactive decay the two nuclides, the mother and the daughter will in most cases, be different chemical elements and may therefore be chemically, physically or mechanically separated. In most cases the mother nuclide is bound to a column material, and the daughter is eluted either by liquid or gas flushing through the column, leaving the mother nuclei untouched. This system constitutes a radionuclide generator. The isolated daughter may then be utilized as a radiotracer directly or as chemically bound in a tracer molecule.

A radiotracer generator is a chemical/physical/mechanical devise, which contains a radionuclide generator and possible additional features for chemically treatment of the daughter nuclide to tailor-make a tracer for a particular purpose. Automation or semi-automation not only reduces manual handling of radioactivity and prevents high doses to the operator, but also lower possibilities for spills and site contamination and render remote operation possible (ref. the e-field concept in the oil industry). Some principle sketches of a radiotracer generator based on a column support for the mother nuclide are shown in figure 2.

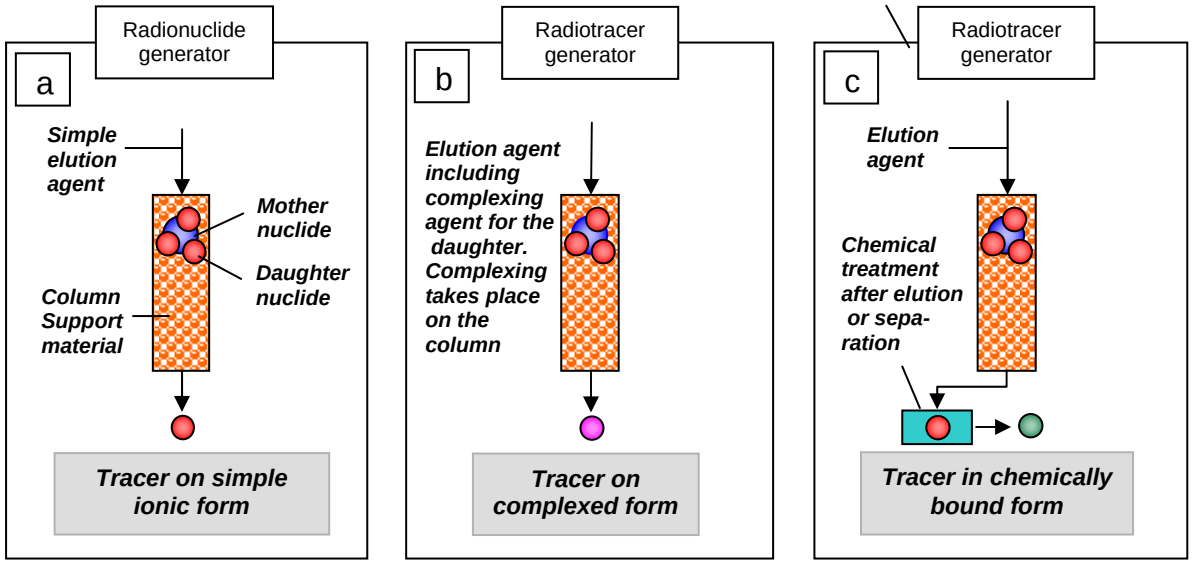

Figure 2 A radiotracer generator may be of varying complexity from a pure radionuclide generator (a) where the eluted radionuclide is used as a tracer directly to a more complex version (c) which may include extensive chemical treatment of the eluted radionuclide before application in tracer experiments

CHOICE OF RADIONUCLIDES

Many of the radionuclide generators' physical properties are set by the half-lives of the two "genetically" related radionuclides. If the half-life of the mother nuclide is long compared to that of the corresponding daughter nuclide, the daughter nuclide can be repeatedly eluted because the inventory of mother radionuclide produces daughter nuclides continuously. The necessary time between elutions is exclusively governed by the half-life of the daughter radionuclide and the radioactivity required for a particular purpose. Generally, this delay time should be longer than one half-life of the daughter nuclide. The lifetime of the generator is governed by the half-life of the mother nuclide, but also by radiolytic damage and other chemical processes, which may reduce the milking efficiency and/or induce too high breakthrough of mother nuclide and thereby affect negatively the operation safety. An operative period of a radionuclide generator is therefore for many systems practically restricted to 2-3 half-lives of the mother radionuclide.

The half-life of the daughter nuclide governs how often the generator may be eluted. It also governs how long the daughter radionuclide will be available as a tracer. A shorter half-life means that the nuclide will decay away faster, and this restricts the use of the tracer, but it also has an advantage concerning waste. In many cases the decay product from the daughter nuclide is an inactive nuclide,

and after a reasonable delay time, there will be no radioactivity for disposal. No radioactive waste will be generated, and the waste may be disposed without precautions taken to radioactivity. High radionuclide purity is therefore crucial. Especially to keep breakthrough of mother nuclide in the eluate to a minimum is important. The relation between activity (Bq) and chemical amount (moles, N) of a radioactive species given in equation 1, and means there will be no need for chemical disposal permission for the inactive decay product of the daughter nuclide.

$N = \frac{T_{1/2}}{\ln 2 \cdot 6.022 \cdot 10^{23}} A$	N: Number of moles A: Activity (Bq) $T_{1/2}$: Half-life (s) $6{,}22 \cdot 10^{23}$: Avogadro's Number	Eqn. 1.

The four nuclear "genetic" related mother-daughter pairs selected in this project are the ones in Table 1. All of these radionuclides have sufficiently good nuclear properties for being a radionuclide generator for industrial purposes. All selected generators will have an operation time of at least one year, and elution more than once in a working shift will be possible. The waste will not be significantly active after one day and the radiation type and energy is well suited for studying mass transport inside non-transparent and thick-walled production equipment like, for instance, gas-oil-water separators and scrubbers.

Table 1 Nuclear properties for the four radionuclides [vi]

Generator	Half-life Mother Nuclide	Half-life Daughter Nuclide	Decay, Radiation energy
$^{68}Ge \rightarrow ^{68}Ga$	270,82 d	67,629 min	β^+, γ 511 keV
$^{113}Sn \rightarrow ^{113m}In$	115,09 d	1,6582 h	IT, γ 391,690 keV
$^{137}Cs \rightarrow ^{137m}Ba$	30,07 y	2,552 min	IT, γ 661,660 keV
$^{144}Ce \rightarrow ^{144}Pr$	284,893 d	17,28 min	β^-, γ 696,513 keV, 2185,682 keV

Gallium

The $^{68}Ge \rightarrow ^{68}Ga$ generator is already commercially available, due to its application in positron emission tomography (PET) analysis in nuclear medicine. The nuclear properties of the mother and daughter radionuclides are, as can be seen in table 1, well suited for process studies in the industry. The half-life of the mother nuclide of 270,82 days offers possibility for a generator with an operation time of 1.5 to 2 years. Further elution every second hour will produce 70 % the generator's total capacity, see figure 3. The two coincident and directionally opposite 511 keV gamma energy with its origin in the annihilation of the beta-plus particle, has perfect energy for penetrating steal walls of a few millimeters to some centimeters. In addition, it gives possibility for homographic studies by PET technology. Due to the relatively short half-life of the daughter nuclide more than

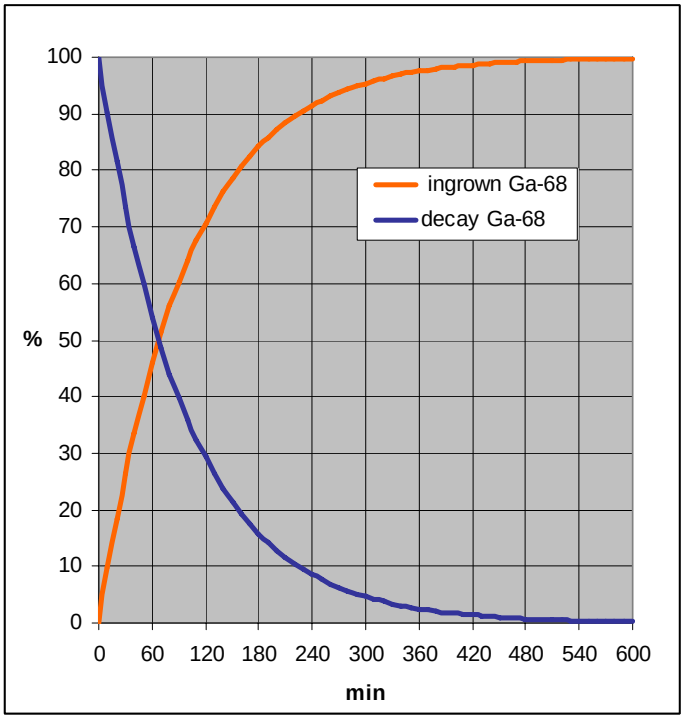

Figure 3 Ingrowths of ^{68}Ga in the generator and decay of the eluted ^{68}Ga.

99 % of the ^{68}Ga-activity will have decayed after ten hours ending up as ^{68}Zn. And since ^{68}Zn is a stabile nuclide, no radioactive waste will be generated.

Since the generator is commercially available, the development of a ^{68}Ga based tracer will concentrate on making suitable gallium tracer chemistry, and on testing some of these generators to foresee that they meet requirements for a radiotracer generator. So far, a generator from China (CIAE) has been tested. After one year of operation the generator showed an elution efficiency of 61 % and a breakthrough of mother nuclide measured to $4 \cdot 10^{-5}$. The column in this generator is made of SnO_2 [vii]. The generator is adequate for this project but breakthrough lower than 10^{-5} would be more desirable.

Indium

The ^{113}Sn→^{113m}In is another commercially available radionuclide generator from nuclear medicine. Its operation time is about 0.5 to 1 year, see table 1. Every third hour ^{113m}In will have grown in to 70 % of the generator's total capacity, see figure 4, and be ready for elution. The 392 keV gamma ray originates from an internal transition from the isomeric state ^{113m}In to the none-radioactive ground state ^{113g}In. The gamma is slightly softer compared to the other radionuclide generators, but still adequate for penetrating thin steel walls. Within 15 hours more than 99 % of ^{113m}In activity will have decayed away.

With ^{113}Sn→^{113m}In generators commercially available, the work on a ^{113m}In based tracer has been concentrated on indium chemistry. A ^{113}Sn→^{113m}In generator distributed delivered by IDB in Holland will be tested in the nearest future.

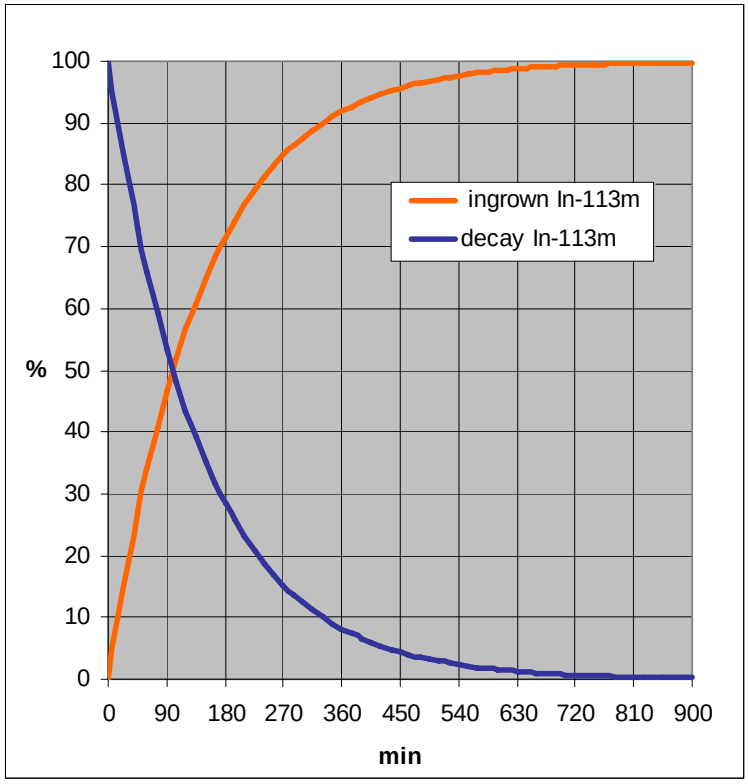

Figure 4 Ingrowths of ^{113m}In in the generator and decay of the eluted ^{113m}In

Barium

There are a few commercially available $^{137}Cs \rightarrow ^{137m}Ba$ radionuclide generators on the market, but they are all small and designed for educational purposes. In an industrial radionuclide generator activities of several GBq may be needed, and this poses strict demands for minimum breakthrough of mother nuclide, resistance of the column material to radiation damage and chemical purity of the eluted daughter nuclide. ^{137}Cs has a half-life of 30 years, se table 1, which indicates a generator of almost "endless" lifetime compared to industrial installations, if radiation damage can be controlled. In reality radiation damage of the column material may restrict the generator's operation time. The relatively short half-life of 2.55 minutes of the daughter nuclide ^{137m}Ba makes multiple injections possible since already after 5 minutes more than 70 % of achievable activity will have grown in, and after 20 minutes more than 99 % of the eluted ^{137m}Ba-activity will have decayed away, se figure 5. ^{137m}Ba decays by internal transition to stable ^{137}Ba, and the 662 keV gamma energy is perfect for studying processes inside steel constructions.

Since there is no commercially available adequate $^{137}Cs \rightarrow ^{137m}Ba$ generator, work here will have to deal with both finding a suitable column material for ^{137}Cs and making a good barium tracer molecule.

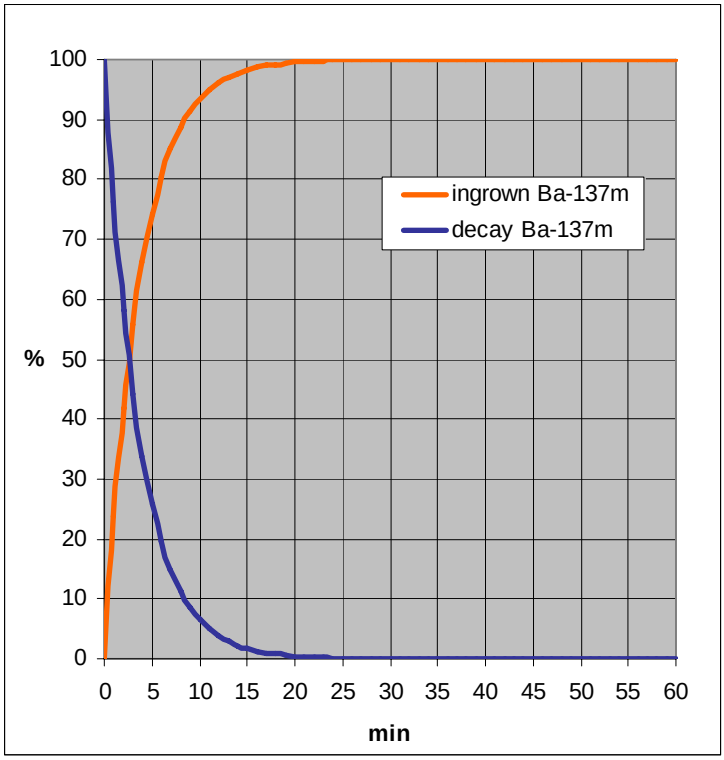

Figure 5 Ingrowths of ^{137m}Ba in the generator and decay of the eluted ^{137m}Ba

Praseodymium

As far as the authors know, there is no commercially available $^{144}Ce \rightarrow ^{144}Pr$ generator. The generator should have an operational time of 1.5 to 2 years, which is about the same as the $^{68}Ge \rightarrow ^{68}Ga$ generator, due to similar half-life of the mother nuclides ^{144}Ce and ^{68}Ge, see table 1. But the shorter life-time of the daughter ^{144}Pr, makes possible elution of the generator 4 times more frequent than for the $^{68}Ge \rightarrow ^{68}Ga$ generator. The 696 kev gamma line is perfect for studying processes inside steel constructions, but the 2186 keV line with about the same intensity may give rise to shielding problems and doses to workers during operation. A solution to this problem would be automatic and unmanned operation. The two gamma lines, however, give possibilities for depth measurement. The decay product of ^{144}Pr is ^{144}Nb, which is a long-lived alfa-particle emitting nuclide with a half-life of $2{,}1 \cdot 10^{15}$ years. The half-life is so long that the nuclide may be regarded as stable, and the isotope exist to a fraction of 23,80 % in naturally occurring neodymium. The radioactive waste produced from this generator will therefore be insignificant as the ^{144}Nb-activity is given by equation2.

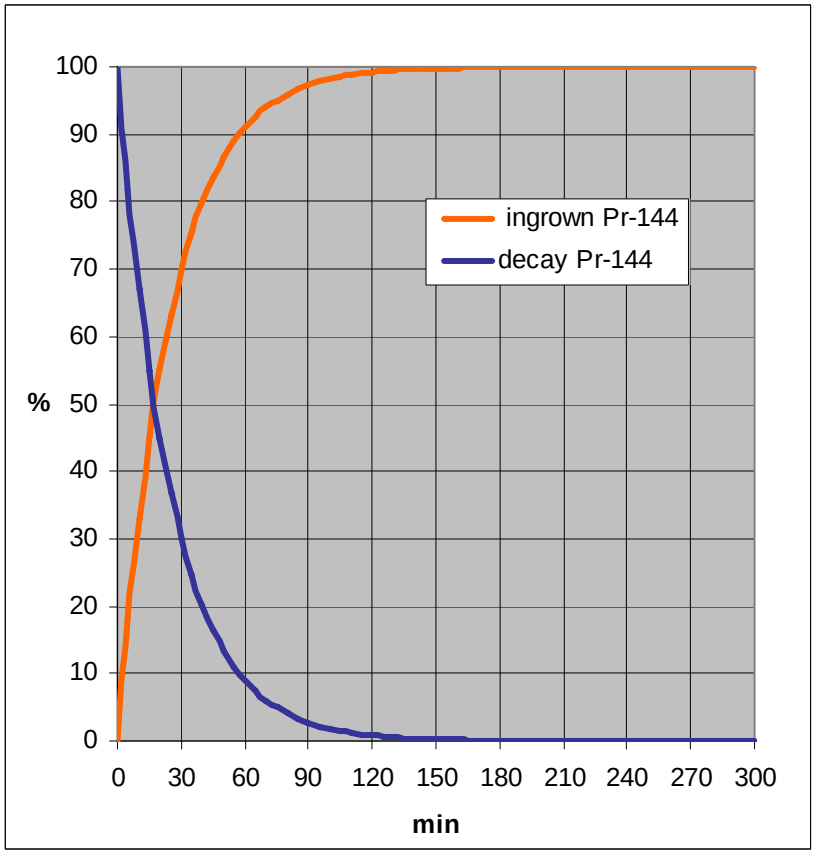

Figure 6 Ingrowths of ^{144}Pr in the generator and decay of the eluted ^{144}Pr

$A^2 = \frac{\ln T^1_{1/2}}{\ln T^2_{1/2}} A^1$	A^1: Activity of ^{144}Pr A^2: Activity of nuclide ^{144}Nb $T^1_{1/2}$: Half-life of nuclide ^{144}Pr $T^2_{1/2}$: Half-life of nuclide ^{144}Nb	Eqn. 2.

As for the $^{137}Cs \rightarrow ^{137m}Ba$ generator, there are both needs for finding a suitable column material for ^{144}Ce and making a good praseodymium tracer molecule in order to create a $^{144}Ce \rightarrow ^{144}Pr$ tracer generator.

SUMMARY

Goals and tasks for the future:

- In those cases where commercially available nuclide generators all ready exists, for instance in the case of the $^{68}Ge \rightarrow ^{68}Ga$ generator and the $^{113}Sn \rightarrow ^{113m}In$ generator, multiple generators have to be tested to examine their ability to meet requirements concerning breakthrough of mother nuclide ($< 10^{-5}$) and chemical purity of daughter nuclide. Their elution chemistry may also need to be changed in order to make a good radiotracer from the eluted daughter nuclide.

- Where commercially available nuclide generators don't exist, like for the mother-daughter pairs $^{137}Cs \rightarrow ^{137m}Ba$ and $^{144}Ce \rightarrow ^{144}Pr$, column materials have to be tested to find a suitable resin, which strongly retains mother nuclide while daughter nuclide may be eluted. These columns, like the commercial ones, will also have to meet the requirements of low breakthrough of mother nuclide and purity of daughter nuclide.
- Develop chemistry for all the daughter elements to make dedicated radiotracers for a particular system; gas-oil-water separators, scrubbers, wells, and for a particular medium; oil, water (solid particles and gas).
- Look for automation possibilities for the radiotracer generators and the chemistry.
- Testing and quality control of the various elaborated radiotracer generator systems.

REFERENCES

1. [1]Bjørnstad, T., Fure, K.: "Industrial Radiotracer Generators for the Petroleum Industry", IAEA CM-report, Vienna, Austria, Aug. 2007
2. [1]Axelsson, G., Barry, B.J., Berne, P., Bjørnstad, T, Cameron, R. Charlton, S., Maggio, G.E., Pang, Z, Thereska, J. and Vitart, X: "Radiotracer Applications in Industry – A Guidebook", IAEA Technical Report Series No 423, IAEA Vienna, Sep. 2004
3. [1]Bjørnstad, T, Hills, A.E., Jin, J-H., Khan, I. and Palige, J.: "Radiotracers and Labelling Compounds for Applications in Industry and Environment", IAEA CM-report, Warsawa, Poland, June 2004, 49 pp.
4. [1]Bjørnstad, T., Dugstad, Ø, Galdiga, C. And Sagen, J.: "Interwell Tracer Technology in Oil Reservoirs; State-of-the-Art", in proc. For the "First International congress on Tracers and Tracing Methods", Nancy, France, May. 29-31, 2001, p. 261-268
5. [1]Zemel, B.: "Tracers in the Oil field", Elsevier Science, Amsterdam (1995)
6. [1]Firestine, Richard. B., Frank Chu, S. Y., Shirley V. S., Baglin, C. M., Zipkin, J.: "Table of Isotopes" , 8. Ed. Ver. 1, Mar. 1996
7. [1]"Ga-68 Generator for the Production of Gallium Ga-68 Chloride Solution", Atom Hightech Co., Ltd, Beijing, China

APPLICATION OF RADIOTRACER METHODOLOGY TO STUDY MIXING AND SEGREGATION IN A ROTARY MIXER IN GLASS INDUSTRY

L. E. B. Brandão[1] , L. Vasconcellos[2] , A. S. de Sousa[1]
[1] Instituto de Engenharia Nuclear IEN/ CNEN-RJ
[2] Instituto de Radioproteção e Dosimetria IRD / CNEN-RJ

ABSTRACT

Radioactive tracers are very suitable to study the homogenization process in a glass industrial rotating mixer because they can be measure through the wall with no disturbs in the mixing process. Tracer studies have been undertaken using a Eirich DZ29 mixer with 5.0 Ton cylindrical rotating chamber (2.8 m diameter and 7rpm), two mixing rotating star, one clockwise (38 rpm) and one anticlockwise (31 rpm) and a drum type rotor (484 rpm) . To measure the quality of final process 140La was used to mark three different components of the mixing process (sand , Sodium Sulfate and Iron Oxide) and two NaI 3"x3" scintillators detectors were used do register the tracer signal outside of the vessel. It was possible to identify a dead zone inside the chamber and segregation in the mixing ´process.

I – INTRODUCTION

The mixing of particulate solids may be defined as any process that tends to eliminate existing inhomogeneity or to reduce a gradient of each component in the blend. The effectiveness of blending depends on physicochemical factors (density, size, chemical form), on the characteristics of mixing devices and their operating conditions. Mixing of solids is invariably accompanied by segregation because small differences in either size or density of granular components lead to flow-induced segregation and the fundamentals of the process are not well understood. Rotary mixers play an important role in the processing of granular solids in the industries, especially in glass industry where mixing applications involve processes that require different materials and long mixing times.

Modeling these mixing and segregation processes requires the confluence of several tools, including continuum and discrete descriptions.

Basically glass is a blend of sand, limestone, dolomite, soda ash but various materials are employed to produce glasses having particular optical properties or for specific purposes. These materials consist of small quantities of discrete particles (different specific gravity) which will initially blend together but which during subsequent handling have been separated out or became segregated to the end that when the batch is introduced into the glass melting furnace. In most cases, the segregation is controlled by adding water in the blend during the mixing process.

The radiotracer technique is especially well suited to the measurement of the quality of mixing in industrials vessels because of radiotracer can be measured accurately directly through the mixer walls using radiation detectors[1,2] A small quantity of marked component is injected in the blend and followed continuously by measuring its concentrations during the operation. This procedure is specially indicated for large scale industry equipment.

II – MATERIALS AND METHODS

The major raw materials used in glass industry are sand, sodium and magnesium carbonate and the composition of all commercially produced glass is very carefully controlled.

In addition to these basic ingredients several other items may be added in order to bring color or improve chemical or physical properties. To obtaining the desired glass composition, the correct material blend must be well calculated and mixed, in our case, 5.0 Ton of materials were mixed each batch.

All the experiments were done in an Eirich Model DZ29 cylindrical mixer with rotating (7 rpm) mixing pan with 2.8 m diameter; 1.2 m height and operated in batchwise mode. Inside the mixer

there are two rapid mixing stars, one clockwise (38 rpm), one anticlockwise (31 rpm) and a drum type rotor (484 rpm).
The rotating mixing pan continually transport the material to the rotating mixing tools, inducing counter-flowing currents of material. A wall-bottom scraper acts as a deflector to the material and prevents residue accumulations on the wall and surface of the mixing pan and both furnishes rapid evacuation when the job is finished [manual].
Three components (sand, sodium sulfate and iron oxide) of the blend with different granulometry and density were used to study the mixing process and a small volume of each one was marked.
As tracer was used ^{131}I for sand and ^{140}La to sodium sulfate and iron oxide. Sand grains was marked using the procedure suggested by Kolar [1]. Sands particles were first covered with a thin layer of silver and then immersed in aqueous solution of $NH_4{}^{131}I$. Sodium sulfate and iron oxide were marked using the method suggested by Brandão [3] using a using Lanthanum oxide of mixed in acrylic resin dissolved in chloroform. Using these methods it was possible to mark particles with 185 MBq for each experiment.
To measure the radiation intensity, two external NaI 3"x3" scintillators detectors, diametrical opposing one to the other, facing the mixer wall had been located 10.0 cm from the wall at the half of mixer height. No collimators were used and lead bricks had been used to block the lateral of the detectors.

III - RESULTS AND DISCUSSION

In all the experiments, the interval of time between two successive counting was 50 milliseconds, with total time of sampling varying between 600 and 650 seconds. In all figures the signal of one detector is plotted in red and the other one is plotted in blue.
In the first experiment sand was used and the signal registered by the detectors is shown in picture 1. The injection was done 40 sec after the acquisition was started and 15 sec after the tracer signal was registered by both detectors. In Fig. 2 show some peaks, this is because the tracer was still concentrated in a small portion of the sand. The curve reaches a constant variation 110 sec after the injection, so the mixing time was fixed equal 120 sec.

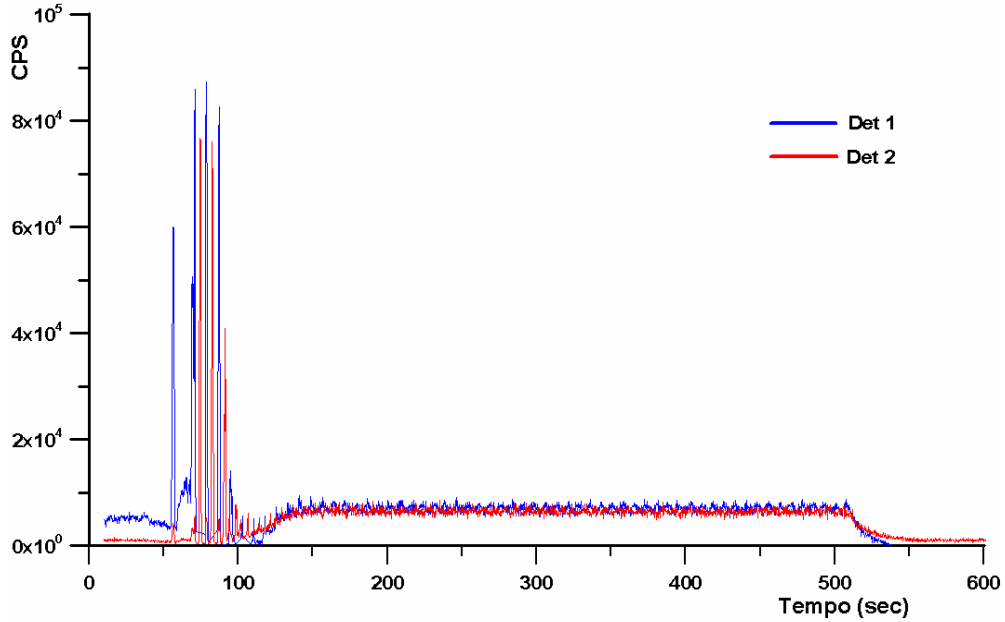

Fig. 1 – Signal registered by scintillators detectors with sand marked with 131I.

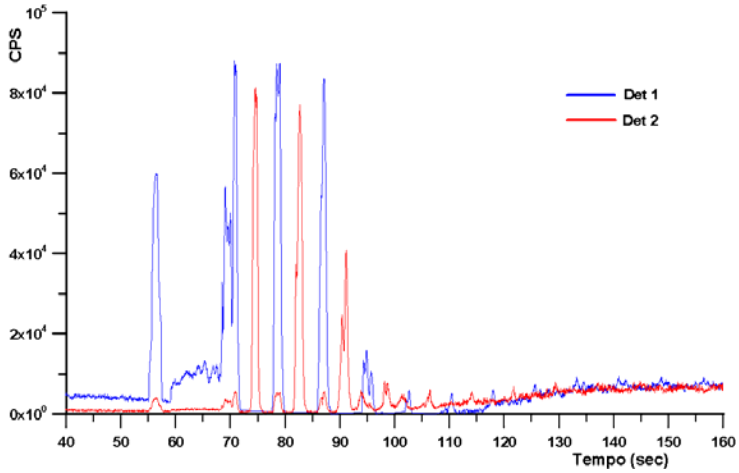

Fig. 2 – Detail showing the beginning of the process inside the mixer.

As the curve show, after the mixing time there is a constant oscillation in the signals registered by both detectors. This is because some portion of tracer wasn´t mixed and was accumulated in a region near the two mixing stars, so this proves a existence of a dead zone inside the mixer. This fact is evident when we visualize the pan evacuation, shown is Fig. 3.
To remove the blend the mixer pas was stopped and the wall-bottom scraper helps the evacuation. When the pan rotating stopped, the oscillations in the detectors signals stopped too and one detector registered a fast removal of the material and the other still registered a signal, constant but not zero. This proves that some marked sand continued inside of the mixer.

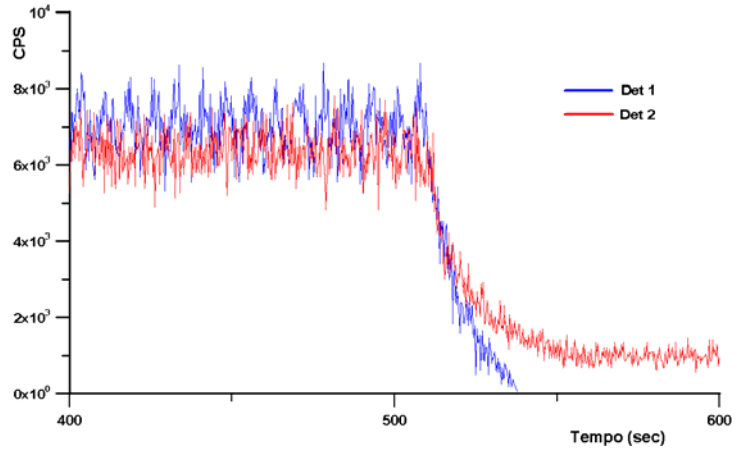

Fig. 3 – The end of the process: the evacuation of mixing pan

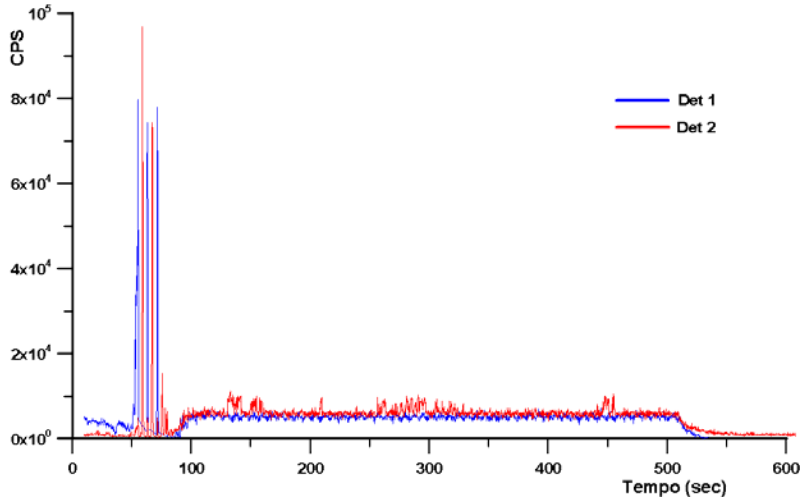

Fig. 4 – Signal registered by the detectors using sodium sulfate marked with 140La

The same situations were registered when Sodium Sulfate was studied. Again, the mixing time equal 120 sec was calculated and was verified an accumulation inside the mixer pan. With sodium sulfate during the process some structures appear for Det. 2 as shown in Fig 5 for t= 320 sec and t= 450 sec. This is because some tracer was being kept in the dead zone.

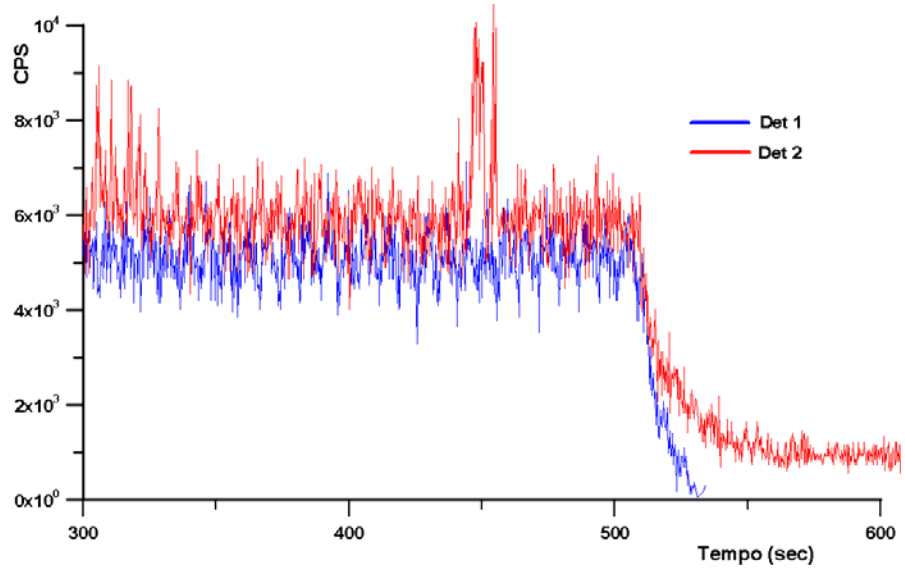

FIG. 5 – Signal registered by detectors for sodium sulfate showing retention.

The situation is totally different in case of iron oxide as shown if Fig. 6. The tracer injection was done in t=10 sec, and only t=35 sec the tracer was registered by the detectors, but the base line is constant until t=150 sec.

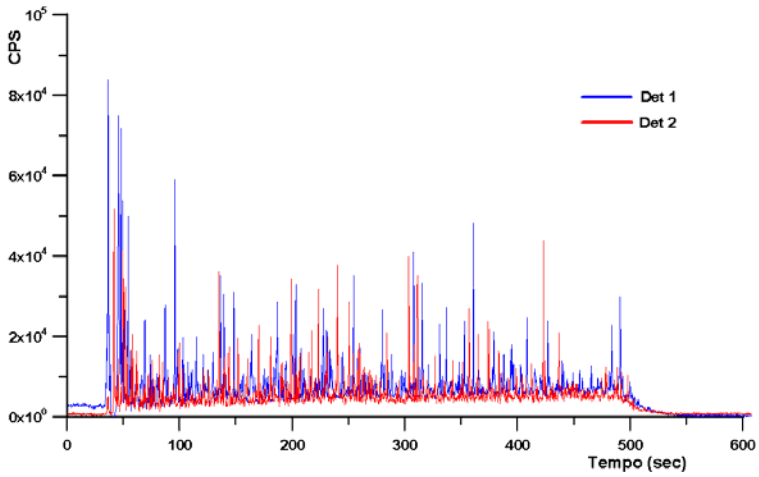

Fig. 6 - Signal registered by detectors for iron oxide marked with 140La.

After this time, there is a small increasing in base line but again the iron oxide was not mixing with the others material this is evident by the great number of peaks registered in both detectors. This situation happens during all the experiment, even after 500 sec the iron oxide was not homogenized, Fig. 7 and Fig. 8.

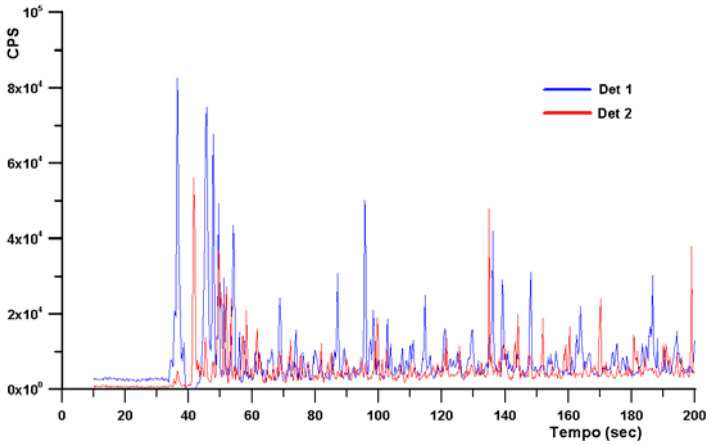

FIG. 7 – Iron oxide segregation during the mixing process.

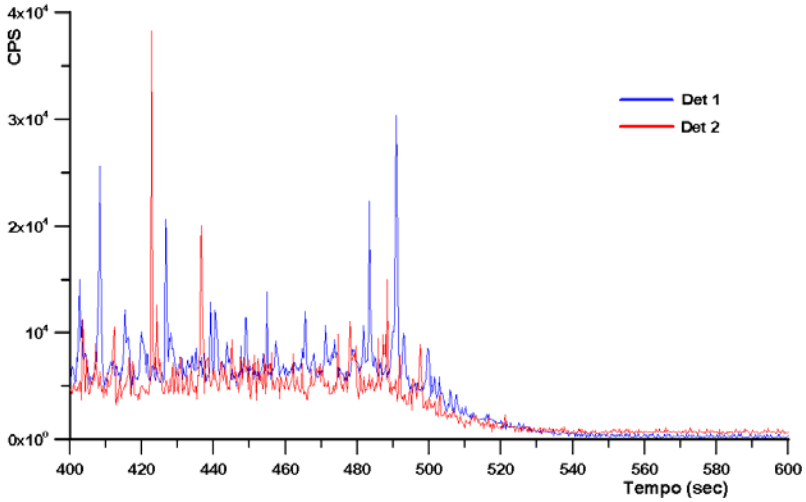

FIG. 8 - The end of the experiment with iron oxide.

Again, in this case, a small part of blend was still inside the mixer pan after the evacuation.

IV - CONCLUSIONS

Mixing of granular solids is a complex phenomenon and is not only determined by the geometric configuration of mixer and mixing star velocities but is dependent on the differences in properties of the particles that are being mixed. The presence of particles with different size, shape, density or surface property adds to the complexity and leads to segregation of particles.
With radioactive tracer technique was possible to determine the mixing time and located a dead zone inside the mixing pan.

V - BIBLIOGRAPHY

1. Z. I. Kolar "Radiotracer aided optimization of batch mixing of solids" Isotopenpraxis 25 (1989) 4 135-138
2. Z.I.Kolar "Utility of radiotracer methodology in scientific research on industrial relevancy" Isotopenpraxis 26 (1990) 9 419-424
3. L. E. B. Brandão " Otimização de unidades de tratamento de águas residuais empregando-se traçadores radioativos" COPPE/URFJ - D. Sc. Engenharia Nuclear 2001

USING TRACER DATA TO IMPROVE PETROLEUM RESERVOIR MODELS

Olaf Huseby[1], Elin Rein[2], Øyvind Dugstad[1] and Jan Sagen[1]
[1] Institute for Energy Technology, Kjeller, Norway
[2] StatoilHydro, Bergen, Norway

ABSTRACT

Numerical reservoir models are extensively used to plan and optimize production from petroleum reservoirs. In order to maximize the effect of enhanced oil recovery (EOR) methods and modern drilling technology (e.g. horizontal/flexible and multi-branched wells), it is important to obtain a proper understanding of the complex geological structures found in most reservoirs. Improved computational capabilities and simulation tools have helped to improve decisions regarding optimum reservoir development. Nevertheless, any reservoir simulation model represents one of many realizations of the real reservoir, and to reduce the inherent uncertainty of the models it is important to include additional data, such as tracer data. Unfortunately, tracers are underexploited as a source of data to understand oil reservoirs, and should be used in a better way, e.g., to locate and quantify bypassed and un-produced oil volumes in the reservoirs. In this paper we address this shortcoming, by illustrating how tracer data can be used in combination with other production data to improve reservoir models. Tracer modeling relies on high-quality tracer data that should always be evaluated for contamination, measurement flaws and misinterpretations. We discuss the issue of water re-injection, and demonstrate how this potential problem can be overcome. The value of tracer-data for simulation model improvements is demonstrated by history matching of a North Sea reservoir case using tracer and production data.

TRACER TESTING AND MODELING IN PETROLEUM RESERVOIRS

Tracers are inert chemical or radioactive compounds that are used to label and track fluids. They can be used to monitor wells, production equipment, as well as fluid movement in the reservoir. In the reservoir, tracers can be used in single well operations, e.g., to evaluate remaining oil in the near-well zone, or in inter-well tracer tests (IWTT), to evaluate fluid movement between injectors and producers. A general review of tracers applied in petroleum reservoirs is given by Zemel (1994).

In the petroleum industry, both radioactive and chemical tracers are used. Typical radioactive tracers are tritiated water (HTO), or radio-labeled hydrocarbon components (e.g., tritiated or carbon-14 labeled methane). Typical chemical tracers are fluorinated benzoic acids for water (Galdiga and Greibrokk, 1998), or perfluorocarbons for gas (Dugstad et al., 1992; Kleven et al., 1996).

Inter-well tracer testing has been established and proven as an efficient technology to obtain information on well-to-well communication, heterogeneities and fluid dynamics. During such tests, chemical or radioactive tracers are used to label water or gas from specific injection wells. The tracers are then subsequently used to trace the fluids as they move through the reservoir together with the injection phase. One of the appealing features of IWTT is that at the first tracer breakthrough in a producer, immediate information on the injector - producer communication is given. In some cases tracers may be injected into specific reservoir zones, to reduce ambiguities in interpretation. For two wells in the field considered here, e.g., different tracers were injected in the annulus and tubing of the wells. A review of inter-well tracer testing is given by Dugstad (2007).

The most common IWTT are performed using non-partitioning tracers. Despite the appealing features of IWTT, they are still underutilized in the petroleum industry and most tracer-tests reported in the open literature are only evaluated in a qualitative manner, and rarely compared to simulation results (Du and Guan, 2005). IWTT are an additional source of data, which should be used in combination with production data (well pressure and production rates). Recently, integration of tracer data and 4D seismic together with production data has shown to give additional understanding of fluid transport in the field (Huseby et al., 2007).

TRACER TRANSPORT CONSERVATION EQUATIONS

Tracers are present in the reservoirs at miniscule quantities, and do not affect the other fluids in the reservoir. For this reason, modeling of tracers may be decoupled from the reservoir simulation itself (Sagen et al., 1996). At each time-step, the flow field is retrieved from the host reservoir simulator to predict tracer flow and production. This modular method allows coupling to any black oil or compositional reservoir simulator, if the necessary information can be obtained from the host reservoir simulator.

Tracers are subject to several physical and chemical effects such as partitioning between liquid phases, adsorption to the solid phase, diffusion, dispersion and radioactive decay. Conditioning of reservoir simulation models to tracer and production data (history matching) requires that all relevant physical effects are included in the formulation of the tracer transport equations, if false conclusions are to be avoided. An adequate formulation of the tracer equations, including partitioning, is therefore important.

Radioactive decay can easily be accounted for by correcting measured concentrations by decayed quantities, and are thus not considered here. Adsorption of the solutes onto the rock surface may also be important, especially in the presence of clay minerals. Adsorption complicates interpretation of tracer data, and in general one would avoid using tracers that interact too much with the solid matrix in the reservoirs. Molecular diffusion may be important, especially when fluid velocities are close to zero. The concentration distribution within phases for partitioning tracers, is governed by partitioning coefficients specific for each tracer and the composition of the fluids in the phase. In general, partitioning coefficients are temperature and pressure dependent, but this may be neglected if temperature and pressure gradients are not too severe.

The tracer mass conservation equation in a reservoir may be written as

$$\frac{\partial}{\partial t}\left[\sum_{i=o,w,g}\phi S_i K_i C_i\right]+\nabla\cdot\left[\sum_{i=o,w,g}\bar{\mathbf{v}}_i K_i C_i\right]-\nabla\cdot\left[\sum_{i=o,w,g}\phi S_i \mathbf{D}_i^*\cdot\nabla(K_i C_i)\right]=0 \qquad (1)$$

where i is the index of phases oil (o), water (w) or gas (g) with saturations S_i, C_i is the tracer concentration in a given phase i , K_i is a coefficient that determine the partitioning of the tracer between the phases, $\mathbf{D}_i^*$ is the dispersion tensor and □ is porosity. The Darcy velocity $\bar{\mathbf{v}}_i$ and the phase saturations are obtained from the flow equations for the phases. These flow equations are solved by a "host" reservoir simulator ("Eclipse Technical Description", 2006), and yield phase pressure and saturations for oil, gas and water. Once the reservoir simulator has solved for flow in a time-step, the tracer movement can thus be obtained by means of Eq. (1). For non-partitioning water tracers, concentrations in oil (and gas) are zero and equation (1) reduces to

$$\frac{\partial}{\partial t}\left(\phi S_w C_w\right)+\nabla\cdot\left(\bar{\mathbf{v}}_w C_w\right)-\nabla\cdot\left(\phi S_w \mathbf{D}_w^*\cdot\nabla C_w\right)=0 \qquad (2)$$

The latter equation is the one solved in the water tracer application considered here.

DESCRIPTION AND EVALUATION OF ORDINARY TRACERS IN A DEMONSTRATION CASE

Injected tracers are an important source of information about flow-paths etc. in a reservoir. However, tracer modeling and quantitative evaluation of tracer data relies on access to high-quality data. In the North Sea field case used for demonstration in this paper, a significant tracer campaign has been carried out, comprising gas and water tracers. We focus on water tracers in this paper, and in the field, 5 chemical water tracers have been injected in 8 wells, 2 tracers (3,4-DFBA and 2,4,5-TFBA) were injected once, 3 tracers (2-FBA, 4-FBA and 2,6-DFBA) were injected twice.

Injection of water is used to maintain the pressure in most North Sea reservoirs, which leads to a significant production of water. For environmental purposes, produced water is re-injected in many North Sea petroleum reservoirs. As a consequence, tracer mass in the produced water is also re-injected as the water is re-injected. Re-injection of water therefore leads to a potential for misinterpretation of tracer results. A simple procedure to avoid such misinterpretations is to

compare produced tracer concentrations to concentrations in the re-injected water. If measured concentrations in a producer are larger than the injection water concentration, we know that it is due to an intended injection of a tracer pulse.

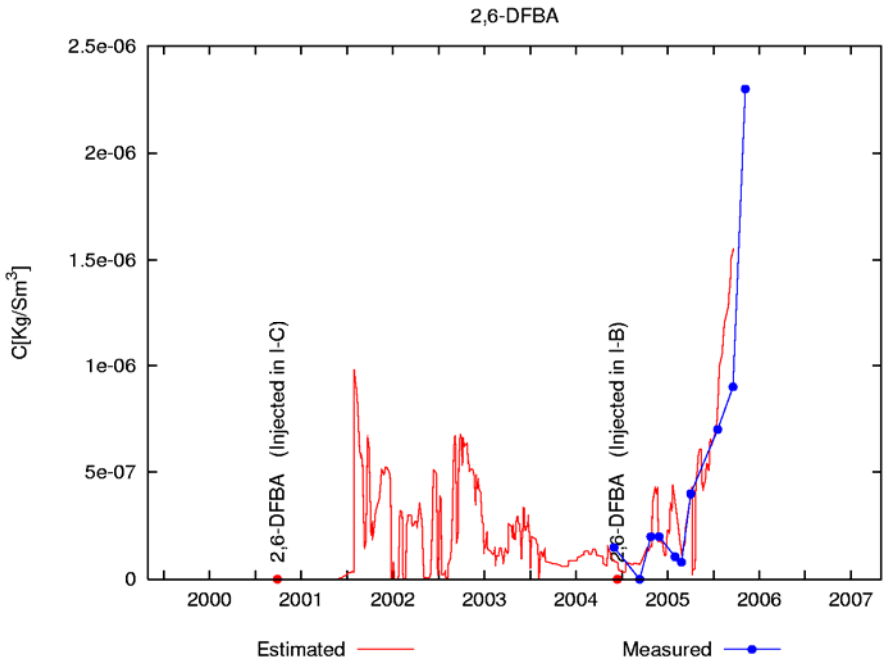

Figure 1 Estimated (red curve) and measured (blue curve) concentrations of the 2,6-DFBA tracer in field case example discussed in the text. This tracer has been injected twice, first in injector I-C and later in injector I-B. Water from I-B is re-injected and yields a significant concentration background in the injection water. By comparing the values in the figure to measurements in the producers, it can be determined if a tracer response is due to the background or if it represents an intended injection.

In the field example studied here, tracer concentrations in the injection water were measured from mid 2004. Fortunately, previous re-injected mass can be estimated from produced water volumes and production well tracer concentrations. A procedure to estimate ordinary tracer concentrations in the injection water is described in Huseby et al. (2007). Such curves were estimated for all water tracers in the field case studied here, and were used to decide whether tracer observations were due to water re-injection, or to primary injections in a single well. When tracer simulation results are given later the re-injection concentration curves for the various tracers are added to the figures for comparison.

Such curves were estimated for all ordinary water tracers in the field, and used to decide whether tracer observations are due to intended primary injections or water re-injection. As an example of re-injection water concentration curves obtained from these estimations, measured 2,6-DFBA concentrations in the injection water in the field are compared to the estimated values in Figure 1. The estimated and measured values compare well for times when measurements exist, which suggest that the estimates are fair and can be used for times when measurements are lacking.

TRACER MODELING RESULTS FROM THE ORIGINAL MODEL

A numerical simulation model of the field was made available for this study. This simulation model had been conditioned to production data, such as pressure measurements and water-cut, and represents the base-case of our study. Water-cut data is a common way of representing water-production in petroleum reservoirs. It is defined as the fraction of produced water vs. the sum of produced water and oil, with a scale from zero to one, where zero represents zero water production and one represents zero oil-production.

The matching of production data implies that the model has been tuned to represent a likely scenario given that set of data. To check if tracer data can give additional information, we added

tracers in the modeling. Tracer injections were simulated by adding tracers in the model's injectors at times when real tracer injections took place. In the following we only consider tracers in wells where the measured concentrations are above concentrations in the injection water. The non-zero injection water concentrations due to re-injection of produced water are displayed with a red line in Figure 2 and Figure 3.

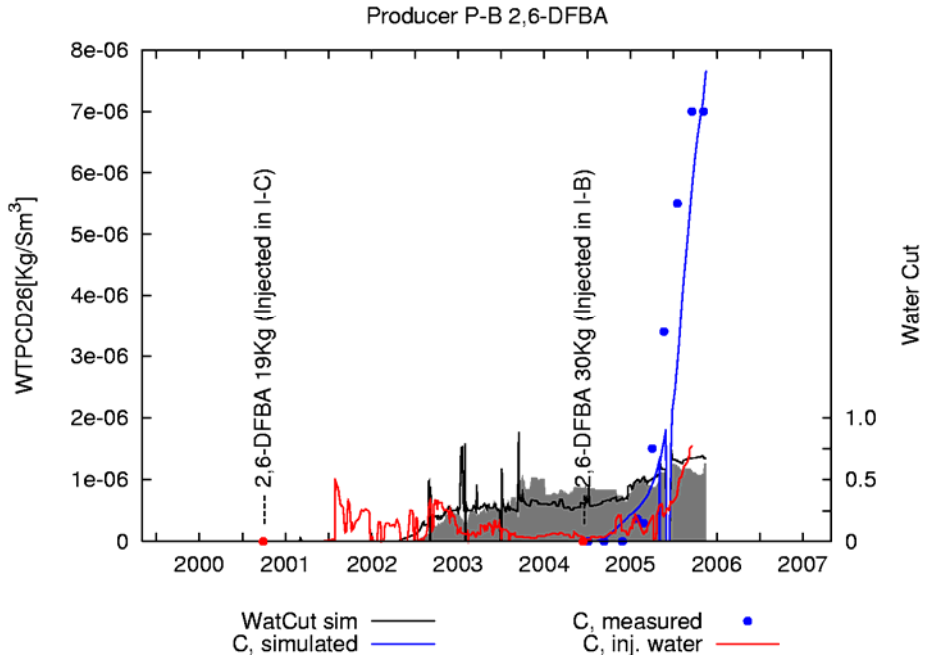

Figure 2 Basecase tracer simulation results for the production well P-B. The curves give measured (blue points), and simulated (blue line) tracer concentrations. The red lines are the estimated concentrations in the injection water, due to re-injection of produced water. The gray filled curves and black lines are measured and simulated water cut, respectively, given for comparison.

All numerical simulation results are sensitive to the grid size and orientation. The tracer transport is subject to numerical smearing (or numerical dispersion) that depends on grid-size and the chosen numerical scheme. Numerical smearing may be overcome by introducing a separate grid for the tracer or by using numerical schemes that reduce the effect (Sagen et al., 1996). A separate refinement of the tracer-grid was not available in the numerical simulations performed here. Refinement of the reservoir grid is not practical because it significantly increases the execution times for the simulations. In the simulation results described below, a second order numerical scheme was therefore the only practical means available to reduce the effect of numerical smearing.
When reservoir models have been conditioned to pressure and water-cut, overall production of water and oil is well described. The most important additional information gained from water tracers, is the location of the origin of produced water. When the base case correctly captures the origin of water, tracer data does not give additional information. In such cases, tracers may be seen as a confirmation of the matching based on pressure and water rates.
An example of a well where this is the case, is given in producer P-B, displayed in Figure 2. The observed and simulated water cut (gray filled curve and black line, respectively) in Figure 2 match well. Similarly, the observed and simulated response of the 2,6-DFBA tracer, injected in injector I-B, match well. This shows that the fluid movement in the reservoir model in the area between injector I-B and producer P-B correctly captures the in-situ fluid movements in the reservoir in this region. For this well-pair, the information from the tracer data confirms the existing base-case model, and does not justify any changes to the base-case in this well-pair.

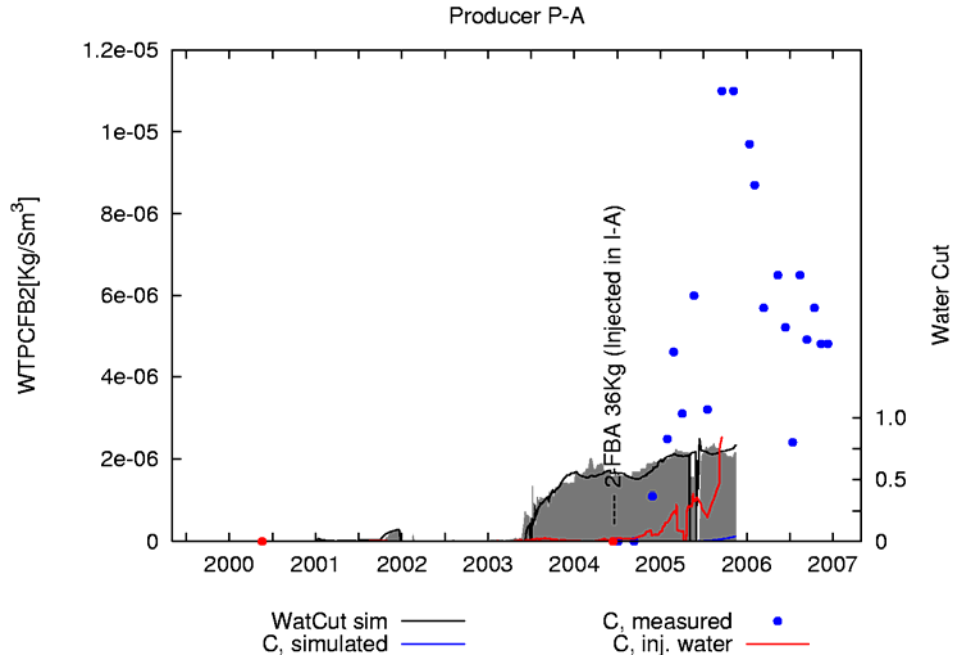

Figure 3 Basecase tracer simulation results for the production well P-A. The figures show measured (blue points), and simulated (blue line) tracer concentrations. The mismatch between the blue line representing simulated tracer concentrations (can hardly be seen) and the measurements, indicate a potential for model improvement. The red lines are the estimated concentrations in the injection water, due to re-injection of produced water. The gray filled curves and black lines are measured and simulated water cut, respectively, given for comparison.

An example where tracer data contradicts the existing base-case model is given in Figure 3. The observed and simulated water cut (gray filled curve and black line, respectively) in Figure 3 match well. On the other hand, the observed and simulated response of the 2-FBA tracer, injected in injector I-A, does not match well in this case. The simulations predict a much later breakthrough and smaller concentrations than the measurements (the curve can hardly be seen in Figure 3). This shows that even if the simulation predicts a correct amount of produced water in the well, the origin of this water is incorrect in the base case model. This tracer therefore reveals a potential for model improvement. We will therefore try to improve the reservoir model in the area between injector I-A and producer P-A.

MODEL IMPROVEMENT FROM TRACER DATA

The mismatch of simulated and measured ordinary tracers seen for 2-FBA, tracing I-A water, in producer P-A (Figure 3) is likely due to model-features in the region between I-A and P-A. The reservoir used here is separated in several vertical formations, with varying vertical communication. The injector I-A injects in several of these formations, but the producer P-A produces solely from the upper formation, and this formation is not in communication with the lower formation. The origin of the mismatch is therefore likely located on the path from I-A to P-A, in the upper formation, represented by the top layers in the reservoir model.

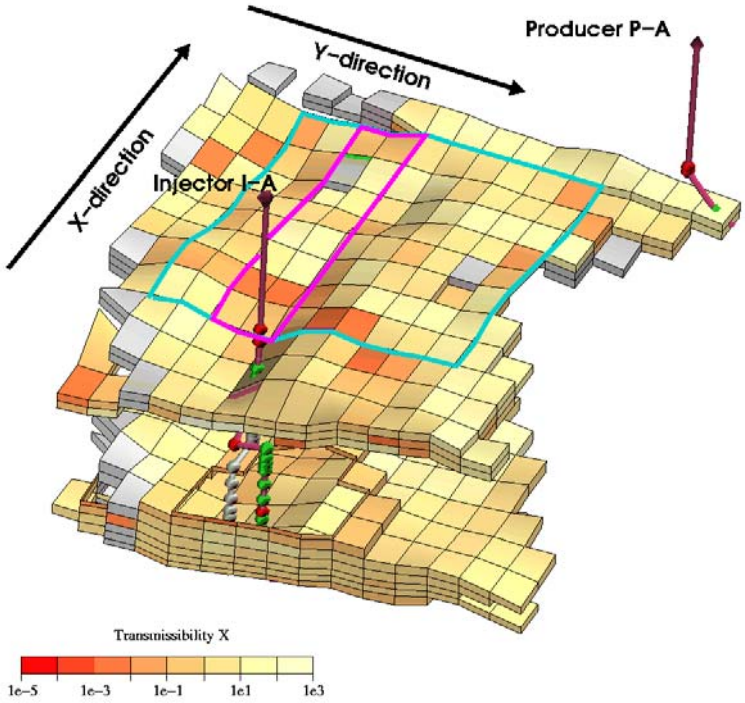

Figure 4 Reservoir grid geometry in the region between the injector I-A and the producer P-A in the example case. To enhance the visibility of the layers, grid blocks with a zero concentration of 2-FBA are not displayed. The plotted quantity in the magnified grid is transmissibility in the x-direction, i.e. normal to the orange low-transmissibility blocks. Two modifications to the base case are investigated. Case I: the x-transmissibility is increased in the large area indicated by the cyan lines. Case II: the x-transmissibility is increased in the small area indicated by the pink lines.

An illustration of the reservoir grid in the relevant region is given in Figure 4. The upper layers in the model correspond to fluvial channels in the y-direction in Figure 4. The channels are stochastically generated, and the location of the channels and cross-communication between the channels represents one of many possible scenarios. In Figure 4 the channel bounds can be seen as orange colored areas, representing low x-direction transmissibility. The tracer arrives at the producer about 4 months after injection and about 6% of the injected mass is produced in one year (until 2006). This indicates that there is good communication between the injector and the producer; however, the simulation model does not capture this. A natural hypothesis for matching vs. measured data is therefore to improve the communication in the x-direction.

To improve communication across the channels, the x-direction transmissibility was increased in the region. Two modifications to the base case were investigated: In case I the x-transmissibility is increased in the large area indicated by the cyan lines in Figure 4. In case II the x-transmissibility is increased in the small area indicated by the pink lines in Figure 4.

Increasing the transmissibility in the large region (Case I) improved the tracer match significantly (green line in Figure 5) but unfortunately corrupted the water-cut match (green line in Figure 6). When a narrower region was used (Case II) the tracer match was improved significantly (black line in Figure 5) without corruption of the water-cut match (black line in Figure 6).

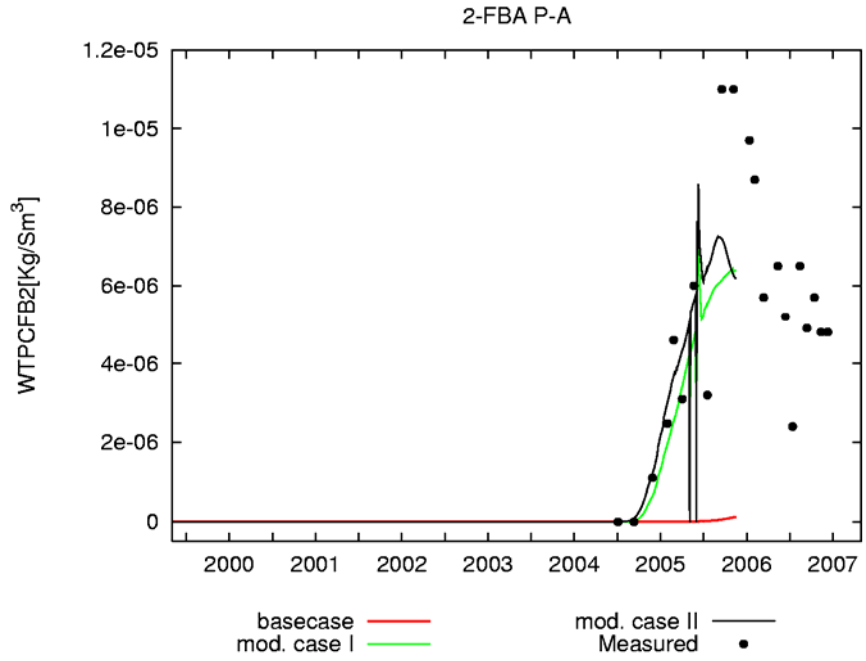

Figure 5 Effect of model modifications on simulated 2-FBA tracer results in the example reservoir case. In the base-case (red curve) concentrations are barley larger than zero. The 2-FBA match is much better when the transmissibility is increased in the large area (case I Figure 4) as shown by the green line. When the transmissibility is increased in the smaller area (case II in Figure 4) the 2-FBA match is even better.

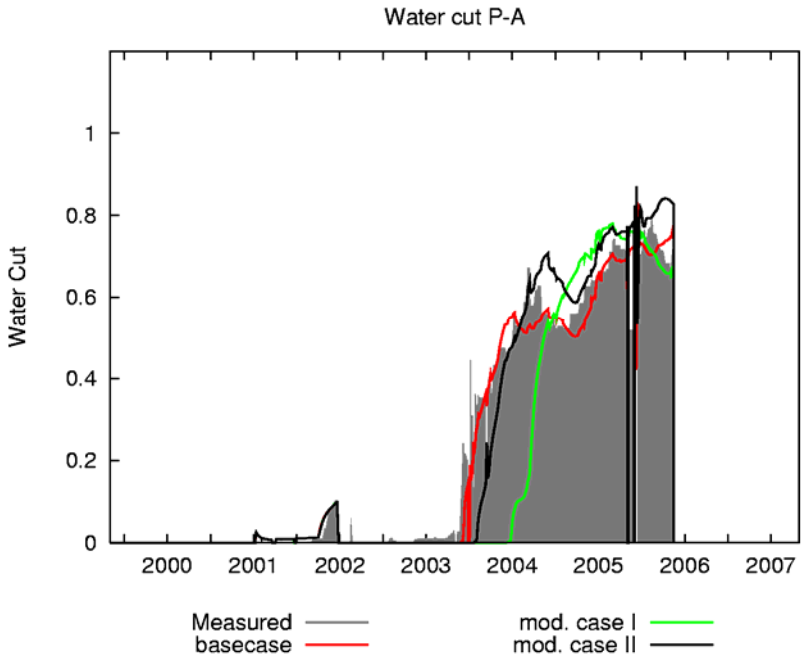

Figure 6 Effect of the model modifications on the water cut in the example reservoir case. The base-case water cut match (red line) was very good. The modified case I yields much better 2-FBA match (cf. the green line Figure 5) but the water-cut match is unsatisfactory (green line). When the transmissibility is increased in a smaller area (case II in Figure 4) the 2-FBA match is even better (black line in Figure 5), and in this case the good water-cut match is also preserved (black line).

The important effect of the modifications on the tracer results suggests that the model results are sensitive to the location and communication across the channels. The particular channel realization in the model probably underestimates the communication from the injector to the producer. The

sensitivity to the modifications shows that a different channel realization should be able to capture the tracer behavior, while honoring the other production data.

CONCLUDING REMARKS

In this paper we have demonstrated that tracers can give important information about geological features in petroleum reservoirs. Potential misinterpretation issues originating from re-use of tracers and water re-injection can be overcome by comparing measured tracer concentrations to injection water concentrations. If the latter are not measured, fair estimates may be obtained by calculating the mass balance of tracers measured in production wells. When measured and simulated tracer concentrations match, these data confirm model conditioning based on production data. In the example presented here, a mismatch was identified between measured and simulated tracer concentrations. A modification of the model was able to capture both production data and tracer data. The particular realization of channels underestimates the communication between the injector and producer pair in the example, but the sensitivity to the modifications indicates that, in an updated model, a different channel realization may capture both tracer and production data. The modifications based on tracer data thus suggest an effort to improve the reservoir model, which may be important for subsequent production strategy decisions.

ACKNOWLEDGEMENT

Partial financial support by the Research Council of Norway, through Petromaks grant no. 176000/S30 is gratefully acknowledged.

REFERENCES

1) Du, Y. and Guan L.: “Inter-well Tracer Tests: Lessons Learned from Past Field Studies”. SPE Paper Number 93140. SPE Asia Pacific Oil and Gas Conference and Exhibition, 5-7 April, Jakarta, Indonesia, 2005.
2) Dugstad Ø.: “Well-to-Well Tracer Tests”. Chapter 6 (pp. 651-683), Petroleum Engineering Handbook, Vol. 5 - Reservoir Engineering and Petrophysics by Edward D. Holstein (Ed.) SPE, Richardson, Texas, 2007.
3) Dugstad, Ø., Bjørnstad, T., and Hundere, I.A.: “Measurements and Application of Partition Coefficients of Compounds Suitable for Tracing Gas Injected into Oil Reservoirs”. Revue de l’Institut Francais du P´etrole, Vol. 47 Num. 2, pp. 205-215, 1992.
4) Dugstad, Ø., Bjørnstad, T., and Hundere, I.A.: “Measurements and Application of Partition Coefficients of Compounds Suitable for Tracing Gas Injected into Oil Reservoirs”. Revue de l’Institut Francais du P´etrole, Vol. 47 Num. 2, pp. 205-215, 1992.
5) Eclipse Technical Description 2006A, Schlumberger, 2006.
6) Huseby, O., Andersen, M., Svorstøl, I., and Dugstad, Ø.: “Improved Understanding of Reservoir Fluid Dynamics in the North Sea Snorre Field by Combining Tracers, 4D Seismic, and Production Data”. SPE Paper Number 105288. SPE Middle East Oil and Gas Show and Conference, Kingdom of Bahrain, 11-14 March, 2007.
7) Galdiga, C.U., Greibrokk, T: "Ultra-trace determination of fluorinated aromatic carboxylic acids in aqueous reservoir fluids using solid-phase extraction in combination with gas chromatography-mass spectrometry". Journal of Chromatography A, 793 (2), pp. 297-306, 1998.
8) Kleven, R., Høvring, O., Opdal, S.T., Bjørnstad, T., Dugstad, Ø., and Hundere, I.A.: “Non-Radioactive Tracing of Injection Gas in Reservoirs”. SPE Paper Number 35651. SPE Gas Technology Symposium, Calgary, Canada, 28 April-1 May, 1996.
9) Sagen, J., Cvetkovic B., Brendesdal, E., Halvorsen, G., You, Y.L., and Bjornstad, T.: “Reservoir Chemical-Thermal Simulation with Tracers”. SPE Paper Number 36921. SPE European Petroleum Conference, Milan, Italy, 22- 24 October, 1996.
10) Zemel B.: Tracers in the Oil Field. Elsevier, New York, 1994.

TRACERS FOR ENHANCED OIL RECOVERY IN NORTHEAST BRAZIL

Maria Aparecida de Melo Petrobras
Ivonete Pereira Gonzalez da Silva Petrobras
Amenônia Maria Ferreira Pinto CDTN

ABSTRACT

The use of tracer substances for petroleum reservoir characterization has grown a lot over the last years. The information obtained through this technology is crucial for reservoir management and results in actions of great economical and environmental impact for petroleum production. The objective of this technology is to supply information concerning the distribution and path of the fluids involved in the petroleum reservoir, defining the flow direction tendencies and allowing the evaluation of the swept efficiency of the recovery processes. This technology has the advantage of being the only tool that accesses the reservoir supplying direct information without causing physiochemical modifications to the system. As such, a great effort has been made to develop methodologies for quantitative interpretation of tracer tests in petroleum reservoirs. To this end, this work presents a tracer application for a pilot project of petroleum advanced recovery in a field in Northeast Brazil. The target reservoir was loosing pressure resulting in a low oil production. The problem was diagnosed as probable preferential channels releasing the injected water. These had been formed due to the rock heterogeneity and/or the viscosity difference between the phases displaced (oil) and displacement (water). A treatment was designed to block these preferential channels thereby maintaining the injected water advancing front correcting the injectivity profile. Two different tracers were used, the first injected in the original reservoir condition. This tracer would be recovered from the production wells indicating the existence and flow path of the preferential channels. The second tracer was injected after the blocking treatment had been applied. The results obtained demonstrated that the use of tracers is an indispensable tool for the evaluation of the recovery processes.

INTRODUCTION

In the petroleum industry, the lack of direct access to the reservoirs and the inexistence of any other detector that permeates through the channels of the formation is a challenge to reservoir management. Tracers are now a very important characterization tool and have become indispensable in the evaluation of petroleum recovery methods in both the laboratory and the field. The tracers are pumped into the injection wells, they pass through the flow channels of the reservoir following the water way in the direction of the production wells, where they are detected and quantified in the effluents [1-4]. Once identified a balance mass is made between the input and recovered tracer and the result associated to the transport phenomena, allows the hydrodynamic characterizing of the swept channels.

The application of this technology in petroleum reservoirs provides information concerning the distribution and path of the involved fluids, defining the flow directional tendencies and permits the evaluation of the swept efficiency of the recovery processes [5-8].

This information is crucial for the planning and evaluation of projects of advanced recovery (tertiary recovery), reducing the inherent risks of these processes and increasing the production efficiency [6, 11]. The objective of this work is to present a test using tracers in the planning and evaluation of an advanced recovery project (tertiary recovery) in a field in Northeast Brazil. The used process aims at controlling the injected water profile by blocking the preferential channels [6-8]. These have been formed due to the rock heterogeneity and/or the viscosity difference between the phases displaced (oil) and displacement (water). In this work two different tracers were used. The first tracer was injected in the original area, before the application of the blocking process, to determine the main existing preferential channels and the second tracer, injected after the application of the blocking process, to evaluate the modification in the porous media caused by the blocking process. This work presents the pilot project area selection, followed by the results of the

first tracer injection (before the process) and of the second tracer injection (to determine the success of the blocking process).

DEVELOPMENT

1- Pilot area selection

The selected site (Figure 01 and Table I) for this pilot project is located in the water injection block of the field. This pilot consists of a single injector (named A at Figure 1) and 8 producers (B to I) distributed in a non regular pattern. The water/oil ratio has been increasing in these wells, with a consequential reduction in the oil production. Figure 1 also shows a structural map of the production area.

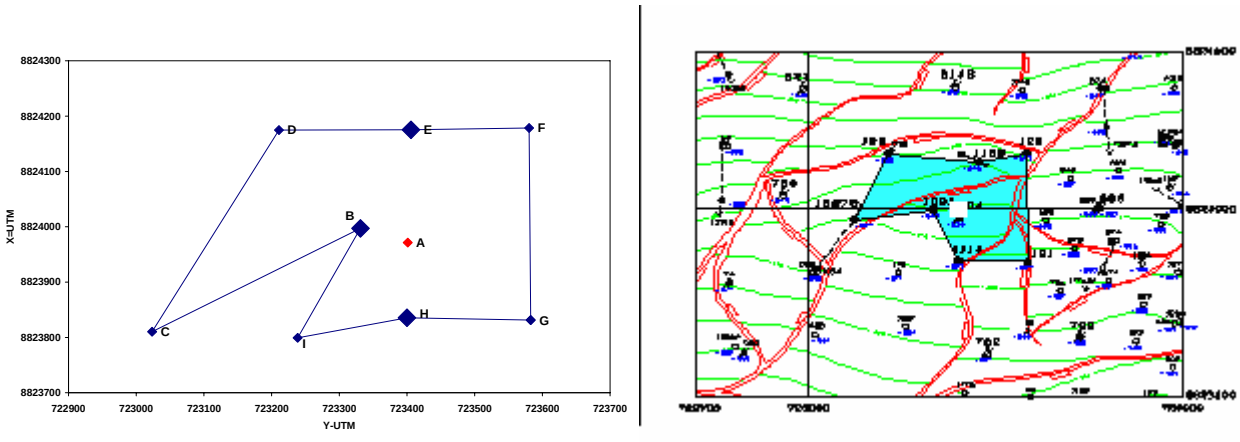

Figure 01: Pilot area selection

In this selected area, there are 3 sub-zones. In the first sub-zone, fine and very fine sandstones dominate. In the second sub-zone, large grained sandstones and conglomerates dominate. In the third sub-zone, very large grained conglomerates dominate. The heterogeneity of the reservoir rock increases with the increase of the perm-porous complexities of the system hindering the swept efficiency (horizontal and vertical) in the water injection process, where they are usually channels (Figure 02). From the structural point of view, the injection well A is in a lower layer in relation to the production wells, except for well B. This condition doesn't prevent the reaction to the water injection in the production wells, because the existent faults are permeable.

Table I – Initial production data of the pilot wells.

Well	Total flow rate (m^3/d)	Oil flow rate (m^3/d)	Water flow rate (m^3/d)	Amount of water (%)
A	83	-	-	-
B	52.0	1.0	51.0	98.1
C	20.0	8.0	12.0	60.0
D	30.0	7.5	22.5	75.0
E	55.0	3.9	51.1	92.9
F	2.0	1.2	0.8	40.0
G	9.0	2.5	6.5	72.2
H	35.0	2.8	32.2	92.0
I	85.0	5.1	79.9	94.0
Total	288.0	32.0	256.0	-

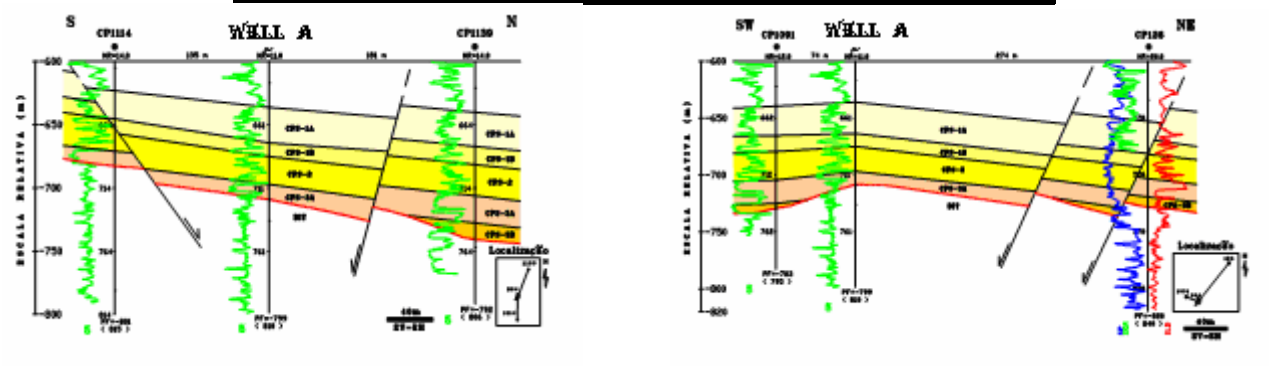

Figure 02: Cross Section South-north and Southeast-northwest

During the selection of the area, a study of mathematical simulation of stream lines using IMEX [12] was also made to evaluate the area drainage plan and to evaluate the possibility to exclude or not well B that was the closest to the injection well. This resulted in a large geometric distortion of the pilot. After the evaluation (Figures 3 and 4), the team opted to maintain well B open during the treatments. Initially the outlying wells were not considered, as it was assumed that the injection and production flow rates of the pilot's wells would be maintained.

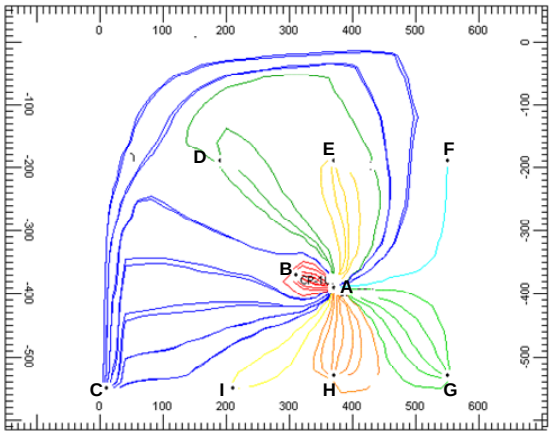

Figure 03: Stream lines of the pilot considering the real flow rates and with well B

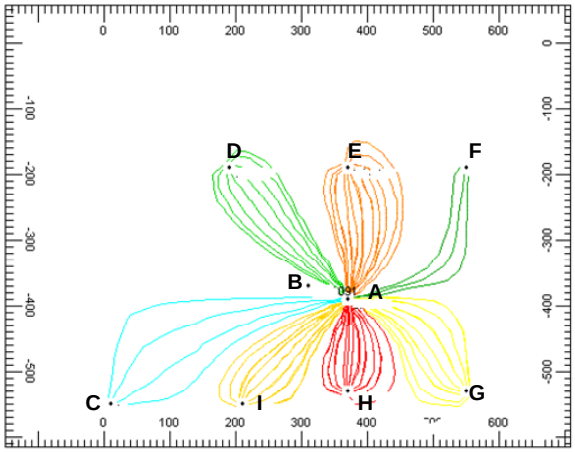

Figure 04: Stream lines of the pilot considering the real flow rates and without well B

2. First tracer (Fluorescent): before treatment

The fluorescent tracer injection was made before the channel blockage process with the objective of hydrodynamically characterizing the area and to identify the preferential channels. The fluorescent tracer injection was made in well A on December 18, 2001. This Fluorescenin was detected in wells H and B after 7 and 9 days respectively (Table II and Figure 5). In spite of the tracer appear in these wells in a relatively short time, demonstrating that there were two preferential channels, both very well defined in these directions, the mass balance indicated that only 10 and 13% of the total injected tracer was produced from the respective wells. This shows that about 77% of the injected tracer might have flowed in other directions.

Considering a flow rate of 83 m^3/d of injected water in the injection well A and the fluorescent tracer resident times in the reservoir, the volumes of the slug were calculated for the injection process. This corresponds to the space of the respective channels to be filled by the blocking product

The concentration profiles presented by the tracers (Figure 5) in wells B and H were very well defined, and match with results typically found in the literature. We can also observe two secondary peaks, one in profile H and another in profile B. These secondary peaks are linked to the presence of the injected water through other zones. The objective of the test was to check the natural selection process therefore, we opted to work with all the zones and subzones open.

Table II: Result (appearance dates and produced mass) in each production well following the fluorescent tracer injection in the injection well CP-804

Well	Appearance date	Residence time (day)	Produced mass (%)
B	25/12/2001	7	10,1
C	-	-	-
D	-	-	-
E	-	-	-
F	-	-	-
G	-	-	-
H	27/12/2001	9	12,8
I	-	-	-
Total	-	-	22,9

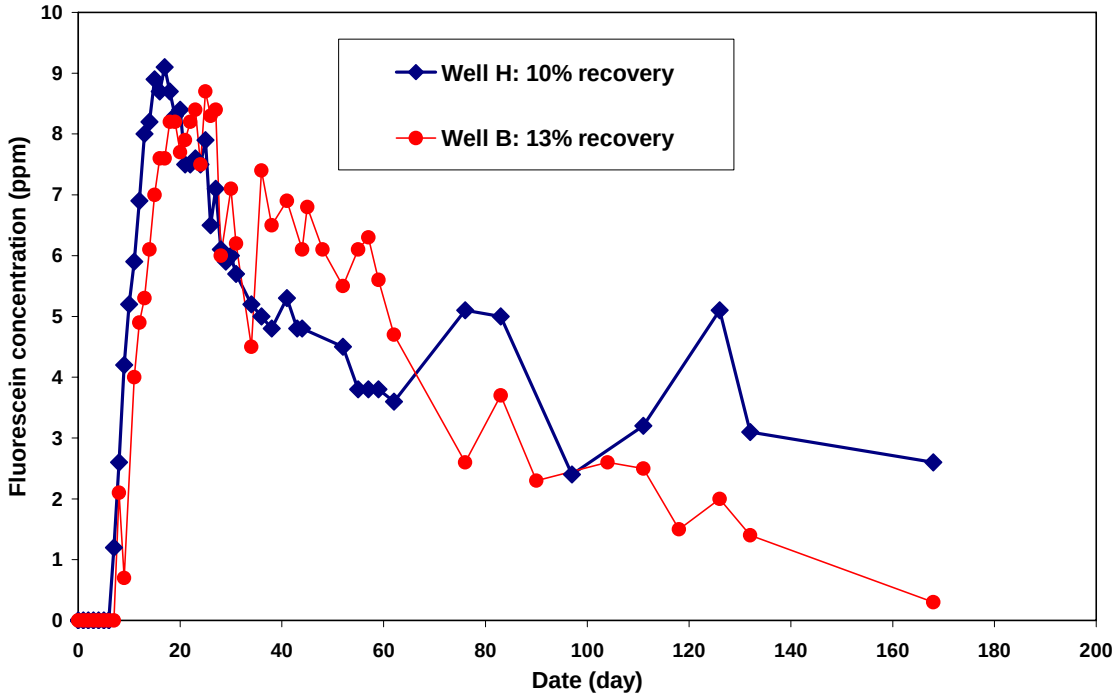

Figure 5: Concentration profiles of the fluorescent tracer in wells B and H

3. Second tracer (Radioactive): after treatment

Figures 6 and 7 show the results of the fluorescent tracer, which was injected before the treatment, and the radioactive tracer, injected after the treatment. Notice that in Figure 6, the profiles of the tracers injected before and after treatment indicate that there has been a blocking of the preferential channel between well H and the injection well. The quantity of the tracer collected before (10%) and after the treatment (1,2%) was significantly reduced, indicating that the channel had been blocked.

On the other hand, Figure 7 indicates that the preferential channel between well B and the injection well had not been blocked, which was also confirmed by the well's production data. This fact shows that the project crew's doubt regarding this well was valid. Perhaps it would have been better to have left the well closed following this process. The process was to test the natural vertical selectivity of the well behavior in view of the multilayer of the reservoir. The geometric irregularity of the pilot (horizontal heterogeneity), associated to well A, was not a good strategy for this operation and it hindered the treatment evaluation.

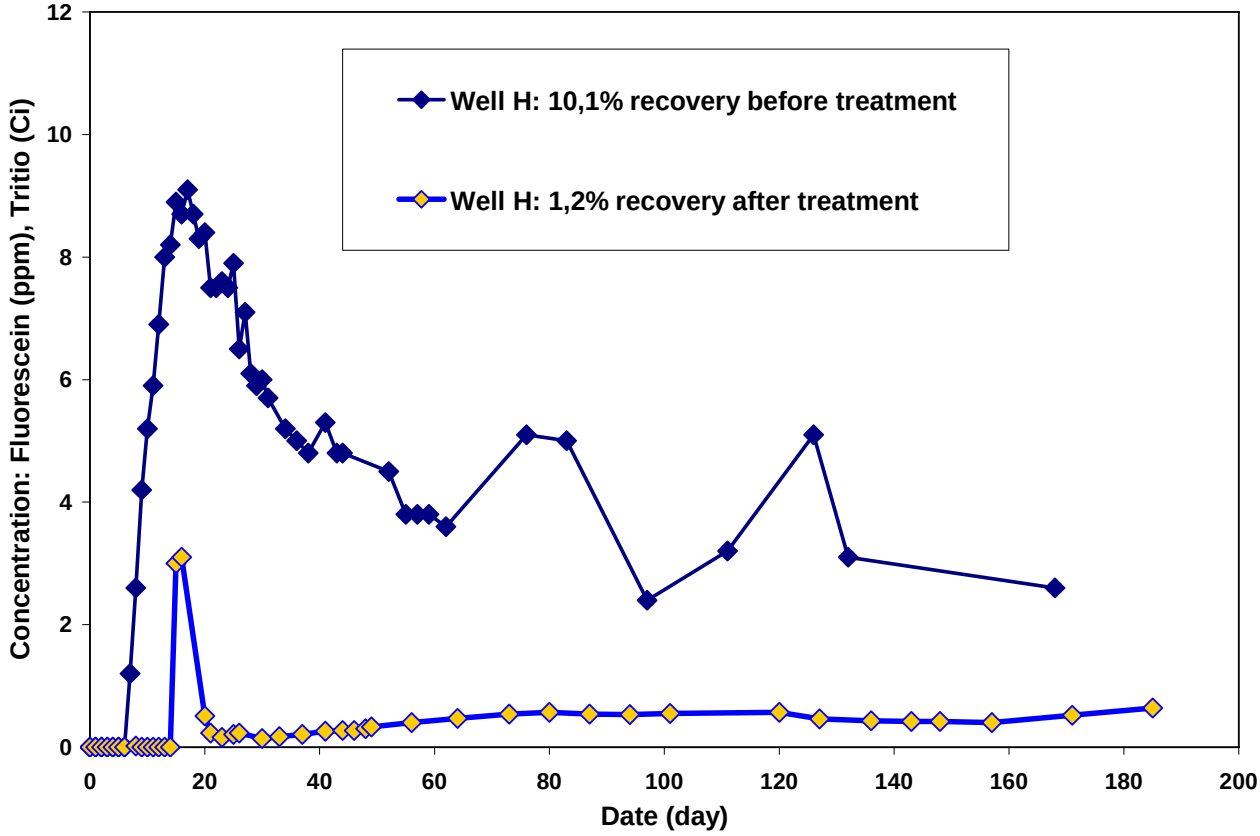

Figure 6: Results of the tracers in well H before (fluorescent) and after (radioactive) the blocking treatment

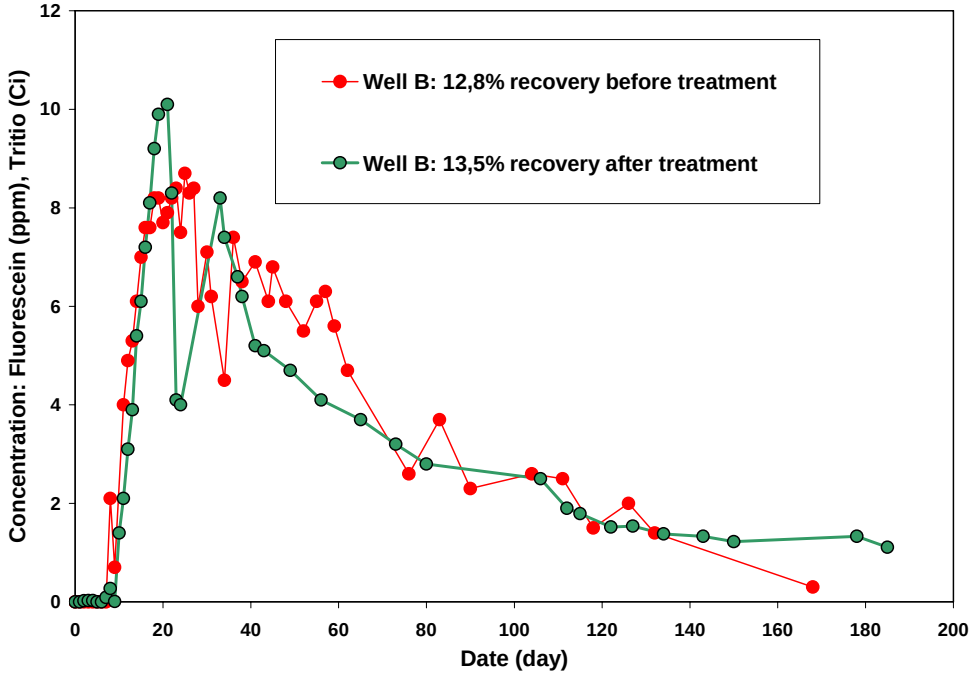

Figure 7: Results of the tracers in well B before (fluorescent) and after (radioactive) the blocking treatment.

CONCLUSION

The blocking treatment applied to the target reservoir was shown to be effective in blocking the preferential channels and hydrodynamically modifying the test area as seen in the results of the tracers before and after the treatment in well H (Figure 6).
This work confirms the importance of water-soluble tracers as a tool to increase the technico-economical and environmental efficiencies of petroleum production, through the optimization of the reservoir drainage area. This optimization is crucial in water injection projects (secondary recovery) and in projects of petroleum advanced recovery (tertiary recovery) always with a focus on energy efficiency.

REFFERENCES

1. Brigham, W.E.; Abbaszadeh, M.D. Tracer testing for reservoir description. USA, 1981. SPE 14102, SPE Distinguished Author Series, Richardson, USA: SPE Librarian, 1983.
2. Agca, C.; Pope, G. A. & Sepehrnoori, K. Modelling and Analysis of tracer flow in oil reservoir. J. Pet. Sci. Eng., 4, 1990 (3-19).
3. Tor, B.: "Selection of Tracer for Oil and Gas Reservoir Evaluation," report, Project IFE-Tracer Research Club, IFE/KR/E-91/009, IFE, Norway (1991).
4. ZEMEL, Bernard. Tracers in the oil field. Amsterdam: Elsevier Science B.V., 1995.
5. Du, Y.; Guan, L. Interwell tracer test: Lessons learned from past field studies. In: ASIA PACIFIC OIL & GAS CONFERENCE AND EXIBITHION, 2005, Jacarta. SPE 93140, Richardson, USA: SPE Librarian, 2005.
6. Melo, M.A, Holleben, C.R., Silva, I.P.G., Correia, A.B., Silva, G.A., Rosa, A.J., Junior, A.G.L., Lima, J.C., Evaluation of Polymer Injection Projects in Brazil, SPE 94 898, 2005.
7. Almeida, A. R., Aplicação da técnica de transformação integral a problemas de injeção de traçadores em reservatório de petróleo, Tese de mestrado, UFRJ-Engenharia Mecânica, 04/1994.
8. Lake, L.W.; "Enhanced Oil Recovery"; Prentice Hall, Englewood Cliffs, New Jersey 1989.9. Ogata, A.; Banks, R.B., A solution of the differential equation of longitudinal dispersion in porous media. U.S. Geology Surv. Prof. Pap., p. 441, 1961.
9. Arya, A.et al., Dispersion and reservoir heterogeneity, SPE 14364, Las Vegas, 22-25 Sept. 1985.
10. 16- Abbaszadeh-Dehghani, M.. Analysis of Unit Mobility Ratio Well-to-well tracer flow to determine reservoir heterogeneity. PhD dissertation, Stanfod University.
11. Abbaszadeh-Dehghani, M.. & Brigham, W.E.; Analysis of Well-to-well tracer flow to determine reservoir layering. J. Pet. Tech., Out 1984 (1753-1762) heterogeneity. PhD dissertation, Stanfod University.
12. CMG (COMPUTER MODELLING GROUP), "IMEX User's Manual", Calgary, Alberta, Canada, 2007.

ACKNOWLEDGEMENTS

The authors wish to thank the field team for their commitment in all phases of the application of the process.

RADIOLABELLED $[NI(CN)_4]^{2-}$ FOR WATER TRACING: SYNTHESIS AND QUALITY EXAMINATION

Kjersti Jevanord and Tor Bjørnstad
Institute for Energy Technology (IFE), Kjeller, Norway

ABSTRACT

The article describes the synthesis of the non-radiolabelled and the ^{14}C- and ^{63}Ni-labelled potential water tracer $Ni(CN)_4^{2-}$ and the quality assurance experiments performed on the synthesis product. These experiments include HPLC with UV detection on the non-radiolabelled product and paper electrophoresis both on the radiolabelled product detected with a scanner (or position sensitive) detector and on the non-radiolabelled product detected with neutron activation analysis of Ni.

INTRODUCTION

Cyanide, CN^-, is known to be a strongly bound ligand in many metal complexes resulting in high stability constants of the complexes. Previous reports of and with the cobalthexacyanide complex, $[Co(CN)_6]^{3-}$ as a water tracer [1,2,3], led us to conclude that such cyanide complexes with high complex constants may be applicable water tracers for oil reservoirs. However, serious limitations may apply [4].

The cobalthexacyanide studies have been followed in the authors' laboratory by similar investigations of other metal cyanide complexes like $[Ni(CN)_4]^{2-}$ with the possible radiolabels ^{63}Ni and ^{14}C, $[Fe(CN)_6]^{3-}$ with the possible radiolabels ^{55}Fe, ^{59}Fe and ^{14}C, $[Ag(CN)_2]^-$ with the possible radiolabels ^{110m}Ag and ^{14}C and $Au(CN)_4^-$ with the possible radiolabels ^{195m}Au and ^{14}C [5, 6]. In addition, the two latter complexes may be used as non-radioactive tracers in combination with molecular enrichment techniques and sensitive detection techniques for Ag and Au, respectively.

To the authors' knowledge there are no other published literature report describing the use of radiolabelled $Ni(CN)_4^{2-}$ as a water tracer and no other reference on laboratory testing for its potential tracer properties.

Nickel-tetracyanide, $Ni(CN)_4^{2-}$, is reported to have a total stability (or complex) constant of $\beta_4 \approx 31$ [7]. This may be sufficient to be interesting for water tracing. However, the main key parameter is really not the value of the total complex constant β_4 but rather the difference between β_4 and β_3. This value is not known.

The present paper is one in a sequence of papers on metal cyanide complexes for water tracing and will exclusively deal with the synthesis and quality investigations of radiolabelled $Ni(CN)_4^{2-}$.

EXPERIMENTAL

Synthesis of $Ni(CN)_4^{2-}$ and quality check on HPLC

Synthesis: The starting point for the synthesis was the procedure given in ref. [8]. It is straight forward and takes place in the following steps:

- Dissolve $NiCl_2$ and KCN separately both in synthetic formation water (Table 1) and distilled water.
- Precipitate bluish $Ni(CN)_2$ by adding KCN-solution to the corresponding $NiCl_2$-solution in stoechiometric amounts according to the eqn:

$$Ni^{2+} + 2CN^- \leftrightarrows Ni(CN)_{2(s)}$$

- Dissolve the bluish $Ni(CN)_2$-precipitate and form the complex $Ni(CN)_4^{2-}$ by further addition of an equivalent amount + 15% surplus of the KCN-solution according to the eqn.

$$Ni(CN)_{2(s)} + 2CN^- \leftrightarrows Ni(CN)_4^{2-}{}_{(aq)}$$

The reactions are exothermic, and the solution must be cooled during the synthesis. The solution now becomes yellow and transparent.

Table 1. Recipe of synthetic sea water. The salts are dissolved in 10 L of distilled water

Compound	Amount (g)	Compound	Amount (g)
KCl	6.3	$SrCl_2 \cdot 6H_2O$	4.4
$CaCl_2 \cdot 2H_2O$	38.1	$NaHCO_3$	2.1
$MgCl_2 \cdot 6H_2O$	25.5	Na_2SO_4	0.5
$BaCl_2 \cdot 6H_2O$	0.9	NaCl	280

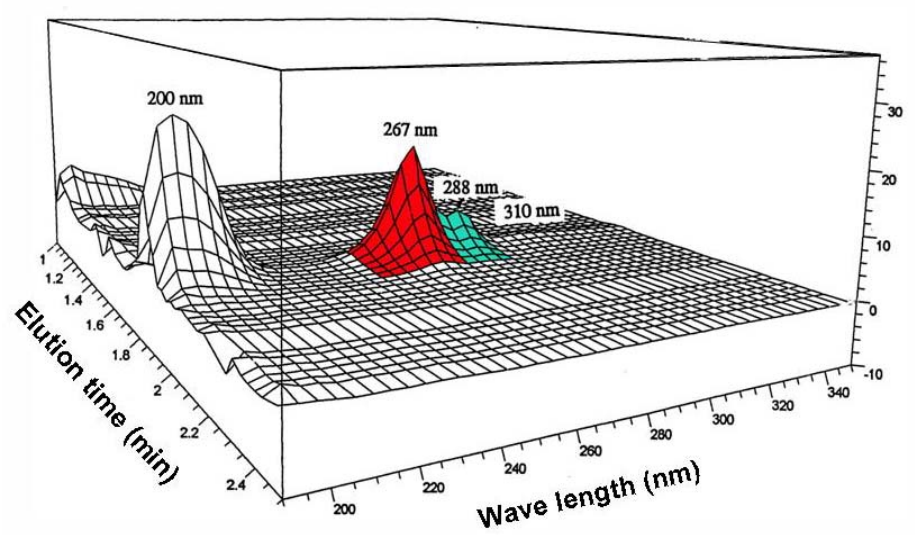

Figure 1. UV spectrum of $Ni(CN)_4^{2-}$ complex

HPLC analysis: $Ni(CN)_4^{2-}$ absorbs UV-light at different wavelengths, but has extra absorbance at 267 and 288 nm (Fig.1). The absorbance ratio at these two wavelengths is used to determine the quality of the synthesized complex by comparing with a solution of commercial $K_2Ni(CN)_4$, here called the standard.

All experimental parameters are summarized in Table 2.

Table 2. Experimental parameters for quality check of synthesized $Ni(CN)_4^{2-}$ with HPLC

Parameter	Parameter information
Instrument	Hewlett Packard, series 1050, with diode array detector
Columns	1. C8-column: Hewlett Packard, MOS Hypersil, 5µm particle size, dimension 200x2.1 mm, Part. No. 79916MO-572 2. C18-column: Waters, µ-Bondapak, 10µm particle size, dimension 300x3.9 mm, Part. No. 27324
Ion-pair reagents	Tetrabuthyl-ammonium-hydrogen-sulphate (TBAHS)
Mobile phase	30% acetonitrile and 70% TBAHS, isocratic elution
Experimental values	Flow rate: 1 ml/min, injection volume: 5µL, retention time C8-column: ~1.7 min, retention time C18-column: ~ 2.9 min,
Samples for analysis	Synthesized $Ni(CN)_4^{2-}$ (test sample) and commercial $Ni(CN)_4^{2-}$ (standard)

Results are given below.

Synthesis of Ni(^{14}CN)$(CN)_3^{2-}$ and quality check with HT paper electrophore-sis and thermal neutron activation analysis

In order to provide a more thorough evaluation of the quality of the product from the described synthetic procedure, we have applied two other independent analytical methods,- high-tension paper electrophoresis for separation and detection both with position-sensitive radiation detector and with thermal neutron activation analysis on cut sections of the chromatography paper.

The synthesis followed the main steps described previously, but with the following details: 1.619 g of $NiCl_2$ and 2.038 g of KCN were dissolved separately in 5 mL distilled water. 250 µL of each solution was mixed together during magnetic stirring. 500 µL of a solution of $^{14}CN^-$ with an activity concentration of 9.25 MBq/mL was added to the reaction mixture.

Electrophoresis: The electrophoretic mobility is expressed by the migration rate u of the ion in an electric field at equilibrium:

$$u = \frac{q_1 \cdot E \cdot (1 - \kappa r)}{6 \cdot r \cdot \pi \cdot \eta} \qquad \text{(Eqn 1)}$$

where q_1 = ionic charge of complex, E = the field strength, r = effective radius of the complex, η = viscosity of solution and κ a complex parameter expressed by

$$\kappa = \frac{\sqrt{8 \cdot \pi \cdot q_2^2 \cdot I}}{\varepsilon \cdot k \cdot T} \qquad \text{(Eqn 2)}$$

Here, q_2 = ionic charge of the counter-ion of the complex, I = ionic strength of the solution, ε = relative permittivity of the solution, k = Boltzmann's constant and T = absolute temperature of the solution.

The setup of the electrophoresis experiment including the position-sensitive detector is illustrated in Fig.2a and b.

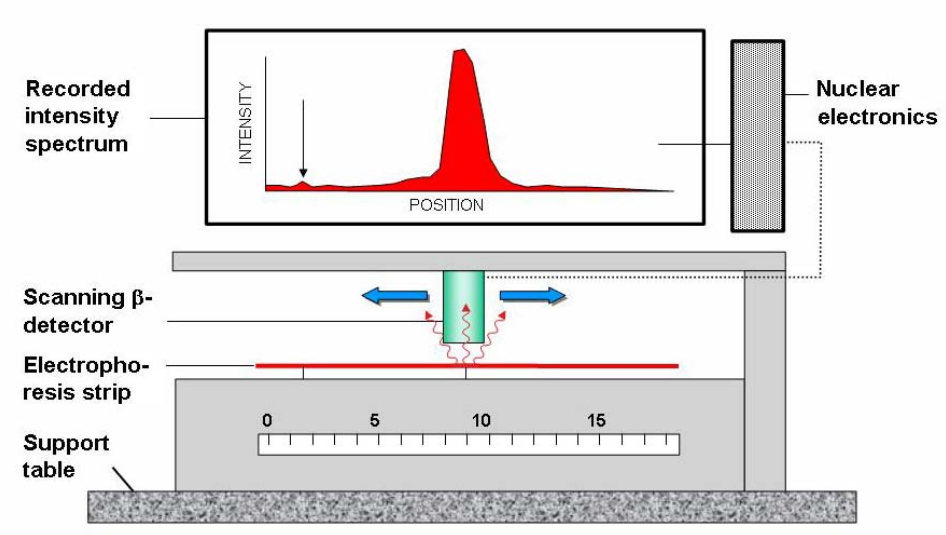

Figure 2a. Experimental setup of the high-tension paper electrophoresis experiment

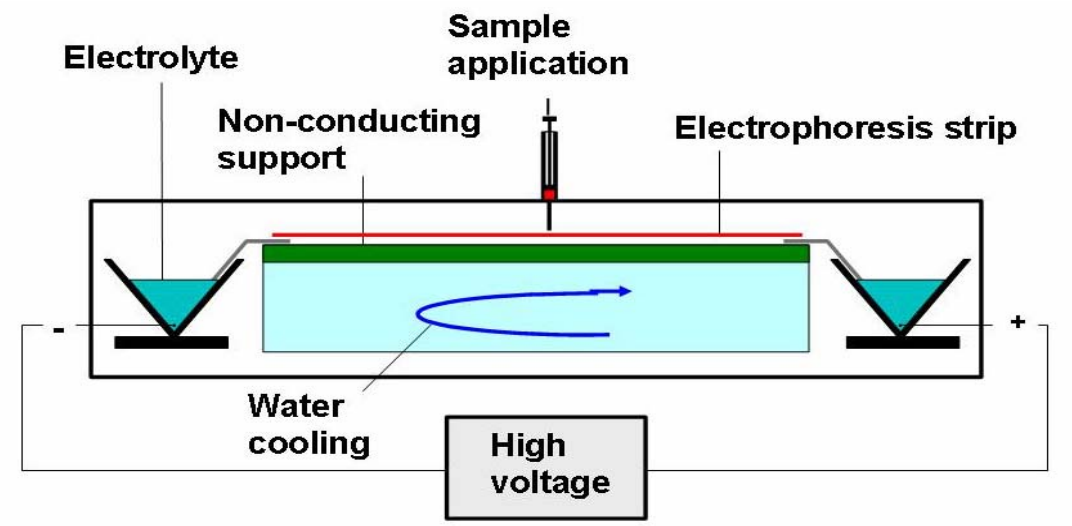

Figure 2b. Sketch of detection system used to record the distribution of 14C-activity on the electrophoresis strip.

Equipment and experimental parameters are further described in Table 3 below.

Table 3. Experimental parameters for quality check of synthesized $Ni(^{14}CN)(CN)_3^{2-}$ with HT paper electrophoresis.

Parameter	Parameter information
Equipment	– Electrophoresis equipment: Shandon HT paper electrophoresis – Electrophoresis paper: Whatman No.1, dimension 58x2.5 cm – β-scanner: GITA, type 2P No.92.
Solutions	– Commercial $K_2Ni(CN)_4$ in distilled water (standard) – Synthesised $Ni(^{14}CN)(CN)_3^{2-}$ in distilled water (test sample) – 1M LiOH, 1M NaOH and conc. NH_3
Buffer	– Phosphate buffer [9], adjusted by LiOH, NaOH or NH_3 to pH7 – Barbiturate buffer composed of 10.0 g sodium-5,5-diethylbarbiturate + 6.5 g sodium acetate + 8.0 g sodium-octaneoate + 68.1 mL 0.1 M HCl. Ph is adjusted to pH7 by NaOH. The salt and acid mixture was dissolved in distilled water and diluted to 2000 mL
Running parameters	HT = 6000 V for phosphate buffer and 4000 V for barbiturate buffer. Analysis time 5 or 15 min. Application volume: 5 μL of the test sample and/or the standard

After the various electrophoresis runs the paper strips containing ^{14}C-activity were analysed on the β-scanner. Chromatography papers containing the non-radioactive standard were sectioned into 1cm broad paper strips and analysed by thermal neutron activation analysis (NAA) for their contents of Ni with γ-spectroscopy using a Ge(Li)-detector. Only relative concentrations were of interest. Parameters for NAA are described in Table 4 below.

Table 4. Experimental parameters for analysis of non-radioactive $Ni(CN)_4^{2-}$ on an electrophoresis paper with NAA

Nuclear characteristics	Nuclear reaction	$^{64}Ni(n_{th}, \gamma)^{65}Ni$
	Reaction cross section	1.49 b
	Natural abundance of ^{64}Ni	0.926 %
	Half-life of ^{65}Ni	2.52 h
	Major γ-lines from ^{65}Ni	1481.9 keV (23.0 %) 1115.58 keV (14.8 %)
Equipment	– Nuclear reactor: JEEP II at IFE, Kjeller – Detector: Canberra Ge(Li), model GC3518 – High-tension: Ortec, model 459 – Linear amplifier: Canberra model 2026 – Multichannel analyser: Ortec	
Running parameters	Neutron flux: ~ 10^{13} n/cm^{2}s Irradiation time: 15 min Counting time: 5 or 15 min.	

Results are given below.

RESULTS AND DISCUSSION

HPLC experiments

The HPLC experiments were performed to investigate if the Ni-complex contains the correct number of CN-ligands (4) by comparing the synthesized compound with a solution of a commercial chemical. Results for the UV diode array detection are given in Fig.3 below.

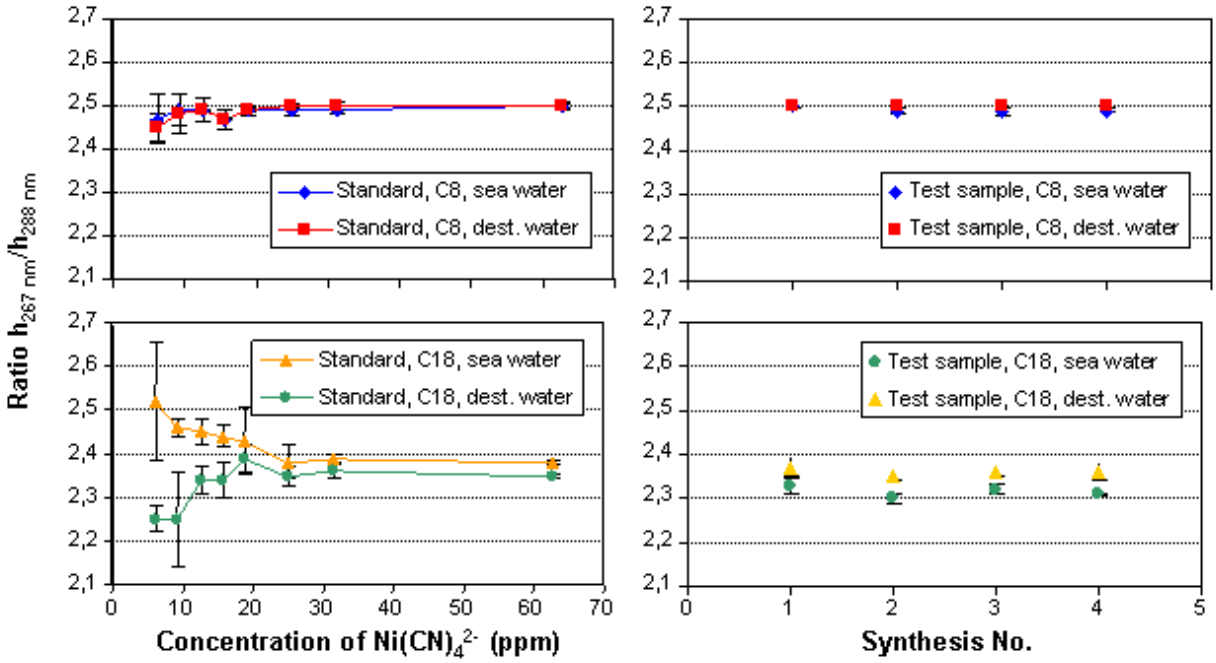

Figure 3. The ratio of the heights of the fluorescence peaks for $Ni(CN)_4^{2-}$ at 267 nm and 288 nm has been analysed with ion pair chromatography on HPLC with UV diode array detector for our synthesized product and compared to those for dissolved commercial chemical $K_2Ni(CN)_4$. Curves to the left represent the commercial product on C8 and C18 chromatogra-phic columns and data to the right represent the corresponding synthesized product after four individual syntheses.

The best and most consistent results were obtained with the C8-solumn which gives a height ratio for the 267 nm and 288 nm fluorescence peaks of about 2.5 both for the commercial and the

synthesized product. These findings strongly suggest that the Ni-complex with the correct number of CN-ligands has been formed in the synthesis.

Electrophoresis experiments

Introductory experiments showed that the barbiturate buffer adjusted to various pH-values around neutrality did not work sufficiently well. The reproducibility was relatively poor and the peaks too broad. In addition, the sodium content of the barbiturate buffer excluded its use in the NAA-experiments because of too high production of the strongly radioactive ^{24}Na in the activation process. This radiation will completely overshadow the radiation from produced ^{65}Ni. Hence, the phosphate buffer was used throughout the experiments.

Figures 5a-d show typical electrophoresis spectra for cases where the pH has been adjusted with various bases. As can be seen, in Fig. 5a, b and d, where pH has been adjusted to 7.0-7.1 with different agents, the main peak has a shoulder to the right suggesting that two different components are present. Fig. 5c shows a more complex pattern. At least three components seem to be involved.

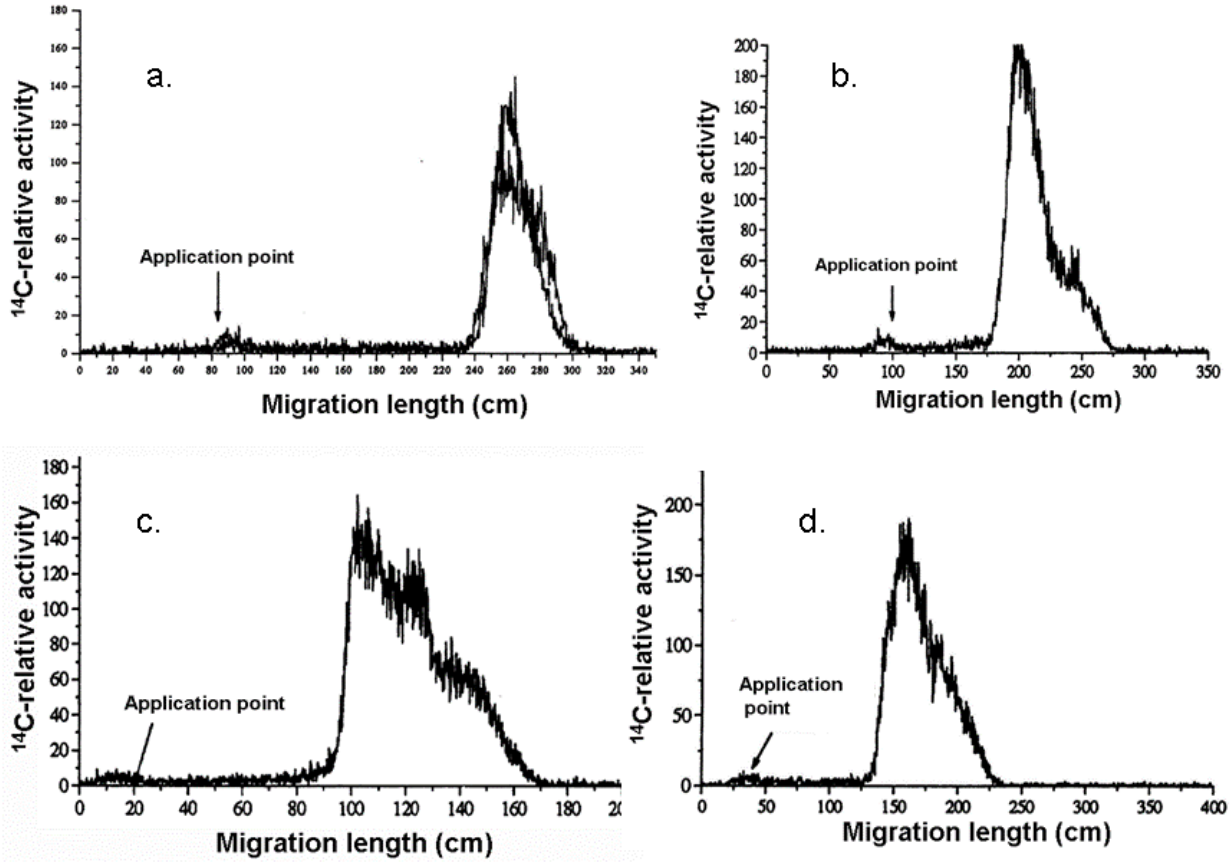

Figure 4. Electrophoresis spectra of synthesized Ni(^{14}CN)(CN)$_3^{2-}$ in phosphate buffer where a. pH adjusted to 7.0 with NaOH, b. pH adjusted to 7.1 by NH_3, c. pH adjusted to 8.3 by NH_3 and d. ph adjusted to 7.1 with LiOH.

Our interpretation is as follows: We anticipate that the shoulder component is unreacted CN^- since CN^- was added in surplus amount during the synthesis and no attempts have been made to remove it before the electrophoresis. Eqn 1 shows that the migration rate is a function of the ionic charge and ionic radius where the first is above and the latter below the fraction line. Accordingly, and based on the charge only, CN^- with $q_1 = 1$, should move at a slower speed than $Ni(CN)_4^{2-}$ where $q_1 = 2$ in an electric field. However, based on the ionic radius, where $r_{Ni\text{-}complex} > r_{CN}$, the CN^--ion will move at a higher speed than $Ni(CN)_4^{2-}$. The result is that the two ions might migrate with comparable speed. Unfortunately, a separate experiment exclusively on CN^- to support this idea was not performed.

An example of results from the NAA detection of Ni on the electrophoresis strip after sectioning in 1 cm broad bands, neutron activation of the strips and γ-counting of ^{65}Ni on high-resolution semiconductor detector is given in Fig.6. The relatively poor resolution is attributed to low amount of Ni which leads to poor counting statistics. The results do not constitute a strong support to those from the HPLC-experiments. On the other hand, results are not in disagreement.

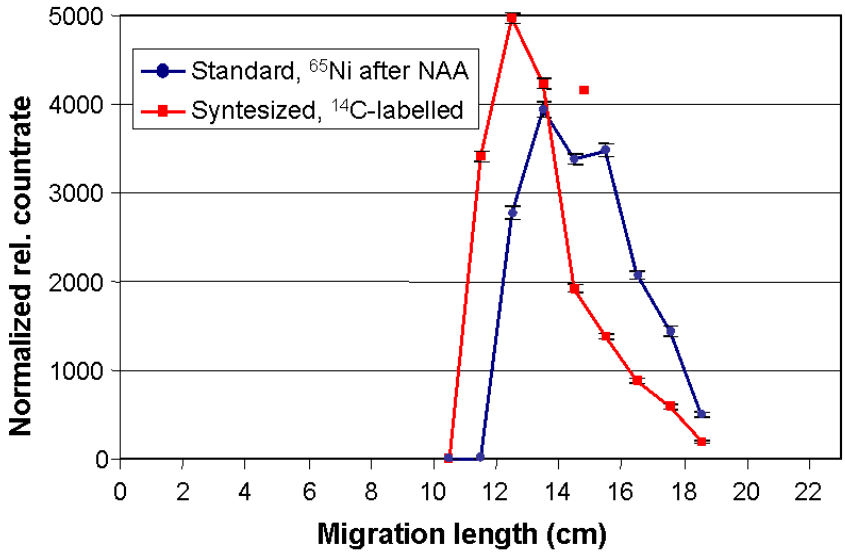

Fig. 6. Electrophoresis spectrum of synthesized Ni(^{14}CN)$(CN)_3^{2-}$ compared to that of commercial (standard) $Ni(CN)_4^{2-}$ where the latter is analysed by NAA on Ni.

CONCLUSION

The final conclusion on this subject is that the results strongly indicate the formation of the $Ni(CN)_4^{2-}$-complex in the synthesis, and there are no strong signs of complexes with different number of ligands. On this basis we have concluded that we can safely regard the synthesis product as being $Ni(CN)_4^{2-}$ and use it in the form of the ^{63}Ni-labelled version in the further investigations of the thermal stability and flow properties of the complex and in development of analytical methods including separation and enrichment from ultra-dilute concentrations in field samples. The latter subject is published in another paper in the present conference proceedings [9].

REFERENCES

[1]. Sternau, R.; Schwarz, J.; Mercado, A.;Harpaz, Y.; Nir, A. and Halevy, E.: „Radioisotope Tracers in Large-Scale Recharge Studies of Groundwater“, in „Proc. Symp. Isotopes in Hydrology“, IAEA/IUGG, Vienna, 14-18 Nov., 1966, p.489-505

[2]. Frissel, M.J.; Poelstra, P.; Harmsen, K. and Bolt, G.H.: „Tracing Soil Moisture Migration with ^{36}Cl, ^{60}Co and Tritium“, in “Isotopes and Radiation Techniques in Soil Physics and Irrigation Studies 1973”, IAEA, Vienna 1974, p. 145-148.

[3]. Lebecka, J.; Tomza, I. and Trzebicka, B.: „Tracing of Underground Waters by means of $K_3{}^{60}Co(CN)_6$”, Freiberger Forschungshefte Geowissenschaften, C417, (1985)155-159.

[4]. Bjørnstad, T.; Michelsen, O.B. and Eriksen, D.Ø.; “Safe application of radiolabelled cobalthexacyanides as water tracers in oil reservoirs”, Research Report IFE/KR/F-97/037, 64 pp, 1997, restricted distribution.

[5]. Jevanord, K.: “Radioaktive cyanidkomplekser av innskuddsmetaller som vanntracere i petroleumsvirksomheten: Utvikling av radiokjemiske analysemetoder”, MSc-Thesis, University of Oslo and Institute for Energy Technology (IFE), 1997, pp. 75 + 67, in Norwegian..

[6]. Røv, L.: ”Cyanidkomplekser av gull og nikkel som mulige vanntracere i petroleumsvirksomheten: Statisk sorpsjonstest mot utvalgte reservoarbergarter”, MSc-Thesis,

University of Oslo and Institute for Energy Technology (IFE), 1999, pp. 51 + 43, in Norwegian.
[7]. Smith, R.M. and Martell, A. E.: “Critical stability constants: Volume 4: Inorganic complexes”, New York, NY: Plenum Press, 1976
[8]. Durrant, P. J. and Durrant, B.: “Introduction to Advanced Inorganic Chemistry”, Wiley, New York, 1962, p.1048.
[9]. Jevanord, K. and Bjørnstad, T.: “Separation, enrichment and analysis of radiolabelled Ni(CN)42- in laboratory and field samples”, in proc. TRACER5-Conference, Tiradentes, Brazil, 2-6 Nov. 2008

.

PROFILE ANALYSIS OF FLUIDS DISPLACEMNT IN A PHASE SEPARATION TANK APPLYING THE RADIOTRACER TECHNIQUE

Ricardo E. de Miranda Candeiro[1], Luis E. Barreira Brandão[1] e Verginia R. Crispim[2]
[1] Instituto de Engenharia Nuclear (IEN / CNEN)
Caixa Postal 68550
21945-970 Ilha do Fundão, Rio de Janeiro, RJ
ricardocandeiro@ien.gov.br
brandao@ien.gov.br
[2] Universidade Federal do Rio de Janeiro/COPPE
Programa de Engenharia Nuclear.
Caixa Postal 68509
21941-972 Rio de Janeiro, RJ
verginia@con.ufrj.br

ABSTRACT

This paper aims at studying and evaluating a phase separator tank (organic/liquid) applying the radiotracers technique. This technique is based on the study of material transport and identification of operational problems in industrial tanks and has great advantages due to the interventions done without influencing on the normal operation. In the studied case, to evaluate the fluid hydrodynamic behaviour inside the tank, the radiotracer 82Br in the aqueous solution of potassium bromide (KBr), and for the radiotracer passage registration, four scintillation detectors of NaI (2 x 2)" were used. For methodology was possible to analyze the unit response and also to identify the operational problems.

INTRODUCTION

In the last decades, several studies involving radioisotopes have been applied to the industrial area. Then, methodologies that come to the contribution of the appropriate industrial installation are of great interest to the market. The tracer technique allows an evaluation in real time of a unit without alteration in the production line and is mainly applied in complex processes, such as, in the optimization of the treatment stations effluents, in production processes in petrochemical industries of cement, cellulose, metallurgy, etc.

METHODOLOGY

The measures of the residence time distribution functions have been an important tool for the study of several systems. Its main advantage is to allow describing the real conditions of the tracer displacement in the system by means of statistical functions. Establishing the study in a liquid system, each element of fluid that is coming out from this system has a "history", that is, what occurred since the injection until the exit of the unit [1]. The residence time of each fluid element is defined in statistical terms and for describing the displacement profile of the flux some probability density functions that give information on the fluid behaviour while displacing through the system are defined.
Thus, for an open system with volume V and flow rate Q constant in all moments, mean residence time is defined as the mean time take by the tracer to go through the whole tank [2, 3, 4, 5]. The mean residence time is given by:

$$\tau = \int_{t+\Delta t}^{t} t \cdot E(t)dt = \frac{V}{Q}$$

The functions are:

- E(t): the external age distribution represents the probability that an element of the fluid went through the tank, that is, the fraction of the exit flow having an age between a determined time t and another t + Δt. Considering that a determined tracer volume is injected in the system during a very short time and that for each time t_n are registered in the detector counting $C_n(t)$, then, the definition of the function E(t) is given by:

$$E(t) = \frac{C(t)}{\int_{t+\Delta t}^{t} C(t)\,dt}$$

- I(t): is such that I(t)Δt represents the fraction of the fluid elements within the tank, with ages between t and t + Δt. The function is normalised as:

$$\int_{t+\Delta t}^{t} I(t)dt = 1$$

- Λ(t): the function is defined as the fraction of the fluid elements with age t, which leaves the system between t and t + Δt. The function is the relation between the fraction of fluid elements that left the unit with age t and the fraction of elements that still remain inside the unit, given by Equation 4. The function has a characteristic format, where initially the curve is crescent, indicating the tracer removal, after the curve reaches the level region in which the material is removed and the material that is inside the system is moving constantly, and in the end of the curve tends to the infinite indicating that there is no more tracers inside the system.

$$\Lambda(t) = \frac{1}{\tau} \cdot \frac{E(t)}{I(t)}$$

The radiotracer ^{82}Br was used, in the form of KBr aqueous solution, produced by the reaction (n, γ) supplied by the IEN Reactor Argonauta. The activity to be inserted in the tank of measure was 1,4 x 10^8 Bq. Bromium-82 was chosen due to its sensitivity to detection and has several γ rays that range from 0,55 MeV to 1,31 MeV, besides its physic-chemical characteristics are similar to the mean that is being studied, once in aqueous mean, it is easily diluted, and is not absorbed by the tank walls and does not suffer any chemical reaction [1]. The other factor refers to the short half life ($T_{1/2}$ = 36 h) that avoids the "memory effect".

TANK OF MEASURE SEPARATION PHASE OF RESIDENCE TIME DISTRIBUTION FUNCTIONS

A rectangular tank used for studies of liquid separation phases (organic/aqueous) was used for the profile study of the displacement material marked by the radiotracer technique. The tank shown in figure 1 is composed of two rectangular compartments; a smaller one (12 x 24 x 12) cm that has the function of mixer and has the fluid entrance in the inferior part and the exit in the superior part. The second compartment (77 x 24 x 33) cm is connected to the smaller, projected in order to allow the phases separation. The last compartment has a denser effluent located in the inferior part and the lightest one in the superior part.

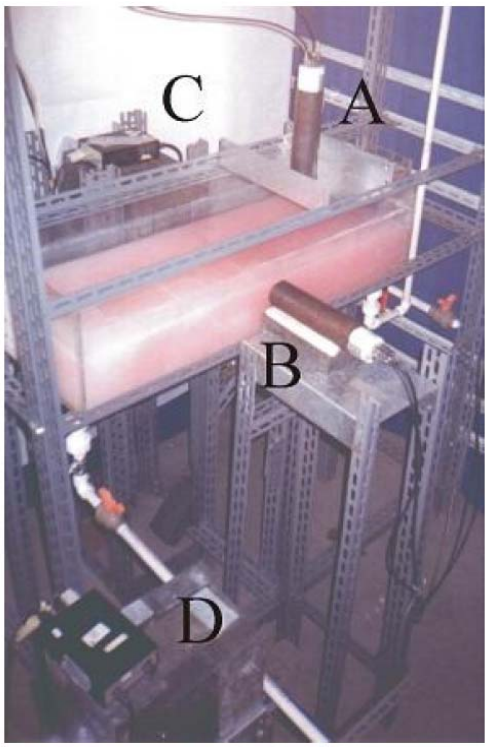

Figure1.Configuration and identification of detectors A, B, C and D

For the profile study of the displacement of the radiotracer inserted in the separation tank, four detectors were employed and located at a distance of 80 cm from the input. The detector A, without collimation, was positioned in the superior part of the tank. The detectors B and C, positioning each of one side of the separation tank were used as a reference of the movement situation marked in the interior of the tank. Considering that detector B was not shielded neither collimated and the detector C was shielded by a lead wall whose thickness was 10 cm and collimated with an opening of 1,2 cm of diameter. The detector D, near the exit, was used in order to measure the mean residence time and for determine the characteristic curve of the whole separation tank.

The experiments were carried out considering a fix volume of 50 L of water and entrance and exit constant flows of (1,00 ± 0,02) L/min, considering that the theoretical mean residence time was estimated in τteo = (50,0 ± 0,6) min, according to the calculation made by equation 1. For the detectors group lined in the tank, the experimental mean residence time, τexp, calculated for detector D was of de (31,8 ± 0,5) min. For test, a time of interval of 2 seconds and a total acquiring time of 7200 seconds were used.

NON - COLLIMATED SUPERIOR DETECTOR –A

For detector A, the curves DTR were use focusing on studying the tracer behaviour in the superficial region of the tank. By the analysis of curve E(t), it was noticed that in the beginning of the curve, figure 2(a), around t = 180 s and t = 270 s, a small fraction of the marked material moved faster than the other parts of the fluid, that is, a small fraction of the tracer was canalised fast. Another peak of bigger intensity around t = 400 s and t = 500 s, was also evident, indicating that more material was canalised. In approximately t = 1500 s and t = 3500 s, it was observed the presence of a faster passage of the tracer and identified by the absence of the characteristic time of the exponential curve of a perfect mixer, where there is a constant removal. From t = 3500 s, the curve presents a exponential behaviour until reaching the base line.

In curve $\Lambda(t)$, Figure 2(b), it was observed that in the beginning, around t = 180 s and t = 270 s and t = 400 s and t = 500 s, there are two peaks of small intensity that are related to two canalisations observed in curve E(t). After that, it is observed that between t = 1500 s and t = 3000 s, the curve is crescent, identifying that a bigger quantity of the marked material leaves the region of sensibility in

relation to the fraction of the material that is in its inner part. For values of time bigger than t = 4000 s, it is observed a decrease in the crescent curve and the presence of a small peaks indicating that more marked material is in the inner part of tank and that this fraction is recirculating until there is no more material inside the tank and then the curve tends to the infinite.

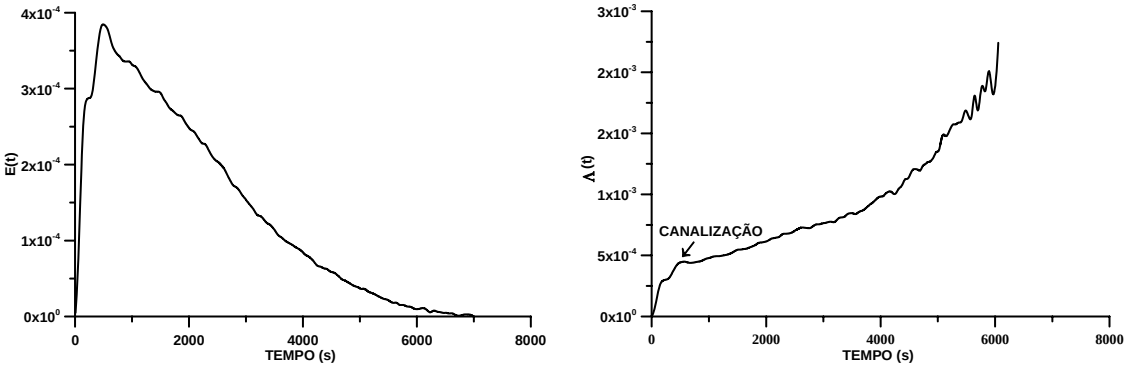

Figure2. (a) Curve E(t) of detector A. (b) Curve Λ(t) of detector A.

LATERAL DETECTORS: COLLIMATED AND NON-COLLIMATED–DETECTORS B AND C

The responses of the DTR curves, referring to detectors B (non collimated) and C (collimated) were put at the same graphic as a reference for the observation profile of the tracer dislocation in the interior of the separation tank, considering its different regions of sensibility and as a consequence of the register of the cloud passage to the identification of several phenomena as shown in Figure 3.

According to detector C responses, as observed in Figure 3(a), one fraction of the radiotracer passed with a higher velocity than the rest of the fluid and that passage was identified as around t = 210 s, by the existence of a peak formation in the beginning of the curve making evident a direct canalisation. In the interval around t = 500 s and t = 3500 s, the material is removed in a constant way so the curve in this interval acts as a perfect mixer, being then a decreasing exponential. Between t = 4000 s and t = 4600 s it is presented a small level, where there was no movement of the material in the region presented, indicating that there is a retention zone. Now for times superior to t = 4500 s peaks of small intensity are presented, making evident small internal circulations, for this phenomenon, the curve shows a light decay until reaching the base line.

In curve Λ(t) that refers to detector C, Figure 3(b), it was also observed, at the same interval around t = 210 s, the formation of a peak, indicating then a canalisation. The level is identified in the region of the curve with an interval around t = 500 s and t = 3500 s, what represents a constant removal of the material. In the end of the curve, from t = 4000 s, some structures in peaks are observed, this sequence indicates a fraction of the material that passed by the sensible region of the detector and began moving in the same region, characterizing then a recirculation of the material. The curve also increases slowly due to the fact that the material remains inside the tank, after that, it assumes a characteristic behaviour of a crescent curve and tends to infinite.

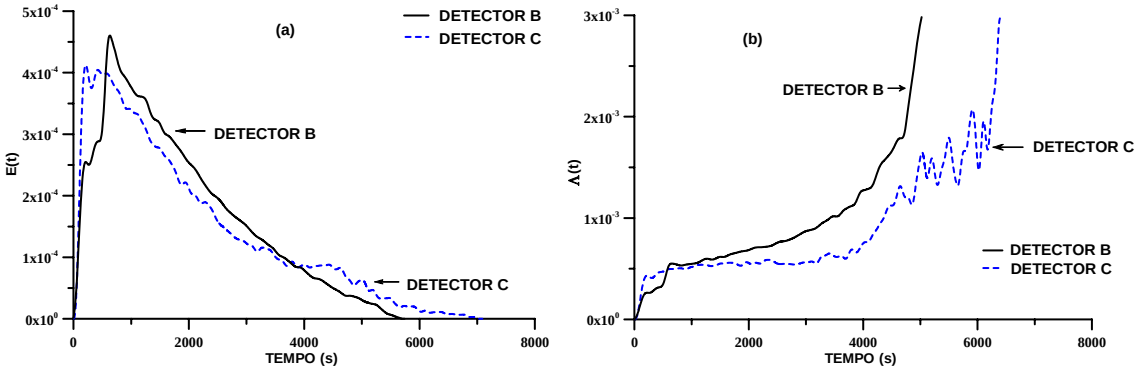

Figure3. (a) Curves E (t) of detectors B and C. (b) Curves Λ(t) of detectors B e C.

In curve E (t) of detector B, Figure 3(a), the canalization phenomenon was also observed, at the same interval around t = 210 s, registering then, a small fraction of the tracer that is removed in a faster way. The smallest intensity of the peak is due to the non-collimation, so the biggest region of the detector sensibility makes impossible to identify some phenomena. In the interval around t = 1000 s and t = 4000 s, the curve presents an exponential with bigger inclination, making evident that the material displaces faster.

In curve Λ(t) of detector B, Figure 3(b), the canalisation was observed by a peak of small intensity followed by a small level around t = 200 s and t = 280 s. Next, for the interval around t = 900 s and t = 4000 s, curve Λ(t) presents a fast removal of the material indicated by the crescent curve, showing that there is more material being released than inside the tank Around t = 4000 s and t = 4800 s, it is observed the presence of small recirculations, this kind of phenomenon is less evident in curve E(t), due to the detector big region of sensibility

NON-COLLIMATED DETECTOR IN THE TANK EXIT OF DTECTOR D

The detector was placed in the exit aiming at registering all the hydrodynamic behavior of the tracer inside the place where the experimental medium residence time was measured and whose value was τexp = (31.8 ± 0.5) m, and being aware of the system operating in stationary system, the residence time was τteo = (50 ± 0.6) m, what meant a difference of approximately 36 %. Curves DTR for the detector located in the tank exit are presented in Figure 4.

In the beginning of curve E (t), Figure 4 (a), the phenomenon of canalisation was observed through the two peaks that were formed around t1 = 300 s and t2 = 800 s, and they refer to a fast removal of the radioactive tracer. In the region around t = 1200 s and t = 4000 s, the curve follows the exponential behaviour of a perfect mixer through a decrescent exponential indicating a constant movement of the radiotracer. After a time around t = 4000 s until reaching the base line, the curve indicating a light decrease in the curve, representing a small exit of the material that was in the retention zone.

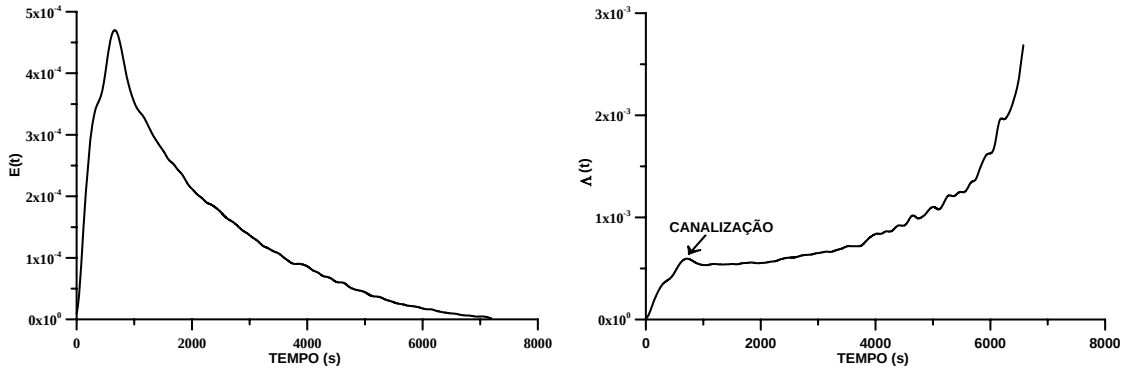

Figure 4. (a) Curve E (t) of detector D(b) Curve Λ(t) of detector D.

In the studied case, Figure 4(b), curve Λ(t) presents in the beginning, mainly around t = 650 s and t = 780 s, a format of two peaks, making evident a fast exit of the material marked in the tank. Around t = 1000 s and t = 4000 s, there is the presence of a level that indicates a constant removal of the material, which is a characteristic of the perfect For times between t = 4000 s and t = 6500 s, the curve is crescent, presenting a series of peaks of low intensity that make evident the exit of the material that was kept in one region of the tank. For times superior to t = 6500 s, there is no presence of tracer movement internally, presenting according to the theory that the curve tends to infinite

CONCLUSION

The use of the radiotracer technique was very efficient in the profile study of the radiotracer displacement inside the phase separation tank, besides the technique presents a very versatile methodology for the different conditions of the study. Another advantage is that this technique allows to measure in real time, the functions of distribution of residence time and also the medium residence time. Then, it was observed, according to the sensibility region of each detector, the radiotracer movement, and identifying operational problems in the tank was possible as well.

ACKNOWLEDMENTS

The authors are grateful to the Nuclear Engineering Institute for their help and more specifically, to the Radiotracers Laboratory, and to the Argonauta and Cíclotron Division as well.

REFERENCES

1. R.E.M. Candeiro, Medida de Tempo de Residência em Tanques Industriais, usando uma Unidade Estanque para Detector Estanque Submerso. Tese de Mestrado, COPPE/UFRJ, Rio de Janeiro, Brasil (2003).
2. P.V. DANCKWERTS, Continuous Flow Systems – Distributions of Residence Times, Chem. Eng. Sc, 2, n.2, pp. 1-18, (1953).
3. K.B. BISCHOFF and E.A. McCRACKEN, Tracer Test in Flow Systems, Industrial & Engineering Chemistry Fundamentals, 58, n.7, pp. 18-31, (1966).
4. Guidebook on Radioisotope Tracers in Industry, N. 316, Technical Reports Series IAEA, Vienna, Áustria (1990).
5. D.M. HIMMELBLAU and K.B.BISCHOFF, Process Analysis and Simulation - Deterministic Systems. John Wiley & Sons, Inc, New York, USA (1968).

STUDIES ON SEPARATION OF TRACER CONCENTRATIONS OF RADIOLABELLED $[CO(CN)_6]^{3-}$ FROM RADIOLABELLED SCN^- IN WATER SAMPLES

Tor Bjørnstad, Dag Ø. Eriksen and Gonglai Yan
Institute for Energy Technology (IFE), Kjeller, Norway

ABSTRACT

The use of radiolabelled $[Co(CN)_6]^{3-}$ as a water tracer in oilfield operations demands an efficient procedure for separation and analysis of the complex. This article describes two possible methods for enrichment of the Co-complex from collected 1 L samples of produced brine and its separation from the radiolabelled water tracer SCN^- which may be used simultaneously. The methods are based on solvent extraction with amine ion pair reagents and on anion exchange with tertiary amine-based resins. The overall best performance is obtained with anion exchange using Dowex 2x8 resin. Absorption yield of $[Co(CN)_6]^{3-}$ is ~ 100% while any simultaneously fixed SCN^- can be selectively removed by 0.1 M ClO_4^-. Raffinate containing SCN^- is loaded with high yield onto a BioRad AG1 resin. $[Co(CN)_6]^{3-}$ is stripped by 5 M NH_4NO_3 to an efficiency of 75% while SCN^- is stripped by 2.8M ClO_4^-. For collected elution volumes of 10 mL, the total enrichment factors of $[Co(CN)_6]^{3-}$ and SCN- are > 75 and > 65, respectively. These numbers can be further improved by carefully selecting the respective elution bands.

INTRODUCTION

We have previously reported on experimentally derived properties for the $[Co(CN)_6]^{3-}$ complex [1-3]. This complex is of interest as a basic carrier of the five different radionuclides ^{56}Co, ^{57}Co, ^{58}Co, ^{60}Co and ^{14}C. Here, the first four are gamma-emitters while the latter is a pure beta-emitter. This labelling offers the possibility of five different radiolabelled water tracers. In addition, the relatively high cross-section for thermal neutron capture of stable ^{59}Co (37.2 barn), makes it very sensitive to neutron activation analysis. Thus, the non-labelled molecule may also be used as a water tracer.

One prerequisite for its use as a water tracer in petroleum reservoirs is that it survives the reservoir conditions without substantial degradation or reactions. Thermal and chemical stability were measured in various actual chemical environments with various substrates present. The substrates were solid substances which the tracer is likely to contact during field operations. Typically, they are reservoir rocks like sandstone, calcite and clay and other solid substances like steel, corroded steel, grease and scale ($BaSO_4$). For the complex $[Co(CN)_6]^{3-}$ high degree of sorption was found on some forms of rust. In addition, thermal degradation seems to accelerate at temperatures higher than 90°C. Dynamic experiments in porous media below 90°C shows that this complex is a near ideal water tracer. However, it shows, as expected, some degree of anion exclusion behaviour due to the three negative charges.

In real field situations it may be used in areas where $^{35}SCN^-$ or $S^{14}CN^-$ have been applied simultaneously. Since the thiocyanate tracers have to be analysed by liquid scintillation counting (LSC) the presence of $[Co(CN)_6]^{3-}$, regardless of the radiolabel, will disturb the counting of the thiocyanate. For gamma-emitting labels the analysis may be performed by gamma spectrometry, but if the label on the $[Co(CN)_6]^{3-}$ is ^{14}C, there will be a mutual disturbance of the two radiolabelled complexes. Therefore, there is a need to develop radiochemical procedures to separate cobalthexacyanide and thiocyanate on tracer level in produced water. Results from attempts on this separation are reported here.

OBJECTIVES

The aim in this study was to develop a method for quantitative analysis using 1000 mL seawater (as a mimic of produced water) containing a mixture of SCN^- and $[Co(CN)_6]^{3-}$ by enrichment procedures and preconcentration into samples small enough to be measured by LSC. The sample volume for LSC should not exceed 8-10 ml since this is normally the maximum water sample volume dissolved by modern scintillation cocktails (12 mL) for ordinary 22 mL scintillation vials.

METHODS

Test sequence

The main hypothesis was to take advantage of the difference in anionic charges to obtain a separation. The test sequence contained the following main points:

1. Screening tests to find a selective separation procedure for $[Co(CN)_6]^{3-}$ by the use of ^{60}Co-labelled complex as a tracer. The separation is based on either solvent extraction or ion exchange techniques.
2. Tests of different stripping or elution agents in order to minimize the degree of quenching in the final counting samples
3. Checking the absorption and stripping/elution characteristics of SCN^- in the $[Co(CN)_6]^{3-}$ method
4. Perform separation experiments on a real sample containing both tracers labelled with ^{60}Co and ^{14}C, respectively.

Radioactivity measurements

In this laboratory screening experiments with ^{60}Co were measured with gamma spectroscopy using a lead-shielded high-resolution semiconductor detector coupled to a PC multichannel analyser operated by the MAESTRO acquisition software from ORTEC. ^{14}C was measured with a Beckman LS 3000 liquid scintillation counter.

Solvent extraction

The procedure was as follows: A series of 5 mL samples of seawater were doped with tracer amounts of ^{60}Co-labelled $[Co(CN)_6]^{3-}$ and pH-adjusted in the range pH 1-7 by addition of HCl. Each sample was then contacted in a separatory funnel with 5 mL of organic phase (kerosene) containing the extraction agent. The funnel was then vigorously shaken by a mechanical shaking machine for a predetermined time of 3 min at room temperature, which is sufficient time to reach extraction equilibrium. After phase separation (by gravity), 1 mL samples of both phases were extracted from both phases and measured for radioactivity. For the high gamma energies of ^{60}Co (1173 keV and 1332 keV), correction for difference in sample density is not needed. In addition, when equal volumes of the two phases are used in the counting procedures, the distribution coefficients D-values) can be determined from the raw counting rates by the formula

$$D = \frac{R_{org}}{R_{aq}} \tag{1}$$

where R_{org} = net counting rate of the organic sample and R_{aq} = net counting rate of the aqueous sample.

The extracted amount from one extraction operation is expressed as %E by the formula

$$\%E = \frac{D}{\frac{V_{aq}}{V_{org}} + D} \cdot 100\% \tag{2a}$$

For high values of D one can obtain a substantial volume reduction and enrichment factor by using a volume ratio V_{aq}/V_{org} = 10 or higher. Here, since equal volumes have been used of the aqueous and organic phase also during extraction, the formula reduces to

$$\%E = \frac{D}{1 + D} \cdot 100\% \tag{2b}$$

For even further enrichment, one needs to strip the activity back to an aqueous phase with a high stripping efficiency and perform a new extraction sequence on this strip solution with a volume ratio $V_{aq}/V_{org} >> 1$. As an example: For D = 10 and V_{aq}/V_{org} = 10, one obtain a volume reduction of

10 and an enrichment factor of 5 after 1 extraction. After a stripping with 100% efficiency and a new extraction with the same volume ratio, one has obtained a volume reduction of 100 and an enrichment factor of 25. For higher D-values the enrichment factor will be higher.

We have therefore also screened the stripping efficiency with a few stripping agents.

The extractions performed here are based on so-called ion pair formation, and the extraction agents are all amines of different kind which, as a rule, has been conditioned with 0.1M H_2SO_4. Data for extraction and stripping systems are found in Table 1.

Table 5. Extraction and stripping systems

Extractant	Type	Producer	Concentration	Stripping agent tested
Primene JM-T	Primary amine	Rohm and Haas	10 % in kerosene	No stripping
Amberlite LA-2	Secondary amine			1.8M H_2SO_4, 3.5M H_2SO_4 6M $NH_3$1M $K_2(COO)_2$
Amberlite LA-2*)				
Alamine 336 (>95% trioctylamine TOA)	Tertiary amine	Henkel Corp.		

*) Without pre-treatment with 0.1 M H_2SO_4

Anion exchange

The general procedure was as follows: Resin was immersed in water for 24 hours for full swelling before loading onto the polyethylene column. The resin was then washed with 10M HCl to convert it into the Cl^--form followed by ion exchanged water until pH = 7.
For experiments where the main purpose was separation of $[Co(CN)_6]^{3-}$, the column had dimensions Ø = 5 mm and L = 25 mm to a resin volume of 0.5 mL. For the experiments where the main purpose was absorption of SCN^-, the column dimensions were Ø = 6mm and L = 300 mm to a resin volume of 8.5 mL. This latter procedure was based on earlier experiments by Bjørnstad et al. [4].
100-1000 mL of seawater containing radiotracer was passed through the columns. Flow rates were kept at ca. 0.5 mL/min.

Absorption yield is expressed by percent absorbed and calculated by

$$Y_{abs} = \frac{R_{cs,feed} \cdot \frac{V_{ts,feed}}{V_{cs,feed}} - R_{cs,raf} \cdot \frac{V_{ts,raf}}{V_{cs,raf}}}{R_{cs,feed} \cdot \frac{V_{ts,feed}}{V_{cs,feed}}} \cdot 100\% \qquad (3)$$

where R_{cs} denotes the net sample counting rate, V_{ts} the total phase volume, V_{cs} the counting sample volume and the subscripts feed and raf denote the feed (or input) solution and raffinate, respectively.

Elution yield is determined by

$$Y_{elut} = \frac{R_{cs,elut} \cdot \frac{V_{ts,elut}}{V_{cs,elut}}}{R_{cs,feed} \cdot \frac{V_{ts,feed}}{V_{cs,feed}} \cdot \frac{Y_{abs}}{100}} \cdot 100\% \qquad (4)$$

where the subscript elut denotes the eluate.

The separation factor of $[Co(CN)_6]^{3-}$ and SCN^- in the complete ion exchange procedure (feed + elution) is then defined as

$$\alpha_{Co}^{SCN} = \frac{Y_{abs,SCN} \cdot Y_{elut,SCN}}{Y_{abs,Co} \cdot Y_{elut,Co}} \qquad (5)$$

All anion exchangers are of the amine type. The main parameters are given in Table 2.

Table 6. Anion exchangers used

Resin	Type	Producer	Elution agents
Amberlite IR45, 50-100 mesh	Weak base, $-NH_2$	Rohm and Haas	No elutions performed
Lewatit MP60, 50-100 mesh		Bayer AG	
Dowex 1x2, 50-100 mesh	Strong base, quaternary amine	Dow Chemical	4M NH_4Cl+2M HCL, 12M HCL, 65% HNO_3
Dowex 1x2, 200-400 mesh			NH_4Cl (saturated), 65% HNO_3
Dowex 2x8, 100-200 mesh			70% $HClO_4$, HI (conc.), 96% H_2SO^4, 12M HCl, 32.5% HNO_3, 2.5M NH_4NO_3, 5M NH_4NO_3, 7.5M NH_4NO_3, 10M NH_4NO_3

RESULTS

Solvent extraction

Results from the extraction of $[Co(CN)_6]^{3-}$ are shown in Fig.1. The primary amine, Primene JM-T, extracted only minor amounts at pH=1. At higher pH-values the extraction was not detectable. The secondary amine, Amberlite LA-2, without H_2SO_4 pre-treatment shows, as expected, a reasonably high extraction at pH=1, but has a strongly falling tendency towards higher pH-values while the same resin with H_2SO_4 pre-treatment maintains a high extraction yield until pH=5 but decreases at higher pH-values. Only the tertiary amine extractant, Alamine 336, extracted the Co-complex strongly (near 100%) over the whole pH-range 1-7.

Since Alamine 336 contains a basic nitrogen atom, it typically can react with a variety of inorganic and organic acids to form amine salts, which are capable of undergoing ion exchange reactions with a host of other anions. As such, Alamine 336 is a liquid ion exchanger operated in a solvent extraction system. The general reactions, which are shown below, illustrates in the two steps protonation and exchange:

Protonation:

$$[R_3N]_{org} + [HA]_{aq} \leftrightarrows [R_3NH^+A^-]_{org}$$

$$[R_3N]_{org} + [HCl]_{aq} \leftrightarrows [R_3NH^+Cl^-]_{org}$$

Exchange:

$$[R_3NH^+A^-]_{org} + [B^-]_{aq} \leftrightarrows [R_3NH^+B^-]_{org} + [A^-]_{aq}$$

$$3[R_3NH^+Cl^-]_{org} + [Co(CN)_6]^{3-}{}_{aq} \leftrightarrows \{[R_3NH^+]_3[Co(CN)_6]^{3-}\}_{org} + 3[Cl^-]_{aq}$$

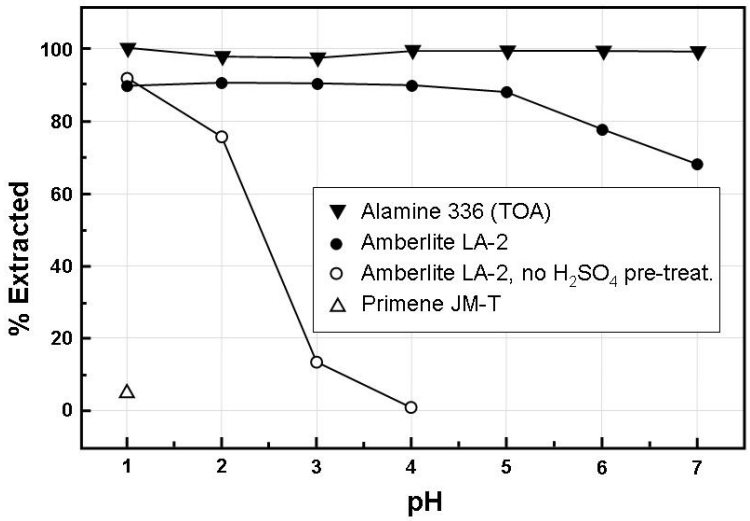

Figure 1. Extraction yield for the complex $[Co(CN)_6]^{3-}$ as a function of pH with 4 different extraction agents (10%) in kerosene.

After extraction, the organic phases containing Amberlite LA-2 or Alamine 336 were tested for stripping by the agents listed in Table 1. NH_3 could be used for stripping Co-complex from the Amberlite phases while $K_2(COO)_2$ (potassium oxal-ate) could be used for stripping Co-complex from both for the Amberlite and Alamine phases. For Alamine 336, for instance, the type of stripping agents to be used depends on the overall recovery process, but in general basic stripping agents, which reverse the protonation reaction, give the best stripping efficiency. The equations below show two alternative reaction routes for the stripping action by $K_2(COO)_2$ for recovery of $[Co(CN)_6]^{3-}$ from Alamine 336:

Stripping, two alterna-tive mecha-nisms:

$$2\{[R_3NH^+]_3[Co(CN)_6]^{3-}\}_{org} + 3[K_2(COO)_2]_{aq} \leftrightarrows 3[R_3N]_{org} + 3[H_2(COO)_2]_{aq+org} + 2K_3[Co(CN)_6]_{aq}$$

$$2\{[R_3NH^+]_3[Co(CN)_6]^{3-}\}_{org} + 3[K_2(COO)_2]_{aq} \leftrightarrows 3\{[R_3NH^+]_2[(COO)_2^{2-}]\}_{org} + 2\{K_3[Co(CN)_6]\}$$

Anion exchange

$[Co(CN)_6]^{3-}$: The ion exchange yields for the resins listed in Table 2 are given in Table 3 below. It is obvious from the figures in Table 3 that the strong base resins are superior to the weak base ones. Although both Dowex 1 and Dowex 2 are strong bases and quaternary amines, there is a difference in the functional groups: The functional (or ionogenic) group of Dowex 1 is $–CH_2\text{-}N^+(CH_3)_3$ while for Dowex 2 the composition of the ionogenic group is $–CH_2\text{-}N^+(CH_3)_2\text{-}C_2H_4OH$. This latter structure implies that the base strength is somewhat lower than for the first structure. This is not seen in the ion exchange yield but became evident in the succeeding stripping process.

Table 4 shows that elution of $[Co(CN)_6]^{3-}$ from the Dowex 2 resin is easier than from the Dowex 1 resin both for strong HNO_3 and HCl elution agent solutions reflecting the somewhat weaker basicity of Dowex 2.

More detailed results for complex elution from Dowex 2 by various concentrations of NH_4NO_3 and HNO_3 are shown in Fig.2 below.

Table 7. Ion exchange yields for tracer concentration of $[Co(CN)_6]^{3-}$ on various ion exchange resins with a feed volume of 100 mL

Anion resin	Anion exchange yield, Y_{abs} (%)
Amberlite IR45	40.7
Lewatit MP60	2.6
Dowex 1x2 (50-100 mesh)	95.9
Dowex 1x2 (200-400 mesh)	100
Dowex 2x8 (100-200 mesh)	100

Table 4. Elution yields for tracer concentration of $[Co(CN)_6]^{3-}$ from Dowex 1x2 and Dowex 2x8 with two different strong mineral acids

Elution agent	Elution yield, Y_{elut} (%)	
	Dowex 1	Dowex 2
12 M HCl	24.7	63.4
14.5 M HNO_3	52.3	80.3

For a strong base exchanger the effect of NO_3^- should be dominant relative to the acidity of the elution solution. Therefore, the data for Na_4NO_3 and HNO_3 elution should be closely overlapping.

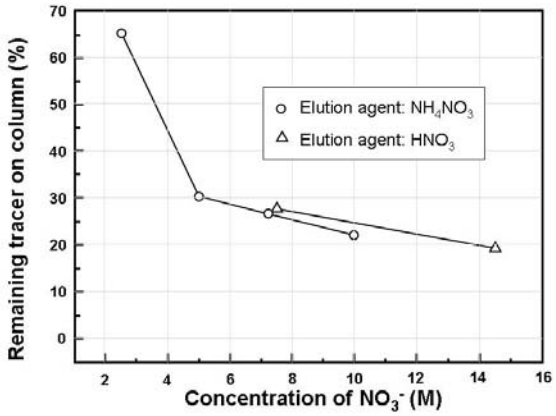

Figure 2. Results from elution of $[Co(CN)_6]^{3-}$ from Dowex 2x8 (100-200 mesh) with different concentrations of NH_4NO_3 (2.5M, 5M, 7.5M and 10M) and HNO_3 (7.25M and 14.5M).

SCN^-: A method for isolation and up-concentration of SCN^- from seawater (produced water) has previously been worked out by Bjørnstad et al. [1]. It is based on the use of the anion exchange resin BioRad AG1, which is in principle equivalent to Dowex 1. It was now necessary to check the performance of SCN^- on the Dowex 2x8 resin with the column dimension described earlier, and to investigate the separation factor from $[Co(CN)_6]^{3-}$ with various elution solutions. Results of elution yields and separation factors are found in Table 5. Fig.3 illustrates the absorption characteristics for $[Co(CN)_6]^{3-}$ and SCN^- on the Dowex 2x8 column and compare these data to the sorption characteristics of SCN^- on the BioRad AG1 column.

Table 5. Elution efficiency of $[Co(CN)_6]^{3-}$ and SCN^- on a (ø=5, l=25 mm) Dowex 2x8 (100-200 mesh) column and the separation factors obtained between the radiotracers for a selection of elution agents

Elution agent	Elution yield, Y_{elut} (%)		Separation factor α_{Co}^{SCN}
	$[Co(CN)_6]^{3-}$	SCN^-	
Na_3PO_4 (saturated)	≈ 0	3.4	-
1M NH_4NO_3	5	85	17.0
1.5M NH_4NO_3	7	95	13.6
0.1M $NaClO_4$	2	60	30.0
0.2M KI	5	88	17.6

It is obvious from the data that SCN^- experiences a rather fast breakthrough on the 0.5 mL Dowex 2x8 column, so the separation from $[Co(CN)_6]^{3-}$ will be substantial already in the absorption process.

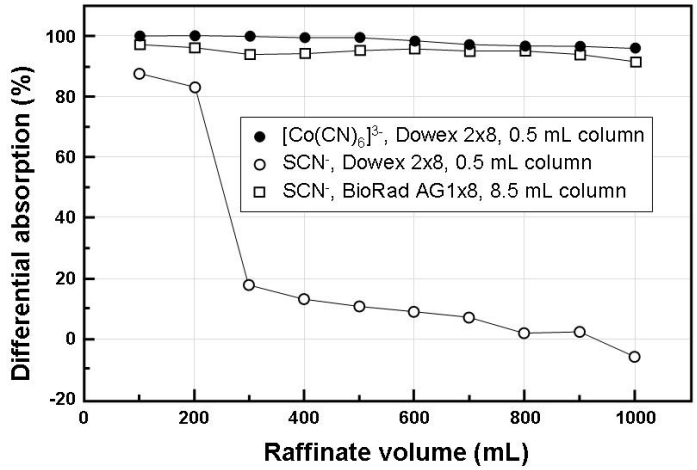

Figure 3. Absorption yield of [Co(CN)6]3- and SCN- on the 0.5 mL Dowex 2x8 (100-200 mesh) column, and for SCN- on the 8.5 mL BioRad AG1 column, as a function of raffinate volume (or original sample size) for tracer-containing seawater samples

DISCUSSION AND CONCLUSIONS

Both solvent extraction and ion exchange procedures may be used for trapping, enrichment and separation of $[Co(CN)_6]^{3-}$ and SCN- tracers from saline waters (seawater of formation water). It seems, however, that the ion exchange procedures are the less labour-intensive. We therefore put most emphasis on the discussion of the ion exchange results in the following.

The results reported here indicate a higher extraction of $[Co(CN)_6]^{3-}$ with strong basic extractants than with weak ones for the experimental conditions used here. This is valid both for the liquid extraction agents and for the solid anion exchangers tested.

$[Co(CN)_6]^{3-}$ is more strongly absorbed by Dowex 1x2 than Dowex 2x8 although the absorption yield are close to 100% for both at the conditions used here. Their relative absorption strengths appear through their ability to release the tracer again by various elution agents. The difference in the degree of cross-linking between the Dowex 1x2 and Dowex 2x8 resin would favour the kinetics of the x2-resin [5]. However, for reasonable flow rates the kinetics is not an issue. Since the Dowex 2x8 resin shows the highest elution yield (which we previously have concluded is due to the difference in the functional groups), we recommend using the Dowex 2x8 resin for the actual separation process.

The remaining SCN^- on the Dowex 2x8 ion exchanger after sample loading may be eluted selectively and with high elution efficiency by 10 mL of 0.1M $NaClO_4$. This eluate may be added to the raffinate after the sample loading process and used as a feed to the BioRad AG1 column for separation and enrichment of the SCN^- tracer along the lines outlined in ref. [4]. From a 1000 mL sample, the total recovery (chemical yield) is >65%. Since the volume is reduced by a factor 100, the enrichment factor is > 65. By optimising the process, it is probably possible to double this figure, especially by selecting carefully only the elution volume containing the bulk of the tracer peak. In this way the volume may probably be reduced by a factor 2-3 and the chemical yield only slightly reduced.

$[Co(CN)_6]^{3-}$ may be stripped from Dowex 2x8 by, for instance, 10 ml 5M NH_4NO_3 (acceptable for modern scintillation cocktails) with an efficiency of 75%. The overall chemical yield will therefore be >75%. From the same sample size as for SCN^- above, the volume reduction will amount to a factor 100 and the corresponding enrichment factor to >75. Also this figure is possible to improve by optimization of the procedure along the same lines as described for SCN^- above.

REFERENCES:

[1]. T. Bjørnstad, O.B. Michelsen and D.Ø. Eriksen; "Safe application of radiolabelled cobalthexacyanides as water tracers in oil reservoirs", Research Report IFE/KR/F-97/037, 64 pp, 1997, restricted distribution.

[2]. T. Bjørnstad, G.E. Maggio, B.J. Barry, G. Axelsson and Z. Pang; in "Radiotracer Applications in Industry – A Guidebook", Technical Report Series No. 423, IAEA, Vienna, 2004, Chapter 6: "Tracers in oilfields and geothermal reservoirs", p. 165-280.

[3]. T. Bjørnstad; in "2nd RCM Report on Validation of Tracers and Software for Interwell Investigations", IAEA meeting Grenoble, France 25-29 September 2006, p. 62-65.

[4]. T. Bjørnstad, E. Brendsdal, O.B. Michelsen, S.A. Rogde; "Analysis of radiolabelled thiocyanate tracer in oil field brines", Nucl. Instr. Meth., A299, (1990), 629-633

[5]. F. Helfferich; "Ion exchange", Chap.24, p.250-322, McGraw –Hill Book Company, Inc., New York, 1962.

ANALYTICAL MODEL FOR TRACER TRANSPORT IN FORMATIONS HAVING CONDUCTIVE GEOLOGICAL FAULTS32

Manuel Coronado and Jetzabeth Ramírez-Sabag
Instituto Mexicano del Petróleo,
Eje Central Lázaro Cárdenas 152, 07730 México D.F., Mexico

ABSTRACT

Hydrocarbon recovery in oil reservoirs is importantly affected by the presence of geologic faults since they modify fluid motion. Therefore it becomes very relevant for injection and flooding recovery projects to know with opportunity the presence of such heterogeneities and take their impact into account. Tracer tests are a tool to dynamically characterize the conduit or flow barrier fault behavior. Although diverse analytical models have been developed to describe tracer transport in geological conductive faults, only few of them capture the fact that injection and production wells are regularly located off the fracture plane, and consequently, they do not take in consideration the tracer path that run outside the fault. This work is an extension of a previous analytical model that describes this situation. The system assumes three coupled regions in a bi-dimensional horizontal plane associated to the injector-to-fault, fault, and fault-to-production-well zones. In this new approach, (i) the region coupling is introduced as a tracer source coming from the previous region, (ii) the fault section is taken as an open flow system, and (iii) the fault self is treated as a fractured porous medium. The model considers uniform velocity and hydrodynamic dispersion different in each region. The initial condition is a Dirac delta pulse at the injection site. The equations are analytically solved in Laplace space and the inverse transform is evaluated numerically by the Stehfest algorithm. Presently, the model has not been fully finished, but some preliminary results are shown. A sensitivity analysis of the tracer breakthrough curve with respect to the system parameters are still to be done. We believe this model will be very useful in faulted reservoir tracer test interpretation.

1.- INTRODUCTION

Determining the presence of main communication channels in underground formations and particularly in oil reservoir is of primary interest. Fluid flooding and improved oil recovery processes in oil fields are dramatically affected by them. Highly conductive channels are generally undesired since they seriously reduce flood sweep efficiency by providing direct underground flow paths that hinder the injection fluid for getting inside the porous rocks and push some of the remaining oil out. When these channels are known, they can be taken into account, or in some circumstances sealed. Geological faults work frequently as transverse flow barriers but also as longitudinal flow conduits depending on the fault structure. Faults commonly have a low permeability central core slide surrounded by damaged zones at both sides. Frequently, these zones are high permeability regions (Caine et al., 1999), and fluids can easily move along them.

Inter-well tracer tests constitute a fundamental technique to dynamically determine the presence of relevant conductive channels in underground formations such as in aquifers, geothermal fields and oil reservoirs. In such a test, a tracer is introduced in the formation through an injection well, and its appearance is observed in the surrounding production wells. From the tracer breakthrough curves fundamental information on the conduction channels can be obtained. Many analytical and numerical models have been developed to describe inter-well tracer transport in underground formations. However, only few analytical models capture the common feature in oil reservoirs, that the injection or production wells in the formation are located outside the fault plane (Houseworth, 2004; Coronado and Ramírez-Sabag, 2008). Therefore, the inter-well tracer flow path comprehends

[1] Work presented at the *5th International Conference on Tracer and Tracing Methods*, Tiradentes, Brazil from 2 to 6 November 2008

not only the section along the fault but also a section from the injection well to the fault, and a section from the fault to a production well. These two additional path sections have in general non-negligible length, and definitively impact the final tracer breakthrough curve. In Houseworth's (2004) report the first path section was not present and tracer longitudinal dispersion was not taken into account. In the work by Coronado and Ramírez-Sabag (2008) those ingredients were introduced but the fault was considered as a closed flow system connecting the injection and the production wells, and the diffusive coupling between the fracture network and the rock matrix in the fault region was neglected. These last two ingredients have been incorporated in this new model, as will be shown below.

2.- Model description

The bi-dimensional XY-system considers the flow in a reservoir section comprehending a fluid injector, a production well and a conductive fault dividing the path between them, as shown in Figure 1. The magnitude of the fluid flow going outside the fault section in consideration depends on the reservoir features beyond our injector-fault-producer system. We will examine two particular cases. A strong injection case, when the left outwards flow in Figure 1 goes outside the fault section, and a weak injection case, when the injector has a negligible effect on the fault flow, and the left outwards flow goes in reality into the fault section.

In order to take account that the system is open (i.e. the total fluid flow along the path between the injection and production well is not constant) a scheme to decouple the three regions has been designed. Each region is treated independently from the other. As illustrated in Figure 2 the space variable for Region 1 is named x, and thus the injector is located at $x = 0$ and the fault at $x = L_1$. The second region corresponds to the fault section, and it is described by the space variable y. The tracer source, due to the tracer arriving from Region 1, is set at $y = 0$, and the total length path along the fault is L_2. At $y = L_2$ the fraction F of the tracer goes to the production well in the third region, and the rest of tracer continues along the fault. Region 3 is described by the space variable z. The source due to the tracer arriving from Region 2 is located at $z = 0$ and the production well at $z = L_3$.

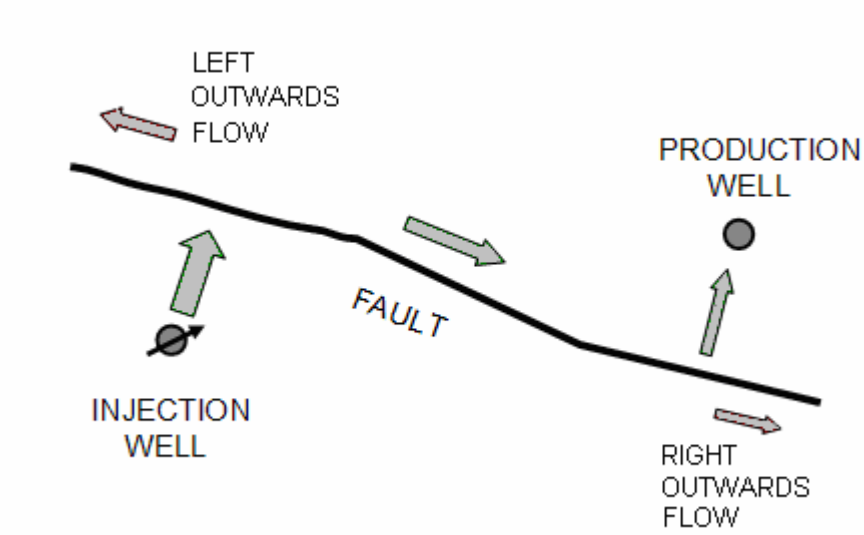

Figure 1- Schematic representation of the fluid flow in the (injection well) –fault– (production well) system under consideration.

The tracer transport is described by the tracer concentration in each region, $C_1(x,t)$, $C_2(y,t)$ and $C_3(z,t)$. The porous media in Region 1 and Region 3 is assumed homogeneous and non-fractured, while in Region 2 homogeneous and fractured. The physical phenomena to be considered are (i) advection, (ii) longitudinal hydrodynamic dispersion and additionally (iii) diffusive fransfer

between fractures and matrix rock in Region 2. The velocity pattern inside each region section is uniform given by

REGION 1: $-u_1$ for $x<0$ and u_1 for $x>0$

REGION 2: $-u_2$ for $y<0$ and u_2 for $y>0$ strong injection

u_2 for $y<0$ and u_2 for $y>0$ weak injection

REGION 3: u_3 for all z

The assumptions $|u_{2,L}|=u_2$ and $u_{2,R}=u_2$ are done in order to simplify the calculations while keeping the main tracer transport features. The dispersion coefficient will be constant given by $D_i=\alpha_i|u_i|$, where α_i is the dispersivity in the i-Region. The corresponding equations as well as the boundary and initial conditions for each region are described below.

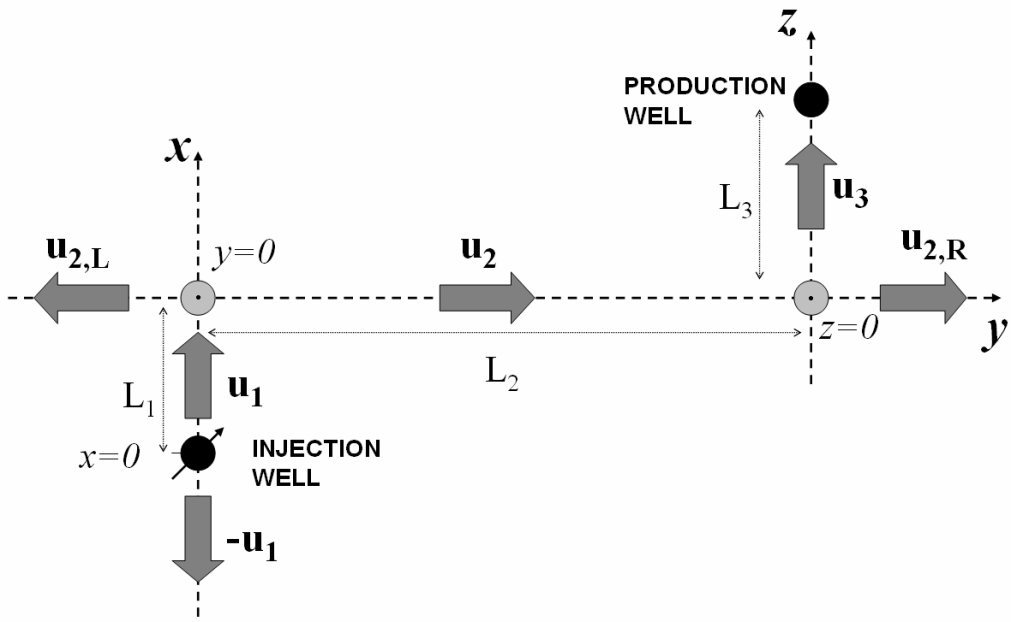

Figure 2- Diagram of the three independent path regions described by the variables x, y and z respectively. The main velocity pattern for the strong injection case is illustrated.

2.1- Region 1

The one-dimensional tracer transport problem involved here is a classical problem. It considers the initial condition

$$C_1(x,t=0)=\frac{m}{A_1\phi_1}\delta(x), \tag{1}$$

where m is the tracer mass injected, A_i the macroscopic channel cross-section and ϕ_i the porosity in Region i. The boundary conditions are $C_1(x\to\pm\infty,\ t)=0$. The advection-dispersion equation for this region is

$$\frac{\partial C_1}{\partial t}+u_1(x)\frac{\partial C_1}{\partial x}-D_1\frac{\partial^2 C_1}{\partial x^2}=0, \tag{2}$$

where $u_1(x)$ is a step-wise function, u_1 for $x\geq 0$ and $-u_1$ for $x<0$. The Laplace transform of Eq. (2) yields

$$s\overline{C_1}(x,s)+u_1(x)\frac{\partial \overline{C}_1(x,s)}{\partial x}-D_1\frac{\partial^2 \overline{C}_1(x,s)}{\partial x^2}=\frac{m}{A_1\phi_1}\delta(x). \tag{3}$$

This equation can be solved for $x<0$ and for $x>0$ separately, and then the solutions put together at $x=0$ by the tracer concentration continuity condition $\overline{C}_1(x=0_-,s)=\overline{C}_1(x=0_+,s)$ and the tracer flow jump condition

$$-D_1\left[\left.\frac{\partial\overline{C}_1}{\partial x}\right|_{x=0_-}-\left.\frac{\partial\overline{C}_1}{\partial x}\right|_{x=0_+}\right]+2u_1\overline{C}_1(x=0)=\frac{m}{A_1\phi_1}. \tag{4}$$

The solution is given by

$$\overline{C}_1(x,s)=B(s)\exp(\gamma\,|\,x\,|), \tag{5}$$

with $\gamma=\dfrac{u_1}{2D_1}\left[1-\sqrt{1+4sD_1/u_1^2}\right]$ and $B(s)=\dfrac{m/A_1\phi_1}{1+\sqrt{1+4sD_1/u_1^2}}$. The tracer mass rate arriving at the point $x=L_1$ is $\overset{\circ}{M}_1=A_1\phi_1J_1(x=L_1,t)$, where J is the tracer mass flux.

2.2- Region 2

This region corresponds to a fractured porous media, and thus the well known double-porosity model is used (Maloszewski, 1985; Coronado et al., 2007). The tracer population in the fracture network is $C_f(y,t)$ and in the matrix rock $C_m(y,w,t)$. The transport equations are the standard,

$$\frac{\partial C_f}{\partial t}+u_2(y)\frac{\partial C_f}{\partial y}-D_f\frac{\partial^2C_f}{\partial y^2}-\left.\frac{\phi_mD_m}{b}\frac{\partial C_m}{\partial w}\right|_{w=b}=S_2(t)\delta(y) \tag{6}$$

$$\frac{\partial C_m}{\partial t}-\frac{D_m}{R}\frac{\partial^2C_m}{\partial w^2}=0, \tag{7}$$

except by the source term. Here $u_2(y)$ is a step-wise function, R is a tracer retardation factor due to rock adsorption/desorption and $S_2(t)$ the tracer source that gives the amount of tracer arriving from Region 1 per unit of channel cross-section.

$$S_2(t)=(A_1\phi_1/A_2\phi_2)J_1(x=L_1,t) \tag{8}$$

The Dirac delta function $\delta(y)$ locates the source at $y=0$. The initial condition is that no tracer is present in Region 2 at $t=0$. The equation is solved by the Laplace transform technique. It appears in terms of the quantities

$$\xi_\pm(s)=\frac{u_2}{2D_f}\left[1\pm\sqrt{1+4\sigma D_f/u_2^2}\right],\ \sigma(s)=s+\sqrt{s}\left(\frac{\phi_mD_m}{b}\right)\sqrt{\frac{R}{D_m}}\tanh\left[\sqrt{sR/D_m}\,(E/2-b)\right],$$

where $2b$ is the effective fracture width, and E the effective matrix block size.

For the strong injection case it yields

$$\overline{C}_f(y,s)=\begin{cases}Y(s)\exp(-\xi_-y) & y<0\\ Y(s)\exp(\xi_-y) & y>0\end{cases}\quad\text{with}\quad Y(s)=\frac{\overline{S}_2/u_2}{1+\sqrt{1+4\sigma D_f/u_2^2}}. \tag{9a}$$

And for the weak injection case it holds

$$\overline{C}_f(y,s)=\begin{cases}Y(s)\exp(\xi_+y) & y<0\\ Y(s)\exp(\xi_-y) & y>0\end{cases}\quad\text{with}\quad Y(s)=\frac{\overline{S}_2/u_2}{\sqrt{1+4\sigma D_f/u_2^2}}. \tag{9b}$$

2.3- Region 3

This region represents the tracer path from the fault zone to the production well. It corresponds to a non-fractured media with similar properties as Region 1. At production well the Danckwerts discharge condition is imposed (it means vanishing tracer dispersive flow), $\left(\partial C_3/\partial z\right)_{z=L_1} = 0$. A tracer source taking into account the tracer arriving from Region 2 is introduced at $z = 0$. The left boundary condition is $C_3(z \to -\infty, t) = 0$ and no tracer at initial time is introduced. The tracer transport equation is

$$\frac{\partial C_3}{\partial t} + u_3 \frac{\partial C_3}{\partial z} - D_3 \frac{\partial^2 C_3}{\partial z^2} = S_3(t)\delta(z), \qquad (10)$$

with $S_3(t) = \dfrac{A_2\phi_2 F}{A_3\phi_3} J_2(y = L_2, t)$ and $\eta_{\pm} = \dfrac{u_3}{2D_3}[1 \pm \sqrt{1 + 4sD_3/u_3^2}]$. Here F is the fraction of the tracer amount coming from Region 2 that goes into Region 3. For $0 \le z \le L_3$ the final solution for the strong injection case is

$$\overline{C}_3 = \frac{mF}{4A_3\phi_3} \exp(\gamma L_1 + \xi_- L_2 + \eta_- L_3) \left[\exp[\eta_-(z - L_3)] - \left(\frac{\eta_-}{\eta_+}\right) \exp[\eta_+(z - L_3)] \right], \qquad (11)$$

and for weak injection it results the same expression but multiplied by the factor $\left([1 + \sqrt{1 + 4\sigma D_f/u_2^2}]/\sqrt{1 + 4\sigma D_f/u_2^2}\right)$. After the Laplace inverse transformation this expression for $\overline{C}_3$ provides the tracer concentration space profile and tracer breakthrough curve at the production well. Here the inverse will be calculated numerically employing the Stehfest algorithm.

3.- THE SOLUTION

Before numerically evaluating the Laplace inverse of $\overline{C}_i(x,s)$ we introduce the dimensionless variables $x_D = x/L$, $y_D = y/L$, $z_D = z/L$, $t_D = t/tc$ and $s_D = st_c$. Here L is an estimated length for the total tracer path length between injection and production wells, $L = L_1 + L_2 + L_3$, and t_c is a characteristic total tracer transit time. Further, we employ the dimensionless parameters

$$a_i = \alpha_i / L \;, \quad b_i = u_i tc / L \;, \quad d_i = L_i / L, \qquad (12a)$$

$$\beta = \frac{\phi_m L}{b}\sqrt{\frac{RD_m}{(L^2/t_c)}}, \quad \Theta = \sqrt{\frac{R(L^2/t_c)}{D_m}}\left(\frac{E}{2L} - \frac{b}{L}\right), \quad \frac{q_1}{q_2}, \quad F\frac{q_3}{q_2} \qquad (12b)$$

where $q_i/q_2 = u_i A_i \phi_i / u_2 A_2 \phi_2$ is fluid flow ratio of Region i and Region 2. All together they are 12 parameters. In order to analyze the model the sensitivity of the tracer breakthrough to these parameter should be examined. From this examination the relevant parameters can be obtained. At the present model development stage we have numerical solve the equations, and the mentioned analysis is still underway. A plot of the solution in terms of the space variables is shown in Figure 3 for the case of weak injection. In this figure the lengths $d_1 = 0.1$, $d_2 = 0.7$ and $d_3 = 0.2$ were chosen, together with the parameter values $a_i = 0.05$, $b_i = 0.2$, $\beta = 0$, $\Theta = 15$, $q1/q2 = 1$ and $Fq_3/q_2 = 1$ In graphs (A), (B) and (C) the three regions for 6 different times {0.01, 0.05, 0.15, 0.4, 3, 5} following the color sequence {gray, cyan, blue, green, red, orange} are displayed. In (D) the final region composition is shown for the times 3 and 5. Here l_D is the space variable. The dotted

curves in (D) correspond to a Dirac delta pulse flowing directly from the injection site in a porous medium (no source coupling approach).

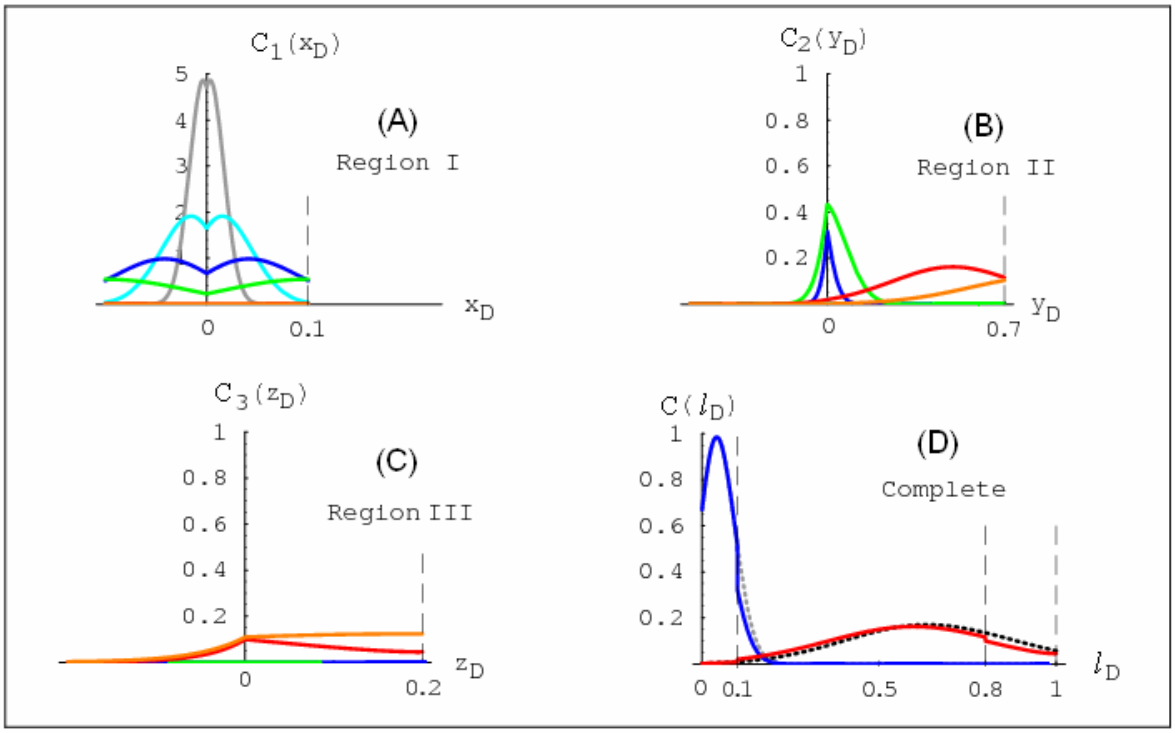

Figure 3.- Tracer concentration as function of space in the three regions in (A), (B) and (C) for six different times. In (D) the composed final tracer profile is shown for times 3 (blue) and 5 (red). The color sequence is maintained in the four plots.

Plots of the tracer breakthrough curve are presented in Figure 4. The (A), (B), (C) correspond to the three regions. In (A) the positions $x_D = 0.04$ (dotted) and $x_D = d_1$ (green) are shown. In Plot (B) the tracer concentration at $y_D = 0$ (green) and at $y_D = d_2$ (blue) is displayed. The dotted curve represents the case of a pulse in a single region system (no source coupling approach). In Plot (C) the tracer breakthrough at $z_D = 0$ (blue) and $z_D = d_3$ are shown.

SUMMARY AND DISCUSSION

A model has been developed to describe tracer transport in a faulted reservoir that considers an open flow fault and fractured porous medium in the fault region. The mathematical model has been established, in which a source coupling between regions has been introduced. The equations are analytically solved in Laplace space. Presently the inverse transformation is numerically evaluated. In the next future the model parameter sensitivity will be examined. In the limiting case of single porous media (the three regions have the same properties) a small difference is observed between the new source-coupling approach and the standard model.

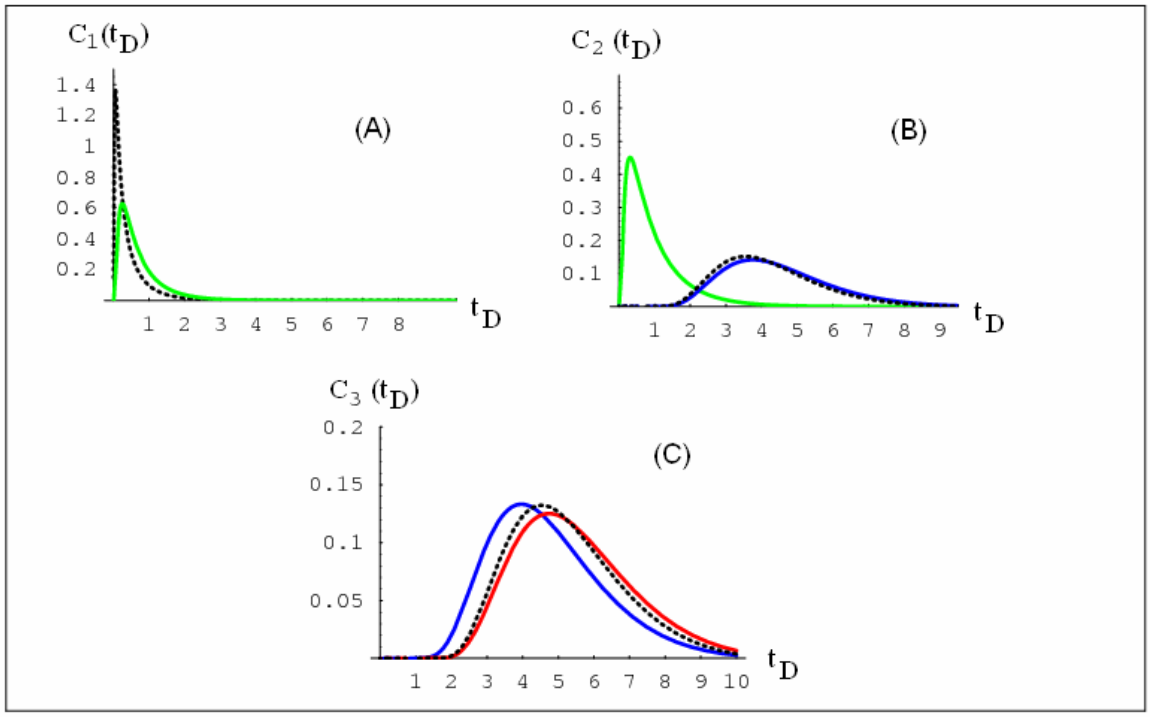

Figure 4.- Tracer breakthrough curves at different positions. The plots (A), (B) and (C) correspond to Regions 1, 2 and 3 respectively.

REFERENCES

1. Caine, J.S., Evans, J.P., Forster, C.B., 1996. Fault zone architecture and permeability structure. Geology, 24 (11): 1025-1028.
2. Coronado and Ramírez-Sabag, 2008, Analytical model for tracer transport in reservoirs having a conductive geological fault, paper accepted for publication in J. Pet. Sc. Eng.
3. Coronado M., Ramírez-Sabag J., Valdiviezo-Mijangos O., 2007. On the boundary conditions in tracer transport models for fractured porous underground formations, Rev. Mex. Física, 53, (4) 260-269.
4. Houseworth, J.E., 2004. An analytical model for solute transport in unsaturated flow through a single fracture and porous rock matrix. Lawrence Berkeley National Laboratory, paper LBNL-56342. http://repositories.cdlib.org/lbnl/LBNL-56342.
5. Maloszewski P. y Zuber A., 1985. On the theory of tracer experiments in fissured Rocks with a porous matrix, J. Hydrology, 79, 33-358.

RTD OF THE GAS PHASE IN A 130 M³ SELF-AERATED FLOTATION CELL

Francisco Díaz[1], Juan Yianatos[2], Felipe Contreras[2]
1 Nuclear Applications Department, Chilean Commission of Nuclear Energy,
P.O. Box 188-D, Santiago, Chile
2 Chemical Engineering Department, Santa Maria University,
P.O. Box 110-V, Valparaíso, Chile

ABSTRACT

In this work the direct measurement of the gas residence time distribution in an industrial 130 m³ self-aerated flotation cell is presented. For this purpose a radioactive tracer gas was produced in the 5 MW Nuclear Reactor from Chilean Nuclear Energy Commission.
The gas selected was Freon 13B1, which contains Br with a 36 hours mean life activation, which was compatible with the required times for preparation, activation, manipulation, transport and application of the gas tracer in the industrial flotation process.
The gas tracer was injected as an impulse signal at the gas (air) inlet point, located at the top of the cell, from which the gas tracer circulates first through the rotor, where the bubble dispersion occurs, and then the gas becomes well distributed over the whole cross-section area before leaving the cell.
The transient response curves obtained from these experiences showed that the air entering the cell was preferentially circulated around the upper half of the cell. It was found that the presence of circulating gas near the bottom of the large size flotation cell was not significant, therefore that gas short-circuiting into tailings was negligible. Also, it was found that the mean gas residence time was less than 20% of the pulp mean residence time, while the mixing conditions were similar for gas and pulp.

INTRODUCTION

The dramatic increase in size of industrial flotation cells, in the last years, poses new challenges related to equipment design, in terms of mixing, gas dispersion and pulp circulation, which need to be addressed.
In flotation processes the gas flowrate (typically air) is a key variable which provides the gas surface required for selective mineral particles capture and transport. For this purpose the gas flowrate must be firstly dispersed into small bubbles and the bubble swarm contacted with the pulp (mineral suspension) in order to collect the mineral particles of interest. As a result particle–bubble aggregates are generated, which are less dense than the medium, thus allowing the separation of collected minerals by true flotation. Measurement of the gas residence time distribution (RTD) is relevant because it allows the evaluation of the gas mean residence time as well as the effective gas holdup in the cell. Presence of gas recirculation through the rotor and gas short-circuiting into tailings can also be identified.
Several studies have been reported on the gas dispersion in laboratory, pilot and plant flotation cells, using gas-liquid and gas-pulp systems (i.e. Deglon et al., 2000, Gomez and Finch, 2002; Schwarz and Alexander, 2005; Dahlke et al., 2005; Nesset et al, 2006).
Measurement of the gas residence time distribution RTD in laboratory scale cells has been reported by Gal-Or and William (1966) and Thijert et al. (1992) using Helium as the gaseous tracer and thermal conductivity for Helium detection at the exit point. The gas RTD in laboratory flotation columns was measured by Molerus and Kurtin (1986) using Argon as the gaseous tracer to eliminate absorption effects in water, and the concentration of gaseous tracer exiting at the column head was measured by means of a gas spectrometer. Washi and Nojima (1990) used Freon 12 as the gaseous tracer, and to observe the concentration response, a part of the exhaust gas was continuously sampled, and gas was introduced into a FID gas-chromatograph. In these works, the importance of the gas dispersion measurement has been emphasized, because it gives new insights for correlating hydrodynamics with metallurgical performance, providing opportunities for process improvement.

Characterization of large flotation cells has been reported mainly in terms of pulp properties, liquid and solids mixing characteristics and gas dispersion (Yianatos et al., 2001, 2005, 2008; Yianatos, 2007). For example, cells of 45 m³, 130 m³ and 160 m³ has been evaluated under normal operating conditions, where local measurements of gas holdup, superficial gas rate and bubble size have been performed. However, the information on gas residence time distribution as well as gas spatial distribution inside industrial flotation equipments is rather scarce. Yianatos et al, (1994) measured the gas RTD in pilot and industrial flotation columns. For this purpose a radioactive gaseous tracer Kripton-85 was selected. Kripton-85 is a beta emitter and also has a low gamma radiation emission (514 KeV, 0.41%), with a half life of 10.7 year, which allows for a large storage time.
On the other hand, theoretical efforts have been made using CFD (Weber et al, 1999) as well as experimental designs where 3D measurements has been reported on bubble size distribution in laboratory and pilot cells (i.e. Grau and Heiskanen, 2002, 2003, 2005; Hernandez-Aguilar et al, 2004), and gas holdup measurements in a pilot flotation cell of 2.8 m^3 (Gorain et al, 1995).
In summary, there is a lack of data reported on gas RTD, as well as gas back-mixing and short-circuiting, in industrial flotation cells.
In this study, a suitable technique to measure the actual gas RTD, as well as to observe the gas circulation and short-circuiting in large size industrial flotation cells, is presented.

EXPERIMENTAL

The experimental work was developed at El Teniente Division, Codelco-Chile, in the rougher flotation circuit consisting of 4 parallel banks. Each bank consists of seven 130m³ self-aerated mechanical cells. The gas RTD was measured in the first cell of the third bank.

TRACER GAS SELECTION AND DEVELOPMENT

Bromine Tri-Fluor-Methane (CF_3Br), also called Freon 13B1, was selected as the gaseous tracer because is an inert gas which only contains Bromine (Br) as activating element with a half life of 36 hours, which is compatible with times required for preparation, activation, manipulation, transport and gas application in the industrial plant (International Atomic Energy Agency, 1990).
The gas was firstly stored in a stainless steel tank of special design, Fig. 1, and then activated by direct irradiation in a 5MW Nuclear Reactor, RECH-1, of the Chilean Commission of Nuclear Energy. The time for gas activation depends on the amount of tracer or activity required for each particular application.
After neutrons irradiation in the nuclear reactor the radioactive gaseous tracer was transferred into a stainless steel cylinder of special design, Fig. 2, which was used for the radioactive tracer transport to the industry, where the gas was finally transferred to the injection device. Figure 3 shows the system for radioactive gas transfer and storage into the transport cylinders. The gas transfer was developed by means of vacuum provided by mechanical displacement and cooling.

Fig. 1 Tank for gas storage and irradiation

Fig. 2 Cylinder for radioactive gaseous tracer transport

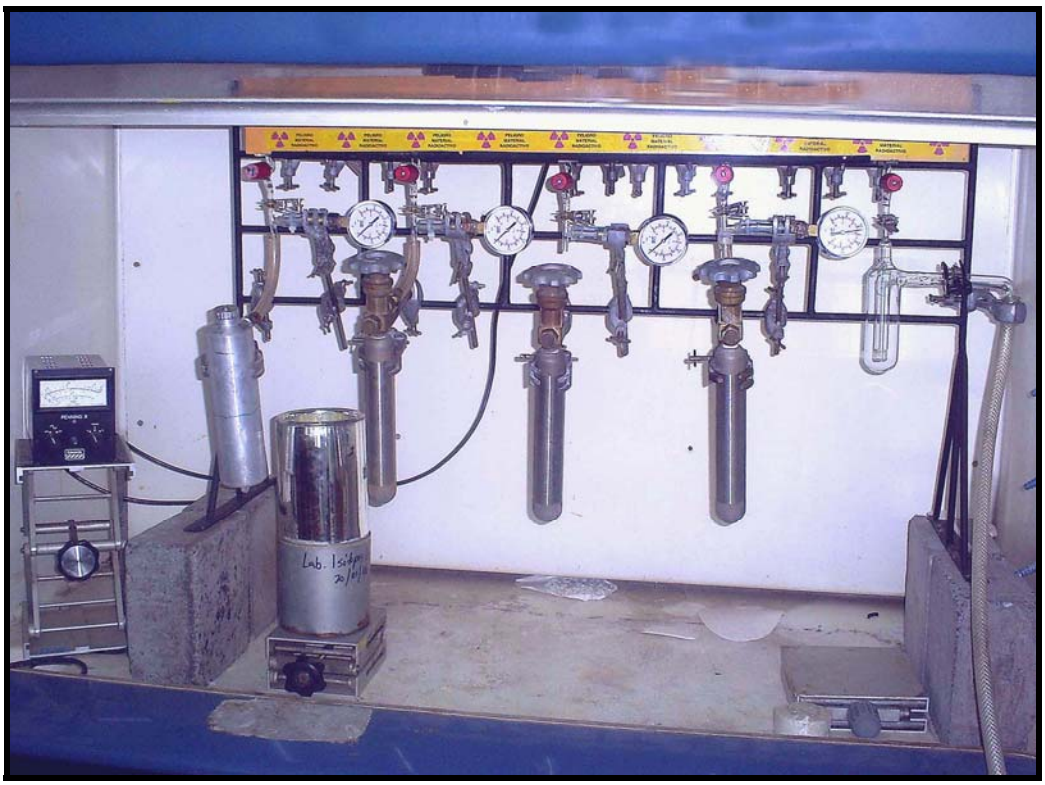

Fig. 3 System of radioactive gas transfer and storage in transport cylinders

In summary, the procedure for production and application of the radioactive gaseous tracer consists of:

- Gas storage in the irradiation tank
- Gas irradiation in the nuclear reactor
- Radioactive gas storage in transport cylinders
- Radioactive gas storage in the injection device
- Radioactive gaseous tracer injection

INJECTION SYSTEM

The injection system, shown in Fig. 4, consists of a cylinder where the gas contained in the transport container was transferred by means of a valve system which allows the regulation of the proper charge of radioactive gas tracer for each experience, using mechanical vacuum and cooling. For the present study 10 mCi (0.37 GBq) of Br-82 was required in Freon 13B1. The radioactive tracer technique consists of the injection of a gas impulse signal through the gas (air) inlet, consisting of a 25.4cm (12 in.) pipe located at the top of the cell, Fig. 5, which allowed the tracer to circulate first through the rotor, thus being well distributed over the whole cross-section area before leaving the cell upwards by froth overflowing and collapse.

Fig. 4 Gas injection system

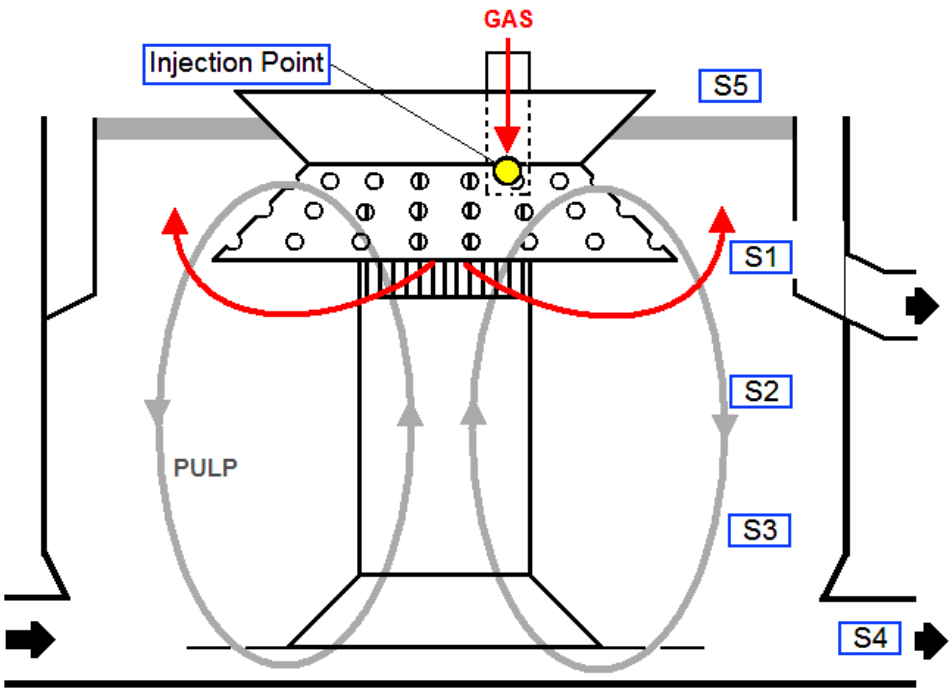

Fig. 5 Cut view of the industrial flotation cell

ON-LINE CONCENTRATION MEASUREMENT OF GASEOUS TRACER

The tracer concentration inside the cell, as well as the presence of tracer leaving the cell at the concentrate and tailings streams, was on-line recorded by non-invasive sensors, provided with scintillating crystal sensors of NaI(Tl) of 1x1.5inch, Saphymo-SRAT (Massy, France).
After the gas impulse injection, the tracer response inside the cell was measured by means of three sensors: S1, S2 and S3, located at 70, 220 and 370cm below the cell lip level, respectively. Also, sensor S4 was located on the tailings flow discharge pipe (450cm below the cell lip level), and sensor S5 was located 10cm above the top of the froth to observe the upper gas discharge. Figure 5 shows the location of each sensor in the cell.

RESULTS AND DISCUSSION

Figure 6 shows the transient concentration of radioactive gas at different locations inside the cell. Sensor S1 shows the larger concentration of radioactive gas tracer in the annular section located below the pulp/froth interface, in front of the rotor discharge. This sensor see the gas tracer moving from the rotor directly upwards to the pulp/froth interface as well as the fraction of gas which firstly moves downwards, entrained by the pulp circulation, but finally return to the upper part of the cell. Sensor S2 also see a significant fraction of tracer recycling through the annular section below the rotor discharge level. Finally, sensor S3, located at 0.8m above the bottom level, showed that the amount of gas tracer reaching that level was negligible. The last observation was also confirmed by the reading of sensor S5, located out of the cell on the discharge pipe, where the presence of gas tracer was nil.
These observations confirm that the gas bubbles did not recycle through the false bottom into the riser tube, as the case of pulp recycling. Thus, it was observed that the gas preferentially concentrates in the upper part of the cell before leaving the cell throughout the froth.

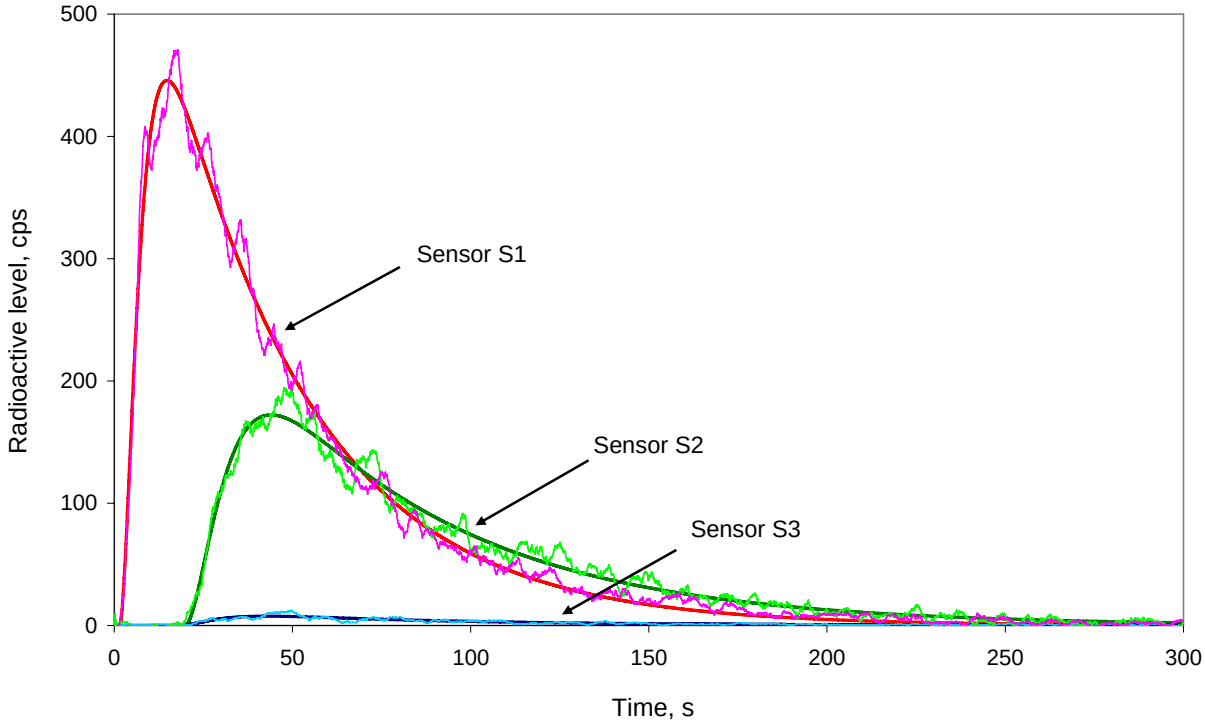

Fig. 6 Transient gas concentration inside the cell

LOCAL GAS HOLDUP MEASUREMENT

In order to estimate the gas holdup in the cell, for calibration purposes, local gas holdup measurements were performed using a manual device, Fig. 7, as described by Yianatos et al. (2001).

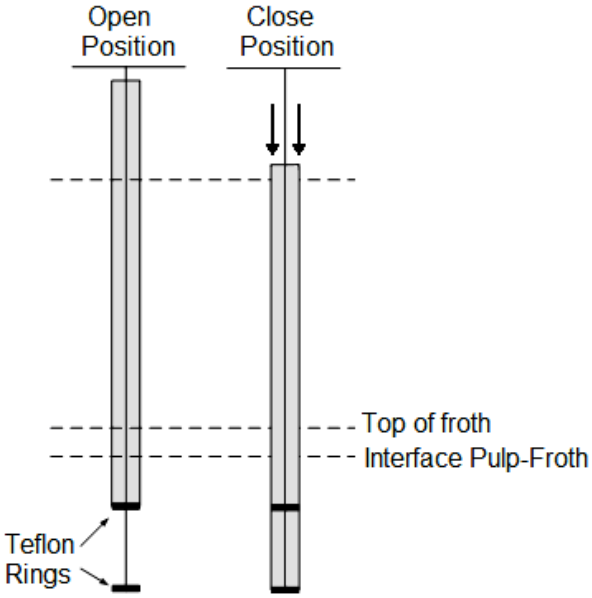

Fig. 7 Local gas holdup measurement

Table 1 shows the gas holdup observed at 60cm below the cell lip, for two radii (1.91 and 2.56m), and superficial gas rate of 1.3 cm/s, referred to the cell cross-section at the pulp-froth interface level. The overall gas volumetric flowrate entering the cell was evaluated at the cell air admission pipe, Fig. 5, by means of a digital gas velocity meter TSI, model 8360-M-6B. Thus, the radial gas profile in the admission pipe was directly measured and the overall gas flowrate was calculated by integration. From Table 1 a slight decrease in gas holdup, less than 1%, was observed at the higher radii approaching the cell wall.

Table 1. Air holdup measurement

Deep [m]	Radius [m]	Gas Concentration %	Mean [m]	Standard Deviation
0,6	1,91	14,6	14,3	0,46
		14,6		
		13,8		
	2,56	13,8	13,5	0,46
		13,0		
		13,8		

GAS CONCENTRATION ESTIMATION FROM RADIOACTIVE TRACER MEASUREMENTS

The three sensors installed inside the cell were equally collimated to observe the pulp at different levels directly. Measurement of local radioactivity (cps) was then proportional to the relative amount of tracer in the surroundings of the scintillating crystal sensors. Thus, the integration of the total radiation observed at each local sensor during tracer tests allowed the estimation of the relative presence of gaseous tracer at a certain level in the cell.

Table 2 shows the resulting data from sensors S1, S2 and S3, in terms of total local radiation (area under the curve, Fig. 6), local gas volumetric fraction relative to sensor S1, and the normalized gas holdup calculated by calibration, using the direct measurement of gas holdup (ε_G=14%) near sensor S1, at 70cm below the cell lip level.

Table 2. Gas holdup estimation (reference: ε_G =14% at 70 cm)

		Experience 1			Experience 2			Experience 3		
Sensor	Deep	Area	Volume Fraction	Normalized holdup %	Area	Volume Fraction	Normalized holdup	Area	Volume Fraction	Normalized holdup
1	70	2,54E+07	1,00	14,00	1,92E+07	1,00	14,00	5,92E+07	1,00	14,00
2	220	1,38E+07	0,54	7,61	1,11E+07	0,58	8,12	2,91E+07	0,49	6,90
3	370	5,85E+05	0,023	0,32	4,50E+05	0,023	0,33	1,32E+06	0,022	0,31
4	450	0,00E+00	0,00	0	0,00E+00	0,00	0	0,00E+00	0,00	0
5	-10	3,67E+07	1,44	--	2,49E+07	1,30	--	7,79E+07	3,07	--

The area under the curve calculated for sensors S4 and S5, was not directly comparable with the area of internal sensors, because geometry and transmittance (medium) between the gaseous tracer and sensors was different. Even so, the observation of a nil signal in sensor S4 (tailings pulp discharge) confirms that the presence of tracer near the bottom of the cell was also negligible and there was no gas circulation into the riser tube.

Figure 8 shows the gas holdup profile estimated along the pulp zone in a 130 m^3 flotation cell.

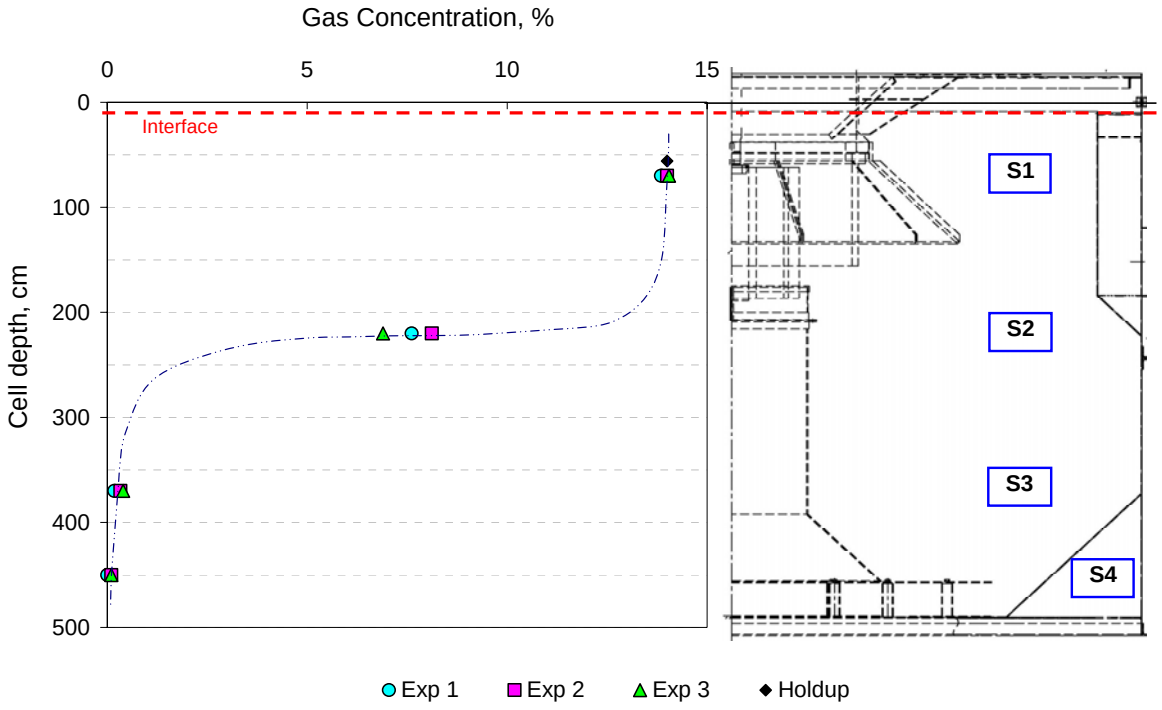

Fig. 8 Gas holdup profile in an industrial flotation cell

RESIDENCE TIME DISTRIBUTION OF THE GAS PHASE

Figure 9 shows the data registered in one of the three tests on gas residence time distribution observed at the gas output sensors S4 and S5.

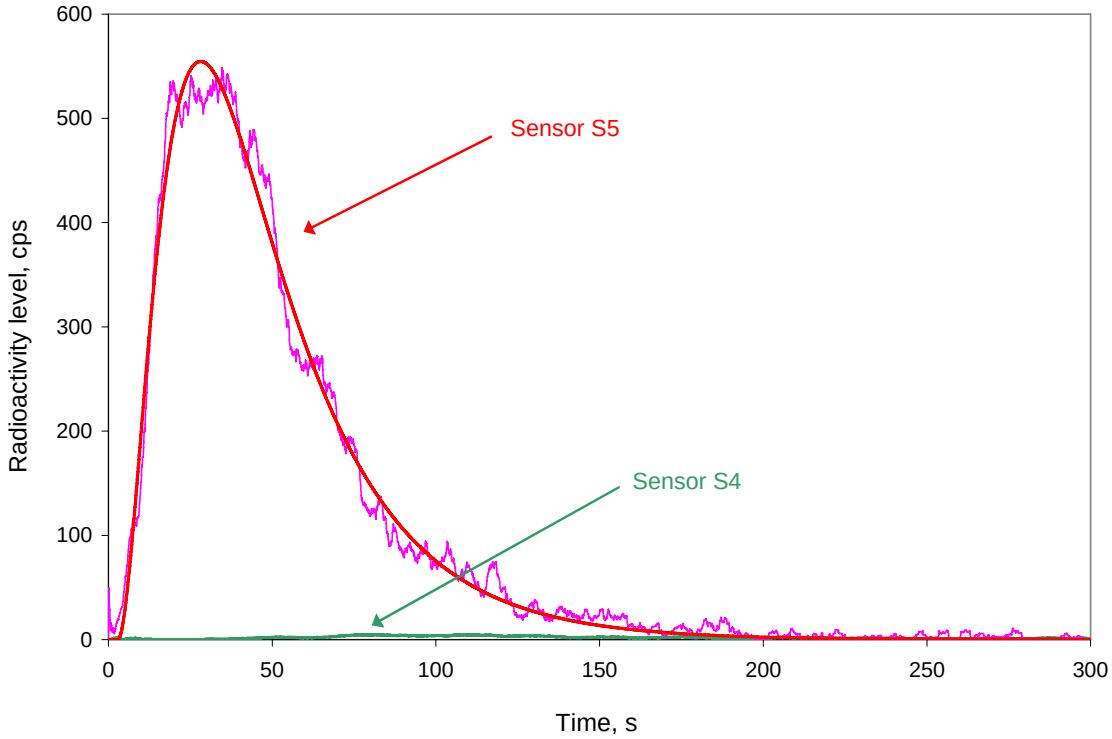

Fig. 9 Gas residence time distribution data and model fit (sensor 5)

Also, in order to characterize the gas mixing a tank in series model, Eq. (1), consisting of one large perfect mixer in series with two small perfect mixers, was used to fit the experimental data. This kind of model has been used to describe the pulp mixing in single mechanical cells and columns (Yianatos et al., 2005, 2007).

$$E(t) = \frac{\left[\frac{-(t-\tau_P)}{\tau_S} - \alpha\right] e^{\left[\frac{-(t-\tau_P)}{\tau_S}\right]} + \alpha e^{\left[\frac{-(t-\tau_P)}{\tau_L}\right]}}{(\tau_L - \tau_S)}$$

where

$$\alpha = \frac{\tau_L}{(\tau_L - \tau_S)}. \qquad (1)$$

where T_L is the residence time of the large mixer, T_S is the residence time of the small mixer and T_P is the lag time.

Numerical results for the three gaseous tracer tests, developed in the 130m^3 rougher flotation cell, are presented in Table 3. The mean residence time was 51.1±2.2 seconds, which shows good repeatability. Comparison of these results with the mean pulp residence time, typically around 300 seconds for this type of operation, showed that the gas residence time was less than 20% of the pulp residence time. Also, the good model fit, Fig. 6, and results presented in Table 3 showed that the gas mixing characteristics are similar to the pulp mixing.

Table 3. Residence time distribution model parameters (Eq. 1)

Experience	Tau large, τ_L	Tau small, τ_S	Delay, τ_P	Mean residence time [s]
1	29.61	8.48	6.84	53.41
2	36.97	4.35	5.24	50.91
3	29.07	8.53	2.85	48.98
			Average	51.1 ± 2.2

CONCLUSIONS

From direct measurements of gas residence time distribution in a 130 m^3 flotation cell, using the radioactive gas tracer Freon 13B1, was observed:

- the gas bubbles preferentially concentrate in the upper part of the cell
- the gas bubbles recycle through the false bottom into the riser tube was negligible
- the amount of gas reported to the tailings was nil
- the gas residence time was less than 20% of the pulp residence time
- the gas mixing was similar to that of the pulp

Also, the local gas holdup below the pulp-froth interface was directly measured and it was about 14%.

ACKNOWLEDGEMENTS

The authors are grateful to El Teniente Division Codelco-Chile for providing access to their plant and for valuable assistance in the experimental work. Funding for process modelling and control research is provided by CONICYT, project Fondecyt 1070106, Santa María University, project 270522, and Chilean Commission of Nuclear Energy.

REFERENCES

1. Dahlke, R., Gomez, C., Finch, J., 2005. Operating range of a flotation cell determined from gas holdup vs. gas rate. Minerals Engineering, Vol. 18, 977-980.
2. Deglon, D., Egya-Mensah, D. and Franzidis, J., 2000. Review of hydrodynamics and gas dispersion in flotation cells on South African platinum concentrators. Minerals Engineering, Vol.13 (3), 235-244.
3. Gal-Or, B., William, R., 1966. Gas Residence Time in Agitated Gas-Liquid Contactor. Experimental Test of Mass Transfer Model. Ind. Eng. Chem. Proc. Des. Dev., 5(1),15-19.
4. Grau, R., Heiskanen, K., 2003. Gas dispersion measurements in a flotation cell. Minerals Engineering, 16 (11), 1081-1089.
5. Grau, R., Heiskanen, K., 2002. Visual technique for measuring bubble size in flotation machines. Minerals Engineering, 15 (7), 507-513.
6. Grau, R., Heiskanen, K., 2005. Bubble size distribution in laboratory scale flotation cells. Minerals Engineering, 18 (12), 1164-1172.
7. Gomez, C., Finch, J., 2002. Gas dispersion measurements in flotation machines. CIMM Bulletin, Vol. 95, 1066, 73–78.
8. Gorain B., Franzidis J., Manlapig E., 1995. Studies on impeller type, impeller speed and air flow rate in an industrial flotation cell, Part 2: Effect on gas hold-up, Minerals Engineering, Vol. 8, 1557–1570.

9. Hernandez-Aguilar, J.R., Coleman, R.G., Gomez, C.O. and Finch, J.A., 2004. A comparison between capillary and imaging techniques for sizing bubbles in flotation systems. Minerals Engineering, Vol. 17, 53–61.
10. International Atomic Energy Agency. Guidebook on Radioisotopes Tracers in Industry. Reports Series Nº 16, Vienna. 1990.
11. Molerus, O., and Kurtin, M., 1986. Chemical Engineering Science, Vol. 41 (10), 2693-2698.
12. Nesset J.E., Hernandez-Aguilar J.R., Acuna C., Gomez C.O. and Finch J.A., 2006. Some gas dispersion characteristics of mechanical flotation machines, Minerals Engineering, Vol.19, 807–815.
13. Schwarz S., and Alexander D., 2005. Gas dispersion measurements in industrial flotation cells, Minerals Engineering, Vol. 19, 554–560.
14. Thijert, M. and Oyevaar, M., Kuper, W., Westerterp, K., 1992. Residence time distribution of the gas phase in a mechanically agitated gas-liquid reactor. Chemical Engineering Science, Vol. 47 (13/14), 3339-3346.
15. Wachi and Nojima, 1990. Gas-phase dispersion in bubble columns. Chemical Engineering Science, Vol. 45 (4), 901-905.
16. Weber, A., Walker, C., Redden, L., 1999. Scale up and design of large-scale flotation equipment. In Advances in Flotation Technology, Annual SME Meeting, Parekh, B.K., and Miller, J.D., Eds., SME Inc. Pub., USA, pp. 353-369.
17. Yianatos J., Bergh, L., Tello, K., Díaz. F., Villanueva, A., 2008. Residence time distribution in single big industrial flotation cells. Minerals & Metallurgical Processing Journal, Vol. 25 (1), 46-52.
18. Yianatos J., 2007. Fluid flow and kinetic modelling in flotation related processes: columns and mechanically agitated cells. Chemical Engineering Research and Design, Vol. 85 (A12), 1-13.
19. Yianatos, J., Bergh, L., Díaz, F., Rodríguez J., 2005. Mixing characteristics of industrial flotation equipments. Chemical Engineering Science, Vol. 60 (8/9), 2273-2282.
20. Yianatos, J., Bergh, L., Condori, P., Aguilera J., 2001. Hydrodynamic and metallurgical characterization of industrial flotation banks for control purposes. . Minerals Engineering, Vol.14 (9), 1033-1046.
21. Yianatos, J., Bergh, L., Durán, O., Díaz, F., Heresi, N., 1994. Measurement of residence time distribution of the gas phase in flotation columns. Minerals Engineering, Vol.7 (2/3), 333-344.

APPLICATION OF RADIOACTIVE TRACERS IN PULP FOLLOW UP DURING A DIGESTER BLOWING IN A MULTIPLE BATCH-DIGESTER PULP MILL

Francisco Díaz V.[33], Darren Ledermann M.[34], Hernán Arriagada C.[35]

ABSTRACT

The bottom blow pipelines at Arauco Pulp Mill Line 1 Plant presented severe damage at the blow valves in a repetitive fashion after performing a major process and piping modification in March 2007. The geometry of the blow tank, where top and bottom blow pipelines discharge gas and liquor from the digesters, was modified in such a way that top and bottom blow line flows faced each other in the circular tank. Several tests were performed on-site to determine the cause of the damages. In all tests, liquor appeared downstream of the valves in situations where the line should have been empty. Such phenomena could have been explained by choked flow in the lines or by crossing liquor flows at the blow tank head.

To determine the real cause of the appearance of liquor in the lines, an iodine-based radioactive tracer was added during the filling phase of one of seven digesters to its feed material so as to follow the flow of the outgoing liquor during the discharge phase. Sensors were placed at all bottom blow lines and at top and bottom blow inlets near the blow tank head so as to monitor possible crossing flows. This test was performed twice, injecting the tracer on two different digesters so as to measure the phenomena under slightly different circumstances. Gathered data showed the presence of crossing flows among the top and bottom blow lines, causing liquor to appear in pipelines that should have been free of any fluid. Choked flow was ruled out due to these results.

By performing two tests it was possible to determine that the phenomena was not restricted to the discharge of one digester vessel, but was associated to all seven digesters in the plant because of the geometric configuration of the nozzles at the blow tank. Due to the characteristics of the tracer used in the tests, it was possible to determine that top blow flows, which should be mainly gas, carried more liquid than expected. Also, by analyzing signal intensity at the discharge sensor it was possible to quantitatively determine the degree of homogenization of the mixing in the digester. In the end, crossing liquor flows were ruled as the cause for the problem in plant operation thanks to the application of tracing techniques, leading to a final design solution for blow tank and pipeline geometry.

I. INTRODUCTION

The bottom blow pipelines at Arauco Pulp Mill Line 1 Plant presented severe damage at the blow valves in a repetitive fashion after performing a major process and piping modification in March 2007. The geometry of the blow tank, where top and bottom blow pipelines discharge gas and liquor from the digesters, was modified in such a way that top and bottom blow line flows faced each other in the circular tank [1]. Several tests were performed on-site to determine the cause of the damages. In all tests, liquor appeared downstream of the valves in situations where the line should have been empty. Such phenomena could have been explained by choked flow in the lines or by crossing liquor flows at the blow tank head.

The fact that two completely different mechanisms could be causing the appearance of liquor at the blow valves complicated the decision on what corrective measures could be taken, since both mechanisms would require completely different solutions. Therefore, it was of the utmost importance to rule out which filling mechanism was causing the liquor to appear in the lines so as to perform the right corrections during the March 2008 full mill stop [2]. For this purpose, a radioactive tracer test was performed in order to verify which one was the active filling mechanism at the mill.

[33] Industry and Environment Section Chief, Comisión Chilena de Energía Nuclear. fdiaz@cchen.cl
[34] Mechanical Engineer, AMEC-Cade Engineering Consultants. darren.ledermann@amec.com
[35] Chief of Engineering and Construction, Celulosa Arauco y Constitución. harriagada@arauco.cl

II. PROCEDURE

The main objective of the test was to determine the effective destination of the blown up pulp since it was clear that not all of the blown material actually reached the blow tank. The test was designed so as to answer this question with the available resources. The test was performed with the use of 11 radioactive tracer sensors connected to a portable logging computer and an iodine-based tracer, I-131 (1.85 GBq) like NaI, that was manually injected into a particular digester during its chip fill phase. The choice of the sensor positioning and the digester to be marked with the tracer was made so as to effectively study the behavior of the points that had been subject more frequently to failures since the major design change of the mill [3].

The aforementioned procedure allowed the test to show whether the flows were effectively crossing among top and bottom blow lines at the blow tank. This placement also allowed the testers to determine which lines were more prone to receive liquors from the crossing flows. The procedure considered performing the top and bottom blows from the injected digester and then the blowing of the next digester in the sequence, which was free from any tracer. This allowed the testers to check the behavior of the system in a more global way. This was done in two days, first tracing digester number 6 and logging the behavior during the blows of digesters 6 and 7 (which share common blow lines) and later tracing digester number 6 and logging the behavior during the blows of digesters 7 and 1 (which do not share any blow lines at all). In this way, the behavior of common and uncommon lines was tested for further analysis.

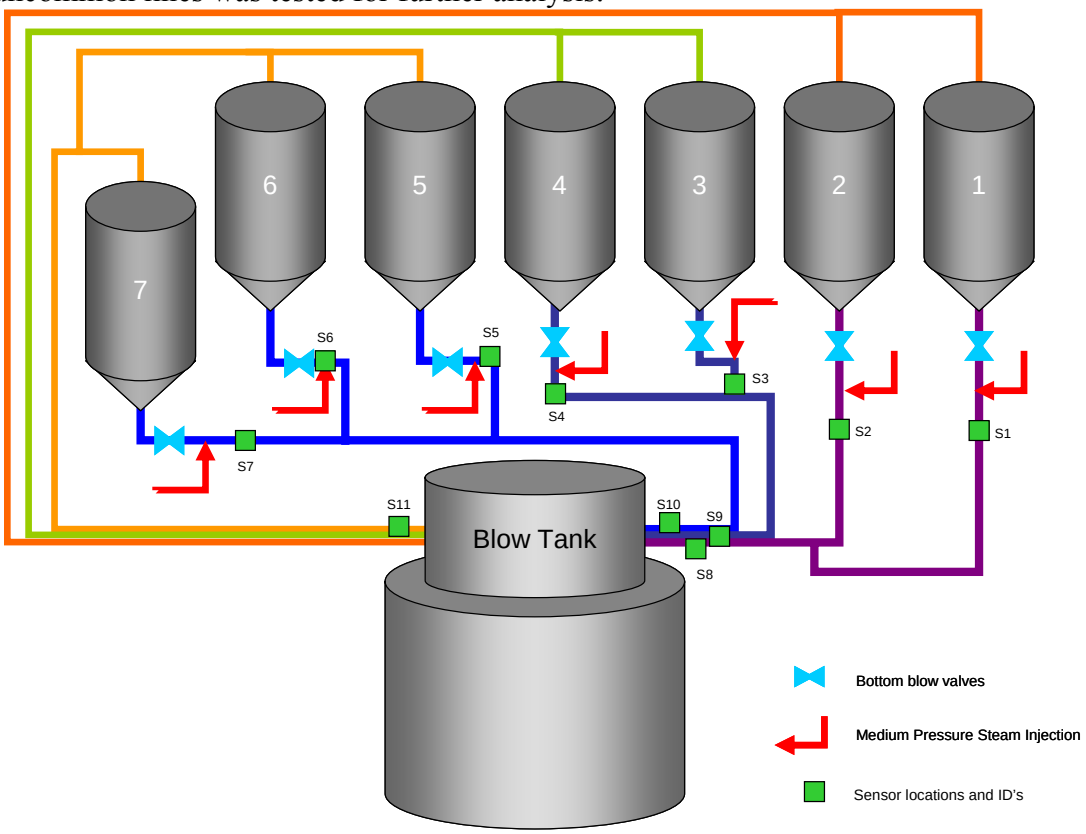

Figure 1. Schematic showing the plant connections and sensor placement

III. PERFORMING OF TESTS

Tests were carried over by injecting the tracer into the objective digester during the chip fill phase of the process. The cooking of the chips takes place for about two hours, in which all of the elements are mixed inside the digester while heat and pressure builds up to temperatures of around 180°C and pressures reaching 7 bar. This allows for the tracer to be homogeneously mixed with all other elements during this time period. Once cooking is completed, the digester is top blown in order to reduce its internal pressure from 7 to 5.6 bar by releasing gas into the blow tank, loosening the contained mass inside to allow for an easier flow during the bottom blow. After the top blow is

done, the bottom blow starts, releasing the pulp from the digester into the blow tank. The test is therefore designed to check for unwanted liquid flow in the top blow operation and to check for liquids reaching the bottom sections of all bottom blow lines.
Logging of tracer measuring was performed in a combined effort with the plant control room operators in order to ensure proper logging of the results. All process variables were kept at normal operating values for the measurements to be a faithful representation of the ongoing process. The tests were performed in two separate days due to the long time elapsed between the chip filling and the actual blow. Consecutive tests were not considered since it was necessary to isolate the source of the traced liquids and this was not possible if two consecutive tests were performed. The delay between tests allowed for all pipes to be tracer free for the second test, not altering the results.
Base signals were recorded previous to the logging of the actual tests. This allowed identifying the natural radiation present at the site that could be monitored by the sensors, therefore allowing this effect to be accounted for in the interpretation of the results.

Figure 2: (a) Manual tracer injection at chip fill bin
(b) Sensor placement in bottom blow line

IV. RESULTS

The measured results of both tests could be read and interpreted in many ways. One of them was to represent all of the sensors' data simultaneously in independent graphs. Due to the large signal variation, it was impractical to overlap all of the data into independent streams in a single graph. The other way was to isolate the events for each sensor and assign the event to its "physical" location for a given instance of the test. Both ways were used to interpret the data since each way of representation seemed simpler to understand for a fraction of the analyzing team. This does not alter the interpreted results, but demonstrates that there is no standard way of presenting such test results for simplifying the analysis, proving that the best way to present data is in a way in which you can interpret the given data. Figure 3 is an example of a physical representation of the signals measured during the bottom blow of digester 6 with the tracer injected in digester 6. The measured data allowed determining the presence of crossing flows and the destination of such flows.

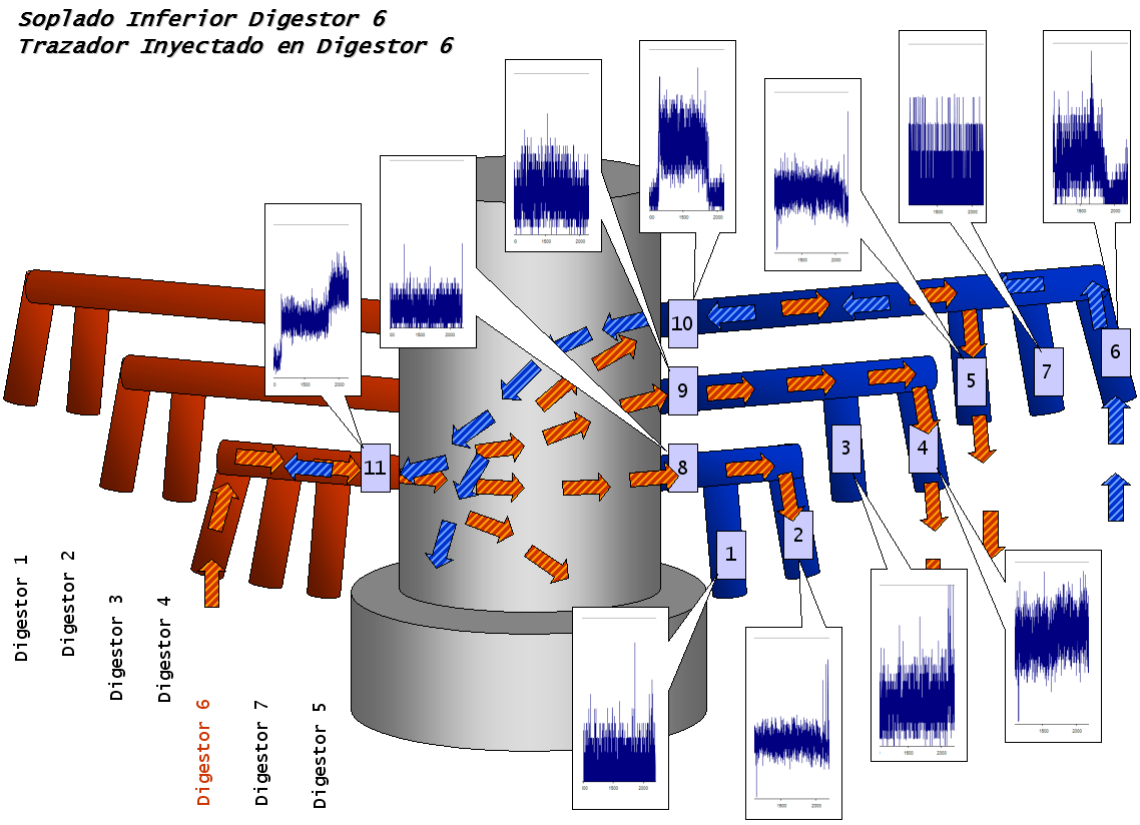

Figure 3: Example of graphical representation of results for a given event

V. ANALYSIS

A proper interpretation of the results is only possible by combining process knowledge with experience from the performing of previous other tracer tests. In this particular case, several events that were pointed out by the tracing experts as anomalies were actually devised as normal operating conditions by the process experts and vice versa. This integration of skills allowed the analyzing team to realize that the problem of crossing flows was far worse than originally expected, completely ruling out choked flow or internal flow blocking theories. Flow of considerable amounts of liquids was identified in the top blow processes from both traced digesters, in circumstances that these flows should consist mainly of gases. Signal peaks were measured during the top blow in both the sensors placed at the exit of the top blow line and in the sensors placed at the exit of the bottom blow lines. Even though it is impossible to perform a mass balance out of the performed test, sensors arrayed in the bottom blow lines proved that liquors exhausted in the top blows was sufficient enough to fill the lower horizontal section of several bottom blow lines, accounting for more than three meters of 12” pipes filled with cross flowing liquors. The measuring of the events occurring during the blows of the next digester in the sequence allowed to identify that more liquid entered the bottom blow lines from crossing flows. It should be noted that this was observed by a reduction of signal levels in the bottom line sensors, since part of the measured traced liquid diluted with untraced liquid from the unmarked digester. It was not possible to determine the level reached by the liquors in the bottom blow pipe since the sensors were placed in the horizontal part of the line, so once this part was filled with traced liquor, any rise in liquor level was not going to be reflected in the measurements. This leads to the idea that if new tests are to be carried out, sensors could be placed in the vertical portion of the pipes to measure if traced liquor passes on filling the horizontal line and, if enough liquid passes on, a one-point measurement of the level could be established to determine the height of the liquor column.

As a side product of the test, the measurements obtained for the bottom blow line of the traced digester were able to account for the homogenization level of the mixing of the chips and chemicals

in the digester during the cooking process. The graph in Figure 4 shows one of these measurements. Said measurement monitored continuously the flow of the outgoing traced pulp into the blow tank, so, if the mixing process inside the digester was perfect, a regular decaying signal should be observed. However, the process is not a perfect mixing one. Note that, prior to the starting of the blow, there is a constantly rising level metered by the sensor. This corresponds to base radiation detected by the sensor caused by the large mass of traced pulp that lied directly next to the sensor. Once the blow starts, there is a notorious rise and drop of the signal level. This occurs because, at first, a traced plug exits the digester, followed by a plug of pulp with the poorest mixing level within the digester, explaining the decrease in tracer signal. After such plug exits the digester, the signal recovers to a new higher level to finally decrease as the blow progresses and ends. Thanks to this interpretation of results, it could be determined that the mixing in the digester occurred within the expected levels of operation.

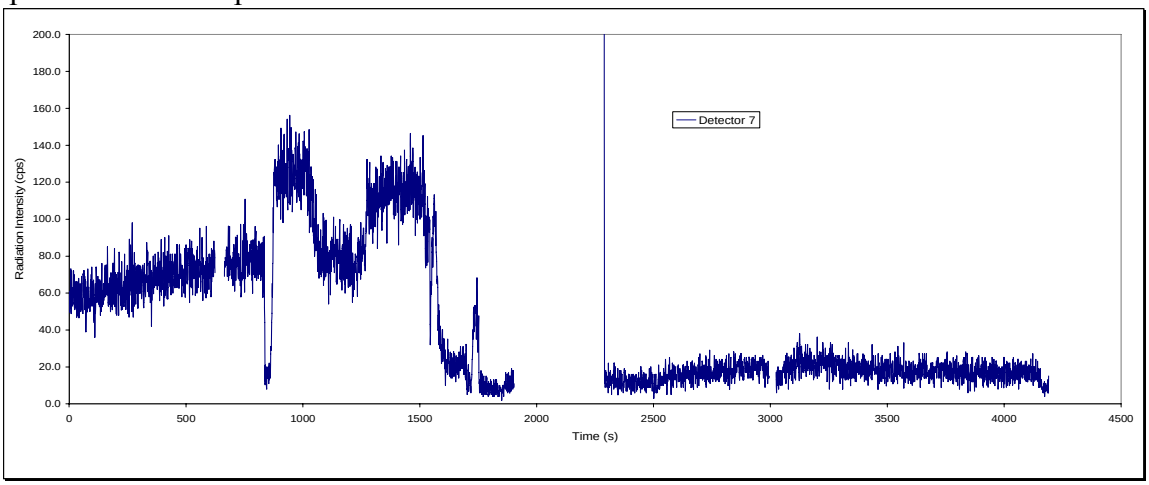

Figure 4: Signal metering of the bottom blow line of digester 7 during the consecutive top and bottom blows of digesters 7 and 1

VI. CONCLUSIONS

Thanks to the results derived from the radioactive tracer tests, the main cause for the presence of unwanted liquor in the bottom blow lines of Line 1 of Arauco Pulp Mill was ruled to be crossing flows generated at the blow tank due to its geometry. The success of the tests allowed taking the right decision on which way to modify the existing piping and blow tank geometry during the full mill stoppage of March 2008. The test also allowed verifying the way mixing is performed inside the traced digesters. Despite the fact that this was the first effort in Chile to perform a radioactive tracer test in a pulp mill, results were satisfying thanks to the combined effort of mill personnel and tracing experts. It should be noted that a correct analysis of the data was only possible by combining the expertise from both the process and tracing areas, since each group on its own would have most certainly missed details that could have mislead the analysis of the results. This experience is a great example on how cooperation among teams allows for satisfying results while performing a complicated task such as a tracer test in a normally running pulp mill.

VIII. ACKNOWLEDGEMENTS

The authors would like to thank Arauco's Line 1 Fiberline manager Felipe Quintana, AMEC-Cade's consultants Alejandro Steiner and Jukka Kiviaho, and CCHEN's Industry and Environment team for making this experience possible.

IX. REFERENCES

[1] R. E. Bergstrom, Pulp and Paper Manufacture: The Pulping of Wood, McGraw-Hill, 1969.

[2] D. Ledermann, Procedimientos, Objetivos y Resultados Obtenidos en la Realización de Pruebas de Trazado Radioactivo en la Línea 1 de Planta Arauco. CADE-IDEPE internal report for Arauco Project N°2135, November 2007.
[3] International Atomic Energy Agency. Guidebook on Radioisotopes Tracers in Industry. Reports Series Nº 16, Vienna. 1990.

COMPARATIVE STUDY OF THE CATALYTIC POWDER BEHAVIOR AT TWO DIFFERENT RISERS OF FCC PLANTS.

Francisco Pablo Ramírez García[36], Taller de Física de Radiaciones,
Facultad de Ciencias, UNAM.

RESUME

Comparative studies of the flow behavior of the catalytic powder at the "RISER" at two Fluid Catalytic Cracking ("FCC") Plants were made, using four radioisotope methods; radiotracers, gamma scanning, tomography and correlation flow measurement. These techniques allowed determining the internal behavior of the catalyst and reaction gases inside the RISER.
The internal behavior can be seeN in eight graphs, three for the radiotracers, two for the gamma scanning and three groups of tomographs obtained from two FCC Plants.
Time contact of the charge and catalyst at the RISER were measureD with radiotracers, the variations of density a long the RISER's vertical axis were obtained with gamma scanning and several horizontal tomographyc cuts were obtained at different heights of the RISER. With this information, acquired from the two different RISER Plant design (denominated FCCI and FCCII), it was possible to evaluate and compare their fluid behavior, that sustained the following assertions:
Reaction gases and catalyst at the Riser have different residence time distribution.
Deficient mixture between the reaction gases and the catalyst that are due to canalizations at the two RISERs, showing that there are volumes were the catalyst is too concentrated and others were it is diluted, these volumes were along the vertical axis and were also manifested in the horizontal cuts.
Under the last observation, and the analysis of the tomograph obtained, above the nozzle section were supposed that the nozzle section did not operate uniformly, for this reason it was necessary to measure the flow rate of water vapor and of the charge at each independent nozzle, that injects the charge to the RISER. To satisfy this aim the method "correlation flow measurement" was employed, finding that all flow rates were different, the worse case was nozzle 6, at FCCII, which had a flow double than the mean average of the other five nozzles.
After adjusting the control flow valves, for the charge and water vapor, for each nozzle, it was possible to increase 17% the production of gasoline, at FCCI. Also, it was possible to find out hydrodynamic design differences between both designs.
This work was done at the IMP for PEMEX in 1998 and 1999.

BACKGROUND

The reasons that gave origin to this study were:
The convenience of obtaining, under stable conditions, the behavior of: the catalyst and reactive gases in the RISER of two FCC Plants, the FCCI has a design know as Model "F" and the FCCII is known as Model "UOF" or UltraOrthoFlow, located at "Miguel Hidalgo" Refinery, PEMEX.
Having for both plants FCCI and FCCII Plants the same determinations in their RISERs, will allow a comparative analysis of the behavior of the catalyst and reactive gases.
In addition, to investigate if there were hydrodynamical differences in the operation between the nozzles of load of unit FCCI and the nozzles installed in unit FCCII.
After satisfying the first points, it was decided to adjust the flows of feed and dispersion vapor at each nozzle for unit FFCI and evaluate their impact.

INTRODUCTION

The methods Gamma Scanning, Radiotracers and Tomography have proven their utility in the study of FCC units (Ref. 1, 2 & 3), not only because they can be used during the normal operation of the plants but because they allow obtaining data on the densities of the mixture of fluids, their concentrations and their times of residence. All these characteristics provide information on the

[36] Colaborate with the Instituto Mexicano del Petróleo (IMP), until 2003.

hydrodynamic state of the reactors of units FCC. For these aims the two FCC units at the Refinery "Miguel Hidalgo" were chosen. Also to take advantage of the knowledge obtained in previous reports (Ref. 4 to 9).

RADIOISOTOPE METHODS APPLIED

The techniques applied to determine the Hydrodynamic state of the catalyst and reactive gases inside the RISER, were:
Radiotracers to measure the Residence time distribution, which allows knowing the existence of canalizations, dead volumes and mean residence time of reaction gases and catalyst in the RISER.
Gamma Scanning that gives the density of the mixture of catalyst and reaction gases along the RISER's height.
Computerized Axial Tomography to obtain the transversal cuts of the RISER, allowing identification of the existence of high and low densities of the catalyst and reaction gases mixture, that suggest possible canalizations of the reaction vapors.
Correlation flow velocity measurement to determine the flow rate of feed and water vapor that receives each nozzle.

DESIGN CHARACTERISTICS OF THE TWO FCC RISERS MODELS "F" & "UOF"

CHARACTERISTIC	MODEL F	MODEL UOF
Capacity (BPD)	40,000	40,000
Catalyst Inventory (Ton)	180,000	230,000
RISER's length* boot-crossover	111' 3½"	114' 3"
Catalyst flow (Ton/min)	25	27
Distance* Regenerator-RISER	19' 0"	23' 0"
Distance* PV2-RISER	13' 0"	13' 6"
Separation Boot-Nozzles	18' 9 ½"	22' 3"
Separation Nozzles 1 – Nozzles 2	10´ 0"	-
Separation first to second RISER's expansion	10´ 0"	38' 0"
Ø Before first expansion	32"	32"
Ø Before second expansion	40"	50"
Ø After second expansion	48"	63"
Ø Crossover	48"	63"
Nozzles number	6 at level 1 6 at level 2	6 Only one level
Angular position of the nozzles	0°, 50°, 160°, 210°, 260° y 310°	30°, 90°, 150°, 210°, 270° y 330°
Nozzle inclination to wall	30°	30°
Nozzle type	horizontal slot nozzle	FULLJET nozzle
Ø Nozzle tube	Level 1 4" Level 2 6"	6"
Elevation water vapor nozzle at boot	10 ½"	8"
Ø water vapor nozzle tube at boot	0.815"	1"
Distributor of feed and water vapor	Comb	Ring
Separation to the nozzles	15 m	2 m

* Lengths are from center to center Ø Internal diameter

GRAPHICAL RESULTS

The results are presented as graphs since they are easily interpreted.

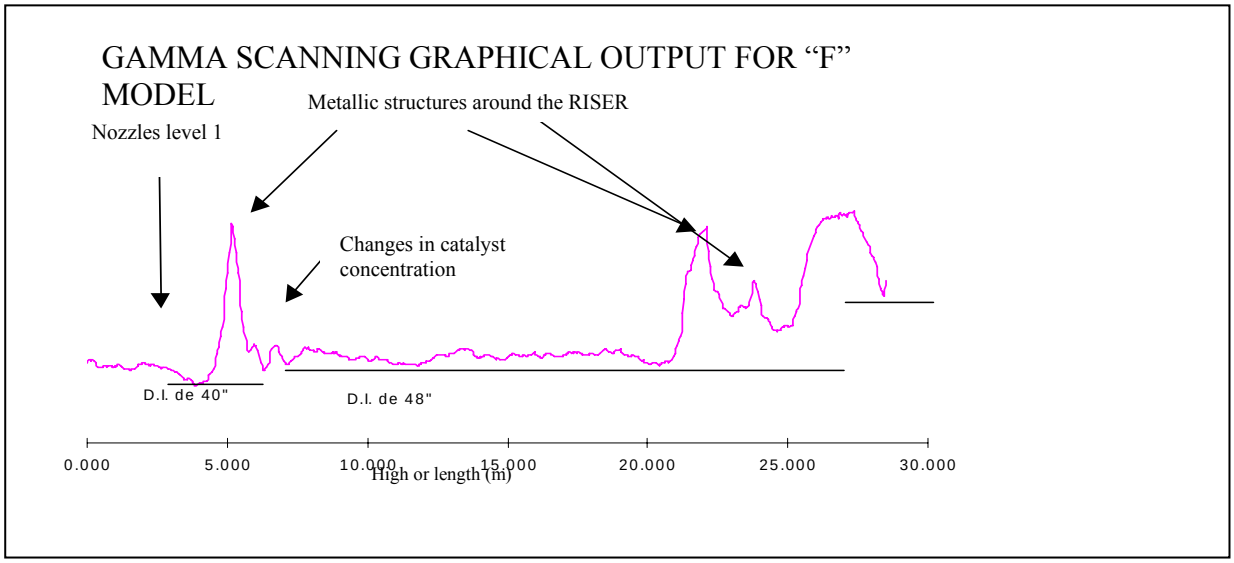

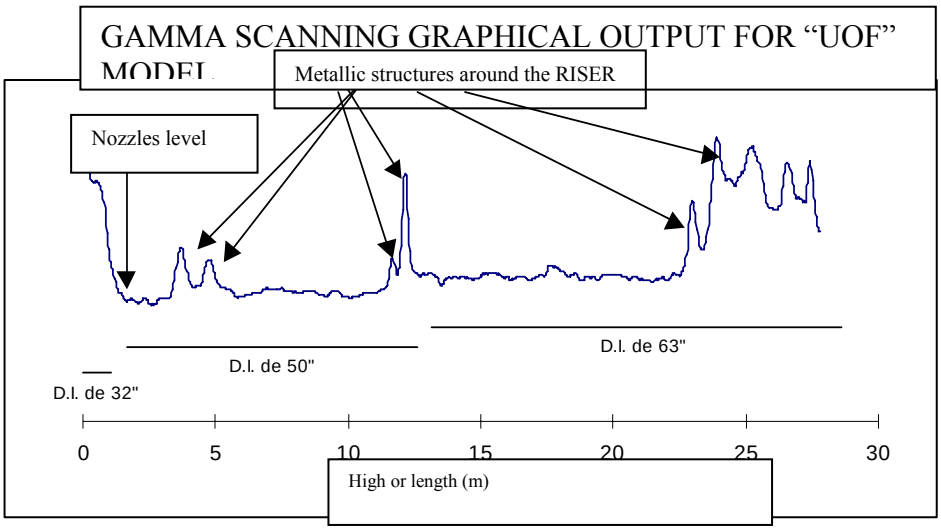

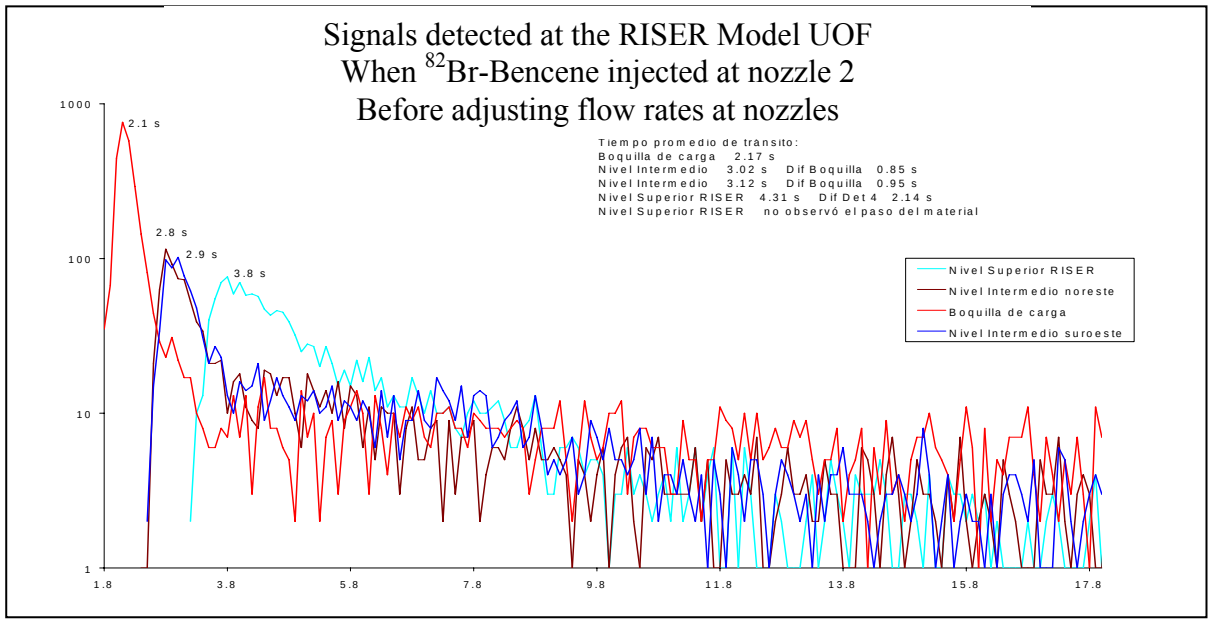

Signals detected at the RISER Model F
When ^{82}Br-Bencene injected at nozzle 4

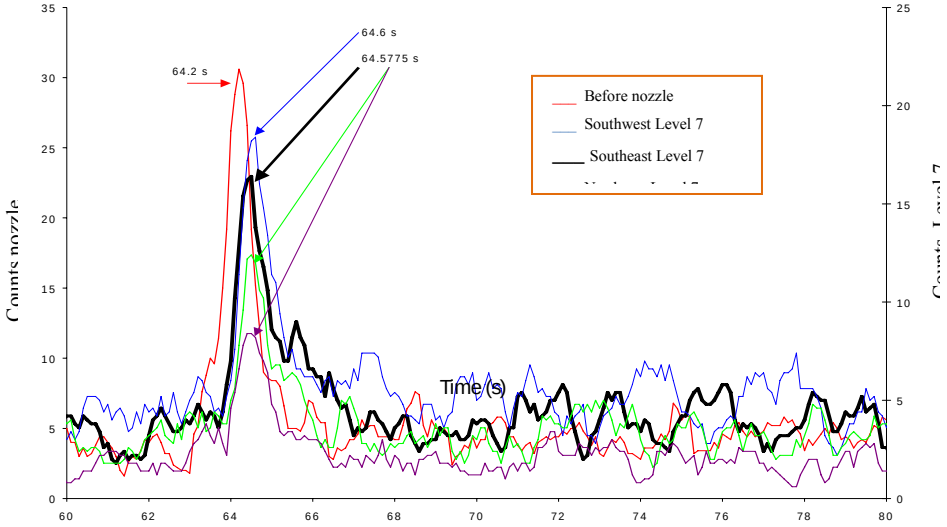

Signals detected at Riser Model F
When activated catalyst (^{140}La) injected at boot

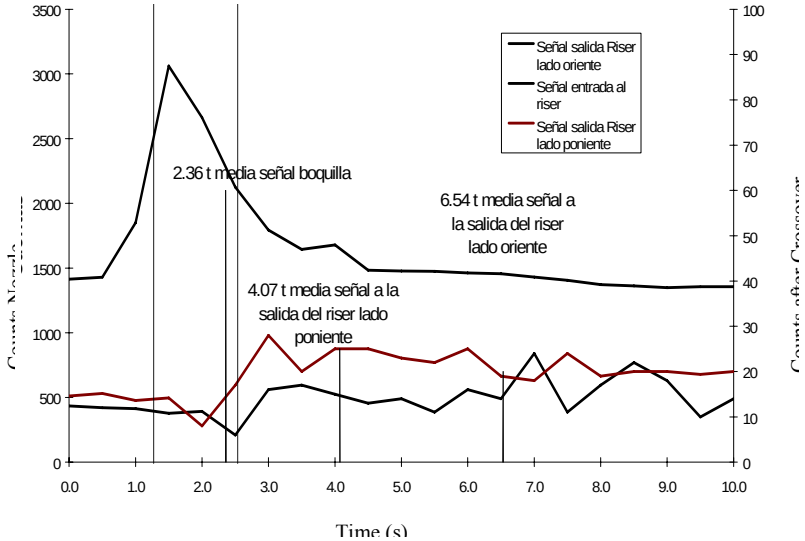

TOMOGRAFIAS MODELO UOF

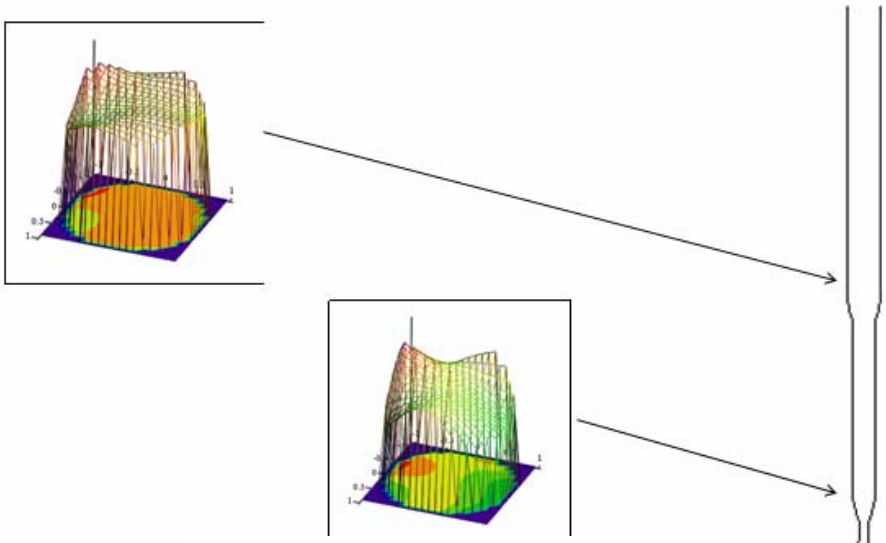

TOMOGRAPHIES OBTAINED AT
RISER MODEL “UOF”

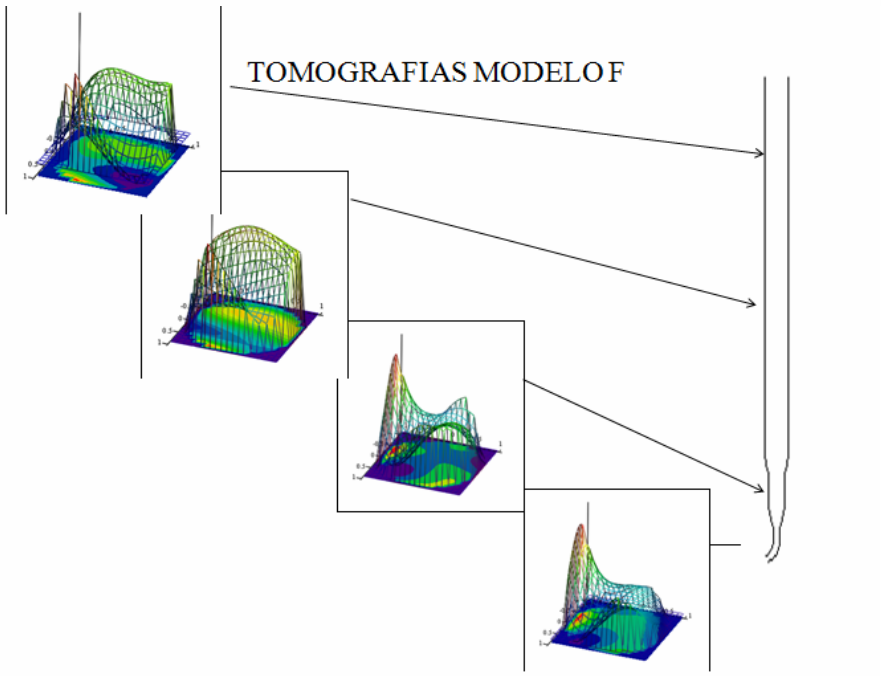

TOMOGRAPHIES OBTAINED AT RISER
MODEL “F”
AFTER MOVING FEED & VAPOR FLOW

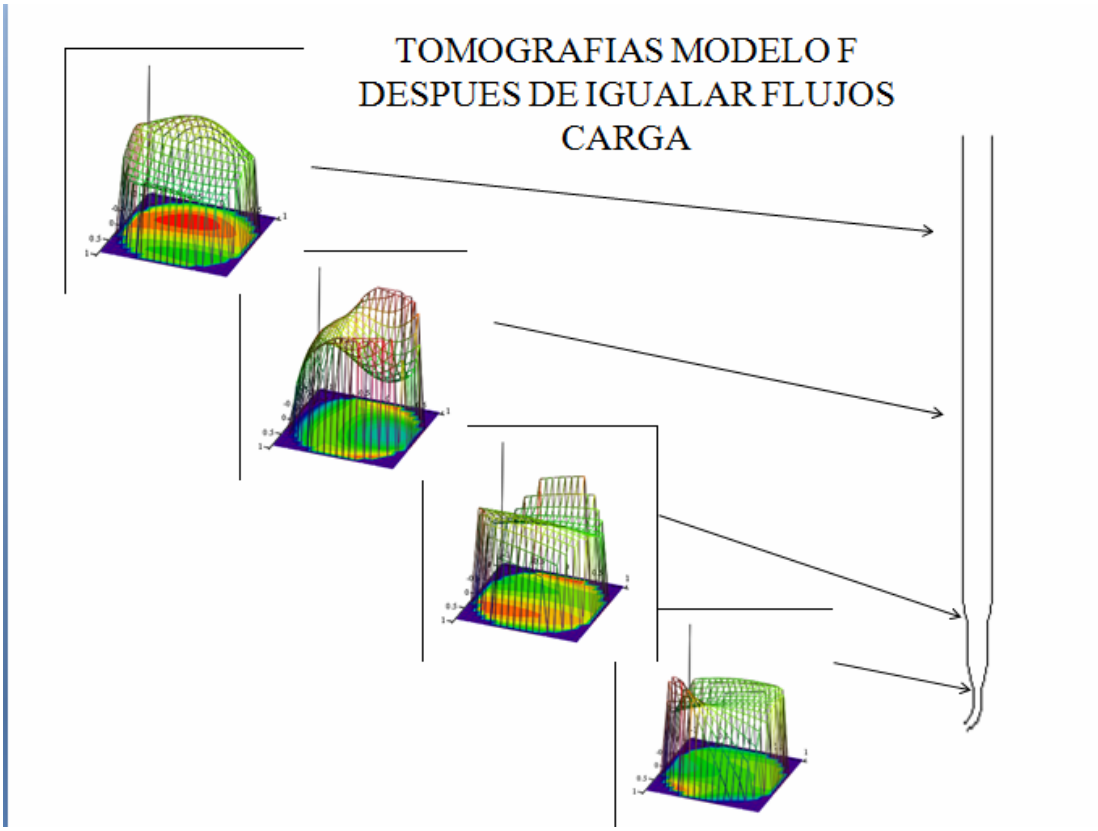

CONCLUSIONS

The time of contact between the charge and catalyst was determined, the variations of density at different horizontal cuts, which are equivalent to tomographs at different heights, as well as the variation of the density along the vertical axis, or symmetrical axis, all of them of the "RISER", for each FCC Plant.

From these studies it was concluded that:

1. There is a deficient mixture between the reaction gases and catalyst at the RISER
2. There are canalizations in both RISERS.

So it was decided to investigate the flows that arrive at each nozzle of the RISER at FCCI

The measures of the flow rates of feed and water vapor were made using the crosscorrelation flow measurement technique.

After adjusting the control flow valves, for the charge and water vapor, for each nozzle, it was possible to increase 17% the production of gasoline, at FCCI. Also, it was possible to find out hydrodynamical design differences between both designs.

REFERENCES

1 "Employing radiotracer diagnostic technology to support FCCU revamps", AIChE FCC Operations Symposium, March 2000.

2 Wang, S.J., Geldart, D., Beck M. and Dyakowski, T. "A behavior of catalyst powder flowing a dipleg" Proc. 1st World Congr. Industrial Process Tomography, Buxton, U.K., 1999, pp. 147-152.

3 Rerouin C., Nevicato D., Forissier M.,Wild G. and Bernard J.R., Ind. Eng. Chem.Res., 1997, 36, p. 4504-4515.

4 Ramírez G., F. P., Cortés I., M. E. et al., Informe "Determinación del Nivel de Catalizador, Planta FCC-2, Refinería de Salamanca, Gto.", Instituto Mexicano del Petróleo, 1995.

5 Ramírez G., F. P., Cortés I., M. E. et al., Informe “Estudio de Radiotrazado y Tomografía del Convertidor Catalítico, Planta FCC, Refinería de Minatitlán, Ver.”, Instituto Mexicano del Petróleo, 1996.
6 Ramírez G., F. P., Cortés I., M. E. et al., Informe “Estudio de Verificación de la Reparación con Radiotrazado y Tomografía del Convertidor Catalítico, Planta FCC, Refinería de Minatitlán, Ver.”, Instituto Mexicano del Petróleo, 1996.
7 Ramírez G., F. P., Cortés I., M. E. et al., Informe “Estudio de Radiotrazado y Gammagrafía Longitudinal Electrónica para determinar el nivel de Catalizador en el Separador del Convertidor Catalítico, Planta FCC1, Refinería de Cadereyta, N.L.”, Instituto Mexicano del Petróleo, 1997.
8 Ramírez G., F. P., Cortés I., M. E. et al., Informe “Estudio de Radiotrazado y Gammagrafía Longitudinal Electrónica para determinar Flujos en el RISER del Convertidor Catalítico, Planta FCC1, Refinería de Cadereyta, N.L.”, Instituto Mexicano del Petróleo, 1997.
9 Ramírez G., F. P., Cortés I., M. E. et al., Informe “Estudio de Radiotrazado, Gammagrafía Longitudinal Electrónica y Tomografía del Convertidor Catalítico de DOS Plantas FCC, Refinería de Tula, Hgo.”, Instituto Mexicano del Petróleo, 1997.
10 Ramírez G., F. P., Cortés I., M. E. et al., Informe Final “Estudio de las Unidades FCC, Refinería de Tula, Hgo.”, Instituto Mexicano del Petróleo, Diciembre 1998.

DEVELOPMENT OF NEW AND ALTERNATIVE TRACERS FOR OIL RESERVOIRS

Láuris. L. Silva[1], Cláudio. L. Donnici[1], José. D. Ayala[1], Cíntia H. Freitas[2], Rubens. M. Moreira[2], Amenônia. F. Pinto[2].
[1] Universidade Federal de Minas Gerais - ICEX- Depto de Química (UFMG / QUÍMICA)
Av. Presidente Antônio Carlos, 6627- Campus Pampulha
31270-901, Belo Horizonte, MG
laurislsilva@yahoo.com.br
[2] Centro de Desenvolvimento da Tecnologia Nuclear (CDTN/CNEN)
Av. Presidente Antônio Carlos, 6627- Campus Pampulha
31270-901, Belo Horizonte, MG

ABSTRACT

A possible application of great interest involving lanthanide elements is the use of their complexes as activable tracers under neutron irradiation in order to evaluate the efficiency of the petroleum production processes. For this purpose, tracers must be soluble in the aqueous phase and be insoluble in the organic phase, must not adsorbed on the internal microporous rock formations and be easily detectable. The lanthanides are characterized by the high neutron cross sections and, if it is complexed, it may be used as activable tracers. In this way they can be injected in the petroleum reservoir in their natural state (non-radioactive), the samples being subsequently irradiated in a nuclear reactor, producing enough activities with characteristics that allow their identification even in very low concentrations. Lanthanide complexes with DTPA and thiodicarboxylic acid ligands are an alternative to the development of these novel tracers since their properties may be chemically adjusted.

1. INTRODUCTION

The oil industry plays an important role in the economic development of many countries. Efforts are made to get maximum oil recovery from a producing well as drilling cost is very high and success rate is low. When formation pressure drops due to oil production, pumping is sometimes used or fluids are injected in order to maintain the formation pressure and push the oil towards producing well. The exploitation of oil by operations involving the application of external energy or modifications of reservoir characteristics is most commonly termed ‘‘enhanced oil recovery’’ (EOR).[1] The fluid most commonly injected is water which should be previously treated so that no physical or chemical alterations occur in the reservoir. The efficiency of the water flow process highly depends on the rock characteristics. It will generally be less efficient if heterogeneities are present in the reservoir, such as permeability barriers which prevent a good displacement of the petroleum by the injected water [2,3]. Generally, the injected fluid is labelled with a tracer (radioactive or non-radioactive) and the produced fluid from the well(s) of interest is sampled and analyzed to determine the tracer response. A variety of materials were used as a water tracer in early works on streams, underground caverns, groundwater and oilfields. [1]

A tracer is any substance which, when incorporated in the mass of a system (an industrial process, an environmental compartment, a living organism, etc) allows the investigation of its behavior in a particular physical, chemical, biological, or of another natural process. The most important characteristic of tracers is that they behave as close as possible to the material to be studied and they possess characteristics that make them detectable even if in low concentrations. The most used non-isotopic water tracers consist of specific chemical compounds soluble in water, easily identifiable and which can be measured by means of high sensitivity analytical techniques. They may be organic, ionic or dye compounds. In some cases, a simple chemical analysis of ions transported by water due to dissolution of materials naturally present in the environment or to accidental contamination may provide valuable information. However, these analyses should be carried out with much care especially when the water originates from lithologically heterogeneous agents [3].The isotopic tracers can be divided in four groups: purposedy added radioactive tracers; activable tracers

(formed by non-radioactive nuclides whose concentration is determined through neutron activation analysis); natural radioactive tracers and stable isotopes from water elements. The group of activable tracers is of great interest, since they can be introduced in the system to be studied in their inactive state and then sampled and dosed through neutron activation. Besides, they might eliminate the biggest problem involving radioactive tracers in field works: the safety of high activities handled under relatively precarious conditions, the possible radioisotopes decay during long work, as well as the logistic difficulties involved in the transport of radioactive materials to isolated regions, sometimes in the oceans[4]. Based on tracer behavior, certain transport parameters within the reservoir may be assumed. In other words, based on an appropriate interpretation of the transference functions between the injection and the production well, evinced by results obtained in experiments with tracers, it is possible to diagnose possible inefficiencies in the secondary recovery process and take the adequate decisions to correct their causes[4].

2. TRACER BEHAVIOR IN PETROLEUM RESERVOIRS

The fluid flow is anisotropic in most reservoirs. The structures of the reservoir are often extended in layers containing significant heterogeneities which lead to directional variations in the flow extension. And in this point the tracer technology plays an important role, the tracer movement reflects the movement of injected fluid. It is important to make sure that the tracer properties are as similar as possible to the characteristics of the ideal tracer.[3] Due to the great variable diversity, it is not possible to select a universal tracer which adapts satisfactorily to all conditions. In case of groundwaters circulating through porous agents along tortuous trajectories, tracers require more severe conditions for the following reasons:

a) the possibility of tracer retention by solid material is very high, partly due to contact with the solid surfaces and, on the other hand, to the sluggishness of the existent flows;

b) the velocity variation of the tracer due to the difference between the size of its molecules and that of water molecules, as well as the attraction they may suffer by the electrical charges existent on the pore internal surfaces cause a longitudinal and transversal dispersion of the tracer which does not coincide with that of water;

c) transport differences due to the molecular diffusion and osmotic pressure of the tracer [3].

No radioisotope species acts as an ideal tracer hence its selection should be carried out according to the characteristics of the process to be studied [5]. A promising group of non-sorbing tracers are metal ions strongly complexed to organic anions, which yield a negatively charged complex. A metal ion could be chosen which, in its non-complexed form, is very insoluble in groundwater and thus no severe background concentrations problem would arise.[6] The lanthanide elements may be used as tracers (activable) since they present good solubility in water, when complexed, and the nuclides have high neutron cross sections, which allow their detection in extremely low concentrations by means of the Neutron Activation Analysis (NAA)[7]. Nevertheless, it is important to point out that for them to behave as good tracers the ideal is that they behave similar to water and that there is no partition in any other phase, unless this can be quantified[5].

The solubilization of the lanthanides must be guaranteed along their trajectory through the microcanals and micropores in the reservoir. This is the central problem of this application, taking in to account the extended surface available for the adsorption of the lanthanides (which retain positive charges) by the negatively charged clays deposited on the internal surfaces of the pores/canals. Therefore it becomes absolutely necessary to use chelating ligands to shield the radionuclides[7], such as the azo-carboxylic – DTPA and thiodicarboxylic acids. The present work describes the systematization of the processes to obtain azo-carboxylate and thiacarboxylic processes aimed at using them in partition tests between the phases existent in the petroleum reservoir.

3. METHODOLOGY

Synthesis of Thiocarboxylic acids[8]

These compounds have the general formula R-S-Y-COOH, at the present time they are proceeding basically according with the reaction:

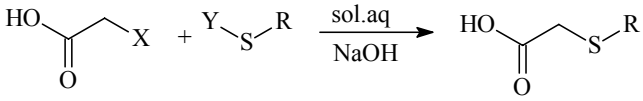

General reaction procedure: addition of the halogen substituted acid which was dissolved in NaOH solution to the corresponding thiolates (Y-S-R) also dissolved in NaOH, followed by magnetic stirring at room temperature for 20 to 34 h (or, alternatively, reflux during 8 h). Then diluted H_2SO_4 was added to the reacting system until pH = 2. If no immediate precipitation occurs, the reacting mixture is thrice extracted with dichloromethane (3 x 1000 mL) and ethylic ether (3 x 1000 mL). In the later case the whole organic extract is dried with anhydrous sodium sulfate, filtrated to eliminate the drying agent, and concentrated in a rotary evaporator. The dried and pure ligands have been obtained as colorless solids with a yield ranging from 63% to 91%. The obtained thiodicarboxylic acids were then characterized spectrometrically by means of Infrared (IR) and Nuclear Magnetic Resonance of hydrogen (NMR of ^{1}H) and of carbon- 13 (NMR of ^{13}C).

Lanthanoid complexation

The two ligands tested thus far were: DTPA - diethylenetriaminopentaacetic acid and thiodicarboxylic acid, whose structural formulas are as following :

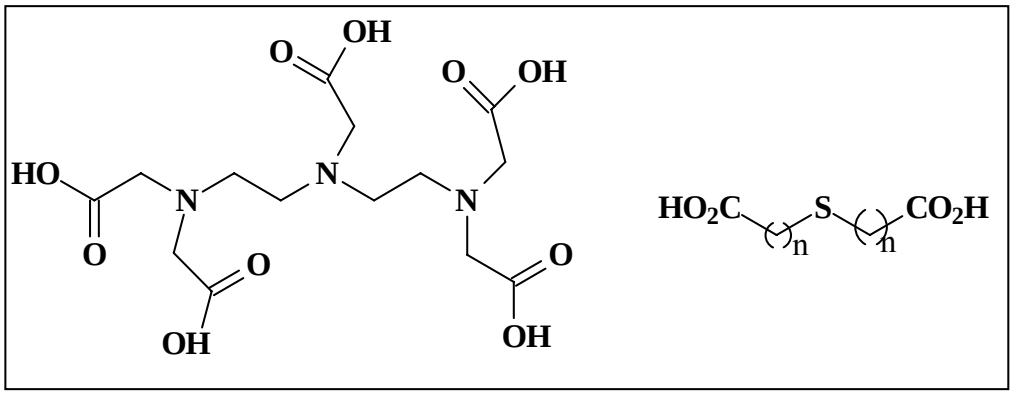

The occurrence of complexation can be checked by infrared spectrometry. The spectra of the above aminopolicarboxylic e thiodicarboxylic acids show an absorption band at the 1700-1600 cm-1 wave number range. It can be seen in Figures 1 and 2 that this band shifts to a lower range in the case of europium complexed with DTPA and thiodicarboxylic acid.

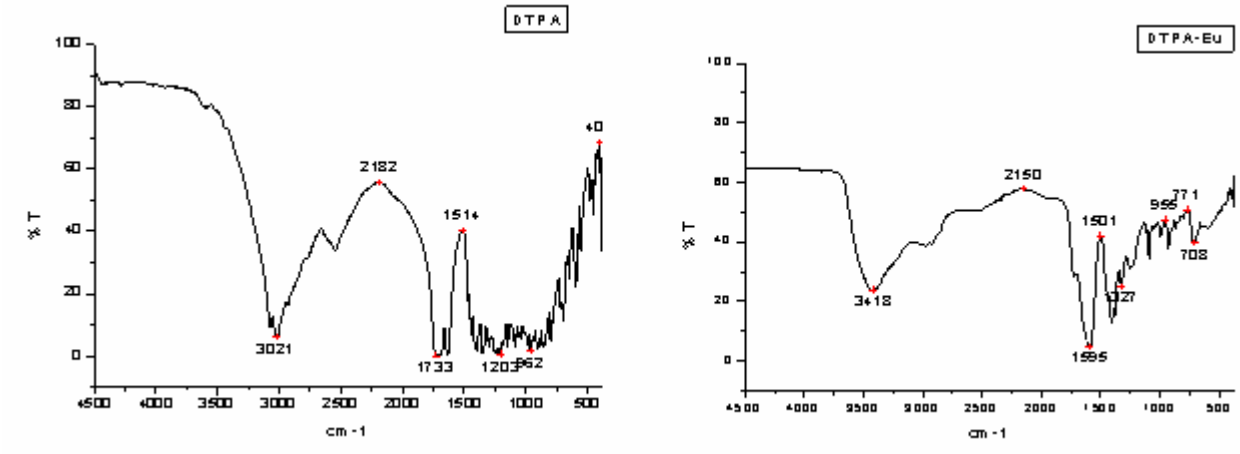

Figure 1 – Infrared spectra of DTPA and Eu-DTPA (1:1)

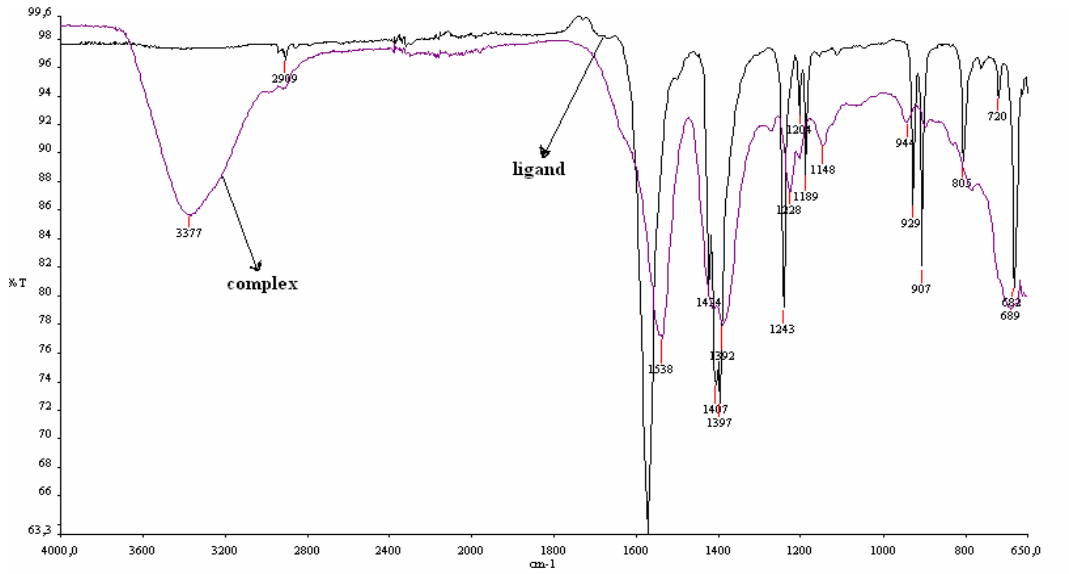

Figure 2 – Infrared spectra of Thiodicarboxylic acid and complex Eu-Thiodicarboxylic (1:1)

The complexation yield of the lanthanides La, Eu and Dy with the ligand DTPA was determined using high performace liquid chromatography (HPLC) methodology and this way the non-complexed ion was determined (Figure 3)9.

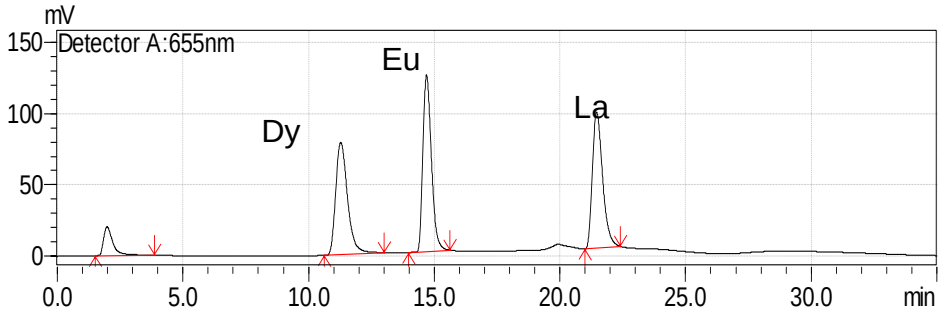

Figure 3. Chromatogram of Ln.DTPA complex

The analyses for the ionic exchange chromatography technique were performed with an α-hydroxyisobutyric acid buffer as eluent, using a cation exchange column. The contents were quantified and determined in an elution gradient after pos-column complexation reaction with arsenazo III spectrophotometry detection.

2.3- Analysis in bench test with a core sample

The lanthanide concentration for Neutron Activation Analysis (NAA) was determined before and after contact with the phases of the system. In the case of tracer partition between water and a solid, the process is called sorption (comprising adsorption and desorption). The bench test with a core sample showed a possible adsorption of the tracer in the solid phase, see Figure 4:

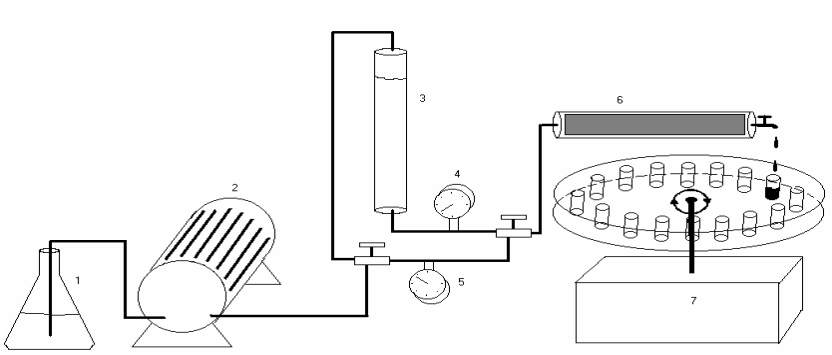

Figure 4. Experimental model with core sample: water reservoir (1), constant outflow pump (2), recipient for storing the tracer solution (3), pressure gauges (4,5), core sample (6), sample collection system (7).

Tritium was used for comparison since it behaves a nearly ideal tracer and is a reference for the evaluation of the performances of the other tracers. The tritium analyses were carried out by means of the Liquid Scintillation technique.

4. RESULTS AND DISCUSSION

In order to determine the occurrence of a partition for a solid, tritium and the complexes were simultaneously injected in the body test apparatus. A possible adsorption of the tracer in the solid phase was observed as shown in Figure 5. The results obtained in the core sample bench test experiment for the solution of the tracers Dy-DTPA, Eu-DTPA and tritium are shown, respectively, in Figures 5, and 6 see below:

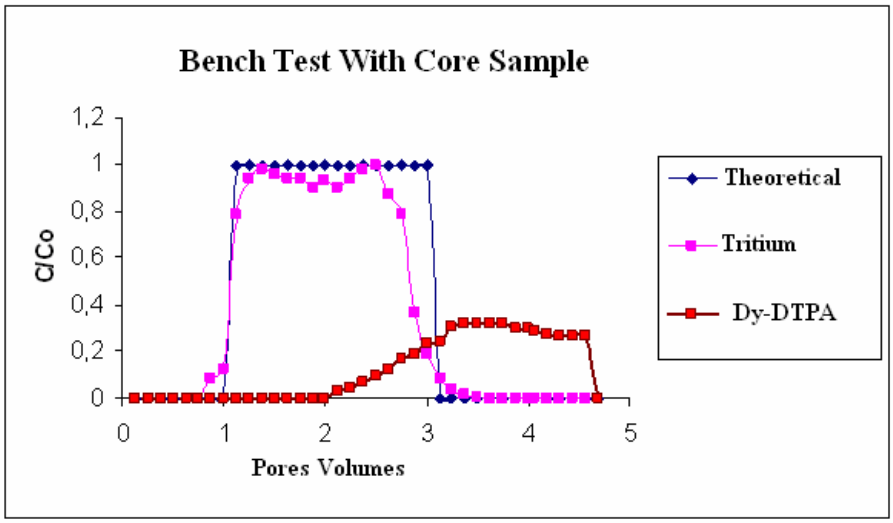

Figure 5. Bench test with tritium + Dy-DTPA

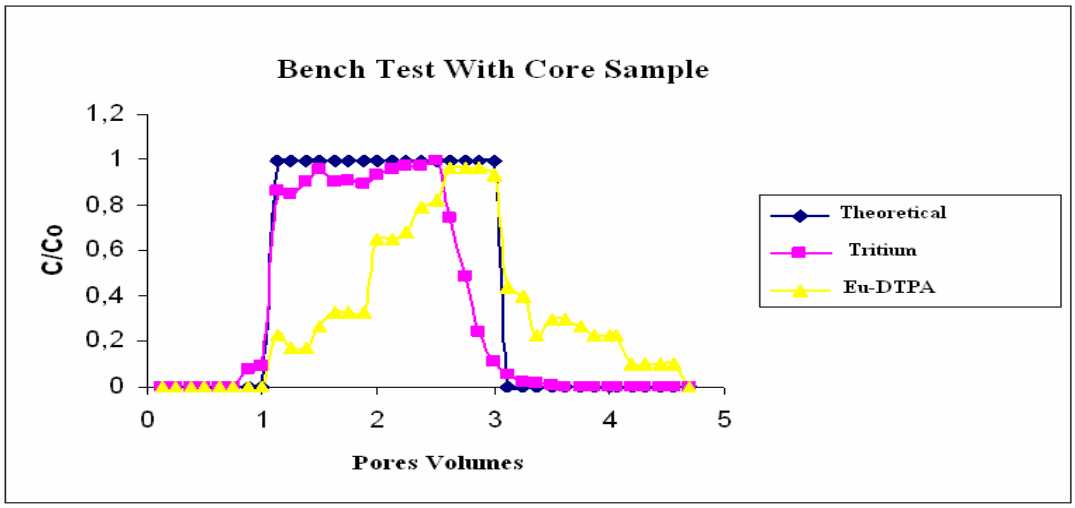

Figure 6. Bench test with tritium + Eu-DTPA

For the core test runs, the entrance and exit functions of both tritium and the complexed lanthanides did not coincided, even for dysprosium, which show adsorption of the complex, and for europium, which shows there were no delays with respect to tritium, that is, the absence of adsorption of the complexes by the rock walls. The latter demonstrates the possible applicability of these Eu-DTPA complex as tracers.

The stability the complex of the lanthanide Eu with the ligand thiodicarboxylic acid was determined using thermogravimetric analysis (TGA), the results obtained in the thermogravimetric analysis (TGA) is shown in Figure 7 see below:

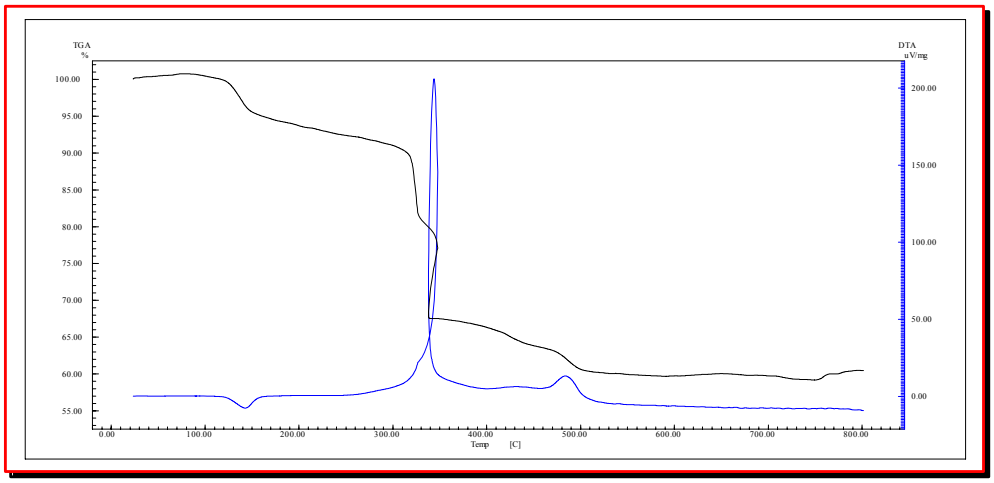

___ DTA of the Eu[$S(CH_2COOH)_2$]
___ TGA of the Eu[$S(CH_2COOH)_2$]

Figure 7. Thermogravimetric analysis with Eu-Thiodicarboxylic acid

The results of this thermoanalytical technique confirm an effective complexation between the ions and the ligand. According to the thermogravimetric analysis, the complex Eu[$S(CH_2COOH)_2$] is stable up to approximately 120°C, a very important feature to test this complex as tracer in oil reservoirs, where the temperature is around 70°C. In temperature of 345°C, the decomposition process occurs with an extremely exothermic effect, with a release of energy of 5985 kJ mol^{-1} (7.6 kJ g^{-1}). This energy is almost twice of the quantity released by detonation of the TNT (4.18 kJ g^{-1}).

5. CONCLUSION

The High Performace Liquid Chromatography (HPLC) can be defined as a suitable technique to determination of the efficiency of the complexation methods, which presented free lanthanides Eu and Dy concentrations lower to the quantification limit of the equipment used, and lanthanide La presented the highest percentage the free lanthanum (88,5%) dissolved in aqueous solution. The characterization of the complexes formed, by means of the Infrared (IR) spectrometry, indicated the disappearance of the characteristic bands of the axial deformation of the hydroxylic group, with intermolecular hydrogen interactions and it is observed a broad band which is characteristic of hydration water, besides a displacement of carboxylate bands towards lower ν values is noticed. The caracterization of the complex Eu-thiodicarboxylic acids by thermogravimetric analysis (TGA) corroborates an effective complexation between the metals and the ligand and it is noteworthy that the complex is stable up to approximately 120°C, a very important feature to test this complex as tracer in oil reservoirs, where the temperature is around 70^{o}C. The results of both analytical techniques confirm an effective complexation between the metals and the ligand.

The results of the core tests, determined for two analytical techniques: Neutron Activation Analysis (NAA) for the lanthanide complexes, plus the Liquid Scintillation Spectrometry (LSS) for the tritium water injected simultaneously as Eu-DTPA reference tracer, showed:

1) an almost null percentage of complexed lanthanides dissolved in aqueous solution;

2) small evidence of sorption of the tracers on the internal surfaces of the rock formation pores since there was no displacement between the complexed lanthanide and reference tracer responses, whose behavior reflects faithfully the water flow outlet. With these results two features of a good tracer were fulfilled: a behavior as similarity as possible as the fluid whose behavior it tracers (water) and detectability even if only in low concentrations. The excellent behavior reproduction of tritiated water by the tracers tested in the core runs are one of the inside a shielding of europium by the ligand DTPA.

The partition process of the tracer on the oil/water interface should now be carried out to simulated by physical analogue of the Flow Injection Analysis (FIA), by usual partition coefficient determination techniques. Experiments in real petroleum fields should now be carried out to evaluate the performance in situ of the Eu-DTPA complex in reservoirs during the injection water process, as a final step their homologation as activable tracers to estimate the efficiency of the secondary recovery of petroleum.

ACKNOWLEDGMENTS

Thanks to CAPES and CNPq for scholar ships and to FAPEMIG (CEX 817/06; APQ 4911-5.02/07) for financial support.

6. REFERENCES

[1]- Ahmad, M.; Tasneem, M. A.; Rafiq, M.; Khan, I. H.; Farooq, M.; Sajjad, M. I. Applied Radiation and Isotopes 2003, 58, 611.

[2] MILANI, E. J. et al. Petróleo na margem continental brasileira: geologia, exploração, resultados e perspectivas. Brazilian Journal of Geophysics, v. 18, n. 3, p. 352-396, 2000.

[3] BJ∅RNSTAD, T.; MAGGIO, G. E. Radiotracer technology as applied to interwell communication in oilfields. (Manuscript for publication in IAEA Technical Report Series: “Radiotracers and Sealed Sources Applicaton in Industry”), Vienna, 2000.

[4] PLATA BEDMAR, A. Isótopos en hidrologia. Madrid: Alhambra, 1972. 328p. (Zairos, 8)

[5] FREITAS, C. H. Partição de Complexos de Lantanídeos entre Fases de um Reservatório de Petróleo. 2007. (Dissertação de Mestrado) - Centro de Desenvolvimento da Tecnologia Nuclear.

[6] Byegard. J.; Sharnemark. G.; Skalberg. M.; Journal of Radioanalytical and Nuclear Chemistry . 1999, 241, 281.

[7] MOREIRA, R. M. et al. Desenvolvimento de Metodologia de Multitraçadores para Caracterização de Reservatórios de Petróleo – Multitracer. Belo Horizonte: CDTN, 2005. 104p.

[8] Furukawa, N., Ogawa, S., Kawai, T. J. Chem. Soc. Perkin Trans. 1984,1,1849.
[9] Souza, F. F. Inovação e modernização industrial para recuperação de metais de valores minerais. Belo Horizonte: CDTN, 1999. (Relatório).

SYNTHESIS OF THE INDIUM COMPLEXES FOR USING AS AN ACTIVABLE TRACER IN THE OIL SECONDARY RECUPERATION

Júnia de O. Alves[1] (IC)*, Rubens M. Moreira[1] (PQ)
oliver_junia@yahoo.com.br
[1] Centro de Desenvolvimento da Tecnologia Nuclear
Serviço de Meio Ambiente e Técnicas Nucleares
Rua Professor Mário Werneck s/n – Caixa Postal 941,
CEP 30123-970, Belo Horizonte, MG, Brazil.

ABSTRACT

Oil is found in the environment, impregnated in the sedimentary rock pores: the reservoirs. Such reservoirs are layers of natural gas, oil and water, submitted to high pressure. As the exploited loses pressure, it is necessary to introduce fluids in the reservoir in order to push the oil towards producer wells. Water's commonly used for this purpose, and tracers that are soluble in it provide information on the efficiency of this recovery procedure. In this paper the performace of complexed indium that can be used with activable tracer (i.e. analysed buy NAA after being sampled in the producer well) is tested in the laboratory. The tracer is used to evaluate the secondary recuperation of the oil and in this present paper studied tracer is Indium
Key words: Activable Tracer, Indium.

INTRODUCTION

The tracer is incorporated to a substance which will be named marked material and it allows to investigate the behavior of such material. It is necessary that the tracer has a behavior equal to or very similar to the substance to which it was addtioned in order to carry out this study. (Plata, 1972).
Three kinds of tracers are observed: the stable, the radioactive and the activable ones.
In this paper, the tracer in focus is an activable tracer, Indium is a metal with high cross section due and because of that it is easily analyzed by neutronic activation. An activable tracer has great advantages in relation to others and it can be used in small concentrations and it is not necessary to work with radioactive material in the field.
The tracer is incorporated to the liquid injected in the process of secondary recuperation. The function of this liquid is to push as much as possible the oil located in the rock pores of the formation. However, the injected liquid can not totally scan the reservoir in function of the differences of impermeability, faults and other characteristics that make some regions not to be achieved by the created flux. The use of tracers is the most efficient way to inform about the process, since differently from some other kinds of tests that offer accurate information, this method integrates the influence of all characteristics that interfere on the flux between the injection point and the sampling. The tracer will follow the liquid injected in all changes that it suffers while leaking through the reservoir.

OBJECTIVE

Synthesis of the indium complexes in order this metal can be used as a activable tracer in the water leaking by porous means.

EXPERIMENTAL PART

Synthesis of the complex of In3+ with legand 2,2'-Bipyridin (Bipy)

Reagents

Indium chloride,, P.A of Aldrich – pureness 98%; 2,2'-bipyridin, P.A of Vetec - pureness 99,5%; Hexan, P.A da Vetec used for previous treatment Tetrahydrofuran (THF), P.A of Vetec – pureness 99% was treated previously.

Methodology

The complex was syntherized in tube Schlenk. It was prepared a solution with 1,2g (5,0mmol) of indium chloride (III) and 50mL Tetrahydrofuran (THF), dry. This solution was prepared in na atmosphere of hydrogene. Next, it was additioned 1,7g of the ligand Bipyridin (~10 mmol) and it was observed a formation of a white precipitate. The reaction remained on constant agitation and at room temperature 180 minutes. After this time, the solvent was evaporated IN THE VACCUM LINE. The resulting white solid was washed with Hexan and filtrated in vaccum. It was obtained from the reaction 2,35 grams of the complex..

synthesis of the complex In^{3+} with the ligand etylenediaminetetraacetic (EDTA)

Reagents

Indium chloride, P.A of Aldrich – pureness 98%; EDTA Bisodic P.A of Quimica Moderna– pureness 99-100%, Sodium hydroxide, P.A of Fluka – Biochemika.

Methodology

It was dilluted 0,2215g (1mmol) of indium chloride (III) in 50mL of distillated water. It was added a solution with 0,336g (1mmol) of EDTA dissodic in the previous solution, the pH of the resulting solution was adjusted to pH 6 addtioning slowly drops of a dilluted solution of sodium hydroxide. The solution remained on magnetic agitation for 30 minutes and was volumeted for 500mL.

RESULTS AND DISCUSSION

To characterize the first complex, (In-Bipy), it was done some comparisions between the ligand and also the obtained compound.

The fusion/decomposition points were determined in a digital set of Microquímica Equipamentos Ltda, model MQAPF-302. The fusion range of the ligand was 70-72ºC and for the product it was not observed fusion until 250ºC. The comparision of both values can suggest that a new compound was transformed during the synthesis

The vibrational spectra in the region of the infrared (IR) were obtained from pellets of KBr, pressed under vaccuum. The equipment used was a spectrometer with transformed of Fourier Perkin Elmer– Spectrum 100, in the region between 4000 and 400 cm-1. The resolution was of 4 cm-1. With the spectra of the ligand (Figure 1) and also of the complex (Figure 2) it is possible to make comparisons between both of them.

By observing the spectra, three common regions were revealed and identified as: A, B and C. Band A refers to the axial modification of the C-H of the aromatic (3080cm-1-3010cm-1), bands B refer to the axial deformation of the ring C-C and C-N (1600cm-1-1430cm-1) and band C is related to the angular deformation out the angular plan C-H (~750cm-1). It is noticed that bands B in the product spectrum and of the ligand are very different and it may have happened due to complexion of the atoms of nitrogen to the metal indium. Another region that is also different is the region circled in red, when observed, it is perceived that the spectrum of the product is cleaner and with less intense bands, the band circled in blue, which is observed in the spectrum of the ligand, is not observed in the spectrum of the product.. All these differences indicate the formation of the complex In-Bipy.

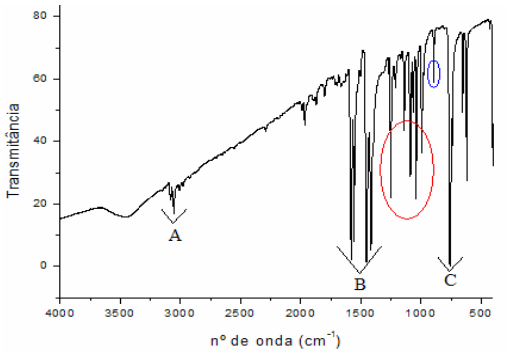

Figure1: Vibrational Spectrum of the ligand 2,2'-Biypiridin.

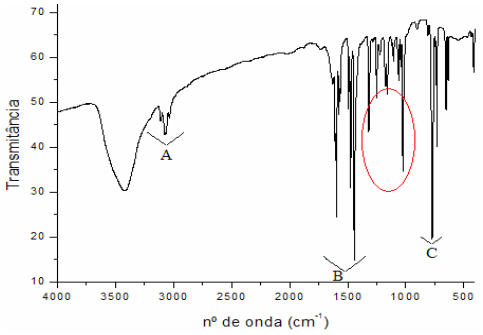

Figure 2: Vibrational Spectrum of the complex of the complex In-Bipy.

The spectra of RMN of 1H for bypiridin and for the syntherized complex were obtained D2O. The experiments were acquired in a spectrometer of RMN AVANCE DRX 400 of Bruker in a probe of inverted detection of 5mm. With the spectra, it was observed that the same signs that existed in the ligand appeared in the spectrum of the product.. It happens because the molecule that originates such signs is bypiridin, linked or not to the metal. A very interesting difference is the fact that all the signs of the spectrum of the complex present a chemical displacement (δ) bigger in relation to signs of the ligand of the spectrum and it occurs because in the formation of the complex, the ligand donates electrons to the metal, so the hydrogens are more unprotected and consequently have a higher δ.

The thermal analysis was made in the thermoscale Mettler Toledo of the Department of Chemistry, in air atmosphere and with heat reason of 10,00ºC/min.

The curve TG presented three mass losses and a residue of 25,035%. The first loss was of 16,756%, the second 42,691% and the third was of 16,060%. The residue TG is indium oxide (III) what was proved by the analyses of diffraction of x-rays. The analyses was made by using the method of powder, impregnating a diffractrometer manufactored by Rigaku, model Geigerflex, semi-automatic and x-ray tubes of cooper.

The first loss is probably the exit of the three chlorides and they can leave as Cl2 or HCl, considering that it was an air atmosphere The second and the third losses represent together 58,751% of the complex and it is equal to two molecules of bipyridin

According to the results and the information of the literature, it is proposed a new structure for the formed complex, it is known that

the metal is complexed with two

molecules of bipyridin,

In forms octaedric complexes,

The other ligand present in the reactional mean is chloride.
However, the complex obtained can be [In(BIPY)2Cl2]Cl (Figure 3).

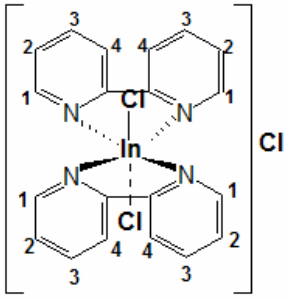

Figure 3: Structure proposed for the complex [In(BIPY)2Cl2]Cl.

A primary analysis of C, N and H was done and the numerical value was calculated based on the structure proposed by the complex, $C_{20}H_{16}N_4$ (Table 1).

Table1: Complex analytical data, theorethical, experimental and relative mistake *

	%H	%C	%N
Therethical	2,99	44,9	10,5
Experimental	2,51	38,3	8,72
Relative mistake	16,0	14,7	16,9

*Relative mistake (%) = $[(V_T - V_E)/V_T]100$

V_T = Therethical value
V_E = Experimental Value

The complex of In-EDTA was not possible to characterize but it was observed an evidence of complextion, which was possible with the expectrometry analysis in the region of the ultraviolet
The ligand spectra (Figure 5) and the complex (Figure 6) in aqueous solution were submitted in an spectrometer by Shimadzu Corporation, model UV-2401 (PC) S.

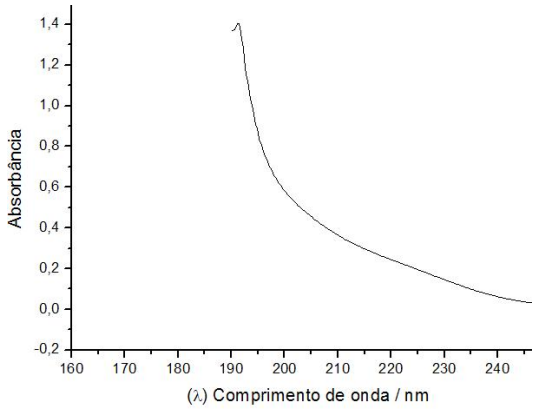

Figure 5: Absorption Spectrum of the EDTA ligand in the ultraviolet region.

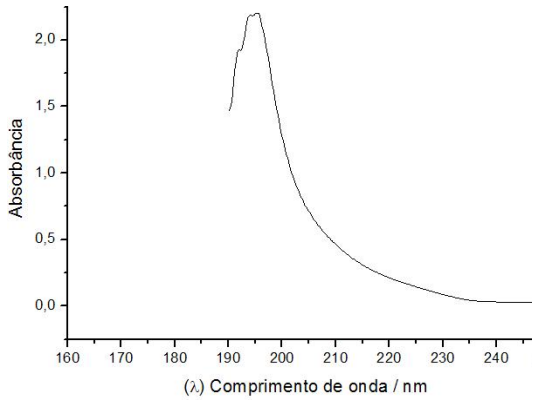

Figure 6: Absorption spectrum of the complex In-EDTA in the ultraviolet region

Figures 5 and 6 allow to infer that the complextion occurred since the absorption bands are considerably different.

The ligand spectrum presents a maximum around 190nm and the complex spectrum presents three maximums, considering that one of them can is near 190nm what can mean that exists an excess of the ligand in the solution. Both of the other peaks are near 195nm.
Based on literature information, it is known that indium tends to form octaedric complexes, so one structure was proposed with the proportion of 1:1 (Figure 7).

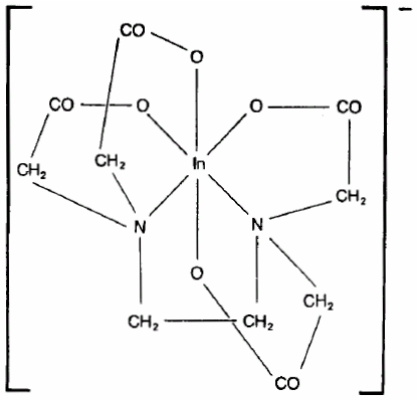

Figure 7: Structure of the In-EDTA complex in aqueous solution (Chrysikopoulos and Kruger, 1986).

DISPLACEMENT TEST IN POROUS CORE

One of he procedures for the evaluation of the tracer availability is the (BENCH TEST). It consists of tracer displacement together with water through a specimen that simulates the reservoir rock. The specimen is cylindrical sample of sandstone previously treated and encapsulated with impermeable material and resistant to pression. A scheme of the mounting is shown in Figure 8.

The first complex to be tested was the In-Bipy complex. In the tracer vase a solution of this complex and tritiated water. This solution was prepared with concentration of 1,9x10-3mol/L of complex and activity of 10200 Bq/L tritium.

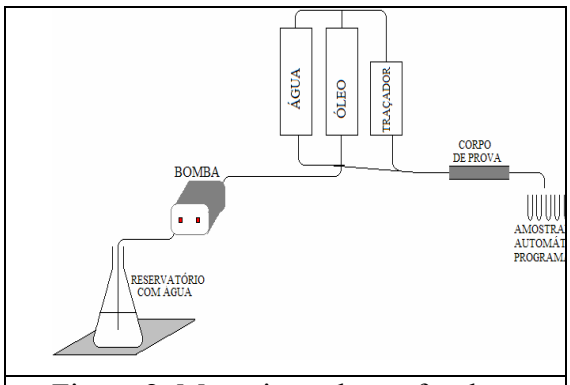

Figure 8: Mounting scheme for the tracers availability test.

When the tracers pass through the specimen, it is possible to know if the tracer is good or not, since it is adequate, it will behave similarly to the ideal tracer, tritium. The bench test consists simply of the injection of pure water, next, the injection of a solution with the tracers and then the injection of pure water. Thus, the form of the curve concentration normalized of the tracers X sample will have the profile of a degree function FUNÇÃO DEGRAU.

Forty samples were collected and sent for analyses. To quantify the tritium it was used a spectrometer of Liquid Cintillation Perkin Elmer / Wallac – 1220 Quantulus and to quantify In, it was used a TRIGA nuclear reactor IPR-R1 from CDTN/CNEN. The metal was quantified by the Neutron Activation Analysis technique. The concentrations were normalized and a curve Concentration X Sample was constituted. (Figure 9).

It is observed that a delay of the tracer in relation to the tritium occurred and it indicates that the tracer was absorbed by the rock of the specimen.

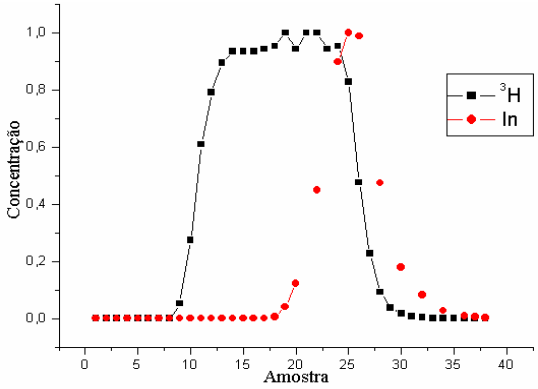

Figure 9: Experimental curve for Tritium (tracer of reference) and for the In-Bipy complex (sytherised tracer).

The tracer viability test using the In-EDTA was also done. In this case, one solution of this complex and tritiated water was put in the tracer VASE. This solution was prepared with concentration 2,0x10-3mol/L of the complex (as described in the procedures) and activity of 10200 Bq/L of tritium.

The collected samples were sent for analyses. To quantify tritium, it was used a Spectrometer of Liquid Cintillation Perkin Elmer / Wallac – 1220 Quantulus and to quantify indium it was used a Spectrometer of Atomic Absorption e Perkin Elmer, model 5000. The concentrations were normalized and it was constituted the curve Concentration X Sample (Figure 10).

The tracer had a perfect behavior, that is, behaved in a similar way of the ideal tracer by using the complex In-EDTA,

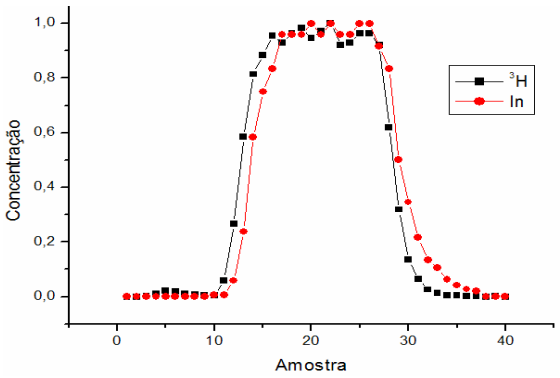

Figure 10: Experimental curve for tritium (tracer of reference) and for the In-EDTA complex (sytherized tracer).

CONCLUSION

Observing the infrared spectra and RMN, it was noticed that indium was complexed with the ligand bipyridin.. After having the other results, it was possible to propose a structure which has not been proved yet.

The displacement test in porous core for the In-EDTA complex was not satisfactory due to the delay of the complex in relation to tritium, what indicates that it will not be able to use the complex as tracer in underground water, what does not mean that the complex can not be used in surface water where the absorption phenomenon is observed.

The In-EDTA complex was not very well characterized, complextion was made evident by the analysis in the ultraviolet region. The structure of the complex was proposed based on literature information.

The displacement test in porous core for the In-EDTA complex was excellent, the tracer was not stuck in the specimen and during all the process behaved in a similar way to tritium. Thus, it was concluded that it will be able to use this complex in oil wells on order to evaluate the process efficiency for secondary recuperation.

REFERENCES

1) BEHRENS, H.; MOSER, H.; WILDNER, E. Investigation of groundwater flow with the aid of indium-EDTA-complex using neutron activation for the determination of the tracer. Journal of Radioanalytical Chemistry, vol 38, p 491-498, 1977.

2) CHRYSIKOPOULOS, C. V.;KRUGER, P. Chelated Indium Activable Tracer for Geothermal Reservoirs. 1986. 94f. Stanford University, Stanford, California.

3) DYSON, R. M.; LAWRANCE, G. A.; MÄCKEC, H.; MAEDERB, M. Stability investigations of medically relevant complexes by the simultaneous analysis of series of spectrophotometric titrations. Polyhedron 18, p 3243-3251, 1999.

4) DONNICI, C. L.; OLIVEIRA, I. M. F.; TEMBA, E. S. C.; CASTRO, M. C. R. Metodos sintéticos para preparação de 2,2'-Bipiridinas substituídas. Quím. Nova vol.25 no.4, 2002.

5) LEE, J. D. Química inorgânica: um novo texto conciso. 3ª ed, São Paulo, Edgard Blücher, 1980, 507p.

6) MARTINS, P. F. F. Desenvolvimento de traçadores ativáveis para aplicação em recuperação secundária de reservatório de petróleo. 2005. 101f. Tese (Mestrado em Ciência e tecnologia das Radiações Minerais e Materiais – Meio ambiente com aplicações de Técnicas Nucleares.) – Centro de Desenvolvimento da Tecnologia Nuclear

7) PLATA BEDMAR, A. Isótopos en hidrologia, 8ª ed, Madri, Zairos, 1972. 328 p.

8) PEREIRA, E. H. T. Desenvolvimento de metodologia de multitraçadores para a caracterização de reservatórios de petróleo-multitracer. Belo Horizonte: CDTN, 2005. 25p. (Relatório Final de Bolsista do CTPetro).

9) RODRIGUES, C. J. Síntese, caracterização e estudo térmico de complexos de alumínio(III), gálio(III) e índio(III). 2004. 106f. Tese (Mestrado em Química)-Departamento de Química, Universidade Federal de Minas Gerais.
10) SHRIVER, D.F.; ATKINS, P. Química Inorgânica, 3ªed, Porto Alegre, Bookman, 2003.
11) SILVESTEIN, R. M.; BASSLER, G. C.; MORRILL, T. C. Identificação espectrométrica de Compostos Orgânicos, 3ª ed, Rio de Janeiro, Guanabara, 1979. 299p.
12) SOLOMONS, T. W. G.; FRYHLE, C. B. Química Orgânica, 7ªed, Rio de janeiro, LTC, 2000. 645 p.
13) WOOD, S. A.; SAMSON, I. M. The aqueous geochemistry of gallium, germanium, indium and scandium. Ore Geology Reviews 28, p 57-102, 2006.
14) http://pt.wikipedia.org/ wiki/índio, acesso em 17-04-07.
15)http://www.maxwell.lambda.ele.puc-rio.br/cgi-bin/PRG_0599.EXE/4774_3.PDF. O elemento químico índio, acesso em 17-04-07.

COMPARISON OF SEVERAL MODELS/SOFTWARE FOR INTERPRETATION OF A TRACER TEST IN A FIVE-SPOT LABORATORY SET-UP

Ph. Berne[1], J.P. Leclerc[2]
[1] CEA, LITEN, L2T, F-38054 Grenoble, France
[2] LSGC, Nancy-Université, CNRS - 1 rue Grandville, BP 20451, 54001 Nancy Cedex, France

ABSTRACT

A laboratory-scale mock-up for interwell tracer experiments was designed and built. It allowed to generate tracer data in an approximate five-spot arrangement. The experimental results were used to test various modelling tools: the analytical Brigham model, the semi-analytical streamline-based software Poro and the finite-element package Comsol. Respecting model assumptions proved crucial with the Brigham model, which may be a serious limitation in real oilfield experiments. The other tools were found reasonably effective and yielded identical values for porosity and dispersion length.

INTRODUCTION

Interwell tracer tests are an interesting tool for the characterization and analysis of oil or geothermal fields. The interpretation of tracer tests is now fairly well mastered in many industrial situations (IAEA, 2004), but remains rather challenging in the case of interwell tests, for several reasons:

- the natural medium involved is usually complex and knowledge of its properties frequently rather poor,
- tracer recovery is often low,
- the time scales are large, which means that the restitution curves will more often than not be incomplete.

The tracer practitioner can fortunately use various modelling tools to overcome these problems and usefully exploit the experimental data. Their domain of validity is however not always quite clear, nor are standard practices always soundly established. The approach in the present work (part of the Coordinated Research Project: "validation of tracers and software for interwell investigations" initiated by the International Atomic Energy Agency) is therefore twofold:

- generate experimental data in a simple, well-defined test facility using a five-spot pattern,
- use these data to assess various modelling tools, from purely analytical to purely computational: the Brigham model, a streamline-based software (Poro) and a finite-element code (Comsol).

EXPERIMENTAL

The experimental rig was a large rectangular tank, 2 m in length, 1 m in depth and 0.95 m in width. The tank was separated in three parts by perforated plates (Figures 1 and 2), the central part (1.60 m long) being filled with sand. The sand layer was deposited manually. Porosity was thought to be about 35%; mass median grain diameter was 0.75 mm. The sand layer was saturated with water up to a height of 0.80 m.

Five perforated tubes were installed in the sand bed, approximately following a five-spot pattern (the centre tube was actually nearer the well 1-well 4 line). The tubes were 40 mm in diameter and 1 mm in thickness. The central tube was used as an injector. The injection flow rate was imposed by a constant-level tank equipped with a calibrated orifice. The other tubes were used as producers, the production flow rates being controlled by a peristaltic pump. Injector-producer distance was approximately 40 cm.

Three experiments were made, during which the water table was kept stagnant (another one was attempted with an overall movement of the water table but was found inexploitable). Injection flow rate was 107 cm^3/min during the first two experiments, 184 cm^3/min during the last one. Production flow rate in each producer was always ¼ of injection flow rate.

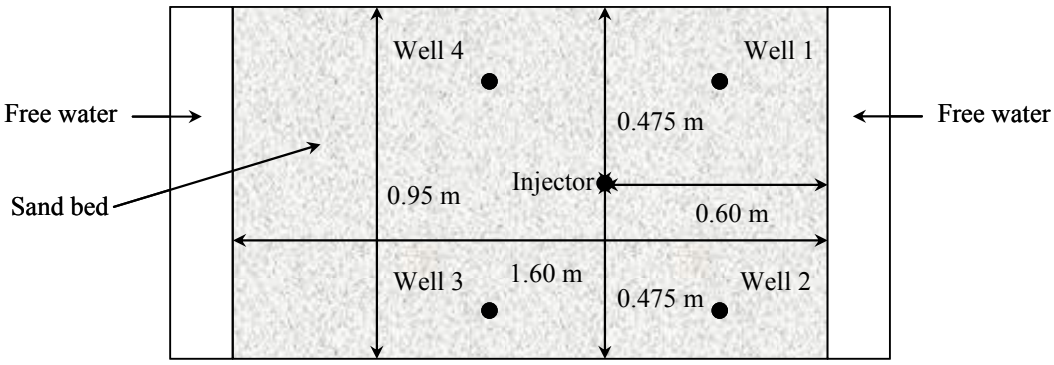

Figure 1: Top view of the experimental setup.

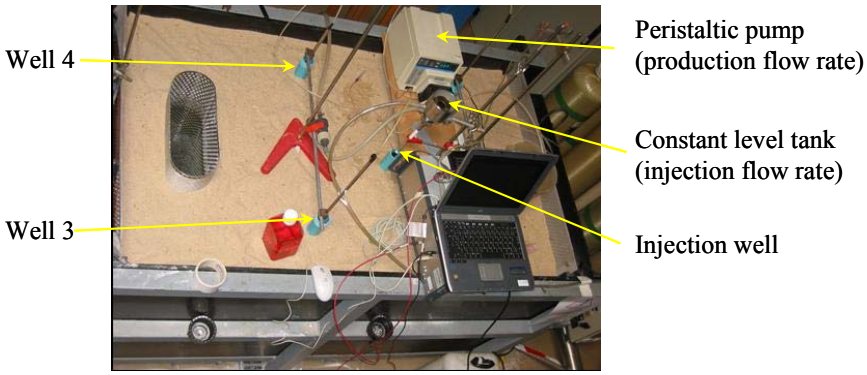

Figure 2: Photograph of the experimental setup.

Rhodamine WT was used as a fluorescent tracer. A mass of 20 to 40 mg was introduced in the injector well during each experiment. During two hours after tracer injection, water in the injector well was circulated in a closed loop by an external pump so as to homogenize tracer concentration. Samples were periodically taken from the producer wells and analysed with a spectrofluorometer.

All three experiments were found exploitable. The first experiment gave very good results (Figure 3 left); because the injector well was not exactly at the centre of the producer wells, different restitution curves were obtained in wells 1-3 and 2-4. The restitution curves were found to evolve in the next experiments and to differ more and more (Figure 3 right). In all cases, tracer recovery was more than 80%; the missing 20% were thought within measurement uncertainties. Further analysis however revealed that the time- and area-normalized curves were remarkably close together (Figure 4). The flow pattern was therefore deduced to be the same during all the experiments, the difference in the restitution curves being due to unequal distribution of the tracer in the injector tube in spite of the homogenization system mentioned above.

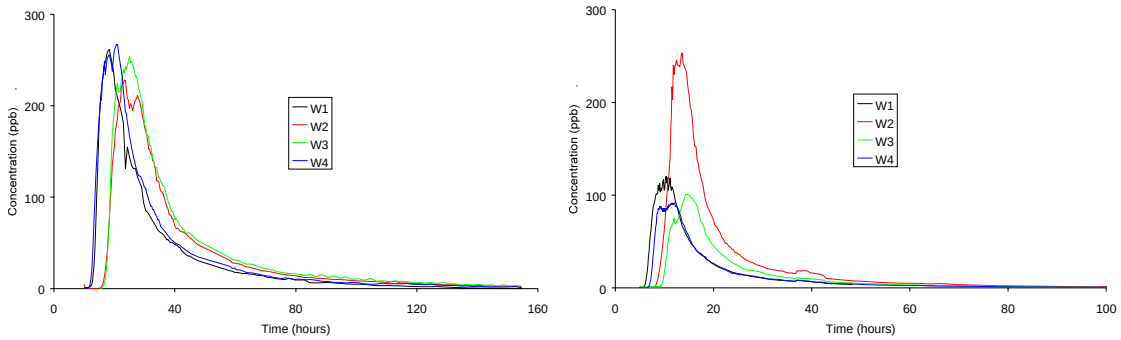

Figure 3: Tracer restitution curvesleft: first experiment - right: third experiment.

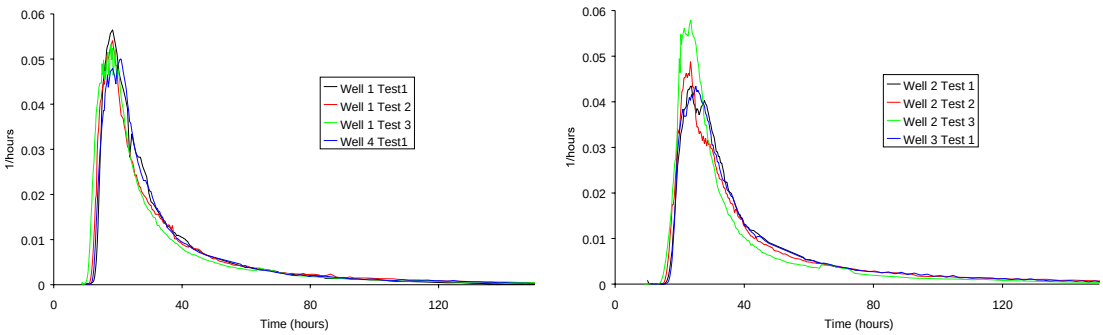

Figure 4: Comparison of normalized tracer breakthrough curvesleft: well 1 – right: well 2.

MODELS

The Brigham model

The Brigham model predicts tracer breakthrough in a homogeneous, repetitive and balanced five-spot pattern (Tang, 2005). It is based on an empirical correlation for step response in a producer well, in the case of a non-dispersive medium:

$$\log\left[\log\left(\frac{1.07}{1.07-F(Q_{pv})}\right)\right] = -0.0041 + 0.581\log(Q_{pv} - 0.72) \qquad (1)$$

where $F(Q_{pv})$ is the response to a unit step and Q_{pv} is the injected pore volume; impulse response can be calculated as dF/dQ_{pv}. Equation (1) is valid in the $0.72 < Q_{pv} < 2.29$ range; $F(Q_{pv})$ is respectively equal to 0 and 1 below and above that range). Dispersion can be introduced thanks to the following convolution product:

$$C(Q_{pv}) = C_m \int_{0.72}^{Q_{pv}} \frac{dF(\chi)}{d\chi} \exp\left[-\frac{3L(\chi - Q_{pv})^2}{\pi^2 \alpha}\right] d\chi \qquad (2)$$

where $C(Q_{pv})$ is the impulse response, L the injector-producer distance, α the dispersion length. Maximum concentration C_m is given by a semi-empirical relationship:

$$C_m = \frac{m}{\beta L^{1.5} \alpha^{0.5} h \varepsilon} \qquad (3)$$

where m is the injected tracer mass, h and ε respectively the height and the porosity of the layer of porous medium (unit water saturation is assumed). β is a coefficient given as 4.10^{-4} ppm.ft^2.lb^{-1} in Tang (2005).

The advantage of this model is its fairly simple analytical formulation. It should however be borne in mind that it is, strictly speaking, only valid under rather stringent assumptions. In particular, the five-spot pattern should be repetitive.

Another small imperfection is the fact that Equation (1) predicts total tracer recovery at $Q_{pv} = 2.29$. This means that, beyond that point, tailing will only be due to the dispersion term in equation (2), whereas in reality it is also due to the multiplicity of paths linking the injector and the producer. It can therefore be expected that the tails in experimental restitution curves will be poorly represented.

The model was programmed using the Fortran language and a Levenberg-Marquardt optimisation routine from the IMSL library. It was tested against the monolayer results reported by Tang (Figure 2 in his paper).

The Poro software

The Poro Tracersim software, developed by Somaruga et al. (2008), assumes a single layer of porous medium with uniform porosity (and water saturation), permeability and dispersivity. Permeability can be anisotropic. Injector and producer wells are defined by their positions and flow rates. The velocity of water at each point in the computation domain is the sum of the contributions from all the wells, calculated using a potential flow equation. Faults can also be introduced and are taken into account by the image-well method.
The user is requested to select an injector-producer pair. A set of streamlines is then computed using the calculated velocity field. Tracer is introduced in the injector and transported by combined advection and dispersion along each streamline. The contributions from all the streamlines are summed up in the producer well, generating the "fractional recovery curve" i.e. the area-normalised tracer restitution curve.
The software is found user-friendly and fairly fast (typical computation time on a standard laptop: less than 1 min.) thanks to the semi-analytical formulation of velocity and tracer transport. No provision is however made for parameter optimisation, that has to be performed manually.

The Comsol package

Comsol Multiphysics (Comsol, 2005) is a well-known finite-element package for solving coupled systems of partial differential equations. The "earth science module" was used in the present work, more specifically the pre-programmed (steady-state) Darcy flow and (transient) solute transport equations.
Only two-dimensional calculations were made. Default solver settings were used all along.
The built-in mesh generator was used. Computation results were systematically checked for mesh independence, that was typically achieved with a few thousand elements. Maximum computation time was about 6 min. on a standard desktop PC.
Parameter optimisation was again performed manually.

Cross-comparison

Consistency of the various tools was first checked on a true five-spot configuration. The Brigham model was obviously used just as it is. A total of 30 wells (15 injectors and 15 producers) were used in Poro to create at least a part of a repetitive five-spot (an attempt was made at using faults to impose symmetrical boundary conditions on a five-well arrangement but failed). A $1/8^{th}$ five-spot computational domain containing 4600 elements was used with Comsol. Dispersion length α was varied from 10^{-1} to 10^{-4} L even though the Poro calculation failed in the latter case.
The results are shown on Figure 5. The Brigham formulation is obviously inadequate at large dispersion length ($\alpha = 0.1L$ - it predicts non-zero concentration at $t = 0$). In all the other cases, agreement with the Comsol results is quite good. Comparison with Poro is only acceptable. The reason may lie in the well arrangement that is not truly an infinite, repetitive five-spot.

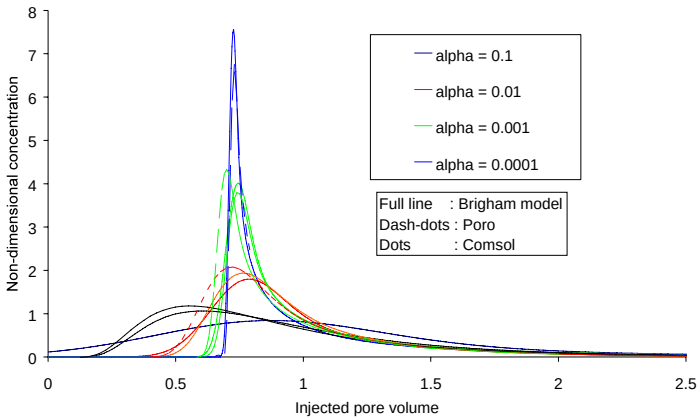

Figure 5: Cross-comparison of Brigham model/Poro software/Comsol code.

ANALYSIS OF THE EXPERIMENTAL RESULTS

A few preliminary comments

The unknown parameters that can be determined from the present tracer experiments are the following:

- dispersion length α ,
- porosity ε , as the 35% value reported above is no more than a crude estimate,
- tracer mass m_i injected towards production well i .

The first two quantities should be the same for all production wells since some care was taken to make the sand bed as homogeneous as possible. In this way, our tracer experiment is not typical of oilfield tracer practice, where uniform properties cannot reasonably be assumed. Another difference is the non-uniform distribution of tracer in the injection well. In a real oilfield experiment, the strong pressure drop contrast between the injection well and the porous formation would probably force the tracer to distribute evenly.

The Brigham model

The Brigham model offers potential for the determination of all the parameters mentioned above. This was done by non-linear fitting of the model against all four tracer recovery curves. A typical result is shown on Figure 6; optimised parameters are reported in Table1.

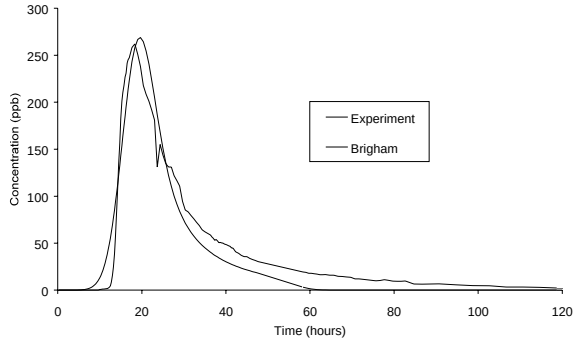

Figure 6: Comparison of experimental tracer recovery curve with Brigham model
Test 1, production well 1.

The Brigham model fits the experimental data reasonably well except, as expected, for the tail part of the curve.

Table 1: Optimised parameters.

Eperiment	Test 1	Test 2	Test 3
ε (%)	58	57	54
α (mm)	5.2	5.6	4.3
% tracer, well 1	22	24	19
% tracer, well 2	25	35	46
% tracer, well 3	27	24	19
% tracer, well 4	26	17	16

Tests 1 and 2, made with identical flow rates, yield the same porosity value. Optimised value for test 3 is slightly lower, which suggests that accessible porosity might depend slightly on flow rate. This effect is however small and perhaps not significant. At any rate, the order of magnitude (close to 60%) appears very large. This point will be commented in more detail later.

Dispersion length is in the millimetre range, which is plausible since the size of sand grains is also roughly millimetric. The same trend as with porosity is observed.
Optimised percentages of tracer recovery are close to the values calculated from the zero-order moments of the experimental tracer recovery curves.

The Poro software

The basic output from the Poro software is the area-normalised tracer recovery curve in a production well. This means that:

- only parameters ε and α are accessible,
- as the area-normalised recovery curves from all the tests are identical, it will be necessary to treat one test only – for instance the first one.

A Poro model was built consisting of the five wells in their exact positions and of two fault lines representing the boundaries of the sand bed nearest the wells (the other boundaries were assumed remote enough to have little influence). Parameter optimisation was done manually.
Excellent fit was obtained with ε equal to 40% and α to 6 mm (Figure 7). Both values are perfectly reasonable for a layer of millimetre-sized sand.

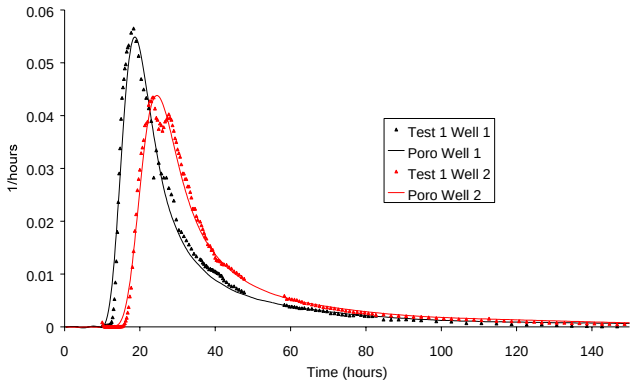

Figure 7: Comparison of experimental tracer recovery curve with Poro software
Test 1, production wells 1 and 2.

The Poro simulation offers a way of understanding why the Brigham model failed to predict a likely value for porosity. Figure 8 shows the streamlines connecting the wells predicted by Poro. It clearly shows that the tracer explores a much larger space between the injector and a producer than the mere rectangle it would sweep in a true five-spot (illustrated on Figure 7 for well 1), hence the overestimation of porosity.

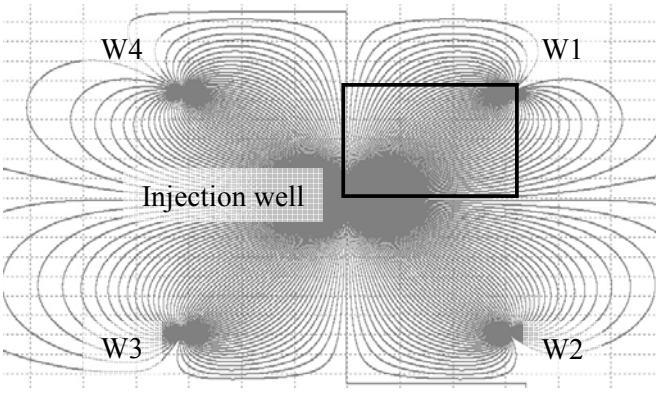

Figure 8: Streamlines predicted by Poro.

The Comsol package

The Comsol software is theoretically able to take into account all relevant phenomena including the tracer flow in the injector well. However, since it was not desired to have a complex porous/non porous coupled model, it was preferred to use the tracer recovery curves from the first experiment

only, in which the problem of unequal tracer distribution was avoided. The porous medium only was therefore simulated, with a 4000-element mesh. Water velocity was imposed at the circumference of all the wells; a top-hat tracer concentration history was imposed at the injection well (actual injected tracer mass was respected); null concentration gradient was imposed at the production wells.
Porosity and dispersion length were the variable parameters in the calculation. Sensivity of the model was checked – especially regarding dispersion length since CFD models are prone to numerical dispersion, which would have made parameter adjustment impossible. Optimal values of 40% and 6 mm were again obtained (see Figure 9).

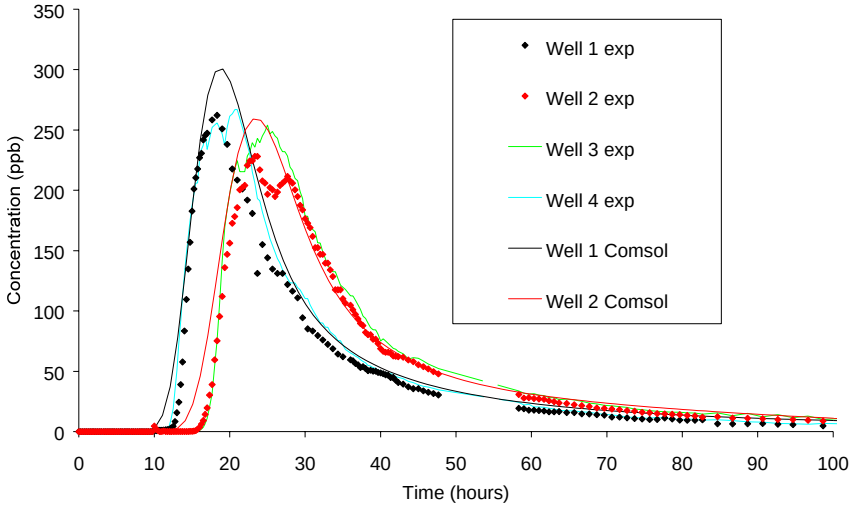

Figure 9: Tracer recovery curves predicted by Comsol.

CONCLUSION

The following points have been established in the present work:

- A laboratory scale setup for interwell tracer experiments has been designed and built approximating a five-spot injector/producers arrangement; tracer recovery curves have been acquired and analysed; apart from an unexpected problem of unequal tracer distribution, they have been found consistent and exploitable.
- Simulation of these data has been attempted with three different tools: a purely analytical model, a semi-analytical model and a numerical code. In all cases, parameter optimisation has allowed good reproduction of the experimental data. Main adjustable parameters were porosity and dispersion length.
- The analytical model (Brigham model) predicted unrealistic high porosity (60%). The cause for this problem is that model assumptions (repetitive five-spot pattern) are not exactly respected in the experimental setup. This observation may have some importance in real oilfield experiments since i) true five-spot configuration is probably rarely encountered ii) “porosity” would actually mean oil saturation, a parameter of foremost importance to the oil engineer.
- The other models (Poro and Comsol software) yielded identical optimised values with a reasonable computation effort. These values were thought to be correct. Whether a CFD code like Comsol can be used in a real-life, complex case remains to be checked.

ACKNOWLEDGEMENTS

The authors are grateful to the International Atomic Energy Agency (IAEA) for initiating and partially funding this work.

REFERENCES

1. COMSOL, 2005, Comsol multiphysics: user's guide, Version 3.2.
2. IAEA, 2004, Radiotracer applications in industry – A guidebook. Technical Report Series n° 423, International Atomic Energy Agency, Vienna, Austria.
3. Somaruga, C., Crespo, E., Uribe, G., 2008, PORO TracerSim Version 1.1 – User Manual. Neuquén, Argentina.
4. Tang, J., 2005, Extended Brigham model for residual oil saturation measurement by partitioning tracer tests. SPE Journal, June 2005, paper 84874, pp. 175-183.

TRACERS FOR WORMHOLE CHARACTERIZATION AND GEL TREATMENT DESIGN AND EVALUATION, IN OIL SECONDARY RECOVERY

M.B. Peralta, C. Procak, M.V. de la Fuente y C. Somaruga

Facultad de Ingeniería, Universidad Nacional del Comahue,

Buenos Aires 1400, (8300) Neuquén, Argentina

Abstract

Heavy oil production in unconsolidated sands constitutes a complex task because of the oil - sand combined production. During the primary exploitation, the voids generated by the sand extraction contribute to increase the drainage volume of the wells and so the oil production. In contrast, during the secondary recovery of oil, when water is injected for pushing the remaining oil, the ends of the voids located far from the production wells (known as wormholes due to their resemblance) may be reached by the water injection. In consequence, the injected water will be being channeled between the injector and the producer, without pushing the oil banks. The usual corrective treatment consists of the wormhole plugging employing gels. During the gel treatment design, precise values of permeability and volume of the wormhole are necessary for optimizing the gel viscosity and quantity. For this reason, a pre-gel tracer test was carried out. Also after the gel injection a second tracer test was conducted for evaluating the gel corrective action. In both cases, the tracer records have showed extremely short breakthrough times and excessive mixing. Several models were analyzed for reproducing the tracer behavior and parameters evaluation. The best behavior was shown by a simple perfect mixing model, with mixers in series and diffusive exchange with the walls.

Introduction

The increasing productivity of heavy oil in unconsolidated sandy reservoirs is attributed to the development of high-porosity tubes termed "wormholes"(Fig.1).

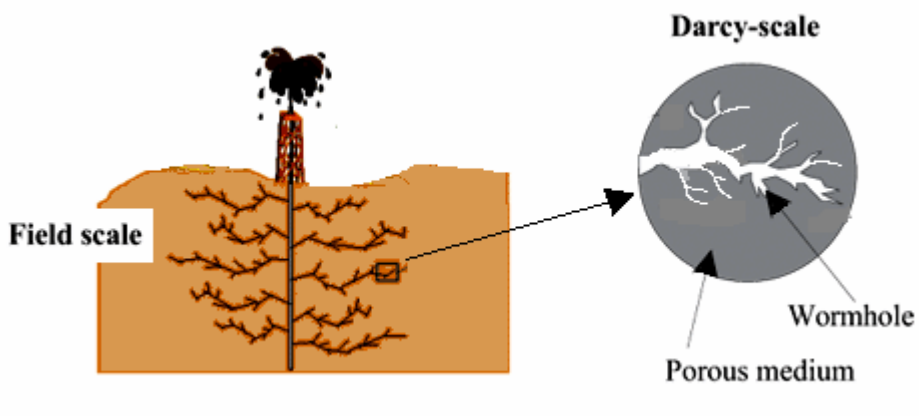

Figure 1. Wormhole development (Field scale and Darcy scale)

High sand production is typical at the starting of the operation. After this, the sand production decreases while the oil production increases[1]. This situation continues up to the reservoir pressure depletion. At this stage, a water injection plan may be started in selected wells, for pressure recovering. A very frequent problem appears when wormholes have progressed deeply, because the injector wormholes can intercept the producer

wormholes, bypassing the injected water. The most extended solution for these problems is the wormhole plugging by gel injection. McDiarmid et al[2], have reported a complete and successful experience on gel treatment. They also show results from a tracer test that was conducted for preliminary wormhole characterization.

Now, in this paper, we show results obtained by using tracers for preliminary (pre-gel) and post-gel wormhole characterization The aim was to provide information for the gel treatment design and also for the gel treatment evaluation. Complementary, we have proposed and analyzed several elementary models for reproducing, as well as possible, the tracer transport problem. We suspect that the tracer transport in wormholes shows special features that can not be captured by most of conventional models.

Interwell tracer tests

Interwell tracer tests are especially appropriate for evaluating the effectiveness of gel treatments. It is a consequence of the sensitivity of the tracer transport in relation to the permeability and thickness of the watered layers. The permeability controls the tracer particles residence time between a pair of injector-productor wells and the product "permeability-thickness", controls the "mass flow rate" of the tracer that is being conducted through the layer (assuming a constant pressure drop). As an example, during a water flooding project, the interwell tracer tests permit us to recognize the problem of "water channeling", which is evidenced by very small values of mean residence time. Complementary, the measured tracer concentrations in the productor well, reveal the mass flow rate of the tracer that is being produced. This is related to the permeability-thickness of the channeled layer. In conclusion, it is possible to characterize the water channeling problem, by mean of two parameters:

1. residence time distribution (or the first moment of the distribution, i.e. the mean residence time)
2. tracer mass produced (rate and cumulative production)

Since gel treatments procure to seal the channeled layers (diverting the water injection to the unswept zones), the effectiveness of the treatment would be evident if the post polymer values for mean residence time and "recovered tracer mass" are compared to those corresponding to the pre polymer tests. Here, due to possible differences in flow conditions between the pre-polymer and post polymer tests, for comparative purposes only, the tracer records will be written in terms of fractional daily tracer recovery (Fdtr) and fractional accumulated tracer recovered (Fatr), which are defined as:

$$Fdtr = \frac{1}{m_{tracer-inj}} \frac{\Delta m_{tracer-rec}}{\Delta t} = \frac{C_{tracer-sample} \cdot \ q_{water-producer}}{m_{tracer-inj}} \quad (1)$$

$$Fatr = \frac{1}{m_{tracer-inj}} \int_0^t C_{tracer-sample} \cdot \ q_{water-producer} \ dt \quad (2)$$

where,

$m_{tracer\text{-}inj}$ is the tracer mass injected.

$C_{tracer\text{-}sample}$ is the measured concentration in a producer.

$q_{water\text{-}producer}$ is the water flow rate of the producer.

$\Delta m_{tracer\text{-}rec}$ is the tracer mass recovered in the time Δt.

If channeling conditions are present between a pair injector- producer (verified with a tracer, previous to the polymer treatment), many different scenarios can be expected for the post polymer tracer test:

1. No tracer is detected in a lapsed time similar to the pre polymer tracer test. If an increasing oil production is observed, this is the optimal case.
2. Tracer is detected and the mean residence time is longer that in the pre polymer test. Here the polymer has sealed the most channeled layer and the tracer traveled through a less permeable layer. If this less permeable layer was water saturated before the polymer injection (and that had been evident in the pre polymer tracer test), then the layer was not sealed by the polymer and so, the polymer was insufficient. On the other hand, if this layer was oil saturated before the polymer injection, it should not have been evident in the pre polymer tracer test and consequently an incremental oil production should have been verified, after the polymer injection. Obviously, in this case, the polymer is working appropriately.
3. Tracer is detected and the mean residence time is smaller than in the pre-polymer test. This case is possible only when the lapsed time between both tracer tests has been very long, so that the layer sweeping could have been completed increasing the channeling conditions. Obviously, the polymer would have been ineffective for sealing the layer.

Wormhole evidence in the oilfield

The first indication of water channeling along wormholes was the sharp reduction of tracer production in the P7 well at the end of May 2007 (Fig.2). This first tracer (sodium fluorescein) was injected at the beginning of the water injection project. Until May 2007 no evidence of channeling was observed. A breakthrough time of 4 months was interpreted

as reasonable, taking into account the elevated contrast of viscosities between oil and water. After May 2007, the pressure and water flow rate of the injector became very unstable (Fig.3). Finally, only water was produced after September 2th, notably increasing its rate after October 5th. The facts described above are interpreted as wormhole evidence, especially the tracer behavior. In fact, the tracer was injected when the wormholes were not bypassing water (because the injector and producer wormholes had not intercepted each other yet). In consequence the tracer invaded an unaltered zone, in which it started to progress in a conventional way (between pores). When the injector wormhole reached the producer wormhole, the water injected was channeled along them. After this, mostly water (with little tracer) was conducted along the wormholes. The tracer had been trapped in the unaltered zones.

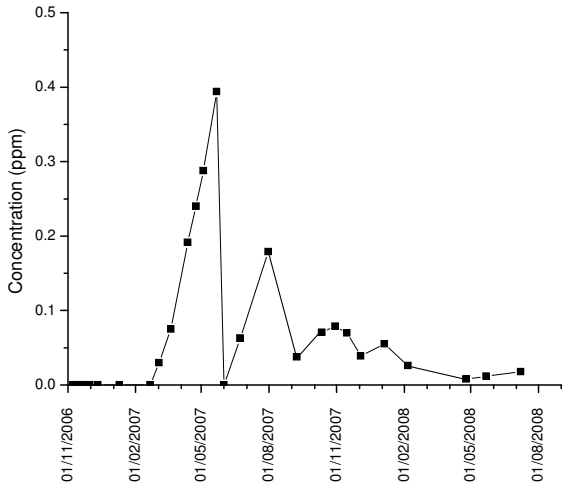

Figure 2. Tracer concentration in the producer well P7.

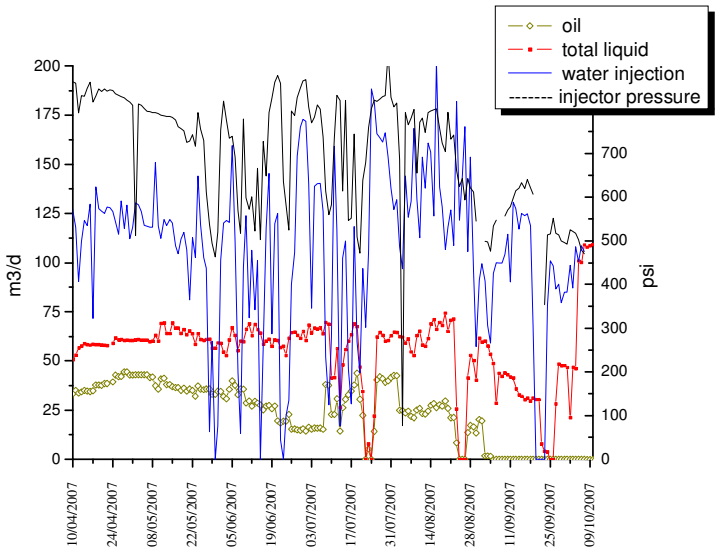

Figure 3. Production records of well P7 and injection parameters of the well I10.

Wormhole characterization and plugging

The evidence shown above allowed the oil company to choose an appropriate corrective treatment employing gels. Complementarily, a second tracer campaign was started in order to characterize the wormhole and so, facilitate the gel treatment design. Ammonium thiocyanate was injected on October 2007 for this purpose. On February 2008 a gel treatment was started. The gel effects were not clear yet, but the reduction of the bottom pressure was a good sign. However, some doubts were persisting in relation to the evolution of the oil rate production (Fig.4). For this reason, the company decided to begin a third tracer campaign so as to evaluate (and assure) the gel effectiveness. Therefore, isopropilic alcohol was injected on 2008 July 7th. The corrective effect of the gel is evident, when the post-gel and the pre-gel tracer records are compared (Fig.5).

Tracer transport in wormholes

At a first stage, we procured to capture the main features of the tracer transport in wormholes, employing the semi quantitative methods of Danckwerts[3], which are based on knowing the "residence time distribution" of the tracer (RTD). The "age" of an element of fluid is defined as the time elapsed since it entered the system. During an experiment with tracers, all fluids elements entering a system can be marked, monitoring then the output signal for these tagged particles. Several possibilities can be observed.

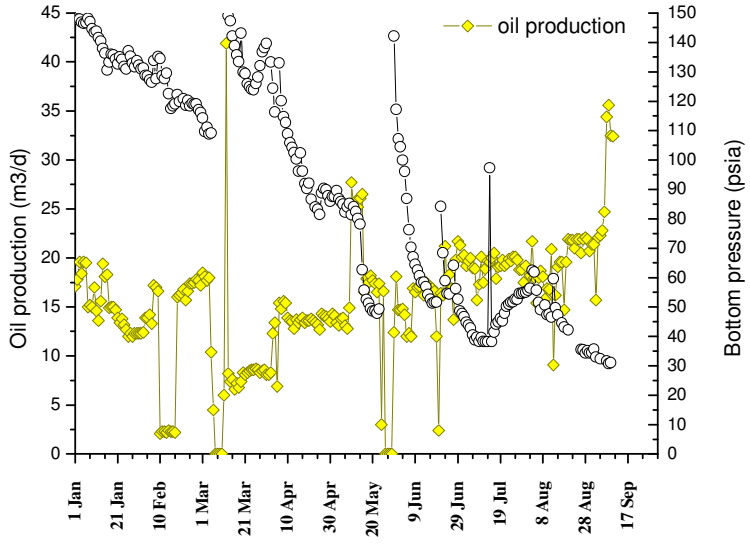

Figure 4. Production records of well P7 before and after the gel treatment.

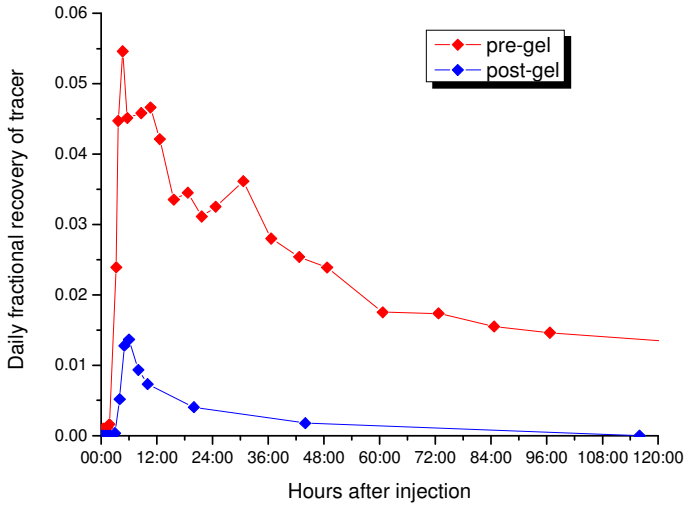

Figure 5. Pre-gel and post-gel tracer records.

If the system had plug flow, no tagged fluid would be seen until a time elapsed equal to the mean residence time of the system, at which point all the elements would leave. The other extreme can be described by perfect mixing. This shape is obtained since the instantaneous mixing of the tracer at time zero gives a certain initial concentration, which is then “washed out” of the system by the continued inflow of no traced fluid.

In our case, we were forced to incorporate mass exchanges between a main flow and a stagnant fluid or a porous solid phase. Special models have been developed for such cases, on the basis of either axially dispersed plug flow concept or perfect mixers in series model. A brief description of each of them is given.

Axial dispersed plug flow with exchange model.

This model comprises one main stream described by the convection-dispersion equation with open/closed boundary conditions, plus a no-flow zone exchanging with the main stream (Fig.6). The parameters given by the model are:

- τ , is in this model only, the total volume of the system divided by the flow rate,
- Pe , is the usual Péclet number,
- N, is a mass transfer coefficient, and
- φ, is the ratio of the cross section of the main stream to the total cross section.

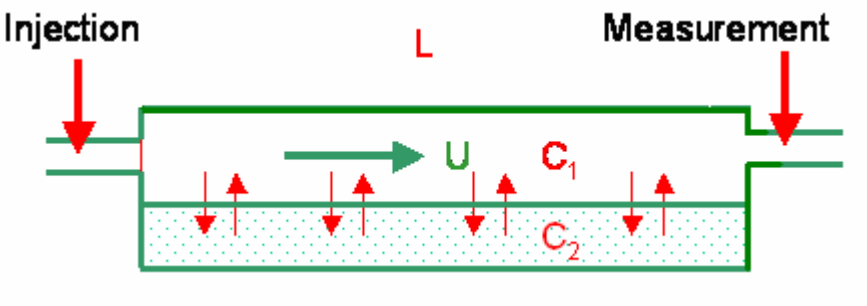

Fig. 6: Axial Dispersed Plug Flow with Exchange

Perfect mixers in series with exchange model

This model consists of a series of (J) perfect mixers with a total volume (V), fed by the flow rate (Q), each perfect mixer being now connected to another one with an exchange flow rate of (αQ) (Fig.7). The total volume of the main stream is V_1 and the total volume of exchange cells is V_2. The parameters given by the model are:

- τ, is the total volume of the main stream divided by the flow rate,
- T_m, is the exchange time constant,
- K , is the ratio of V_1 to V_2, and
- J, is the number of tanks.

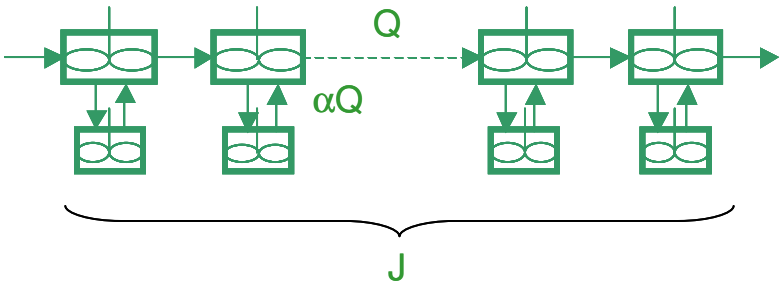

Fig. 7: Perfect mixers in series with exchange

<u>Models behavior</u>

The pre-gel tracer record was best described by an **Axial dispersed plug flow with exchange model,** and the post-gel condition by a **Perfect mixers in series with exchange model.** A RTD software provided by IAEA[4] was used, obtaining the curves and corresponding parameters shown in Figs. 8 and 9. These curves are:

- the signal at the inlet, E(t),
- the signal measured at the outlet, S(t) as:

$$S_{(t)} = \frac{C_{(t)}}{\int_0^{\infty} C_{(t)}\,dt} \tag{3}$$

- the impulse response of the model, H(t).

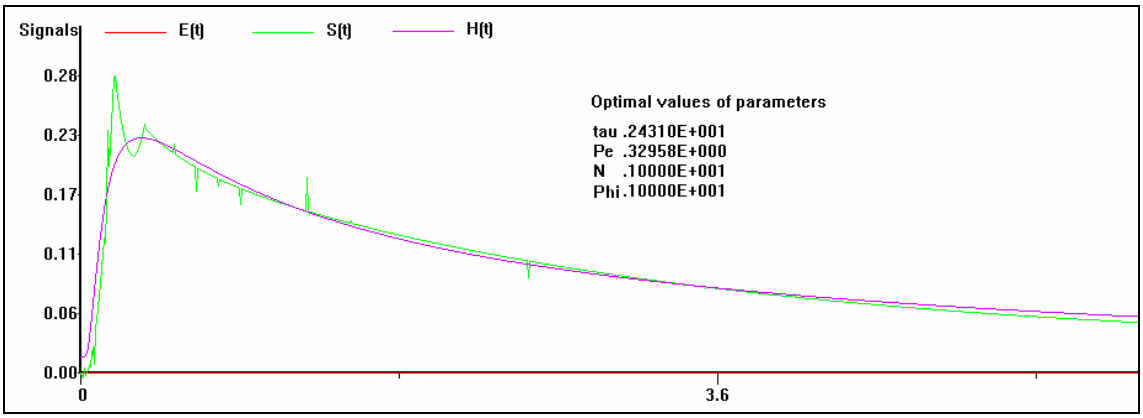

Fig. 8. Experimental and simulated pre-gel tracer records

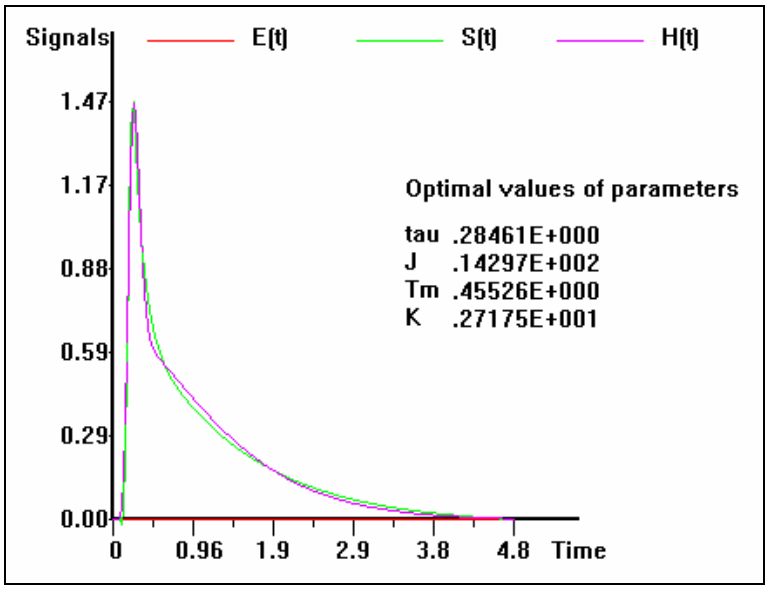

Fig. 9. Experimental and simulated post-gel tracer records

Discussion

The two cases described above, can be analysed based on the results given by both the RTD software and the experiments carried out.

- In the pre-gel tracer test an important recovery of tracer was verified (close to 18%). The channelled water flow rate was calculated, obtaining 18 m^3/day. From the fitted τ, the channelled volume was 43.74 m^3. The wormhole behaves as a tube with strong exchange with a stagnant region. It was interpreted as a deep tracer invasion by

diffusion on the sand walls. This may be intensified by the unconsolidated character of the sand.

- In the post-gel tracer test the recovered tracer was very little (only 0.62%). In consequence a lower channelled flow rate was calculated (0.62 m^3/day). From the fitted τ, a channeled volume close to 0.18 m^3 was estimated. The shape of the curve (and the model that permit to reproduce it, in the best way) suggests a more orientated flow, but in a reduced zone. It is evident that the gel has plugged the channel (almost totally), but it has also sealed the wormhole walls pores, reducing as a result the tracer exchange with the sandy media.
- Even though the tracers have showed to be adequate for evaluating the gel treatment, more work must be performed in relation to the model refining. This paper serves as a first approximation in this field.

References

1. Larry Lines, Sandy Chen, P. F. Daley and Joan Embleton. **"**Seismic pursuit of wormholes**".** *The Leading Edge*; May 2003; v. 22; no. 5; p. 459-461; DOI: 10.1190/1.1579580 © 2003 Society of Exploration Geophysicists
2. Allan McDiarmid, Ivor Alexander, Andy Ion and Jeffrey Thompson. "Experience of a Reservoir Waterflood Failure and Remediation Treatment in the Stag Reservoir, Australia". Paper SPE 72117. Presented in SPE Asia Pacific Improved Oil Recovery Conference. Kuala Lumpur Malaysia, 8-9 October 2001.
3. Danckwerts P V. "Continuous flow systems. Distribution of residence times". *Chem. Eng. Sci.* **2**:1-13, 1953
4. Radiotracer Residence Time Distribution Method for Industrial and Environmental Applications. Training Course Series 31. IAEA. Vienna 2008.

Hydrodynamic Characteristics of SDU Enterprise "Heriberto Duquesne" by the radiotracer method.

Griffith J, Derivet M; Cuesta J, Flores J, Valdés J.

Instituto Cubano de Investigaciones Azucareras (ICINAZ), MINAZ
Carretera Central M. Prieto Km 21/2 Boyeros, C. Habana

E-mail:amaderivet@infomed.sld.cu
E-mail: jose@ceaden.edu.cu

Abstract.

Preliminary results achieved in the evaluation of the hydrodynamic characteristics of the settling dissolute unit (SDU) at the wastewater treatment plant located in the molasses enterprise "Heriberto Duquesne" working in continuous regime employing distillery slops diluted with water are presented.

Tc-99m was employed as tracer, its injection was performed instantaneously with the treated distillery slop fluid and the monitoring of the tracer through different areas of the unit was carried out with the help of radiation detectors. The control of specific parameters of the fluid as pH, conductivity, temperature, Brix (dissolved solids), Chemical Oxygen Demand (COD) and Settling Index was performed through the discrete sampling method.

Results achieved during the evaluation have shown that the pattern flow is far away from the theoretical one that is expected for a settling unit, the hydrodynamic model reflects the combination of a Tank in series flow with interchangeable "dead "zones due baffle design and the irregular fluid inlet to the system.

Recommendations are presented in order to eliminate the above mentioned deficiencies with the aim to increase the efficiency of the settling unit.

Introduction.

The wastewater treatment plant (WWTP) of the Sugar Enterprise "Heriberto Duquesne" located at the city of Remedios, province Villa Clara constructed according ICIDCA Technology /1/ is conceived for the treatment of 800 m^3 distillery slops with the aim to reduce the pollution in the discharge of these waste to the environment.

One of the main units of this WWTP is the Settling Dissolute installation destined for elimination of solids after the neutralization and alkalization with liming milk (4 Bx) of the diluted distillery slops. The settling process that takes place in this unit leads to the reduction of the polluted charge and the efficiency of this process depends mainly on the velocity, settling time and the design of the installation, with the objective to reach a high degree of solid-liquid separation in a determine hydraulic retention time.

Taking in account this premise it was decided to carry out an evaluation of the hydrodynamic characteristics of this unit controlling the main parameters of this process in order to verify if the

hydrodynamic model was close to the regimen of dispersed plug flow that should take place in this type of installation with the employment of the radiotracer method/2,3/

Material and methods.

- ^{99m}Tc ($T_{1/2}$ = 6.02 h, Energy = 140 KeV) as pertechnetate from a radioisotope generator of $^{99}Mo/^{99m}Tc$ was used as tracer. The injection of 150 mCi was performed at the inlet of the distillery slop fluid at the right side of the zone delimited by the baffle of the SDU (see scheme in figure 1).
- For the continuous monitoring of tracer activity the detection system from FORCE Technology composed by 6 INa scintillation detectors coupled to a portable laptop with the PM4 software for the visualization of activity vs time after injection, was employed.
- Distillery slop was urea and milk lime, dissolution with water was performed in a separate way at the proper zone delimited by the baffle.
- pH measurements were carried out with the PROFLINE ph-meter, conductivity with the help of PORTMEAS conductimeter, Brix through an ABBE refractmeter and in the determination of the settling index, the "GENESYS" spectrophotometer was used. COD determination was carried out by the standard method.
- With the aim to evaluate in all the extension the SDU and verify some results reached in early tests related to the time and degree of fluid homogenization, several detectors were situated in different zones of the installation as schematically is shown in figure 1

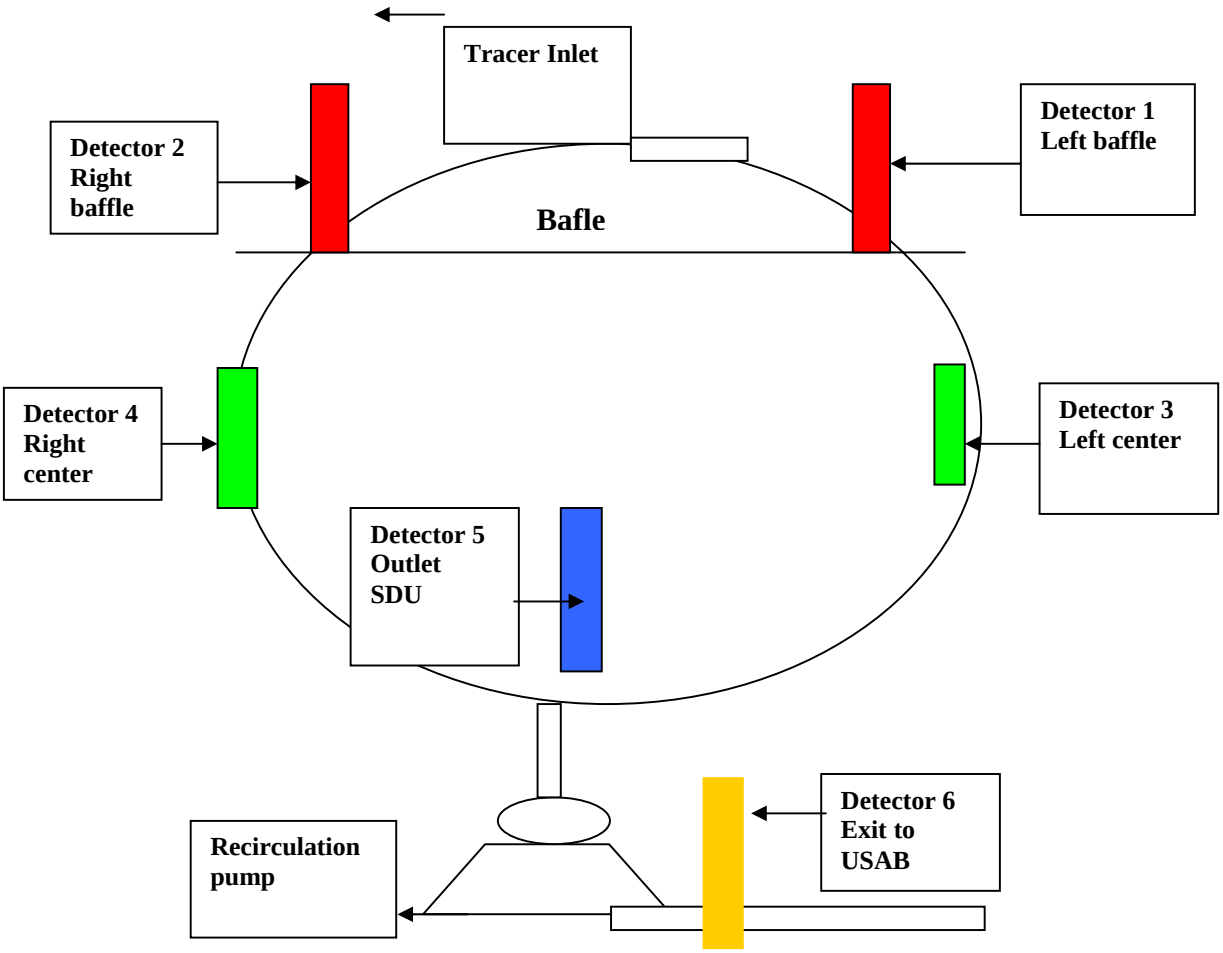

Fig. 1 Scheme installation detectors and tracer injection (Tc-99m) at the SDU.

- DTS PRO /4/ software was employed for response curve processing..

Results.

In figures 2, 3 and 4 are shown the response curves from tracer inlet obtained by detectors situated in the above mentioned zones. Detector #6 situated at the fluid pipe exit to the USAB reactors was collimated and achieve a lower count rate.

Due the unexpected retention time at the baffle region derived from the form of the response curves detectors #1 and 2, the response curves of detectors # 3, 4, 5 and 6, reflect a pattern flow far away from the dispersed plug flow that should be took place in this type of installation taking in account the proper essence of the settling process.

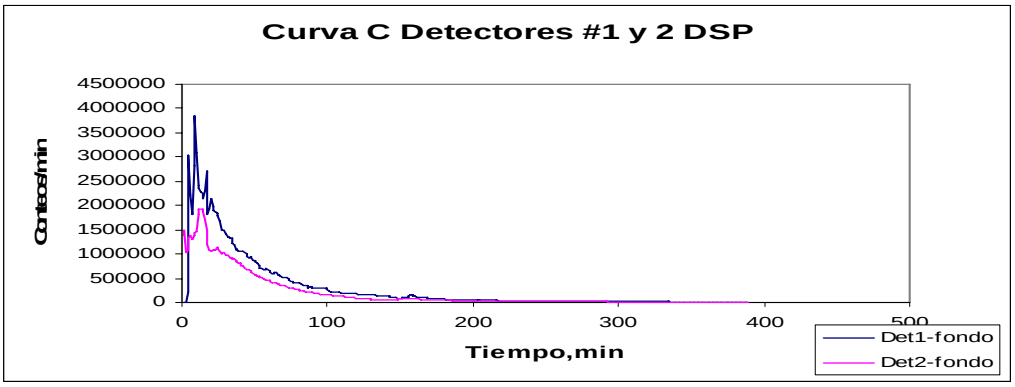

Fig.2 Response Curves Detectors #1 (Left Baffle) and #2 (Right Baffle) SDU.

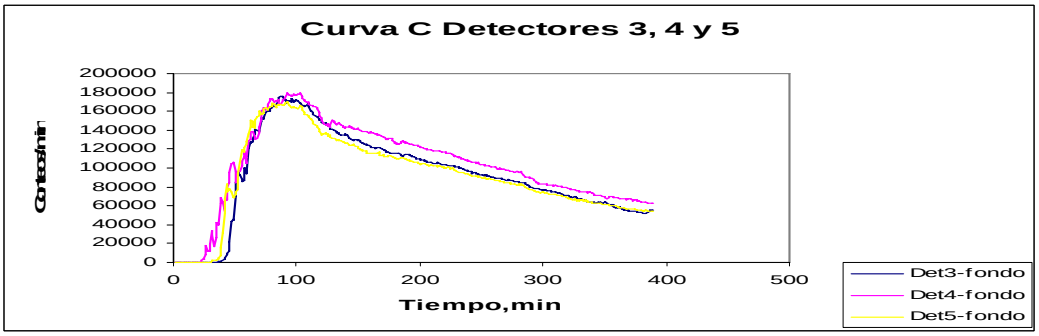

Fig.3 Response Curves detectors #3,4 and 5.

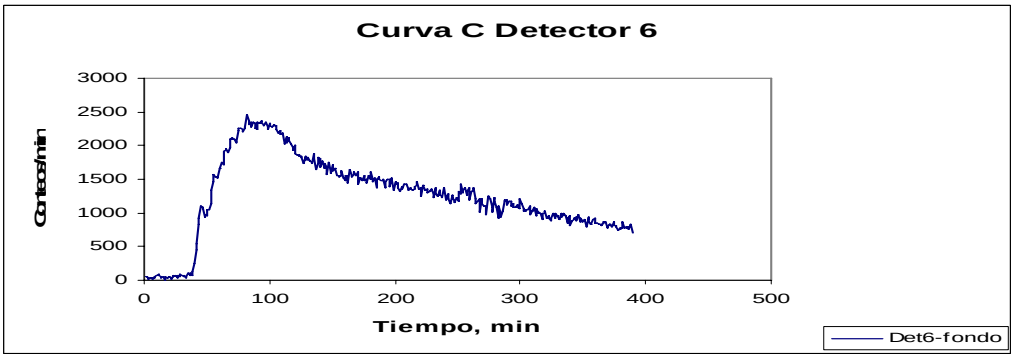

Fig.4 Response Curve Detector #6 (Collimated situated at the pipe exit to USAB).

A first adjustment of response curves to theoretical models of Residence Time Distribution (RTD) was carried out with the employment of the DTSPRO software. The main parameters of this distribution are shown in Table No.1. The response curves from detectors #1 and #2 located at the baffle region, the theoretical model that better adjust to the experimental curve is the one that compromise a perfect mixing cell (J=6) connected to a tank in series with recirculation (Fig.5)

In the case of the response curves from detectors # 3,4,5 and 6, the theoretical model fits well to system that compromises two parallel block, one perfect mixing cells and the other a tank in series exchanging with a dead zone (Fig.6)

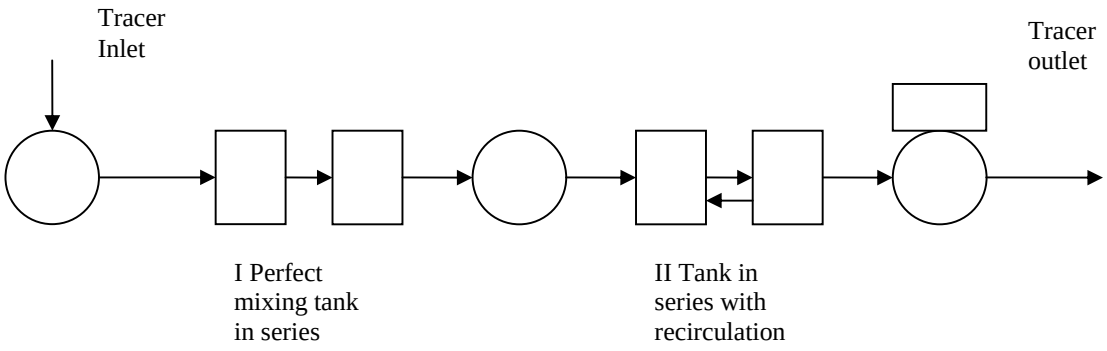

Fig.5 Scheme theoretical model flow pattern detectors #1 and 2.

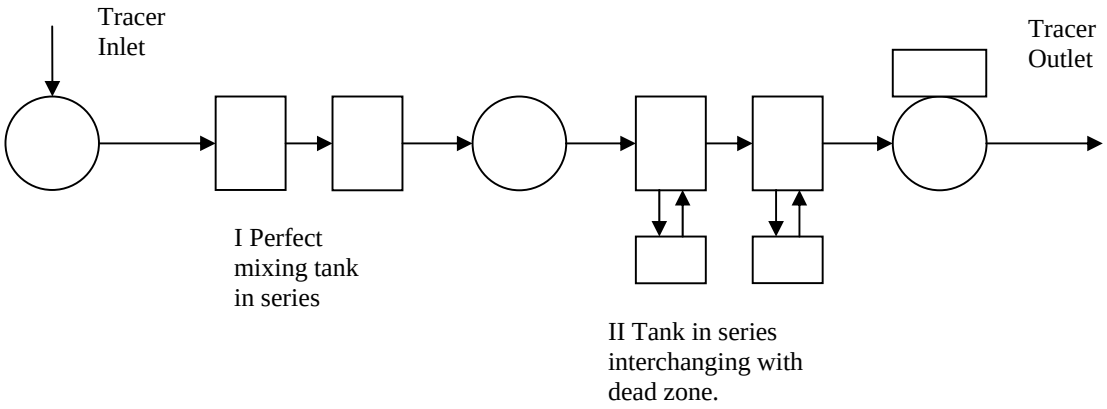

Fig.6 Scheme theoretical model flow pattern detectors #3,4,5 and 6.

Table No.1 Parameters RTD curves at the position of detectors

Parameters RTD curves	Detector #1	Detector #2	Detector #3	Detector #4	Detector #5	Detector #6
1st moment (Residence time), min.	60	56	188	187	185	187
2nd. moment	8195	7370	43945	44239	43270	44056
(Dispersion)	4588	4228	8537	8937	8949	9099

Example of the fitness of the experimental curves to the proposed theoretical models are shown in figures 7 and 8 for detector #1 (located relative far away from tracer inlet) and detector #5 (outlet of the SDU). Visually it can be observed that the adjustment seems adequate and demonstrate that the model describes the flow pattern in this part of the unit.

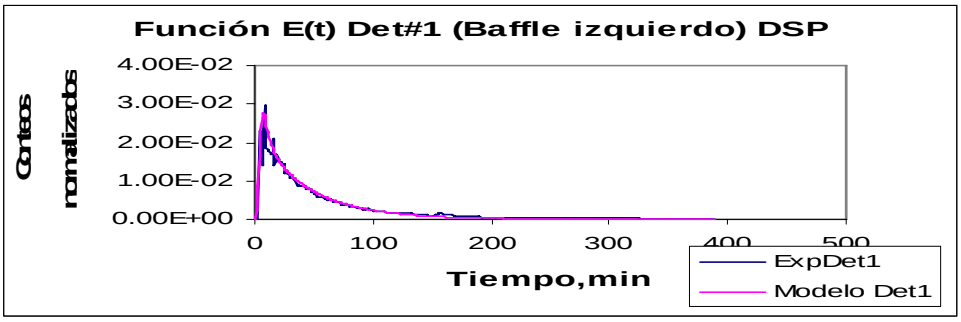

Fig. 7 RTD Curve Detector #1

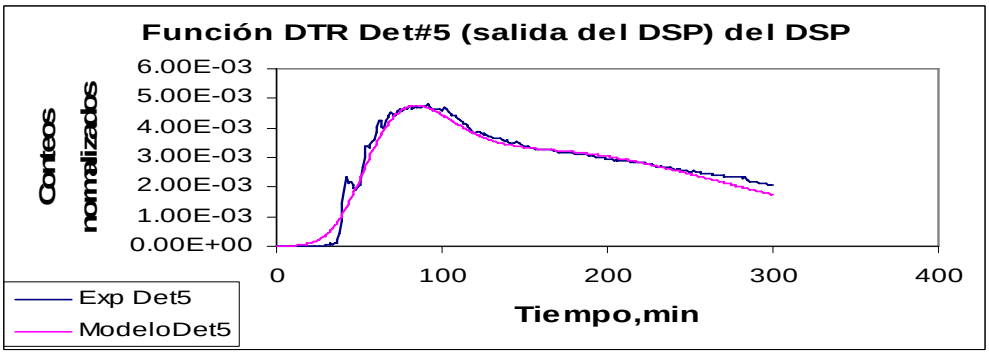

Fig.8 RTD Curve Detector #5.

Results of the chemical analysis performed upon the discrete samples drawn out at the inlet and outlet of the fluid during the evaluation are presented in Tables No. 2 and No.3

Table No.2 Values of the analytical parameter of inlet samples of SDU

Time sampling	pH	Conductivity, mS	Brix	Absorbance (720nm)	Temperature ^{o}C	COD (g/l)
11.15 am	4.46	11.99	5.25	2.413	28	32.63
12.15 pm	4.46	9.94	3.50	2.317	27	-
1.15 pm	4.10	14.18	5.00	2.735	29	-
2.15 pm (*)	9.30	3.13	1.30	1.079	25	0.897
3.15 pm	4.09	13.38	4.75	2.749	30	38.41
4.15 pm	4.08	14.61	4.25	2.451	32	40.38
5.15 pm	4.09	14.80	4.75	2.467	32	41.28

(*) Sample that evidently suffer some problem when was taken.

Table No.3 Values of the analytical parameter of outlet samples of SDU

Time sampling	pH	Conductivity mS	Brix	Absorbance (720nm) No centrifuged	Absorbance (720nm) centrifuged	Temperature ^{o}C	COD (g/l)
11.45 am	4.90	9.75	3.25	2.037	1.424	23	18.84
12.45 pm	4.89	9.54	3.25	2.042	1.501	23	-
1.45 pm	4.90	9.24	3.25	2.127	1.427	22	20.64
2.45 pm	4.90	9.13	2.75	2.294	1.426	23	-
3.45 pm	4.88	9.20	2.50	2.285	1.412	23	-
4.45 pm	4.84	8.71	2.75	2.205	1.303	24	-
5.45 pm	4.79	8.75	3.25	-	1.282	24	12.56

Taking in account that the measurement of the absorbance at the wave length of 720nm is proportional to the degree of turbidity of the fluid, the comparison of the values obtained for inlet samples and those corresponding to the outlet samples displaced 3hours (residence time of the SDU), could be used as a criterion to evaluate the Settling Efficiency (SE) at the DSU. The following expression was used with this objective:

$\%SE = ((ABS_{INLET} - ABS_{OUTLET})/(ABS_{INLET}))x100$
where:
%ES, percent settling efficiency
ABS_{INLET}, Absorbance inlet sample at 72 0nm.
ABS_{OUTLET}, Absorbance outlet sample at 720nm displaced 3 hours respect to the inlet sample.

Additionally, with the aim to evaluate the efficiency of the settling process in ideal conditions we introduce the concept of Settling Index (SI) in witch we compare the absorbance of the outlet sample no centrifuged with the proper sample centrifuged that practically eliminates all the turbidity. The method is based in the following expression:

$\%S = (ABS_{NC} - ABS_{C})/ABS_{NC})x100.$
Where:
%SI, percent of Settling Index.
ABS_{NC}, Absorbance at 720nm of the no centrifuged outlet sample
ABS_{C}, Absorbance at 720nm of the centrifuged outlet sample.

In Table No.4 are shown values obtained for %SE and %SI of samples during the evaluation of SDU.

Table No.4 Determination of %SI and %SE

No. Sample (time)	ABS inlet sample	ABS outlet sample no centrifuged	ABS outlet sample centrifuged	% Settling Efficiency	% Settling Index
1. (11.15am)	2.413	2.294	1.424	4.93	37.92
2. (12.15pm)	2.317	2.285	1.412	1.38	38.05
3. (1.15pm)	2.735	2.205	1.303	19.37	40.90

These results show that the values of % of Settling efficiency are far away from the % of Settling Index, indicating that the unit is not working as expected.

Results Discussion.

According to these preliminary results the flow pattern of SDU does not corresponds to the dispersed plug flow that should take place in the settling process.

This anomalous behavior in our criterion is due the retention of the fluid at the zone delimited by the baffle and the route of the fluid inlet through the corner of that zone and not by the center. This situation allows that the fluid moves more faster by the right side than the left side in such way that the time of appearance of the tracer (Table No.5) in the left side of SDU where detector #3 is located is much larger even than the time of appearance at the outlet of the unit where detector #5 was situated.

Table 5. Time of appearance of tracer.

No. Detectors	Position of detector at the SDU	Time of appearance of tracer. (min.)
#3	Left Central Side	37
#4	Right Central Side	23
#5	SDU Outlet	31
#6	Pipe Exit to USAB reactor	44

Another fact that also has a markedly influence is the baffle design. According to the design the travel of the fluid from the baffle zone to the center of the SDU occurs through an aperture (gap) situated at the bottom along the whole wall of the baffle, this condition the possibility of short-circuiting of the fluid by the right side of the zone delimited by the baffle that is much closer to the fluid inlet.

In order to achieve a more homogeneous distribution of the fluid from the baffle zone, the inlet of the fluid should be by the center of that zone and gaps should be situated equidistant at the left and right side at the bottom of the baffle walls. With this design the fluid is obligated to emerge at the same time to the other part of the SDU.

Nevertheless these deficiencies, according the analytical parameters performed during the evaluation a certain degree of suspended and dissolved solids was removed. This fact evidence that the approximation of the flow pattern to the expected model undoubtedly will contribute to increase the efficiency of the SDU.

Conclusions:

- The flow pattern of the SDU installed at the WWTP " Heriberto Duquesne" does not corresponds to the dispersed plug flow that should take place in this type of installation.
- The % of Settling efficiency at the SDU is low and is relative far away from the Settling index.
- There are evidences that nevertheless the detected deficiencies, certain separation of suspended and dissolved solids was achieved at the SDU during the evaluation.
- The relative high residence time at the zone delimited by the baffle, indicated an irregular inlet of the fluid to the system or problems with the baffle design.

Recommendations:

- To take in account the proposal to carry out the inlet of the fluid by the center of the zone delimited by the baffle.
- Redesign of the aperture located at the bottom of the baffle through the construction of equidistant gaps on the bottom at the right and left side baffle walls.

References:

1. Obaya, C y Col. Tratamiento combinado de la vinaza de destilería y residuales azucareros en reactores USAB. Tecnología de Agua, 78-85 (2004)
2. LEVENSPIEL O, Ingeniería de las Reacciones Químicas 2da. Edición. Ed. Reverté (1974)
3. GUIDEBOOK ON RADIOSOTOPE TRACERS IN INDUSTRY. Technical Reports Series No. 316, IAEA, Vienna (1990).
4. LECLERC J.P DTS PRO V4.2 A software for interpretation of Tracer Experiments in Industrial Processes. PROGEPI, France (1998).

Acknowledgements:

- To the International Atomic Energy Agency (IAEA) for the support in the execution of this work as a part of the l ProjectoCUB/8/021.

IMPLEMENTATION AND AUTOMATIZATION OF A FLOW-THROUGH EXPERIMENTAL SETUP FOR THE EVALUATION OF NEW TRACERS FOR OIL RESERVOIR CHARACTERIZATION

Bruno Resende Debien[1], Aimoré Dutra, Letícia Tasmo Perigolo and Rubens Martins Moreira
Centro de Desenvolvimento da Tecnologia Nuclear (CDTN / CNEN - MG)
[1]brunodebien@yahoo.com.br

ABSTRACT

One of the greatest challenges facing petroleum extraction is to increase its fractional recovery as much as possible. Injection of fluids – especially water – is the most commonly applied method to reach that goal, since it forces the remaining oil to leave the rock formation. Therefore, it is necessary to evaluate the performance of this process and the most efficient tool used for this purpose is the injection of tracers, which are able to provide information about the behaviour of the injected fluid inside the reservoir. However, before their application in the field, tracers must be experimentally evaluated in the laboratory, aiming to guarantee its effectiveness. One of the most important parameters that must be investigated is their interaction with reservoir rocks. The present paper describes an automated laboratory column experiment designed to study sorption characteristics of compounds synthesised in CDTN on consolidated sandstone samples from the Botucatu formation. The system performance was investigated using the NaCl as reference tracer – since its behavior is in quite good agreement with tritiated water, considered the ideal tracer for water phases – and confirmed that the construction and automatization of the system for flow-through tests were successful.

INTRODUCTION

Nowadays petroleum is one of the most important energy sources of the planet, and is also the raw material for more than six thousand different products. For these reasons it has became one of the main natural resources all around the world.

At the beginning of its exploration, oil gushes spontaneously from the production wells, forced by the elevated original pressure within the formation. After a rather short period, it becomes necessary the injection of fluids (mainly water) in specific wells, denominated injection wells, in order to extract the remaining amount of oil in place. The implementation of this method, called secondary recovery, can increase the fraction of oil extracted up to around 40%. Because of this expressive value, any technique that provides information of the fluid behaviour inside the reservoir (as the use of tracers) becomes crucial for evaluating exploration's strategies, resulting in economic gain (IAEA 2002).

Tracer is any compound that can be added to the mass of a substance in order to provide information about the behavior of the latter in a chemical, biological or physical process (BEDMAR, 1972). They are used to investigate water flow inside the reservoir, aiming to optimize its secondary recovery. Tritiated water (3H-O-H) is considered the ideal tracer for studies involving aqueous phases. It has been used in many countries to characterize their petroleum reservoirs, including Brazil, where only CDTN had already applied it (MOREIRA, 2005).

Furthermore, other promising options (as K35SCN, tiocarboxilic acids and some inorganic complexes) are being studied at CDTN, in order to allow simultaneous investigations of the several flows present in the same reservoir (MOREIRA, 2005). However, these optional compounds should be previously tested in laboratory, to verify if they will work satisfactorily in the field. One of the most important requirements that a certain compound must fulfill in order to be applied as a passive tracer is following water molecules without sticking to the rock surfaces.

Sorption is the general term used to define the retention of a compound at a solid surface, which results in a retardation of the solute compared to water movement. Among the general methods applied to investigate that phenomenon, laboratory flow-through (or column) method is the second

most frequently used, and allows the determination of distribution factor (Kd) value considering chemical and hydrodynamic effects (EPA, 1999).
The present paper describes an automated experimental setup designed to perform laboratory flow-through tests aiming to study the interaction between developed tracers and petroleum reservoir rocks.

EXPERIMENTAL SECTION

FIG. 1 shows a schematic diagram of the experimental apparatus, which was designed and constructed at CDTN. The experiment consists in injecting a pulse of the compound solution (also containing a reference tracer) through a horizontal porous core (only the longitudinal flow is allowed) and monitoring its concentration at the column outlet as a function of time. All column experiments were conducted at room temperature.

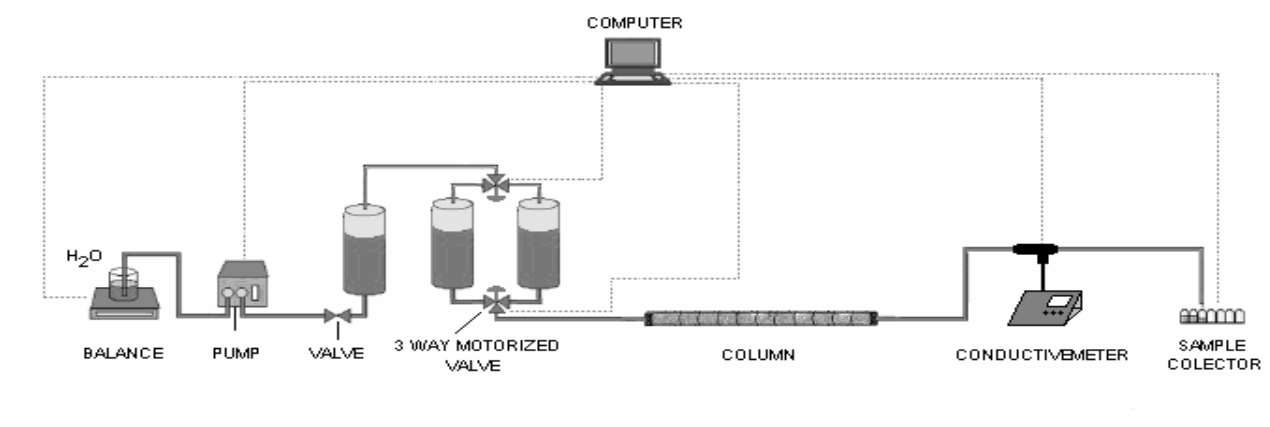

FIGURE 1 – Experimental setup for column experiments.

In order to facilitate the interpretation of the results, a rectangular tracer pulse is commonly used, often preceded and followed by distilled water injection. These feeding solutions (distilled water and tracer solution) were pumped by a dual plunger pump, at a constant flow rate of 1 mL/min, and two home made motorized three way valves (FIG. 2) were coupled up to allow the fluid selection.

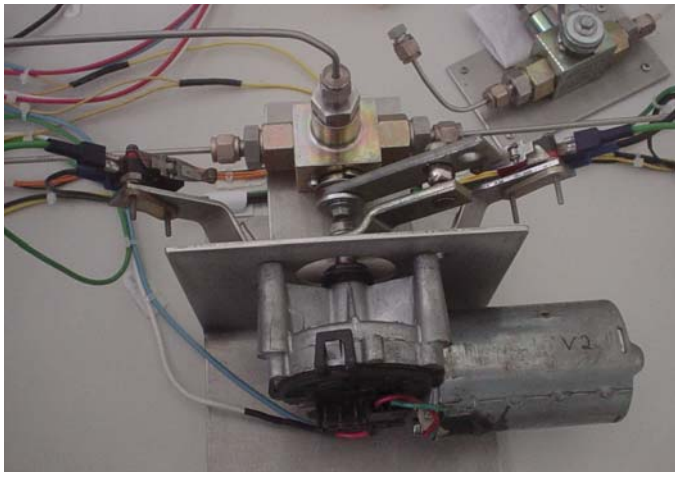

FIGURE 2 – Picture of the home made motorized three way valve.

The columns used in flow-through experiments are usually consolidated samples of cylindrical geometry from the reservoir rocks or other representative rocks. The 24.7 cm long column used in this study is a sample of sandstone from the Botucatu formation, constituted mainly of quartz containing a small amount of feldspar and cemented by silica, similar to the majority of the

reservoirs rocks found widespread. It was saturated with water prior to the runs, and its properties can be seen in TAB. I.

TABLE I – Column properties

Length (cm)	Diameter (mm)	Total volune (cm^3)	Porous volume (cm^3)	Permeability - water (mD)
24,7	37,2	268,32	64,2	598

The column exit was connected to an automatic sample collector, and the collected aliquots were monitored in order to determine the concentration of the injected compounds. Experimental results are commonly presented as breakthrough curves (BTC's); i. e. a graph of the tracer's relative concentration versus injected pore volumes. A reference tracer – usually tritiated water, considered the ideal tracer for aqueous phase study – is injected with the compound under investigation, and the comparison of both BTC´s allows the evaluation of the latter's dynamic behaviour. Tritiated water replacement as reference tracer by NaCl was tested, due the lower cost of the latter, and to the simplicity of its measurement via a conductivity meter equipped with a flow-through cell that could produce information online.

A specific computer program named Condutix N (FIG. 3), developed in Liberty Basic language, is responsible for data acquisition and controling the sample collector, the pump and the motorized three way valves.

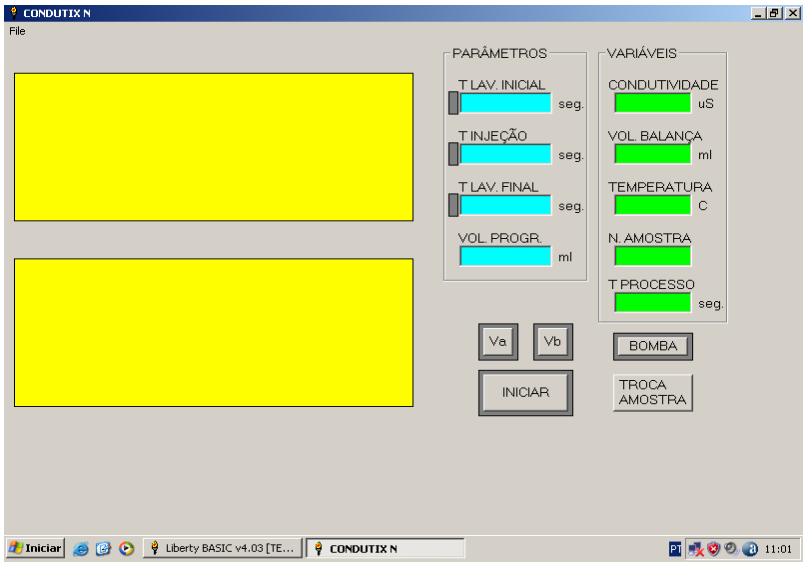

FIGURE 3 – Picture of the Condutix N main window.

RESULTS

3.1) Reference tracer

Simultaneous injection of tritiated water and NaCl was performed in order to examine the possibility of replacing the former by the latter as reference tracer in laboratory flow-through experiments. At that point the system was not automatized yet, and the detection of both compounds was accomplished in the samples collected at the column exit. The comparison of their BTC's can be seen in FIG. 4.

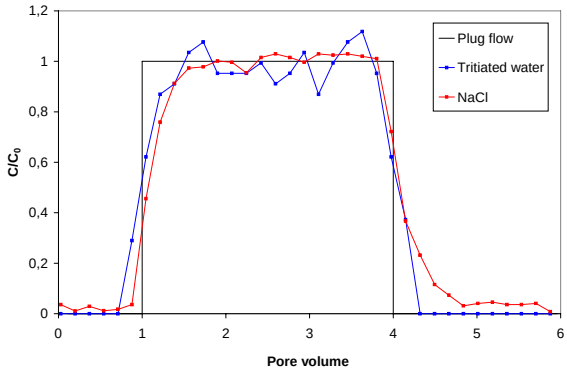

FIGURE 4 – Comparison of tritiated water and NaCl breakthrough curves.

The black curve represents an ideal plug flow (D = 0), and the other curves correspond to tritiated water and NaCl. They exhibit smoother gradients due to the dispersion that occurs inside porous media. Despite the small differences that can be seen in the graph of FIG. 4, both BTC's are quite similar, suggesting no retardation of the NaCl relatively to tritiated water, confirming the potential of the former to be used as reference tracer.

3.2) Flow through cell position

Once the NaCl was confirmed as the reference tracer to be used in order to evaluate the experimental setup, a flow cell conductivity meter was connected to the column exit in order to ease the NaCl detection. Samples were also collected immediately downstream the cell and measured in a batch conductivity meter. Besides, runs without the flow cell were performed, with a batch-wise NaCl measurement. The continuous and batch measurements (with and without the flow cell connected in the experimental setup) were compared aiming to verify whether the cell did not cause any interference in the values obtained. Results are presented in FIG. 5.
NaCl BTC's for continuous and batch measurements are in quite good agreement, as can be seen in the graph of FIG. 5. It demonstrates that the presence of the flow cell in the experimental setup does not cause any interference to the results. However, it only happens whem the flow cell is at horizontal position, because it changes the hydrodynamic behavior of the compound when vertically positioned.

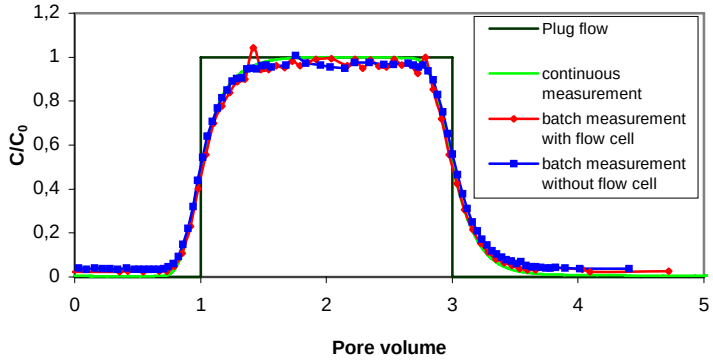

FIGURE 5 – Comparison of NaCl BTCs for continuous (flow), and for batch measurements with and without flow cell.

3.3) Experimental setup automatization

At this point the system setup automatization was completed, and the experimental data obtained could be saved in the computer as a text file, whose format is presented in FIG.6.

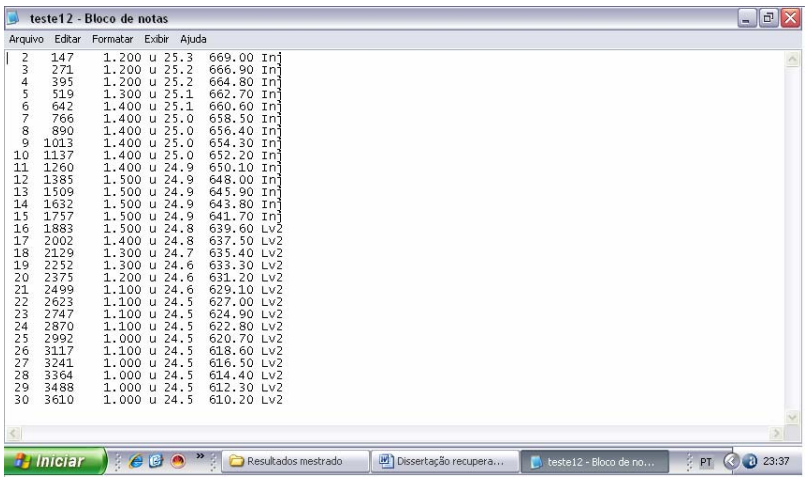

FIGURE 6 – Text file created by the Condutix N, containing experimental data.

Columns are not labeled, but they are related, respectively, to the vial number, experimental time, conductivity, temperature and mass values measured.

Once the pump outflow is able to negatively influence the stabilization of the balance measurements, compromising the transmission of data to the computer, the operational range of the pump had to be established. It can be seen in FIG. 7 that this parameter must be kept below 5 mL/min in order to guarantee a proper response of the experimental setup.

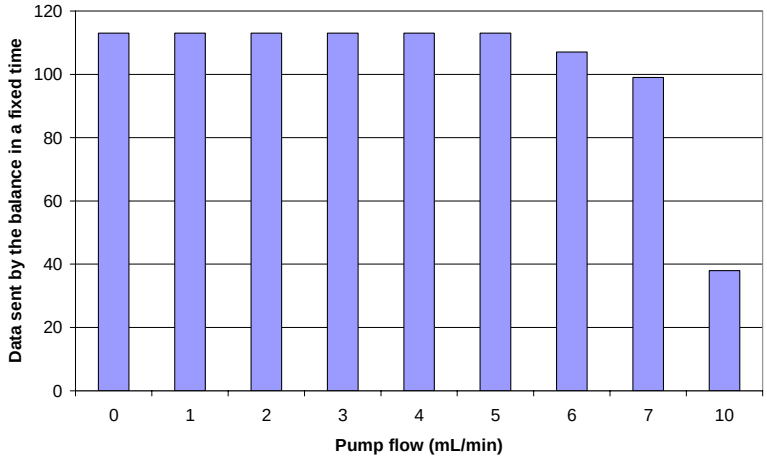

FIGURE 7 – Influence of the pump flow in the frequency of data sent by the balance to the computer.

Finally, aiming to validate the results obtained by the automated experimental setup, breakthrough curves from automatizated and manually controled tests were compared (FIG. 8).

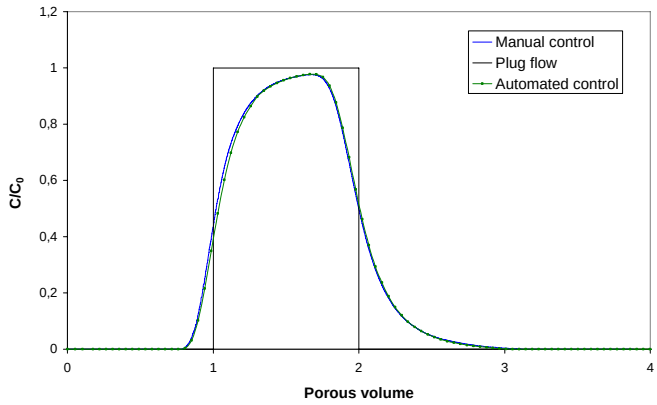

FIGURE 8 – Comparison of BTC's from both manual and automated controlled experiments.

As can be seen in the graph of FIG. 8, the automatization of the experimental setup for flow-through tests was a success.

CONCLUSION

In this paper the experimental setup constructed and automated at CDTN to carry out laboratory flow-through experiments was presented. That system allows the study of the sorption characteristics of compounds on geological materials such as soils, sediments and rocks, becoming a useful tool for evaluating the performance of tracers before their injection in field tests, increasing the chance of success in their application.

ACKNOWLEDGMENTS

The authors gratefully acknowledge the CNEN and CTPETRO/FINEP, which provided financial support.

REFERENCES

1. BEDMAR, A.P. Consideraciones generales sobre trazadores. In: Isótopos en hidrologia. Espanha: Alhambra, 1972. Cap. 2.
2. EPA – ENVIRONMENTAL PROTECTION AGENCY. Understanding variation in partition coefficient, K_d, values – volume 1: the K_d model, methods of measurement and application of chemical reaction codes. United States of America: EPA, 1999 (402-R-99-004A)
3. IAEA - INTERNATIONAL ATOMIC ENERGY AGENCY. Tracers in oilfields and geothermal reservoirs. In: Radiotracer applications in industrial processing, oil and geothermal reservoirs – a guidebook. Viena, 2002. Cap. 6.
4. MOREIRA, R. M. Desenvolvimento de metodologia de multitraçadores para caracterização de reservatórios de petróleo – Multitracer. Belo Horizonte: Centro de Desenvolvimento da Tecnologia Nuclear, 2005.

METHODOLOGY FOR INJECTION OF RADIOACTIVE TRACER IN OIL RESERVOIRS

Alberto Avellar Barreto, Amenônia Maria Ferreira Pinto, Rubens Martins Moreira, Bruno Carvalho Garcia
Centro de Desenvolvimento da Tecnologia Nuclear - CDTN

ABSTRACT

The oil recuperation rate in oil reservoirs, if any case of intervention occurs, is of approximately 25%. So, an injection of different flows in the reservoir aiming at expelling the residual oil from the pores that are kept was used. The use of tracers is a great tool to help in this work. The Nuclear Technology Development Center (CDTN) and the Brazilian company named Petróleo Brasileiro SA (PETROBRÁS) have been studying the Oil reservoirs by applying the radioactive tracers. The information of such studies aims at increasing the understanding of the injection fluid, usually water. In this work, it is presented the methodology used at CDTN for the injection of radioactive tracers in oil reservoirs. This methodology was developed following the principles of radioprotection defined by the Nuclear Energy National Commission (CDTN). Cylinder samplers are used to store and transport tracers to oil fields. The procedures are described in order to prepare the scheme for the tracer injection; for the tracer transportation until the place for injection; for carrying out the tracer injection operation and for performing the sampling in the producing wells. Also, the advantages in relation to methods used previously and the main difficulties faced along the execution of the whole tracer injection process in works performed by the CDTN staff are related.

INTRODUCTION

Oil is considered a non renewable energy source. It is a raw material for oil and petrochemistry industries resulting in many other kinds of material. It is known that the oil recuperation rate in oil reservoirs, if any case of intervention occurs, is of approximately 25%. So, an injection of different flows in the reservoir aiming at expelling the residual oil from the pores that are kept was used. The use of tracers is a great tool to help in this work. Such techniques can increase the extraction coefficient until 50% from the original volume of the oil reservoir.

The Nuclear Technology Development Center (CDTN), an Institute of Nuclear Commission of Brazil (CNEN), has been applying tracers in several works in Brazil. In the beginning, the applications were used to help in environmental problems like: aquifer contamination, study of hydrodynamic mixing zones (coast problems) and pollutant discharges into surface waters. In the last years, CDTN and the Brazilian company named Petróleo Brasileiro SA (PETROBRÁS) have been studying the Oil reservoirs by applying the radioactive tracers. The information of such studies aims at increasing the understanding of the injection fluid, usually water. These studies are part of a great project that is developed in the CDTN with the objective of to investigate, to synthesize and to test new compounds that can be used like tracers.

The works with radioactive tracers implying some cares, the methodology used at CDTN for the injection of radioactive tracers in oil reservoirs was developed following the principles of radioprotection defined by CNEN. This methodology use cylinder samplers to store and transport tracers to oil fields. The objective of this document is to describe the procedures for preparing the scheme for the tracer injection: to transfer the tracer to the cylinders, to transport the tracer until the place for injection; to carry out the tracer injection operation and to perform the sampling in the producing wells. Also, the advantages in relation to methods used previously and the main difficulties faced along the execution of the whole tracer injection process in works performed by the CDTN staff are related.

METHODOLOGY

An application of radioactive tracer needs to follow some steps. After to decide what and how much tracer will be used, the first step is to store this tracer in a safety recipient. Some accessories are necessary to perform the operations of fulfill the tracer in the recipient and to inject the tracer in the well. These equipments must be tested in laboratory to prevent some leak during the work of injection.

Components and accessories

We have been using double-ended cylinders (Fig. 01) to stored, to transport and to inject the tracer. Their main characteristics are (TM Swagelok Company; 2003A):

- Body made of seamless tubing provides consistent wall thickness, size, and capacity;
- Smooth internal neck transition allows easy cleaning and eliminates trapped fluids;
- Cold-formed female NPT threads provide greater strength;
- Heavy-wall end connections provide strength and resist flaring.

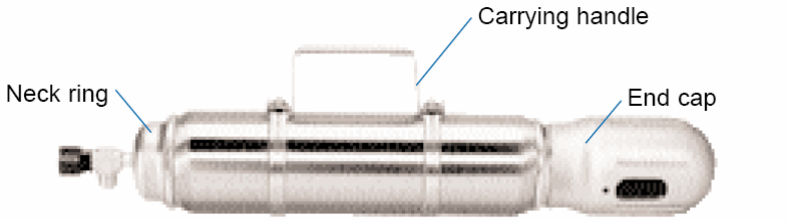

Figure 01 – Sample cylinders and accessories (TM Swagelok Company; 2003A).

In Fig. 01 can be observed the carrying handle, this accessory provides a convenient way to carry sample. Other importants accessories are the caps and plugs that are used to protect the tube fitting or NPT end.

In ours works we have been used two types of cylinders:

- Cylinder A: size of 3785 cm^3 (1 gal); working pressure of 3000 psig (210 bar).
- Cylinder B: size of 500 cm^3 (1 gal); working pressure of 5000 psig (344 bar).

The needle valves connected to the end of cylinders are projected to working pressure of 5000 psig (344 bar). Some of them are showed in Fig. 02 and Fig. 03.

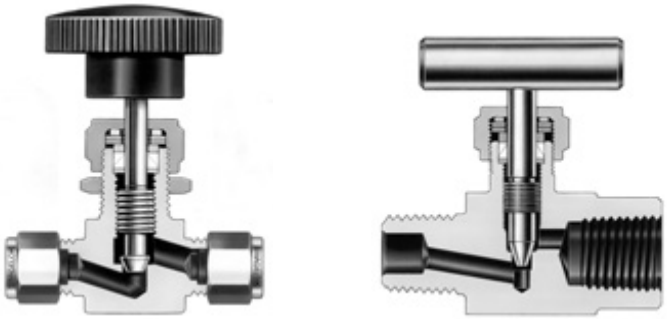

Figure 2 – Needle valves (TM Swagelok Company; 2003B).

The hoses produced to work in high pressure (5000 psig – 344 bar), used during the injection process, are showed in Fig. 03.

The pressure tests

The complete system (cylinders + valves + hoses) is tested in laboratory before be used in the field. During these tests the system is fulfill with water and then, a working pressure is applied (up to 5000 psig).

Figure 03 – Pressure test: cylinders, valves and hoses.

Storing the tracer in the cylinder

The radioactive material (tritium) is supplied in ampoules. After defined the quantity to be injected, this material must be stored in the sample cylinders. Some illustrations of this process are showed in Fig. 04. First the ampoule is cut and the necessary material is collected using a syringe. Then this material is diluted and injected in a dispositive that is connected to the cylinder. A water flux is promoted from a reservoir to complete the cylinder volume. A scheme of this apparatus is described in Fig. 05.

Figure 04 – Storing process of the tracer.

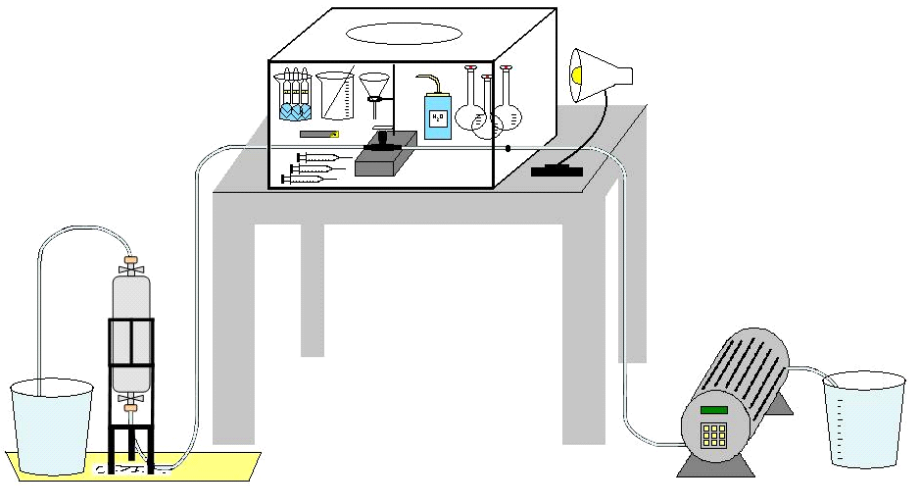

Figure 05 – Scheme to Storing process of the tracer.

Transporting the tracer

The cylinder with the radioactive tracer has to be sent to the point of injection, so it must be used again only in the injector well. It is necessary be sure about the integrity of the cylinder during its way from the CDTN to the field. A transport container was developed in CDTN to do that task. This container has sufficiently foam to absorb all the fluid transported in the cylinder. The container was passed by some tests to verify its resistance. These tests are defined by CNEN. Another function of the container is be used like a kind of platform during the operation of injection. Again, if some leak happens, the fluid will be stored in the foam.

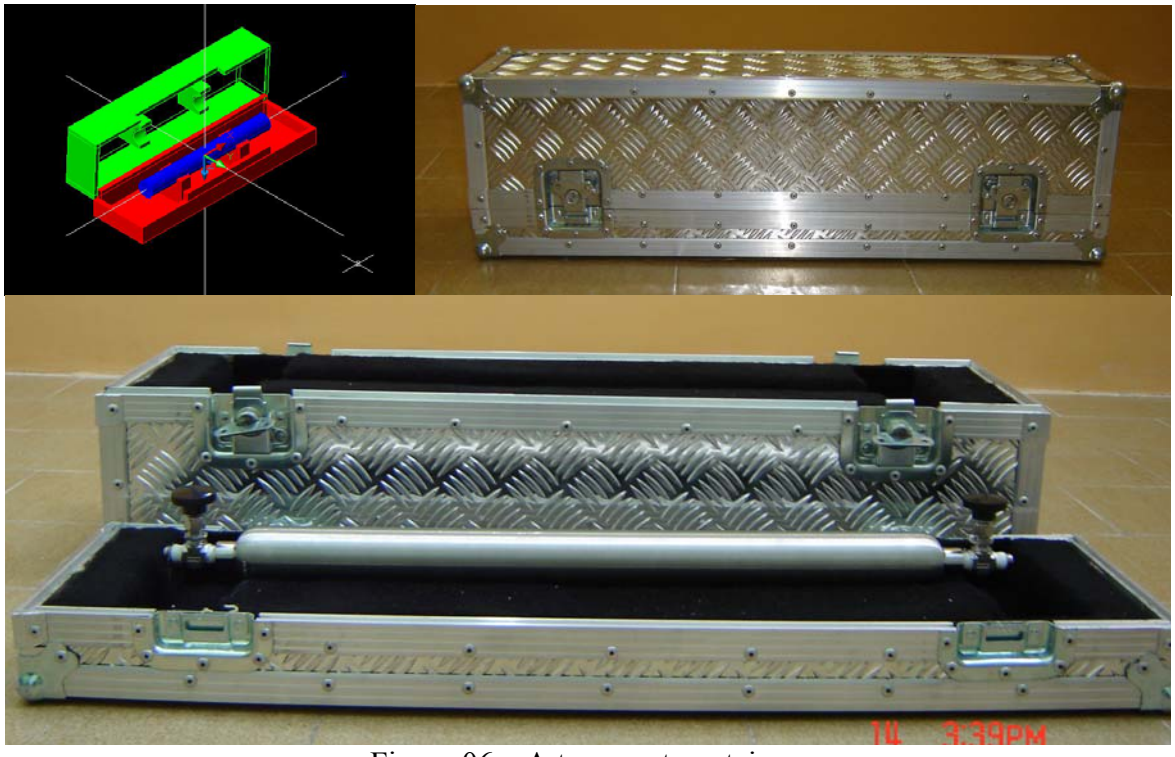

Figure 06 – A transport container.

Injecting the tracer in the well

The process of injection of the tracer uses the system of valves and tubes existing in the water injection well. It is an easy operation: stop the water injection; connect the hoses like is indicated in Fig. 07; open the bypass system; leave the flux through the cylinder during some minutes; close the bypass system; and open the system of water injection again.

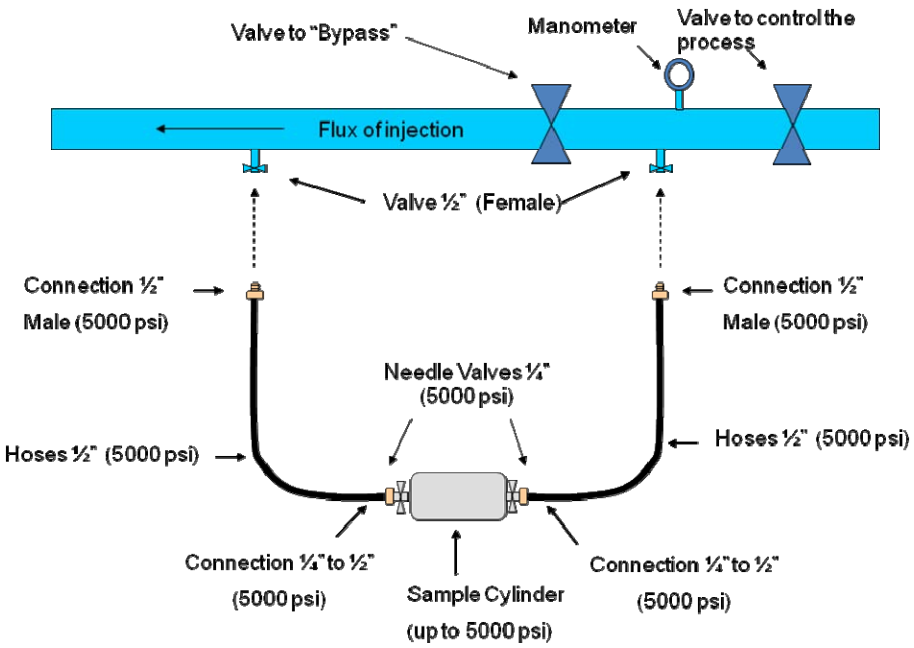

Figure 07 – scheme of the bypass system.

After the injection operation we must investigate about leaks and then return the cylinder to the container. All the others components (hoses, tools, etc) must be stored adequately.

The operations illustrated in Fig.08 were performed in field using the bypass system. The container used to transport the cylinder was an old type.

Figure 08 – scheme of the bypass in the field.

The curve showed in Fig. 09 was constructed using results of the analysis of samples collected in the field where were done the injections.

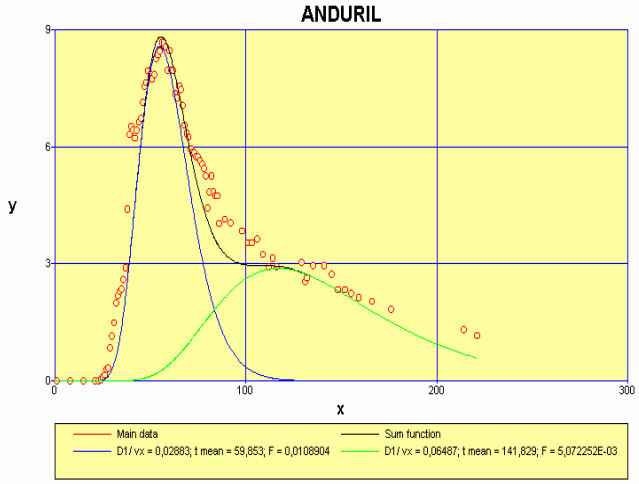

Figure 09 – Break-through curve.

Collect and analysis of samples

After the injection, the process of collect of sample begins. In the well (field), fuel bags (Fig.10) are used to do this collect. Then, these bags are used in the process of separating water from the oil. Water samples are extracted from the bags and they are analyzed in CDTN.
The main techniques used to process the samples are High Performance Liquid Chromatography (HPLC) and Liquid Scintillation. Some of equipments used in these process are illustrated in Fig. 11.

Figure 10 – Fuel bag (left); analysis process.

Figure 11 – Equipments used to the analysis.

CONCLUDING REMARKS

The methodology to injected radioactive tracers described in this work has been developed during the last years. The difficulties passed during the field works were important to teach us some practical details.

REFERENCES

1. MACINTYRE, A. J. Bombas e Instalações de bombeamento. Rio de Janeiro, Guanabara, 1987.
2. Parker Hannifin Corporation (1999). Technologia Hidráulica Industrial. Apostila M2001 BR. Parker Trainning. Jacareí, SP – Brasil. Found in www.swagelok.com.
3. TM Swagelok Company (2003A). Sample Cylinders, Accessories and Outage Tubes. MS-01-177. U.S.A., MI. Found in www.swagelok.com.
4. TM Swagelok Company (2003B). Integral-Bonnet Needle Valves. MS-01-164. U.S.A., MI. Found in www.swagelok.com.
5. TM Swagelok Company (2004). Swagelok Products Compliant with the Transportable Pressure Equipment Directive (TPED). MS-02-193-E. U.S.A., MI. Found in www.swagelok.com.

3.4. MS – Measurement Section

MS03	Determining tritium in new tracers research Raquel M. Mingote , Eliane S. C. Temba and Rubens M. Moreira
MS04	Determining tritium in new tracers research Radon determination in different matrices using LSC Eliane S. C. Temba, Raquel M. Mingote and Amenônia M. F. Pinto
MS05	222Rn determination in water samples by using liquid scintillation spectrometry with different cocktails Thiago C. Oliveira, Raquel M. Mingote and Rubens M. Moreira

5th International Conference on Tracers and Tracing Methods - TRACER 5
Tiradentes, MG, Brazil, November 2 to 6, 2008

DETERMINING TRITIUM IN NEW TRACERS RESEARCH

Raquel M. Mingote[1], Eliane S. C. Temba[1] and Rubens M. Moreira[2]

[1,2] Centro de Desenvolvimento da Tecnologia Nuclear (CDTN / CNEN - MG)
[1] Serviço de Química e Radioquímica, [2] Serviço de Meio Ambiente e Técnicas Nucleares,
Caixa Postal 941, 30123-970 Belo Horizonte, MG
mingote@cdtn.br, esct@cdtn.br, rubens@cdtn.br

ABSTRACT

Tritium determination is important in several applications, such as groundwater survey, quantification of aquifer recharge, and oil recovery from reservoirs, in which tritiated water is used to tag injection fluids. Since an oil field has many injection and production wells, it is necessary to use more than one tracer to discriminate the individual contribution of different injection in production wells. The development of a variety of tracers for use in oil fields is an objective of the research group at CDTN. Tritiated water, considered as an ideal tracer, is used as a reference for the behavior analysis of the behavior of the new tracers in tests carried out in reduced physical model of the reservoir aimed at verifying the occurrence of diverse interactions that may occur with the tracer during the investigation process. To determine tracer response the tritium content in the samples is measured by liquid scintillation spectrometry. This work presents the methodology employed in this analysis, improvements that have been made and also those that are still required. A low background liquid scintillation system detector, Perkin Elmer-Wallac Quantulus 1220, has been used. Due to the low volume of samples usually obtained in such tests, small polyethylene vials have been used. Since the sample characteristics varied with the characteristics of the tracer studied, the use of quenching correction methods and changes in the sample load capacity were needed.

1. INTRODUCTION

Tritiated water has the longest history of use as a tracer of waterfloods. The characteristics and dynamics of various process may be evaluated such as groundwater survey, quantification of aquifer recharge and oil recovery from reservoirs. The research in tracer methodology as applied to oilfield production requires the development of different tracers for optimizing oil recovery from more and more complex reservoir situations [1]. The development of a variety of tracers for use in oil fields is an objective of the research group at CDTN [2]. Test are carried out in reduced physical model of the reservoir aimed at verifying the occurrence of diverse interactions that may occur with the tracer during the investigation process. To evaluate the performance of newly developed tracers, tritiated water (HTO) is used as a reference water tracer since it be considered an ideal tracer.

This work presents the methodology employed in tritium determination by liquid scintillation spectrometry (LSC). Some optimizations of the counting performance for tritium determinations in water samples by direct counting were previously defined [3]. Since the sample characteristics varies with the characteristics of the tracer studied, adjustments in the routine procedure were needed. Usually a low volume of samples is obtained in new tracer performance tests, therefore the direct counting is recommended in order to avoid uncertainties due to chemical separation. The most important processes that interfere in tritium determination are chemiluminescence, photoluminescence, color quenching, chemical quenching and physical quenching. Evaluation of quenching effect is necessary in order to calculate counting efficiency. Were also considered other aspects that affect the counting rate like luminescence and sample stability.

2. MATERIALS AND METHODS

A low background liquid scintillation system detector, Perkin Elmer-Wallac Quantulus 1220, was used with the counting tritium configuration and counting window from channel 50 to 200. All samples were prepared in 7 mL polyethylene vial using OptiPhase Hisafe 3 LSC cocktail and counted into 20 mL polyethylene vial, both with caps. This second vial was used as an adapter to hold the small vial. Before counting, the vials were stored into a closed box placed at ambient temperature (20-30 ^{o}C) for at least 24 hours to allow decay of chemi- and photoluminescence [3]. The counting time for each sample was 60 minutes divided into 2 cycles with 3 repeats of 10 minutes each.

To asses the counting efficiency a stock solution of tritiated water, 2554 $\pm$ 1 Bq kg^{-1}, made by gravimetric dilution of a certified reference solution [4] was made. The background was evaluated by using a very old water (dead water), previously distilled, from Thermas Antônio Carlos, Poços de Caldas, Brazil. The quenching was identified by measuring (15 seconds) the external quench parameter SQP(E). The quenching correction was applied to samples with SQP(E) value out range of $\overline{SQP} \pm 2S$, where $\overline{SQP}$ is the mean value and S is the standard deviation to blank background and tritium standard vials. The standard addition technique to calculate the counting efficiency for each individual sample by the addition of standard tritium solution to each sample was used. Also 200 μL (about 110 Bq) of the stock solution of tritiated water made by appropriated dilution of a certified reference solution [5] was used.

3. RESULTS AND DISCUSSION

Quenching and stability of sample/cocktail mixture are important aspects that must be taken into account. It is known that occurs phase separation with the ingrowth the salinity and decrease of pH. So, before the counting, the vial is checked for phase separation. Due to

the low volume of samples usually obtained in performance tests, small polyethylene vials have been used. The sample/cocktail ratio was defined by $f = 40\ \%$, value usually applied at environmental and saline samples to avoid phase separation. Where $f = \frac{V_a}{V_a + V_c} \cdot 100$, V_a and V_c are the sample and cocktail volume, respectively. A sample load of 2.0 mL and 3.0 mL cocktail was used.

The use of 20 mL polyethylene vial as an adapter to hold the small vial showed to be an alternative to vented pico holder (supplied by Perkin Elmer). This can be confirmed by the good performance obtained: tritium counting efficiency of 0.343$\pm$0.001, blank background of 0.97$\pm$0.14 cpm and SQP(E) of 749$\pm$6.

On the account that the sample characteristics vary with the tracer studied, the use of quenching correction methods and changes in the sample load capacity can be necessary. On account that the quenching agent may change from one sample batch to another according to the tracer characteristics, the standard addition technique was chose to avoid quenching curve errors. The usual quenching curve technique to calculate the counting efficiency is applied only for routine analysis by using an appropriated quenching agent.

It was observed the luminescence through the random coincidence spectrum (counting window from channel 50 to 200). The waiting time of 1 day for the counting was adequate and no correction was necessary.

The limit of detection[6] was calculated for each individual sample. For colored samples the counting efficiency decrease until about three times. The effect in the limit of detection was of 0.02 to 0.50 Bq mL^{-1} to unquenched and quenched samples, respectively.

4. CONCLUSIONS

The choise of an appropriated sample/cocktail ratio and the efficiency determination for each individual sample is recommended to prevent errors in the analysis. As a consequence, mistakes in performance evaluation of the new tracers can be avoided since the tritium content is used as a reference water tracer.

ACKNOWLEDGMENTS

The authors are grateful the staff of CDTN/CNEN for their contribution to the realization of this work.

REFERENCES

1. IAEA, “Radiotracer technology as applied to industry,” Tech. Rep. IAEA-TECDOC-1262, International Atomic Energy Agency, Vienna, (2001). 1.

2. R. M. Moreira, “Development of alternative tracers for oil reservoirs,” (2007). 1.

3. E. S. C. Temba, R. M. Mingote, and R. M. Moreira, “Tritium determination in aqueous samples by using LSC Quantulus in CDTN, Brazil,” in *2007 International Nuclear Atlantic Conference - INAC 2007*, (Santos, SP, Brazil), Associação Brasileira de Energia Nuclear - ABEN (September 30 to October 5, 2007). `http://www.inac2007.com.br/dvd/pdf_dvd/E04_1148.pdf`. 1., 2.

4. H-3 Radioactive Standard, “Standard reference material 4926E.” National Institute of Standards & Technology - NIST. Reference date September 03, 1998. 2.

5. Tritiated water, “185 MBq ml^{-1}, 5 mCi code TRS3(19).” Amersham International. 2.

6. L. A. Currie, “Limits for qualitative detection and quantitative determination: application to radiochemistry,” *Anal. Chem.*, vol. **40**, no. 3, pp. 586–593, (1968). 3.

5th International Conference on Tracers and Tracing Methods - TRACER 5
Tiradentes, MG, Brazil, November 2 to 6, 2008

RADON DETERMINATION IN DIFFERENT MATRICES BY USING LSC

Eliane S. C. Temba[1], Raquel M. Mingote[1] and Amenônia M. F. Pinto[2]

[1,2]Centro de Desenvolvimento da Tecnologia Nuclear (CDTN / CNEN - MG)
[1]Serviço de Química e Radioquímica, [2]Serviço de Meio Ambiente e Técnicas Nucleares,
Caixa Postal 941, 30123-970 Belo Horizonte, MG
esct@cdtn.br, mingote@cdtn.br, amfp@cdtn.br

ABSTRACT

In this work procedures applied for the determination of ^{222}Rn in different matrices by using liquid scintillation spectrometry (LSC) are presented. Measurements in a Botucatu sandstone sample to evaluate the radon emanation, and in vaseline oil for future application in oil reservoir studies were performed. In the case of sandstone sample, glass vial containing the solid sample supported by a sheet of polypropylene non-woven cloth and filled with the scintillation cocktail was measured using a low-level liquid scintillation counter. The estimated detection limit was 1 Bq kg^{-1} considering an alpha counting efficiency of 100 % and the region of the radon and its progeny. A low diffusion polyethylene vial was used to the vaseline oil sample and a detection limit of 0.08 Bq L^{-1} and a counting efficiency of 89 %, accounting the ^{214}Po counting region only, were attained. The present study indicated that LSC is a suitable method to determine ^{222}Rn in vaseline oil samples. For the solid samples, modifications are needed in order to increase the sensibility of the technique.

1. INTRODUCTION

^{222}Rn is an isotope of the ^{238}U natural radioactive decay series what makes it an important natural tracer. ^{222}Rn itself decays of ^{226}Ra by an alpha - particle decay with a half-life of 3.8 days to a series of short-lived daughter products (^{218}Po, ^{214}Pb, ^{214}Bi, ^{214}Po). This work aimed at evaluating the viability of measuring ^{222}Rn by using liquid scintillation spectrometry (LSC) in two different kinds of samples, sandstone and vaseline oil, for future application in oil reservoir studies.

The objective was to evaluate the radon emanation from a Botucatu sandstone of Brazil sample to use in reduced physical model of oil reservoir. Botucatu sandstones are fine to medium in grain size, quartzarenites in composition and are usually present in low levels of radium. The ^{222}Rn emanation coefficient is defined as the fraction of radon atoms formed in the solid matrix, that are able to escape and are free to migrate. The structure of the porosity and the moisture content of the ^{226}Ra bearing material are determined by the distribution of ^{226}Ra [1]. Actually, radon emanation from a material depends on many factors and the radon emanation coefficient is not an indicative of radium content. According to the UNSCEAR 2000 Report [2], typical emanation coefficients for rocks and soils range from 0.05 to 0.7.

The methodology for sandstone was based on the work of Buzinny (1996) [3], in which the radon was absorbed in special charcoal canisters from air. The canister was connected to a Teflon vial and after an adequate time to diffusion of the ^{222}Rn to the scintillation cocktail, this was analyzed by using LSC. Moreover, a procedure to radon determination in vaseline was tested in order to use a pharmaceutical grade vaseline oil as simulation liquid for oil reservoir.

2. MATERIALS AND METHODS

A low-level liquid scintillation system detector Perkin Elmer-Wallac Quantulus 1220 was used for the measurements. For the efficiency determination, a ^{226}Ra solution with an activity of 2.18$\pm$0.26 Bq mL^{-1}, prepared by gravimetric dissolution from NIST-SRM-4967A ^{226}Ra standard solution was used.

Sandstone sample

The proposed methodology here was to use a sheet of polypropylene non-woven cloth to contain the sandstone sample inside the vial previously filled with scintillation cocktail. The sheet was put under the vial cap so that much there was no contact between the sample and the scintillation cocktail. The counting parameters were:

- Sample: 5 g of the Botucatu sandstone, Brazil.
- Vial: Glass vial with urea screw caps.
- Scintillation cocktail: Ultima Gold AB from Perkin Elmer. The volume used for the scintillation cocktail was 8 mL, which avoided a direct contact with the sample.
- Counting conditions: The samples were counted for 180 minutes, first after the equilibrium between radon and its progeny was attained (3 hours) and then after 6 days of sample preparation. The PSA=95 and counting window in the α region of 700-900 channel were used.

Vaseline sample

In order to determine radon in vaseline oil, the following counting parameters were used:

- Sample: 10 mL of the pharmaceutical grade vaseline oil

- Scintillation cocktail: 12 mL of the Optiscint Hisafe, from Perkin Elmer, an immiscible DIN-based scintillation cocktail is suitable for all organic samples.
- Vial: Low diffusion polyethylene vial, from Perkin Elmer.
- Counting conditions: The samples were counted for 60 minutes, each vial, in the selected counting windows 700-900 (^{222}Rn + ^{218}Po + ^{214}Po) and 835-900 channels (^{214}Po). The PSA=100 and a delay time for counting of 3 hours and 24 days after sample preparation were used.
- Background: For background estimation, it was prepared a blank sample with vaseline and scintillation cocktail, whose ratio was 10/12.

3. RESULTS AND DISCUSSIONS

Sandstone sample

Glass vial was used to avoid losses of radon by diffusion through the walls of the vial. Although it is known that it presents background counts greater than the polyethylene Teflon-coated ones, it permits a good visualization of the sample.

Figure 1 shows the alpha spectrum with the scintillation cocktail Ultima Gold AB obtained by diffusion of a ^{226}Ra standard solution (5 Bq) through the sheet of polypropylene non-woven cloth after delay time of 3 hours. The counting window was set to 700-900 channels according to the alpha region of ^{222}Rn and its progeny.

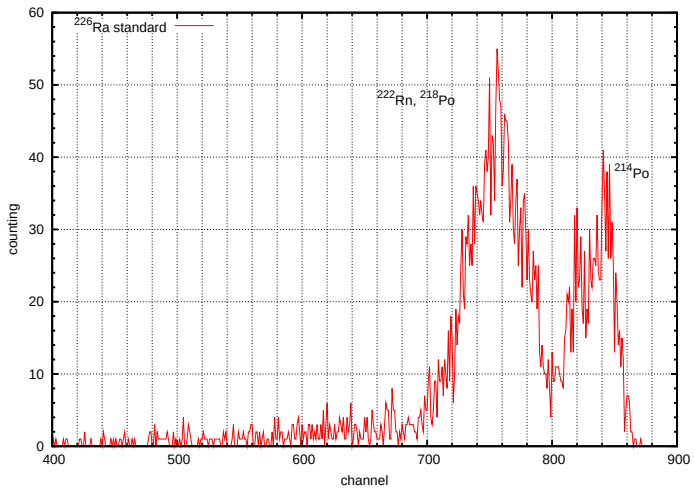

Figure 1. ^{226}Ra standard diffusion spectrum by using Ultima Gold AB

Initially, the cocktail Ultima Gold AB was chosen due to its specific design to the α/β discrimination. However, it is shown a high alpha background counting. This can be due to the presence of some ^{226}Ra impurity as observed by Salonen (1997) [4]. Also the great background in the α region may be due to the beta interference in the PSA selected, which needs to be better studied. The background counts obtained from 8 mL of three different cocktails were shown in Table 1. All cocktails are di-isopropylnaftalene based, that enables good α/β discrimination.

Table 1. Alpha background counts for different cocktails in glass vial

Scintillation cocktail	Counting rate, cpm
Ultima Gold AB	0.670 ± 0.062
Optiphase Hisafe3	0.045 ± 0.016
Optiscint Hisafe	0.097 ± 0.023

Counting time: 180 minutes, Counting window: 700-900 channel

Due to the adsorption/equilibrium time between the sandstone and the scintillation cocktail be unknown, the samples were counted twice, first waiting 3 hours of the sample preparation, when the equilibrium between radon and its progeny was reached. Then the counting was repeated after 6 days. The obtained results showed that 3 hours is a waiting time proper for the radon determination.

The estimated detection limit was 1 Bq kg^{-1} considering an alpha counting efficiency of 100 % and 5 g of sample, calculated according to Currie (1968) [5]. Radon emanation measurements of the Botucatu sandstone and also of the certified soil sample IAEA-375, with a ^{226}Ra content of 20 ± 2 Bq kg^{-1}, were carried out. The ^{222}Rn activity obtained for both samples were below the estimated detection limit (1 Bq kg^{-1}). The low radon emanation measurements were confirmed with results obtained using AlphaGuard radon gas monitor.

Although the proposed procedure was not suitable for determining low radon emanation coefficient, the results showed that this raw Botucatu sandstone sample is not proper as the reduced physical model of oil reservoir in studies using radon as natural tracer. The utilization of polyethylene Teflon-coated vials and consequently lower background could increase the sensibility of the method. Another scintillation cocktails must be tested and a calibration procedure needs to be established. In addition, the used small sample quantity is the most limitative factor for the sensibility of the technique.

Vaseline samples

Teflon-coated polyethylene vial and Optiscint scintillation cocktail which is designed for organic samples were used. Figure 2 shows the spectrum of the ^{222}Rn and its progeny ob-

tained by using a ^{226}Ra solution standard. The observed efficiencies were 299 % for the region of 700-900 channels, corresponding to 3 alpha decays (^{222}Rn, ^{218}Po and ^{218}Po). However, by accounting only the region of ^{214}Po, the counting efficiency was 89 %, corresponding to 1 alpha decay. The efficiency was slight lower than the other alphas, as observed by Salonen (2006) [6] on the aqueous samples. This fact was attributed to the short half-life of ^{214}Po (164 μs), so some counts are lost during the dead time of the spectrometer. Considering the higher counting efficiency in alpha region, the PSA value needs be better defined to minimize the beta interference.

Values of SQP(E) quenching parameter obtained above 900 showed an unquenched sample. The background counting observed for this sample was 0.0068 cpm in the region 700-900 channels and 0.017 cpm in the region 835-900 channels (the region of ^{214}Po). The detection limit obtained was 0.10 Bq L^{-1} to the region of 700-900 channels and 0.08 Bq L^{-1} to the region of 835-900 channels, calculated according to Currie (1968) [5].

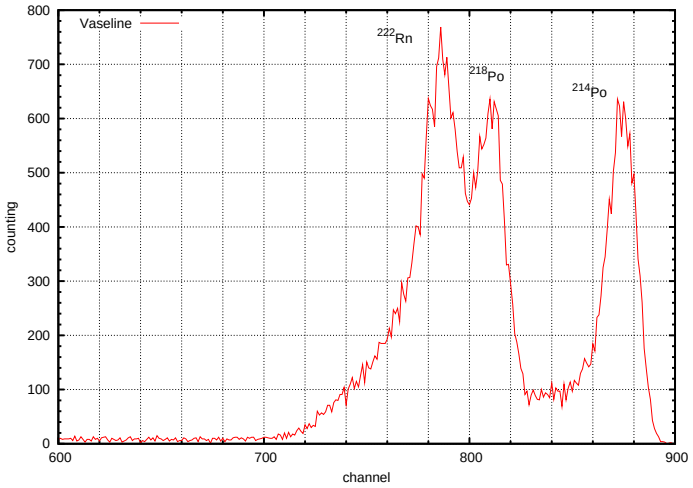

Figure 2. ^{226}Ra standard spectrum in liquid vaseline

4. CONCLUSIONS

The main advantage of procedures described here are its simplicity and the possibility of obtaining results in a relatively short time. The present study indicated that LSC is a suitable method to determine ^{222}Rn in vaseline oil samples. For the solid samples, modifications are needed in order to increase the sensibility of the technique.

ACKNOWLEDGMENTS

The authors are very grateful to the staff of CDTN/CNEN for their support to the realization of this work.

REFERENCES

1. E. M. El-Afifi, S. M. Khalifa, and H. F. Aly, "Assesssment of the ^{226}Ra content and ^{222}Rn emanation fraction of te-norm wastes at certain sites of petroleum and gas production in Egypt," *J. Radioanal. Nucl. Chem.*, vol. **260**, no. 1, pp. 221–224, (2004). 1.

2. UNSCEAR, "Sources and effects of ionizing radiation." United Nations, (2000). 1.

3. M. G. Buzinny, "A new approach to determining ^{222}Rn in air using liquid scintillation counting," in *Liquid Scintillation Spectrometry 1994 - Int. Conf. on Advances in LSC* (G. Cook, D. Harkness, G. MacKenzie, B. Miller, and M. Scott, eds.), (Glasgow), pp. 137–140, Radiocarbon, (1996). 1.

4. L. Salonen and H. Hukkanen, "Advantages of low-background liquid scintillation alpha-spectrometry and pulse shape analysis in measuring ^{222}Rn, uranium and ^{226}Ra in groundwater samples," *J. Radioanal. Nucl. Chem.*, vol. **226**, no. 1-2, pp. 67–74, (1997). 3.

5. L. A. Curie, "Limits for qualitative detection and quantitative determination: application to radiochemistry," *Anal. Chem.*, vol. **40**, no. 3, pp. 586–593, (1968). 3., 3.

6. L. Salonen, "Alpha/beta liquid scintillation spectrometry in surveying finnish groundwater samples," *Radiochemistry (Transl. of Radiokhimiya)*, vol. **48**, pp. 606–612, (2006). 3.

5th International Conference on Tracers and Tracing Methods - TRACER 5
Tiradentes, MG, Brazil, November 2 to 6, 2008

^{222}Rn DETERMINATION IN BRINE SAMPLES BY USING LIQUID SCINTILLATION SPECTROMETRY

Thiago C. Oliveira[1], Raquel M. Mingote[1] and Rubens M. Moreira[2]

[1,2] Centro de Desenvolvimento da Tecnologia Nuclear (CDTN / CNEN - MG)
[1] Serviço de Química e Radioquímica, [2] Serviço de Meio Ambiente e Técnicas Nucleares,
Caixa Postal 941, 30123-970 Belo Horizonte, MG
tco@cdtn.br, mingote@cdtn.br, rubens@cdtn.br

ABSTRACT

Liquid scintillation spectrometry is the most common technique used for ^{222}Rn determinaton in environmental aqueous sample. The purpose of the present work is to analyze the interference of the salinity in the ^{222}Rn determination in brine water by using two different kinds of cocktail: Ultima Gold AB and Optiscint. Both cocktails were found to be suitable, however the Optiscint is recommended due to its quenching resistance.

Keywords: radon, liquid scintillation spectrometry, brine samples

1. INTRODUCTION

^{222}Rn is a radioactive noble gas which is widely found in the environment. Produced in rocks and soil from the decay of ^{226}Ra, radon is an alpha-particle emitter with a half-life of 3.8 days and decays to a series of short-lived daughter products (^{218}Po, ^{214}Pb, ^{214}Bi, ^{214}Po). It exists at low concentrations in surface waters, whereas its concentration in groundwaters can have greater orders of magnitude. The liquid scintillation spectrometry (LSC) is a technique widely utilized for radon determination in water [1, 2, 3]. The two main advantages of this technique were alpha counting efficiency about to 90 % (^{214}Po region) and an easy sample preparation.

Radon is recognized as a being potentially important natural partitioning tracer [4] that makes it possible to be used as a tracer in oil reservoirs. Information about the reservoir structure may be obtained by produced water composition which is a salty brine generated during the oil production. The salts content is usually higher than the seawater salinity and varies widely between fields or even within the same field.

The aim of the present work is to evaluate the salinity effect in the radon determination by using LSC. The performance of two di-isopropylnaphthalene-based (DIN) liquid scintillation cocktails were tested. This solvent is nonflammable, biodegradable, safer to use and enables good alpha/beta discrimination. The first cocktail, Ultima Gold AB, is aqueous-miscible and

specifically designed for alpha/beta discrimination. The second, Optiscint, is suitable for all organic samples.

2. MATERIALS AND METHODS

It was used Teflon-coated polyethylene vials and the cocktails Ultima Gold AB and Optiscint, all supplied by Perkin Elmer. A low background liquid scintillation system detector, Perkin Elmer - Wallac Quantulus 1220, equipped with an anticoicidence guard counter and pulse shape analyzer was used.

The used counting parameters were previous defined [5] for water samples. The selected pulse shape analyzer values (PSA) were 95 and 85 for Ultima Gold AB and Optiscint, respectively. The counting window was defined by ^{214}Po region, from 700 to 800 channel and from 900 to 950 channel for Ultima Gold AB and Optiscint, respectively. The sample/cocktail ratio for water sample was 10/12 mL for both cocktails. Due to the salts content, the used sample/cocktail ratio was 8/12, which is usually applied to saline water as seawater samples.

In order to verify the salinity effect in radon determination by using LSC, high brine samples (40 to 120 g L^{-1}) were prepared using “pro analysis” grade reagents. The ions present in brine samples of Campos Basin, Na^+ (30 %), K^+ (1 %), Mg^{2+} (3.7 %), Cl^- (55 %), $SO_4{}^{-2}$ (7.7 %) [6], were considered the most important.

The radon counting efficiency was evaluated by using a ^{226}Ra standard solution according to Salonen (1993) [7] methodology for both cocktails. In order to know the contributions of ^{226}Ra and ^{210}Po in the α spectrum, N_2 was bubbled through the ^{226}Ra standard solution (1 Bq) for 4 hours. Then, the cocktail was added and immediately counted for establishing the blank during 60 minutes (3 x 20 minutes). The ^{226}Ra standard samples were measured after 25-30 days to determine radon counting efficiency.

3. RESULTS AND DISCUSSION

Table 1 shows the salinity effect in radon determination. It was observed a phase separation and a non-transparent emulsion for all samples when the Ultima Gold AB cocktail was used. If a phase separation is shown, then a decrease in counting efficiency is to be expected due to the inhomogeneous distribution of the radioelement in the total volume of the counting vial. However, on account of the high solubility of radon in the organic compounds, the decrease in the radon counting efficiency was significant only for high salts concentration. We consider that the decrease of the counting efficiency by using the cocktail Ultima Gold AB occured mainly due to the physical quenching. The poor resolution observed in the sample spectra (Fig. 1) is typical of quenching presence.

On other hand, the cocktail Optiscint showed a high SQP(E) quenching parameter, that was evidenced by good resolution presented to all samples (Fig. 2). The lower counting efficiency compared to Ultima Gold AB cocktail is due to the partitioning radon between the organic and aqueous phases into vial.

Table 1. Radon determination by using the cocktails Ultima Gold AB and Optiscint

Cocktail	Salinity ($g\,L^{-1}$)	Efficiency (%)	Background (cpm)	SQP(E)	LLD ($Bq\,L^{-1}$)
Ultima Gold AB	40	87	0.05	795	0.04
	80	86	0.02	795	0.03
	120	61	0.10	790	0.08
Optiscint	40	68		944	
	80	68	0.02	937	0.04
	120	64		942	

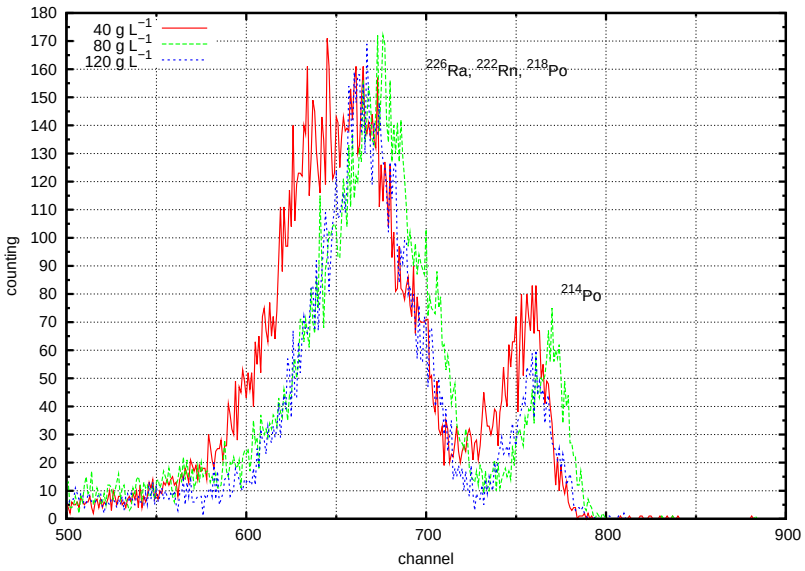

Figure 1. Alpha spectra of ^{226}Ra standard by using Ultima Gold AB for brine samples

4. CONCLUSIONS

Taking into account the data obtained in this study, both cocktails (Ultima Gold AB and Optiscint) can be used for radon determination in brine samples. However, the cocktail Optiscint is recommended due to its better resistance to the quenching.

ACKNOWLEDGMENTS

The authors are grateful to the staff of CDTN/CNEN for their contribution to this work.

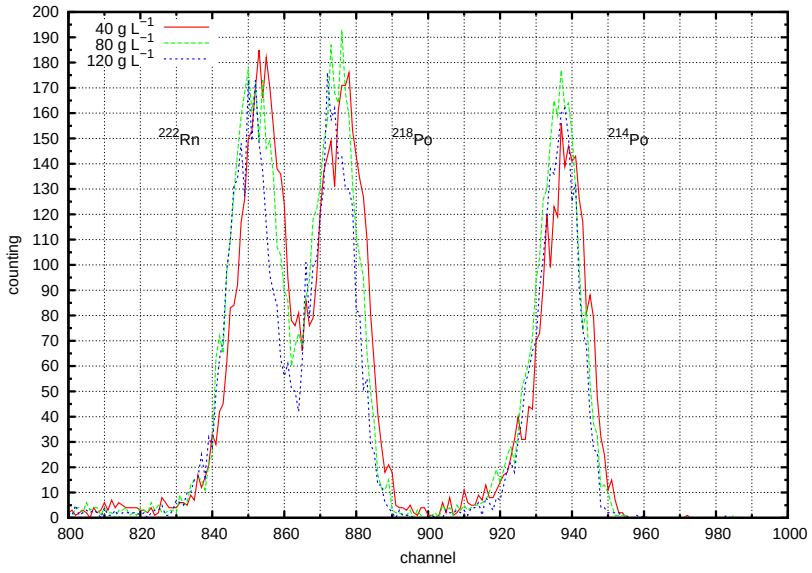

Figure 2. Alpha spectra of ^{226}Ra standard by using Optiscint for brine samples

REFERENCES

1. M. Forte, R. Rusconi, E. Di-Caprio, S. Bellinzona, and G. Sgorbati, "Natural radionuclides measurements in drinking water by liquid scintillation counting. methods and results," in *Environmental Chemical Analysis* (P. Warwick, ed.), vol. **II**, pp. 128–142, Royal Chemical Society, (2003). 1.

2. M. G. López, A. M. Sánchez, and V. G. Escobar, "Application of ultra-low liquid scintillation of the determination of ^{222}Rn in groundwater," *J. Radioanal. Nucl. Chem.*, vol. **261**, no. 3, pp. 631–636, (2004). 1.

3. J. M. Pates and N. J. Mullinger, "Determination of ^{222}Rn in fresh water: Development of a robust method of analysis by α/β separation liquid scintillation spectrometry," *Appl. Radiat. Isot.*, vol. **65**, pp. 92–103, (2007). 1.

4. L. Semprini, S. O. Hopkins, and R. B. Tasker, "Laboratory, field and modeling studies of radon-222 as a natural tracer for monitoring (NAPL) contamination," *Transport in Porous Media*, vol. **38**, pp. 223–240, (2000). 1.

5. T. C. de Oliveira, "Estabelecimento de metodologia para determinação de ^{222}Rn por espectrometria de cintilação em líquido para aplicação em reservatórios de petróleo," Dissertação (Mestrado em Ciência e Tecnologia das Radiações, Minerais e Materiais), Centro de Desenvolvimento da Tecnologia Nuclear CDTN-CNEN, Belo Horizonte, (2008). In Portuguese. 2.

6. A. A. Rocha, N. Miekeley, C. L. P. Silveira, and M. C. M. Bezerra, “Determinação de fósforo orgânico em águas de produção petrolífera por ICP- AES e ICP- MS após pré-concentração em coluna de sílica-c_{18},” *Quim. Nova*, vol. **21**, no. 5, pp. 584–589, (1998). In Portuguese. 2.

7. L. Salonen, “Measurement of low levels of ^{222}Rn in water with different commercial liquid scintillation counters and pulse-shape analysis,” in *Liquid Scintillation Spectrometry 1992 - Int. Conf. on Advances in LSC* (J. E. Noakes, F. Schönhofer, and H. A. Polach, eds.), pp. 361–372, RADIOCARBON, (1993). 2.